SOVIET PHYSICS

JETP

A translation of the Journal of Experimental and Theoretical Physics of the USSR.

SOVIET PHYSICS JETP VOL. 36 (9), NO. 2, pp. 239-451 AUGUST, 1959

INTERMEDIATE-ENERGY PHOTODEUTERONS FROM C^{12} *AND* Be^9

V. P. CHIZHOV and L. A. KUL'CHITSKIĬ

Leningrad Physico-Technical Institute, Academy of Sciences, U.S.S.R.

Submitted to JETP editor June 26, 1958

J. Exptl. Theoret. Phys. (U.S.S.R.) **36**, 345-352 (February, 1959)

The energy distributions of deuterons and protons and the energy dependences of the ratios of the deuteron to proton yields in the photodisintegration of C^{12} and Be^9 are presented. Bremsstrahlung from a synchrotron was used, with $E_{\gamma\,max} = 80$ Mev in the case of C^{12} and $E_{\gamma\,max} = 90$ Mev in the case of Be^9. The angular distributions of deuterons and protons from Be^9 are also given. A semi-empirical analysis of the results for deuterons is carried out on the assumption that the deuterons are formed in the so-called "pick-up" process. The experimental results obtained by other investigators are also analyzed.

1. INTRODUCTION

INVESTIGATIONS of deuterons produced in photonuclear reactions usually establish the ratio of the deuteron yield to the proton yield over a single and often quite broad energy range.[1,2] Only reference 3 has reported the ratio of the deuteron yield to the proton yield as a function of the energies of these particles for a few elements. We possess extremely scanty information on the angular distributions of photodeuterons.

In the investigations that have been mentioned it was determined that the ratio between the photodeuteron and photoproton yields ranges from a few percent to a few tens percent. Such large ratios cannot be accounted for by the statistical theory of nuclear reactions. The authors of reference 3 suggest without obtaining numerical estimates that the experimental results may be accounted for if deuterons are produced by the so-called pick-up process.*

It was necessary to make a detailed study of the relative photodeuteron yields as a function of energy, as well as of the energy and angular distributions. We shall give these relations for deuterons produced through the photodisintegration of C^{12} by bremsstrahlung with $E_{\gamma\,max} = 80$ Mev and of Be^9 with $E_{\gamma\,max} = 90$ Mev. The results are interpreted by means of the pick-up deuteron reaction, which means that a two-stage mechanism is assumed for the (γ, d) reaction. In the first stage the quantum is absorbed by a single nucleon in the nucleus. In the second stage, this nucleon, which is now regarded as free, snatches a complementary nucleon from the same nucleus with sufficient momentum so that a deuteron can be formed and escape from the nucleus as a bound system.

2. EXPERIMENTAL TECHNIQUE AND RESULTS

Particles ejected from nuclei as a result of photodisintegration were detected and identified by means of two independent telescopes, each of which consisted of two scintillation counters connected in coincidence and serving as spectrometers. In each recorded event, therefore, a particle passed through the thin crystal of the first counter, losing the energy $\Delta E \sim dE/dx$, and lost its residual energy E in the second crystal. The pairs of pulses, which

*The term "pick-up" is used in the foreign literature to designate the capture of a nucleon.

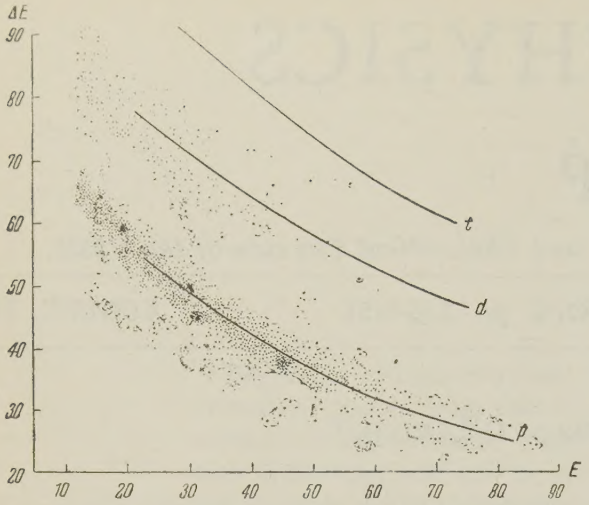

FIG. 1. Relation between energy ΔE absorbed in first telescope crystal and energy E absorbed in second crystal for particles of different masses: p – protons, d – deuterons, t – tritons.

were proportional to $\Delta E \sim dE/dx$ and E, respectively, were separated in time by a delay line, after which they passed to the oscilloscope plates and were finally photographed. The switching circuit provided for triggering of the oscilloscope beam only when a gamma-ray beam was associated with coincident pulses from the telescope counters.

When the energy resolution of the scintillation counters is sufficiently good, rapid and reliable particle identification results from an analysis of pulses proportional to E and ΔE, respectively. Adequate energy resolution for this purpose was achieved only by using NaI(Tl) crystals as scintillators. The thin crystal of the first counter had a thickness of about 0.8 mm and the energy resolution for alpha particles from a polonium source was better than 10%. The crystal of the second counter was thick enough to stop protons with energy ~60 Mev and the energy resolution for the gamma-ray line of the Cs^{137} source was 10 – 12%. Figure 1 gives a typical picture of the separation of protons and deuterons from Be^9. Each point represents a particle which lost the energy ΔE in the first crystal and its entire residual energy E in the second crystal. The solid curves were calculated for protons, deuterons and tritons. Points representing electrons differ markedly from all other points and are not shown in the figure. It is evident that points which can be ascribed to tritons make an extremely small contribution. In this experiment protons with energies above 50 Mev and deuterons with energies above 18 Mev are analyzed; these thresholds make it unnecessary to supply a correction for the absorption of energy in the target, air and materials protecting the NaI(Tl) crystals.

Some of our experimental data were reported at a conference on nuclear reactions at low and intermediate energies.[4] Figure 2 shows the energy distributions of deuterons and protons from Be^9 with the telescope at 90° to the direction of the gamma-ray beam. The abscissas are particle energies E in Mev and the ordinates are the numbers of protons $N_p(E_p, \theta = 90°)$ and of deuterons $N_d(E_d, \theta = 90°)$ in arbitrary units per 1-Mev energy interval and per unit radiation dose. Analogous data for C^{12} using the same notation are shown in Fig. 3. In both figures the heights of the rectangles represent the maximum statistical errors while the widths represent the particle energy in-

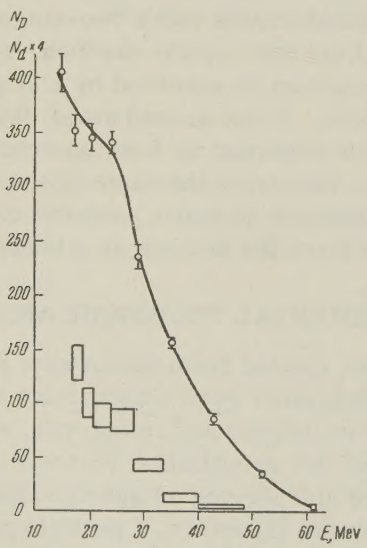

FIG. 2. Energy distributions; o – photoprotons and □ – photodeuterons from Be^9 with $E_{\gamma\,max}$ = 90 Mev. The scale of the ordinate axis for deuterons is enlarged by a factor of 4.

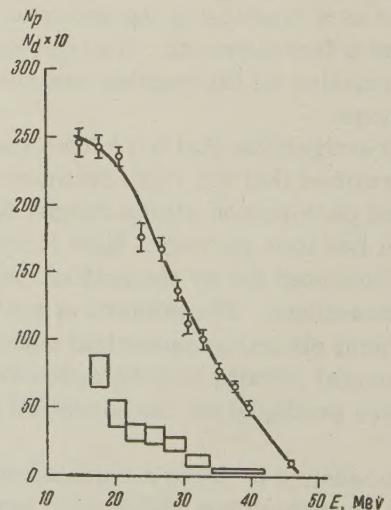

FIG. 3. Energy distributions: o – photoprotons and □ – photodeuterons from C^{12} with $E_{\gamma\,max}$ = 80 Mev. The scale of the ordinate axis for deuterons is enlarged by a factor of 10.

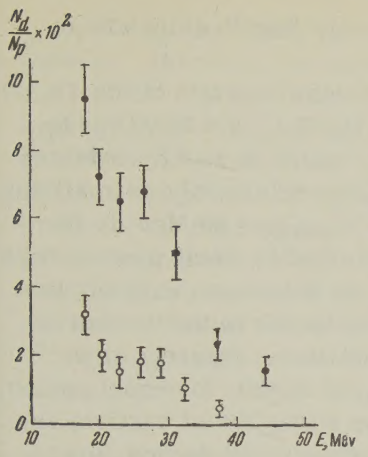

FIG. 4. Ratio of the number of photodeuterons to the number of photoprotons with the same energy, as a function of energy: o – for C^{12} and • – for Be^9.

tervals. The continuous lines are smoothed curves of experimental proton energy distributions.

Figure 4 gives the ratio

$$\frac{N_d(E_d, \theta = 90^\circ)}{N_p(E_p, \theta = 90^\circ)}$$

with $E_p = E_d$, as a function of the energy $E = E_p = E_d$ of these particles for Be^9 and C^{12}. The relative yield of deuterons from Be^9 is seen to be considerably greater than that from C^{12}. Figure 5 gives three points of the angular distributions of photodeuterons and photoprotons from Be^9 in the laboratory coordinate system. Normalization was performed by superimposing the points for deuteron and proton emission at 90° to the gamma-ray beam. The measurements include deuterons with $E_d > 18$ Mev and protons with $E_p > 16$ Mev. Figure 5 shows that the angular distributions of deuterons and protons are similar with their peaks shifted to at least 50 – 60°.

3. DISCUSSION OF EXPERIMENTAL RESULTS

As has been stated in Sec. 1, we are assuming a two-stage mechanism for the (γ, d) reaction with a gamma quantum absorbed by a single nucleon of the nucleus in the first stage, after which this nucleon is regarded as free. We may then represent the second stage of the deuteron production process as the pick-up by the free proton or neutron of its complement in the same nucleus, following Chew and Goldberger,[5] who give the angular dependence of the pick-up cross section and the dependence on incident nucleon energy. Following these authors we can write the cross section $d\sigma_{pd}/d\Omega$ for nucleon pick-up by another nucleon to form a deuteron as

$$d\sigma_{pd}/d\Omega \sim \frac{K}{k} N(\mathbf{n}) F(q), \qquad (1)$$

where K and k are, respectively, the momentum

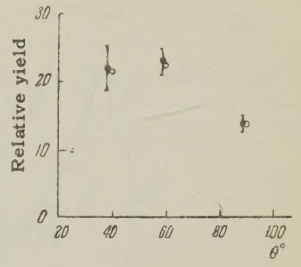

FIG. 5. Angular distributions of photodeuterons (solid circles) and of photoprotons (open circles) from Be^9.

of the outgoing deuteron and of the incident nucleon, $N(\mathbf{n})$ is the distribution function of nucleon momentum $\mathbf{n}$ inside the nucleus and $F(q)$ is a function of relative nucleon momentum in the outgoing deuteron. The last factor possesses much weaker angular and energy dependence than $N(\mathbf{n})$ and will represent a constant in our subsequent applications of (1). The energy distribution of deuterons produced through the bombardment of light nuclei by monoenergetic protons and neutrons[6,7] indicates that in (p, d) and (n, d) reactions deuteron production mainly leaves the residual nucleus in its ground state or in weakly excited states (roughly speaking, up to 5 or 6 Mev). The cross section for the production of deuterons which leave the nucleus in higher excited states falls off sharply, and, as the excitation energy of the residual nucleus increases, it reaches an approximately constant value at $\kappa \approx 0.1 - 0.5$ of the cross section for the production of deuterons that leave the nucleus in its ground state or a weakly excited state. Equation (1) has been confirmed experimentally to a certain extent.[6,7] At present we have no detailed experimental data showing the dependence of the pick-up cross section on incident nucleon energy and shall use (1) as a rough approximation. In our case of continuous bremsstrahlung (also giving the proton energy distributions in the form of the continuous spectra shown in Figs. 2 and 3) the deuterons in any narrow energy interval from E_{d_0} to $E_{d_0} + \Delta E_d$ detected by a telescope at $\theta = 90^\circ$ to the gamma-ray beam are formed by protons and neutrons emitted from nuclei at all angles and at all energies above some minimum. There is no ground for assuming that the (γ, n) cross section[8] is very different from the (γ, p) cross section or that the (n, d) cross section[7] is very different from the (p, d) cross section.[6]

We shall also assume that the energy distribution of high-energy photoneutrons does not differ greatly in shape from that of the photoproton energy distribution and we shall hereinafter speak only of (γ, p) and (p, d) reactions. In virtue of the foregoing we can then estimate the (γ, d) cross section and the deuteron energy distribution from the following expressions:

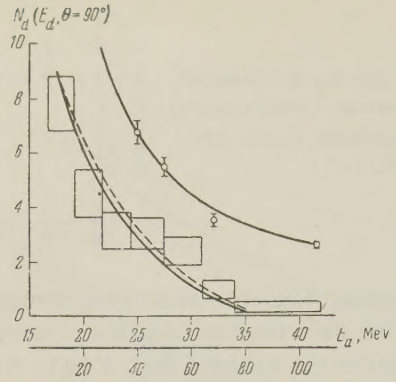

FIG. 6. Experimental and calculated energy distributions of photodeuterons from C^{12}: o – experimental values for $E_{\gamma max}$ = 300 Mev (lower abscissas), rectangles – for $E_{\gamma max}$ = 80 Mev (upper abscissas); the heights of the rectangles represent the statistical errors and the widths represent the energy intervals.

$$\int_0^{\vartheta_0}\int_0^{2\pi}\int_{E_{d_0}}^{E_{d_0}+\Delta E_d} \frac{d\sigma_{\gamma d}(E_d, \vartheta', \varphi')}{d\Omega dE_d} d\Omega dE_d$$

$$= \int_0^{\pi}\int_0^{2\pi}\int_{E_{p\,\min}}^{E_{p\,\max}} \frac{d\sigma_{\gamma p}(E_p, \vartheta, \varphi)}{d\Omega dE_p} P_{pd} d\Omega dE_p; \qquad (2)$$

$$P_{pd} = \frac{\varkappa}{\pi R^2}\int_0^{\vartheta_0}\int_0^{2\pi}\int_{E_{d_0}}^{E_{d_0}+\Delta E_d} \frac{d\sigma_{pd}(E_p, E_d)}{d\Omega dE_d} d\Omega dE_d. \qquad (3)$$

Here P_{pd} is the pick-up probability, $d\sigma_{pd}(E_p, E_d)/d\Omega\, dE_d$ is the cross section for the production of deuterons of energy E_d emitted at the angles ϑ', φ' by nucleons with energy E_p emitted at angles ϑ, φ; $\kappa = 1$ when the residual nucleus is in its ground state or is weakly excited (up to 5 Mev). For more strongly excited residual nuclei $\kappa \approx 0.1 - 0.5$. $E_{p\,min}$ is determined from the equation for the Q reaction.[9] It has been shown experimentally[6] that κ is more or less constant for the angles between proton and deuteron directions that are essential for our calculations. Making the arbitrary assumption that κ is independent of proton energy, and using (1) as the pick-up cross section in (2) with $N(n)$ given experimentally,[6] we obtain roughly the expected energy distribution of photodeuterons from the (γ, d) reaction in C^{12}. Figure 6 gives the calculated and experimental deuteron energy distributions from the (γ, d) reaction in carbon for our case $E_{\gamma max}$ = 80 Mev (the lower solid curve for $\kappa = 0.5$ and the dashed curve for $\kappa = 0.25$) and for $E_{\gamma max}$ = 300 Mev (the upper solid curve for $\kappa = 0.5$). Experimental values were obtained from references 3 and 10 for the last case. The calculated curves were arbitrarily normalized to correspond to the experimental results, which were plotted on an arbitrary scale for each case. It is evident from Fig. 6 that the calculated and experimental deuteron energy distributions are in agreement.

From (2) we can calculate the ratio of the (γ, d) and (γ, p) reactions, $N_d(E_{d_0}, \theta = 90°)/N_p(E_{p_0}, \theta = 90°)$ for $E_{d_0} = E_{p_0}$, which is usually obtained experimentally. Then after arbitrarily normalizing the calculated ratio for $E_{\gamma max}$ = 80 Mev to the experimental results obtained by using gamma rays with $E_{\gamma max}$ = 80 Mev we determine uniquely the ratio of the number of deuterons to the number of protons for $E_{\gamma max}$ = 300 Mev. Figure 7 gives $N_d(E_d, \theta = 90°)/N_p(E_p, \theta = 90°)$ for equal proton and deuteron energies as a function of particle energy E. The lower continuous and dashed curves represent the calculated ratios for $E_{\gamma max}$ = 80 Mev using $\kappa = 0.5$ and 0.25, respectively. These curves were normalized at an arbitrary point. The upper continuous and dashed curves represent, after the first normalization, the uniquely determined ratio $N_d(E_d, \theta = 90°)/N_p(E_p, \theta = 90°)$ for $E_{\gamma max}$ = 300 Mev with $\kappa = 0.5$ and 0.25, respectively. The experimental values for $E_{\gamma max}$ = 300 Mev were taken from reference 3. It is evident from Fig. 7 that the calculation based on the two-stage (γ, d) mechanism that N_d/N_p shows a considerable tendency to grow as the maximum gamma-ray energy increases, which is also in agreement with experiment.

A more direct test of the pick-up mechanism in (γ, d) reactions would be provided by comparing with experiment the ratio N_d/N_p calculated from (2) after substituting the experimental values of the pick-up cross section $d\sigma_{pd}/d\Omega\, dE_d$. This would require experimental values of the pick-up cross section over broad intervals of proton energy val-

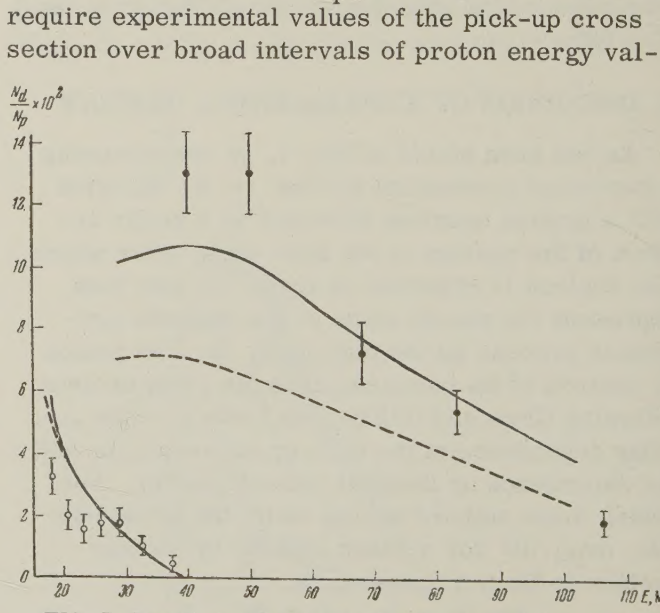

FIG. 7. Experimental and calculated ratios of the number of photodeuterons to the number of photoprotons from C^{12} as functions of particle energy: o – with $E_{\gamma max}$ = 80 Mev and • – with $E_{\gamma max}$ = 300 Mev.

ues and angles, which we unfortunately do not yet possess. However, we may attempt a rough estimate of the (γ, d) cross section in C^{12}, using experimental values of the (p, d) reaction from reference 6 or reference 11 extrapolated by means of (1) to the proton energies and angles required in (2). If (1) represents the actual energy and angular dependences of the (p, d) cross section even roughly, we may expect that the calculated and experimental values of the ratio N_d/N_p for C^{12} will agree in order of magnitude. Some indication that this extrapolation may be justified lies in the fact that when we use (1) to extrapolate the cross sections obtained from references 6 and 11 to the cross sections for the same proton energy and deuteron emission angle the numerical values are very close. The accompanying table gives the experimental values of $N_d(E_d, \theta = 90°)/N_p(E_p, \theta = 90°)$ which were represented in Fig. 7 and the corresponding calculated ratios using the experimental value of the (p, d) cross section[11] with $\kappa = 0.25$ and $r_0 = 1.4 \times 10^{-13}$ cm. The average statistical error of the experimental ratios is ±20%, while the minimum of the (p, d) cross section taken from Ref. 11 is ±50%. Assuming identical photoproton and photoneutron contributions to deuteron production, it is better to compare the calculated ratios given in the table with halved values of the experimental results in the table. The calculated and experimental ratios are seen to be of the same order of magnitude.

$E_{\gamma\,max} = 80$ Mev			$E_{\gamma max} = 300$ Mev		
E_p, E_d, Mev	$N_d(E_d, \theta=90°)/N_p(E_p, \theta=90°)$, %		E_p, E_d, Mev	$N_d(E_d, \theta=90°)/N_p(E_p, \theta=90°)$, %	
	Experimental	Calculated		Experimental	Calculated
18	3.2	7.3	40	13	10.4
20.5	2	5.2	50	13	9.5
23	1.5	4.0	68	7	7.3
26	1.8	3.0	83	5.4	5.6
29	1.8	2.0			
32.5	1	1.2			

All of the foregoing estimates agree qualitatively with experimental results. Further study of the angular distributions of photodeuterons may provide additional information on the (γ, d) reaction.

The authors wish to thank the synchrotron group of the Physico-Technical Institute of the Academy of Sciences under the direction of N. N. Chernov for their assistance and cooperation.

[1] B. Forkman, Ark. f. Fysik **11**, 265 (1956).

[2] L. S. Ring, Jr., Phys. Rev. **99**, 137 (1955).

[3] DeWire, Silverman, and Wolfe, Phys. Rev. **92**, 519 (1953).

[4] Bazhanov, Volkov, Komar, Kul'chitskiĭ, Chizhov, and Yavor, Тр. Всесоюзной конференции по ядерным реакциям при малых и средних энергиях (Trans. All-Union Conference on Low-Energy and Intermediate-Energy Nuclear Reactions) Moscow, 1957, Acad. Sci. Press, 1958.

[5] G. F. Chew and M. L. Goldberger, Phys. Rev. **77**, 470 (1950).

[6] W. Selove, Phys. Rev. **101**, 231 (1956).

[7] J. C. Hadley and H. York, Phys. Rev. **80**, 345 (1950).

[8] A. P. Gorbunov and V. M. Spiridonov, J. Exptl. Theoret. Phys. (U.S.S.R.) **34**, 862 (1958), Soviet Phys. JETP **7**, 596 (1958).

[9] R. D. Evans, The Atomic Nucleus, McGraw-Hill Book Co., New York, 1955, p. 408.

[10] J. C. Keck, Phys. Rev. **85**, 410 (1952).

[11] R. Britten, Phys. Rev. **88**, 283 (1952).

Translated by I. Emin
62

LIFETIME OF THE FIRST EXCITED STATE IN Be^{10}

A. N. BOYARKINA and A. F. TULINOV

Institute of Nuclear Physics, Moscow State University

Submitted to JETP editor June 27, 1958

J. Exptl. Theoret. Phys. (U.S.S.R.) **36**, 353-361 (February, 1959)

A method is described for measuring the lifetime of nuclear excited states, using the recoil nuclei, together with an experiment to find the lifetime τ of the 3.37-Mev excited state in Be^{10}. An upper limit for τ of 8×10^{-14} sec is obtained.

1. INTRODUCTION

EXPERIMENTAL investigation of γ-ray transition probabilities are an important source of information about nuclear structure. For light nuclei, the excitation energies of even the lowest states are rather large and the lifetimes of these states usually less than 10^{-10}sec, so that direct methods of obtaining τ, based on decay schemes, are not applicable. To measure short lifetimes, indirect methods must be used, such as measuring widths Γ in resonance reactions, resonance scattering of γ-rays, and the Doppler shift method.

Unfortunately, none of these methods can be applied over a wide range of conditions. Thus, in the first of those mentioned above the width Γ can be measured only for levels close to the dissociation energy of the nucleus. Resonance scattering of γ rays can be used only with stable isotopes occurring naturally with a reasonable abundance. The Doppler-shift method can be more generally applied, but technical difficulties limit its usefulness.

A new method has recently been proposed[1] for measuring the lifetimes of excited states in light nuclei. It has about the same range of applicability as does the Doppler shift method, but the technical difficulties involved are less.

The present paper is devoted to a theoretical exposition of this method and a description of an experiment to measure the lifetime of the first excited state in Be^{10}.

2. DESCRIPTION OF THE METHOD

The distinguishing characteristic of reactions involving light nuclei is that the kinetic energy of the recoil nucleus is comparable with the kinetic energy of the lighter component. This circumstance, together with the fact that light nuclei undergo little multiple scattering in thin targets, has the consequence that in a reaction both the direction in which the light component is emitted and the direction in which the nucleus recoils can be fixed.

If the light particle is observed to be emitted in a certain direction, there is a discrete spectrum of angles in which the nucleus could have recoiled, each angle corresponding to a definite energy level of this nucleus.[2] For the ground state, the direction of recoil is uniquely determined. Nuclei recoiling in an excited state had a momentum p_0 given to them during the reaction, and then get some more momentum p_γ when the γ ray is emitted. Usually, the condition $p_\gamma \ll p_0$ holds. Nuclei recoiling in a definite excited state will then be emitted in a cone with angle $\Phi_0 = p_\gamma / p_0$. The fact that Φ_0 depends on the speed of the nucleus when the γ ray was emitted can be used to find the lifetime of the excited state in question.

Let us assume that just after passing through a thin target the recoil nuclei must pass through an absorbing layer of material where they slow down and lose energy. Two cases must be considered: (1) The lifetime τ is small, so that decay occurs before the nuclei slow down; then the size of the cone will be determined by the angle Φ_0. (2) The lifetime τ is large,* so that decay occurs after the nuclei have been slowed down. In this case the angle of the cone Φ_d will be determined by the relation $\Phi_d = p_\gamma / p_d$, where p_d is the momentum of the recoil nucleus upon emerging from the absorbing layer.

It is clear that if the γ ray is emitted while the nucleus is slowing down, the angle of the cone and the angular distribution of recoil nuclei within the cone will be connected in some unique way with the value of τ.

The value of τ can be determined experimen-

*Actually we consider only values of τ which are small compared to the time of flight of the nucleus from the target to the detector (about 20 cm.).

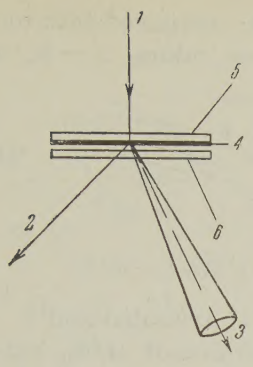

FIG. 1. Schematic of the experiment: 1 – incident beam; 2 – light particle; 3 – recoil nucleus; 4 – target; 5 – backing; 6 – compensating layer.

tally as follows: We count the number of nuclei passing through a small slit on the axis of the cone both when the decelerating layer is present and when it is absent. Since the ratio δ of these two counting rates is a function of τ, the value of the latter can then be calculated. As a decelerating layer we can use the target backing. Then δ is the ratio of the counting rates observed in two target positions differing by 180°.

The considerations above are valid only when we can neglect multiple scattering and the energy straggling in the nuclei due to the backing. If these effects cannot be neglected, the experimental setup must be changed so that these effects are the same in the two positions of the target. This can be achieved by putting a second layer of material, of the same thickness and composition as the target backing, a short distance from the target and parallel to it (see Fig. 1).

Let the target position shown in Fig. 1 be A, and let position B be obtained from A by rotation through 180°. For lifetimes $\tau \geq 10^{-10}$ sec the recoil nuclei travel a distance ~ 0.01 mm. Hence all the decays occur before the compensating layer is reached and the number of nuclei counted in position A will remain independent of lifetime. In this case, δ, the ratio of the counting rate in position B to that in position A, is still a suitable quantity to measure for finding τ.

From the qualitative considerations above, it is clear that the range of lifetimes τ which can be measured is determined by how long the nuclei are decelerated in matter ($10^{-12} - 10^{-14}$ sec). As is well known, the range of lifetimes covered by the Doppler-shift method is about the same. There is, however, a difference between the cases to which the two methods can be applied. Thus, the Doppler-shift technique can be applied to transitions between excited states. The method described here can be applied only to transitions to the ground state. On the other hand, if we differentiate between the various energy particles produced in the reaction, we can investigate transition probabilities for levels

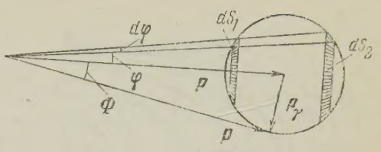

FIG. 2. Angular distribution of recoil nuclei due to γ emission.

lying close together, which is very difficult to do with the Doppler-shift method.

The purpose of the following argument is to obtain the functional relation between δ and τ. Suppose that just before the γ ray was emitted the recoil nucleus had momentum p and that the γ ray gave it an extra momentum p_γ. The distribution function of the nuclei within the cone can then be found from Fig. 2. From this drawing it is clear that the ends of the vectors $\mathbf{P} = \mathbf{p} + \mathbf{p}_\gamma$ will lie on the surface of a sphere of radius p_γ. Since the γ rays are emitted more or less isotropically, the fraction of nuclei scattered through an angle φ into the solid angle $d\varphi$ will be given by the ratio of the total area of the shaded spherical surface in the figure to the total area of the sphere:

$$dN / N = (ds_1 + ds_2) / 4\pi p_\gamma^2. \qquad (1)$$

Remembering that $p_\gamma \ll p_0$, the distribution function $\psi(\varphi)$ of the recoil nuclei in the cone can easily be found, Normalizing $\psi(\varphi)$ so that

$$\int_0^\Phi 2\pi\psi(\varphi)\sin\varphi d\varphi = 1,$$

where $\Phi = p_\gamma / p$, we find that the distribution function has the form

$$\psi(\varphi) = 1 / 2\pi\Phi\sqrt{\Phi^2 - \varphi^2}. \qquad (2)$$

Let the lifetime τ be comparable with the time of deceleration, and let the target be in position B. Then the distribution function will have two components, one due to nuclei decaying in the target backing, and the second due to nuclei that emit γ rays after leaving the backing. Neglecting multiple scattering for the time being, let us find these two distribution functions, which we denote by f_1 and f_2.

Assume that the total range R of a particle in matter is proportional to its speed, $R = \alpha v$.[3] Then from the exponential character of the decay it is easy to show that the probability that a nucleus decays in a layer of the backing having thickness dx and distant x from the target is given by the formula

$$U(x)\,dx = (\lambda\alpha / R)(1 - x/R)^{\lambda\alpha - 1}dx, \qquad (3)$$

where $\lambda = \ln 2/\tau$. Since $p = p_0(1 - x/R)$, formula (2) gives the distribution of recoil nuclei decaying in the layer dx:

$$\psi(x, \varphi) = (1 - x/R)^2 / 2\pi\Phi_0\sqrt{\Phi_0^2 - \varphi^2(1 - x/R)^2}. \qquad (4)$$

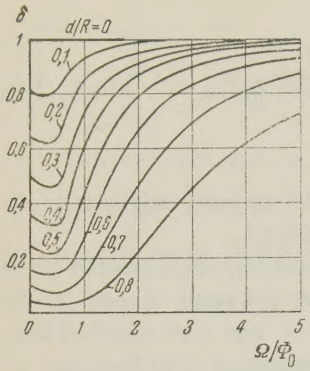

FIG. 3. Dependence of δ on Ω/Φ_0 for various values of the parameter d/R.

The function f_1 is then given by the following:

$$f_1 = \begin{cases} \int_0^d \psi(x, \varphi)\, U(x)\, dx & \text{for } 0 < \varphi \leqslant \Phi_0, \\ \int_{R(1-\Phi_0/\varphi)}^d \psi(x, \varphi)\, U(x)\, dx & \text{for } \Phi_0 < \varphi \leqslant \frac{\Phi_0}{1-d/R}. \end{cases} \tag{5}$$

From (3) it is easy to show that the probability a nucleus decays after passing through a backing of thickness d is $(1-d/R)^{\lambda\alpha}$; hence

$$f_2 = \psi(d, \varphi)\,(1-d/R)^{\lambda\alpha}. \tag{6}$$

Denote the total distribution by $f_B = f_1 + f_2$. If the target is in position A, the distribution function f_A can easily be found from f_B by going to the limit $\tau \to \infty$. It has the form:

$$f_A = 1/2\pi\Phi_0 \sqrt{\Phi_0^2 - \varphi^2}. \tag{7}$$

Now let us take into account multiple scattering in the backing. The distribution function for multiple scattering with dispersion Ω^2 can be written

$$w = (1/2\pi\Omega^2) \exp\{-\varphi^2/2\Omega^2\}. \tag{8}$$

The functions f_B and f_A should be replaced by F_B and F_A, which take on the following values at $\varphi = 0$:

$$F_B(0) = 2\pi \int_0^{\Phi_0/(1-d/R)} f_B(\varphi)\, w(\varphi)\, \varphi d\varphi, \tag{9}$$

$$F_A(0) = 2\pi \int_0^{\Phi_0} f_A(\varphi)\, w(\varphi)\, \varphi d\varphi. \tag{10}$$

The slit in front of the counter has previously been assumed small enough that we can take $\delta = F_B(0)/F_A(0)$. τ enters the expression for δ through the decay constant λ appearing in (5) and (6). The integral in (9) cannot be expressed in terms of elementary functions and must be found by numerical integration.

To get an idea how sensitive the method is, we can consider the values of δ in two extreme cases:

(1) The lifetime τ is small compared with the deceleration time. Evidently, for this case $\delta = 1$.

(2) The lifetime τ is large compared with the deceleration time. In this case, taking $\lambda \to 0$, we obtain

$$\delta = \left(1 - \frac{d}{R}\right) e^{-z_d^2} \int_0^{z_d} e^{t^2} dt \Big/ e^{-z_0^2} \int_0^{z_0} e^{t^2} dt, \tag{11}$$

where

$$z_0 = \Phi_0/\sqrt{2\Omega},\ z_d = \Phi_0/\sqrt{2\Omega}\,(1-d/R).$$

(the integrals occurring in (11) are tabulated[4]).

Figure 3 shows δ as a function of Ω/Φ_0 calculated from formula (11) for various values of d/R. From this figure it is clear that δ is most sensitive to changes in τ for large values of d/R and small values of Ω/Φ_0. These quantities are not independent. At present, the relationship between them cannot be written down in the general case. This can be done, however, for light nuclei when the recoil nuclei and the nuclei in the decelerating layer have masses about 20 and the energy of the recoil nucleus is of order 1 Mev.

With an accuracy sufficient for our purposes, the theory of multiple scattering[5] gives the relation

$$\frac{\Omega}{\Phi_0} = 2\sqrt{\pi N \rho Z_T v \alpha}\, \frac{Z_{nuc}^{1/3} c\hbar}{E_\gamma} \left(\frac{d/R}{1-d/R}\right)^{1/2}. \tag{12}$$

In this formula, N is Avogadro's number, ρ is the density of the decelerating material, Z_T is its atomic number, v and Z_{nuc} are the speed and charge of the recoil nuclei, E_γ is the energy of the γ ray, c is the velocity of light, and h is Planck's constant. From (12) we see that the relation between Ω/Φ_0 and d/R depends critically on the value of E_γ. It is the value of E_γ which gives the fundamental limitation on the applicability of this method. Substituting values into (12) typical for light nuclei it is easy to see that in order for δ to be less than 0.8 it is necessary that E_γ be more than 1.2 Mev. This is not a serious limitation.

The analysis carried out above shows that for sufficiently large excitation energies, δ varies over a fairly wide range.

3. APPARATUS AND MEASUREMENTS

We measured the lifetime of the first excited state in Be^{10}, as formed in the reaction $Be^9(d, p)Be^{10}$. To our knowledge, the lifetime of this state had not been measured before. It is possible to calculate the wave functions of the ground and first excited states of the Be^{10} nucleus in various nuclear models, and from these wave functions the matrix element for the transition between them, so that an experimental measure of the lifetime would have theoretical interest.

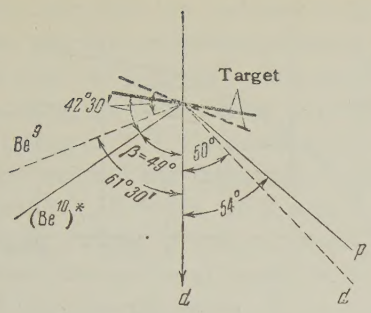

FIG. 4. Angles used in measuring Ω.

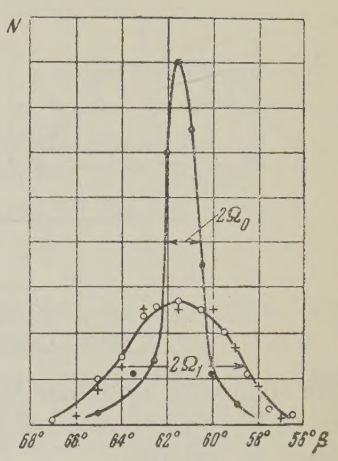

FIG. 5 Angular distribution of recoil nuclei in the elastic scattering of deuterons on Be^9 nuclei.

The incident beam of 4 Mev deuterons was obtained from the cyclotron of the Scientific Research Institute for Nuclear Physics, Moscow State University. Near the target the beam had a diameter of 6 mm and intensity about 10^{-7} amp. The target was a layer of beryllium on an aluminum backing situated at the center of the scattering chamber. The positions of the detectors used to count the protons and recoil nuclei could be varied continuously without breaking the vacuum.[6] The recoil nuclei were detected by an electron multiplier. The protons were registered by a proportional counter.

Pulses from both counters were fed into a coincidence circuit. There was a large unwanted counting rate in the multiplier, due to slow particles coming from the surface of the target[7] and to recoil nuclei from deuteron scattering on aluminum. To minimize the number of accidental coincidences, thin organic films were placed before the entrance to the multiplier. The thickness of the films was chosen so that aluminum recoil nuclei were absorbed while Be^{10} nuclei were transmitted.

The backing and absorbing layers were of aluminum stretched on suitable frames. The frames were mounted so as to make the aluminum foils accurately parallel. The mounting was also such that either foil could be removed at will. The distance between the foils was 1 mm. The angle between the target and the beam could be adjusted to a fraction of a degree. The aluminum layers were prepared by evaporating aluminum in vacuum onto an organic film glued to a thin rubber ring.[8] After the aluminum had been deposited, half of its surface was covered by a shield and beryllium deposited on the other half. The organic film was then dissolved in amyl acetate. The aluminum foil was glued onto two frames so that one carried a layer of aluminum and beryllium while the other carried only aluminum, the aluminum layers being of about the same thickness. The thickness of the compensating layer was measured by comparing the number of deuterons elastically scattered from it with the number scattered from a thicker foil of known thickness. The thickness of the beryllium target was determined by comparing it with a control sample which could be weighed. Particular attention was paid to the uniformity of the layers. Only films with mirror-like surfaces were used.

The experiment was carried out in two steps. First we measured the mean angle of multiple scattering Ω, which is required for the calculations, and compared the thicknesses of the backing and compensating layers. To do this we used the elastic scattering of deuterons from Be^9 nuclei. The second stage was the measurement of δ. This used the reaction $Be^9(d, p)Be^{10}$. In order that the quantity Ω, which was measured for Be^9 nuclei, could be used with Be^{10} it was necessary to choose the angles at which deuterons, protons and recoil nuclei were emitted so that the energies of the Be^9 and Be^{10} nuclei were the same. The geometry used in the experiments is shown in Fig. 4. The Be^9 and Be^{10} nuclei had energy 550 kev. In both cases the angle between the plane of the target and the direction of the recoil nuclei was 42°30′.

Figure 5 shows the measured angular distribution of Be^9 nuclei after elastic scattering. The sharp peak corresponds to target position A without the compensating layer. The wide peak was obtained with the compensating plate in place, the crosses referring to position A and the circles to position B. The thickness of the compensating layer was (55 ± 2) μg/cm². The thickness of the beryllium target was 10 μg/cm². Since the target was at an angle 42°30′ to the direction of the recoil nuclei, we conclude that the recoil nuclei passed through a compensating layer of effective thickness 82 μg/cm². The slit in front of the counter had dimensions 4×4 mm., which corresponded to a solid angle (1×1)°. The slit in front of the multiplier had dimensions 2×36 mm (0.5×9)°. The width of the high peak was determined essentially by the size of the slits and the width of the beam, i.e., by factors that are unaffected by the presence of

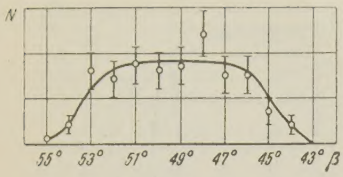

FIG. 6. Angular distribution of the recoil nuclei in the reaction $Be^9(d,p)Be^{10*}$.

	1	2	3	4
A	75×4	112×4	61×4	71×4
B	74×4	116×4	54×4	74×4

the scattering aluminum layer. The mean angle of multiple scattering can be obtained approximately from the relation

$$\Omega = \sqrt{\Omega_1^2 - \Omega_0^2}.$$

In our case $2\Omega_0 = (1.5 \pm 0.2)°$; $2\Omega_1 = (6 \pm 0.5)°$, so that $\Omega = (2.9 \pm 0.3)°$. To compare the thicknesses of the backing and compensating layer, we measured the coincidence counting rate at the peak (61°30′) for the two target positions A and B. The results of several reversals of the target showed that the difference was less than 5%.

The angular distribution of recoil nuclei from the reaction $Be^9(d,p)Be^{10*}$ with target position B is shown in Fig. 6. The slit in front of the counter was 8×8 mm, that in front of the multiplier was 4×20 mm. From the diagram it is evicent that the peak has a full width of about 8°, which is approximately what was expected. The distribution shown corresponds to nuclei recoiling in the first excited state of Be^{10}; nuclei recoiling in the ground state travel in directions around $\beta = 62°$. There could have been little admixture of nuclei in the higher excited states because of the absorber in front of the counter for slow protons.

The angle $\beta = 49°$ was chosen to measure δ. The slits in front of the counter and multiplier were of the same size, 8×8 mm (2×2°). The number of coincidence counts in positions A and B were measured for the same number of counts in the beam integrator. The results are shown in column 1 of the table. This was repeated at the angles used to compare the thicknesses of the aluminum layers. The results are shown in column 2. The whole procedure was then repeated with the results shown in columns 3 and 4. The number of counts in the integrator for each column was arbitrary.

From the table we can see that sithin the statistical errors the thicknesses of the layers are the same. From columns 1 and 3 we get

$$\delta = 0.93 \pm 0.08.$$

Figure 7 shows the functional dependence of δ on $\lambda\alpha$, as calculated from formulas (9) and (10) with the parameters $\Omega = 2.9°$; $\Phi_0 = 2°$; $d/R = 0.6$. The range R of the recoil nuclei was found from the formula $R = \alpha v$, where α was taken to be 4×10^{-13} sec.[9] The value $\delta = 0.93$ corresponds to $\lambda\alpha = 7.2$, but the statistical errors in measuring δ are such that we can only say $\lambda\alpha > 5$. This gives an upper limit to the lifetime $\tau < 8 \times 10^{-14}$ sec.

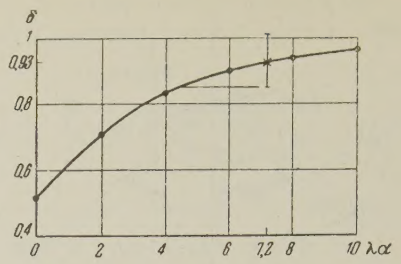

FIG. 7. Determination of limiting value of of $\lambda\alpha$.

4. DISCUSSION OF THE RESULTS

Inglis[10] and Kurath[11] have shown that for the lightest nuclei (up to O^{16}) the shell model gives a satisfactory account of the level schemes, magnetic dipole moments of the ground states, and the probabilities of magnetic dipole γ ray transitions. The constant in the spin-orbit interaction increases monotonically with increasing number the nucleons in the nucleus. For Be^{10} we have $a/K \approx 5$ where a is the constant in the spin-orbit coupling and K is the exchange integral for the central interaction between two nucleons. The first excited state in Be^{10} (3.37 Mev) has spin J = 2, isotopic spin T = 1, while the ground state has J = 0 and T = 1.[12] Both states have positive parity so the transition is pure E2.

To calculate τ we use the relation $\tau = 6.58 \times 10^{-16}/\Gamma$, where Γ is the width of the excited state in electron volts and τ is in seconds. For an E2 transition the formula for Γ can be put in the form[13]

$$\Gamma = 8.1 \cdot 10^{-5} E^5 |\langle JT \| H^{(2)} \| J'T' \rangle|^2,$$

where E is the energy of the transition in mev and $\langle JT \| H^{(2)} \| J'T' \rangle$ is the reduced matrix element for an electric quadrupole transition from a state J, T to a state J′, T′. Denote the wave functions of the J, T and J′, T′ states in the L-S representation by $\{c_i\}$ and $\{b_i\}$ respectively, where i and j are indices labelling the supermultiplet state.[14] Then the expression for Γ has the form

$$\Gamma = 8.1 \cdot 10^{-5} E^5 \left| \sum_{ij} c_i b_j \langle (L_i S_i) JT \| H^{(2)} \| (L_j' S_j') J'T' \rangle \right|^2. \quad (13)$$

To calculate the reduced matrix elements in (13) we use the relations given in reference,[13] and $\langle r^2 \rangle = 10^{-25}$ cm^2. The wave functions were calculated for a centrally symmetric interaction consisting of 80% Majorana and 20% Bartlett forces, the ratio of the integrals for the central interaction being L/K = 6.8. a/K was taken to be 4.75. For these values of the parameters, $\tau = 2.1 \times 10^{-13}$ sec. Decreasing the strength of the spin orbit interaction decreases the value of τ, which reaches a value 1.4×10^{-13} sec in the extreme case of L-S coupling. For the limiting case of j-j coupling the corresponding matrix element is zero.

In view of the difference between the measured and computed values of τ for all possible values of a/K, it becomes interesting to look at the agreement between experimental and theoretical values for other E2 transitions.

Experimental values of τ for pure E2 transitions in the P-shell are known for C^{12} (4.43 mev $\rightarrow$ 0), C^{12} (16.1 mev $\rightarrow$ 0) and B^{10} (0.72 mev $\rightarrow$ 0). The experimental value τ_{exp} for the 4.43 mev $\rightarrow$ 0 transition in C^{12} is 5.25×10^{-14} sec.[15] With the reasonable value for the strength of the spin-orbit coupling $a/K \approx 6$ and with $\langle r^2 \rangle = 5.7 \times 10^{-26}$ cm^2 [16] the shell model gives the value $\tau_{theor} \approx 2.5 \times 10^{-13}$ sec. For the transition 16.1 Mev $\rightarrow$ 0 in C^{12}, $\tau_{exp} = 9 \times 10^{-16}$ sec[15] while $\tau_{theor} = 1.2 \times 10^{-15}$ sec. For the case B^{10}, $\tau_{exp} = 1.05 \times 10^{-9}$ sec[15] while for $a/K > 4$ and the larger value $\langle r^2 \rangle = 10^{-25}$ cm^2, $\tau_{theor} = 2 - 3 \times 10^{-9}$ sec.[11]

Thus in the third and first cases τ_{exp} is substantially smaller than τ_{theor}, while in the second case the two values agree.

The suggestion has been made[11] that the smallness of τ_{exp} compared to τ_{theor} is due to collective motions in the nucleus. In reference 17 it is pointed out that collective motions should have an effect on τ only for transitions where the isotopic spin does not change. The transitions C^{12} (4.43 Mev $\rightarrow$ 0) and B^{10} (0.72 Mev $\rightarrow$ 0) are just of this type. The isotopic spin changes in the transition C^{12} (16.1 Mev $\rightarrow$ 0) and accordingly the values τ_{exp} and τ_{theor} agree. In our case, the isotopic spin does not change in the Be^{10} (3.37 Mev $\rightarrow$ 0) transition (T = T' = 1), so the discrepancy between the experimental and theoretical values of the lifetime is not surprising and supports the conjecture that collective effects exist in light nuclei.

In conclusion the authors would like to express their gratitude to S. S. Vasil'ev and V. G. Neudachin for fruitful discussions, and to Yu. V. Koshelyaev, A. A. Danilov, and V. P. Khlapov for their assistance in carrying out the experimental part of this work.

[1] A. F. Tulinov, J. Exptl. Theoret. Phys. (U.S.S.R.) **32**, 1568 (1957); Soviet Phys. JETP **5**, 1277 (1957).

[2] A. F. Tulinov, J. Exptl. Theoret. Phys. (U.S.S.R.) **31**, 698 (1956); Soviet Phys. JETP **4**, 596 (1957).

[3] P. M. S. Blackett and C. H. Lees, Proc. Roy. Soc. (London) **A134**, 658 (1932).

[4] K. A. Karpov, Таблицы функции $w(z)$ в комплексной области (Tables of the Function w(z) in the Complex Plane) AN SSSR (1954).

[5] N. Bohr, Passage of Atomic Particles Through Matter (Russian Translation) IIL 1950.

[6] A. F. Tulinov, Приборы и техника эксперимента (Instruments and Meas. Engg.) **1**, 112 (1957).

[7] Akishin, Boyarkina and Tulinov, Приборы и техника эксперимента (Instruments and Meas. Engg.), in press.

[8] P. A. Il'chenko, J. Tech. Phys. (U.S.S.R.) **24**, 1136 (1954).

[9] Ya. A. Teplova and A. F. Tulinov, Вестник ЛГУ (Bull., Moscow State University Report), in press.

[10] D. R. Inglis, Revs. Modern Phys. **25**, 390 (1953).

[11] D. Kurath, Phys. Rev. **101**, 216 (1956); **106**, 975 (1957).

[12] F. Ajzenberg and T. Lauritsen, Revs. Modern Phys. **27**, 77 (1955).

[13] A. Lane and L. Radicati, Proc. Phys. Soc. (London) **A67**, 167 (1954).

[14] E. Feenberg and M. Phillips, Phys. Rev. **51**, 597 (1937).

[15] Swann, Metzger and Rasmussen, Bull. Am. Phys. Soc. Ser. II **2**, 29 (1957).

[16] R. Hofstadter, Revs. Modern Phys. **28**, 214 (1956).

[17] V. V. Balashov and A. F. Tulinov, J. Exptl. Theoret. Phys. (U.S.S.R.) **36**, 615 (1959), this issue, p. 426.

Translated by R. Krotkov
63

SPECTRUM OF THE INTERNAL CONVERSION ELECTRONS ACCOMPANYING THE ALPHA DECAY OF Pu^{238} *AND* Pu^{240}

E. F. TRETYAKOV, L. N. KONDRAT' EV, G. I. KHLEBNIKOV, and L. L. GOL' DIN

Submitted to JETP editor June 14, 1958

J. Exptl. Theoret. Phys. (U.S.S.R.) **36**, 362-366 (February, 1959)

The spectrum of conversion electrons accompanying the alpha decay of Pu^{238} and Pu^{240} was studied by means of a high-transmission magnetic spectrometer with toroidal field shape, which measured α-e coincidences. Transitions from the 6+ excited levels were detected, and the multipolarity and more precise energy values were determined for transitions from the 4+ and 2+ levels.

THE decay of nonspherical even-even nuclei is of especially great interest for the theory of alpha decay because of its simplicity. Exact energy values for excited levels are essential for the theory of nonspherical nuclei. The decay of Pu^{238} and Pu^{240} are especially interesting because these nuclei lie in a region of almost constant eccentricity and reveal alpha decay to a well-developed system of rotational levels. The alpha decay of these nuclei (and of the levels of daughter nuclei resulting from alpha decay) was studied by means of alpha spectrometry, γ-γ coincidences, and internal conversion electrons accompanying alpha decay. The last method gives the most exact values of the energy levels and permits determination of radiation multipolarity but has thus far been applied only to the strongest transitions. In the present work we have investigated the conversion electron spectra of Pu^{238} and Pu^{240}.

EXPERIMENTAL TECHNIQUE

Measurements were performed by means of a beta spectrometer with a toroidal magnetic field utilizing α-e coincidences.[1] The only difference from the procedure described in references 1 and 2 was that in studying weak lines we obtained more rigorous amplitude discrimination of beta-counter pulses (using a scintillation counter with a stilbene crystal). This strongly reduced the background of scattered electrons resulting from the basic transitions. Electron energies were determined by comparison with the energies of conversion electrons associated with the transitions $2+ \rightarrow 0$ (43.5 kev) and $4+ \rightarrow 2+$ (99.8 kev) in U^{234} (daughter nucleus Pu^{238}). Accurate values of these energies have been given in reference 3.

CONVERSION SPECTRUM OF Pu^{238}

In studying the conversion spectrum of Pu^{238} we used a 40 μc source of 1 cm diameter. Our conversion spectrum (which is actually the spectrum of the daughter nucleus U^{234}) is shown in Fig. 1, where the lines are interpreted. Figure 2 shows the level scheme of U^{234} and Table I gives previously available as well as new numerical data. The intensities of peaks 4 and 5, which are associated with the conversion of 99.8-kev radiation in the L_{II} and L_{III} subshells, as well as the absence of conversion in the L_I subshell, provide reliable evidence of the electric quadrupole character of this transition. We also attempted to detect a direct transition from the 143.3-kev level to the ground state, the intensity of which is less than 2×10^{-4} of the intensity of the transition to the 2+ level. These data provide reliable evidence that the 143.3-kev level possesses spin 4 and positive parity. We also investigated the conversion electrons associated with the $6+ \rightarrow 4+$ transition, which had previously been known only through gamma emission and alpha spectrometry. The detected transition energy was 152.6 ± 0.3 kev, giving a level of 295.9 ± 0.4 kev. Although the L_{II} and L_{III} conversion lines of this transition were poorly resolved the statistics are adequate for the resolution of peak 8 into its components. This is undoubtedly an E2 transition. The intensity of conversion emission from the 6+ level is about 0.025 of that from the 4+ level to the 2+ level. Considering the energy dependence of the conversion coefficients and taking the value 0.13%[4] as the intensity of alpha decay to the 4+ level, we obtain $(4.3 \pm 0.4) \times 10^{-3}$% for the intensity of alpha decay to the 6+ level, which is in good agreement with references 3 and 4.

TABLE I. U^{234} energy levels and Pu^{238} alpha line intensities

Alpha line	Spin and parity of level	From alpha spectroscopy: Line intensity, % [a]	From alpha spectroscopy: Line intensity, % [b]	From alpha spectroscopy: Level energy, kev [a]	From alpha spectroscopy: Level energy, kev [b]	From gamma spectroscopy: Intensity, % [a]	From gamma spectroscopy: Energy, kev [a]	From conversion electrons: Energy, kev [a]	From conversion electrons: Energy, kev Our data	From conversion electrons: Intensity,% Our data
α_0	0+	71.1	72	0	0		0	0	0	
α_{44}	2+	28.7	28	43.7 ± 1	43		43.8	43.50	43.50 *	
α_{143}	4+	0.13	$9.5 \cdot 10^{-2}$	141.5 ± 1	145		143	143.31	143.31 *	
α_{296}	6+	$5 \cdot 10^{-3}$		288 ± 5		$4 \cdot 10^{-3}$	296.4		295.9 ± 0.4	$(4.3 \pm 0.4) \cdot 10^{-3}$
α_{499}						$7 \cdot 10^{-6}$	499			

*These values were taken from reference 3 and were used to calibrate the spectrometer.

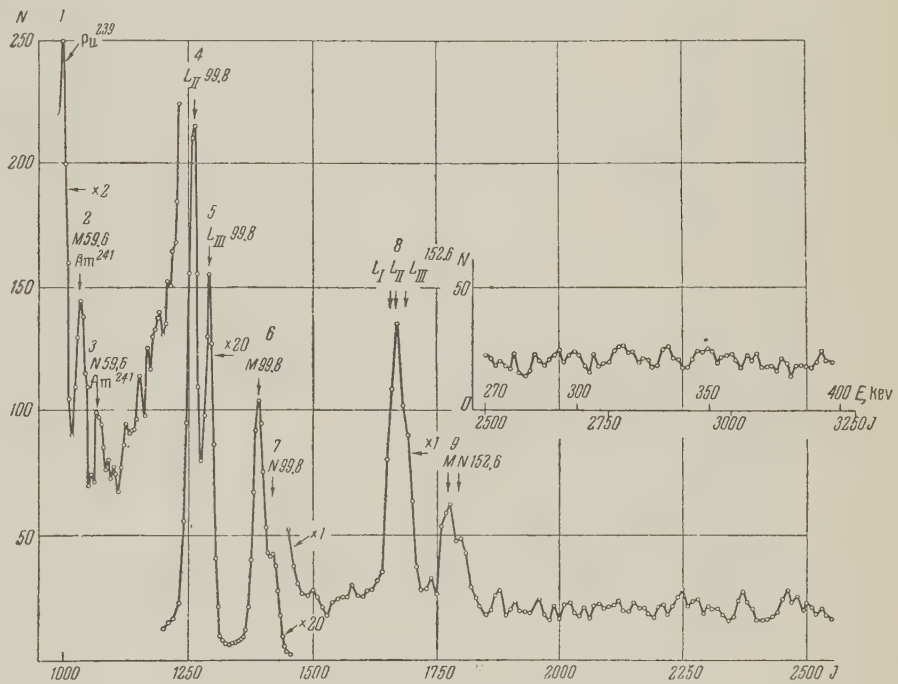

FIG. 1. Spectrum of conversion electrons accompanying the alpha decay of Pu^{238}. (Different portions of the spectrum were plotted on different scales.) Abscissas represent the current I through the spectrometer coil (in arbitrary units) and electron energy E_e. Ordinates represent the number of $e-\alpha$ coincidences. Line 1 represents the conversion of 51.7-kev radiation in the N shell.

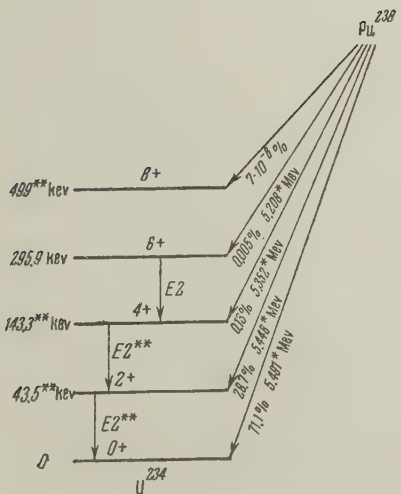

FIG. 2. Level scheme of U^{234}. *—according to reference 4 (alpha spectrum); **—according to reference 3 ($\gamma-\gamma$ coincidences).

CONVERSION SPECTRUM OF Pu^{240}

We had at our disposal only a rather weak (5 μc) thick Pu^{240} source, so that recording of the spectrum required a relatively long time. Figure 3 shows the spectrum of conversion electrons in the 20 — 220 kev region accompanying alpha decay. Figure 4 shows the level scheme of the daughter nucleus U^{236}, and Table II gives the numerical data taken from the literature and that obtained in the present work.

Conversion intensities in the L_{II} and L_{III} subshells indicate that transitions from the first excited level to the ground level and from the second to the first excited level are of the E2 type. The transition energies are 45.3 ± 0.2 kev and 103.6 ± 0.3 kev, respectively.

The high transmission and the low background

TABLE II. U^{236} energy levels and Pu^{240} alpha line intensities

Alpha line	Spin and parity of level	From alpha-particle spectroscopy: Alpha-line intensity, % [3]	[4]	Level energy, kev [3]	[4]	From conversion electron studies: Level energy, kev [7]	Our data	Intensity, % Our data
α_0	0+	75.5	75.5	0	0	0	0	
α_{45}	2+	24.5	24.4	45	45	45.6	45.3±0.2	
α_{149}	4+	0.1	0.091	151	147±2	149.6	148.9±0.4	
α_{210}?	1—?		$2.7\cdot10^{-3}$		210±8			
α_{239}?	3—?		$3.1\cdot10^{-3}$		239±8			
α_{309}	6+		$3.2\cdot10^{-3}$		313±5		309±1.5	$(2+1)\cdot10^{-3}$

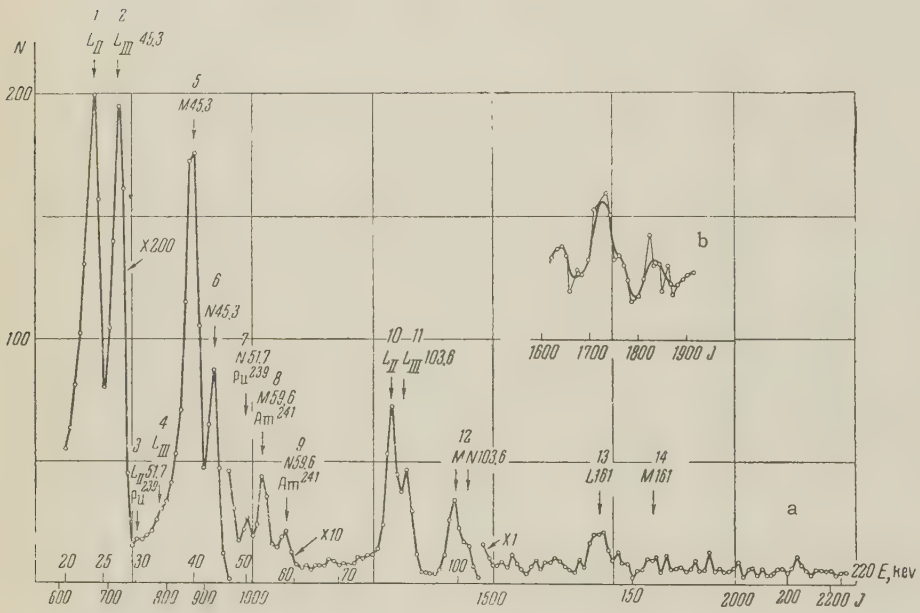

FIG. 3. Spectrum of conversion electrons accompanying the alpha decay of Pu^{240}. (Different portions of the spectrum were plotted on different scales.) The upper right-hand corner shows the spectrum around 140 kev summed over all exposures. The exposure times were 24 min in a and 60 min in b. Coordinates represent the same quantities as in Fig. 1.

level of our spectrometer permitted the detecting of a 6+ → 4+ transition. We were unable to determine the multipolarity of this transition, but the value 6+ for the spin is confirmed by the absence of transitions to lower excited levels. We measured the transition energy at 160 ± 1.5 kev, which gives 309 ± 1.5 kev for the energy of the excited 6+ level. The intensity of this transition is 1/60 of the intensity of the 4+ → 2+ transition. Taking the intensity of alpha decay to the 4+ level as 9.1×10^{-2}%, we obtain $(2 \pm 1) \times 10^{-3}$% for the intensity of alpha decay to the 6+ level.

Two more alpha lines (α_{210} and α_{239}) were reported in reference 6, where it was suggested that they belonged to Pu^{240}. We were unable to detect any conversion electrons associated with radiation from such levels, but it must be noted that if these are actually 1− and 3− levels, as was suggested in reference 6, they would emit E1 radiation and we would have been unable to detect conversion

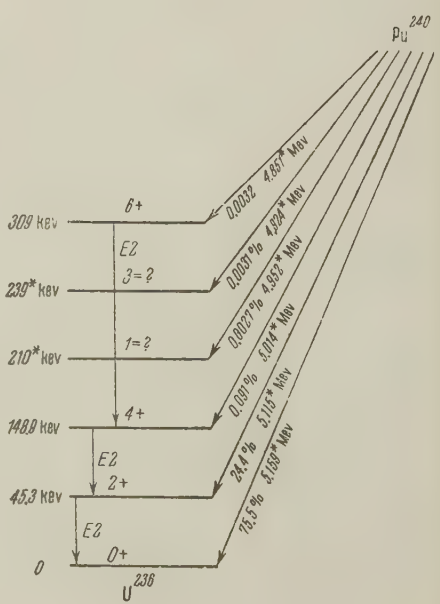

FIG. 4. Level scheme of U^{236}. * — according to reference 5.

electrons because of the small conversion coefficients for E1 transitions.

Comparison of Tables I and II indicates a "loss of individuality" of even-even nuclides that is characteristic of this portion of the periodic table. Energy levels are given by the familiar formula

$$E_{\text{rot}} = aI(I+1) + b[I(I+1)]^2,$$

where the first term is the principal one and the second term serves as a correction. The best values of the constants a and b for U^{234} are: a = 7.29 kev and b = −0.006 kev; for U^{236}: a = 7.60 kev and b = −0.0075 kev.

The authors wish to thank G. I. Grishuk, V. F. Konyaev, and Yu. N. Chernov for assistance with the experiments.

[1] Tretyakov, Gol'din, and Grishuk, Приборы и техника эксперимента (Instruments and Meas. Engg.) **6**, 22 (1957).

[2] Tretyakov, Grishuk and Gol'din, J. Exptl. Theoret. Phys. (U.S.S.R.) **34**, 811 (1958), Soviet Physics JETP **7**, 560 (1958).

[3] J. Perlman and J. O. Rasmussen, U.C.R.L. — 3424.

[4] Kondrat'ev, Novikova, Dedov, and Gol'din, Izv. Akad. Nauk SSSR, Ser. Fiz. **21**, 907 (1957), Columbia Tech. Transl. p. 909.

[5] F. Asaro and J. Perlman, Phys. Rev. **94**, 381 (1954).

[6] Kondrat'ev, Novikova, Sobolev, and Gol'din, J. Exptl. Theoret. Phys. (U.S.S.R.) **31**, 771 (1956), Soviet Phys. JETP **4**, 645 (1957).

[7] P. S. Samoilov, Атомная энергия (Atomic Energy) **4**, 81 (1958).

Translated by I. Emin
64

CASCADE α-PARTICLES IN STARS PRODUCED BY 360 and 660 Mev PROTONS

V. I. OSTROUMOV, N. A. PERFILOV, and R. A. FILOV

Radium Institute, Academy of Sciences, U.S.S.R.

Submitted to JETP editor June 28, 1958

J. Exptl. Theoret. Phys. (U.S.S.R.) **36**, 367-375 (February, 1959)

Stars containing tracks of α particles with energies above 30 Mev were studied in nuclear emulsions irradiated by 360 and 660 Mev protons. The effective cross section for production of these stars, the angular distribution of fast α particles, and the relative probability of their emission from light and heavy emulsion nuclei were determined. A similarity was found between the emission of cascade α particles and of fragments from nuclei as a result of bombardment with protons, which seems to indicate that both processes have an identical mechanism.

INTRODUCTION

In a series of experiments on the interaction of high-energy protons with nuclei of emulsion, it was found that α particles are emitted in stars with an energy and angular distribution which contradicts the assumption that we are dealing with an evaporation process.[1,2] The energy spectrum of these particles has a long tail in the high-energy region. The direction of emission of α particles is correlated with the direction of the primary protons. The majority of them are emitted in the forward direction, and the degree of anisotropy increases with increasing kinetic energy of the α particles. As is well known, a similar picture is valid for nucleons ejected from the nucleus during the cascade stage of the nuclear interaction with the primary proton. The appearance of fast α particles is therefore also connected with the development of the nuclear cascade in the nucleus, although the mechanism of the transfer of considerable kinetic energy to a complex consisting of our nucleons is unclear.

Even heavier particles, called fragments, are observed in nuclear disintegrations, the cross sections of these events being smaller by approximately one order of magnitude.[3-6] At present, there are no well-founded ideas about the fragmentation process which could explain all experimental facts. It is reasonable to assume that the process of emission of all multi-charged particles (among them α particles) is basically similar. There are no special reasons to believe that the emission of a He nucleus in the cascade process has different causes and is connected with a basically different mechanism, than the emission, let us say, of a Li and Be nucleus. The study of inelastic interactions between high-energy nucleons with nuclei, which give rise to cascade α particles, will therefore be helpful for the study of the fragmentation mechanism, and has, of course, its own intrinsic interest. Experiments with α particles can be carried out in better conditions, and their results can be interpreted more exclusively, than experiments on the study of fragments since, in the latter case, the observed variety of particles, the identification of which is not always possible, makes it difficult to reduce the experimental data.

In the present work, we studied stars in a nuclear emulsion containing tracks of fast α particles. The results of observations were, whenever possible, compared with the corresponding data on fragments given in reference 5.

EXPERIMENTAL METHOD

Fine-grain nuclear emulsion P-9, sensitive to protons in the energy range 30 — 40 Mev, was used in the experiment. The emulsions were irradiated, using the Joint Institute for Nuclear Research synchrocyclotron, by the collimated external proton beam incident perpendicularly to the surface of the emulsion. The energy of the protons was 660 and 360 Mev. The lower energy value was obtained by slowing the protons down in a copper absorber.

Stars containing tracks of α particles with energy higher than 30 Mev were noted in scanning the emulsion. Only those cases where the particles stopped in the emulsion and where the inclination of their tracks with respect to the plane of emulsion was not larger than 7° (in undeveloped emulsion) were selected for further analysis. The visual selection of such tracks did not cause any

difficulties, since the type of emulsions chosen had good discriminating power for singly- and doubly-charged particles. However, our data contained a certain number of tracks of fast Li nuclei which could not be easily distinguished from the tracks of α particles. Checking 70 randomly-chosen tracks of particles with charge larger than unity over the length of 300 μ by the method of counting the number of intervals of the ocular scale obscured by grain,[7] it was found that the admixture of triply charged particles in our experiment amounted to less than 15%. The energy of α particles was determined from the track length using the range energy curves for protons.[8] The transition coefficient from the range in air to the range in emulsion was taken as 2000.

In the observed stars, we measured the angle between the projection of the track of a fast α particle on the emulsion plane and the direction of the bombarding beam. Since the chosen tracks have a small inclination to that plane, such a procedure gives the angular distribution of cascade α-particles per unit solid angle accurately enough. Necessary corrections for the finite thickness of the chosen spherical zone were applied.

For the lower energy limit of recorded α particles (30 Mev), it could be confirmed that the majority of found tracks were not related to the process of evaporation of nuclei, which substantially simplifies the analysis of experimental results. For the estimate of the cross section for the production of α particles with energy larger than 30 Mev in nuclear interactions of fast protons, we measured the frequency of occurrence of such cases among all stars found in the emulsion. The cross section for star production for 360-Mev protons was taken from the work of Bernardini et al.,[9] and that for 660-Mev protons from the work of Grigor'ev and Solov'eva.[10]

EXPERIMENTAL RESULTS

All observed cases were divided into three groups. All stars having the track of the recoil nucleus were ascribed to the first group. We assumed that these represent the result of disintegration of heavy nuclei of the emulsion. For brevity, we shall call these cases H stars. To the second group belong stars without a visible track of the recoil nucleus, with total charge of emitted particles smaller than 8e, and which contained at least one track of an α-particle with energy smaller than 8 Mev, or of a proton with energy smaller than 4 Mev. These stars were assumed to represent events involving light nuclei (L-stars). Finally, the third group contains disintegration not falling within anyone of the two former groups. The number of stars in each of the three groups is given in Table I.

TABLE I

Proton energy, Mev	Group I H stars	Group II L stars	Group III H and L stars	Total stars	σ_T, mbn	σ_L, mbn
360	397	68	203	668	85±15	17±6
660	363	77	160	600	120±25	18±6

Observations of the disintegrations in the gelatine layer, produced by fast protons, indicate that the fraction of stars involving light nuclei showing a track of the residual nucleus is smaller than 20 — 25%.[11,12] If we assume that about 20% of all stars visible in the emulsion involve light nuclei, it is found that the admixture of L-stars in the first group is smaller than 10%. It is obvious that a certain number of stars involving Ag and Br nuclei is present in the second group. From the data of references 2 and 3, the fraction of H stars with less than seven prongs containing sub-barrier particles amounts to about 5 to 10% of the total number of heavy nuclei disintegration. All of these corrections therefore compensate roughly each other, and the intensities of the first and second group represents accurately enough the real relation of probabilities of appearance of L and H stars containing a fast α particle.

The number of L stars in the third group can be estimated by the following methods:

(1) From the angular distribution of fast α particles. We shall assume that the distribution is identical for all L stars of the second and third groups. Such an assumption is not correct for H stars, since, the presence or absence of the visible track of the recoil nucleus may be due to a change of direction of the emission of a fast particle.

To determine the fraction k of α particles emitted in the forward direction in H stars of the third group, we plotted the dependence k(R) for H stars of the first group (R is the length of the recoil nucleus track). Extrapolation of this plot to the value R = 0 gives the value of K for H stars of the third group. The fraction of L stars in this group will then be equal to

$$x = (k_0 - k_T)/(k_L - k_T), \qquad (1)$$

where the indices O, L, and H refer correspondingly to the stars of the third, second, and first groups.

(2) From the multiplicity distribution of stars. The multiplicity distribution of stars of the third

TABLE II

Proton energy, Mev	x, % Method 1	2	3	4	Average x
360	31	34	54	—	(40±10)%
660	15	16	11	17	(15± 3)%

group represents a mixture of two distributions (for L and H stars), having statistical weights equal to x and 1 − x respectively. The value of x is formed by simple calculation under the assumption that the multiplicity of L and H stars is independent of the above criterion of dividing the stars into groups.

(3) Form the value of the ratio α/p of the number of doubly-charged particles to the number of singly-charged particles in L and H stars. In writing this expression, it is also assumed that the value of α/p is similar to that in stars produced on nuclei of one type (L and H), independently of the number of the group. It is easy to obtain the formula for x:

$$x = \frac{[(\alpha/p)_0 - (\alpha/p)_T]\,[1 + (\alpha/p)_L]\,n_T}{[(\alpha/p)_L - (\alpha/p)_0]\,[1 + (\alpha/p)_T]\,n_L} \qquad (2)$$

where n is the mean multiplicity of a star, and where the indices O, L, T, have the same sense as in Eq. (1).

(4) In the experiment with 660-Mev protons it was possible to estimate the fraction of L stars containing tracks of low-energy particles from the ratio to the total number of stars involving C, O, and N nuclei, and making use of the observations of Serebnikov, who studied stars in a layer of gelatine.[12] The fraction of light L stars with sub-barrier particles is probably not changed markedly in the case of the emission of an α particle with energy > 30 Mev.

Results of the calculations of the fraction of L stars in the third group, as obtained by each of the three methods, are given in Table II.

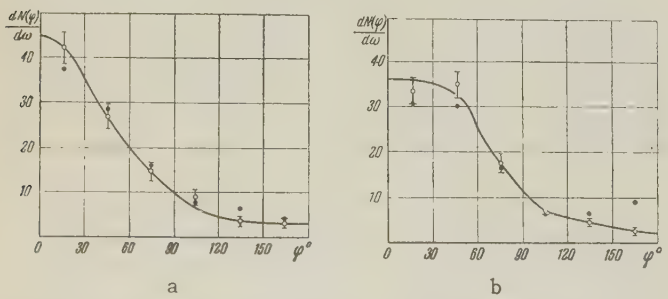

FIG. 1. Angular distribution of α particles with E > 30 Mev, calculated per unit solid angle (H nuclei) a – for 660-Mev protons, b – for 360-Mev protons. Black dots – data of reference 5.

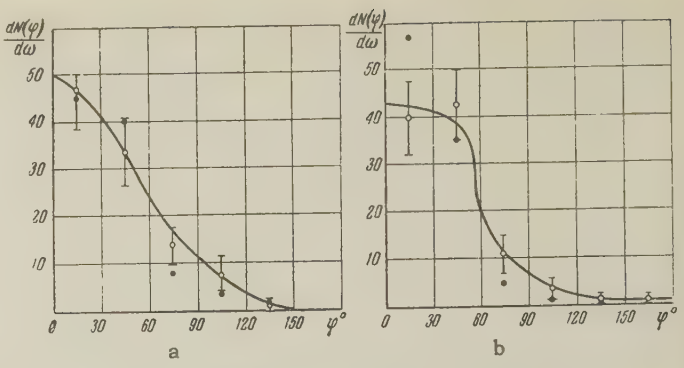

FIG. 2. Same as Fig. 1 for L nuclei.

Knowing the values of x, it is possible to distribute all stars of the third group statistically among the L and H groups, and to determine the relative cross sections for the production of fast α particles on heavy and light nuclei of the emulsion.

The cross section for the production of stars containing α particles are given in Table I (last two columns), calculated as averages of our data and the data of reference 2. The given errors include the errors in the determination of x and the error in the identification of stars according to the tracks of the recoil nuclei, assumed to be equal to 10%.

Apart from stars with one fast α particle (in the following we shall call them α stars, while the cases with emission of a fragment will be called f stars), five cases with two tracks of α particles of more than 30 Mev, satisfying the assumed criterion of selection, were found for 660-Mev incident protons, and four such cases for 360-Mev protons. If we assume the total star production cross section on T nuclei to be equal to unity, then the cross sections for the production of α and 2α stars relative to it equal 0.11 and 0.008 respectively. Among α stars, cases are found in which a track of the fragment may be observed (αf stars). In the course of the experiment, 28 and 15 such stars were found for proton energies of 660 and 360 Mev, respectively. Two stars of the type 2αf were found with the 660-Mev proton beam. Consequently,

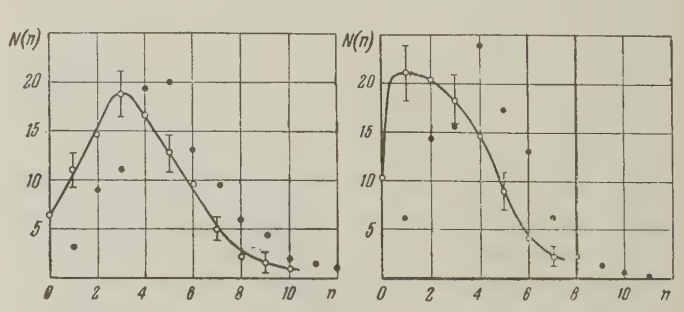

FIG. 3. Multiplicity distribution of α stars (H nuclei): a – for 660-Mev protons, b – for 360-Mev protons. Black dots – the same for f stars (data of reference 5).

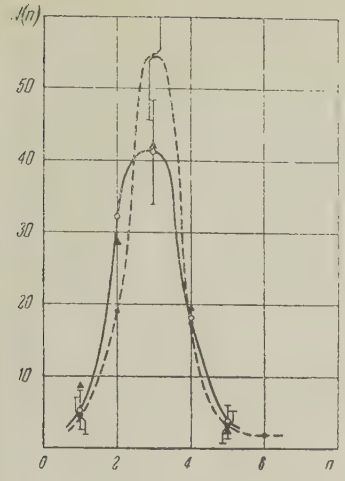

FIG. 4. Multiplicity distribution of α stars for L nuclei: solid curve – for 660-Mev protons, dashed curve – for 360-Mev protons. Triangles – multiplicity distribution of f stars for 660-Mev protons.

the ratio of the production cross sections for stars of the type α, αf, and α2f by 660-Mev protons is 1 : 0.04 : 0.003. The angular distribution of α particles is given in Figs. 1 and 2.

The multiplicity distribution of α-stars for H and L nuclei separately are given in Figs. 3 and 4. It is interesting to note that the mean multiplicity in α stars produced on H nuclei is apparently decreasing with increasing energy of the α particles (Table III).

For L stars, the mean multiplicity remains constant in all cases, and is equal to 2.8 ± 0.2 for 660-Mev protons, and to 3.0 ± 0.2 for 360-Mev protons (without the fast α particle).

Data on the relative emission probability of a fast α-particle from H and L nuclei for a different number of black prongs in the star are given in Figs. 5 and 6. This probability w_α is determined from the formula

$$w_\alpha(n) = \sigma_\alpha \alpha_n / \sigma_0, \qquad (3)$$

where σ_α and σ_0 are the cross section for the production of α-stars and the total star production cross section respectively, and α_n is the

TABLE III. Multiplicity of α-stars

Proton energy, Mev	E_α, Mev			Total for α stars	Mean number of black prongs in normal H stars
	30÷50	50÷80	>80		
360	2.6±0,1*	2.3±0.1	2.0±0.4	2.5±0.1	2,5±0.1
660	3.7±0,1	3.6±0.1	3.2±0.3	3.6±0.1	3.6±0.1

*The fast α particle is not counted among the black prongs.

fraction of α stars with the multiplicity n among all α stars. (Here and throughout, the fast α particle is not included in the number of tracks.) The values of α_n are taken from the graphs in Figs. 3 and 4, and the multiplicity distribution of normal stars is taken from reference 13 (H nuclei and 660-Mev protons), from reference 9 (360-Mev protons, H nuclei), reference 12 (660-Mev protons, L nuclei) and reference 11 (360-Mev protons, L nuclei). The errors shown in the figures correspond to statistical errors, and do not include the error in the determination of σ_α and σ_0.

DISCUSSION OF RESULTS

The data on α stars obtained in the course of the experiment were compared with the results of an investigation of the fragmentation process carried out in reference 5 for the same energies of bombarding protons. Such a comparison has meaning only under the condition that the observed α particles are not due to evaporation of the excited nuclei. Estimates based on the energy spectrum of α particles show that the number of evaporated particles among all those detected is not larger than 10%. The angular distribution of particles with energy > 30 Mev indicates also a small admixture of evaporated component.

With increasing proton energy, the effective cross section for the emission of fragments form H-nuclei increases sharply.[5] The cross section

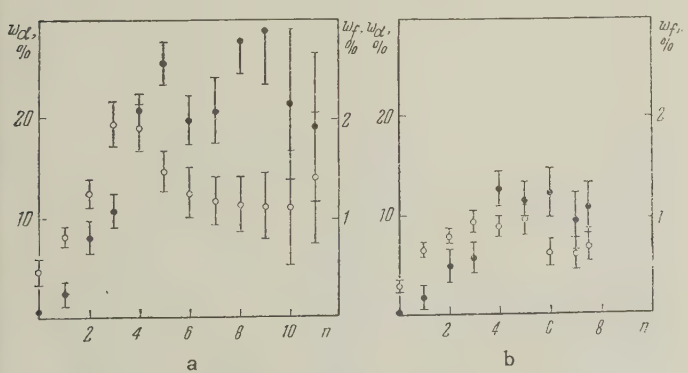

FIG. 5. The relative probability of emission of α particles (light circles) and fragments (filled circles) and the dependence on the number of prongs in the star (H nuclei) for a – 660-Mev and b – 360-Mev protons.

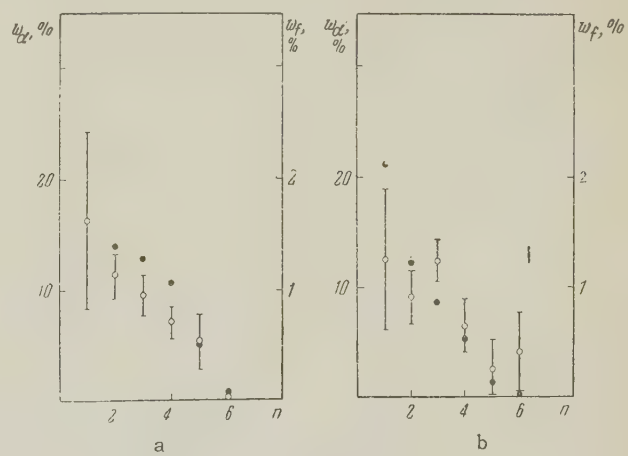

FIG. 6. Same as Fig. 5 for L nuclei.

for the emission of α particles increases less markedly, as can be seen from Table I. The cross section for fragment production on light nuclei does not vary with increasing energy of the beam, and this is the case also for the cross section for emission of fast α particles. Evidently, such difference in the energy dependence of the cross section for light and heavy nuclei is connected with different transparency of the nuclei for fast protons and with a different degree of development of the internal cascade process. It can be noted that the ratio of the cross section for the production of 1, 2, etc. fragments in α stars is approximately the same as that given in reference 5 for f stars, if we assume that the emission of a fast α particle is equivalent to the emission of a fragment.

The multiplicity distributions of α and f stars, similar to each other, are markedly different from the distribution of normal stars which do not contain tracks of a fast α particle or fragment. It can be seen from Figs. 5 and 6 that the relative probability of the production of an α particle on a H nucleus increases with increasing dimensions of the star, attaining a maximum and then falling off slowly. To a lesser extent, a similar behavior may be observed for the emission of fragments as well. An increase of the relative probability of the emission of α particles and fragments is due, we believe, to the increased number of collisions between nucleons in the cascade stage of the disintegration process, and to the increase in the number of the secondary nucleons responsible for the appearance of these multiply-charged particles. The fall-off in the curves $w_\alpha(n)$ and $w_f(n)$ for large n is due to the fact that, in a strongly developed cascade, colliding nucleons have, on the average, small energies which are not sufficient for imparting to the α particles or to the fragment the necessary energy. The relation between the energy of α-particles and the mean multiplicity in an α-star (Table II) indicates also that the more energetical α particles are emitted under the action of cascade nucleons of higher energies. The maximum of curve $w_\alpha(n)$ should therefore shift to the left with increasing energy of detected α particles. An experimental check showed that the shift of the curves $w_\alpha(n)$ constructed for α-particles of various energies really takes place. Data of reference 5 indicate that the mean multiplicity of f stars increases slightly if we consider events with emission of fragments having a long range. Such a conclusion should, however, yet be verified, since the observed variation of the mean multiplicity in f stars with varying range of the fragments lies within the limits of statistical fluctuations.

Special attention should be given to the practically identical angular distributions of α-particles and fragments in all four compared cases. Such a similarity is hardly due to chance, and the fact undoubtedly should be taken into account in considering any hypothesis proposed for the explanation of fragment emission. Observation also shows that the angular distribution of cascade α particles depends on their kinetic energy. In our experiment, the angular distribution of cascade α-particles with energy > 30 Mev was measured. It is probable, that in varying the energy limit, the angular characteristics of α particles will also change. The question therefore arises as to why the angular distribution of α-particles with energy > 30 Mev and of fragments with kinetic energy > 1 to 2 Mev per nucleon[5] are identical.

One can attempt to explain this fact by assuming that the observed particles are emitted from the nucleus as a result of an elastic (quasi-elastic) collision of a fast nucleon with a nucleon complex.[14] We shall assume that nucleons of the same energies are responsible for the emission of α-particles and fragments (consequently the angular spread of these nucleons with respect to the direction of the beam is the same in both cases). The ratio of the kinetic energies of the particles emitted at the same angle to the beam will then be equal to

$$\varepsilon_f / \varepsilon_\alpha = 25 / [(M_f / m) + 1]^2, \quad (\varepsilon_f = E_f/M_f, \quad \varepsilon_\alpha = E_\alpha/M_\alpha). \tag{4}$$

where M_α and M_f are the masses of α particles and fragments respectively, E_α and E_f their energy, and m the nucleonic mass.

In our experiment, the minimum value of ϵ_α is equal to 7.5 Mev. We have then for a particle with a mass $M_f = 9$ (Be nucleus), $\epsilon_f = 2$ Mev; for the B^{10} nucleus we have $\epsilon_f = 1.6$ Mev, etc. The values of the lower limit of the recorded multi-charged particles calculated according to formula (4) will be 1 to 2 Mev per nucleon, which corresponds to the conditions of the experiments of reference 5.

On the basis of the available experimental data, it is of course impossible to maintain that the mechanism of fragment production is essentially due to collisions. Keeping the hypothesis of elastic ejection of nucleon complexes from the nucleus, it should, for instance, be explained why there is no unique dependence of the energy of multi-charged particles on the angle of their emission. Alpha particles as well as fragments have a markedly smaller kinetic energy than they should possess at a given angle of their emission. The contribution of secondary nucleons does not remove the difficulty, since, in that case, the deviations would

be spread uniformly both towards smaller and longer angles.

To determine the mechanism of emission of fragments and fast α particles, further work is necessary. In particular, it would be interesting to have data on the energy and angular distribution of fragments with a given charge, to find the connection between the emission of a multiply-charged particle and of a fast proton, etc. Analysis of the results of experiments of similar type, and comparison with the data on the emission of fast α particles, will make it possible to approach the solution of this problem.

The authors would like to express their gratitude to O. V. Lozhkin, and U. I. Serebrennikov, who helped in carrying out the work and took part in discussing the results.

[1] H. Muirhead and W. G. Rosser, Phil. Mag. **46**, 658 (1955).

[2] P. A. Vaganov and V. I. Ostroumov, J. Exptl. Theoret. Phys. (U.S.S.R.) **33**, 1131 (1957), Soviet Phys. JETP **6**, 871 (1958).

[3] S. O. C. Sorensen, Phil. Mag. **42**, 188 (1951).

[4] D. Perkins, Proc. Roy. Soc. **203**, 399 (1950).

[5] O. V. Lozhkin and N. A. Perfilov, J. Exptl. Theoret. Phys. (U.S.S.R.) **31**, 913 (1956), Soviet Phys. JETP **4**, 790 (1957). O. V. Lozhkin, Dissertation, Radium Institute, Academy of Sciences, U.S.S.R. 1957.

[6] V. M. Sidorov and E. L. Grigoriev, J. Exptl. Theoret. Phys. (U.S.S.R.) **33**, 1179 (1957), Soviet Phys. JETP **6**, 906 (1959).

[7] Yu. I. Serebrennikov, Научно-информ. бюлл. Ленинградского политехнического ин-та (Sci. Info. Bull., Leningrad Polytech. Inst.) **12**, 85 (1957).

[8] E. Segrè (editor), Experimental Nuclear Physics, Vol. I, p. 156, N. Y., Wiley, 1953.

[9] Bernardini, Booth, and Lindenbaum, Phys. Rev. **88**, 1017 (1952).

[10] E. L. Grigor'ev, and L. I. Solov'eva, J. Exptl. Theoret. Phys. (U.S.S.R.) **31**, 932 (1956), Soviet Phys. JETP **4**, 801 (1957).

[11] Blau, Oliver, and Smith, Phys. Rev. **91**, 949 (1953).

[12] Yu. I. Serebrennikov, Научно-информ. бюлл. Ленинградского политехнического ин-та (Sci. Info. Bull., Leningrad Polytech. Inst.) **12**, 75 (1957).

[13] V. I. Ostroumov, J. Exptl. Theoret. Phys. (U.S.S.R.) **32**, 3 (1957), Soviet Phys. JETP **5**, 12 (1957).

[14] D. I. Blokhintsev, J. Exptl. Theoret. Phys. (U.S.S.R.) **33**, 1295 (1957), Soviet Phys. JETP **6**, 995 (1959).

Translated by H. Kasha
65

SLIPPING OF BERYLLIUM SINGLE CRYSTALS AT LOW TEMPERATURES. III*

R. I. GARBER, I. A. GINDIN, and Yu V. SHUBIN

Physico-Technical Institute, Academy of Sciences, Ukrainian S.S.R.

Submitted to JETP editor July 16, 1958

J. Exptl. Theoret. Phys. (U.S.S.R.) **36**, 376-384 (February, 1959)

Especially pure (99.98%) beryllium single crystals were deformed at 20° and 77°K. Slipping along the basal plane (0001) has been detected at 20° as well as at 77°K. Two deformations stages are discerned: an initial stage, when the displacement occurs in a thin layer adjacent to the slip band, and a later stage when the deformation is localized at the slip band. In regions between the bands, twisting has been detected which increases with the deformation. The twist of the blocks in the early stages may be ascribed to the effect of residual strains. In the later stages, when the rotation reaches 3°, one is forced to assume that twinning takes place during slip. The large magnitude of the relative displacement in the second stage may be explained by violation of continuity with subsequent healing of the contacts.

WE have shown elsewhere[1,2] that single crystals of commercial beryllium, 99.7% pure, have a plasticity, particularly basal slip along (0001) plane, not only at room temperature but also at lower temperatures. We have found as the results of these investigations that the first microcracks (along the planes of the prisms and second-order pyramids) are formed as a consequence of non-uniform shear along individual basal slip bands. At low temperature, the non-uniformity of the shear increases, leading to an increase in brittleness. The non-uniformity in shear can be assumed to be due to impurities and that the shear would be more uniform in pure beryllium.

In this project we have investigated basal slip of single crystals of especially pure beryllium (99.98%) at low temperatures (20 and 77°K), at which brittleness of this metal manifests itself most.

1. SPECIMENS AND INVESTIGATION PROCEDURE

Single crystals were grown from the melt by slowly cooling pre-purified beryllium in vacuo.† The method of preparation of single-crystal specimens was described in detail in earlier papers.[1,2]

The samples were oriented in such a way that the basal plane (0001) made an angle of 45° to the direction of the deforming forces, while the direction of the shear in the case of basal slip — the first-order diagonal $[11\bar{2}0]$ was parallel to one of the side faces of the specimen (Fig. 1). The specimens were deformed by uniaxial compression in a machine provided with a special fixture for low-temperature testing.[3,4] The speed of deformation was constant at 0.03 mm/sec. The compression was carried out in sequence to δ = 0.1, 0.3, 0.7, 0.9, 1.7, and 6%. The sample was subjected after each step to x-ray, micro-interference, and electron-microscopic investigation by methods described in references 1, 2, and 5. In addition, it was possible to determine the overall picture of the slip at various stages of deformation from the displacement of scribe marks scratched beforehand on one of the lateral faces of the specimen, coinciding with the $(1\bar{1}00)$ shear plane. These data were compared with the profile of the face of the specimen, perpendicular to shear plane (face ah, Fig. 1). To draw the profile of this face, use was made of an electron-microscopic photograph with a lacquer replica contrasted with chromium.

Usually the angle and the direction of contrast-

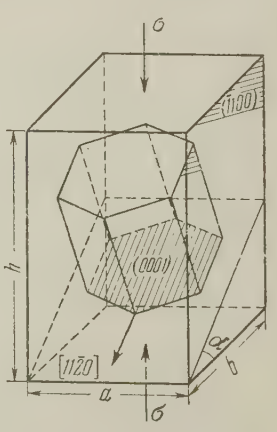

FIG. 1. Crystallographic orientation of the slip elements (α = 45°).

*For parts I and II see references 1 and 2.

†The pre-purified beryllium was graciously furnished to us by V. E. Ivanov and V. M. Amonenko.

ing are determined from the shadows produced by the magnesium-oxide crystals that settle on the replica that during the combustion of a magnesium ribbon.[6] In this case, however, an exact determination of the length of the shadow is difficult because of the arbitrary placement of the cubic crystals of the replica. To increase the accuracy of the drawn profile, spherical particles were deposited on the replica. These particles were obtained from a 1% solution of coloxylin in amyl acetate by atomizing the solution in air.*

Drops of the solution, suspended in air, contract into spheres on the order of 0.1 μ in diameter after the evaporation of the amyl acetate. Under suitably chosen conditions one or two spheres settle on the replica within the field of view of the electron microscope. By measuring the radius of the sphere R and the length of the shadow H it is possible to determine the contrasting angle from the following formula

$$\alpha_1 = 2 \tan^{-1} (R/H) \qquad (1)$$

2. RESULTS AND DISCUSSION

Unlike technical beryllium, in which slip is observed only at 77°K and above,† basal slip in pure beryllium occurs even at 20°K. It manifests itself in the form of thin straight-line tracks on the lateral faces of the specimen. The appearance of the first band is preceded by a stage of block formation, which is observed from the fragmentation of the Laue dots and deformation without formation of slip tracks. However, in pure beryllium this process is weakly pronounced. For example, it was noted with the aid of an electron-microscope that in pure beryllium the first bands appear at 77°K after 0.3% compression, while in technical beryllium the bands arise only after 3% compression. Furthermore, in pure beryllium the yield point is more than 10 times lower. The lower resistance of single-crystal pure beryllium to shear combines with the weak development of the block formation in the initial stage of deformation. The table lists the mechanical characteristics of beryllium crystals of various purity at 20 and 77°K.

Purification of beryllium leads to a reduction of deformation in block formation and to an increase in the overall plasticity. The slip tracks of pure beryllium at low temperatures are similar in external appearance to the slip tracks of technical

Test temperature (degrees K)	Purity of beryllium (percentage) by weight)	Deformation prior to appearance of bands (percent)	Yield	Total residual compression (percent)	Ultimate strength
20	99.7	No slip bands observed.		2.4	48.0
	99.98	2.0	14.0	8.8	37.0
77	99.7	3.0	42.0	6.0	52.0
	99.98	0.3	3.4	22.0	34.0

beryllium at 200°C and above. This is explained by the fact that the deformation by block formation, which precedes the basal slip, is sufficiently small in either case. The prismatic slip which occurs in technical beryllium at 400°C is observed in pure beryllium at 77°K. As the compression stress increases, the number of slip bands and the displacement in each band also increase. Lines scratched beforehand on a polished lateral face of the specimen bend and shift during the compression process.

3. INVESTIGATION OF THE PROFILE OF THE SPECIMEN SURFACE

Figure 2a shows an electron-microscope photograph of a portion of the face parallel to the $(\bar{1}100)$ shear plane of the specimen, deformed 0.3% (at 77°K) by a compression stress of 3.4 kg/mm^2. The black lines at 45° to the vertical axis of the specimen are the tracks of basal slip bands. The scribe marks intersect the slip track. At the initial stage of the deformation, the shear is not observed directly on the slip band. As the distance from the track of the band increases, the shear increases and reaches a maximum at a distance of 0.4 μ. The remaining portion of the crystal shifts as a whole and therefore the scratch remains straight. Thus, the curved portion of the scribe mark near the slip plane shows a region in which the shear deformation, usually ascribed to the slip band, is concentrated. Figure 2b shows schematically details of an electron-microscope photograph (Fig. 2), in which the reproduction does not show the scribe marks with sufficient contrast). The residual relative shear in this region is

$$\gamma = S_n / b_0 = 0.63,$$

where b_0 is the thickness of the shear region, and S_n the displacement of the scribe mark in the direction of the shear. The straight sections of the scribe marks on both sides of each slippage band are no longer parallel after the deformation. This could be explained by the influence of the remain-

*The procedure of determining the angle of contrasting with the aid of coloxylin small spheres was developed by I. M. Fishman, and will be described in detail elsewhere.

†At 77°K only weak basal slip occurs in technical beryllium.

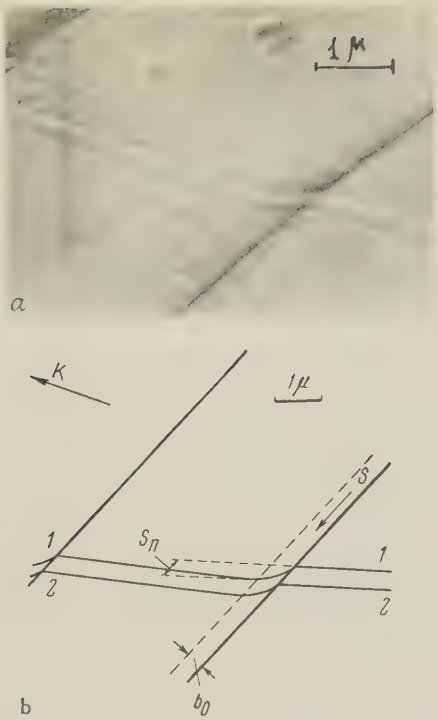

FIG. 2. a) cracks of the basal slip bands on the shear plane (1100) (See Fig. 1). Temperature 77°K. Deformation 0.3%. The curved lines near the slip bands are the scratch marks. b) arrangement of the details of the photograph. Dotted line illustrates the region of the localization of the shear, 1–1 and 2–2 are the scribe marks.

ing elastic stresses which have opposite signs on both sides of each band.[7] In this case the elastic relative shear is

$$\gamma_1 = \tan \varphi_1 - \tan (\varphi_1 - \alpha_1),$$

where φ_1 is the angle between the normal (N-N) to the slip band and the initial direction of the scribe mark (B-B), and α_2 is the angle of rotation of the scribe mark, which equals approximately half the angle between the directions of the straight segments of the scribe mark (B_1-B_1) on both sides of the band after deformation (see Fig. 3). From Fig. 2a we obtain $\alpha_2 \approx 1°$ when $\varphi_1 = 35°$, which yields $\gamma_1 = 0.026$. This value of α_1 corresponds approximately to the yield point.

Further deformation leads to localization of the shear on the slip band. The scribe marks break and the tracks of the slip band shift a considerable distance from each other. Figures 4a and 4b show an electron-microscope photograph and a diagram of a portion of the lateral face of the specimen, deformed by 6% at 77°K.* The compression was 8.5 kg/mm^2 before unloading. The

*The specimen was repolished after 1.7% compression and fresh scribe marks were scratched on the side surface. Thus the shift of the marks on Fig. 4 corresponds to a deformation of 4.3% of a specimen previously deformed by 1.7%.

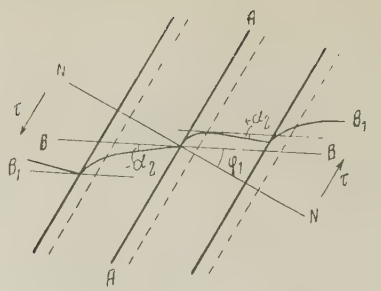

FIG. 3. Illustrating the calculation of the residual elastic stress. A – A) tracks of slip bands on the (1100) shear plane; N – N) normal to the slip plane; B – B) initial position of scribe mark; $B_1 - B_1$) position of scribe mark after a small plastic deformation ($\delta = 0.3\%$); τ) direction of shear.

shear along the slip plane reached a considerable value (2.5 μ). Distortions near the slip plane manifests themselves more sharply. The photograph shows clearly the complicated relief of this region.

A striking fact is that the sections of the scribe marks adjacent to the band are less curved in Fig. 4 than in Fig. 2. This is apparently due to localization of the shear in the band. The relative rotation of the straight sections of the marks indicates an increase in the residual stress.* The residual relative shear at this stage of basal slip is difficult to estimate, since the thickness of the deformed layer is very small. It is found thus that, in sufficiently pure beryllium, a shear that is concentrated in the slip band occurs at 77°K. In commercial beryllium, a similar shear is observed only at temperatures exceeding 400°C.[2]

From the data obtained it follows at in beryllium the initial stage of the basal slip is localized in the region adjacent to the slip band and covers a layer several hundreds or thousands atomic distances thick. Starting with a certain stress, the slip is concentrated in the slip band and is characterized by a large relative shear.

The slip should result in a change in the profile of the lateral face of the specimen (face ah of Fig. 1). Rosenhain[9] has observed in a single crystal of iron a sawtooth contour, corresponding to

*Large local distortions occur in certain sections of the face bh (see Fig. 1), leading to a considerable increase in the angle of rotation of the scribe marks, α_2 (see Fig. 3). Figure 5 shows the corresponding electron-microscope photograph. In this case $\alpha_2 \approx 3°$, corresponding to $\gamma_1 \approx 0.067$. So large a value cannot be atributed to the influence of the residual stress alone. The rotation of the marks may reflect in addition to the residual stress, also the rotation of the crystal through twinning in slip, similar to that described by Brilliantov and Obreimov.[8] It is important to note that in our case we deal with slip along the basal plane of a hexagonal crystal, slip considered by most authors as purely translational. In reference 8, however, the substance investigated was rock salt, in which the slip may be more complicated.

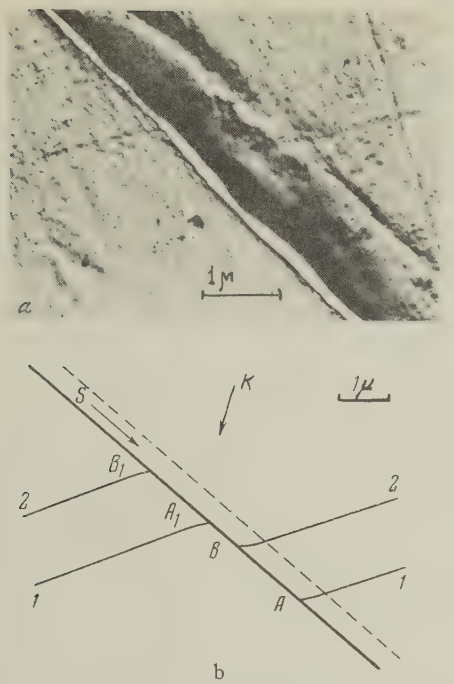

FIG. 4 (A, B). Tracks of the basal slip bands at 77°K. Deformation 6%. The shear is localized on the slip plane and amounts to 2.5 μ. $AA_1 \simeq BB_1$.

"pure" slip. Greenland,[10] however, found in a mercury single crystal a profile that evidences non-uniform shear of various layers of the crystal. In beryllium one can observe two types of profiles, a smooth one at the start of the deformation and a rough (sawtooth) one at a certain stage of deformation. Micro-interference investigations confirm this statement (Fig. 6). In a specimen compressed by 0.3% at 77°K, the interference bands curve smoothly along the slip track, and the absolute shear displacement amounts to, on the average, one interference fringe (0.22 μ) (Fig. 6a). In a specimen compressed by 6% at 77°K, the interference fringes break up on the slip tracks, the absolute shear displacement amounts to 9 or 10 interference fringes (2 — 2.25 μ) (Fig. 6b).

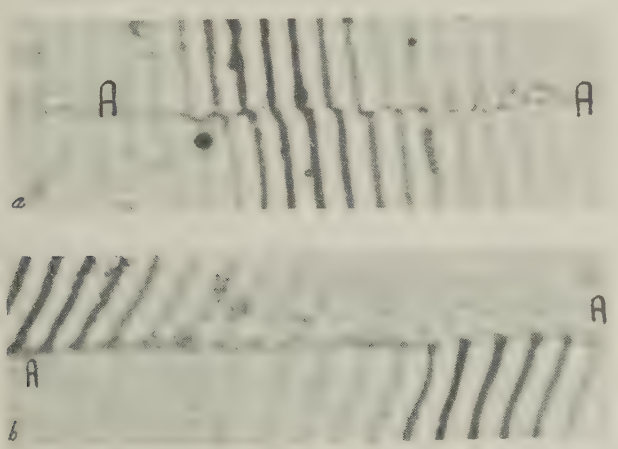

FIG. 6. Interference fringes on the ah face (Fig. 1). Temperature 77°K. A — A) track of slip band, a) deformation 0.3%, b) deformation 6% (×1000).

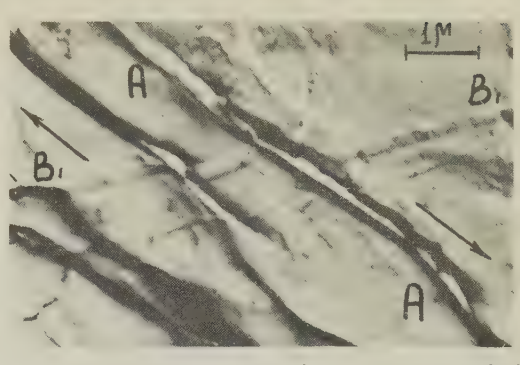

FIG. 5. Illustrating mechanical twinning in basal slip. A — A) tracks of the basal slip band; $B_1 - B_1$) position of the scribe mark after plastic deformation (δ = 6%).

It was shown earlier[2] that one of the causes of brittle fracture of single-crystal commercial beryllium is non-uniform shear along the basal slip band. The uneven shear manifests itself in the different displacement of the scribe marks that cross one slip band. In the case of pure beryllium no unevenness in shear is observed even if the shear is in the slip band and amounts to 3 to 5 μ. The elimination of impurities from the beryllium contributes to the greater uniformity of the shear in basal slip, eliminates the appearance of microcracks along the planes of the second-order prisms and pyramids at various stages of deformation, and consequently raises the plasticity of the crystal.

The plasticity of purified beryllium single crystals manifests itself also in the fact that at 77°K, along with single slip bands, stacks consisting of many closely-spaced slip bands are produced. The appearance of such stacks is observed even at 0.7% deformation. The stack is 10 to 15 μ thick, and the shear displacement is 0.5 to 0.8 μ. Figure 7 shows electron-microscope photographs of a stack of basal slip bands in a specimen deformed 0.7% at 77°K. An electron-microscope investigation of the

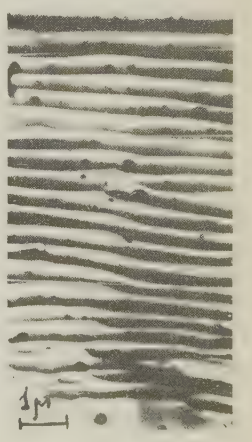

FIG. 7. Group of basal slip bands on the ah face (Fig. 1) at 77°K and 0.7% deformation.

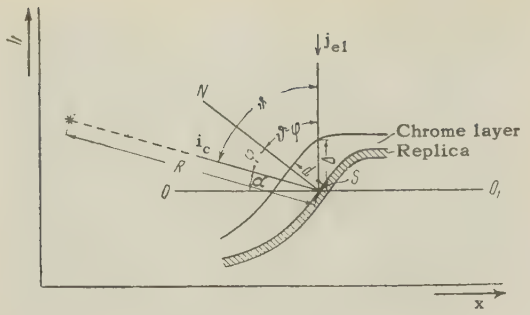

FIG. 8. Illustrating the determination of the profile. i_c – contrast direction, j_{e1} – direction of electron beam, $\alpha_1 = 15°$ – angle between the contrast direction and the undeformed face. OO_1 – undeformed face, S – surface element of the replica, N – normal to the surface element of the replica, φ – angle between the normal to the surface element and the contrast direction.

structure of the stack was made with the aid of chrome-stained lacquer replicas. A photograph of Fig. 7 was used to draw a profile of the slip-band stack.

4. INVESTIGATION OF THE PROFILE BY PHOTOMETRY OF THE ELECTRON-MICROSCOPE PICTURE

Let an element S of the surface of the replica be arbitrarily oriented relative to the beam i_c of the contrasting substance (Fig. 8). The amount of substance condensing on the surface element is determined from the expression

$$q = dQ/dS = Q\cos\varphi/4\pi R^2, \tag{2}$$

where Q is the total amount of evaporating substance, R is the distance from the evaporator to the surface element S of the replica (R is considerably greater than the linear dimensions of the replica), and φ is the angle between the direction of i_c and the normal to the surface element S.

If the replica is examined in an electron microscope, the electron beam passes through a stained layer of thickness

$$\Delta = \frac{d}{\cos(\vartheta-\varphi)} = \frac{Q\cos\varphi}{4\pi R^2\rho\cos(\vartheta-\varphi)}, \tag{3}$$

where d is the thickness of the layer of stained substance in the normal direction to the surface element S of the replica, and R is the density of the stained substance.

The electron beam is partly absorbed in the layer Δ and is scattered (one can neglect the absorption in the lacquer replica compared with the absorption in the chromium). The intensity of the electron beam after passage through a layer Δ is

$$J_\Delta = J_0 e^{-\mu\Delta}, \tag{4}$$

where μ is the absorption coefficient. Since

$$dh/dx = \tan(\vartheta-\varphi), \tag{5}$$

(cf. Fig. 8), the ordinates of the profile h can be determined from

$$h = \frac{1}{\beta}\int_0^x f(x)\,dx, \tag{6}$$

where $\beta = \mu Q/4\pi R^2\rho$ is a constant, and

$$f(x) = \ln\frac{J_0}{J_\Delta}\cdot\frac{\sin(\vartheta-\varphi)}{\cos\varphi}, \tag{7}$$

which follows from (2), (3), and (4).

It is not necessary to determine β in order to calculate h, since $\vartheta = \varphi$ for a horizontally-placed element S of the replica (see Fig. 8), i.e., we have from (3) and (4)

$$\ln(J_0/J_{\Delta h}) = \beta\cos\vartheta. \tag{8}$$

Here $J_{\Delta h}$ is the intensity of the electron beam passing through the horizontal portion of the replica.

Inserting into (6) the value of β from (8), we get

$$h = \cot\vartheta\left[\int_0^x\left(\frac{\ln(J_0/J_\Delta)}{\ln(J_0/J_{\Delta h})}-1\right)dx\right]. \tag{9}$$

The density D of the photographic plate is portional, within a definite exposure interval, to the intensity of the electron beam. One can therefore express the integrand f(x) in (9) as follows:

$$f(x) = \frac{\ln(D_{max}/D)}{\ln(D_{max}/D_h)} - 1. \tag{10}$$

It must be noted that D_{max} is the density produced in an electron-microscope plate by an electron beam that has experienced no scattering or absorption, i.e., that has passed through a section of the replica on which there is no contrasting substance. In our case such a spot is the shadow region produced by the coloxylin sphere, placed on the replica to determine the direction and angle of contrast. D_h is the density on the horizontal portion of the replica, while D is the density of the replica at the point with the given value of x. Thus, to determine the profile of the face it is enough to carry out a photometric measurement of the electron-microscope plate, find f(x), and integrate (9). In other words, the area bounded by the curve at f(x) for various values of x will yield all the points of the sought profile of the individual slip band.

Figure 9 shows the profile of a stack of slip

bands in pure beryllium. It is seen that the profile is smooth (as in the case of single bands during the earlier stage of deformation). The thickness b of an elementary band in the stack, in the case of a 0.7% deformation, is estimated to be 700 A, while the absolute shear ($\Delta S = b - a$) on the band is approximately 200 A. Consequently, the relative shear in the region adjacent to the slip band is $\gamma = \Delta S/b = 0.3$. In the case of a single band, $\gamma = 0.6$ at $\delta = 0.3\%$. For a uniform overall deformation in the stack, the shear at each band is somewhat smaller than in individual slip bands, this being compensated for by the closer placement of the bands in the stack.

5. INTERPRETATION OF THE PHENOMENA

It is interesting to compare the data obtained with the results of investigations on the fine structure of slip bands of the following plastic metals; mercury,[10] zinc,[11] and aluminum.[12] In these metals the profile is believed by the authors to be smooth and the average shear per band is believed to be several thousands of angstroms. The relative shear per band is several units. Since these data pertain to the initial stage of deformation, one can conclude that pure beryllium exhibits typical plastic properties at low degrees of compression.

The observed phenomena can be interpreted in terms of the dislocation theory as follows. In the initial stage shearing occurs of an entire stack of glide planes, which leads to bending of the lines near the future slip bands, as can be seen from Fig. 2. The resolving power of the electron-microscope would permit observation of steps not less than 100 A on the curved portion of the scribe line. Judging from Fig. 2a, no such steps appear, and consequently we can assume that the adjacent glide planes does not exceed 100 A. This corresponds to a linear density of 10^6 per centimeter of the edge dislocations in a direction perpendicular to the glide planes. Assuming that the distance between the dislocations in each glide plane is of the same order, we obtain a figure of 10^{12} per cm^2 for the dislocation density in this zone.

As the relative shear reaches 0.6, corresponding, under these assumptions, to an emergence of 20 dislocations on the lateral surface of the crystal at each glide plane, the active planes become stronger, since some of the dislocation stick together. As the stresses increase further, this leads to localization of the deformation on one the glide planes. The region of localization of large shear displacements is usually called a slip band, as was done in the present paper.

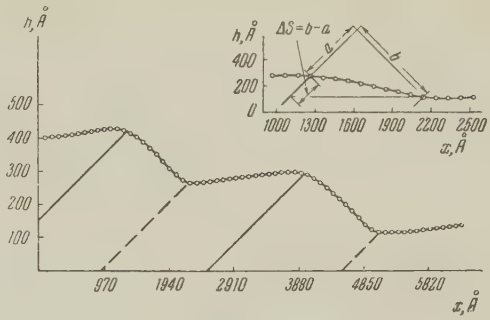

FIG. 9. Profile of a stack of slip bands in pure beryllium (cf. Fig. 7). b) thickness of elementary band in the pocket, equal to 700 A, ΔS) absolute shear in band, equal to 200 A. The relative shear is $\gamma = 0.3$.

The shear localized in a slip band at 77°K reaches several microns, which amounts to approximately 10^4 atomic distances. It is hard to believe that a regular motion of so large a number of dislocations is possible without a noticeable strengthening. It is therefore more probable that the localized shear is due to damage to the continuity with subsequent healing of the contacts.[13]

6. CONCLUSIONS

1. In crystals of 99.98% pure beryllium a clearly pronounced slip is observed along the (0001) basal plane, beginning with the temperature of liquid hydrogen (20°K).

2. The character of the slip differs substantially at different stages of deformation. At small degress of compression, there is no shear directly on the band, and the slip takes places in layers adjacent to the band. The remaining part of the crystal, between the two bands, moves as a whole. The residual stresses produce an elastic shear of opposite sign in the layers of the crystal adjacent to the band. At considerable degrees of compression, the slip is concentrated on the band and is characterized by a large relative shear. A characteristic feature of this stage is the development of a sawtooth profile in the crystal face, which, in the case of basal slip,[8] can be considered as the result of twinning along planes with large indices which combines with the break in the continuity and a subsequent healing of the contacts over the slip surface.[13]

3. The non-uniformity of the shear is due to the presence of impurities; purification of the beryllium makes for more uniform shear along each slip band, leading in turn to an increase in the plasticity of the metal. At 77°K one observes a formation of stacks of basal slip bands.

A method was developed for plotting the face

profiles of deformed crystals, which makes it possible to determine the principal parameters of the fine structure of single and multiple slip bands.

The authors expressed their gratitude to I. M. Fishman for preparing and contrasting of the replicas and taking the electron-microscope photographs.

[1] Garber, Gindin, Kogan, and Lazarev, Физика металлов и металловедение (Phys. of Metals and Metal Research) 3, 529 (1955).

[2] Garber, Gindin, Kovalev, and Shubin, Физика металлов и металловедение (Phys. of Metals and Metal Research) 7, No. 3 (1957).

[3] Garber, Gindin, Konstantinovskiĭ, Malik, Polyakov, and Startsev, Заводск. лабор. (Plant Laboratory) 19, 857 (1953).

[4] Gindin, Khotkevich, and Starodubov, Физика металлов и металловедение (Phys. of Metals and Metal Research), 1958 (in press).

[5] Garber, Gindin, Kogan, and Lazarev, Izv. Akad. Nauk SSSR, Ser. Fiz. 20, 639 (1956), Columbia Techn. Transl. p. 580.

[6] I. S. Brokhin and L. M. Bursuk, Заводск. лабор. (Plant Laboratory) 10, 1225 (1951).

[7] I. V. Obreimov and L. V. Shubnikov, Жур. Русск. Физ. Об. (J. Russ. Phys. Soc.) 58, 817 (1926).

[8] N. A. Brilliantov and I. V. Obreimov, J. Exptl. Theoret. Phys. (U.S.S.R.) 7, 978 (1937).

[9] V. Rosenhain, Introduction to Physical Metallurgy, 1916 (cf. C. S. Barret, Structure of Metals, Russ. Transl., Metallurgizdat, 1948, p. 370, McGraw-Hill, N.Y., 1943).

[10] K. M. Greenland, Proc. Roy. Soc. A163, 28 (1937).

[11] S. L. Hoyt, Trans. AIME, 75a, 116 (1927).

[12] R. D. Heidenreich and W. Shockley. Report of a Conference on Strength of Solids, London, Phys. Soc., 1948, p. 57.

[13] Garber, Gindin, and Polyakov. International Conference on Mechanical Properties of Nonmetals, Leningrad, May, 1958.

Translated by J. G. Adashko
66

DISSOCIATION OF THE MOLECULAR ION H_2^+ IN COLLISIONS WITH GASES

N. V. FEDORENKO, V. V. AFROSIMOV, R. N. IL'IN, and D. M. KAMINKER

Leningrad Physico-Technical Institute, Academy of Sciences, U.S.S.R.

Submitted to JETP editor July 29, 1958

J. Exptl. Theoret. Phys. (U.S.S.R.) **36**, 385-392 (February, 1959)

We have measured the cross section σ_{H^+} for proton production resulting from the dissociation of molecular hydrogen ions H_2^+ in single collisions occurring in helium, argon, hydrogen and air. The energy T of the H_2^+ ions varied between 5 and 180 kev. For hydrogen and helium the $\sigma_{H^+}(T)$ curves possess two maxima, while for argon and air they rise monotonically. The angular distribution of primary 24-kev H_2^+ ions scattered in argon without change of e/m was investigated as well as the angular distributions of H^+ and H^- ions resulting from dissociation. It is concluded that with decrease of the distance of closest approach between the nuclei of the colliding particles the relative probability of scattering with dissociation increases.

INTRODUCTION

In investigations of inelastic collisions associated with changes of e/m for the molecular ion H_2^+ the following possible processes must be considered:

$$H_2^+ \rightarrow H_2^0; \quad \text{(I)}$$

$$H_2^+ \rightarrow H^0 + H^0; \quad \text{(II)}$$

$$H_2^+ \rightarrow H^- + H^+; \quad \text{(III)}$$

$$H_2^+ \rightarrow H^- + H^0; \quad \text{(IV)}$$

$$H_2^+ \rightarrow H^- + H^-; \quad \text{(V)}$$

$$H_2^+ \rightarrow H^+ + H^0; \quad \text{(VI)}$$

$$H_2^+ \rightarrow H^+ + H^+. \quad \text{(VII)}$$

Process (I) is ordinary charge transfer with the capture of a single electron from the target atom. Processes (II) — (VII) are different dissociation modes of the molecular ion H_2^+ resulting in the formation of the atomic particles H^+, H^0, and H^-; (II) — (V) are dissociation processes with electron capture; (VI) is dissociation without electron transfer and (VII) is dissociation with the H_2^+ ion losing an electron.

The sum of the cross sections for processes (II) — (VII) gives the total dissocation cross section σ_d. The cross section for proton production σ_{H^+} is the sum of the cross sections for the processes (III), (VI), and (VII). σ_0, the cross section for the production of neutral particles, is the sum of the cross sections for processes (I), (II), (IV), and (VI). σ_{H^-}, the cross section for the production of H^- ions, is the sum of the cross sections for processes (III), (IV), and (V).

The principal role in the dissociation of the H_2^+ ion at kilovolt energies is evidently played by the processes (II), (VI), and (VII). Processes leading to the production of fast negative ions possess small cross sections.[1] The energy expended in each of processes (I) — (VII) varies depending on the electronic and vibrational excitation energies of the two colliding particles.

The theory of molecular ion dissociation through collisions with atoms is not highly developed. The cross sections for (VI) and (VII) at high velocities in the Born approximation have been estimated only in a brief paper by Salpeter.[2] Effat's experimental results,[3] obtained with a cyclotron, are in satisfactory agreement with Salpeter's theory. The total cross section σ_{H^+} for proton production from the dissociation of H_2^+ ions in nitrogen, argon, neon, and hydrogen has been measured by Fedorenko[4] at 5 — 25 kev. Damodaran[5] measured σ_0 and σ_{H^+} in a few gases at 100 — 200 kev. Very little information is available regarding the cross sections for H_2^+ dissociation at low energies.[6,7]

In the present work we measured the proton-production cross sections at energies intermediate between those used in references 4 and 5, in the atomic gases helium and argon and molecular gases hydrogen and air.

1. DESCRIPTION OF APPARATUS

Measurements were obtained with the mass-spectrometric apparatus which was described in earlier papers by our group.[8,9] We shall give a brief description of the present experiment. A monoenergetic H_2^+ ion beam obtained by means

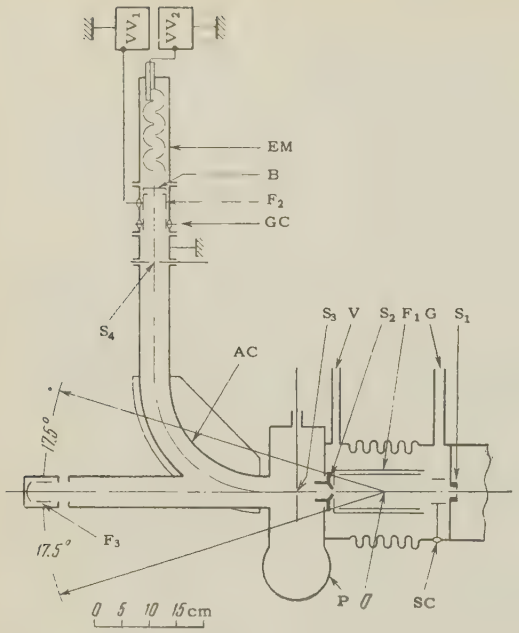

FIG. 1. Diagram of collision chamber and analyzer. AC – analyzing chamber; O – geometric center of rotation of analyzer; S_1 – entrance slit of collision chamber; S_2 – exit slit of collision chamber; S_3 – collimating slit for investigating ion scattering; S_4 – exit slit of analyzer; F_1 – collector of primary ions; F_2 – collector of analyzer; F_3 – collector of fast neutron particles; B – bottom of collector F_2; EM – electron multiplier; VV_1 and VV_2 – vacuum-tube voltmeters; GC – guard condensers; P – diffusion pump; G and V – tubes for gas inlet and vacuum gauge connection.

of a magnetic monochromator entered a collision chamber filled with the investigated gas and was subjected to e/m analysis in the magnetic field. The primary beam entering the collision chamber possessed initial divergence less than 0.5° in both the horizontal and vertical directions. A schematic horizontal section of the collision chamber and analyzer are shown in Fig. 1. For investigations of ion scattering the analyzer can be rotated around a vertical axis passing through the geometric center of the collision chamber through the angular range $-17.5° < \theta < 17.5°$ from the primary-beam direction. The entrance slit S_1 of the collision chamber was 1 mm wide and 3 mm long. Slits S_2 and S_3 served for collimation of scattered ion beams. The analyzer was rotated and the widths of the slits were varied without affecting the vacuum. Variation of the magnetic field strength in the analyzer can be used to send to collector F_2 either primary H_2^+ ions or H^+ and H^- ions resulting from H_2^+ dissociation in the collision chamber. The adjustable slit S_4 was used to determine the geometric widths of spectral lines, which were considerably smaller than the inlet aperture of collector F_2. The current to F_2 was measured by a vacuum-tube voltmeter of sensitivity 1×10^{-14} amp per scale division. Sensitivity was increased by the use of a measuring scheme which consisted of an open electron multiplier connected to the input of a vacuum-tube voltmeter; the sensitivity of this system was 1×10^{-17} amp per division. For the measurement of very small currents the bottom of F_2 was raised by means of flexible bellows and the ion beam entered the electron multiplier. A similar measuring scheme was previously used by the authors of the present paper to investigate the scattering of secondary ions[10] and in the present instance was used to investigate the scattering of fast ions. The primary beam passing through the collision chamber was measured by F_1 with rotation of the analyzer through the angle $\theta = \pm 5°$, in which position practically the entire primary beam was captured by F_1. The primary current of $1 \times 10^{-8} - 1 \times 10^{-6}$ amp was measured by a galvanometer. Collector F_3 was used to detect fast neutral particles produced from H_2^+ ions.

2. INVESTIGATION OF SCATTERING

For the investigation of scattering we used a procedure similar to that described in references 11 and 12. The first collimating slit S_2 was 1.5 mm wide and 6 mm long; the dimensions of the cecond collimating slit S_3 were 0.25 and 2.0 mm, respectively. The angular resolution of the measuring scheme as a whole was $\sim 2.3°$.

After the collision chamber was filled with gas we observed some broadening of primary H_2^+ ion lines and the appearance of atomic H^+ and H^- ions resulting from H_2^+ dissociation. We investigated (1) the angular distribution of primary H_2^+ ions with the collision chamber pumped down to its ultimate vacuum, i.e., the shape of the beam; (2) the angular distribution of H_2^+ ions and the angular distributions of H^+ and H^- ions after the collision chamber was filled with gas. For each case separately we determined the angular distribution

$$f(\theta) = i_2 / i_1, \qquad (1)$$

where θ is the angle of ion deflection due to rotation of the analyzer, i_1 is the primary current in the collision chamber and i_2 is the current to F_2. We used the data to compare the angular distributions for H_2^+, H^+ and H^- obtained with completely identical geometry.

3. TOTAL CROSS SECTIONS σ_{H^+} FOR PROTON PRODUCTION

Preliminary scattering experiments showed that a large fraction of the protons resulting from H_2^+ dissociation are deflected through small angles

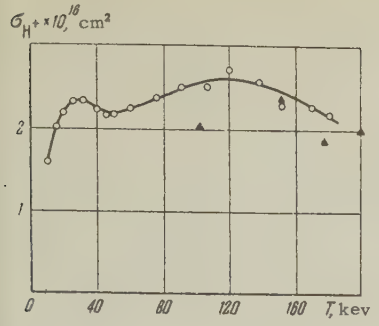

FIG. 2. Proton production cross section in helium as a function of H_2^+ energy; ▲ – data from reference 5.

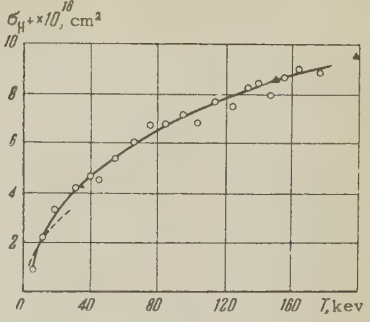

FIG. 3. Proton production cross section in argon as a function of H_2^+ energy; ▲ – data from reference 5; dashed line – curve taken from reference 4.

from the primary beam direction. Therefore, as in references 4, 5, and 8, σ_{H^+} was determined by means of a collision chamber with a wide entrance slit. The second collimating slit S_3 was removed and the width of slit S_2 was increased to 4.5 mm. It was determined experimentally that further increase of the slit width does not produce an appreciable increase of the proton current to F_2. For the measurement of σ_{H^+} the analyzer was set in the position $\theta = 0°$. Proton production cross sections were determined from the formula

$$\sigma_{H^+} = i_2 / i_1 nlk, \qquad (2)$$

where n is the atomic concentration of the given gas in the collision chamber; i_2 is the proton current measured by F_2; i_1 is the primary H_2^+ ion current in the collision chamber; l is the length of the collision chamber (16 cm); k is the so-called "penetration coefficient" of the analyzer, which is the ratio of primary beam currents measured by F_2 and F_1 when the collision chamber is filled with gas. The value of k characterizes the attenuation of the primary ion beam through elastic and inelastic scattering; in our work k varied from 0.85 to 0.95. The conditions for single collisions between primary ions and gas ions, resulting in dissociation, were established by investigating the ratio $i_2/i_1 = \varphi(p)$ for protons entering F_2. The principal measurements were obtained at the pressure $p \approx 1.5 \times 10^{-4}$ mm over a linear portion of this relation. Differential pumping maintained the pressure below 5×10^{-6} mm in other portions of the apparatus.

The purity of the investigated gas was monitored by a separate analyzer, which was previously used to investigate the charges of secondary ions produced through the ionization of gas atoms by the ion beam.[13] Random errors in determining σ_{H^+} are estimated at ±12%, combining errors in measuring the gas pressure (±6%) and the ion current (±6%).

Equation (2) was also used to determine σ_{H^-}, but we regard the value obtained for the latter as approximate since the $\sigma_{H^-}(p)$ curve did not possess a well-defined linear portion.

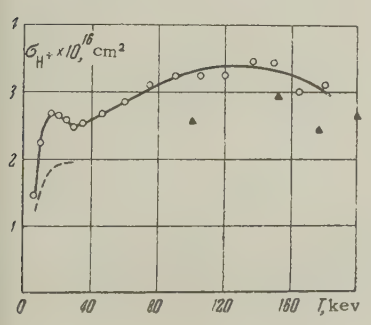

FIG. 4. Proton production cross section in hydrogen as a function of H_2^+ energy ▲ – data from reference 5; dashed line – curve from reference 4.

4. EXPERIMENTAL RESULTS AND DISCUSSION

1. Proton and H^- Production Cross Sections

The dependences of σ_{H^+} on H_2^+ ion energy in helium, argon, hydrogen, and air are shown in Figs. 2, 3, 4, and 5. The cross sections were calculated for a single primary molecular ion per gas molecule. All of the figures also show the values of σ_{H^+} taken from Damodaran's data[5*] and Figs. 3, 4, and 5 give the corresponding curves taken from Fedorenko's work.[4] All of the experimental data for argon show satisfactory consistency, whereas for the other gases the spread of experimental results somewhat exceeds the limits of the random-measurement errors indicated in the respective papers. The curves obtained in the present work give higher values of the cross sections for a single H_2^+ energy. We note that in reference 4 the penetration coefficient of the analyzer did not exceed 0.35, so that, as indicated in the present work, the values of σ_{H^+} could be too low. The same inadequacy of the experimental procedure could have existed in reference 5 because of the relatively narrow entrance slit of the collision chamber.

It is evident from Figs. 3 and 5 that σ_{H^+} in argon and air increases continuously over the en-

*Using the data of reference 5, σ_{H^+} can be determined from the ratio σ_{H^+}/σ_d. However, in determining the total dissociation cross section σ_d in reference 5 the experimental data are interpreted inaccurately, since the author neglects the possibility that H_2^0 molecules resulting from ordinary charge transfer can enter the neutral-particle detector together with H^0 atoms.

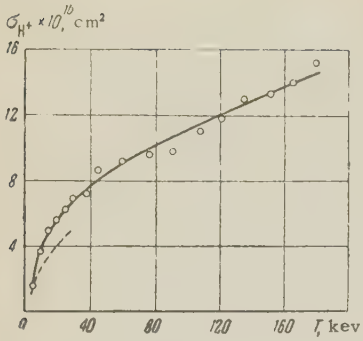

FIG. 5. Proton production cross section in air as a function of H_2^+ energy; ▲ – data from reference 5 for nitrogen; dashed line – curve from reference 4 for nitrogen.

tire investigated energy range. For hydrogen and helium $\sigma_{H^+}(T)$ shows a broad peak between 100 and 160 kev. Also, the same curves reveal an additional narrow peak, at ~15 kev for hydrogen and ~30 kev for helium. These narrow peaks are not very sharply defined and in general fall within the limits of error mentioned above. However, frequent repetition of measurements in this range confirmed without exception the existence of these peaks of $\sigma_{H^+}(T)$ for hydrogen and helium.

The cross section for the production of negative ions was measured only in argon, giving $\sigma_{H^-} \approx 1.6 \times 10^{-18}$ cm² at 12 kev. A rapid continuous reduction of σ_{H^-} is observed as the energy is increased up to 180 kev.

According to general theoretical concepts, the dissociation of molecular ions possessing energies of thousands of volts in collisions with atoms should proceed mainly through electron transitions to excited levels, observing the Franck-Condon principle. Dissociation due to the excitation of vibrational states plays an essential part at lower energies. It is known from the most recent work on the ionization of atoms by ionic impact[8,14-17] that in the kilovolt range ionization cross sections in heavy gases can attain values $\sim 1 \times 10^{-15}$ cm² and the excitation of both colliding particles is observed. Therefore large cross sections for the dissociation of the molecular ion H_2^+ are not unexpected.

It appears to us that some characteristics of the $\sigma_{H^+}(T)$ curves can be explained qualitatively from a consideration of the theoretical potential energy curves for electron states of H_2^+.[18] The narrow first peak of the σ_{H^+} curves for hydrogen and helium can be attributed to a transition from $^2\Sigma_g$, the ground state of H_2^+, to the repulsive state $^2\Sigma_u$, with the production of a proton and of a hydrogen atom in an unexcited state. The broad second peak, at a higher energy, can be associated with a transition of H_2^+ to various excited states or to a fully ionized state with the production of two protons and an electron. The cross sections σ_{H^+} in argon and air are considerably larger than in hydrogen and helium; this apparently results from the relatively large probability of H_2^+ excitation in passing through the complex electron cloud of a target atom.

2. Angular Distributions

In the light gases hydrogen and helium H_2^+ ions with energies $T \gtrsim 100$ kev are scattered without dissociation, and the atomic ions H^+ and H^- resulting from the dissociation are deflected very little from the primary beam direction. We shall therefore give only the clearest data for scattering in argon at 24 kev, the curves for which are shown in Fig. 6. A logarithmic scale is used for the angular distribution $f(\theta)$.

The angular distribution curves were compared more conveniently by making them coincide at $\theta = 0°$. The small amount of broadening of the H_2^+ angular distribution for a gas-filled collision chamber is evidence that H_2^+ ions are scattered without change of e/m. It is quite evident that the angular distributions of H^+ and H^- ions resulting from dissociation are flatter. Similar results were previously obtained by Fedorenko[11] in a study of N_2^+ scattering in neon and of H_2^+ and H_3^+ scattering in krypton.

These results permit the general conclusion that the relative probability of scattering with dissociation increases with reduction of the distance of closest approach between a molecular ion and gas atom. This conclusion is supported by the following considerations. Classical concepts can be used to interpret data on the scattering of atomic particles at kilovolt energies outside of the small-

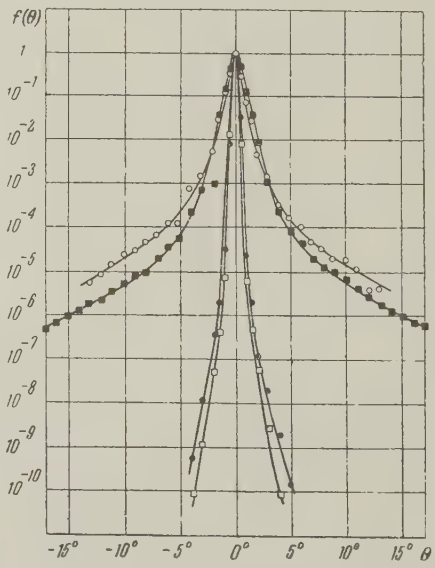

FIG. 6. Angular distributions: □ – for primary H_2^+ ions, with the collision chamber at a pressure of 5×10^{-6} mm; ●, ■, ○ – for H_2^+, H^+ and H^-, with the collision chamber filled with argon at 1.5×10^{-4} mm.

angle region.[10-12,19,20] Specifically, increase of the deflection angle corresponds to reduction of the impact parameter and of the distance of closest approach of the colliding particles. In addition, elastic and inelastic scattering angles differ very little when the inelastic energy loss is small compared to the kinetic energy of relative motion of the colliding particles.

The two atomic particles resulting from the dissociation of H_2^+ during their separation acquire additional kinetic energy as the H_2^+ ion makes its transition to a repulsive state; however this energy does not exceed 10 ev per particle even when two protons are produced. The magnitude of the additional energy can be used to determine a corresponding change of direction, which in our case is computed to be less than 1.6°. Therefore the different shapes of the angular distribution curves in Fig. 6 cannot be attributed only to mutual repulsion of the atomic particles produced by dissociation. Indeed, it is evident that as the deflection angle is varied a redistribution of the relative probabilities of different types of scattering is observed. Inelastic scattering with dissociation becomes relatively more probable as θ increases. Ionic scattering without dissociation, which is elastic when unaccompanied by excitation, occurs principally at small angles.

In our earlier studies of primary ion scattering with the loss of electrons,[12] and of the scattering of secondary ions derived from gas atoms,[17] it was determined that a reduction of the distance of closest approach of the colliding nuclei is accompanied by increased relative probability of inelastic processes requiring the expenditure of relatively large amounts of energy. The results of the present work show that this phenomenological law can evidently be extended to the dissociation of molecular ions and we presume that it is a general property of atomic collisions.

In conclusion it is a pleasant obligation to thank O. B. Firsov and V. M. Dukel'skiĭ for discussions.

[1] Fogel', Krupnik, and Ankudinov, J. Tech. Phys. (U.S.S.R.) **26**, 1208 (1956), Soviet Phys. JTP **1**, 1181 (1956).

[2] E. E. Salpeter, Proc. Phys. Soc. (London) **A63**, 1295 (1950).

[3] K. E. A. Effat, Proc. Phys. Soc. (London) **A65**, 433 (1952).

[4] N. V. Fedorenko, J. Tech. Phys. (U.S.S.R.) **24**, 769 (1954).

[5] K. K. Damodaran, Proc. Roy. Soc. (London) **A239**, 382 (1957).

[6] Lamar, Samson, and Compton, Phys. Rev. **48**, 886 (1935).

[7] S. E. Kupriyanov and V. K. Potapov, J. Exptl. Theoret. Phys. (U.S.S.R.) **33**, 311 (1957), Soviet Phys. JETP **6**, 244 (1958).

[8] D. M. Kaminker and N. V. Fedorenko, J. Tech. Phys. (U.S.S.R.) **25**, 1843 (1955).

[9] N. V. Fedorenko, Proceedings of the Third International Conference on Ionization Phenomena in Gases, Venice, 1957, p. 295.

[10] V. V. Afrosimov and N. V. Fedorenko, J. Tech. Phys. (U.S.S.R.) **27**, 2573 (1957), Soviet Phys. JTP **2**, 2391 (1957).

[11] N. V. Fedorenko, J. Tech. Phys. (U.S.S.R.) **24**, 784 (1954).

[12] D. M. Kaminker and N. V. Fedorenko, J. Tech. Phys. (U.S.S.R.) **25**, 2239 (1955).

[13] N. V. Fedorenko and V. V. Afrosimov, J. Tech. Phys. (U.S.S.R.) **26**, 1941 (1956), Soviet Phys. JTP **1**, 1872 (1956).

[14] N. V. Fedorenko, J. Tech. Phys. (U.S.S.R.) **24**, 2113 (1954).

[15] Fedorenko, Afrosimov and Kaminker, J. Tech. Phys. (U.S.S.R.) **26**, 1929 (1956), Soviet Phys. JTP **1**, 1861 (1956).

[16] H. B. Gilbody and J. B. Hasted, Proc. Roy. Soc. (London) **A240**, 382 (1957).

[17] V. V. Afrosimov and N. V. Fedorenko, J. Tech. Phys. (U.S.S.R.) **27**, 2557 (1957), Soviet Phys. JTP **2**, 2378 (1957).

[18] H. S. W. Massey and E. H. S. Burhop, Electronic and Ionic Impact Phenomena (Oxford, 1952), Russ. Transl., Moscow, 1958.

[19] Carbone, Fuls, and Everhart, Phys. Rev. **102**, 1524 (1956).

[20] O. V. Firsov, J. Exptl. Theoret. Phys. (U.S.S.R.) **34**, 447 (1958), Soviet Phys. JETP **7**, 308 (1958).

Translated by I. Emin
67

RELATIVE PROBABILITIES FOR THE PHOTOEFFECT IN SHELLS AND SUBSHELLS OF AN ATOM

E. P. GRIGOR' EV and A. V. ZOLOTAVIN

Leningrad State University

Submitted to JETP editor August 16, 1958

J. Exptl. Theoret. Phys. (U.S.S.R.) **36**, 393-400 (February, 1959)

The relative intensities of the K, $L_I + L_{II}$, L_{III} and M+N photoelectric lines produced in various targets by γ rays from several radioactive isotopes were measured by a γ ray spectrometer of resolving power 0.4%. The results are compared with theoretical calculations.

1. INTRODUCTION

In spite of the considerable amount of work on the photoeffect, there is up to now no formula for accurate calculation of the probability of this process for arbitrary energy of the x-rays or γ rays. The process of emission of an electron from the K shell has been considered in greatest detail. For the nonrelativistic case, Heitler[1] gave a formula for the photoelectric cross section in Born approximation. Stobbe[2] and Hall[3] obtained more accurate results. Using relativistic wave functions, Sauter[4] and Hulme[5] obtained formulae for the photoeffect in Born approximation. A simple formula was derived by Hall[6] for the case $h\nu \gg mc^2$. The most accurate calculations of τ_K have been carried out by Hulme et al.[7] for three elements and two γ-ray energies. Formulae for the coefficients of photoabsorption in the L_I, $L_{II} + L_{III}$ and M shells have been given by Stobbe and Hall.[2,3]

2. SURVEY OF EXPERIMENTAL DATA

In so far as experimental results for the relative probabilities of the photoeffect will be given in this article, we first consider similar investigations. We know of three projects carried out with the view of checking theoretical predictions about the relative probabilities of the photoeffect, as well as a series of studies in which relative probabilities of the photoeffect in the K and L shells of the atom were obtained from the study of γ-ray spectra of radioactive elements. A general feature of these works is insufficient resolving power of the apparatus and rather thick targets,

(a) Marty[8] measured the ratio of absorption coefficients τ_K/τ_L for energies of 140 and 411 kev, and drew conclusions concerning the agreement of experimental results with those calculated from Hall's formula for the relativistic case. Our own[9] investigation of the influence of target thickness makes us believe that the results for τ_K/τ_L obtained there are too low.

(b) Davidson and Latyshev[10] determined the ratio τ_K/τ_L for 2614-kev γ rays. This value was 4.8 for Pb and 5.3 for Ta. Later[11,12] Latyshev gave slightly different values, 4.9 and 5.4 respectively. Since the error in the experiments, according to our estimate, constitutes $\sim 20\%$, this difference is not meaningful.

(c) Bazin[13] measured the photoabsorption coefficients for the K_{α_1}-line of molybdenum, $h\nu = 17.5$ kev, in several targets.

The results of this investigation were as follows:

$$\tau_K/(\tau_L+\tau_M) = 11.3 \text{ for sulphur}$$
$$\tau_K/(\tau_L+\tau_M) = 9.4 \text{ for chromium}$$
$$\tau_L/(\tau_M+\tau_N) = 1.8 \text{ for selenium}$$
$$\tau_L/\tau_M = 2.6,\ \tau_L/(\tau_M+\tau_N) = 2.1 \text{ for silver.}$$

Unfortunately, the probable errors in these numbers are not given, but clearly they are appreciable.

(d) Of the works in which the main object was not the study of the photoeffect, the article of Navakov, Hultberg and Anderson[14] should be noted. Here the γ rays coming from the decay of Bi^{206} were studied. A uranium target of thickness 3 mg/cm^2 was employed. For 516 and 880 kev γ rays the ratios τ_K/τ_L were the same and equal to 5.5.

It should be noted that in the works considered, comparison of the results obtained with theoretical ones was somewhat loosely carried out. This was because the influence of the angular distributions of photoelectrons from the various shells and subshells of the atom was not taken into account. This remark applies, to some extent, to our work as well. A complete answer to the problem of the probabili-

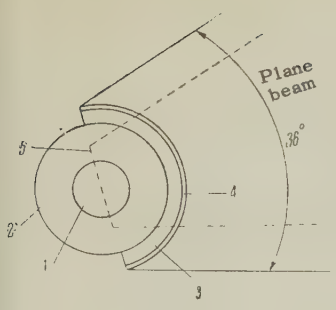

FIG. 1. Arrangement of the source of photoelectrons: 1 – radioactive material ($0.3 \leq \phi \leq 0.5$), 2 – cylindrical ampoule ($1.0 \leq \phi \leq 3.0$), 3 – backing of the target (d = 0.2), 4 – target, 5 – usual position of the source of conversion electrons. The height of the source was 35 mm, the width 1 mm.

ties of the photoeffect in various shells of the atom would be provided by measuring the intensities of the photoelectron lines at various angles, and averaging the results, after which they could be compared with theoretical predictions.

3. EXPERIMENTAL CONDITIONS

The results of the study of the photoeffect given below were obtained by us in continuing during the past five years work on the study of the decay of various isotopes. The measurements were carried out using a β spectrometer with a relative half-width of 0.4% for the spread coming from the apparatus.[15]

In our experiments, the photoelectron lines arising as a result of absorption of monochromatic γ rays in the K, $L_{I,II,III}$ and M+N shells of various elements were studied. The half-width of the photoelectron lines was measured to within 0.4 – 0.8%, depending upon the energy of the photoelectrons. In our experiments, a source with axial symmetry[16,17] was employed (see Fig. 1.) and a thin target.

From comparison of our relative γ-ray intensities with the data obtained by other methods, we conclude that, within a wide energy interval (0.1 – 2.0 Mev), the angular distribution of the photoelectrons – which changes with the γ-ray energy – does not affect the results to more than 15%. From this it follows that if there is any difference in the angular distribution of photoelectrons, for example, from the L_{II} and L_{III} subshells in comparison with L_I one, then it does not show up in our experiments. We note that the theory indicates that the angular distribution of photoelectrons from the K and L_I shells will be similar, and that those from the L_{II} and L_{III} ones will be more isotropic.[3]

In the study of the photoeffect from the L shell of medium atoms (Z ~ 50), and from M and N shells of heavy atoms (Z ~ 80), difficulties arise in the behavior of the background behind the lines, since it is influenced by the photoelectrons emitted from the K shells of the atoms of the material used either as backing of the target or in the ampule

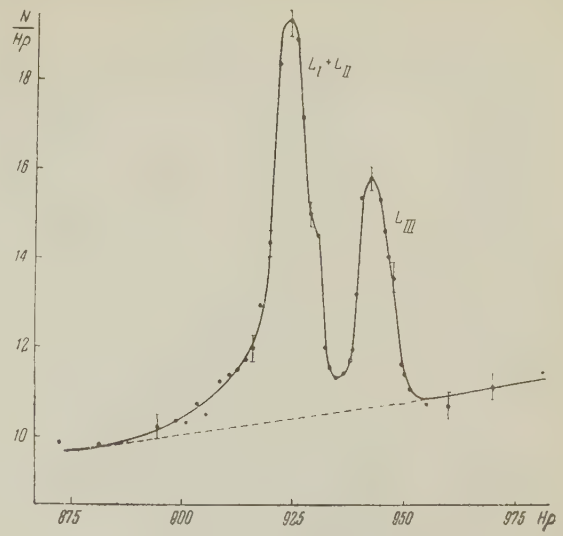

FIG. 2. $L_I + L_{II}$ and L_{III} photoelectron lines from the 86.6-kev Tb^{160} γ rays. The target was 0.25 mg/cm² Bi.

containing the radioactive source. Thus, in our use of a brass cylindrical ampule with wall-thickness 0.5 mm and superimposed target backing of 0.2 mm thick aluminum, a noticeable jump occurred in the background in the places where the K peaks of the photoelectrons of copper and zinc should occur.

In our experiments, we usually measured the background behind the peaks of the photoelectrons, and we used aluminum both in the ampule and backing. The thickness of the targets was varied from 0.03 to 13 mg/cm², to avoid distortion in the relative intensities: Targets with surface thickness < 0.3, < 1, and 3 – 13 mg/cm² were used in the region of photoelectron energies 30 – 100 kev, up to to 200 kev, and above 500 kev, respectively.

4. THE RATIO $(\tau_{L_I} + \tau_{L_{II}})/\tau_{L_{III}}$

Up till now, none of the experimental data in the literature can be compared with the theoretically predicted relative probabilities of the photoeffect from the L_I, L_{II} and L_{III} subshells of the atom for γ rays of energy greater than 20 kev. The high resolving power of the spectrometer and the use of thin targets made it possible to differentiate either partially or completely, L_I, L_{II} and L_{III} lines in measurement with the bismuth target. Since the L_{II} line of Bi is energetically nearer to the L_I than L_{III} line, we can make a very reliable determination of the ratio $(\tau_{L_I} + \tau_{L_{II}})/\tau_{L_{III}}$. We choose this ratio to compare with the formula of Stobbe,[2] considering the ratio of photoabsorption coefficients $\tau_{L_{II}}$ and $\tau_{L_{III}}$ to be 0.45 : 1 corresponding to the number of electrons in p states in the L_{II} and L_{III} subshells of the atom, and following the theoretical work of Phillips,[18] which

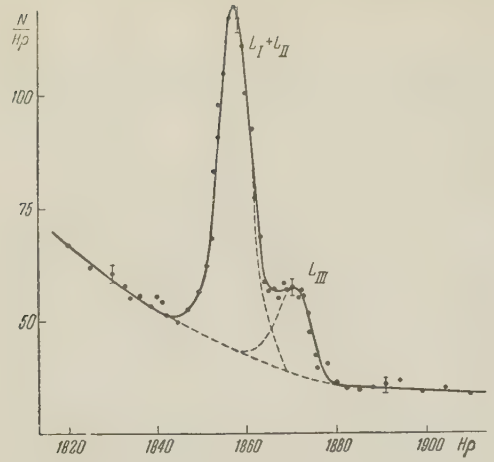

FIG. 3. $L_I + L_{II}$ and L_{III} photoelectron lines from the 265 kev Se^{75} γ rays. The target was 0.1 mg/cm² Bi.

determined this ratio as a function of Z, using relativistic wave functions. The validity of this formula was checked by Patten[19] for energies near to the threshold for absorption by the L subshells and for large Z of order 79 — 83. Examples of measured $L_I + L_{II}$ and L_{III} photoelectron lines are given in Figs. 2 and 3. From the formulae of Stobbe it follows that

$$\frac{\tau_{L_I}}{\tau_{L_{II}}+\tau_{L_{III}}}=\frac{h\nu}{h\nu_2}\,\frac{1+3\,(h\nu_2/h\nu)}{3+8\,(h\nu_2/h\nu)},$$

where $h\nu$ is the γ-ray energy, $h\nu_2 = \frac{1}{4}(Z-s_2)^2\,Ry$, s_2 is the Slater screening constant for 2s or 2p electrons, equal to 4.15 for all Z larger than 10, Ry is the Rydberg constant, (13.61 ev), and Z is the charge of the element in which the photoeffect takes place. With $\tau_{L_{II}}/\tau_{L_{III}} = 0.45$, we obtain

$$(\tau_{L_I}+\tau_{L_{II}})/\tau_{L_{III}} = 0.45+1.45\tau_{L_I}/(\tau_{L_{II}}+\tau_{L_{III}}).$$

In Table I we give calculated and experimental ratios for four cases.

TABLE I. Experimental and theoretical values of $(\tau_{L_I}+\tau_{L_{II}})/\tau_{L_{III}}$ for Z = 83 (0.1 mg/cm² Bi target, Se^{75} and Tb^{160} γ-ray sources)

hν	Theory	Experiment
86.6	2.51	2.6±0.5
121.2	3.33	3.8±0.8
136.2	3.66	3.9±0.3
265.0	6.28	5.0±0.5

Comparison of these numbers shows that the experimental values coincide with the theoretical ones for small energies, but already at an energy of 265 kev, they diverge more than the limits of experimental error.

5. THE RATIO τ_L/τ_M

We did not succeed in establishing any regularity in the ratio τ_L/τ_M. The mean value from experiments carried out with γ rays of various energies and with various targets was equal to $\tau_L/\tau_M = 3.5 \pm 0.5$. It was obtained from very careful measurements of the photoelectron lines from 411-kev γ-rays from Au^{198} on a thorium target, of 364-kev γ-rays from J^{131} on a bismuth target, etc. The ratios τ_L/τ_M, obtained with large errors, did not go outside the limits of the magnitude indicated, which is in agreement with the value $\tau_L/\tau_M = 4$ used in other work. The value $\tau_L/\tau_M = 3.5$ was used by us where it was not possible to separate the M line from the L line.

6. THE RATIO τ_K/τ_L

Our experimental data on the ratio τ_K/τ_L for various targets and $h\nu$ are collected in Table II.

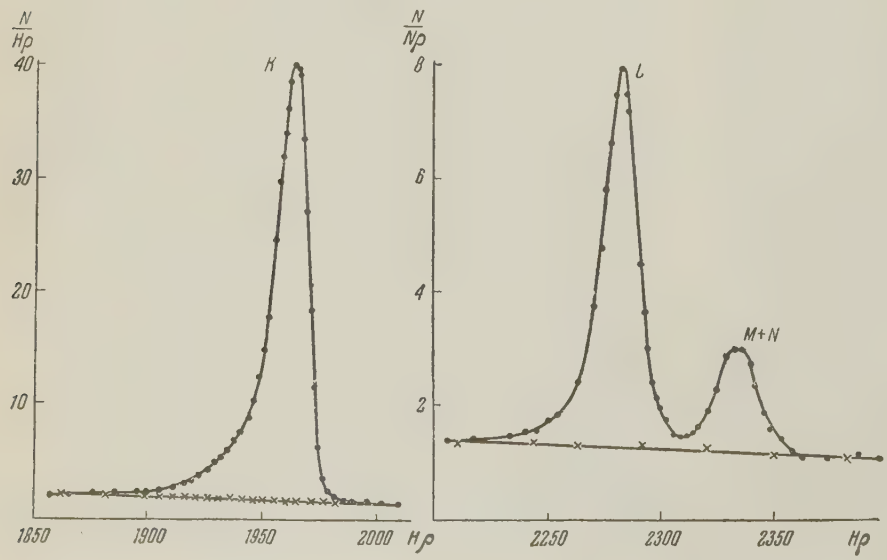

FIG. 4. K, L and M + N photoelectron peaks from the 364 kev J^{131} γ rays. The ampoule was of aluminum. A 3 mg/cm² Bi target was used.

TABLE II. Experimental values of τ_K/τ_L and of the proportion of the absorption coefficient coming from the K-shell to the total photoabsorption coefficient as a function of target material and γ-ray energy

Target	Target thickness, mg/cm²	hν, kev	τ_K/τ_L	τ_K/τ, %**	Target	Target thickness, mg/cm²	hν, kev	τ_K/τ_L	τ_K/τ, %**
Ag	0.25	121	8.3±1.0	86.5±2.2	Au	7.7	1180	5.1 ±1.0	79.8±4.0
Ag	0.25	136	7.0±0.8	84.6±2.0	Pb	13	549	4.7 ±0.2*	82.5±0.8
Ag	1.0	121	7.8±0.8	86.0±1.9	Pb	13	1696	5.1 ±0.3*	83.8±1.0
Ag	1.0	136	7.1±0.6	84.4±1.9	Bi	0.1	121	4.7 ±0.5	78.3±3.0
Ag	1.0	265	9.0±0.9	87.4±1.8	Bi	0.1	136	5.0 ±0.4	79.6±2.0
Ag	1.0	401	8.8±1.0	87.2±2.1	Bi	0.1	265	4.9 ±0.5	79.1±2.6
Ag	3.0	280	10.2±1.0	90.7±1.3	Bi	3	364	5.9 ±0.2	82.2±0.4
Sb	1.0	280	9.3±0.3	88.5±0.9	Bi	3	637	6.0 ±0.2	82.4±0.7
Pt	3.0	603	5.8±0.5	81.8±2.0	Th	3	411	5.2 ±0.6	80.2±2.5
Au	7.7	298	5.6±1.0	81.2±4.0	Th	3	513	4.85±0.1*	83.0±0.4
Au	7.7	878	5.7±1.0	81.5±4.0	Th	3	603	6.9 ±1.2	84.4±3.1
Au	7.7	967	5.9±1.0	82.1±4.0					

*—More accurate values of the ratio $\tau_K/\tau_L + \tau_M$ are given.

**—Here τ_L/τ_M has been taken as 3.5

Figure 4 shows the results.

From the experimental results, the dependence of τ_K/τ_L on Z was constructed (Fig. 5). The mean value of τ_K/τ_L for given Z and for energies greater than 200 kev is plotted along the ordinate. The growth in this ratio with decreasing Z shows up very clearly. For comparison, a curve for τ_K/τ_{L_I} obtained from Hall's relativistic formula[6] is given. For the ratio $\tau_K/\tau_{L_I} + \tau_{L_{II}} + \tau_{L_{III}}$ this curve would be somewhat lower because the contribution of the L_{II} and L_{III} subshells to the photoeffect is not very large. The experimental points begin to deviate strongly from the curve in the region $Z \sim 50$. In Fig. 6 we show the dependence of τ_K/τ_L on γ-ray energy for a group of heavy elements of nearly equal Z, and a comparison with values calculated from both nonrelativistic and relativistic formulae is given. The latter formula predicts the ratio τ_K/τ_{L_I} to be independent of energy. In the region of low γ-ray energy, the calculated ratio $\tau_K/\tau_{L_I+L_{II}+L_{III}}$ should decrease somewhat on account of the contribution of the L_{II} and L_{III} subshells, which grows with decreasing energy. The experimental points lie between the two calculated curves, and not along either. A similar picture is obtained for silver (Z=47) and antimony (Z=51) (see Fig. 7). In both this case and the former one, the ratio τ_K/τ_L is noticeably lower in the energy region 100 — 200 kev; this effect cannot be explained by experimental error. Thus, it is established that the experimental ratio τ_K/τ_L disagrees with the theoretical one both in

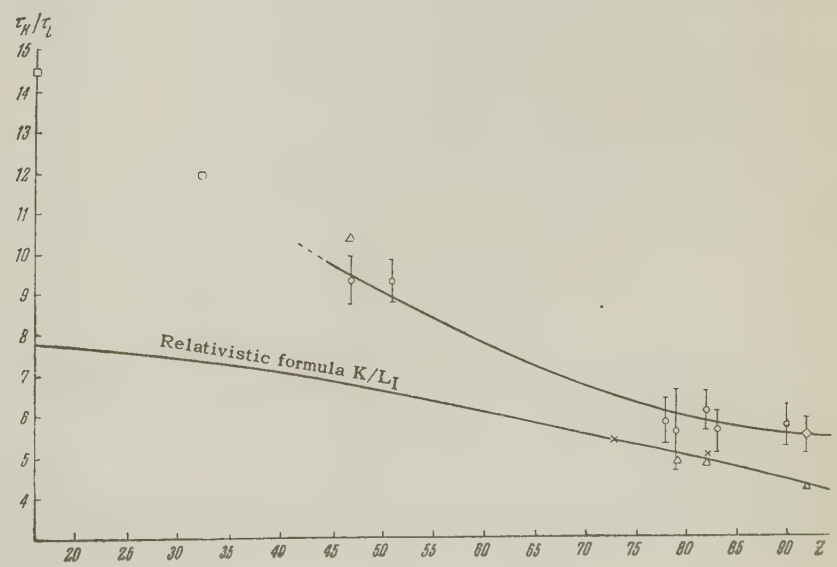

FIG. 5. τ_K/τ_L as a function of Z. The points represent mean values for γ rays of energies greater than 200 kev; ○ — our results, × — results of Latyshev[10] with hν = 2614 kev, □ — results of Bazin[13] with hν = 17.5 kev, Δ — results of Marty[8] with hν = 411 kev, ◊ — results of Navakov et al.[14] with hν = 516 and 880 kev. In the results of Marty[8] and Bazin[13] corrections have been introduced for the M shell. The values of τ_K/τ_L in the work of Bazin may change at higher energies.

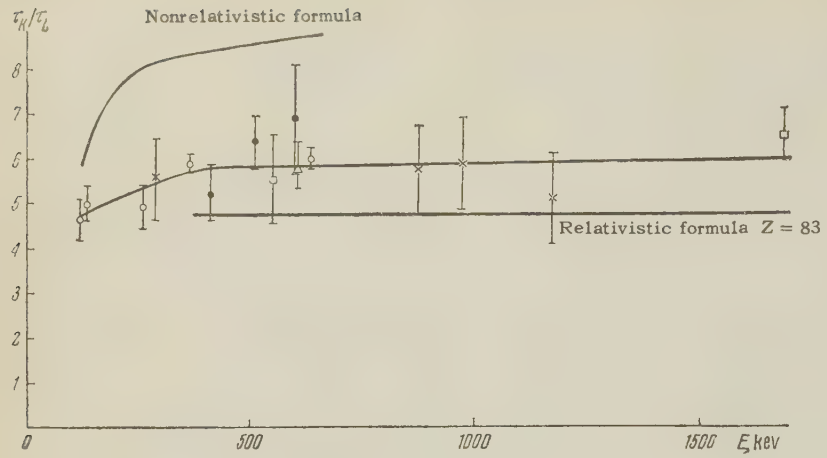

FIG. 6. τ_K/τ_L as a function of γ-ray energy for targets made out of heavy elements: ● – 3 mg/cm² Th, ○ – 0.5 mg/cm² Bi, □ – 13 mg/cm² Pb, × – 7.7 mg/cm² Au, Δ – 3 mg/cm² Pt.

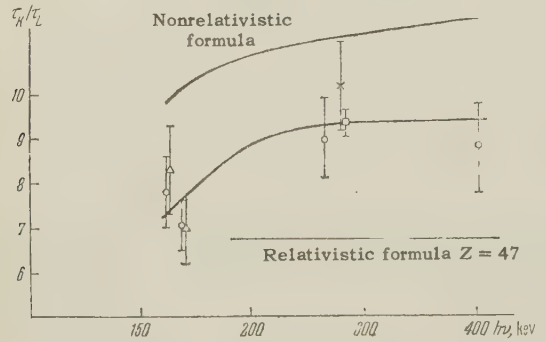

FIG. 7. τ_K/τ_L as a function of γ ray energy for silver (Z = 47) and antimony (Z = 51) targets. Δ – 0.25 mg/cm² Ag, ○ – 1 mg/cm² Ag, × – 3 mg/cm² Ag, □ – 0.3 mg/cm² Sb.

the case of relativistic and in the case of nonrelativistic calculations.

7. THE SHARE OF τ_K IN THE TOTAL ABSORPTION COEFFICIENT τ

From the experimental data given in Table II, and use of the ratio $\tau_L/\tau_M = 3.5$ and the curve given in Fig. 5, we can calculate the share of the K-shell absorption coefficient τ_K in the total absorption coefficient. This ratio is shown in Fig. 8 as a function of Z, for energies greater than 200 kev. The points on the graph are mean values for a given Z. The smooth curve drawn through the experimental points is close to the curve calculated from Allen's formula[20]

$$\frac{\tau_K}{\tau} = \frac{100}{1.13 - [(Z-1)/81] \cdot 0.07}$$

in the region of high Z, but diverges noticeably from it in the region $Z \sim 50$.

The results obtained in this work may be useful in the study of relative γ-ray intensities using photoelectrons. This method is used increasingly widely in nuclear spectroscopy.

In conclusion, the authors would like to express their gratitude to those colleagues who took part in different stages of the work. The authors are sincerely grateful to Prof. B. S. Dzhelepov for valuable remarks, made in discussions of the present articles. The authors thank N. A. Bonch-Osmolovskiĭ for the possibility of seeing his survey paper on the photoeffect before publication.

[1] W. Heitler, The Quantum Theory of Radiation Oxford, 1954.
[2] M. Stobbe, Ann. Physik **7**, 661 (1930).
[3] H. Hall, Revs. Modern Phys. **8**, 358 (1936).
[4] P. Sauter, Ann. Physik **11**, 454 (1931).
[5] H. R. Hulme, Proc. Roy. Soc. (London) **A133**, 381 (1931).
[6] H. Hall, Phys. Rev. **45**, 620 (1934); **84**, 167 (1951).
[7] Hulme, McDougall, Buckingham, and Fowler, Proc. Roy. Soc. (London) **A149**, 131 (1935).
[8] N. Marty, J. Phys. Rad. **13**, 401 (1952); Compt. rend. **234**, 938 (1952).
[9] Grigor'ev, Zolotavin, Klement'ev and Sinitsyn, Izv. Akad. Nauk SSSR, Ser. Fiz. **23** (1959), in press.
[10] Z. S. Davidson and G. D. Latyshev, J. Phys. (U.S.S.R.) 6, **15** (1942).

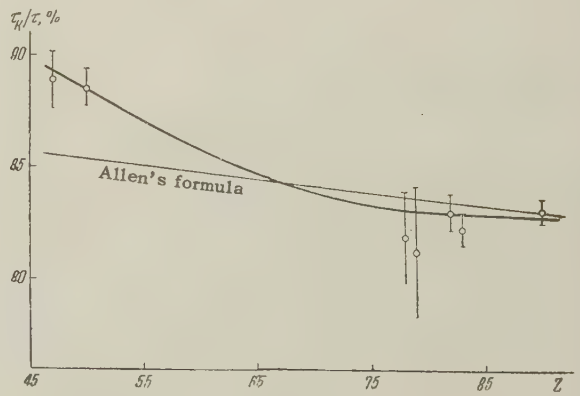

FIG. 8. Absorption coefficients for the K shell τ_K in percent of the total absorption coefficient τ as a function of Z.

[11] G. D. Latyshev, J. Exptl. Theoret. Phys. (U.S.S.R.) **14**, 65 (1944).
[12] G. D. Latyshev, Revs. Modern Phys. **19**, 132 (1947).
[13] A. P. Bazin, J. Exptl. Theoret. Phys. (U.S.S.R.) **14**, 23 (1944).
[14] Navakov, Hultberg, and Andersson, Arkiv Fys. **13**, 117 (1958).
[15] A. V. Zolotavin, Izv. Akad. Nauk SSSR, Ser. Fiz. **18**, 127 (1954).
[16] Zolotavin, Grigor'ev, and Abroyan, Izv. Akad. Nauk SSSR, Ser. Fiz. **20**, 289 (1956), [Columbia Tech. Transl. p. 271].
[17] Avotina, Grigor'ev, Zolotavin, and Kratsik, Dokl. Akad. Nauk SSSR **119**, 1127 (1958), Soviet Phys. "Doklady" **3**, 368 (1958).
[18] M. Phillips, Phys. Rev. **45**, 132 (1934).
[19] C. G. Patten, Phys. Rev. **45**, 131 (1934).
[20] K. Siegbahn, Beta and Gamma Ray Spectroscopy, Amsterdam (1955).

Translated by G. E. Brown
68

MEASUREMENT OF THE NOISE OF CYCLIC REMAGNETIZATION OF FERROMAGNETIC SUBSTANCES AT LOW TEMPERATURES

N. N. KOLACHEVSKIĬ

Moscow Physico-Technical Institute

Submitted to JETP editor August 19, 1959

J. Exptl. Theoret. Phys. (U.S.S.R.) **36**, 401-403 (February, 1959)

We present the result of measurements of the noise due to cyclic remagnetization of ferromagnetic cores at temperatures between 2° and 300°K. No dependence of the noise on the temperature was detected.

INTRODUCTION

THE fact that the reversal of magnetization of ferromagnetic specimens is not repetitive from cycle to cycle leads to the appearance of a dc component in the spectrum of the emf's induced in an indicator coil wound on the remagnetized core.[1] This may be caused by thermal flucations in the parameters that determine the position of the boundary between the domains.[2*] Owing to these flucations, the instants at which the voltage pulses are produced by the jump-like changes in the magnetic moment of the specimen upon its remagnetization (the Barkhausen effect) and also the time behavior of these pulses, may differ from cycle to cycle. However, such an explanation of the phenomenon should lead to a temperature dependence of the noise of cyclic remagnetization.

It was indicated in reference 5 that, in the temperature interval from 90°K (liquid nitrogen) to the corresponding Curie points, many ferromagnetic specimens (such as permalloy or nickel) display no variation whatever of the noise on the temperature, except for the variation caused by the temperature dependence of the average change in the magnetic moment in the Barkhausen effect.

To change substantially the influence of the thermal flucations on the remagnetization processes, we have measured the noise due to cyclic remagnetization at a temperature of 2°K (liquid helium, which boils at 24 mm Hg).

EXPERIMENTAL SETUP

The noise-measuring circuit is shown in Fig. 1. The spectrum analyzer measures the rms noise voltage at 1 to 200 kcs in a bandwidth of 15 cycles. Two indicator coils, 50 turns each, are wound on the specimens subject to remagnetization. These coils are connected in opposition to cancel the discrete components of the spectrum. Since the noise is incoherent, the noise power in these coils is additive. The solenoid with the specimen and the indicator coils is placed in a Dewar vessel with liquid helium.

In addition to measuring the cyclic remagnetization noise, we determined the average of the voltage pulses, corresponding to the average change in the magnetic moment in each elementary remagnetization event, occuring when the specimen is subjected to quasi-static remagnetization, and the voltage from the indicator coils was fed to an oscillograph. The time behavior (waveform) of the voltage pulses was also observed.

The specimens used were plates of single-crystal silicon iron (3%), the anisotropy and electric-resistivity constant of which have a low temperature dependence at low temperatures. The plates were cut out by the electric-spark method parallel to the [1 0 0] axis, with subsequent annealing in vacuo. The dimensions of the specimens were 32 × 0.65 × 0.3 mm. Two identical specimens were used under each indicator coil. The magnetization was effected with a common solenoid, 80 mm long and 30 mm in diameter, which produced a maximum field of 40 oersteds.

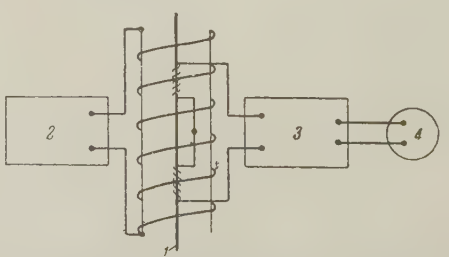

FIG. 1. Diagram of the experiment; 1) specimen, 2) generator ZG-10, 3) spectrum analyzer, 4) galvanometer.

*The possibility of such fluctuations is indicated also in references 3 and 4.

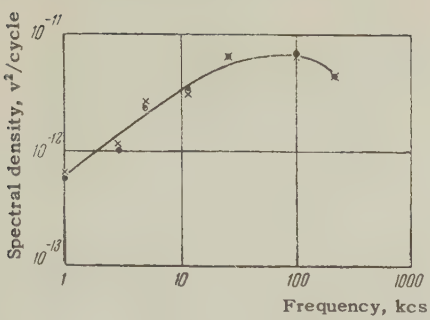

FIG. 2. Noise spectrum for a single-crystal specimen of silicon iron; × – 2°K, • – 300°K.

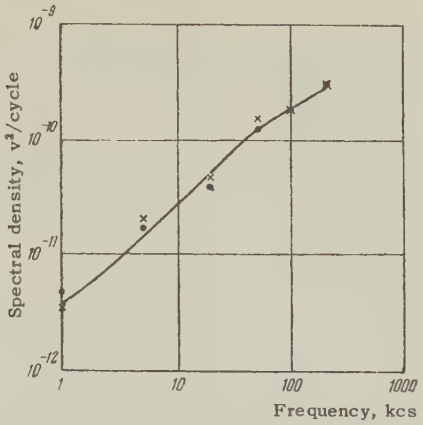

FIG. 3. Noise spectrum for polycrystalline specimen of silicon iron. Average grain dimension 5 mm; × – 2°K, • – 300°K.

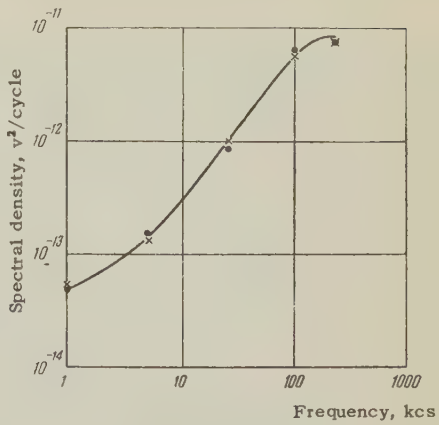

FIG. 4. Noise spectrum for a specimen of unannealed 78% permalloy; × – 2°K, • – 300°K.

To check our results we made analogous measurements on specimens of polycrystalline textured silicon steel, cut in the form of strips 0.3 mm thick, and on unannealed permalloy wire 0.2 mm in diameter. The length of the specimen was determined by the dimensions of the solenoid.

MEASUREMENT RESULTS

Figures 2, 3, and 4 give the cyclic-remagnetization noise spectra at room temperature and at 2°K. The value of the remagnetizing field was chosen such as to saturate the specimen (40 oersteds for all specimens). The frequency of the remagnetizing field was 2 kcs in all cases. As can be seen from the curves, the results of the measurements at room temperature and at the temperature of liquid helium are the same for all specimens. An observation of the oscillograms of the remagnetization pulses and a measurement of their average area also showed no differences in these temperatures. The average volume of the remagnetized region, corresponding to the average value of the voltage pulse, was on the order of 10^{-11} cm^3 for silicon steel and 10^{-10} cm^3 for permalloy.

The results obtained give grounds for concluding that the cyclic remagnetization noise is not due to thermal fluctuations.

[1] A. A. Grachev, Dokl. Akad. Nauk SSSR **71**, 269 (1950).

[2] G. S. Gorelik, Izv. Akad. Nauk SSSR, Ser. Fiz. **14**, 174 (1950).

[3] L. Neel, J. phys. et radium, **11** 49 (1950).

[4] L. Neel, J. phys. et radium **12**, 339 (1951).

[5] N. N. Kolachevskiĭ, Сб. тр. МФТИ (Coll. of Papers, Moscow Physico-technical Inst.) No. 2, (1958).

Translated by J. G. Adashko
69

INVESTIGATION OF THE NATURE AND SPECTRA OF PARTICLES PRODUCED BY HIGH-ENERGY NUCLEONS

A. I. ALIKHANOV, G. P. ELISEEV, V. Sh. KAMALYAN, V. A. LYUBIMOV, B. N. MOISEEV, and A. A. KHRIMYAN

Submitted to JETP editor August 20, 1958

J. Exptl. Theoret. Phys. (U.S.S.R.) **36**, 404-410 (February, 1959)

The nature and the momentum spectrum of secondary particles produced in lead by high-energy cosmic ray particles were investigated at an altitude of 3250 m above sea level, using a magnetic mass spectrometer and a multi-layer proportional counter.

In the present article we report the results of an investigation of the nature and the spectra of particles produced by fast nucleons of cosmic radiation at the altitude of 3200 m above sea level (Aragats, Armenia).

The cross section of the apparatus in two perpendicular views is shown in Fig. 1. The instrument consists of a mass spectrometer (with a magnetic field of 6850 Oe), an additional hodoscopic arrangement placed above the spectrometer,[1] and a five-layer, thin-wall proportional counter.[2] The construction of the instrument makes it possible to observe nuclear disintegrations produced by fast nucleons in the lead generating layers placed in the gaps A, B, C, D, F of the hodoscope arrangement, and also to determine the momenta, the specific ionization, and the character of passage of the secondary products of the stars through the lead and copper absorbers placed below the spectrometer. The mean standard deviation of the determination of momentum amounted to 3, 13, and 65% for 0.2 Bev/c, 1 Bev/c and 5 Bev/c, respectively. The specific ionization of separate particles was determined with the average accuracy of ±14%.

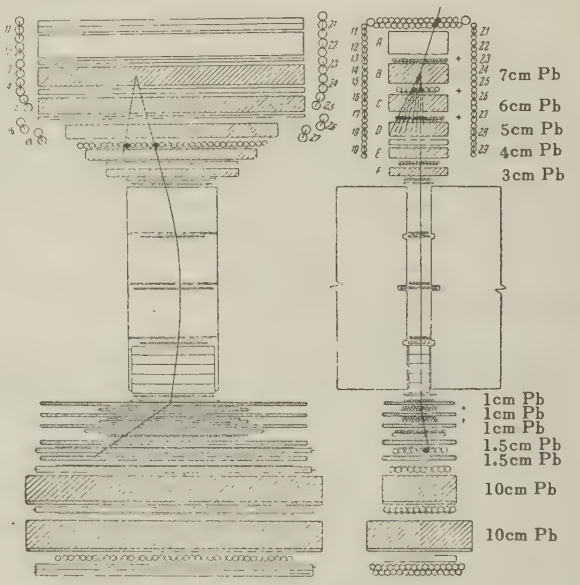

FIG. 1. Schematic diagram of the mass spectrometer in two perpendicular cross sections. A trajectory of a K^+ meson is shown in the diagram (Table I, case 133–122.).

RESULTS OF MEASUREMENTS

Two main series of measurements were carried out: with generators 10 cm and 25 cm, and a check experiment "without generators."* The results of measurements are divided into groups: (A) particles clearly produced in the generators by neutral radiation, and (B) products of stars produced by charged particles, and single charged particles passing through the generators;† μ mesons were excluded by the momentum-range method.

The results of measurements of momenta and of specific ionization of secondary particles produced by neutral radiation in a lead generator 25 cm thick are given in Fig. 2a. The results of analogous measurements of the particles of the group B are given in Fig. 2b.

The accuracy of the measurements of the momentum and ionization of particles makes it possible to separate $\pi^{\pm}$ and $K^{\pm}$ mesons and heavy particles in the momentum range up to 700 Mev/c. In the range of larger momenta, the determination of the nature of separate particles is not always possible.

Protons and Deuterons. From the experimental material given in Fig. 2, one can obtain sufficiently complete data on secondary protons and, partially, on deuterons. We shall not discuss the data in detail, since that is not the aim of the present article.

*The total thickness of matter in different series of the control check "without generators" amounted to 0.3 – 2 cm lead.

†Group B also included products of stars produced by neutrons, containing fast particles moving backwards.

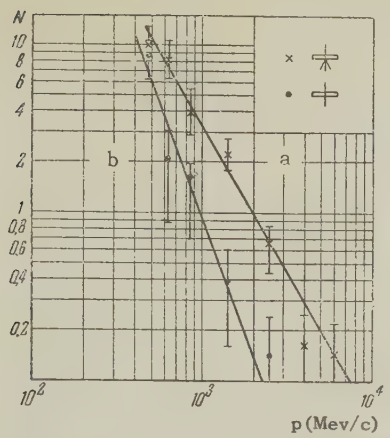

FIG. 3. Differential momentum spectrum of π^- mesons produced by neutrons: a – cascade particles, b – single particles.

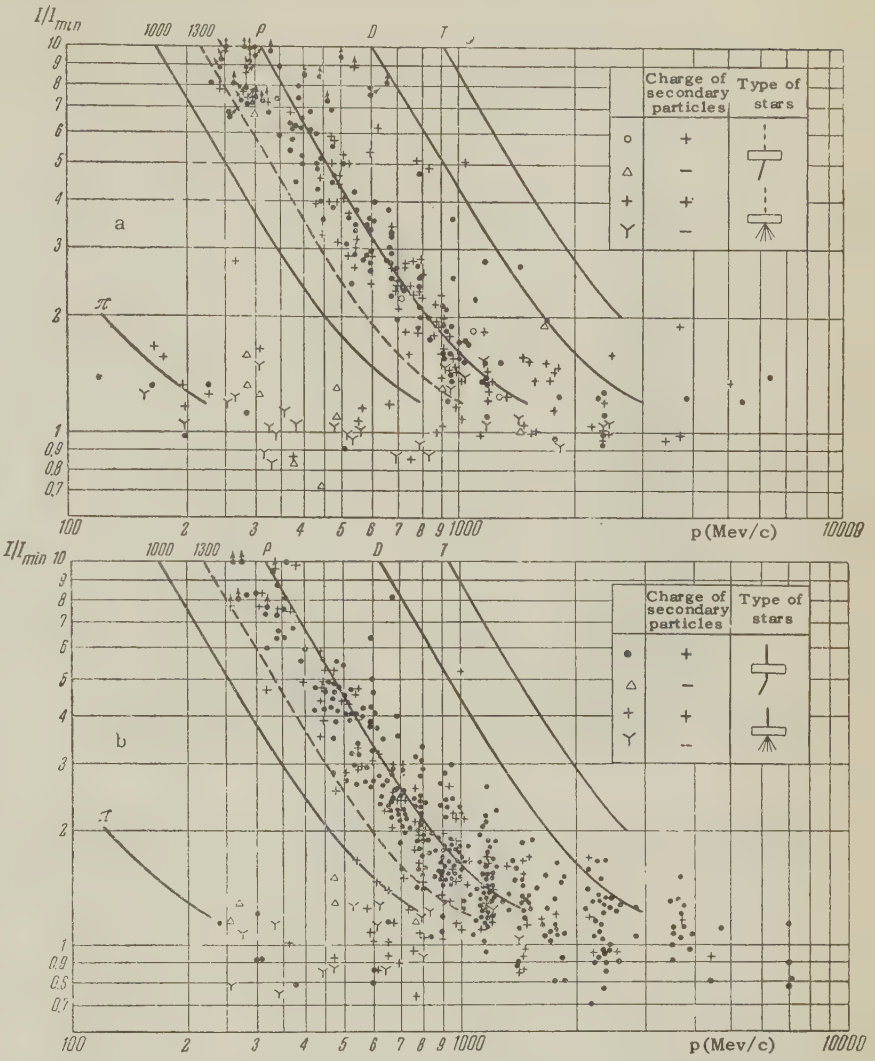

FIG. 2. Results of the measurements of the momentum and ionization of secondary particles observed under 25 cm Pb. a – particles produced by neutrons, b – particles produced by protons. Events in which the specific ionization of the particle was greater than the maximum measurement threshold are denoted by arrows (there is no difference in meaning between light and full circles).

We shall note only that, in two series of measurements in the momentum range 400 – 900 Mev/c, 35 deuterons were observed, 10 of which were produced by protons. According to this data, in the flux of cosmic rays at the altitude of 3250 m in the momentum range 400 – 900 Mev/c there are 3.5 times more neutrons than protons.*

The momentum spectrum of deuterons in the experiment "without generators" in the momentum range > 800 Mev/c (a total of 108 deuterons) can be represented by the expression $N(p) \sim p^{-\gamma}$, where $\gamma \approx 2$.

<u>π mesons</u>. The spectra of π^- mesons with momentum between 400 and 7000 Mev/c produced by neutrons are given in Fig. 3. Spectrum a corresponds to cases where the particle is clearly produced in a multi-prong star (N > 2).† Spectrum b contains particles observed without an accompanying cascade (N = 1). The spectra can be represented by a power function $N(p) \sim p^{-\gamma}$. For spectrum a, $\gamma = 1.7$; for the spectrum of single π^- mesons, $\gamma = 2.4$ (i.e., π^- mesons of large momentum are mainly observed in multi-prong stars. This fact has been mentioned in our ealier paper.[1]

Using the same apparatus, Khrimyan and Asatiani[4] obtained $\gamma = 1.5$ for the spectrum of π^- mesons in multi-prong stars produced by protons. Consequently, the spectrum of π^- mesons produced by fast neutrons is practically identical to the spectrum of π^- mesons produced by fast protons.

We have determined the ratio of the numbers of π^- and π^+ mesons produced by fast neutrons and protons in the momentum interval 125 – 720 Mev/c. Among the secondary particles produced by neutrons, the ratio $N_{\pi^-}/N_{\pi^+} = 89/49$,* i.e., we observed an excess of π^- mesons. In stars produced by protons, the ratio $N_{\pi^-}/N_{\pi^+} = 45/54$.

*The cross sections for the production of deuterons by protons and neutrons used in the estimates were taken from reference 3.

†N – number of observed components of the stars.

*Here we used also our data from reference 1.

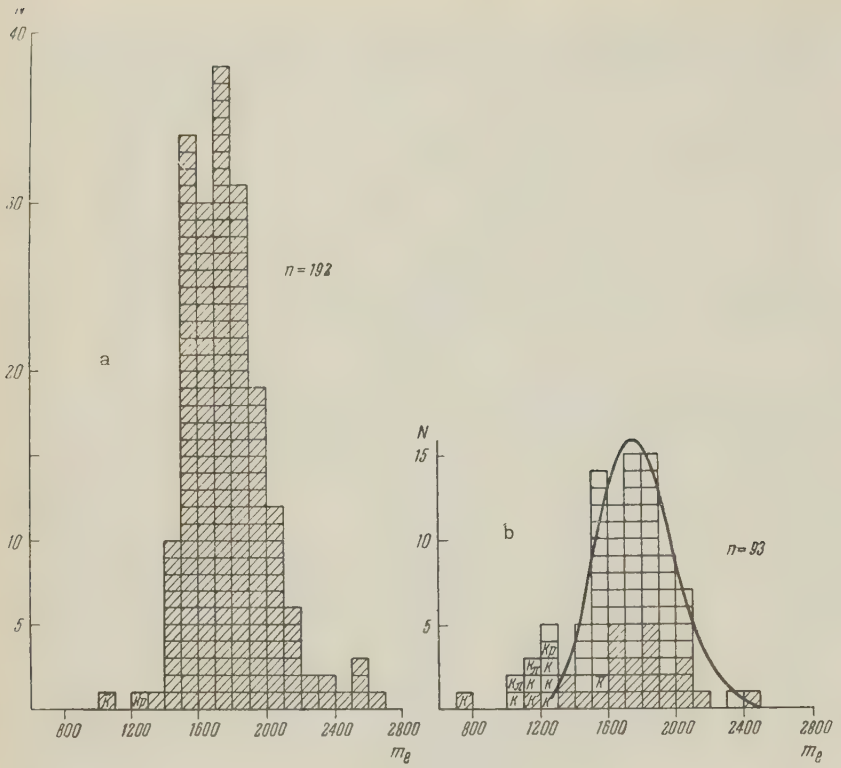

FIG. 4. Mass distribution with particles with momentum in the range 125–720 Mev/c and with ionization in the range 1.3–7 I_{min}, a – single particles produced by neutrons, b – products of multi-prong stars (dashed particles are produced by neutrons).

K mesons. The mass distribution of particles in the momentum range 125 — 720 Mev/c and with ionization 1.3 — 7 I_{min}* is given in Fig. 4. Single particles produced by neutrons are shown in the histogram a. The majority of these particles are protons. Secondary products of multi-prong stars produced by fast neutrons are represented in the histogram b. Particles produced by neutrons are shown crosshatched. This spectrum displays, apart from protons, a group of particles in the mass range 700 — 1300 m_e, the number of which amounts to about 10% of the number of protons. The appearance of these groups of particles cannot be explained by experimental errors since, firstly, a and b are obtained simultaneously using the same apparatus and, secondly, in the series of measurements "without generators" out of 1112 protons traversing the instrument, less than 1% of the particles (7 protons) were recorded by the instrument as particles with mass < 1300 m_e. The distribution of protons observed in the experiment "without generators" is represented by the solid curve in Fig. 4. The distribution is normalized to the total number of particles (n = 93).

In the momentum range $p \leq 720$ Mev/c and ionization range $I \geq 1.3\ I_{min}$, we determined for each particle the probability of that particle being a proton (W_p), K meson (W_K), or π meson (W_π) from the obtained values of momentum, ionization, and range, taking into account the frequency of observation of $\pi^\pm$ and $K^\pm$ mesons and protons. Particles for which $W_K > 5(W_\pi + W_p)$, were assumed to be K mesons. These particles are indicated by a subscript (K, p) or (k, π) in the spectra. Particles for which $K > 10(W_\pi + W_p)$ are denoted by the letter K (negative — by the letter $\bar{K}$).

Detailed data on all $K^\pm$ particles are given in Table I. $K^\pm$ particles observed in weak nuclear disintegrations or without an accompanying cascade which were not given in Fig. 4 are also included in the table.

According to data given in Table I, only 3 $K^\pm$ particles out of 19 observed were negative. The ratio $N_{K^+}/N_{K^-} = 16/3$.

Four K^+ and one K^- particles were produced by neutrons. The remaining (twelve K^+ and two K^-) particles were most probably produced by protons with the ratio $N_{K^\pm}(p)/N_{K^\pm} = 14/5$.

We note that the observed number of large stars produced by neutrons is also smaller (the ratio is 54/108) than the number of stars produced by charged particles. Such an asymmetry can be partly due to the fact that, when working with hodoscopes (and also with cloud chambers), it is impossible to distinguish stars produced by protons from stars produced by neutrons and having fast products moving backwards. The number of such neutron stars in our case, according to the estimate by Khrimyan,[5] amounts to about 30% of all observed neutron stars.

*For $I > 7\ I_{min}$ the electronic equipment was overloaded.

TABLE I

No of event	Sign of charge	p, Mev/c	I/I_{min}	Mass, m_e	Nature of the primary particle and the type of interaction
123—260	+	280	$2.8\ ^{+0.5}_{-0.4}$	735^{+60}_{-105}	Neutral*
81—88	+	315	$4.0\ ^{+1.0}_{-0.4}$	1060^{+140}_{-245}	Charged*
133—122	+	325	$4.65^{+0.8}_{-0.8}$	1210^{+130}_{-130}	Charged*
20—178	+	330	$5.0\ ^{+1.4}_{-0.35}$	1280^{+200}_{-60}	Charged*
21—41	+	450	$2.35^{+0.55}_{-0.25}$	1100^{+150}_{-90}	Charged*
83—34	+	455	$2.95^{+0.55}_{-0.40}$	1290^{+140}_{-110}	Neutral*
199—108	—	480	$1.45^{+0.25}_{-0.20}$	775^{+130}_{-115}	Charged
16—336	—	480	$3.45^{+0.95}_{-0.50}$	1500^{+230}_{-150}	Charged*
37—67	+	495	$26\ ^{+0.5}_{-0.4}$	1290^{+125}_{-125}	Charged*
192—29	+	555	$1.65^{+0.25}_{-0.25}$	1025^{+135}_{-135}	Charged*
179—18(?)	+	620	$1.5\ ^{+0.2}_{-0.2}$	1000^{+160}_{-160}	Charged*
14д—3(?)	+	666	$1.75^{+0.50}_{-0.15}$	1295^{+275}_{-115}	Charged*
72—91	—	680	$1.45^{+0.30}_{-0.15}$	1050^{+240}_{-145}	Neutral
12—272(?)	+	686	$1.65^{+0.25}_{-0.15}$	1230^{+180}_{-120}	Neutral
93—123	+	705	$1.47^{+0.3}_{-0.2}$	1140^{+250}_{-220}	Neutral*
119—34(?)	+	720	$1.5\ ^{+0.2}_{-0.2}$	1200^{+160}_{-240}	Charged*
139—172	+	720	$1.65^{+0.25}_{-0.25}$	1295^{+170}_{-230}	Charged
16a—5(?)	+	720	$1.6\ ^{+0.35}_{-0.20}$	1250^{+260}_{-180}	Charged
35—84(?)	+	720	$1.55^{+0.30}_{-0.15}$	1210^{+240}_{-130}	Charged

(?) Type (K, π?) (K, p?)
*Star

Accounting for this, the ratio of the number of stars produced by protons to the number of stars produced by neutrons equals $N_p/N_n = 1.5$.

π and K mesons in the momentum range 720 to 900 Mev/c. In the momentum range 720 — 900 Mev/c, the separation of K mesons and π mesons is difficult, while the separation of both kinds of particles from protons is still possible, since in that momentum range the ionization of protons, K mesons and π mesons is in the intervals 1.9 — 2.4 I_{min}, 1.2 — 1.4 I_{min}, and 1.03 I_{min}.

In this momentum range we separated a group of 38 particles consisting of a mixture of K and π mesons, out of which 10 were produced by neutrons and were mainly π mesons, while 28 were produced by charged primaries. Out of these 28 particles, 15 stopped in the absorber, which corresponds to a range > 16 cm Pb. Out of these 15 particles, 13 were positive, and these must be considered as different from protons also from range considerations, since protons with momentum 900 Mev/c have a range < 12 cm of Pb. A qualitative division of this group of 28 particles into K and π mesons is possible from the following considerations: Firstly, constructing the spectrum of π mesons produced by protons which, in general, is in good agreement with the law $N \sim p^{-1.6}$ in the range of 720 — 900 Mev/c, one observes an anomalously large number of particles. Such an anomaly in the spectrum of π mesons at sea level was observed by us previously.[2,6] If we assume that this is due to the presence of K mesons, then the group of 28 particles should be divided into (14 ± 5) K mesons and (14 ± 5) π mesons. Secondly, in this group of particles, a large positive excess is observed (22 positive and 6 negative particles), while in the spectrum of π mesons of lower momentum the positive excess is due to K^+ mesons, then this corresponds to a division of the group into (14 ± 5) K mesons and (14 ± 5) π mesons. Thirdly, the specific ionization of positive particles of this group is equal to (1.19 ± 0.03) I_{min}. The specific ionization of negative particles is equal to (1.03 ± 0.07) I_{min}. Hence, assuming a mean specific ionization of K mesons in the momentum range 720 — 900 Mev/c as equal to 1.32 I_{min}, and for π me-

TABLE II

Δp, Mev/c	$\pi^{\pm}$		$K^{\pm}$		p	
	N	%	N	%	N	%
240–480	60	56	8	8	38	36
480—720	58	50	11	10	46	40
720—900	24	~30	14	~15	45	~55

sons as equal to 1.03 I_{min}, we obtain (15 ± 4) K mesons and (13 ± 4) π mesons.

Therefore, in the momentum range 720 — 900 Mev/c, out of 38 π^- and K particles, 14 are most probably K mesons.

The numbers of observed $\pi^{\pm}$ and $K^{\pm}$ mesons and cascade protons in identical momentum ranges are given in Table II. According to these data, in the range of large momenta, the observed number of K mesons increases with increasing momentum. The ratio of the number of observed K mesons to the number of π mesons in the momentum range < 900 Mev/c amounts to about 0.2.

The authors wish to express their deep gratitude to Prof. A. I. Alikhanyan for constant interest in the work, and for his helpful discussion. We would also like to thank V. K. Kosmachevskiĭ, I. P. Karabekyan, B. P. Kanavets, and V. V. Avakyan who helped in the organization and carrying out of the work.

[1] A. V. Khrimyan, Izv. Akad. Nauk SSSR, Ser. Fiz. **19**, 700 (1955), Columbia Techn. Transl. p. 638.

[2] Alikhanov, Lyubimov, and Eliseev, CERN Symposium **2**, 87 (1956).

[3] W. N. Hess and B. J. Meyer, Phys. Rev. **101**, 337 (1956).

[4] T. L. Asatiani and G. B. Khrimyan, J. Exptl. Theoret. Phys. (U.S.S.R.) **33**, 561 (1957), Soviet Phys. JETP **6**, 437 (1958).

[5] G. B. Khrimyan, J. Exptl. Theoret. Phys. (U.S.S.R.) **35**, 1076 (1958), Soviet Phys. JETP **8**, 752 (1959).

[6] Lyubimov, Eliseev, and Kosmachevskiĭ, Izv. Akad. Nauk SSSR, Ser. Fiz. **19**, 720 (1955), Columbia Techn. Transl. p. 652.

Translated by H. Kasha
70

PLASMA ACCELERATION

I. S. SHPIGEL'

P. N. Lebedev Physics Institute, Academy of Sciences, U.S.S.R.

Submitted to JETP editor August 23, 1958

J. Exptl. Theoret. Phys. (U.S.S.R.) 36, 411-415 (February, 1959)

We consider acceleration of plasma in vacuum in an axially symmetric, inhomogeneous, pulsed magnetic field. The density of the plasma bunches is approximately 10^{12} particles/cm^3. The maximum energies for various atomic ions are as follows: nitrogen and oxygen, approximately 190 ev; helium, approximately 280 ev; hydrogen, approximately 120 ev.

1. INTRODUCTION

At the present time the acceleration of charged-particle bunches of high density is of considerable interest. One of the means of solving this problem is the acceleration of quasi-neutral plasma bunches. In contrast with the acceleration of charged particles of one polarity, the production and acceleration of high-density plasma bunches does not require strong focusing forces. In one-shot acceleration by means of electrodynamic forces[1-5] no provisions for extended focusing are necessary.

In the present work we report on attempts to accelerate a plasma in vacuum by means of an axially symmetric, pulsed, inhomogeneous magnetic field. A measured amount of gas is admitted at a definite point in the vacuum volume. Close to this region there is a winding through which a condenser is discharged at the appropriate time. A current is induced in the gas and the acceleration forces result from the interaction of the external magnetic field with the induced current in the gas.

2. DESCRIPTION OF THE APPARATUS

The apparatus (cf. Fig. 1) consists of the vacuum chamber 1 in which the acceleration takes place, the pulsed inlet system and its feed 2, a preliminary ionization system 3, the accelerating coil and its power supply 4, and the control circuit 5.

The vacuum chamber is formed by two coaxial cylinders: the first, which is replaceable (organic glass or pyrex) is 150 mm in diameter and 500 mm long while the second, made of copper, is of the same diameter, but 700 mm long. A pressure of 2 to 4×10^{-5} mm Hg is maintained in the chamber. On one side the copper cylinder is covered by a replaceable brass flange which contains vacuum gaskets for the various probe inputs. The other end is made from a glass cylinder. On the other side the

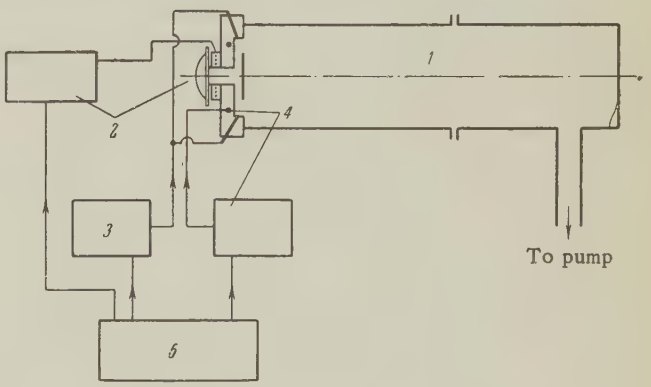

FIG. 1. Block diagram of the apparatus.

glass cylinder there is a flange of organic glass. On this flange (cf. Fig. 2) are mounted the pulsed gas inlet 1 (an electromagnetic valve[6]), the preliminary ionization electrodes 2, the accelerating winding 3, and a disc that provides better distribution of the gas flow 4.

The accelerating coil is cemented inside the disc of organic glass. In these experiments the winding is a single turn. At time t_2, an IM 2.7-50 condenser is discharged through the winding by means of a spark gap. The voltage, U, to which the condenser is charged, varies between 10 and 24 kv. The frequency of the oscillations which re-

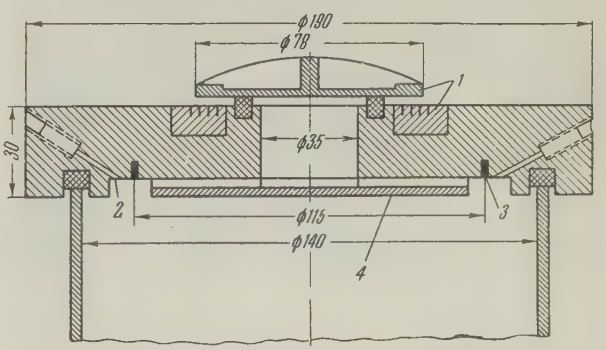

FIG. 2 Cross section of the organic-glass flange.

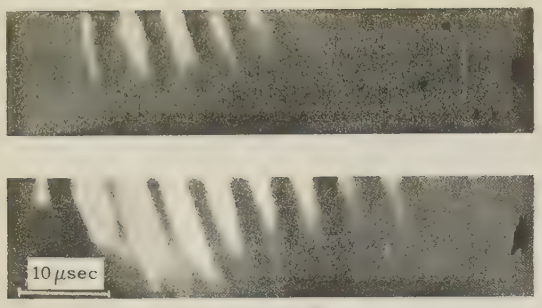

FIG. 3. High-speed photograph showing the motion of the plasma in air. The vertical scale is $\Delta z = 11.5$ cm along the z axis $\tau = 280\,\mu$sec. a) $U_c = 14.5$ kv; b) $U_c = 22.5$ kv.

sult when the condenser is discharged through the single turn is approximately 120 kc/sec; the discharge is a damped oscillatory discharge.

All the elements in the system are operated in a definite time sequence which is determined by a control circuit. At time t_1 the valve opens. The preliminary ionization system is also turned on; this unit is a 500-watt rf generator which operates at 15 Mcs. After a controlled time interval τ, at time t_2 (when the required gas pressure is established near the accelerating coil) the rf generator is turned off and the voltage is applied to the accelerating coil, initiating acceleration of the plasma. A slave sweep on the oscilloscope which is used for observation is triggered by the control circuit 1.5 microseconds before the voltage is applied to the accelerating coil.

3. EXPERIMENTAL RESULTS

The following have been investigated: the plasma velocity along the acceleration axis (the z axis), the nature of the radial motion, the velocity of the wave front, and the relation between pulse duration and plasma density.

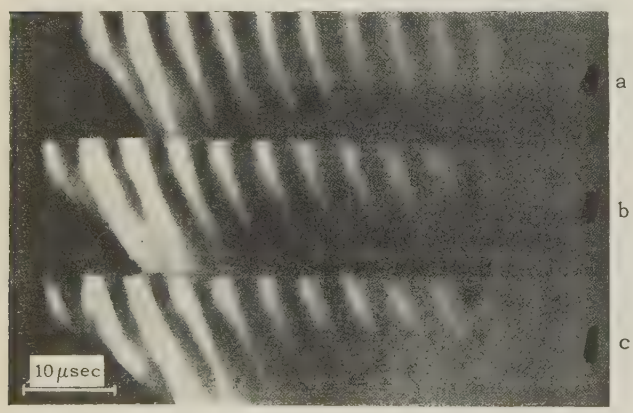

FIG. 4. High-speed photograph of the plasma pressure in helium along the z axis. $\Delta z = 11.5$ cm; $U_c = 22.5$ kv. a) $\tau = 220\,\mu$sec, b) $\tau = 280\,\mu$sec, c) $\tau = 400\,\mu$sec.

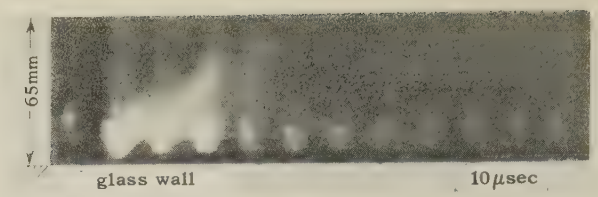

FIG. 5. High speed photograph showing the radial motion of the plasma in air. $U_c = 22.5$ kv, $\tau = 280\,\mu$sec.

(a) Motion of the Plasma Along the Z Axis and Radial Motion

These measurements are carried out by high-speed photography of the luminous plasma, with a CFR-2M camera. To record the motion of the plasma along the acceleration axis the slit of the camera (0.5 cm wide) is oriented along the z axis. The length of the slit, taken from the accelerating coil, is 11.5 cm.

Figure 3 shows typical photographs obtained with air. The sharply defined luminescent plasma bursts are easily distinguished on these photographs. The periodic expulsion of plasma from the acceleration region takes place at twice the frequency of the oscillations in the accelerating turn. The existence of an initial velocity component causes the plasma to collide with the wall of the vacuum chamber at a distance of 4 or 5 cm from the accelerating turn. As a result the plasma velocity in the z direction is reduced (the break in the luminescent band in Fig. 3b).

When the time interval τ is increased a still greater deceleration effect is noted. Figure 4 shows photographs of the motion of a helium plasma in the z direction taken with various values of τ. With $\tau = 280\,\mu$sec (Fig. 4a) there is almost no deceleration whereas when $\tau = 400\,\mu$sec (Fig. 4c) the effect is very large for the initial bursts. Apparently this phenomena is due to the presence of high-density gas in front of the moving plasma. The first pulses remove the gas in front of the plasma so that there is no significant deceleration for subsequent pulses.

Initially the luminescent intensity increases from pulse to pulse; then it falls off. This effect is due to the enhanced conditions for discharge development (the increasing number of free electrons in the discharge region) and the reduction in the amplitude of the oscillations in the accelerating coil. Optimum conditions obtain at about the third or fourth expulsion of the plasma.

The velocity is a maximum for the initial pulses since the accelerating field is large initially and the plasma mass is still small because of incomplete ionization. Later the ionization increases but the currents in the winding and in the plasma have fallen off.

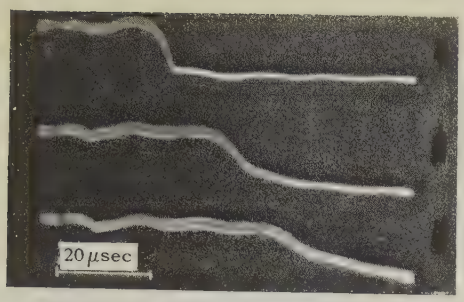

FIG. 6. Pulses at the rf probes for different distances between the probe and the accelerating coil. Plasma in air, U_c = 18 kv, τ = 280 μsec. a) Δz = 21 cm, b) Δz = 51 cm, c) Δz = 76 cm.

Figure 5 shows a high-speed photograph of the radial motion of the plasma. The picture was taken through a radial slit 0.5 cm wide. As is apparent from Fig. 5, in addition to having a v_z component the plasma has a v_r component directed away from the center. After the plasma collides with the wall of the vacuum chamber, v_r changes in both magnitude and direction. Similar photographs are obtained with hydrogen; no significant differences are observed.

This same method is used to measure the velocity of the luminous plasma front; this velocity is related to some effective particle velocity.

The energy of the nitrogen and oxygen ions (air input) obtained from measurements of the corresponding photographs is found to be 80 — 190 ev; for hydrogen and helium ions the range is 40 — 120 ev and 120 — 280 ev, respectively.

(b) Velocity of the Front and Pulse Duration for a Plasma of Given Density.

These measurements are made by means of an rf probe which is sensitive to plasma in the density range from 10^{11} to 10^{13} cm^{-3} and a waveguide which measures plasma densities of 10^{12} cm^{-3}.

The rf probe consists of an inductance circuit which is weakly coupled to a low-power rf oscillator. The tank circuit is tuned to the oscillator frequency. When there is a conducting medium (plasma) inside or outside the probe, the rf eddy currents that arise in the circuit effectively reduce the inductance of the probe and shift the resonant frequency of the circuit toward higher frequencies. As a result of this detuning, the voltage is reduced. The time behavior of the voltage is displayed on an oscilloscope.

The velocity of the plasma front is measured with two rf probes separated by a known distance. One probe is generally kept fixed while the second is moved along the z axis. The velocity is determined from the known distance Δz and the measured time interval ΔT corresponding to the difference in arrival time at the probes. In this case it is possible to determine the velocity of a front for a given density.

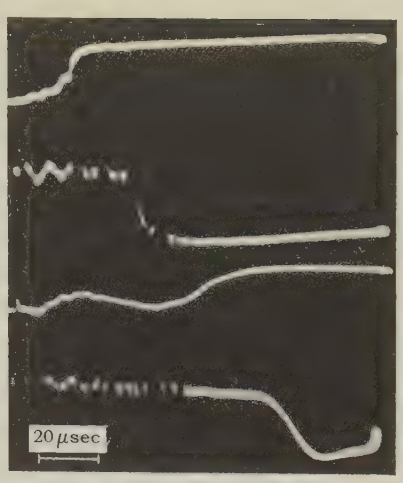

FIG. 7. Change of the pulse shape at the rf probe and starting time as a function of delay time τ and distance from the accelerating coil Δz. Plasma in air, U_c = 20 kv, first probe probe, Δz = 15 cm, second probe, Δz = 33 cm. a) τ = 310 μsec, b) τ = 400 μsec.

A series of oscillograms taken with these probes is shown in Fig. 6. It is apparent that as the distance from the accelerating coil is increased the time delay required for the excitation of the mobile probe increases, the signal front shows more slope, and the amplitude of the signal is reduced. The minimum plasma density which the probe can record is $n_{min} \simeq 10^{11}$ cm^{-3}. The mean plasma velocity, computed from this oscillogram, is approximately 3×10^6 cm/sec. The discrepancy in the velocity measurements by high-speed photographs and rf probes indicates a velocity dispersion effect.

Figure 7 are shows oscillograms of the pulses from the two rf probes taken with air using two different delay times. The pulses in Fig. 7b slope more, start later and the time interval between them is much larger than in Fig. 7a. Similar results, obtained in helium, are shown in Fig. 8. Here the shift of the pulses for both the first and second probes are clearly apparent and the shift of the second probe is much larger. The deceleration effect in helium and hydrogen is much stronger than in air; this is explained by the different thermal velocities of the gases and the resulting higher pressure of the gas in front of the moving plasma for the same values of τ.

Experiments have also been carried out to verify the expulsion of plasma from the acceleration region in individual bunches (density modulation of the plasma as a function of time). However, no density modulation was observed at the discharge frequency,

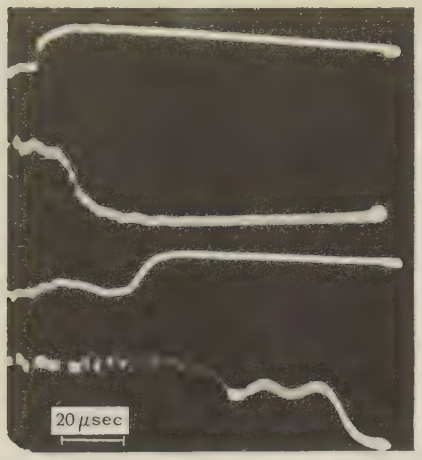

FIG. 8. Change of pulse shape at the rf probe and time of excitation as a function of delay time τ and distance from the accelerating turn. Plasma in helium, $U_c = 20$ kv, distance of the probe to the accelerating turn the same as in Fig. 7. a) $\tau = 190\ \mu$sec, b) $\tau = 280\ \mu$sec.

120 kcs. Apparently this is due to the considerable velocity spread of the ions inside the bunches. The frequency of the oscillations in the accelerating col was then reduced to 56 kcs by increasing the capacity of the condenser. In Fig. 9 are shown oscillograms of the voltage in the rf probe before and after detection and the voltage in the accelerating coil. In the second part of both oscillograms there is visible a clearly defined amplitude modulation of the rf voltage in the probe, indicating a density modulation of the plasma as a function of time at the probe position. At larger value of z the modulation cannot be seen because of the spread in velocity. There is no modulation in the first part of the pulse from the probe because a minimum density $n_{min} > 10^{13}$ cm^{-3} is required for modulation to be observed.

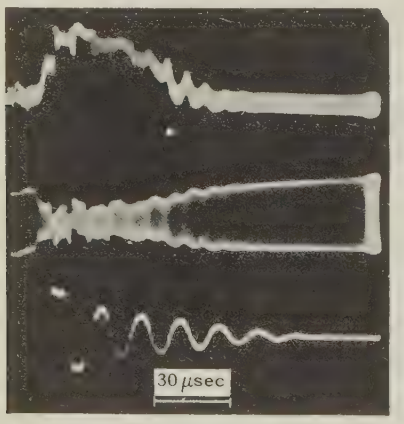

FIG. 9. Oscillogram showing the voltage at the rf probe for motion of the plasma in air with density modulation. $U_c = 15$ kv, $\tau = 260\ \mu$sec. a) voltage at the probe after detection, b) before detection, c) voltage oscillogram for the accelerating coil, f = 58 kcs.

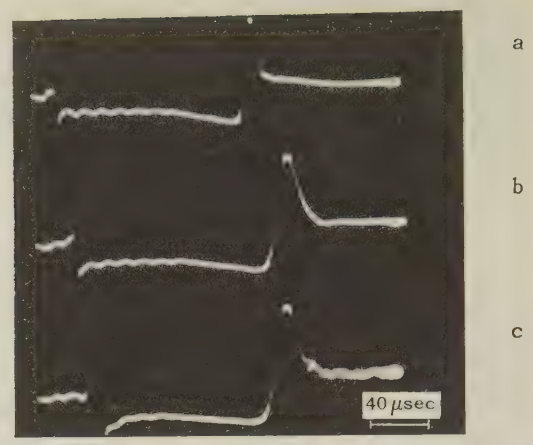

FIG. 10. Detector current pulses from a "radiating" waveguide as a function of distance from the accelerating coil Δz. Plasma in air, $U_c = 20$ kv. a) $\Delta z = 13.5$ cm, b) Δ b) $\Delta z = 34.5$ cm, c) $\Delta z = 56$ cm.

The slope of a given signal front from the rf probe makes it difficult to determine the length of the pulse from a plasma of given density. For this reason a "radiating" waveguide is used. The use of a waveguide in these measurements is based on reflection of radio waves from a plasma when the frequency of the external field is lower than the natural plasma frequency $\omega_0 \sim n^{1/2}$.

The sealed end of the waveguide is introduced inside the chamber. When there was no plasma in the waveguide it was possible to observe a stationary standing-wave distribution due to reflection from the open end. When the plasma appears the radiation is reduced and the standing wave distribution changes. The change in the detector current (proportional to field intensity at any point in the waveguide) is presented on the screen of an oscilloscope. In these measurements the waveguide is driven at 9.4×10^9 cps, corresponding to a plasma density for which total reflection obtains at $n = 10^{12}$ cm^{-3}.

In Fig. 10 are shown oscillograms of plasma pulse lengths for a plasma with $n \geq 10^{12}$, as a function of distance z. The leading edge of the pulse on the last oscillogram exhibits smearing. This is apparently due to the fact that in these measurements the waveguide was located inside a metal tube and there was multiple reflection. The dependence of plasma pulse length on the coordinate z obtained in this work is shown in Fig. 11.

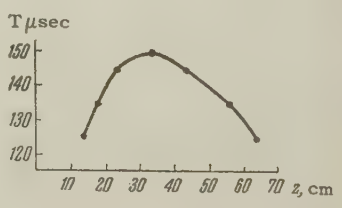

FIG. 11. Dependence of pulse length for a plasma density of 10^{12} cm^{-3} as a function of the distance z between the point of observation and the accelerating coil.

We wish to take this opportunity to thank V. I. Veksler, M. S. Rabinovich, and L. M. Kovrizhnykh for a discussion of the results of the experiment, E. D. Andryukhin for help in carrying out a number of measurements, and E. A. Smirnov for construction of the apparatus.

[1] W. H. Bostick, Phys. Rev. **104**, 292 (1956).
[2] A. C. Kolb, Phys. Rev. **107**, 345 (1957).
[3] L. A. Artsimovich et al., J. Exptl. Theoret. Phys. (U.S.S.R.) **33**, 3 (1957), Soviet Phys. JETP **6**, 1 (1958).
[4] A. I. Morozov, J. Exptl. Theoret. Phys. (U.S.S.R.) **32**, 305 (1957), Soviet Phys. JETP **5**, 215 (1957).
[5] G. S. Janes, Bull. Am. Phys. Soc. **3**, 85 (1958).
[6] I. O. Shpigel', Приборы и техника эксперимента (Inst. and Meas. Engg.) (U.S.S.R.) 1, 1959 (in press).

Translated by H. Lashinsky
71

SCATTERING OF MUONS WITH MOMENTA NEAR 100 Mev/c BY COPPER AND IRON

V. G. KIRILLOV-UGRYUMOV, V. A. DOLGOSHEIN, A. M. MOSKVICHEV, and L. P. MOROZOV

Moscow Engineering-Physics Institute

Submitted to JETP editor August 28, 1958

J. Exptl. Theoret. Phys. (U.S.S.R.) **36**, 416-423 (February, 1959)

A study was made of the scattering of μ mesons by copper plates (for momenta from 85 to 144 Mev/c) and by iron plates (for momenta from 81.2 to 135 Mev/c). The μ-meson angular distribution based on 2,350 scattering events agrees satisfactorily with the distribution for a point nucleus.

1. INTRODUCTION

IT has been reported in a number of papers on the scattering of μ mesons by nuclei that fewer scattering events occurred than had been expected for a Coulomb interaction between the μ mesons and the nuclei. The most complete review of data on μ-meson scattering has been written by Fowler and Wolfendale.[1] In the opinion of these authors there is no anomalous scattering in the low-energy region (below 600 Mev), and the excess reported in individual publications is due to experimental error. This opinion is supported by the results of three recent investigations conducted with slow μ mesons.

Kirillov-Ugryumov and Moskvichev[2] studied the scattering of μ mesons with momenta of 130 ± 16 Mev/c in beryllium plates 1 cm thick, located inside a Wilson chamber. For 2,250 events of μ-meson scattering not a single case was recorded where the scattering was into an angle greater than 6°. The experimental distributions were in good agreement with those computed according to the Moliere theory.

Using a magnetic mass spectrometer, Alikhanyan and Arutyunyan[3] measured μ-meson scattering in lead plates (t = 7 mm). The total μ-meson range was 19 m. Their experimental results were in agreement with the theory of the finite-size nucleus. Further, a negative result in regard to the existence of anomalous scattering was obtained by Chidley et al.,[4] who studied the scattering of 23-Mev μ mesons in a lead plate 0.56 mm thick located inside a propane bubble chamber.

Fukui, Kitamura, and Vataze (private communication) have not discovered any anomalous scattering of μ mesons in the high-energy region (about 1 Bev), even though this result is in conflict with other experimental data and with the theory developed by Fowler and Wolfendale.[1] Essentially these authors are in agreement with the Coulomb interaction theory only when the μ-meson trajectories are selected by recording μ-e decay.

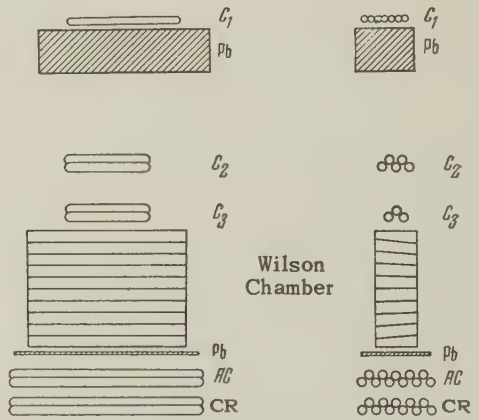

FIG. 1. Diagram of the setup.

In view of the importance of settling once and for all the question of the absence or presence of anomalous scattering, we measured the scattering of μ mesons with momenta from 81.2 to 144 Mev/c by copper and iron plates four millimeters thick. Although the nuclei of these elements contain comparatively large numbers of nucleons it is possible, if the energy and angular interval is properly selected for comparison with the experimental results, to apply the exact Moliere formula without resorting to approximate data on charge distribution in the nuclei.

2. DESCRIPTION OF THE EXPERIMENTAL SETUP

Measurements were made with the setup shown in Fig. 1. The large rectangular Wilson chamber,[5] 55 × 40 × 14 cm working volume, was triggered by a counter telescope, three rows of which (C_1, C_2, and C_3) were in coincidence while the last row, AC, was in anti-coincidence. In order to reduce

the number of miscounts by the anti-coincidence row, a control row CR was connected to a duplicate anti-coincidence circuit. Use of this row reduced the miscounts in the circuit to 0.5%.

The complete unit was operated at sea level. A lead filter 15 cm thick was installed on top of the Wilson chamber to absorb the electronic component of cosmic rays. The μ mesons were scattered in nine plates 4 mm thick placed inside the Wilson chamber. These plates were of copper for one series of measurements and of iron for another. So that decay electrons from μ mesons stopped by the plates would not reach the anti-coincidence row, a lead filter 0.8 cm thick was placed under the chamber. Special precautions were taken to reduce track distortion in the Wilson chamber (temperature stabilization, use of high-speed spark valves). The chamber pictures were obtained by a stereoscopic camera with a 13.5 cm base from a distance of 115 cm. Optical distortion of the angular projections was thus kept to an undetectable minimum.

From the known quantity of material above the Wilson chamber, including the combined thickness of the overhead horizontal partitions of the building housing the apparatus, the rate of operation of the Wilson chamber was computed and this computed rate agreed well with the one observed during the experiment.

3. PARTICLE IDENTIFICATION AND MEASUREMENT OF μ-MESON MOMENTA AND SCATTERING ANGLES

The particles were visually identified by their ionization density and multiple scattering in the plates in the chamber.

The scattering and the ionization density gradient of the μ mesons tracks stopped by the plates in the chamber were appreciably different from those of electron and proton tracks. A calculation of the predicted number of stopped protons indicated that they should amount to less than 2% of the total number of recorded particles. The observed number of particles identified as protons was $(1.5 \pm 0.5)\%$. These particles were excluded from subsequent processing of the scattering data.

The number of stopped μ mesons and the associated decay electrons was in good agreement with the computed number, which took into account the ratio of positive to negative μ mesons, as well as the geometric configuration.

The method of identification used was not suitable for differentiating π from μ mesons. However, calculations applying to our experimental conditions indicated that the admixture of π mesons would amount to less than 1% of the μ mesons stopped.

It can be shown that such an admixture of π mesons introduces practically no change in the expected theoretical angular distribution of the scattered μ mesons. The mass of the particles which were identified as μ mesons was computed from their scattering and range and amounts to $(209 \pm 10)\, m_e$.

Because theoretical angular distributions for μ mesons differ substantially even for neighboring momentum values, accuracy in the measurement of momenta and angles is of great importance in scattering experiments. For this reason we used comparatively thin plates.

The residual range of the μ meson was used to measure its momentum. It was assumed that mesons are scattered and stopped in the middle of a plate. In computing the residual range, we took into account the deviation of the direction, at which the μ mesons entered the plate, from the vertical. For this purpose experimental distributions were plotted for the incident angle θ (from the vertical), the resultant rms values are as follows:

No. of plates from place of stoppage	1	2	3	4	5	6	7	8	9
$(\overline{\theta^2_{exp}})^{1/2}$ in degrees	14.5	12.2	10.5	9	8.5	8	7.5	7	6

It can easily be shown that for non-vertical penetration the effective thickness of a plate exceeds its true thickness by $\sec (\overline{\theta^2_{exp}})^{1/2}$.

Momentum errors caused by inaccuracy in the residual range due to the finite thickness of the plate, as well as by momentum variation within the plate itself, was computed and taken into account when the scattering curves were being constructed. Scattering was studied in the plates, starting with the second plate from the one where the meson was stopped rather than the first, since there would have been too great an error in the momentum measured in the first plate.

Scattering angles were measured in a projection on a plane parallel to the front galss of the chamber. This plane is not the same, in general, as the plane passing through the original direction taken by the particle for which the theoretical distribution of scattering angles is derived. However, thanks to the fact that the chamber was narrow (effective depth 9.5 cm) and high (40 cm), the original direction of a particle cannot be inclined more than $4° - 5°$ from the vertical. Hence, the difference between the projections of the angles on the two planes lies within the range of accuracy with which the angles were measured.

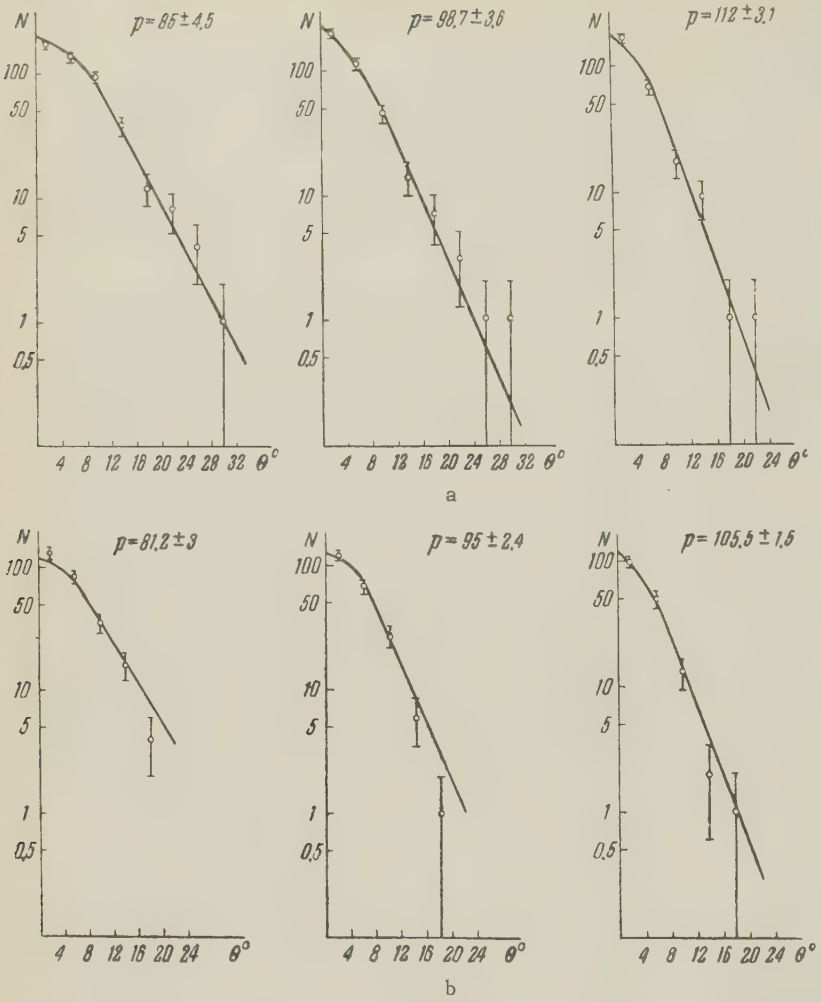

FIG. 2. Differential angular distribution for three momentum intervals: a – copper, b – iron; p is in Mev/c.

The scattering angles were measured repeatedly by several observers. The mean-square error did not exceed 30′.

The geometric dimensions of the detecting apparatus are essential in the measurement of the experimental angular distribution. As Cousins et al.[6] have shown, geometric corrections based on different probabilities for detecting the various angles can lead to incorrect deductions from the experimental data. In this investigation cognizance was taken of the geometric corrections, and they were incorporated in the experimental curves for the angular distribution. Computation of the geometric corrections (cf. Appendix) shows, however, that they have little effect on the form of the curves. This is due to the fact that the chamber is wide enough (55 cm) in relation to the rather narrow solid angle within which μ mesons enter the chamber. Then, too, the shallow depth of the chamber has no effect, since scattering in a plane perpendicular to the plane of photography necessitates no correction in the experimental angular distribution (this holds true for those cases where the angular distribution of scattering can be described as normal).

4. MEASUREMENT RESULTS AND THEIR INTERPRETATION

Two separate series of measurements were made, one with copper and one with iron plates. During the 3,600 hours of operation of the apparatus with copper plates, 475 records were obtained of μ mesons stopped inside the Wilson chamber, and these correspond to 1,460 scattering events with momenta greater than 75 Mev/c. When the iron plates were used, 890 scattering events were recorded.

Differential angular distributions were plotted individually for each group of μ mesons having the same momentum. These experimental data were compared with the theoretical curves computed by the Moliere formulae for a point nucleus. The Moliere theory is applicable to μ meson scattering by copper or iron plates 4 mm thick because the finite dimension of the nucleus begins to be effective only for angles greater than $\lambda\!\!\!^{-}/R$ ($\lambda\!\!\!^{-}$ is the μ meson wavelength and R is the radius of the nucleus). For our momenta this means angles $\sim 25° - 35°$. Comparison of the theoretical predictions of the point nucleus with the experimental

Observed and predicted total scattering events in copper for angles greater than the given angle

θ°≥	0	4	8	12	16	20	24	28
Experiment	1460	678	279	107	42	20	7	2
Theory	1460	705	275	97.6	37.6	15 65	7.55	2.95

data indicates a satisfactory agreement in every angular interval (see Fig. 2).

In addition, a total differential distribution was plotted as a function of dimensionless parameter

$$\varphi_0 = \theta_i / B^{1/2}\xi. \quad (1)$$

Here θ_i is the angle of scattering in radians, B is a slowly varying function of the thickness of the plate and the particle momentum and is equal to

$$B = 2G = 2\left[5.66 + 1.24 \lg \frac{Z^{4/3}A^{-1}t}{1.13\beta^2 + 3.76\,(z/137)^2}\right], \quad (2)$$

where β is the average velocity of the μ mesons in the momentum interval of interest (in our case $\beta = 0.6$, G = 6.56, and B = 13.12), and ξ is given by

$$\xi = 4\pi N e^4 t Z (Z+1) z^2 / (pV)^2; \quad (3)$$

where N is the number of atoms per cm^3, t the thickness of the plate in g/cm^2, Z the charge of the scattering nucleus, z the charge of the particle, p the momentum of the particle, and V its velocity.

Figure 3 shows the total angular distribution for copper and iron versus the dimensionless parameter φ_0. This distribution characterizes scattering over the entire momentum interval from 81.2 to 144 Mev/c.

Application of the χ^2 criterion showed that the experimental values were in good agreement with the theoretical distribution ($p_{\chi^2} = 0.4$). To compare the experimental and theoretical total distributions, values for the entire momentum interval from 85 to 144 Mev/c (in the case of scattering by copper) are listed in the table.

Thus, the analysis of the results of our work indicates satisfactory agreement between experimental and theoretical data in which only the Coulomb interaction between μ mesons and the nucleus is considered.

Earlier measurements of slow μ-meson scattering in copper were made by Alikhanyan and Kirillov-Ugryumov[7] with a magnetic mass spectrometer. It was found that the experimental and predicted distributions were in good agreement in the region of small angles, but for angles greater than 15 there was a small excess of recorded events (23 observed, 15.67 predicted). This discrepancy appears to have been due to the fact that the angle through which the μ mesons entered the Wilson chamber of the mass spectrometer was relatively large, and hence the application of the geometric correction may very well eliminate the discrepancy. For π mesons, the angle of incidence will vary less from the vertical than for μ mesons, and the geometric correction will be correspondingly less. Actually the theoretical and experimental data were found to be in better agreement for π mesons than for μ mesons.

Thus, as in other investigations,[2-4,7] the present investigation has not confirmed the existence of anomalous μ-meson scattering in the low-energy regions.

We take this opportunity to thank Prof. A. I. Alikhanyan for his unfailing interest and valuable comments, B. I. Luchkov for his great help with the investigation, and also to thank F. R. Arutyunyan and M. I. Ter-Mikaelyan, who participated in the analysis.

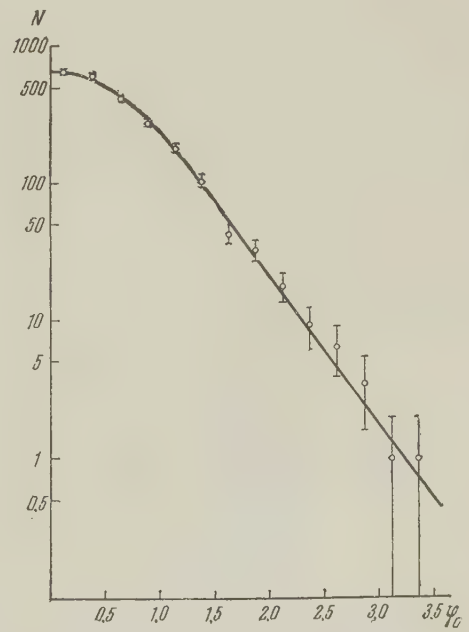

FIG. 3. The total differential distribution for copper and iron vs. the dimensionless parameter φ_0.

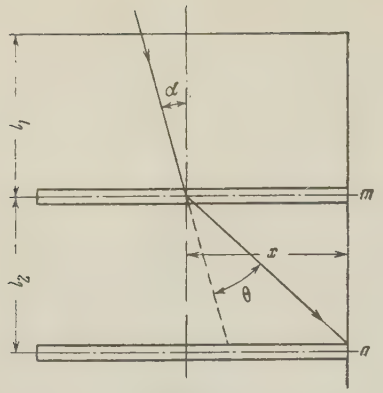

FIG. 4

APPENDIX

COMPUTING GEOMETRIC CORRECTIONS IN THE MEASUREMENT OF ANGLES

Let us consider a point x in plate m, where a μ meson is scattered and is subsequently stopped in plate n (see Fig. 4). Because of the finite dimensions of the telescope, mesons arrive at point x within a given angle of incidence α. If one neglects scattering in the plates in front of plate m, then the angular interval, α, is characterized by the diagram shown in Fig. 5. Since the apparatus is symmetrical, only half of the chamber is considered, i.e., 25.5 cm $\geq x \geq 0$.

Since the range of incidence angles for any x is sufficiently small ($\sim 10°$), the angular distribution of μ mesons within this interval can be considered isotropic. Then the area S in the diagram is proportional to the probability that a μ meson strikes the plate m.

If scattering occurs in plates in front of plate m, then the diagram should be "expanded" along both the x and θ axes. It can be shown with sufficient accuracy that scattering causes an expansion along

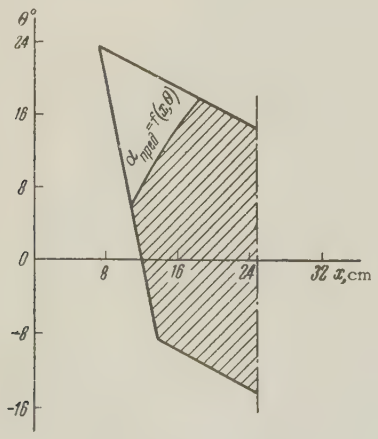

FIG. 5. Angular diagram.

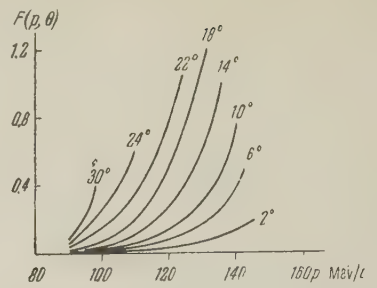

FIG. 6. The geometric correction curve for various angles θ as a function of the momentum of a μ meson at the scattering point.

the θ axis of an amount $\sigma_1 = 0.35\,\sigma$ and along the x axis of $l_1 \tan \sigma_1$, where σ is the mean-square angle for scattering a μ meson with a momentum equal to that of the μ meson stopped in plate n in a thickness t equal to the sum of all the plates before m, while l_1 is the distance from the top of the chamber to plate m.

A meson entering point x in plate m and having the right momentum to be stopped in plate n could be scattered out of the chamber either immediately in plate m or in plates between m and n. To allow for the μ mesons scattered out of the chamber because of both of these possibilities, we assume (in any case we shall overestimate the geometric correction) that scattering into the angle θ at point x in plate m is equivalent to scattering by n-m plates into an angle $\theta_1 = \theta\sqrt{n-m}$. Then the probability that a particle will remain in the chamber will depend on the maximum incidence angle, which is given by

$$x = l_2 \tan(\theta\sqrt{n-m} + \alpha_{max}).$$

The curve $\alpha_{max} = f(x, \theta)$ cuts off a section of the diagram proportional to the number of mesons scattered out of the chamber. Hence the probability for detecting a meson that has the right momentum to be stopped in plate n and is scattered by plate m into an angle θ will be equal to the ratio of the shaded area of the diagram to whole area S.

If the proportion of scattering events in plates m = 1, 2, ... 7 is known from the experimental angular distributions for a given momentum (i.e., for n − m = const), then F(p, θ) can be found, i.e., the correction can be made for the angle θ (see Fig. 6). Consequently, when plotting experimental angular distributions, one should use quantity

$$N = N_{exp}(p, \theta) F(p, \theta),$$

where $N_{exp}(p, \theta)$ is the measured number of scattering events for μ mesons with momentum p into the angle θ.

[1] G. N. Fowler and A. W. Wolfendale, Progress in Elementary Particle and Cosmic Ray Physics, Amsterdam (1958), pp. 123-153.

[2] V. G. Kirillov-Ugryumov and A. M. Moskvichev, J. Exptl. Theoret. Phys. (U.S.S.R.) **34**, 322 (1958), Soviet Phys. JETP **7**, 224 (1958).

[3] A. I. Alikhanyan and F. R. Arutyunyan, J. Exptl. Theoret. Phys. (U.S.S.R.) **36**, 32 (1959), Soviet Phys. **9**, 23 (1959).

[4] Chidley, Hinmann, Goldstein, Summers, and Adler, Can. J. Phys. **36**, 801 (1958).

[5] Kirillov-Ugryumov, Deryagin and Merzon, Приборы и техника эксперимента (Instruments and Meas. Engg.) **3**, 15 (1957).

[6] Cousins, Nash, and Pointon, Nuovo cimento **6**, 1113 (1957).

[7] A. I. Alikhanyan and V. G. Kirillov-Ugryumov, Izv. Akad. Nauk SSSR, ser. fiz. **19**, 737 (1955), Columbia Techn. Transl. p. 667.

Translated by A. Skumanich
72

AN INVESTIGATION OF π^+-μ^+-e^+ DECAY WITH THE AID OF A PROPANE BUBBLE CHAMBER AND SCINTILLATION COUNTERS

M. P. BALANDIN, V. A. MOISEENKO, A. I. MUKHIN, and S. Z. OTVINOVSKIĬ

Joint Institute for Nuclear Research

Submitted to JETP editor August 28, 1958

J. Exptl. Theoret. Phys. (U.S.S.R.) **36**, 424-432 (February, 1959)

The angular distributions of μ^+ mesons and positrons from π^+-μ^+-e^+ decays were investigated with a propane bubble chamber. It was found that the angular distribution of the μ^+ mesons was isotropic, while the angular distribution of the positrons, if described by the expression $(1 - a \cos \theta)/4\pi$, was characterized by the quantity $a = 0.116 \pm 0.035$. This value for a is much smaller than the values obtained in other investigations with propane bubble chambers. Scintillation-counter experiments carried out to determine the cause of this discrepancy showed that the magnitude of anisotropy depends significantly on the degree of purity of the commercial propane sometimes used in bubble chambers. A simultaneous analysis of data obtained with a bubble chamber containing propane of a given composition and scintillation counters showed that the quantity $\lambda(1 - W_c)$ is 0.78 ± 0.26, where W_c is the probability of depolarization of mesons in graphite and λ is a fundamental parameter in the neutrino theory.

INTRODUCTION

AFTER the discovery[1,2] of the non-conservation of parity in weak interactions, a number of publications appeared on the study of μ-e decay. These publications dealt with data obtained both by electronic methods[3,4] of detection and by photographic emulsions.[5,6] During 1957 reports also appeared on the study of μ-e decay with hydrogen[7] and propane[8,9] bubble chambers.

The emulsion and bubble-chamber methods differ from the electronic method of detecting μ-e decay in that (a) in both bubble chambers and emulsions the asymmetry is determined for all the electrons, i.e., without any significant energy cut-off; (b) when the particles are detected with bubble chambers and emulsions, it is possible to investigate the asymmetry of electrons from the μ mesons produced when μ mesons are stopped, i.e., from μ mesons that are altogether longitudinally polarized, while investigation of μ-e decay with scintillation counters depends upon meson beams of an undetermined degree of polarization.

This article (which was nearing completion when similar studies appeared in print[8-11]) describes an investigation whose main purpose was to determine the asymmetry of positrons emitted by μ^+ mesons resulting from the decay of π^+ mesons stopped in a propane bubble chamber. The measured positron asymmetry proved to be much less than that reported by other authors[4,10,11] who also obtained their data by the propane method. The reason for this discrepancy is that sometimes commercial propane is used in bubble chambers, and as is shown here by an experiment with scintillation counters, a difference in the degree of propane purity has a great effect on positron asymmetry.

Moreover, the present experiment with scintillation counters and the same commercial propane as is used in the bubble chamber provide data on the value of the product $\lambda(1 - W_c)$, where λ is a parameter dependent on the coupling constant and W_c is the probability of depolarization of μ^+ mesons in graphite, which was used as a standard.

We have also investigated the angular distribution of the mesons formed from the decay of stopped π^+ mesons.

THE EXPERIMENTAL TECHNIQUE

Figure 1 shows the experimental setup with the bubble chamber, which had an expansion device with a volume limit. A propane bubble chamber[12] 9 cm in diameter was located behind a concrete shield 4 meters thick and in the path of a π^+ meson beam. The π^+ mesons were produced in a polyethylene target located in the path of a 670-Mev proton beam extracted from the accelerator chamber. The mesons that emerged from the target were deflected

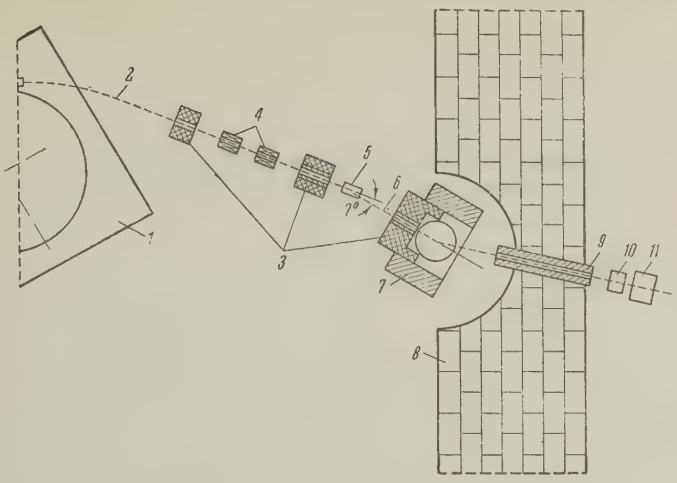

FIG. 1. Experimental setup. 1 – synchrocyclotron vacuum chamber, 2 – extracted proton beam, 3 – lead shield, 4 – quadrupole focusing lens, 5 – polyethylene target, 6 – π^+ meson beam, 7 – deflecting electromagnet, 8 – cast-iron plates in the window of a concrete shield 4 meters thick, 9 – steel collimator, 10 – aluminum filter, 11 – propane bubble chamber.

by an electromagnet and entered a collimator. Photographs were obtained when the average energy of the π^+ mesons at the collimator exit was 170 and 273 Mev, hence with thicknesses of the polyethylene target of 70 and 30 cm respectively, and with angles of 7° and 30° between the π^+ mesons emitted by the target and the direction of the incident proton beam. An aluminum filter 29 cm thick was located directly in front of the chamber to stop the 170 Mev π^+ mesons, and a copper filter 15.5 cm thick was similarly used for the 273 Mev π^+ mesons. To minimize the influence of the stray magnetic field of the synchrocyclotron and deflecting magnet, the bubble chamber was surrounded by a double iron screen. Because of this screening the magnetic field in the operating area of the chamber did not exceed 0.3 oersted. The glass units of the chamber were vertical. The charged particle tracks were photographed on 35 mm film by a stereoscopic camera with two "Yupiter-8" objectives (F = 5.24 cm) at a distance of 45 cm from the central plane of the chamber. The photographic base was 12 cm long and was in a vertical position.

The chamber was filled with commercial propane* which was first purified to rid it of its light fractions (CH_4, C_3H_6). This purification was effected at a temperature of 0°C and was stopped as soon as the saturation pressure of the mixture differed by no more than 0.5 atmosphere from the saturation pressure of propane at the same temperature. The normal working conditions for the bubble chamber were as follows: temperature 62°C, initial pressure 32 atmospheres, and expansion 2.6%. The chamber was in operation for 20 seconds at a time and was under remote control. About 5,000 stereoscopic photographs were obtained.

These photographs were examined and processed, without any reproduction of the stereoscopic pictures, by means of a reprojector[13] whose screen was fixed perpendicular to the optic axes of the objectives in the stereoscopic camera. Nevertheless, both photographs of each stereoscopic pair were used in the examination, to obviate the effect of superimposed tracks and to minimize losses.

The μ^+-meson decay events from stopped π^+ mesons (π^+-μ^+-e^+ events) that concerned us were identified by their characteristic outward appearance (Fig. 2). Out of all the π^+-μ^+-e^+ events, only those could not be interpreted unequivocally for which the direction of μ^+ emission appeared on the reprojector screen to form a small angle to the direction traveled by the π^+ meson before the latter was stopped. This limitation was due to the fact that certain cases, to which we shall henceforth refer as "doubtful," could also be interpreted as due to the decay of μ^+ mesons that had left the collimator (μ^+-e^+ events) and had been scattered 2 – 3.5 mm short of being stopped in the chamber.

To determine the positron asymmetry of π^+-μ^+-e^+ decay we measured directly the angle θ', which is the projection on the vertical plane of the spatial angle θ between the directions of the emissions of the μ^+ meson and the positron. The angular distribution $f(\theta')$ thus obtained is simply related to the distribution $F(\theta, \varphi)$ if the angular distribution of the μ^+ mesons and the azimuthal part of function $F(\theta, \varphi)$ are known. Thus, for example, for an isotropic distribution of the μ^+ mesons we have

$$F(\theta, \varphi) = (1 - a\cos\theta)/4\pi \qquad (1)$$

in which case we find that

$$f(\theta') = \frac{1}{2\pi}\left[1 - a\left(\frac{\pi}{4}\right)^2 \cos\theta'\right] \qquad (2)$$

Use of track coordinates to compute the angle θ gives better accuracy but requires considerably more time. Experience has shown that indirect measurement of the angle θ with the reprojector causes uncontrolled distortion of the angular distribution, particularly in the angular interval $0° \leq \theta \leq 20°$ and $160° \leq \theta \leq 180°$ where a great increase occurs.

The angle θ' was measured directly for both the μ^+-e^+ and the π^+-μ^+-e^+ decays, in which the direction of emission of the μ^+ mesons was believed to be in the direction of the collimated π^+-

*Commercial propane consists of 80% propane (C_3H_8), 10% propylene (C_3H_6), 6% methane (CH_4), and 4% butane (C_4H_{10}).

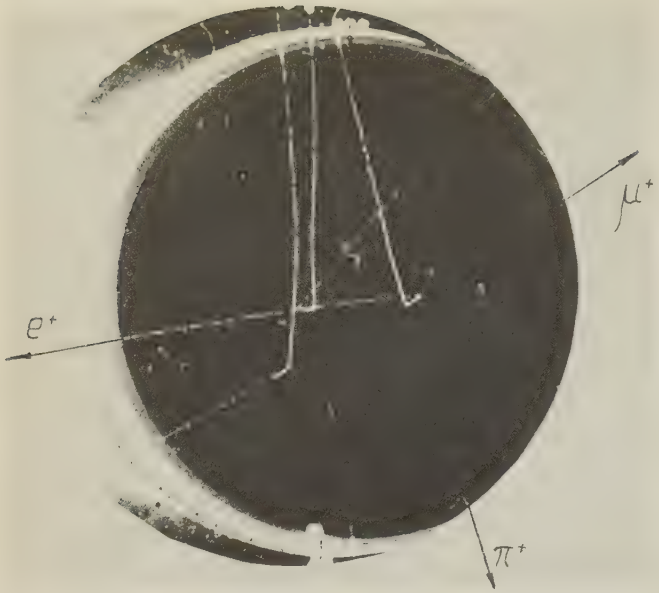

FIG. 2. A typical photograph of a $\pi^+ - \mu^+ - e^+$ decay in the propane bubble chamber.

meson beam. It can be shown that in this case the distribution Eq. (1) is transformed into

$$\xi(\theta') = \frac{1}{2\pi}\left(1 - a\frac{\pi}{4}\cos\theta'\right). \qquad (3)$$

"Doubtful cases were handled as cases of π^+-μ^+-e^+ decay.

All of the photographs were inspected twice independently. To reduce loss during the second inspection we noted in every photograph, besides the events of immediate interest to us, scattering events and stars, since this made possible a more careful review of the stereoscopic shots we had obtained. The first examination disclosed 6,712 cases of π^+-μ^+-e^+ and μ^+-e^+ decay, including "doubtful" ones. During the second examination an additional 346 such cases were found, the combined angular distribution for which is shown in Fig. 3. It is evident from Fig. 3 that the loss of π^+-μ^+-e^+, μ^+-e^+ and "doubtful" events does not depend, roughly speaking, on the angle θ'. If it is also assumed that losses do not depend on the location of the events in the chamber, i.e., that in general they are of a purely random nature, then it can be eas-

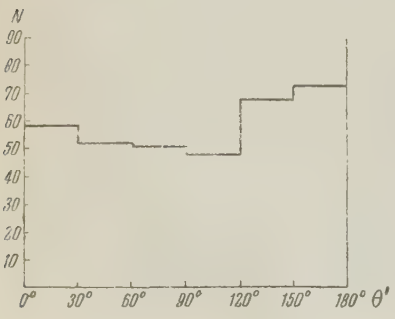

FIG. 3. The angular distribution of positrons for the 346 cases of $\pi^+ - \mu^+ - e^+$, $\mu^+ - e^+$, and "doubtful" events found during a second examination. N is the number of positrons in 30° intervals of the angle θ'.

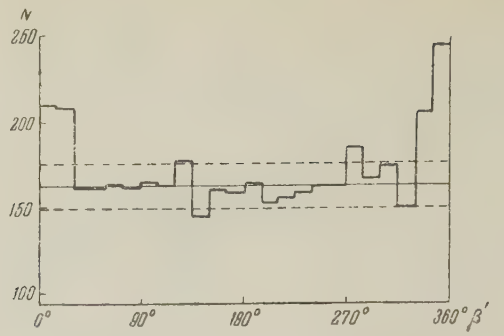

FIG. 4. The angular distribution of μ^+ mesons for 4,107 cases of $\pi^+ - \mu^+ - e^+$ decay (with all "doubtful" cases excluded). N is the number of μ^+ mesons in 15 intervals of the angle β'.

ily demonstrated that a third examination would reveal no more than 50 new cases of π^+-μ^+-e^+ and μ^+-e^+ decay. This number of events, even if there is some dependence of loss on angle θ', could not distort the obtained angular distributions, and therefore the necessity of a third examination is eliminated.

In order to avoid the possibility of distortion due to boundary effects, π^+-μ^+-e^+ and μ^+-e^+ events were considered only when the π^+ or μ^+ mesons were stopped within an area 6 cm in diameter in the center of the chamber.

ANGULAR DISTRIBUTION OF μ^+ MESONS FROM THE DECAY OF MESONS STOPPED IN THE BUBBLE CHAMBER

When our experiments were still in the process of completion, Lattes reported (at the 1957 conference in Varenna, Italy) on the angular distribution of μ^+ mesons from the decay of π^+ mesons stopped in a photographic emulsion. According to his report, more μ^+ mesons are emitted into the rear hemisphere, in relation to the direction of the π^+ meson beam, than into the front hemisphere, and the probability of μ^+-meson emission increases with increasing size of the angle between the direction of their emission and the horizontal plane. To check this result and also to make a correct transition to the spatial angular distribution for the positrons, we attempted to measure the angular distribution of μ^+ mesons from the decay of π^+ mesons that had been emitted from the target at an angle of 7° to the direction of the incident proton beam and that had been stopped in the chamber. We measured the angle β', which was a projection on the vertical plane of the angle β between the direction of the π^+ meson beam and the direction of the μ^+ meson.

Figure 4 shows the angular distribution $\psi(\beta')$ of μ^+ mesons, obtained by processing the 4,107

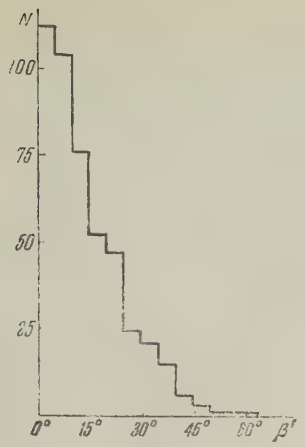

FIG. 5. The angular distribution of μ^+ mesons for "doubtful" cases of decay. N is the number of μ^+ mesons in 5° intervals of the angle β'.

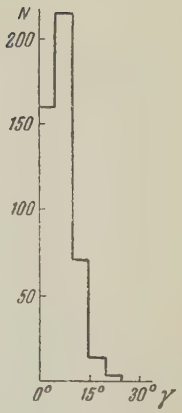

FIG. 7. The angular distribution of μ^+ mesons for "doubtful" cases of decay. N is the number of μ^+ mesons per 5° of γ'.

cases of π^+ meson decay, including "doubtful" cases, for which a separate angular distribution is given in Fig. 5. The solid straight line in Fig. 4 is described by the expression $\psi(\beta') = \overline{N}_\mu$, in which $\overline{N}_\mu$ is the average number of μ^+ mesons in the interval $30° \leq \beta' \leq 330°$, and the broken lines are described by the expression $\psi(\beta') = \overline{N}_\mu \pm \sqrt{\overline{N}_\mu}$. Figure 4 shows that the obtained angular distribution for μ^+ mesons is in good agreement with the isotropic distribution $\psi(\beta') = \overline{N}_\mu$, if one excludes the intervals $0 \leq \beta' \leq 30°$ and $330 \leq \beta' \leq 360°$, where, as is shown in Fig. 5, all the "doubtful" cases are concentrated. Consequently, there is no reason to suppose that the $\psi(\beta')$ angular distribution is not isotropic. If the $\psi(\beta')$ angular distribution is isotropic, the spatial angular distribution of the μ^+ mesons must also be isotropic. On the other hand, if the $\psi(\beta)$ distribution is anisotropic, then one will find anisotropy in the μ^+ mesons with reference to the plane of origin of the π^+ meson, because in this case the π^+ mesons must have a spin and be polarized in a direction perpendicular to the plane of origin, if parity is preserved in strong interactions. For this kind of anisotropy of the spatial angular distribution for the μ^+ mesons, the $\psi(\beta')$ distribution should also be anisotropic, which as is seen from Fig. 4, is not the case. Hence we conclude that the spatial angular distribution for the μ^+ mesons is isotropic. Isotropic angular distributions for μ^+ mesons have also been reported by other authors.[14,15]

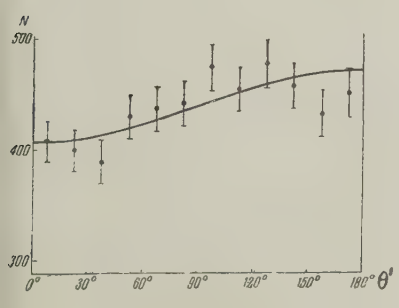

FIG. 6. The angular distribution of positrons for 5,252 cases of $\pi^+ - \mu^+ - e^+$ decay. N is the number of positrons per 15° of θ'.

ANGULAR DISTRIBUTION OF POSITRONS FROM π^+-μ^+-e^+ DECAY

Figure 6 shows the $f(\theta')$ distribution for positrons in 5,252 cases of π^+-μ^+-e^+ decay. The experimental points in this figure are shown with statistical errors. This angular distribution does not include those cases of π^+-μ^+-e^+ decay for which $\gamma' \leq 15°$, where γ' is the projection on the vertical plane of the angle γ between the direction of the μ^+ meson and the direction of the π^+ meson prior to stopping. This has been done because the interval $0 \leq \gamma' \leq 15°$ includes most of the "doubtful" cases, for which Fig. 7 shows a separate angular distribution $\rho(\gamma')$, which confirms our conclusion. Obviously, all of the doubtful cases should be excluded from the general statistical material, in order to eliminate the distortion of the angular distribution $f(\theta')$ due to the fact that the transformation to a spatial angular distribution for positrons from μ^+-e^+ and π^+-μ^+-e^+ decays is described by quite different formulae. Actually, as stated above, all cases were excluded in the angular interval $0 \leq \gamma' \leq 15°$, even those which were not doubtful. This was done to facilitate transformation to the spatial angular distribution.

The solid curve in Fig. 6 is given by Eq. (2), with the coefficient $a = 0.116 \pm 0.035$. The value for this coefficient was found from the ratio

$$a = \frac{8}{\pi} \frac{N'_b - N'_{forw}}{N'_b + N'_{forw}}, \qquad (4)$$

in which N'_{forw} and N'_b represent respectively the numbers of positrons emitted into the forward and back hemispheres with respect to the direction of the μ^+ meson projected onto the vertical plane. From Fig. 6 it is evident that the experimental distribution obtained for the positrons is well described by Eq. (2) when $a = 0.116 \pm 0.035$. This conclusion is also confirmed by the χ^2 criterion. Despite this good agreement, the distribution of the experi-

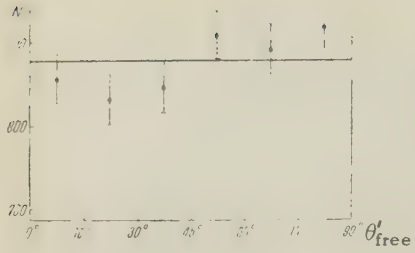

FIG. 8. The angular distribution of positrons for 5,252 cases of $\pi^+ - \mu^+ - e^+$ decay. N is the number of positrons per 15° of θ'_{free}.

mental points in relation to the solid curve is still of interest. One can see that all of the experimental points in the interval $45° \leq \theta' \leq 135°$ lie systematically above the solid curve, but when $0 \leq \theta' \leq 45°$ and $135° \leq \theta' \leq 180°$, they lie systematically below it. This fact becomes still more obvious if the angular distributions shown in Fig. 6 are folded about 90° in the same way as these angular distributions were originally folded about 180°. The angular distributions thus obtained are shown in Fig. 8. The abscissa θ'_{free}, is given by the following relationship

$$\theta'_{free} = \theta' \text{ for } \theta' \leqslant 90° \text{ and } \theta'_{free} = 180° - \theta' \text{ for } \theta' > 90°$$

If the distribution of observed points were entirely random, then the experimental angular distribution would be isotropic after reflection. In fact, however, the number of positrons in the interval $45° \leq \theta'_{free} \leq 90°$ exceeds the number of positrons in the interval $0° \leq \theta'_{free} \leq 45°$ by 179 ± 72. Such a distribution of points may exist, for example, when the loss of $\pi^+ - \mu^+ - e^+$ events in the interval $45° \leq \theta' \leq 135°$ is less than for $0 \leq \theta' \leq 45°$ and $135° \leq \theta' \leq 180°$. The angular distribution in Fig. 3, as well as computations based on it, indicates that even if this effect occurs, it nevertheless is too small to explain the difference of 179 ± 72. It may be that the observed difference is a statistical fluctuation with a probability of 1.5%.

The asymmetry found in our investigation proved to be much less than that reported for "propane" by other authors.[4,10,11] Specifically, in the investigations reported by Alikhanyan et al.[10] and by Barmin et al.,[11] in which propane bubble chambers and the synchrocyclotron of the Joint Institute for Nuclear Research were employed under conditions analogous to ours, the values obtained were $a = 0.19 \pm 0.03$ and 0.22 ± 0.03 respectively. The discrepancy between these data and the value for a obtained by us can hardly be attributed to experimental errors. Therefore, we proposed that the discrepancy be ascribed to a difference in the degree of purity of the commercial propane which was used. To test this idea we measured the asymmetry in the $\mu^+ - e^+$ decay by electronic detection methods.

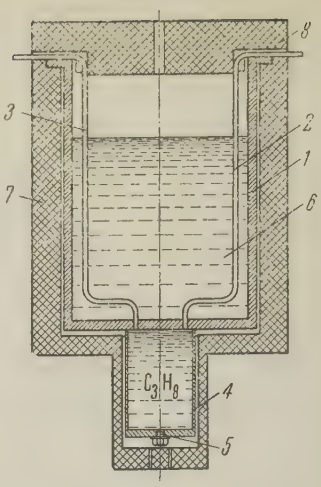

FIG. 9. The propane target. C_3H_8 is liquid propane; 1 – vessel for the refrigerant; 2 – pipe for filling the target with propane; 3 – vent to the atmosphere; 4 – copper foil 0.05 mm thick; 5 – drain plug for the liquid propane; 6 – refrigerant: a mixture of dry ice and alcohol or liquid nitrogen; 7 – polystrene foam jacket; 8 – polystrene lid.

SCINTILLATION-COUNTER STUDY OF THE ASYMMETRY OF POSITRONS FROM μ^+-e^+ DECAY IN PROPANE OF DIFFERENT DEGREES OF PURITY

The asymmetry of positrons from μ^+-e^+ decay was investigated by the scintillation counter method with an apparatus described elsewhere by Mukhin et al.[16]

The μ^+-meson beam employed possessed an energy ~95 Mev, an intensity of 15 cm^{-2} sec^{-1}, and a degree of polarization of 0.81 ± 0.11.[16] The target used to stop the μ^+ mesons consisted of a vessel with two thin plane-parallel walls that contained "propane" of different degrees of purity. This vessel measured $4.5 \times 16 \times 16$ cm and was in the same location with relation to the μ^+ meson beam as the graphite target described by Mukhin et al.[16]

The general appearance of the target is depicted in Fig. 9.

The asymmetry of positrons from μ^+-e^+ decay was determined (a) in "propane" purified of light fractions just as though this "propane" had been intended for use in a bubble chamber, (b) in "propane" that had not undergone any purification, and (c) in the light fractions removed during the purification of the commercial propane.

Asymmetry measurements were performed with a filter in the path of the positrons which had a total equivalent thickness of 13.8 g/cm^2 of polyethylene. This includes the material in the scintillation counters and half of the thickness of the target. Moreover, when the unpurified propane was used, the measurements were performed at the temperature of dry ice (−78.5°C) and at the temperature of liquid nitrogen (−195.8°C). It was discovered that within experimental error the measured asymmetry does not depend on temperature. The obtained asymmetry values were converted to represent the entire positron spectrum by means of

measurements[16] of the dependence of asymmetry on positron energy and are as follows:

unpurified "propane" $a' = 0.147 \pm 0.013$,
purified "propane" $a' = 0.104 \pm 0.014$.

The value of the coefficient a' given here for unpurified propane is the average of the values obtained at the temperatures of $-78.5°$ and $-195.8°$C.

It is obvious from these data that the asymmetry definitely depends on the purity of "propane." The findings verify the suggestions that the discrepancy between the values for a obtained in our investigation and those reported elsewhere[4,10,11] is due to differing degrees of "propane" purity. Our measurements have shown that the small value of asymmetry in purified "propane" is not to be ascribed merely to the fact that the light fraction is characterized by a high degree of asymmetry but rather is due to more complex physico-chemical causes.

DISCUSSION OF THE RESULTS

It is known that the value of $\lambda(1-W_C)$ can be found by simultaneous analysis of data on π^+-μ^+-e^+ and μ^+-e^+ decay obtained both electronically and from emulsions.[12] In principle this kind of analysis could be applied to the stopping of π^+ mesons in a propane bubble chamber, provided that data were available on the relative degree of μ^+ meson depolarization in propane and graphite. At the same time attention should be given to the composition of the "propane," since our investigation indicates that the asymmetry depends markedly on the degree to which the commercial propane has been purified. Since the "propane" used in our electronic experiments had the same composition as that in the propane bubble chamber we are in a good position to evaluate $\lambda(1-W_C)$.

Analysis of the data on π^+-μ^+-e^+ and μ^+-e^+ decays obtained electronically and with the bubble chamber indicate a value for $\lambda(1-W_C) = 0.78 \pm 0.26$. The lack of accuracy in this value, despite the large statistical sample, is due to the low degree of asymmetry in the "propane" used.

The authors deem it their pleasant duty to express their gratitude to B. M. Pontecorvo for his guidance, to M. Ya. Danysh, A. A. Tyapkin, and N. A. Chernikov for their assistance and valuable suggestions during the experimental stage of the investigation, to R. M. Ryndin and S. M. Bilen'kiĭ for reviewing the results, to B. S. Neganov, V. A. Zhukov, and B. D. Balash for their help with the extraction of the π^+-meson beam, and to V. Trifonov and G. Murin for their part in processing the experimental data.

[1] T. D. Lee and C. N. Yang, Phys. Rev. **104**, 254 (1956).

[2] Wu, Ambler, Hayward, Hoppes, and Hudson, Phys. Rev. **105**, 1413 (1957).

[3] Garwin, Lederman, and Weinrich, Phys. Rev. **105**, 1415 (1957).

[4] Swanson, Campbell, Garwin, Sens, Telegdi, Wright, and Yovanovitch, Bull. Am. Phys. Soc. Ser. II, **2**, 205 (1957).

[5] J. I. Friedman and V. L. Telegdi, Phys. Rev. **106**, 1290 (1957).

[6] Gurevich, Kutukova, Mishakov, Nikol'skiĭ, and Surkova, J. Exptl. Theoret. Phys. (U.S.S.R.) **34**, 280 (1958), Soviet Phys. JETP **7**, 195 (1958).

[7] Abashian, Adair, Cool, Erwin, Kopp, Leipuner, Morris, Rahm, Rau, Thorndike, Whittemore, and Willis, Phys. Rev. **105**, 1927 (1957).

[8] Alston, Evans, Morgan, Newport, Williams, and Kirk, Phil. Mag. **2**, 1143 (1957).

[9] Pless, Brenner, Williams, Bizzarri, Hildebrand, Milburn, Shapiro, Strauch, Street, and Young, Phys. Rev. **108**, 159 (1957).

[10] Alikhanyan, Kirillov-Ugryumov, Kotenko, Kuznetsov and Popov, J. Exptl. Theoret. Phys. (U.S.S.R.) **34**, 1101 (1958), Soviet Phys. JETP **7**, 763 (1958).

[11] Barmin, Kanavets, Morozov, and Pershin, J. Theoret. Exptl. Phys. (U.S.S.R.) **34**, 830 (1958), Soviet Phys. JETP **7**, 573 (1958).

[12] M. P. Balandin and V. A. Moiseenko, Тезисы докладов на всесоюзной конференции по физике частиц высоких энергий (Abstracts of Reports at the All-Union Conference on the Physics of High-Energy Particles) Moscow, 1956.

[13] Vasilenko, Kozodaev, Sulyaev, Fillipov, and Shcherbakov, Приборы и техника эксперимента (Instruments and Meas. Engg.) **6**, 34 (1957).

[14] Crewe, Kruse, Miller, and Pondrom, Phys. Rev. **108**, 1531 (1957).

[15] Bogachev, Mikhul, Petrashku and Sidorov, J. Exptl. Theoret. Phys. (U.S.S.R.) **34**, 531 (1958), Soviet Phys. JETP **7**, 367 (1958).

[16] Mukhin, Ozerov, and Pontecorvo, J. Exptl. Theoret. Phys. (U.S.S.R.) **35**, 340 (1958), Soviet Phys. **8**, 237 (1959).

[17] D. H. Wilkinson, Nuovo cimento **6**, 516 (1957).

Translated by A. Skumanich
73

*POSSIBLE SETS OF EXPERIMENTS FOR SIMULTANEOUS ANALYSIS OF DATA ON NUCLEON-NUCLEON SCATTERING AND POLARIZATION IN p-n COLLISIONS AT 635 Mev**

B. M. GOLOVIN, V. P. DZHELEPOV, V. S. NADEZHDIN, and V. I. SATAROV

Joint Institute for Nuclear Research

Submitted to JETP editor September 3, 1958

J. Exptl. Theoret. Phys. (U.S.S.R.) **36**, 433-443 (February, 1959)

It is suggested that n-p and p-p scattering data be analyzed simultaneously to reduce the number of experiments required to reconstruct the scattering amplitudes. Sets of experiments are presented which should yield sufficient information for such analysis. The angular dependence of polarization in p-n collisions at 635 Mev was measured. A difference was detected in the energy and angular dependences of the polarization for states of a nucleon-nucleon system possessing different isotopic spins ($T = 0$ and $T = 1$).

INTRODUCTION

IT is known that the results of all experiments on elastic nucleon scattering can be described by different combinations of five complex coefficients of the scattering amplitude. In the general case nine independent experiments[1] are required for the determination of these coefficients (except for a common phase factor). Because of the unitarity of the scattering matrix the number of necessary experiments can be reduced to five[2] at nucleon energies below the meson-production threshold. At energies above 300 Mev reconstruction of the amplitude from elastic scattering alone requires nine experiments, while eighteen experiments are required to determine the two amplitudes A_{np} and A_{pp} through separate analyses of the data. However, it can be shown that by using the concept of the charge invariance of nuclear forces and by performing the simultaneous analysis of data on p-p and n-p scattering, one can in general reduce to thirteen the number of independent experiments required to reconstruct the p-p and n-p scattering amplitudes except for a common phase factor of the two systems, i.e., to determine nineteen real quantities. The basis for this lies in the fact that, subject to isotopic invariance, scattering in p-p and n-p systems can be described by ten complex functions defined in the angular range $0 \leq \vartheta \leq \pi/2$, which determine nucleon scattering in states with total isotopic spins $T = 0$ and $T = 1$. Therefore the performance of each pair of experiments to determine the same characteristics of the p-p system for $0 \leq \vartheta \leq \pi/2$ and of the n-p system for $0 \leq \vartheta \leq \pi$ provides information concerning three real functions that describe scattering. Two of these functions are determined by nucleon interactions in states with $T = 0$ and $T = 1$, while the third function corresponds to interference between these states. Thus for the purpose of determining all ten complex coefficients of the amplitudes (except for a common phase factor) we must perform six pairs of identical experiments on n-p and p-p scattering, giving eighteen independent equations, and an additional single experiment for the p-p or n-p system. In Appendix 1 we give the analytical expressions relating the quantities to be determined in separate experiments with the coefficients of the scattering amplitude. In Appendix 2 we present sets of experiments which will provide the required information from a minimum number of common experiments (or minimum number of experiments with the n-p system), and we indicate the relative difficulty of such experiments.

POSSIBILITY OF USING P-D SCATTERING DATA

Because of the difficulties encountered in experiments on neutron scattering by free protons some investigators have studied proton scattering by neutrons in p-d collisions. This procedure permits the use of more intense and almost monoenergetic proton beams with a considerably higher degree of polarization than for neutrons. But we must determine whether it is legitimate to use such data instead of data on free n-p scattering. In an earlier paper[3] we considered the conditions under which

*Presented at the 4th session of the Scientific Council of the Joint Institute for Nuclear Research in May, 1958.

n-d scattering data can be used to obtain cross sections for elastic neutron-neutron scattering. We attempted to determine nucleon polarization in the nonrelativistic impulse approximation in the different types of nucleon-deuteron collisions and to establish their relation to polarization in free n-p scattering; our method was similar to that of Tamor.[4]

When the incident nucleon is scattered at angle θ in the laboratory system while the states of the other two nucleons are undetermined, we have the following expression for the polarized cross section $(PQ)(\theta)$:

$$(PQ)_{pd} = (PQ)_{pp} + (PQ)_{pn} + (PQ)_{\text{interf}} I,$$

where $I = I(\theta)$ is a function that is equal to unity for $\theta = 0°$ and decreases rapidly with increasing scattering angle. It is evident from this equation that in the angular region where the integral of $I(\theta)$ is small the polarized cross section for p-d collisions coincides with the sum of the polarized cross sections for p-p and p-n collisions.*

We note finally, that for approximate reconstruction of nucleon-nucleon scattering amplitudes other data on nucleon-deuteron collisions may be useful, since the expressions involved contain combinations of amplitude coefficients which are encountered only in the most complex experiments with free nucleons. Specifically, the expressions that we obtained for the polarized cross section of elastic p-d scattering contain, in addition to the usual Re ae* terms, additional terms of the type Re be*, which are contained only in expressions describing polarization correlations in the scattering of polarized beams.

EXPERIMENTAL PROCEDURE

Figure 1 is a diagram of our experiments on polarization in p-n collisions, using a beam of polarized (635 ± 15)-Mev protons from the synchrocyclotron of the Joint Institute for Nuclear Research. The beam intensity at the target was 4×10^5 sec^{-1} and its degree of polarization was 58 ± 3%.[5] Proton scattering by neutrons was determined from the different counting rates obtained with targets of heavy and light water in thin-walled plexiglas vessels. Elastic p-n scattering events in the range $45° \leq \vartheta \leq 145.7°$ were detected by registering protons and neutrons through two coincidence-connected telescopes that were set up at angles corresponding to nucleon

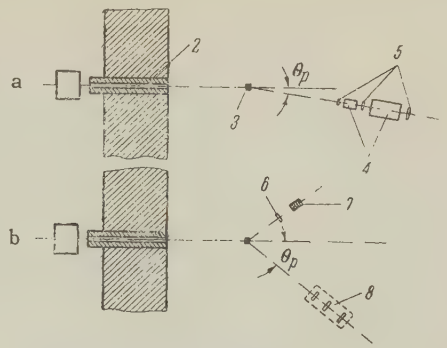

FIG. 1. Arrangement for measurements: a – $\vartheta_p < 57°$ (c.m.s.); b – $45° < \vartheta_p < 145.7°$. 1 – monitor, 2 – collimator, 3 – D_2O or H_2O scatterer, 4 – copper absorbers, 5 – scintillation counters, 6 – anticoincidence counter, 7 – neutron counter, 8 – proton telescope.

flight in elastic collisions. The angular resolution of the system was 7°. Protons were registered by a three-counter telescope with FEU-33 photomultipliers and plastic scintillators. Neutrons were registered by a highly efficient multilayer counter with a liquid scintillator.[6] To obviate the registration of charged particles by this counter it was preceded by a scintillation counter in anticoincidence with the neutron counter. Pulses from all of the scintillation counters were fed to coincidence circuits with 2×10^{-8} sec resolving time. The coincidence and anticoincidence circuits provided for the simultaneous registration of both p-p and p-n scattering. The efficiency of the anticoincidence circuit was frequently checked and found to be at least 99.8%.

The registering procedure described above was unsuitable for the angular region in which one of the scattered particles had low energy; therefore for $18 \leq \vartheta \leq 57$ only elastically scattered protons were registered. Suitable absorbers between the counters prevented registration of inelastically scattered nucleons and mesons. In this case the angular resolution of the telescope was about 4°.

ADJUSTMENT OF APPARATUS

A special effort was made to provide an experimental setup which would obviate false asymmetries arising from (a) inaccurate adjustment of the apparatus with respect to the axis of the beam, (b) bending of the beam in stray magnetic fields, (c) beam inhomogeneities at the targets etc. The possible effect of a magnetic field on the beam was estimated to be small giving a deflection of the beam axis in a stray magnetic field which was less than 10′. The multiplier tubes were placed in iron and permalloy shields to prevent stray magnetic field effects. The efficiency of the shielding was

*Our measurements show that at 635 Mev the integral of $I(\theta)$ becomes insignificant for angles $\theta \geq 8°$.

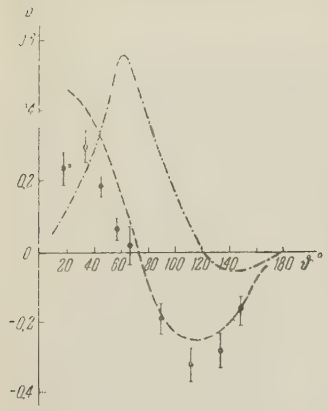

FIG. 2. Angular dependence of polarization in n – p scattering at different energies: dot-dash curve – 95 Mev;[12] dashed curve – 315 Mev;[13] dots – 635 Mev (present work).

considered adequate when no change was observed in the pulse count from a photomultiplier within a magnetic field during gamma irradiation.

Beam uniformity was checked by blackness densities of photographic films exposed at the target position and showed practically no variation across the beam, so far as could be determined from photomicrograms. The position of the center line of the beam was also determined photographically and all of the measuring apparatus was carefully adjusted with respect to this axis. An additional control of correct adjustment was the absence of asymmetry in elastic p-p scattering at c.m. angle 90°, as well as the agreement of p-p asymmetry that we observed at other angles with the asymmetry data given in reference 5 at the same energy.

MEASUREMENTS AND ANALYSIS OF RESULTS

In the range $45° \leq \vartheta \leq 145.7°$ we obtained the anticoincidence counting rates from D_2O and H_2O scatterers to the left and right of the beam axis (looking along the beam). The coincidence setup simultaneously recorded elastic and quasi-elastic p-p scattering events.

The asymmetry of quasi-elastic n-p scattering was determined from the expression

$$\varepsilon_{pn} = \frac{(N_{D_2O} - N_{H_2O})_L - (N_{D_2O} - N_{H_2O})_R}{(N_{D_2O} - N_{H_2O})_L + (N_{D_2O} - N_{H_2O})_R},$$

where N denotes an anticoincidence counting rate (after subtracting the background) with a given scatterer placed in the path of the beam and with the proton telescope located to the left (L) or to the right (R) of the beam. The experiments revealed a symmetrical background on both sides of the beam, and scattering asymmetry with and without correction for the background was identical within the limits of error.

As we have already stated, in the range $18° \leq \vartheta \leq 57°$ only a single (proton) telescope was used. In this case the proton yield from p-n collisions was also determined through the different counting rates from D_2O and H_2O targets. Absorbers of suitable thickness prevented the registration of mesons instead of quasi-elastically scattered protons. In this case N in the expression for ϵ_{pn} is the coincidence counting rate (after subtraction of the background) for a given target and relative telescope position. Control experiments indicated that in these measurements the background resulted mainly from proton scattering at the ends of the collimator and that it was also symmetrical to the left and right of the beam.

An argon-filled ionization chamber served as the monitor in all experiments.

EXPERIMENTAL RESULTS AND DISCUSSION

Some of the quantities involved in the sets of experiments considered in Appendix 2 were previously measured in a number of experiments performed on the synchrocyclotron of the Joint Institute for Nuclear Research. Thus at about 600 Mev we measured the total n-p[7] and p-p[8] cross sections, the differential cross sections for elastic n-p[9] and p-p[10] scattering and the polarization in elastic p-p scattering.[5] During the past year we studied the angular dependence of polarization in p-n scattering in p-d collisions ($E_p = 635$ Mev) and have measured the differential cross sections for elastic neutron scattering by free protons at small angles ($E_n \approx 600$ Mev).[11]

1. The results obtained for the angular dependence of polarization in p-n scattering are given in detail in Fig. 2 together with the statistical errors. This figure also gives the results obtained by other investigators at lower energies. The curve changes markedly from 100 to 300 Mev but much less from 300 to 635 Mev.

A more detailed analysis of the results is planned for a future date; we have considered it useful in the present paper to distinguish the polarized cross sections associated with interactions between nucleons in states with different isotopic spins. The

Asymmetry and polarization of p-n scattering at 635 Mev

ϑ° (c.m. system)	(ε±Δε), %	(P±ΔP), %
18.5	14.1±2.7	24.3±4.8
34.5	17.6±2.6	30.3±4.7
45.7	11.0±1.7	19.0±3.1
56.7	3.8±1.8	6.6±3.1
67.3	1.0±3.0	1.7±5.1
90.0	−11.2±2.6	−19.3±4.6
112.5	−18.6±2.8	−32.1±5.1
134.3	−16.2±2.9	−27.9±5.2
145.7	−10.2±3.3	−17.6±5.8

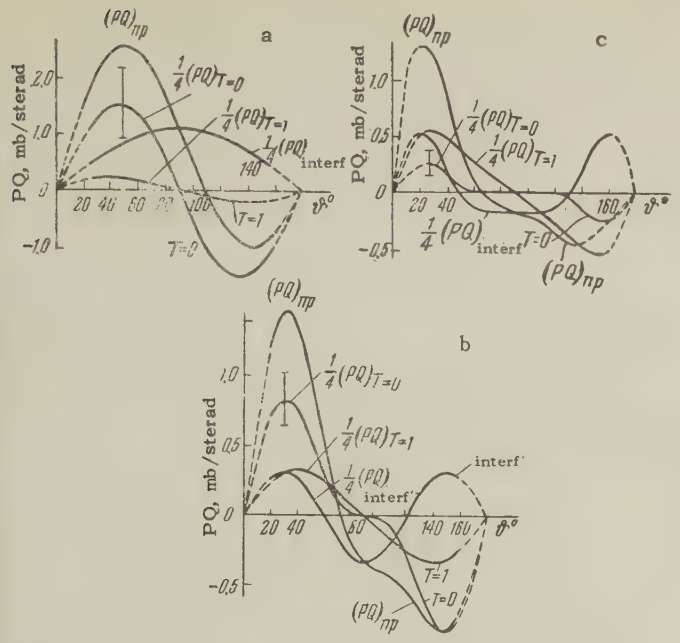

FIG. 3. Angular dependences of polarized n – p scattering cross sections for different isotopic spins at the following energies: a – 95 Mev, b – 315 Mev, c – 635 Mev.

results for three different nucleon energies are given in Fig. 3. All polarized partial cross sections are given with the same weights with which they are included in the polarized n-p scattering cross sections. The relative contributions of polarized partial cross sections in $(PQ)_{np}$ vary markedly with energy; these cross sections for $T = 0$ and $T = 1$ have different energy dependences, $(PQ)_{T=1}$ increasing with energy while $(PQ)_{T=0}$ decreases considerably. The relatively large polarized cross section for $T = 0$ at 635 Mev indicates a significant contribution of noncentral interactions in these states at 600 – 700 Mev just as at 100 – 300 Mev.[14] The observed reduction of polarized cross sections $(PQ)_{T=0}$ with increasing energy, together with previously obtained data on the angular dependence of the elastic scattering cross section for $T = 0$ and on the total cross sections for nucleon interactions in these states, which decrease with energy,[15] provides additional support for Smorodinskiĭ's[16] hypothesis that nucleon interactions for $T = 0$ can be described qualitatively by means of the Born approximation.

2. Polarization results obtained at different energies sometimes provide information about certain characteristics of nucleon interactions, even when a complete analysis is not made.

Let us consider the energy dependence of the polarized cross section $(PQ)_{np}$ at $\vartheta = 90°$ (c.m.), where only one term of $(PQ)_{np}$ remains, which is given by the interference between states with different isotopic spins. Figure 4 gives the data now

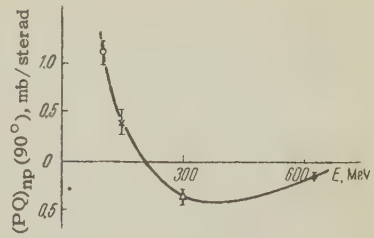

FIG. 4. Energy dependence of the polarized n – p scattering cross section at $\vartheta = 90°$. o – from reference 12, × – from reference 17, Δ – from reference 13, • – the present work.

available on $(PQ)_{np}$ (90°) for different nucleon energies. The sign is seen to change around 200 Mev. The calculations of Signell and Marshak[17] show that at energies up to 150 Mev both S phases diminish while all other phases increase with energy. A comparison of these calculations with a phase analysis of p-p scattering at 300 Mev[18] shows a reversal of the sign of the ^1S phase in the 100 – 300 Mev interval.

On the other hand, according to Wolfenstein[19] the principal role in polarization for n-p scattering near 100 Mev is played by $^3S - {}^3D$ interference. If it is assumed that at high energies an important part is played by the interference of different waves with the ^3S wave, we can conclude that the sign of the phase of the latter wave is reversed near 200 Mev, thus indicating that both S waves behave alike in the given energy region.

The authors are grateful to L. I. Lapidus, R. M. Ryndin and Ya. A. Smorodinskiĭ for discussions of a number of topics involved in the present work and for valuable suggestions.

APPENDIX 1

When nucleon-nucleon scattering amplitudes are written in the form

$$A_{pp} = \alpha_1 + \beta_1 (\sigma_1 \cdot \mathbf{n})(\sigma_2 \cdot \mathbf{n}) + \gamma (\sigma_1 + \sigma_2) \cdot \mathbf{n} + \delta (\sigma_1 \cdot \mathbf{l})(\sigma_2 \cdot \mathbf{l}) + \varepsilon (\sigma_1 \cdot \mathbf{m})(\sigma_2 \cdot \mathbf{m}), \quad (1)$$

$$A_{np} = {}^1/_2 (\alpha_1 + \alpha_0) + {}^1/_2 (\beta_1 + \beta_0)(\sigma_1 \cdot \mathbf{n})(\sigma_2 \cdot \mathbf{n}) + {}^1/_2 (\gamma_1 + \gamma_0)(\sigma_1 + \sigma_2) \cdot \mathbf{n} + {}^1/_2 (\delta_1 + \delta_0)(\sigma_1 \cdot \mathbf{l})(\sigma_2 \cdot \mathbf{l}) + {}^1/_2 (\varepsilon_1 + \varepsilon_0)(\sigma_1 \cdot \mathbf{m})(\sigma_2 \cdot \mathbf{m}), \quad (2)$$

where the subscripts 1 and 0 denote the total isotopic spin of the system, and we introduce the functions

$$a_{1,0} = (\alpha + \beta)_{1,0}; \quad b_{1,0} = (\alpha - \beta)_{1,0}; \quad c_{1,0} = (\delta + \varepsilon)_{1,0}; \quad d_{1,0} = (\delta - \varepsilon)_{1,0}; \quad e_{1,0} = 2\gamma_{1,0} \quad (3)$$

which possess the following symmetry properties under the substitution $\vartheta \leftrightarrow \pi - \vartheta$:

$$a_1(\pi - \vartheta) = -a_1(\vartheta);$$

$$b_1(\pi - \vartheta) = -c_1(\vartheta); \quad c_1(\pi - \vartheta) = -b_1(\vartheta);$$

$$d_1(\pi - \vartheta) = d_1(\vartheta); \quad e_1(\pi - \vartheta) = e_1(\vartheta);$$

$$a_0(\pi - \vartheta) = a_1(\vartheta); \quad b_0(\pi - \vartheta) = c_0(\vartheta); \quad c_0(\pi - \vartheta) = b_0(\vartheta);$$

$$d_0(\pi - \vartheta) = -d_0(\vartheta); \quad e_0(\pi - \vartheta) = -e_0(\vartheta), \quad (4)$$

then, as has already been mentioned, from two experiments where the same quantity for the n-p and p-p systems is measured we can obtain three independent combinations of scattering amplitude coefficients. This enables us to propose a set of thirteen experiments for the purpose of reconstructing the n-p and p-p scattering amplitudes except for a common phase factor of the two amplitudes. The expressions which relate scattering amplitudes to the results of certain basic experiments on elastic nucleon-nucleon scattering are the following:*

1. Elastic scattering cross section:

$$Q_{T=1}(\vartheta) = Q_{pp}(\vartheta)$$
$$= {}^1/_2\{|a_1|^2 + |b_1|^2 + |c_1|^2 + |d_1|^2 + |e_1|^2\}. \quad (5.1)$$
$$Q_{T=0}(\vartheta) = 2[Q_{np}(\vartheta) + Q_{np}(\pi - \vartheta)] - Q_{pp}(\vartheta)$$
$$= {}^1/_2\{|a_0|^2 + |b_0|^2 + |c_0|^2 + |d_0|^2 + |e_0|^2\}, \quad (5.2)$$
$$Q_{\text{interf.}}(\vartheta) = 2[Q_{np}(\vartheta) - Q_{np}(\pi - \vartheta)]$$
$$= \text{Re}\,[a_1 a_0^* + b_1 b_0^* + c_1 c_0^* + d_1 d_0^* + e_1 e_0^*]. \quad (5.3)$$

2. Polarization of angular scattering:

$$(PQ)_{T=1}(\vartheta) = (PQ)_{pp}(\vartheta) = \text{Re}\,a_1 e_1^*, \quad (6.1)$$
$$(PQ)_{T=0}(\vartheta) = 2[(PQ)_{np}(\vartheta) - (PQ)_{np}(\pi - \vartheta)]$$
$$- (PQ)_{pp}(\vartheta) = \text{Re}\,a_0 e_0^*, \quad (6.2)$$
$$(PQ)_{\text{interf.}}(\vartheta) = 2[(PQ)_{np}(\vartheta) + (PQ)_{np}(\pi - \vartheta)]$$
$$= \text{Re}\,(a_1 e_0^* + a_0 e_1^*). \quad (6.3)$$

3. Normal component of polarization correlation:

$$(P_{nn}Q)_{T=1}(\vartheta) = (P_{nn}Q)_{pp}(\vartheta)$$
$$= {}^1/_2\{|a_1|^2 - |b_1|^2 - |c_1|^2 + |d_1|^2 + |e_1|^2\}, \quad (7.1)$$
$$(P_{nn}Q)_{T=0}(\vartheta) = 2[(P_{nn}Q)_{np}(\vartheta)$$
$$+ (P_{nn}Q)_{np}(\pi - \vartheta)] - (P_{nn}Q)_{pp}(\vartheta)$$
$$= {}^1/_2\{|a_0|^2 - |b_0|^2 - |c_0|^2 + |d_0|^2 + |e_0|^2\}, \quad (7.2)$$
$$(P_{nn}Q)_{\text{interf.}}(\vartheta) = 2[(P_{nn}Q)_{np}(\vartheta) - (P_{nn}Q)_{np}(\pi - \vartheta)]$$
$$= \text{Re}\,[a_1 a_0^* - b_1 b_0^* - c_1 c_0^* + d_1 d_0^* + e_1 e_0^*]. \quad (7.3)$$

4. Triple scattering in parallel planes (scattered particle):

$$(D_{nn}Q)_{T=1}(\vartheta) = (D_{nn}Q)_{pp}(\vartheta)$$
$$= {}^1/_2\{|a_1|^2 + |b_1|^2 - |c_1|^2 - |d_1|^2 + |e_1|^2\}, \quad (8.1)$$
$$(D_{nn}Q)_{T=0}(\vartheta) = 2[(D_{nn}Q)_{np}(\vartheta)$$
$$+ (K_{nn}Q)_{np}(\pi - \vartheta)] - (D_{nn}Q)_{pp}(\vartheta)$$
$$= {}^1/_2\{|a_0|^2 + |b_0|^2 - |c_0|^2 - |d_0|^2 + |e_0|^2\}, \quad (8.2)$$
$$(D_{nn}Q)_{\text{interf.}}(\vartheta) = 2[(D_{nn}Q)_{np}(\vartheta) - (K_{nn}Q)_{np}(\pi - \vartheta)]$$
$$= \text{Re}\,[a_1 a_0^* + b_1 b_0^* - c_1 c_0^* - d_1 d_0^* + e_1 e_0^*]. \quad (8.3)$$

5. Triple scattering in parallel planes (recoil particle):

$$(K_{nn}Q)_{T=1}(\vartheta) = (K_{nn}Q)_{pp}(\vartheta)$$
$$= {}^1/_2\{|a_1|^2 - |b_1|^2 + |c_1|^2 - |d_1|^2 + |e_1|^2\}, \quad (9.1)$$
$$(K_{nn}Q)_{T=0}(\vartheta) = 2[(K_{nn}Q)_{np}(\vartheta)$$
$$+ (D_{nn}Q)_{np}(\pi - \vartheta)] - (K_{nn}Q)_{pp}(\vartheta)$$
$$= {}^1/_2\{|a_0|^2 - |b_0|^2 + |c_0|^2 - |d_0|^2 + |e_0|^2\}, \quad (9.2)$$
$$(K_{nn}Q)_{\text{interf.}}(\vartheta) = 2[(K_{nn}Q)_{np}(\vartheta) - (D_{nn}Q)_{np}(\pi - \vartheta)]$$
$$= \text{Re}\,[a_1 a_0^* - b_1 b_0^* + c_1 c_0^* - d_1 d_0^* + e_1 e_0^*]. \quad (9.3)$$

6. Polarization correlation for scattering in mutually perpendicular planes:

$$(P_{ml}Q)_{T=1}(\vartheta) = (P_{ml}Q)_{pp}(\vartheta) = \text{Im}\,d_1 e_1^*, \quad (10.1)$$
$$(P_{ml}Q)_{T=0}(\vartheta) = 2[(P_{ml}Q)_{np}(\vartheta) + (P_{ml}Q)_{np}(\pi - \vartheta)]$$
$$- (P_{ml}Q)_{pp}(\vartheta) = \text{Im}\,d_0 e_0^*, \quad (10.2)$$
$$(P_{ml}Q)_{\text{interf.}}(\vartheta) = 2[(P_{ml}Q)_{np}(\vartheta) - (P_{ml}Q)_{np}(\pi - \vartheta)]$$
$$= \text{Im}\,(d_1 e_0^* + d_0 e_1^*). \quad (10.3)$$

7. Rotation of polarization vector (scattered particle):

$$(D_{xm}Q)_{T=1}(\vartheta) = (D_{xm}Q)_{pp}(\vartheta)$$
$$= -\cos(\vartheta/2)\,\text{Re}\,(a_1^* b_1 + c_1^* d_1) + \sin(\vartheta/2)\,\text{Im}\,b_1^* e_1, \quad (11.1)$$
$$(D_{xm}Q)_{T=0}(\vartheta) = 2[(D_{xm}Q)_{np}(\vartheta)$$
$$- (K_{xl}Q)_{np}(\pi - \vartheta)] - (D_{xm}Q)_{pp}(\vartheta)$$
$$= -\cos(\vartheta/2)\,\text{Re}\,(a_0^* b_0 + c_0^* d_0) + \sin(\vartheta/2)\,\text{Im}\,b_0^* e_0, \quad (11.2)$$
$$(D_{xm}Q)_{\text{interf.}}(\vartheta) = 2[(D_{xm}Q)_{np}(\vartheta) + (K_{xl}Q)_{np}(\pi - \vartheta)]$$
$$= -\cos(\vartheta/2)\,[\text{Re}\,(a_1^* b_0 + a_0^* b_1) + \text{Re}\,(c_1^* d_0 + c_0^* d_1)]$$
$$+ \sin(\vartheta/2)\,\text{Im}\,(b_1^* e_0 + b_0^* e_1). \quad (11.3)$$

8. Rotation of polarization vector (recoil particle):

$$(K_{xl}Q)_{T=1}(\vartheta) = (K_{xl}Q)_{pp}(\vartheta) = \sin(\vartheta/2)\,\text{Re}\,(a_1^* c_1 - b_1^* d_1)$$
$$+ \cos(\vartheta/2)\,\text{Im}\,c_1^* e_1, \quad (12.1)$$
$$(K_{xl}Q)_{T=0}(\vartheta) = 2[(K_{xl}Q)_{np}(\vartheta)$$
$$- (D_{xm}Q)_{np}(\pi - \vartheta)] - (K_{xl}Q)_{pp}(\vartheta)$$
$$= \sin(\vartheta/2)\,\text{Re}\,(a_0^* c_0 - b_0^* d_0) + \cos(\vartheta/2)\,\text{Im}\,c_0^* e_0, \quad (12.2)$$
$$(K_{xl}Q)_{\text{interf.}}(\vartheta) = 2[(K_{xl}Q)_{np}(\vartheta) + (D_{xm}Q)_{np}(\pi - \vartheta)]$$
$$= \sin(\vartheta/2)\,[\text{Re}\,(a_1^* c_0 + a_0^* c_1) - \text{Re}\,(b_1^* d_0 + b_0^* d_1)]$$
$$+ \cos(\vartheta/2)\,\text{Im}\,(c_1^* e_0 + c_0^* e_1). \quad (12.3)$$

9. Influence of longitudinal polarization component of incident beam on transverse component of scattered beam (scattered particle):

$$(D_{zm}Q)_{T=1}(\vartheta) = (D_{zm}Q)_{pp}(\vartheta)$$
$$= \sin(\vartheta/2)\,\text{Re}\,(a_1^* b_1 + c_1^* d_1) + \cos(\vartheta/2)\,\text{Im}\,h_1^* e_1, \quad (13.1)$$
$$(D_{zm}Q)_{T=0}(\vartheta) = 2[(D_{zm}Q)_{np}(\vartheta)$$
$$+ (K_{zl}Q)_{np}(\pi - \vartheta)] - (D_{zm}Q)_{pp}(\vartheta)$$
$$= \sin(\vartheta/2)\,\text{Re}\,(a_0^* b_0 + c_0^* d_0) + \cos(\vartheta/2)\,\text{Im}\,b_0^* e_0, \quad (13.2)$$
$$(D_{zm}Q)_{\text{interf.}}(\vartheta) = 2[(D_{zm}Q)_{np}(\vartheta) - (K_{zl}Q)_{np}(\pi - \vartheta)]$$
$$= \sin(\vartheta/2)\,[\text{Re}\,(a_1^* b_0 + a_0^* b_1) + \text{Re}\,(c_1^* d_0 + c_0^* d_1)]$$
$$+ \cos(\vartheta/2)\,\text{Im}\,(b_1^* e_0 + b_0^* e_1). \quad (13.3)$$

*All expressions are given in nonrelativistic form. The relativistic forms whenever required can be obtained on the basis of Stapp's results,[20] and do not affect the conclusions regarding the reduction of the number of experiments required to reconstruct amplitudes in a simultaneous analysis of n – p and p – p scattering data.

10. Influence of longitudinal polarization component of incident beam on transverse component of scattered beam (recoil particle):

$$(K_{zl}Q)_{T=1}(\vartheta) = (K_{zl}Q)_{pp}(\vartheta) = \cos(\vartheta/2)\,\mathrm{Re}\,(a_1^* c_1 - b_1^* d_1) - \sin(\vartheta/2)\,\mathrm{Im}\,c_1^* e_1, \quad (14.1)$$

$$(K_{zl}Q)_{T=0}(\vartheta) = 2\,[(K_{zl}Q)_{np}(\vartheta) + (D_{zm}Q)_{np}(\pi-\vartheta)] - (K_{zl}Q)_{pp}(\vartheta) = \cos(\vartheta/2)\,\mathrm{Re}\,(a_0^* c_0 - b_0^* d_0) - \sin(\vartheta/2)\,\mathrm{Im}\,c_0^* e_0. \quad (14.2)$$

$$(K_{zl}Q)_{\text{interf}}(\vartheta) = 2\,[(K_{zl}Q)_{np}(\vartheta) - (D_{zm}Q)_{np}(\pi-\vartheta)] = \cos(\vartheta/2)\,[\mathrm{Re}\,(a_1^* c_0 + a_0^* c_1) - \mathrm{Re}\,(b_1^* d_0 + b_0^* d_1)] - \sin(\vartheta/2)\,\mathrm{Im}\,(c_1^* e_0 + c_0^* e_1). \quad (14.3)$$

APPENDIX 2

Let us now consider a possible set of 13 experiments which will permit reconstruction of the scattering amplitude.

Set of experiments No. 1

No.	Experiment	Formulas for analysis	Particle system used in experiment	
			pp	np
1	Polarization of scattering	6.(1–3)	+	+
2	Rotation of polarization vector (scattered particle)	11.(1–3)	+	+
3	The same for recoil particle	12.(1–3)	+	+
4	Polarization correlation for scattering in mutually perpendicular planes	10.(1–3)	+	+
5	Differential cross sections for elastic scattering	5.(1–3)	+	+
6	Correlation of normal polarization components	7.(1–3)	+	+
7	Triple scattering in parallel planes (scattered particle)	8.(1)	+	–

The proposed 13 experiments enable us to obtain a system of 19 equations in the 19 unknowns:

$$|a_1|, |b_1|, |c_1|, |d_1|, |e_1|, \varphi_{e_1}^{a_1}, \varphi_{e_1}^{b_1}, \varphi_{e_1}^{c_1}, \varphi_{e_1}^{d_1};$$

$$|a_0|, |b_0|, |c_0|, |d_0|, |e_0|, \varphi_{e_1}^{a_0}, \varphi_{e_1}^{b_0}, \varphi_{e_1}^{c_0}, \varphi_{e_1}^{d_0}, \varphi_{e_1}^{e_0},$$

$\varphi_{e_1}^{i}$ being the phase difference between i and e_1.

Because of the difficulties involved in performing experiments with an n-p system and the possibility of making fuller use of Eqs. (5), (7), (8), and (9) with a simpler structure, another set of 14 experiments will be of interest, consisting of 9 experiments on a p-p system and only 5 experiments on a n-p system. An example of such a set is the following:

Set of experiments No. 2

No.	Experiment	Formulas for analysis	Particle system used in experiment	
			pp	np
1	Differential cross sections	5.(1–3)	+	+
2	Triple scattering in parallel planes (scattered particle)	8.(1–3)	+	+
3	The same for recoil particle	9.(1–3)	+	+
4	Correlation of normal polarization components	7.(1–3)	+	+
5	Polarization of elastic scattering	6.(1–3)	+	+
6	Polarization correlation for scattering in mutually perpendicular planes	10.(1)	+	–
7	Rotation of polarization vector (scattered particle)	11.(1)	+	–
8	The same for recoil particle	12.(1)	+	–
9	Influence of longitudinal polarization component of incident beam on transverse component of scattered beam (scattered particle)	13.(1)	+	–

In this case the first five pairs of experiments determine the moduli

$$|a_1+e_1|, |a_1-e_1|, |b_1|, |c_1|, |d_1|,$$

$$|a_0+e_0|, |a_0-e_0|, |b_0|, |c_0|, |d_0|$$

and the angles between them: $\varphi_{a_1+e_1}^{a_0+e_0}$, $\varphi_{a_1-e_1}^{a_0-e_0}$, $\varphi_{b_1}^{b_0}$, $\varphi_{e_1}^{e_0}$, $\varphi_{d_1}^{d_0}$.

The four other experiments can be used to determine the angles $\varphi_{e_1}^{a_1+e_1}$, $\varphi_{e_1}^{a_1-e_1}$, $\varphi_{1}^{b_1}$, $\varphi_{e_1}^{c_1}$, $\varphi_{e_1}^{d_1}$. In other words, nine experiments comprise a full set for a p-p system, and the simultaneous analysis of five experiments on n-p scattering, together with the corresponding experiments for the p-p system, can be used to determine the moduli of five functions for a system with T = 0 and the phase differences between the corresponding functions for T = 0 and T = 1.

It must be noted, however, that since the given equations are bilinear with respect to a, b, c, d, and e the solutions obtained from these sets of equations may not be unique. We must therefore obtain additional relations between the quantities to be determined. We have considered two other sets of 14 equations that enable us to obtain such relations. The first of these sets (No. 3) agrees with set No. 2 except that Experiment No. 9 with the p-p system is replaced by Experiment No. 6 with the n-p system. This set of experiments

leads to 20 independent equations for the calculation of the 19 unknowns given above.

Set No. 4 (below) consists of seven pairs of identical experiments with a p-p and a n-p system. The number of n-p experiments is here greater than in the previous set, but the very difficult experiment No. 6 is replaced by two experiments which are much easier from an experimental point of view.

Set of experiments No. 4

No.	Experiment	Formulas for analysis	Particle system used in experiment	
			pp	np
1	Differential cross sections	5.(1–3)	+	+
2	Triple scattering in parallel planes (scattered particles)	8.(1–3)	+	+
3	The same for recoil particle	9.(1–3)	+	+
4	Correlation of normal polarization components	7.(1–3)	+	+
5	Polarization of scattering	6.(1–3)	+	+
6	Rotation of polarization vector (scattered particle)	11.(1–3)	+	+
7	The same for recoil particle	12.(1–3)	+	+

This set of experiments leads to 21 independent equations for 19 unknowns and can thus be very useful for the unique reconstruction of p-p and n-p scattering amplitudes. The indeterminacy of the results can also be reduced by comparing solutions for different scattering angles and energies.

It should be noted that as information concerning scattering amplitudes is accumulated in some instances it may become unnecessary to perform certain experiments of the foregoing sets either over the entire angular range or for individual angles where the form of the amplitude is simpler.

[1] R. Oehme, Phys. Rev. **98**, 216 (1955).

[2] Puzikov, Ryndin and Smorodinskiĭ, J. Exptl. Theoret. Phys. (U.S.S.R.) **32**, 592 (1957), Soviet Phys. JETP **5**, 489 (1957).

[3] B. M. Golovin, Dissertation, Laboratory for Nuclear Problems, Joint Institute for Nuclear Research, 1955.

[4] S. Tamor, Phys. Rev. **97**, 1077 (1955).

[5] Meshcheryakov, Nurushev, and Stoletov, J. Exptl. Theoret. Phys. (U.S.S.R.) **33**, 37 (1957), Soviet Phys. JETP **6**, 28 (1958).

[6] Akimov, Kuznetsov, and Leksin, Приборы и техника эксперимента (Instruments and Measurement Engg.) **2**, 70 (1956).

[7] Dzhelepov, Satarov, and Golovin, Dokl. Akad. Nauk SSSR **104**, 717 (1955).

[8] Dzhelepov, Moskalev, and Medved', Dokl. Akad. Nauk SSSR **104**, 380 (1955).

[9] Yu. M. Kazarinov and Yu. N. Simonov, J. Exptl. Theoret. Phys. (U.S.S.R.) **31**, 169 (1956), Soviet Phys. JETP **4**, 161 (1957); N. S. Amaglobeli and Yu. M. Kazarinov, J. Exptl. Theoret. Phys. (U.S.S.R.) **34**, 53 (1958), Soviet Phys. JETP **7**, 37 (1958).

[10] N. P. Bogachev and I. K. Vzorov, Dokl. Akad. Nauk SSSR **99**, 931 (1954); N. P. Bogachev, Dokl. Akad. Nauk SSSR **108**, 806 (1956), Soviet Phys. "Doklady" **1**, 361 (1956); Bogomolov, Zombkovskiĭ, Nikitin, and Selektor, Symposium CERN **2**, 129 (1956).

[11] Golovin, Dzhelepov, Katyshev, Konin, and Medved', J. Exptl. Theoret. Phys. (U.S.S.R.) **36**, 735 (1959), Soviet Phys. JETP **9** (in press).

[12] Stafford, Whitehead, and Hillman, Nuovo cimento **5**, 1589 (1957).

[13] Chamberlain, Segrè, Tripp, Wiegand, and Ypsilantis, Phys. Rev. **105**, 288 (1957).

[14] L. Wolfenstein, Phys. Rev. **101**, 427 (1956).

[15] Dzhelepov, Golovin, Kazarinov, and Simonov, Symposium CERN **2**, 115 (1956).

[16] Ya. S. Smorodinskiĭ, Introductory article in Проблемы современной физики (Problems of Modern Physics) **7**, 7 (1954).

[17] P. S. Signell and R. E. Marshak, Phys. Rev. **109**, 1229 (1958).

[18] Stapp, Ypsilantis, and Metropolis, Phys. Rev. **105**, 305 (1957).

[19] L. Wolfenstein, Ann. Rev. Nucl. Sci. **6**, 43 (1956).

[20] H. P. Stapp, Phys. Rev. **103**, 425 (1956).

Translated by I. Emin
74

CERTAIN CASES OF ELASTIC SCATTERING OF POSITRONS FROM π^+-μ^+-e^+ DECAY BY EMULSION ELECTRONS

Z. V. MINERVINA and E. A. PESOTSKAYA

Submitted to JETP editor September 4, 1959

J. Exptl. Theoret. Phys. (U.S.S.R.) 36, 444-446 (February, 1959)

We consider π^+-μ^+-e^+ decay events involving two electron tracks originating at the end of a muon track. It is suggested that such cases that occur near the μ-e decay point are due to elastic scattering of positrons by emulsion electrons.

In a systematic scanning of approximately 80,000 π^+-μ^+-e^+ decays in a NIKFI-R emulsion, exposed in the pion beam of the synchrocyclotron of the Joint Institute for Nuclear Research, we observed two events of π^+-μ^+-e^+ decay, in which two electron tracks lead from each end of the track of the stopped muon (Fig. 1).

In the first of these events the angle between the tracks of electrons 1 and 2 was $27 \pm 1°$, the ionization of the two electrons was a minimum, and their energy, determined by the multiple-scattering method, was 51 ± 16 Mev and 3 ± 1 Mev. In the second case the angle between the tracks was $32 \pm 3°$, and the energy of electron 1, having a minimum ionization, was 34 ± 7 Mev. The energy of the second electron could not be determined, since the length of the track was merely ~ 25 microns.

Events in which two electrons were produced at the end of a muon track were also observed before, both in cloud chambers and in emulsion.[1,2] However, these were negative-muon decays in which a slow Auger electron was emitted, through conversion of the meso-atomic x-radiation, along with a fast decay electron. In our case we could not assume the emission of Auger electrons, since here the muons were the decay products of pions stopped in the emulsion, which proves beyond any doubt their positive charge. It is impossible to attribute the apparent paired emission of an electron to an apparent superposition of the end of the background-electron track on the ordinary π^+-μ^+-e^+ decay, since the probability of such an event is rather small under our conditions. In addition to the above events, while scanning electron tracks (in 9000 decays gathered for a different purpose), we observed seven characteristic "forks" of elastic e^+-e^- scattering (Fig. 2). In these cases the track leading from the end of the muon passes a certain distance in the emulsion and splits up; the resultant two relativistic tracks make angles θ_1 and θ_2 with the direction of the initial track.

Table I shows the angles of emergence and the distances from the end of the muon track to the scattering point, observed in our seven events. The left column contains the sums of the three-

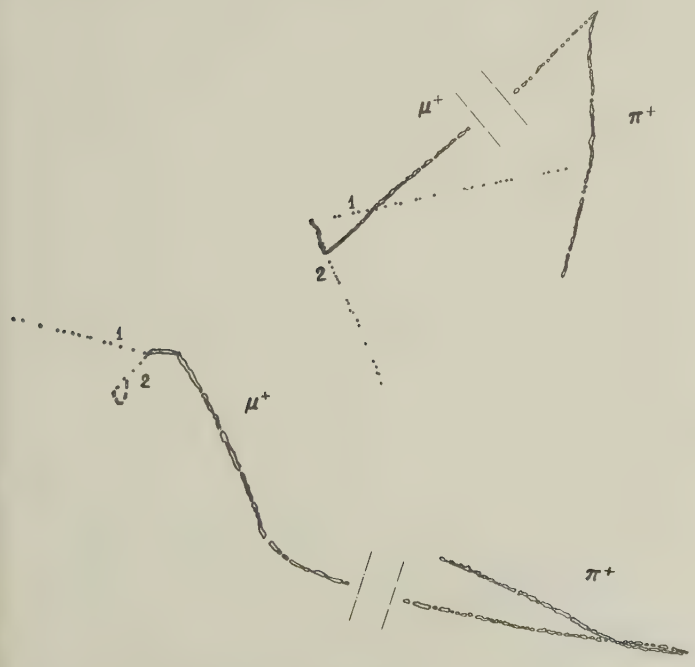

FIG. 1

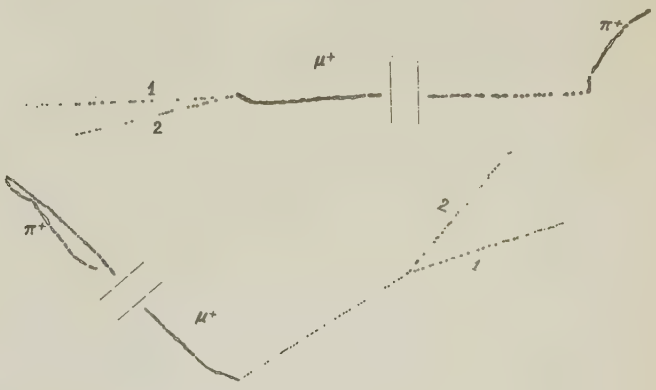

FIG. 2

TABLE I

Event No.	Path of initial particle	$\theta_{1,2}$ (deg)	$\theta_{1,3}$ (deg)	$\theta_{2,3}$ (deg)	Sum of angles (deg)
1	550	11.5	180	169	360.5
2	400	17.5	175	166	358.5
3	275	19.5	169.5	169	358
4	240	41	162.5	157	360.5
5	115	21	171	167.5	359.5
6	15	18	178	161	357
7	5	15.5	—	—	—

TABLE II

Event No.	E_0 (Mev)	E_1 (Mev)	E_2 (Mev)	E_0, by scatter angles, (Mev)
1	27±7	33±5	8±2	26±4
2	17±6	17±2	10±2	18±3
3	31±14	24±11	11±3	32±6
4	11±4	7±1	6±1	5±1
5	—	32±13	17±15	21±4
6	—	36±14	2±1	10±2
7	—	22±4	5±1	—

dimensional angles between the branches of the fork for all cases, in which all three branches of the fork are sufficient long and permit measurement of the angles. The obvious complanarity of these cases is convincing proof that elastic scattering indeed has taken place here.

It is difficult to verify whether the law of conservation of energy holds for these cases, because the tracks, as a rule, are too short and do not permit an accurate determination of the energy. On the average, the statistical accuracy in the determination of the energy is close to 30%. Energies measured with such an accuracy, as seen in Table II, do not contradict each other or the values calculated on the basis of energy and momentum conservation for elastic collisions.

We observed seven such "forks" in a total length of positron track of approvimately 10 meters. If we calculate from this the cross section of the collision between the decay positron and the emulsion electron, we find it to be approximately 6×10^{-27} cm, which is in good agreement with the positron-electron elastic-scattering cross section calculated by the Bhabha formula.[3]

We thus have seven events, for which the appearance of elastic scattering of a decay positron by an emulsion electron is proved with sufficient assurance. From column 2 of Table I it is seen that in the last two cases the e^+-e^- scattering occurred every close to the end of the muon track, at distances of 15 and 5 μ respectively. It is natural to assume that the case of two electron tracks diverging from the end of a muon track, which we have discussed at the beginning (Fig. 1), is indeed an example of a scattering that occurs near the decay point, so close to the end of the muon track that the vertex of a fork coincides with the point of decay. That the angles between the electron tracks do not exceed 90° in either case is also typical of a scattering event.

The probability of e^+-e^- scattering at a distance not exceeding 3 μ at the end of the muon track is 1.5×10^{-6}. The expected number of events of such a scattering is approximately 0.1 or 0.2 This number indicates that the foregoing explanation does not contradict the experiments.

The authors express their indebtedness to A. O. Vaĭsenberg for interest in this project and for a discussion of the result, and also thank V. N. Kuznetsov, A. G. Avalishvili, O. A. Zubkov, and A. K. Krupnov, who observed the foregoing decays.

[1] A. Bennetti and G. Temanini, Nuovo cimento **8**, 693 (1951).

[2] W. F. Fry, Nuovo cimento **10**, 490 (1953).

[3] H. J. Bhabha, Proc. Roy. Soc. **A154**, 195 (1936).

Translated by J. G. Adashko
75

MEASUREMENT OF THE ELECTRICAL RESISTANCE OF METALS IN A MAGNETIC FIELD AS A METHOD OF INVESTIGATING THE FERMI SURFACE

N. E. ALEKSEEVSKIĬ and Yu. P. GAĬDUKOV

Institute for Physical Problems, Academy of Sciences, U.S.S.R.

Submitted to JETP editor October 21, 1958

J. Exptl. Theoret. Phys. (U.S.S.R.) **36**, 447-450 (February, 1959)

Results are given of an investigation of the polar diagrams of resistance for single crystal specimens of Sn, Pb, Tl, Ga, and Na. It is found that for Sn and Pb (as for Au and Cu) the variation of resistance with magnetic field changes from a quadratic relation to complete saturation, as the angle between the field and the crystallographic axes changes. A strong anisotropy of resistance in a magnetic field is also found for Tl and Ga. These results are ascribed to the existence of open Fermi surfaces in these metals.

IT has recently been proposed by Lifshitz, Azbel' and Kaganov[1] and also Chambers[2] that the iso-energetic surfaces for the conduction electrons in metals (the Fermi surfaces) may be complicated topologically, with open sections. Fermi surfaces can be constructed on the basis of data from measurements on the de Haas-van Alphen effect, the anomalous skin effect, and cyclotron resonance.[3] These methods, however, cannot give unambiguous results in cases where one must study directions near to open sections.

It follows from the work of Lifshitz et al. that for open Fermi surfaces it is possible to have a quadratic increase in resistance for some directions of the field, and saturation for others. We showed previously[4] that the increase of the resistance of gold and copper in a magnetic field, $r(H)$, changes considerably with the angle between the field and the crystallographic axes of the specimen: the resistance either increases quadratically with field in the direction corresponding to a sharp maximum on the polar diagram or reaches saturation in the direction of a minimum.

The linear growth law for the resistance of polycrystalline specimens in a magnetic field (Kapitza's law[5]), which has so far no theoretical explanation, can probably be considered[4] as the result of an averaging of the different laws of increase of $r(H)$, observed in single crystals.

We note also that according to the theory of Lifshitz et al., the sharp maxima in the polar diagrams of gold and copper can be attributed to the existence of open Fermi surfaces in these metals.

The appropriate theoretical treatment, explaining these results, was recently given by Lifshitz and Peschanskii.[6]

It seemed of interest to study in detail the angular dependence of $r(H)$ for single crystals of other metals, and we measured specimens of Sn, Pb, Tl, Ga, and Na, as detailed in the table, at 4.2 and 1.5°K.

Figure 1 shows the polar diagrams of the variation of resistance at constant H for specimens Sn-I, Pb-I and Tl. All measurements refer to the magnetic field perpendicular to the measuring current J. Figure 2 shows the variation of $\Delta r_H/r_0 = [r(H) - r_0]/r_0$ (where r_0 is the resistance in zero field) in Sn-I and Pb-I for two fixed directions of the field.

It can be seen from the figures that in the direc-

Specimen	Sn-I	Sn-II	Sn-III	Sn-IV	Sn-V	Pb-I	Pb-II	Tl	Ga	Na
Direction of axis of specimen	[001]	[010]	[110]	[111]	[011]	[111]	[110]	—	—	—
Dimensions, mm:										
length*	22.7	22.1	24.25	18.05	21,28	11.75	6,26	11,61	10,82	—
diameter	1,95	2.04	1,63	2,07	1,53	1.01	0,74	1,97	0.68	—
$r_{4,2°K}/r_{300°K}$	$8.9\cdot10^{-5}$	$10,5\cdot10^{-5}$	$11,4\cdot10^{-5}$	$9,4\cdot10^{-5}$	$4,4\cdot10^{-5}$	$7,2\cdot10^{-5}$	$14\cdot10^{-5}$	$2,6\cdot10^{-4}$	$3,6\cdot10^{-4}$	$2,4\cdot10^{-4}$

*Distance between potential leads.

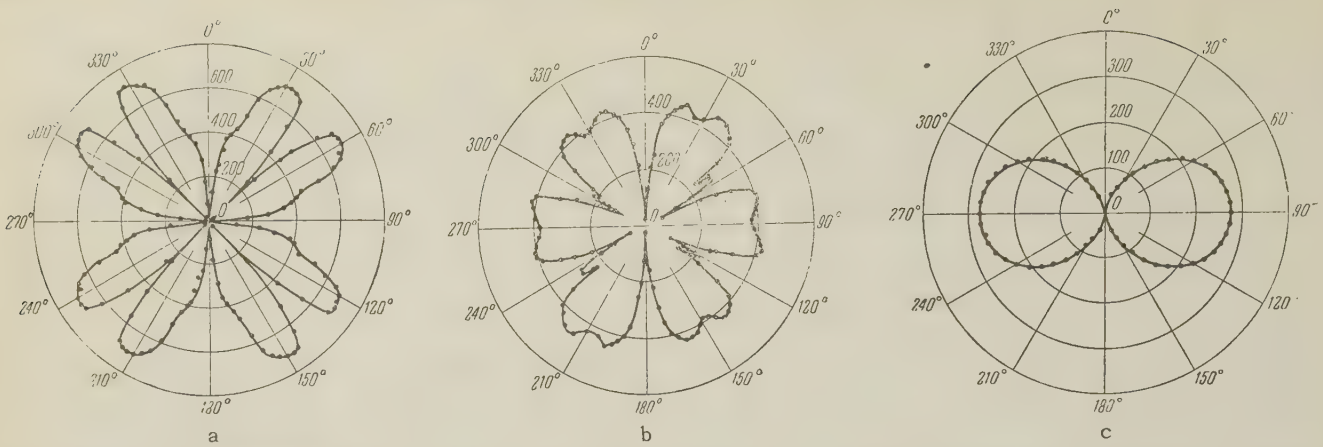

FIG. 1. Polar diagrams of the resistance change $\Delta r_H/r_0$ for constant H as a function of the angle, φ, between the crystallographic axes of the specimen and the direction of the magnetic field. T = 4.2°K. a – specimen Sn-I, H = 23 kOe; b – Pb-I, H = 22.3 kOe; c – Tl, H = 22.3 kOe.

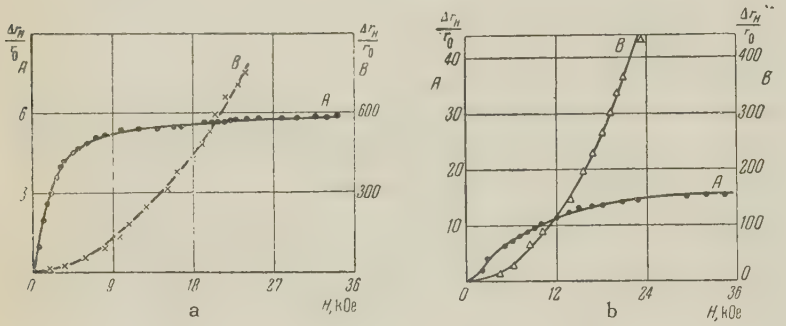

FIG. 2. The resistance change, $\Delta r_H/r_0$, in a magnetic field for fixed angle φ. T = 4.2°K. a – specimen Sn-I; b – Pb-I Curve A – measurements at the minimum (φ = 0°), curves B – at the maximum (φ = 30°) of the corresponding polar diagrams.

tion of the minima of the polar diagrams there is complete saturation, while in the direction of the maxima the resistance continuously increases according to a quadratic relation. A similar behavior was found with Sn-III.

We also found considerable anisotropy in the resistance of Tl and Ga specimens in a magnetic field, and the law of increase, $\Delta r_H/r_0 = AH^n$, for Tl changes at different crystallographic directions from quadratic to linear. For Ga the exponent n, decreases from 2 to 1.6. There appears to be no anisotropy in the resistance of Na in a magnetic field. r(H) is very weakly dependent on the field and tends to saturation ($\Delta r_H/r_0 \approx 1$ in a field $H \simeq 55{,}000$ Oe).

On analyzing our results and those of other authors[7] we can conclude that Au, Cu, Sn, Pb, Tl (and possibly Ga) have open Fermi surfaces, while Al, In, and Na, which show saturation and a very weak anisotropy of r(H), have closed surfaces.

According to the data of Lüthi and Olsen,[8] the resistance of Al increases again on increasing the magnetic field beyond the saturation region. It is not impossible that such an increase may be a consequence of the openness of the Fermi surface. If the dependence of resistance on field in large fields can be represented by the relation

$$\Delta r_H / r_0 = A\,(H/H_0)^2 + B,$$

(where the first term refers to a narrow region of open sections, and the second to closed sections) then for $0 < A \ll B$, when all possible directions are averaged, the resistance will increase again with field after saturation for $H \gg H_0$ [i.e., $A\,(H/H_0)^2 > B$]. Measurements on aluminum single crystals, which we intend to make soon, will enable us to test these ideas.*

The absence of saturation in the direction of a minimum of the polar diagram for Tl and Ga is probably a consequence of the averaging of r(H) over a range of angles close to the minimum. Such an averaging can result from an imperfection of the single crystal or from inhomogeneities of the field. However, strong anisotropy of resistance in a field and different variations of r(H) in the maximum and minimum of the polar diagram are a sufficiently convincing indication of the existence of open Fermi surfaces.

*We should point out that measurements of r(H) on polycrystalline specimens in extremely strong magnetic fields will enable us to show the existence of open sections for all metals in which r(H) shows little anisotropy and rapidly reaches saturation for $H > H_0$ (H_0 is determined from the condition $1/R = 1$, where 1 is the mean free path and R the radius of curvature of the trajectory of an electron in the magnetic field).

On the basis of the data obtained for tin we conclude that the directions of the open sections coincide with the [010], [110] and [001] directions.

Our results on one specimen of copper are not in conflict with the form of Fermi surface proposed by Pippard.[9] Here the directions of the open sections coincide with the main diagonals. It is most likely that gold has a Fermi surface analogous to copper.

The results obtained give us reason to consider that, in addition to the three well known methods for studying the Fermi surface, the measurement of the variation of r(H) for various orientations of single crystals in a magnetic field can serve as a simple and convenient means of showing up open sections.

It is a pleasure to express our thanks to Academician P. L. Kapitza for his constant interest in this work.

[1] Lifshitz, Azbel, and Kaganov, J. Exptl. Theoret. Phys. (U.S.S.R.) **31**, 63 (1956), Soviet Phys. JETP **4**, 41 (1957).

[2] R. G. Chambers, Proc. Roy. Soc. **238**, 344 (1957).

[3] B. I. Berkin, Doctoral Thesis, Physical and Technological Institute of the Academy of Sciences, Ukrainian S.S.R., Khar'kov (1958). M. Ya. Azbel', Doctoral Thesis, Institute for Physical Problems of the Academy of Sciences, U.S.S.R., Moscow (1958).

[4] N. I. Alekseevskiĭ and Yu. P. Gaĭdukov, J. Exptl. Theoret. Phys. (U.S.S.R.) **35**, 554 (1958), Soviet Phys. JETP **8**, 383 (1959).

[5] P. L. Kapitza, Proc. Roy. Soc. **123**, 292 (1929).

[6] I. M. Lifshitz and B. G. Peschanskiĭ, J. Exptl. Theoret. Phys. (U.S.S.R.) **35**, 1251 (1958), Soviet Phys. JETP **8**, 875 (1959).

[7] E. Justi and H. Scheffers, Phys. Z. **39**, 105 (1938). E. S. Borovik, Dokl. Akad. Nauk SSSR **69**, 767 (1949).

[8] B. Lüthi and J. L. Olsen, Nuovo cimento **3**, 840 (1956).

[9] A. B. Pippard, Phil. Trans. Roy. Soc. **250**, 325 (1957).

Translated by R. Berman
76

ON THE THEORY OF ABSORPTION AND DISPERSION OF LIGHT IN CRYSTALS

S. I. PEKAR

Kiev State University

Submitted to JETP editor May 19, 1958

J. Exptl. Theoret. Phys. (U.S.S.R.) 36, 451-464 (February, 1959)

The results of the author's earlier papers[1,2] are generalized to the case of finite lifetime for the excited state of the crystal and to several light-absorption bands. Absorption of light is obtained as a result of the finite lifetime for the excited state with respect to thermal transitions. In the limiting case of a very long exciton wave the dependence of its energy on the direction of propagation has been obtained. A general theory of longitudinal polarization waves in crystals has been developed.. By means of a limiting transition to infinite lifetime for the excited states all the principal results of the earlier paper[1] have been obtained (taking into account the additional remarks of reference 4).

1. FORMULATION OF THE PROBLEM AND THE GENERAL QUANTUM MECHANICAL THEORY

IN our earlier papers[1,2] it was shown that, in the range of exciton absorption of light in crystals, the dispersion has a number of peculiarities: for a given direction of propagation of a plane wave of given frequency and polarization the square of the index of refraction may have not one, but several values (for example, two values in cubic crystals). A proof has been given of the possibility of the existence in the crystal of longitudinal electric waves for which the magnetic field and the electric displacement are both equal to zero. Such waves may be propagated in an unisotropic crystal in certain special directions, and in a cubic crystal in any direction. Essential generalizations were obtained of the fundamental formulas of crystal optics — the Fresnel equations for the passage of light across the boundary between vacuum and the crystal, expressions for the coefficient of reflection of light from the surface of the crystal, formulas expressing the dependence of the indices of refraction on the light frequency, etc.

From the papers referred to above it follows that strong dispersion is possible in the neighborhood of a weak absorption band. In other words, the well-known general relation between the "area under the absorption curve" and the numerator of Sellmeyer's dispersion formula may be violated. This is connected with the fact that, under conditions of steady state illumination of the crystal, the absorption is determined by the finiteness of the lifetime of the exciton with respect to all transitions other than the radiative return of the system to the ground state. For an infinite lifetime of the exciton there will be no absorption at all, no matter how large the value of the oscillator strength of an elementary crystal cell, while the dispersion in this case may be large.[2] Since in the earlier papers the lifetime of the exciton was assumed to be infinite, we were able to calculate in those papers only the dispersion of light, but not its absorption. In the present paper we shall take into account the finite lifetime of the exciton, which will enable us to obtain general formulas for the absorption and corrections to the formulas for the dispersion previously obtained.

In proceeding to set up the Hamiltonian for the system we note that we should not introduce the concept of the dielectric constant of the crystal, since this concept itself is going to be re-examined. Therefore we treat the crystal as a collection of electrons and nuclei interacting with the electromagnetic field in vacuo. The electromagnetic wave perturbing the crystal is assumed to contain many photons and therefore will not be quantized, but will be introduced as a classical perturbing external field defined by a vector potential of the form

$$\mathbf{A} = \mathbf{A}_0 e^{i(\mathbf{k}\cdot\mathbf{r}-\omega t)} + \mathbf{A}_0^* e^{-i(\mathbf{k}\cdot\mathbf{r}-\omega t)}. \qquad (1)$$

The wavelength $2\pi/k$ is assumed to be considerably larger than the lattice constant. $\mathbf{A}$ is assumed to be small and in what follows we take into account effects of order not higher than the first with respect to $\mathbf{A}$.

The operator for the energy of the system may be written in the form $\hat{H} + \hat{W}$; $\hat{H}$ is the usual Schrödinger energy operator for the crystal, consisting of the kinetic energy of the electrons and the nuclei and of the potential energy of their Coulomb (instantaneous) interaction

$$\hat{W} = -\frac{1}{c}\int \hat{\mathbf{P}}\cdot\mathbf{A}\, d\tau = \hat{W}' e^{-i\omega t} + \hat{W}'' e^{i\omega t},$$

where

$$\hat{W}' = -\frac{1}{c}\int \hat{\mathbf{P}}\cdot\mathbf{A}_0 e^{i\mathbf{k}\cdot\mathbf{r}}\, d\tau, \quad \hat{W}'' = -\frac{1}{c}\int \hat{\mathbf{P}}\cdot\mathbf{A}_0^* e^{-i\mathbf{k}\cdot\mathbf{r}}\, d\tau,$$

$$d\tau = dx\, dy\, dz; \tag{2}$$

$\hat{\mathbf{P}}$ is the operator for the dipole moment per unit volume of the dielectric polarization of the crystal (cf. below), while $\hat{\mathbf{P}}$ is the polarization current density. It should be emphasized that the irrotational part of the electric field of the fictitious charges due to the dielectric polarization, E′, represents the Coulomb interaction between the particles of the crystal and, consequently, is contained in $\hat{H}$. E′ should not appear a second time as a perturbation. Thus, **A** describes the macroscopic electric field with the field E′ subtracted.

Let Ψ^0 denote the eigenfunction of $\hat{H}$ which corresponds to the ground state of the crystal, and let $\mathscr{E}^0$ be the energy of the state. This state is not degenerate (we are speaking of a dielectric crystal). Further, let Ψ_m and $\mathscr{E}_m$ be the wave functions and the energies of the excited states of the crystal in the absence of the external perturbation $\hat{W}$. The actually known functions Ψ_m are not exact, but approximate eigenfunctions of $\hat{H}$, since "thermal" transitions between them occur without any external perturbation of the system. Thus, the exciton state, i.e., the excited state which has a single continuous quantum number (the quasi momentum[1]), may as a result of a thermal transition be converted into a "phonon wind" which is a state with many continuous quantum numbers — the momenta of the individual phonons. Thus, the exciton state is only approximately stationary. The same can also be said with respect to the other states appearing in the theory. However, we shall assume that these approximate eigenfunctions of $\hat{H}$ form a sufficiently complete system of orthogonal functions, and this enables us to represent the state of the crystal perturbed by light in the form

$$\Psi = \Psi^0 + \sum_m C_m \Psi_m, \quad |C_m| \ll 1.$$

We assume that the complete dependence on the time is contained in the coefficients C_m. We choose the zero for the energy of the system in such a way that $\mathscr{E}^0 = 0$. Thus, Ψ_0^0 and Ψ_m do not depend on the time. The time-dependent Schrödinger equation leads to the following system of equations for C_m:

$$i\hbar \dot{C}_m = \sum_{m'} H_{mm'} C_{m'} + W_{m0}, \tag{3}$$

where

$$H_{mm'} = \int \Psi_m^* \hat{H} \Psi_{m'}\, d\Omega, \quad W_{m0} = \int \Psi_m^* \hat{W} \Psi^0\, d\Omega,$$

$$d\Omega = \prod_i dx_i\, dy_i\, dz_i. \tag{4}$$

The macroscopic average specific dipole moment due to the dielectric polarization of the crystal can be calculated by means of the formula

$$\mathbf{P}(\mathbf{r}) = \int \Psi^* \Psi \hat{\mathbf{P}}(\mathbf{r})\, d\Omega, \tag{5}$$

where

$$\hat{\mathbf{P}}(\mathbf{r}) = \sum_i e_i (\mathbf{r}_i - \mathbf{r})\, D(\mathbf{r}_i - \mathbf{r}),$$

$$D(\mathbf{r}) = D(xyz) = \begin{cases} 1 & \text{in the range } -1/2 \leqslant x, y, z \leqslant 1/2 \\ 0 & \text{elsewhere} \end{cases} \tag{6}$$

The summation is taken over all the particles of which the crystal is composed; i denotes the particle, e_i denotes its charge, $\mathbf{r}_i$ denotes its coordinate $\mathbf{r}$ is the coordinate of the macroscopic point in the crystal at which the value of the specific dipole moment is evaluated.

The substitution into (5) of Ψ gives up to terms linear in **A**

$$\mathbf{P}(\mathbf{r}) = \sum_m [C_m \mathbf{P}_m(\mathbf{r}) + C_m^* \mathbf{P}_m^*(\mathbf{r})],$$

$$\mathbf{P}_m(\mathbf{r}) = \int \Psi^{0*} \Psi_m \hat{\mathbf{P}}(\mathbf{r})\, d\Omega. \tag{7}$$

It can be shown in a manner completely analogous to that employed in reference 1 for the transition from the ground to the exciton state, that also in the case of a transition to an arbitrary state with quasi-momentum $\mathbf{f}$, i.e., to a state which possesses the translation property $T_{\mathbf{n}}\Psi_m = e^{i\mathbf{f}\cdot\mathbf{n}}\Psi_m$ ($\mathbf{n}$ is the integral lattice vector), one obtains

$$\mathbf{P}_m(\mathbf{r}) = e^{i\mathbf{f}\cdot\mathbf{r}} \mathbf{P}_m(0), \quad \text{if } |\mathbf{f}a_j| \ll \pi; \tag{8}$$

a_j are the lattice constants, j = 1, 2, 3. The vector $\mathbf{f}$ can be used as one of the quantum numbers of the state m.

On substituting (2) and (8) into (4) we obtain

$$W_{m0} = W'_{m0} e^{-i\omega t} + W''_{m0} e^{i\omega t}, \quad W'_{m0} = -\frac{i\omega_m V}{c} \mathbf{P}_m^*(0)\, \mathbf{A}_0 \delta_{\mathbf{k},\mathbf{f}},$$

$$W''_{m0} = -\frac{i\omega_m V}{c} \mathbf{P}_m^*(0)\, \mathbf{A}_0^* \delta_{-\mathbf{k},\mathbf{f}}. \tag{9}$$

Here we have introduced the notation $\omega_m = \mathscr{E}_m/\hbar$, $V = L^3$, L is the size of the cyclic region in which the wave functions Ψ^0 and Ψ_m have been orthonormalized. Each of the components of the vectors $\mathbf{f}$ and $\mathbf{k}$ is an integral multiple of $2\pi/L$.

In solving the system of equations (3) we first introduce into the right hand side of (3), for the sake of simplicity, only the first of the two terms appearing in expression (9) — the term proportional to $e^{-i\omega t}$. The result due to the second term proportional to $e^{i\omega t}$ we shall add at the very end, ob-

taining it by analogy through the substitutions $\mathbf{A}_0 \to \mathbf{A}_0^*$, $\omega \to -\omega$, $\mathbf{k} \to -\mathbf{k}$.

The main task of this section is the determination of the specific polarization of the crystal by means of formulas (7) and (3). In carrying this out it is important to decide what initial conditions are to be adopted for C_m in solving the system of inhomogeneous equations (3). It might appear to be natural to set $C_m = 0$ at time $t = 0$ at which illumination begins, since the system is still in its ground state at that instant. Then, under the perturbing action of the light, C_m varying in accordance with (3) would increase in absolute value with time which, as usual, means that light is absorbed. The process actually occurs in this way, but only during a very short time. This time is considerably shorter than the duration of experiments on the measurement of light absorption in a crystal under conditions of steady-state illumination. Indeed, the increase in the absolute value of C_m with time in accordance with (7) means that the amplitudes of oscillation of the specific dipole moment $\mathbf{P}(\mathbf{r})$ increase with time. In other words, the polarizability of the crystal varies with time. Evidently such a process does not correspond to the experimental conditions of measurement of the steady-state values of the complex dielectric constant of the crystal.

In order that the polarizability of the crystal not depend on the time, the coefficients C_m in formula (7) must vary in time strictly sinusoidally with a frequency ω. The system of equations (7) and (9) does in fact have such a particular solution. However, in this case the absolute values of all the C_m are constant and, consequently, there is no absorption of light at all. This steady-state solution corresponds to such a state of the system when the crystal as a result of absorbing the incident light is heated to such a high temperature that the rate of radiation of light energy equals the absorption rate; the radiation, of course, may have frequencies different from ω. In such a case the energy and the temperature of the crystal will not vary in time. Such a steady state of the system is characterized by optical crystal constants that remain unchanged with time. But evidently this state also does not correspond to the usual conditions of experimental determination of the complex dielectric constant.

The correct initial conditions for C_m must reflect the fact that the usual experimental measurement of the absorption of light in a crystal is necessarily accompanied by the heating of the crystal by the absorbed light (there is no provision for heat removal). Therefore, there appear in the crystal polarization waves of thermal origin with amplitudes that are not proportional to the field of the perturbing light, but depend on the duration of the preceding illumination. The frequencies of these thermal polarization waves have nothing in common with the frequency of the perturbing light. This thermal part of the polarization is also contained in the right-hand side of formula (7), together with the usual polarization which is synchronized with the oscillations of the perturbing light. For the sake of brevity, we shall call the first and second parts of the polarization "thermal" and "synchronous," respectively. It is possible to describe only the synchronous part of the dielectric polarization by means of a complex dielectric constant.

In proceeding to the formulation of the initial conditions for C_m, we shall divide all the excited states of the crystal into two groups. In the first group we shall include a comparatively small number of states into which the system may make transitions directly from the ground state under the action of light; these are such states m for which W_{m0} is appreciable. The second group will include those states for which W_{m0} is negligibly small, and into which phototransitions from the ground state are forbidden; the system may go over into these states by means of thermal transitions from states of the first group. The majority of the states of the crystal belong to the second group. We shall continue to denote the states of the first group by the subscript m, while we shall introduce the subscript q to denote the states of the second group. Further, we assume that for the states of the first group the coefficients C_m attain a steady state, i.e., begin to vary sinusoidally with time in accordance with

$$C_m = A_m e^{-i\omega t}. \tag{10}$$

after the lapse of a short time since the beginning of illumination.

The terms corresponding to these states in the right-hand side of (7) give rise to the synchronous part of the polarization. With respect to the states of the second group we assume that $C_q = 0$ at $t = 0$. This means that at the initial instant of time the temperature of the crystal was equal to zero. As t increases C_q become different from zero as a result of thermal transitions of the system from states of the first group into states of the second group. This corresponds to the heating of the crystal by the absorbed light. The terms in formula (7) containing the coefficients C_q comprise the thermal part of the polarization.

We shall now obtain the solution of the system of equations (3) which satisfies the conditions for-

mulated above. We choose tentatively basis functions Ψ_m that make the matrix $H_{mm'}$ diagonal in the subspace of the functions of the first group. This may be easily done, since the number of states of the first group is not large. As a result, the equations in (3) assume the form:

$$i\hbar\dot{C}_m = \mathscr{E}_m C_m + \sum_q H_{mq} C_q + W'_{m0} e^{-i\omega t}; \qquad (11)$$

$$i\hbar\dot{C}_q = \mathscr{E}_q C_q + \sum_m H_{qm} C_m. \qquad (12)$$

Since Ψ_m and Ψ_q are approximate eigenfunctions of the operator $\hat{H}$, the nondiagonal matrix elements H_{mq} and $H_{qq'}$ are considerably smaller than the diagonal elements $\mathscr{E}_m$ and $\mathscr{E}_q$. We shall regard the diagonal elements as quantities of zero order of smallness, and the nondiagonal elements as quantities of first order. Then it follows from (11), (12) that C_m are quantities of the zero order and C_q are quantities of the first order. Having in mind the determination of C_m from (11) up to terms of the second order inclusive, it is sufficient to retain in (12) terms of only the first order. Therefore, in (12) we have neglected the term $\sum_{q' \neq q} H_{qq'} C_{q'}$.

On substituting (10) into (12) and on taking into account the initial conditions for C_q, we obtain

$$C_q = (e^{-i\omega t} - e^{-i\omega_q t}) \sum_m H_{qm} A_m / (\hbar\omega - \mathscr{E}_q),$$
$$\omega_q = \mathscr{E}_q / \hbar. \qquad (13)$$

On substituting (10) and (13) into (11) we obtain the system of equations for A_m:

$$(\mathscr{E}_m - \hbar\omega) A_m + \sum_{m'} H^a_{mm'} A_{m'} + W'_{m0} = 0, \qquad (14)$$

where

$$H^a_{mm'} = \sum_q H_{mq} H_{qm'} \frac{1 - \exp\{-i(\omega_q - \omega)t\}}{\hbar\omega - \mathscr{E}_q}. \qquad (15)$$

We transform expression (15) in the following way: we make use of the energy $\mathscr{E}_q$ as one of the quantum numbers of the state q, and we denote the set of the remaining quantum numbers by p. Let $\rho_p(\mathscr{E}_q)\,d\mathscr{E}_q$ be the number of states of the system whose energies are contained within the interval $d\mathscr{E}_q$, while the other quantum numbers are equal to p. Then

$$H^a_{mm'} = \sum_p \int H_{mq} H_{qm'} \times \frac{1 - \exp\{-i(\mathscr{E}_q/\hbar - \omega)t\}}{\hbar\omega - \mathscr{E}_q} \rho_p(\mathscr{E}_q)\, d\mathscr{E}_q. \qquad (16)$$

Here the integral has no singularity at $\mathscr{E}_q = \hbar\omega$. If the quantity $(\mathscr{E}_q/\hbar - \omega)t$ is chosen as the new variable of integration then, for not very small values of t, the limits of integration with respect to the new variable can be replaced by $-\infty$ and $+\infty$. By going over from integration along the real axis to integration in the complex plane over the infinite semicircle lying in the lower half plane, it can be easily shown that the integral of the exponential term vanishes. Then, by returning to integration along the real axis, and by deforming the path of integration below the singular point, we obtain

$$H^a_{mm'} = \sum_p \left\{ P \int \frac{H_{mq} H_{qm'}}{\hbar\omega - \mathscr{E}_q} \rho_p(\mathscr{E}_q)\, d\mathscr{E}_q - i\pi\rho_p(\hbar\omega)\,[H_{mq} H_{qm'}]_{\mathscr{E}_q = \hbar\omega} \right\}, \qquad (17)$$

where P denotes the principal value of the integral. Thus, $H^a_{mm'}$ turns out not to depend on the time, and consequently A_m, defined by (14), also turn out to be constant.

In solving (14) in the zeroth approximation we omit the sums containing nondiagonal elements $H^a_{mm'}$. We then introduce these sums as small perturbations and obtain in the next approximation:

$$A_m = -\frac{1}{\mathscr{E}_m + H^a_{mm} - \hbar\omega} \left[W'_{m0} - \sum_{m'}{}' \frac{H^a_{mm'} W'_{m'0}}{\mathscr{E}_{m'} + H^a_{m'm'} - \hbar\omega} \right] \qquad (18)$$

(the prime on the summation sign denotes that the term $m' = m$ should be omitted).

The error in the values of A_m obtained in this manner is of order of magnitude of $(H^a_{mm'})^2$, i.e., $(H_{mq})^4$.

The solutions (10) and (18) have been obtained for the case when in (3) we have taken in place of W_{m0} only the first of the two terms in (9). It is now necessary to take the second term of (9) and to solve the system (3) with this term included. This solution can be immediately written down by analogy with the preceding one: we replace in (10) and (18) ω by $-\omega$, $\mathbf{k}$ by $-\mathbf{k}$, $\mathbf{A}_0$ by $\mathbf{A}_0^*$ and W'_{m0} by W''_{m0}. The final expression for C_m is given by the sum of the two solutions given above. If the values of C_m obtained in this way are substituted into (7), the latter will give the desired specific polarization of the crystal.

In carrying out these calculations it is necessary to keep in mind the following: (1) $W'_{m0} \neq 0$ only if the quasi-momentum of the state m is $\mathbf{f}_m = \mathbf{k}$; $W''_{n0} \neq 0$, only if $\mathbf{f}_m = -\mathbf{k}$; (2) if Ψ_m is an eigenfunction of $\hat{H}$ which corresponds to the quasi-momentum $\mathbf{f}_m = \mathbf{k}$, then $\Psi_n = \Psi_m^*$ is also an eigenfunction of $\hat{H}$ and corresponds to same energy $\mathscr{E}_n = \mathscr{E}_m$, but does not correspond to the quasi-momentum $\mathbf{f}_n = -\mathbf{k}$; (3) since Ψ_0 is assumed to be nondegenerate, it can be considered real. Therefore, in accordance with (7), $\mathbf{P}_n(\mathbf{r}) = \mathbf{P}_m^*(\mathbf{r})$, while in accordance with (9) $W''_{n0} = -W'^*_{m0}$; (4) in accordance with the law of conservation of

quasi-momentum, $H_{mq} \neq 0$ only if the states m and q have the same quasi-momenta: $\mathbf{f}_m = \mathbf{f}_q$; violations of this rule are possible if the crystal contains defects (impurities); (5) if we introduce the notation

$$H^b_{mm'} = -\sum_q H_{mq} H_{qm'} / (\hbar\omega + \mathscr{E}_q), \tag{19}$$

it can be shown that $H^b_{nn'} = H^{b*}_{mm'}$.

By taking into account these remarks we can express the synchronous part of the specific polarization in the following way:

$$\mathbf{P}(\mathbf{r}) = \mathbf{P}_0 e^{i(\mathbf{k}\cdot\mathbf{r}-\omega t)} + \mathbf{P}_0^* e^{-i(\mathbf{k}\cdot\mathbf{r}-\omega t)}, \quad \mathbf{P}_0 = \beta \mathbf{E}_0^{\text{ext}}, \tag{20}$$

where $\mathbf{E}_0^{\text{ext}}$ is the amplitude of the intensity of the external part of the electric field:

$$\mathbf{E}^{\text{ext}} = -\frac{1}{c}\dot{\mathbf{A}} = \mathbf{E}_0^{\text{ext}} e^{i(\mathbf{k}\cdot\mathbf{r}-\omega t)} + \mathbf{E}_0^{*\text{ext}} e^{-i(\mathbf{k}\cdot\mathbf{r}-\omega t)},$$
$$\mathbf{E}_0^{\text{ext}} = \frac{i\omega}{c}\mathbf{A}_0. \tag{21}$$

The complex tensor β is expressed in the following way:

$$\beta = \sum_m [1/(\mathscr{E}_m + H^a_{mm} - \hbar\omega) - 1/(\mathscr{E}_m + H^b_{mm} + \hbar\omega)]\, a_{mm}/\omega$$
$$- \sum_{m,m'}{}' [H^a_{mm'}/(\mathscr{E}_m + H^a_{mm} - \hbar\omega)(\mathscr{E}_{m'} + H^a_{m'm'} - \hbar\omega)$$
$$- H^b_{mm'}/(\mathscr{E}_m + H^b_{mm} + \hbar\omega)$$
$$\times (\mathscr{E}_{m'} + H^b_{m'm'} + \hbar\omega)]\, a_{mm'}/\omega, \tag{22}$$

where $a_{mm'}$ is a tensor of the second rank in three-dimensional coordinate space. This tensor is determined by the relations

$$\mathbf{P}_m(0)\, W'_{m'0} \equiv -\frac{i}{c} a_{mm'} \mathbf{A}_0$$
$$\text{or } (a_{mm'})_{xy} = \omega_{m'} V (\mathbf{P}_m(0))_x (\mathbf{P}^*_{m'}(0))_y. \tag{23}$$

In formula (22), and also everywhere in the following, the subscripts m and m′ denote only those states of the first group for which $\mathbf{f}_m = \mathbf{f}_{m'} = \mathbf{k}$.

In (22) the second term (containing the double summation) is a small correction to the first term. However, if for any two states m and m′ $\mathscr{E}_m = \mathscr{E}_{m'}$ then for $\hbar\omega \approx \mathscr{E}_m$ the corresponding term in the double sum ceases to be small in comparison with the first term. This difficulty can be avoided if in the choice of the basis states of the first group the functions Ψ_m and $\Psi_{m'}$ are replaced by their linear combinations chosen in such a way that $H^a_{mm'} = 0$. Then the "dangerous" term disappears from the double sum.

It should be emphasized that, generally speaking, it is not possible to identify $\mathbf{E}^{\text{ext}}$ with the total macroscopic field $\mathbf{E}$. As we have already explained earlier, the vector potential $\mathbf{A}$ describes the macroscopic field from which we have subtracted the field $\mathbf{E}'$ produced without retardation by the fictitious charges of the dielectric polarization. The field $\mathbf{E}'$ is the field of the Coulomb interaction of the parts of the system; it has already been included in $\hat{H}$ and should not appear a second time as a perturbation. Thus, the second of equations (20) can be re-written

$$\mathbf{P}_0 = \beta(\mathbf{E}_0 - \mathbf{E}'_0). \tag{24}$$

On the other hand, as is well known, the field of the fictitious charges of the dielectric polarization can be expressed in the following way:

$$\mathbf{E}'_0 = -4\pi(\mathbf{P}_0 \cdot \mathbf{s})\,\mathbf{s}, \tag{25}$$

where $\mathbf{s} = \mathbf{k}/k$ is the unit vector normal to the wave front. By eliminating $\mathbf{E}'_0$ from (24) and (25) we obtain the usual expression for the specific polarization in terms of the total macroscopic electric field:

$$\mathbf{P}_0 = \varkappa \mathbf{E}_0, \quad \varkappa = (1 - 4\pi\beta\zeta)^{-1}\beta. \tag{26}$$

Here $\zeta = \overline{\mathbf{ss}}$ is a tensor in three-dimensional coordinate space; its components have the form: $\zeta_{xy} = s_x s_y$. Such a tensor is called a dyad; we shall denote the dyadic product by a bar over both letters.

If into the expression (26) for $\varkappa$ we substitute β from (22), and if we expand the resulting function into partial fractions of the form $C_i/(K_i - \hbar\omega)$, then $\varkappa$ assumes its traditional form:

$$\varkappa = \sum_i C_i/(K_i - \hbar\omega). \tag{27}$$

But the parameters K_i occurring in the dispersion formula, generally speaking, do not coincide with the energy levels of the system $\mathscr{E}_m$ even when the small quantities $H^a_{mm'}$ and $H^b_{mm'}$ are neglected. The relation between K_i and $\mathscr{E}_m$ can be obtained if we actually carry out the expansion mentioned above of $(1 - 4\pi\beta\zeta)^{-1}\beta$ into partial fractions, which is possible in practice only in the simplest cases (cf. the next section of this paper). For a special form of excitons — polarization oscillations of the ionic lattice — such a relationship has been established by the author jointly with Krivoglaz.[3]

In concluding this section we generalize the results obtained above to the case of a field which has an arbitrary spatial variation, but which, as before, oscillates in time harmonically at a frequency ω:

$$\mathbf{E} = \mathbf{f}(\mathbf{r})\, e^{-i\omega t} + \mathbf{f}^*(\mathbf{r})\, e^{i\omega t},$$
$$\mathbf{P} = \mathbf{g}(\mathbf{r})\, e^{-i\omega t} + \mathbf{g}^*(\mathbf{r})\, e^{i\omega t}. \tag{28}$$

To do this we expand the field and the polarization into Fourier series of the form

$$\mathbf{f}(\mathbf{r}) = \sum_{\mathbf{k}} \mathbf{E}_{\mathbf{k}} e^{i\mathbf{k}\cdot\mathbf{r}}, \quad \mathbf{g}(\mathbf{r}) = \sum_{\mathbf{k}} \mathbf{P}_{\mathbf{k}} e^{i\mathbf{k}\cdot\mathbf{r}},$$

$$\text{where } \mathbf{P}_{\mathbf{k}} = \varkappa(\mathbf{k})\,\mathbf{E}_{\mathbf{k}}. \tag{29}$$

Here $\kappa(\mathbf{k})$ is defined by formulas (26) and (22). We assume that $\kappa(\mathbf{k})$ is an analytic function. Then $\kappa(\mathbf{k})\, e^{i\mathbf{k}\cdot\mathbf{r}} = \hat{\kappa}(-i\nabla)\, e^{i\mathbf{k}\cdot\mathbf{r}}$. Consequently, we obtain from (29)

$$\mathbf{g}(\mathbf{r}) = \hat{\varkappa}(-i\nabla)\,\mathbf{f}(\mathbf{r}). \tag{30}$$

It was assumed earlier that the propagation vector of the perturbing light $\mathbf{k}$ in formula (1) is real. In the case when it is complex (damped wave) it may be easily shown by using the general formula (30) that all the results obtained above remain valid, only the complex value of $\mathbf{k}$ should be substituted into them.

Formulas (22), (24), and (26) in principle completely determine the dispersion and the absorption of an electromagnetic wave in a crystal.

2. LIMITING TRANSITION TO MACROSCOPIC ELECTRODYNAMICS

In this section we consider the case of an isolated absorption band, i.e., the case when in the single sum of expression (22) one term predominates over all the others. This may occur either if the coefficient a_{mm} in one of the terms is considerably larger than in the others, or if the value of ω is such that the denominator of one of the terms is close to zero.

It is evident that this is possible only if in (22) $\sum_{m}$ is a discrete sum and not an integral, i.e., if $\mathbf{f}_m = \mathbf{k}$ is the only continuous quantum number that determines the energy $\mathscr{E}_m$; all the other quantum numbers in the expression for $\mathscr{E}_m$ must be discrete. Such states were denoted in reference 1 as exciton states.

By retaining only the dominant term in (22) we obtain

$$\beta = \frac{\overline{Q\mathbf{x}\mathbf{x}^*}}{\mathscr{E} + H^a - \hbar\omega}, \qquad Q \equiv \frac{\omega_m}{\omega} V |\mathbf{P}_m(0)|^2,$$

$$\mathbf{x} \equiv \frac{\mathbf{P}_m(0)}{|\mathbf{P}_m(0)|} \tag{31}$$

(for the sake of brevity we have omitted the subscript m). If we assume the exciton lifetime to be infinite, i.e., if we neglect the small term H^a, (31) coincides with the principal result of reference.[1]

The limiting transition to macroscopic electrodynamics reduces to the assumption that the electric field varies very smoothly in space, i.e., $k \to 0$. It is necessary to require that in this case the magnitude of κ defined by formula (26) should not depend on the direction of $\mathbf{s}$, since the macroscopic specific polarizability tensor should not depend on the direction of incidence of the wave.

It is well known that an arbitrary function of a product of dyads has the following property:

$$F(\overline{\mathbf{x}\mathbf{x}^*}\,\overline{\mathbf{s}\mathbf{s}})\,\overline{\mathbf{x}\mathbf{x}^*} = F(\cos^2\alpha)\,\overline{\mathbf{x}\mathbf{x}^*}, \tag{32}$$

where α is the angle between $\mathbf{x}$ and $\mathbf{s}$. Therefore substitution of (31) into the second of formulas (26) leads to the following result:

$$\varkappa = \left(1 - \frac{4\pi Q\cos^2\alpha}{\mathscr{E} + H^a - \hbar\omega}\right)^{-1} \frac{Q\overline{\mathbf{x}\mathbf{x}^*}}{\mathscr{E} + H^a - \hbar\omega}$$

$$= \frac{Q\overline{\mathbf{x}\mathbf{x}^*}}{\mathscr{E} - 4\pi Q\cos^2\alpha + H^a - \hbar\omega}. \tag{33}$$

By identifying this result with expression (27) and by assuming that $\omega_m/\omega \approx 1$, and therefore by neglecting the dependence of Q on ω we obtain

$$K = \mathscr{E} - 4\pi Q\cos^2\alpha + H^a, \quad C = Q\overline{\mathbf{x}\mathbf{x}^*}. \tag{34}$$

As we have already explained previously, K should not depend on the direction of $\mathbf{s}$, i.e., on α. Then it follows from formula (34) that

$$\mathscr{E} = \mathscr{E}_0 + 4\pi Q\cos^2\alpha. \tag{35}$$

Here $\mathscr{E}_0$ does not depend on the direction of $\mathbf{s}$. Strictly speaking, $\mathscr{E}$ takes on the meaning of exciton energy only if its lifetime is infinite, i.e., when $H^a = 0$. Formula (35) shows that when $\mathbf{f} = \mathbf{k} \to 0$ the energy of the exciton depends on the direction of $\mathbf{f}$, since α is the angle between $\mathbf{f}$ and $\mathbf{x}$. Thus, regarded as a function of the three variables f_x, f_y, f_z, β (but not κ) has a discontinuity at the point $\mathbf{f} = 0$. This, of course, does not exclude the possibility that, for a given direction of $\mathbf{f}$, $\mathscr{E}$ is an analytic function in $|\mathbf{f}|$. The conclusion with respect to the discontinuity in $\mathscr{E}(\mathbf{f})$ follows only if $Q \neq 0$, i.e., $\mathbf{P}_m(0) \neq 0$. Phototransitions are allowed specifically into such states m.

We have already derived Eq. (35) earlier[4] by a completely independent method (by means of a direct calculation of the exciton energy bearing no relation to the theory of dispersion and absorption). In the same paper we have considered cases when in virtue of a definite crystal symmetry the excited state of an elementary crystal cell is degenerate. For such cases we had obtained a generalization of formula (35).

We can now rewrite formula (27) in the form

$$\varkappa = C/(\mathscr{E}_0 + H^a - \hbar\omega), \tag{36}$$

where in H^a we can neglect the first real term of the two terms of expression (17), since it is small in comparison with the other real terms of the denominator. The second term of expression (17)

must be retained since it determines the imaginary part of κ. Formula (36) shows that the region of light absorption, i.e., the region where the real part of κ is important is determined by the relation $\hbar\omega \simeq \mathscr{E}_0$, and not by the usual Bohr frequency formula $\hbar\omega \approx \mathscr{E}$. This is not surprising, since in the preceding section of this article in formulating the initial conditions for C_m and C_q it was explained that the exciton state m under discussion, being a state of the first group, is only an intermediate state in the process of photoexcitation of states of the second group q. Formula (13) shows that only those coefficients C_q will increase monotonically with time which correspond to states of energy $\mathscr{E}_q = \hbar\omega$. Thus the Bohr frequency formula is satisfied for phototransitions into states of the second group which give rise to absorption.

From what has been said above it follows that an experimental investigation of the frequency ω for which the absorption is a maximum allows us to determine, by means of the relation $\hbar\omega = \mathscr{E}_0$, the magnitude of $\mathscr{E}_0$ which, generally speaking, in less than the exciton energy $\mathscr{E}$, since Q is positive in (35). $\mathscr{E}_0$ coincides with the exciton energy only if $\mathbf{s}$ is normal to $\mathbf{x}$.

3. PLANE ELECTROMAGNETIC WAVE. DETERMINATION OF THE INDICES OF REFRACTION

Turning from the case of vanishingly small values of $\mathbf{k}$ to the case of non-zero finite values of $\mathbf{k}$, it should be emphasized that the tensor κ will now depend both on the absolute value and on the direction of the vector $\mathbf{k}$. Whereas in the limiting case $\mathbf{k} \to 0$, the description of the polarization by means of the tensor κ was simpler than by means of the tensor β, since κ did not depend on $\mathbf{k}$ at all, while β depended on the direction of $\mathbf{k}$, now this technical advantage of κ disappears. Now it seems to be more appropriate to describe the polarization by means of the tensor β, since the latter, in accordance with (31), is expressed in terms of the exciton energy $\mathscr{E}(\mathbf{f})$ — a quantity that determines many other phenomena in the crystal. One could try to determine κ without introducing the Hamiltonian for the system; the dependence of κ on $\mathbf{k}$ for the case of small $\mathbf{k}$ can be phenomenologically given in the form of an expansion (polynomial) in k_x, k_y, k_z, as has been done by Ginzburg.[5] But in this case the expansion coefficients remain as unknown parameters in the theory; it is not clear how they could be calculated or related to other physical phenomena. It is particularly inconvenient that the dependence of κ on ω remains completely undetermined. In the present paper we do therefore not make use of the phenomenological method referred to above, but retain the quantum-mechanical discussion utilized in our original papers.[1,2]

We assume that there are no external charges introduced into the crystal which would give rise to an external irrotational field; the only contribution to the irrotational part of the field is made by the field of the fictitious charges of dielectric polarization $\mathbf{E}'$. Then the whole external field $\mathbf{E}^{ext}$ can be obtained as the rotational part of the total macroscopic field $\mathbf{E}$. In the plane-wave case under consideration this corresponds to the following relation between the amplitudes of the fields:

$$\mathbf{E}_0^{ext} = \eta_l \mathbf{E}_0, \text{ where } \eta_{xy} = \delta_{xy} - s_x s_y. \qquad (37)$$

In the first section of this article $\mathbf{E}^{ext}$ was introduced as a given external perturbation. The wave vector $\mathbf{k}$ appeared in it as a given parameter of the perturbing field. It is now necessary to make this perturbing field self-consistent, i.e., to ensure by means of a suitable choice of $\mathbf{k}$ that this field satisfies the system of Maxwell's equations. If we assume, as usual, that the electric field, the displacement, and the magnetic field are proportional to $e^{i(\mathbf{k}\cdot\mathbf{r}-\omega t)}$, where $\mathbf{k} = (\omega n/c)\mathbf{s}$, while n is the index of refraction for the wave, then the system of Maxwell's equations reduces to the following relations:

$$\mathbf{D}_0 = n^2[\mathbf{E}_0 - \mathbf{s}(\mathbf{s}\cdot\mathbf{E}_0)] \equiv n^2\eta_l\mathbf{E}_0,$$
$$\mathbf{D}_0 = \gamma\mathbf{E}_0, \quad \gamma = 1 + 4\pi\beta\eta_l. \qquad (38)$$

One should not identify γ with the usual dielectric constant, since it depends not only on ω but also on the direction of wave propagation $\mathbf{s}$. Moreover, β depends on $\mathbf{f} = \mathbf{k} = (\omega n/c)\mathbf{s}$. Thus γ is a function of the index of refraction n. In this respect Eq. (22) significantly differs from the usual dispersion formula.

If we eliminate $\mathbf{D}_0$ from the system (38) we obtain a system of linear homogeneous equations for the components of $\mathbf{E}_0$. The condition that it have a solution has exactly the same form as in reference 1:

$$(\mathbf{s}, \gamma\mathbf{s})n^4 + [(\mathbf{s}, \gamma^2\mathbf{s}) - (\mathbf{s}, \gamma\mathbf{s})\,\mathrm{Sp}\,\gamma]n^2 + \begin{vmatrix} \gamma_{xx} & \gamma_{xy} & \gamma_{xz} \\ \gamma_{yx} & \gamma_{yy} & \gamma_{yz} \\ \gamma_{zx} & \gamma_{zy} & \gamma_{zz} \end{vmatrix} = 0. \qquad (39)$$

In the usual crystal optics the corresponding equation is a quadratic in n^2; it determines two values of n^2 (double refraction). But in the theory under discussion γ is itself a function of n. Therefore (39) is an equation of higher order with respect to n, it determines not two but more values of n^2,

and the same number of solutions of Maxwell's equations having the form of a plane wave.

We further consider the case when $\hbar\omega$ approaches one of the exciton energy levels $\mathscr{E}_m = \mathscr{E}_0$. Then we can pick out from (22) the term which "resonates," i.e., which has the small denominator $\mathscr{E}_m + H^a_{mm} - \hbar\omega$. This term varies rapidly with ω. We denote the sum of all the remaining terms by β'; it is a slowly varying function of ω and in the region $\hbar\omega \approx \mathscr{E}_m$ can be approximately regarded as a constant. β', generally speaking, is complex, and its imaginary part is a quantity of the second order of smallness. Formula (22) can now be simplified:

$$\beta = \beta' + (Q\overline{\mathbf{x}\mathbf{x}}^* + \alpha)/(\mathscr{E}(\mathbf{k}) + H^a - \hbar\omega),$$

$$\alpha = \sum_{m'}{}'(H^a_{mm'}a_{mm'} + H^a_{m'm}a_{m'm})/\omega(\mathscr{E}_{m'} - \mathscr{E}_m). \qquad (40)$$

Here the summation over m' is taken over all the states except the "resonating" m-th state. Of course, β' and α depend on the direction of wave propagation $\mathbf{s}$.

We assume that for a given direction $\mathbf{k}$ the expansion of $\mathscr{E}(\mathbf{k})$ in powers of k is of the following form:

$$\mathscr{E}(k) = \mathscr{E}_s + \hbar^2k^2/2M_s + \ldots \qquad (41)$$

Here $\mathscr{E}_\mathbf{s}$ and $M_\mathbf{s}$ do not depend on k, but depend on the direction of $\mathbf{k}$, i.e., on $\mathbf{s}$. In the case of an isolated exciton absorption band the dependence of $\mathscr{E}_\mathbf{s}$ on $\mathbf{s}$ is given by formula (35). We shall call $M_\mathbf{s}$ the effective mass of the exciton in the direction $\mathbf{s}$.

If we introduce the notation

$$\gamma' = 1 + 4\pi\beta'\eta, \quad \mu_s = \frac{2M_sc^2}{\hbar\omega}\left(1 - \frac{\mathscr{E}_s + H^a}{\hbar\omega}\right),$$

$$B_s = \frac{8\pi M_sc^2}{\hbar^2\omega^2}[Q\overline{\mathbf{x}\mathbf{x}}^* + \alpha], \qquad (42)$$

then the result of substituting (31) into the expression (38) for γ can be rewritten

$$\gamma = \gamma' + B_s\eta/(n^2 - \mu_s). \qquad (43)$$

This formula differs from the corresponding formula of reference 1 only by the fact that the expression for $\mu_\mathbf{s}$ has acquired in addition to $\mathscr{E}_\mathbf{s}$ the complex term H^a, while the expression for $B_\mathbf{s}$ has acquired the complex additional term α.

If we assume that the exciton lifetime is infinite ($H^a = 0$, $\alpha = 0$), then (42) and (43) reduce exactly to the corresponding equations of reference 1, and yield all the subsequent results of references 1 and 2, subject to the restrictions that follow from reference 4 (cf. also the end of this paper). As has been explained in references 1 and 2, in the case of an infinite exciton lifetime dispersion of light will occur, but there will be no absorption. Thus, absorption appears as a result of taking into account the finite exciton lifetime, which leads to the appearance of additional complex terms H^a and α in the quantities $\mu_\mathbf{s}$ and $B_\mathbf{s}$. As a result, n also acquires an additional complex term, as can be seen from the expressions for n^2, given in references 1 and 2. The formulas derived in references 1 and 2, which express n^2 in terms of $\mu_\mathbf{s}$ and $B_\mathbf{s}$, remain valid, but since $\mu_\mathbf{s}$ and $B_\mathbf{s}$ become complex these formulas begin to describe the case of an absorbing crystal.

The imaginary part of n determines, in a well known way, the damping of a monochromatic wave in space. But, as has been shown in reference 1, several plane waves arise simultaneously in a crystal, each with its own index of refraction and damping coefficient. These waves are coherent and therefore cannot be investigated independently of each other. The total intensity of light is spatially damped nonexponentially. Therefore, strictly speaking, the phenomenological concept of the coefficient of light absorption (the coefficient in the exponential expression for the spatial damping of light intensity) loses its meaning. But the quantities actually measured by experimenters in investigations of light absorption in crystals completely retain their meaning. These include, for example, the reduction in the intensity of light in passing through a plane parallel plate. This can be easily calculated with the aid of the formulas of Sec. 3 of reference 2, provided we introduce the already-mentioned complex terms added to the indices of refraction in the case of a finite exciton lifetime. This will be done in a later paper. In another paper we shall also obtain expressions for H^a and α for specific exciton models.

4. LONGITUDINAL WAVES

Let us investigate the solution of the time-dependent Schrödinger equation for a crystal in the absence of an external perturbing field, i.e., when $\mathbf{A}(\mathbf{r}, t) = 0$. The problem reduces to the solution of the system of equations (11), (12) with $W'_{m0} = 0$. We shall, as before, seek the solutions for C_m in harmonic form (10), but for the coefficients A_m we shall obtain in place of (14) the following system of equations:

$$[\mathscr{E}_m(\mathbf{f}) - \hbar\omega]A_m + \sum_{m'}H^a_{mm'}(\mathbf{f})A_{m'} = 0. \qquad (44)$$

By setting the determinant of this system equal to zero we obtain the values of $\omega(\mathbf{f})$, i.e., the fre-

quencies of the characteristic polarization oscillations of the crystal. By finding, for each root $\omega(\mathbf{f})$ in (44), the coefficients A_m and substituting them into (10), we obtain the corresponding C_m. If these C_m are substituted into (7), and if (8) is taken into account, the following expression is obtained for the polarization eigenwave in the crystal:

$$\mathbf{P}(\mathbf{r}, t) = \mathbf{P}_0 e^{i(\mathbf{f}\cdot\mathbf{r}-\omega t)} + \mathbf{P}_0^* e^{-i(\mathbf{f}\cdot\mathbf{r}-\omega t)};$$

$$\mathbf{P}_0 = \sum_m A_m \mathbf{P}_m(0), \quad \omega = \omega(\mathbf{f}). \tag{45}$$

This result is obtained on the basis of Schrödinger's equation, but without taking into account Maxwell's equations. Therefore, it is now necessary to determine the additional limitations imposed by the latter.

It is clear that if the vector $\mathbf{P}_0$ is not parallel to $\mathbf{f}$, the polarization wave (45) will give rise to a magnetic field and, consequently we shall have $\mathbf{A}(\mathbf{r}, t) \neq 0$. This contradicts the initial assumption of this section of the present article, violates the result (45), and brings us back to the case discussed in the preceding sections. But if the vector $\mathbf{P}_0$ is parallel to $\mathbf{f}$, then in this case, according to Maxwell's equations, the polarization wave (45) will give rise only to an irrotational electric field $\mathbf{E}'$ which is produced without retardation by the fictitious charges of the dielectric polarization, and which is equal to

$$\mathbf{E}' = -4\pi\mathbf{P}. \tag{46}$$

Maxwell's equations will all be satisfied if, in addition to (46), we set

$$\mathbf{D} = \mathbf{H} = \mathbf{E}_\perp = \mathbf{A} = 0, \tag{47}$$

Thus, the solution (45) — (47) satisfies both the Schrödinger equation and Maxwell's equations. It represents a plane longitudinal wave of the electric field $\mathbf{E}'$ and of the polarization. In this case even though $\mathbf{E}'$ is a macroscopic field, it nevertheless represents the Coulomb interaction of the charges of which the crystal is composed and which, consequently, appears in $\hat{H}$, and not in the perturbing operator $\hat{W}$.

The condition $\mathbf{P}_0 \| \mathbf{f}$ determines those directions of $\mathbf{f}$ for which longitudinal waves occur. The number of such direction increases as the symmetry of the crystal becomes higher. It can be shown that, say in a cubic crystal, longitudinal waves can be propagated in an arbitrary direction (it is assumed that the wavelength is considerably greater than the lattice constant).

In the limiting case of long waves it is possible to introduce the concept of the usual macroscopic dielectric constant. In the case of longitudinal waves the latter is equal to zero, since $\mathbf{D} = 0$, while $\mathbf{E} \neq 0$.

It is not difficult to understand why (45) cannot be obtained as one of the solutions of equations (39) and (43). The point is that (39) was obtained as the condition for the existence of such solutions of equations (38) for which $\mathbf{D}$ and $\mathbf{E}_\perp$ differ from zero. But in the case of a longitudinal wave we have just the case $\mathbf{D} = 0$, $\mathbf{E}_\perp = 0$. Therefore the index of refraction of the longitudinal wave does not have to satisfy Eq. (39).

In the case when the system of equations (44) reduces to only one equation (nondiagonal elements of the matrix $H^a_{mm'}$ are neglected and an isolated excited level $\mathscr{E}_m = \mathscr{E}(\mathbf{f})$ is assumed), of the form

$$[\mathscr{E}(\mathbf{f}) + H^a(\mathbf{f}) - \hbar\omega] A_m = 0,$$

we obtain

$$A_m \neq 0, \quad \text{if} \quad \hbar\omega = \mathscr{E}(\mathbf{f}) + H^a(\mathbf{f}). \tag{48}$$

Since H^a is complex (48) means that, for real $\mathbf{f}$, ω is complex. This means that the polarization oscillation will be undamped in space but damped in time; its energy will be converted into the energy of excitation of states q of the second group. But it is possible, on assuming a real value of ω, to obtain a complex $\mathbf{f}$ from (48). We then obtain a polarization oscillation which is stationary in time, but damped in space. Such an oscillation may exist, for example, on the surface of a crystal and be damped out with penetration into the crystal; it is maintained in the steady state by an electromagnetic wave that enters the crystal from the vacuum.

In the case of the limiting transition to the infinite lifetime of the excited state, when $H^a \to 0$, (48) reduces to the corresponding result of reference 1.

In conclusion we note a certain omission made in reference 1. In that paper we have uncritically followed other authors by assuming that the exciton energy $\mathscr{E}(\mathbf{k})$ is an analytic function of the components of the quasi-momentum k_x, k_y, k_z, and we expanded $\mathscr{E}(\mathbf{k})$ in powers of these three arguments. But in our subsequent paper[4] it is shown that the interaction of crystal cells situated far from each other, an interaction due to the irrotational part of the electric field accompanying the exciton wave, gives a finite contribution to the exciton energy $\mathscr{E}(\mathbf{k})$. This additional term is a discontinuous function of k_x, k_y, k_z: its value at $\mathbf{k} = 0$ depends on the direction of the vector $\mathbf{k}$, when its modulus tends to zero. Therefore, the expansion used in reference 1 is not justified. In this paper we use, in place of the foregoing expansion, an expansion in terms of $|\mathbf{k}|$ [Eq. (41)] and

it is emphasized that $\mathscr{E}_{\mathbf{s}}$ and $M_{\mathbf{s}}$ depend on the direction of propagation of the exciton wave $\mathbf{s}$ in accordance with reference 4. Moreover, we obtain all the basic results of reference 1. But certain specific assertions of reference 1 must be corrected. Thus, it is shown in reference 4 that in cubic crystals the magnitude of $\mathscr{E}_{\mathbf{s}}$ is different for excitons with longitudinal and transverse polarization. $M_{\mathbf{s}}$ may also differ for excitons of these types. The energy bands of excitons with transverse polarization must overlap in pairs (we are referring to exciton states into which phototransitions from the ground state of the crystal are allowed). For each pair of overlapping bands the magnitudes of $\mathscr{E}_{\mathbf{s}}$ must coincide, and must not depend on the direction of $\mathbf{s}$, while the magnitudes of $M_{\mathbf{s}}$ must coincide for two bands only in the directions of the edges and the space diagonals of the basic cube.

[1] S. I. Pekar, J. Exptl. Theoret. Phys. (U.S.S.R.) **33**, 1022 (1957), Soviet Phys. JETP **6**, 785 (1958).

[2] S. I. Pekar, J. Exptl. Theoret. Phys. (U.S.S.R.) **34**, 1176 (1958, Soviet Phys. JETP **7**, 813 (1958).

[3] M. A. Krivoglaz and S. I. Pekar, J. Exptl. Theoret. Phys. (U.S.S.R.) **31**, 343 (1956), Soviet Phys. JETP **4**, 286 (1957).

[4] S. I. Pekar, J. Exptl. Theoret. Phys. (U.S.S.R.) **35**, 522 (1958), Soviet Phys. JETP **8**, 360 (1959).

[5] V. L. Ginzburg, J. Exptl. Theoret. Phys. (U.S.S.R.) **34**, 1593 (1958), Soviet Phys. JETP **7**, 1096 (1958).

Translated by G. Volkoff
77

ON THE SCATTERING MATRIX IN AN INDEFINITE METRIC

L. A. MAKSIMOV

Submitted to JETP editor June 7, 1958

J. Exptl. Theoret. Phys. (U.S.S.R.) 36, 465-473 (February, 1959)

A method is presented which, in theories with indefinite metric, excludes all nonphysical states from the initial and final states of the system. The method is applied to the Lee model and the scalar photon model.

1. In a paper by Heisenberg[1] it has been shown with the Lee model that a theory with an indefinite metric can give physically reasonable results if one adds to the initial states of the physical system a definite amplitude of the nonphysical states. This idea has been developed in a paper by Bogolyubov, Medvedev, and Polivanov,[2] who introduce the requirement that the amplitude of the nonphysical states be chosen in such a way that these states not be scattered (standing-wave condition). The essential defect of the recipe developed in references 1 and 2 is that it explicitly dispenses with macroscopic causality: the preparation of the initial state is dependent on the process to be studied. In the present paper a procedure is proposed which evidently does not have this disadvantage.

We can explain the idea of the paper by the example of rotations in three-dimensional Euclidean space. We shall call the xy plane the physical space (Hilbert space I), and shall call the space which supplements this to make the full three-dimensional space the nonphysical space (Hilbert space II). An arbitrary state is represented by a vector which starts at the origin. The manifold of vectors lying in the xy plane forms the manifold of physical states. The S matrix in the three-dimensional space is represented by a rotation of an arbitrary vector around a certain axis through a definite angle. If the axis is perpendicular to the xy plane, the action of the S matrix does not carry vectors that lie in the xy plane out of this plane. This situation illustrates a quantum theory with a definite metric. In order, however, to escape from divergences one must renounce the orthogonality of the axis of the S matrix to the physical space. But then (see Fig. 1) the action of the S matrix (S rotation) carries vectors out of the xy plane, and projections of vectors onto this plane are not conserved; the S matrix loses its physical meaning.

Following Bogolyubov et al.[2] we can restore the physical meaning of the S matrix (i.e., conserve the length of the projection of a vector onto the xy plane) by choosing for each initial physical state a projection along the z axis such that this projection is not changed in absolute value by the S rotation (Fig. 2).

The transformation $a \to a'$ can be called the S matrix for the physical states. In this example we can clearly see the impossibility of a further rotation $b' \to b''$ without a redefinition of the "ghost" component of the state vector.

The idea of the present work also consists of a transformation from S to another matrix S', but of a different form. We call the matrix

$$S' = U^{-1}SU, \tag{1}$$

the S' matrix for the physical states; the matrix U produces a rotation of the xy plane into the plane perpendicular to the axis of S. It is easy to see that the matrix S' takes physical vectors into physical vectors with preservation of lengths (Fig. 3); the rotation U takes a into b, the rotation S takes b into b', and finally U^{-1} takes b' into a'.

In the general case of an indefinite metric the matrix U is a pseudounitary matrix, which transforms the physical space into an invariant subspace of the matrix S isomorphic to the physical space. In other words, the matrix U produces a transformation of the matrix S to a form in which the matrix elements between physical and nonphysical states are zero. Of course not every matrix S can be transformed to such a form. From the point of view used here, however, this means only that the only theories with indefinite metrics that can

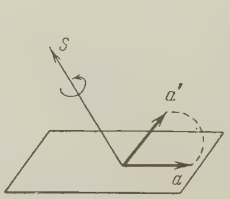

FIG. 1

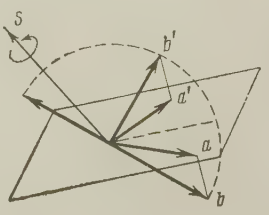

FIG. 2

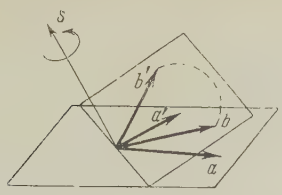

FIG. 3

describe actual processes are those that are such that the transformation U exists.

2. Let us find the equation determining the required pseudounitary transformation for a given form of the S matrix. We find a subspace of states invariant under the transformation S and consisting of vectors of the form

$$\Phi = \begin{pmatrix} F \\ G \end{pmatrix} = \begin{pmatrix} F \\ WF \end{pmatrix}, \tag{2}$$

where the upper row represents the projection onto the physical states, and the lower row the projection onto the space of states supplementing the physical space to the whole space. The transformation S takes the vectors (2) over into vectors of the same form:

$$F_+ = S_{11}F_- + S_{12}WF_-, \tag{3}$$

$$G_+ = WF_+ = S_{21}F_- + S_{22}WF_-, \tag{4}$$

where

$$S_{11} = P_1SP_1,\ S_{12} = P_1SP_2,\ S_{21} = P_2SP_1,\ S_{22} = P_2SP_2, \tag{5}$$

where P_1 and P_2 are operators of projection onto the state-spaces F and G.

Thus the invariant subspace exists if there exists a solution of the equation

$$WS_{11} + WS_{12}W = S_{21} + S_{22}W. \tag{6}$$

If besides this the invariant subspace (2) is a space of vectors with positive norm, then by the pseudounitary transformation U related to W by the equation

$$W = -P_2UP_1 / P_2UP_2 = -U_{21} / U_{22}, \tag{7}$$

it can be transformed into a physical space isomorphic to it, namely

$$U\begin{pmatrix} F \\ WF \end{pmatrix} = \begin{pmatrix} U_{11}F + U_{12}WF \\ 0 \end{pmatrix}. \tag{8}$$

Then it can be verified that the transformation

$$S' = USU^+ \tag{9}$$

takes physical states into physical states. We shall call this transformation the actual S matrix.

The equation (6) is a quadratic equation for the matrix W. It is hard to solve this equation, at least in the general case. In the present paper we succeed in finding the matrix elements of this matrix only for two simple examples — the scattering of a Θ particle by a V particle in the Lee model, and the scattering of a "scalar photon" by an "electron" near the threshold of production of "ghost" states.

3. Let us find the matrix U for the example of the Lee model. In the Lee model one has three particles interacting according to the scheme

$$V \rightleftarrows N + \Theta.$$

Furthermore all the states separate into sectors $(N + z\Theta,\ V + (z-1)\Theta)$, which do not make transitions to each other, so that they can be considered separately. We shall examine the case in which the V particle can exist in two different discrete states, one of which has a negative norm and is called a "ghost" state of the V particle. Repeating the calculation of Heisenberg (Sec. 3.1 of reference 1), we find that the function $\varphi(k)$ which describes the scattering of the Θ particle in the momentum representation obeys the equation [Eq. (68) of reference 1]

$$h^+(E-\omega)\varphi(\omega) = \int_{m_\theta}^{\infty} K(\omega, \omega')\varphi(\omega')\,d\omega + \varphi_{0i}(\omega), \tag{10}$$

where

$$K(\omega, \omega') = -\frac{1}{2}\,\frac{k'}{\omega + \omega' - E - i\gamma}\sqrt{\frac{\omega'}{\omega}},$$

and the function φ_{0i} depends on the initial amplitude of the state $N + 2\Theta$. In what follows we shall for simplicity set $\varphi_{0i} = 0$. The remaining notations are taken from reference 1. The general solution of Eq. (10) has the form (apart from an arbitrary common factor)

$$\varphi(\omega) = \delta(\omega - \omega_p) + x\delta(\omega - \omega_g) + \frac{\chi(\omega)}{h^+(E-\omega)}, \tag{11}$$

where $\omega_{p,g} = E - E_{p,g}$; E_p and E_g are the energies of the physical and ghost states of the V particle. We consider the case $E_p \neq E_g$.

In the stationary theory the S matrix gives the connection between the asymptotic values of converging and diverging waves:

$$\Phi_+ = S\Phi_-. \tag{12}$$

If Φ_+ and Φ_- can be represented in the form

$$\Phi_+ = UF_+,\ \Phi_- = UF_-, \tag{13}$$

where F_+ and F_- are purely physical states and U is a pseudounitary transformation, then, rewriting Eq. (12) in the form

$$F_+ = U^{-1}SUF_-, \tag{14}$$

we get the new scattering matrix

$$S' = U^{-1}SU, \tag{15}$$

which obviously takes physical states into physica states and preserves the norm. We emphasize that from the point of view of the present idea the physical scattering matrix is just the matrix (15), and the matrix (12) is an intermediate stage in the calculation, which is necessary if we wish to keep the old apparatus of the quantum field theory.

The condition (13) means that for the determination of the actual scattering we must choose from among all possible solutions of Eq. (10) those that are transformed by some pseudounitary transformation U^{-1} into expressions that asymptotically do not contain any "ghost" states.

Let us rewrite the function (11) in a form convenient for the pseudounitary transformation. For this purpose we must recall that for the passage to the coordinate representation we have the following correspondence:

$$\delta(\omega - \omega_0) \to \omega_0\left(\frac{1}{r}e^{ik_0 r} - \frac{1}{r}e^{-ik_0 r}\right),$$
$$\frac{1}{2\pi i}\,\frac{1}{\omega - \omega_0 - i\gamma} \to \omega_0\left(\frac{1}{r}e^{ik_0 r}\right). \tag{16}$$

With this in mind, we rewrite Eq. (11) in the form

$$\varphi(\omega) = a'\left[\frac{1}{\omega_p\sqrt{v_p}}\,\delta(\omega - \omega_p)\right]$$
$$+ \chi'_p(\omega)\left[\frac{1}{2\pi i\omega_p\sqrt{v_p}}\cdot\frac{1}{\omega - \omega_p - i\gamma}\right]$$
$$+ b'\left[\frac{1}{\omega_g\sqrt{v_g}}\,\delta(\omega - \omega_g)\right]$$
$$+ \chi'_g(\omega)\left[\frac{1}{2\pi i\omega_g\sqrt{v_g}}\cdot\frac{1}{\omega - \omega_g - i\gamma}\right], \tag{17}$$

$$a' = \omega_p\sqrt{v_p}; \quad b' = x\omega_g\sqrt{v_g}; \quad v_p = k_p/\omega_p; \quad v_g = k_g/\omega_g;$$
$$\chi'_p = \omega_p\sqrt{v_p}g(\omega)\chi(\omega); \quad \chi'_g = -\omega_g\sqrt{v_g}g(\omega)\chi(\omega);$$
$$g(\omega) = 2\pi i\,\frac{(\omega - \omega_p - i\gamma)(\omega - \omega_g - i\gamma)}{(\omega_p - \omega_g)h^+(E - \omega)}; \quad \gamma \to 0. \tag{18}$$

The form (17) is convenient because the coefficients of the square brackets give a direct idea of the fluxes of the converging and diverging waves in the coordinate representation. Writing the expression in columns emphasizes the attribution to different states of the V particle (cf. reference 3). The desired pseudounitary transformation acts on the coefficients of the function (17) and can be represented in the form of a two-rowed pseudounitary matrix:

$$U = \begin{pmatrix} e^{i\alpha}\cosh\theta & e^{i\beta}\sinh\theta \\ e^{i\gamma}\sinh\theta & e^{i\delta}\cosh\theta \end{pmatrix}, \quad \alpha - \beta - \gamma + \delta = 0 \tag{19}$$

We now look for the class of functions (17) which are taken by a transformation of the form (19) into purely physical states at large distances from the origin. This imposes on the amplitudes of the converging and diverging waves the conditions

$$a'e^{i\gamma}\sinh\theta + b'e^{i\delta}\cosh\theta = 0, \tag{20}$$
$$(a' + \chi'_p)e^{i\gamma}\sinh\theta + (b' + \chi'_g)e^{i\delta}\cosh\theta = 0. \tag{21}$$

From this we get

$$\chi'_p(\omega_p)/a' = \chi'_g(\omega_g)/b'$$
$$\text{or} \quad xg(\omega_p)\chi(\omega_p) = -g(\omega_g)\chi(\omega_g). \tag{22}$$

Thus the class of solutions of Eq. (6) in which we are interested has the property that states with different states of the V particle are "scattered" in the same way. This still does not mean the absence of scattering, since there is possible the inelastic process

$$V + \Theta \to N + 2\Theta.$$

The function (11) depends on one parameter x. Equation (22) can be regarded as an equation in the parameter x. Using the integral equation for $\chi(\omega)$,

$$\chi(\omega) = K(\omega, \omega_p) + xK(\omega, \omega_g)$$
$$+ \int K(\omega, \omega')\,\frac{\chi(\omega')}{h^+(E - \omega')}\,d\omega', \tag{23}$$

we rewrite Eq. (22) in the form

$$xg(\omega_p)\left[K(\omega_p, \omega_p) + xK(\omega_p, \omega_g)\right.$$
$$\left. + \int K(\omega_p, \omega')\,\frac{\chi(\omega'; x)}{h^+(E - \omega')}\,d\omega'\right]$$
$$= -g(\omega_g)\left[K(\omega_g, \omega_p) + xK(\omega_g, \omega_g)\right.$$
$$\left. + \int K(\omega_g, \omega')\,\frac{\chi(\omega'; x)}{h^+(E - \omega')}\,d\omega'\right]. \tag{24}$$

By writing $\chi(\omega', x)$ we emphasize the parametric dependence of the solution of Eq. (23) on x. Finding x from Eq. (24), we can recover the form (19) of the matrix, using the condition (20)

$$e^{i(\gamma - \delta)}\tanh\theta = -x\omega_g\sqrt{v_g}/\omega_p\sqrt{v_p}. \tag{25}$$

This equation is solvable if

$$|x| < \omega_p\sqrt{v_p}/\omega_g\sqrt{v_g}. \tag{26}$$

Thus we conclude that in the Lee model one can construct a scheme for calculating final physical states from initial physical states which preserves norms, if among the roots of the equation (24) there are values satisfying the condition (26).

Accordingly, we have shown for the example of the Lee model that under certain conditions the program proposed in Section 1 is feasible. The example considered is, however, a weak one, since in it we deal only with a spherically symmetric,

i.e., a one-dimensional, problem. Therefore it is interesting to examine some other example closer to reality, for instance a model of the type of quantum electrodynamics. Such a model will be considered in the next section.

4. Let us now examine the model in which a spinor field ("electron") interacts with a real scalar field (the "scalar photon"):

$$L = g : \bar{\psi}(x)\varphi(x)\psi(x) :, \tag{27}$$

where the interaction constant is taken to be small.

A Green's function that falls off sufficiently rapidly can be obtained[5] by supposing that the free field obeys an equation containing higher derivatives. For our illustrative purposes it is enough to consider the second-order equation

$$\left(-i\frac{\hat{\partial}}{\partial x}-m\right)\left(-i\frac{\hat{\partial}}{\partial x}-M\right)\psi(x)=0;\ M\gg m \tag{28}$$

(here $\frac{\hat{\partial}}{\partial x}\equiv\sum_{\mu}\gamma^{\mu}\frac{\partial}{\partial x^{\mu}}$), which leads to the Green's function

$$G(p)\sim 1/(\hat{p}-m)(\hat{p}-M). \tag{29}$$

The second-quantized function $\psi(x)$ that leads to the Green's function (29) can be represented as the sum of two fields, one of which satisfies the usual commutation relations, and the other, similar relations, but with the minus sign. This leads to the appearance of states with negative norm, which on physical grounds are not admissible. Thus this model can serve as a simple example of a theory with an indefinite metric, with which one can see the main features of any theory with an indefinite metric.

When a scalar photon is scattered by an electron at energy higher than the threshold, nonphysical states can arise, with the electron in the mass state M, which has a negative norm. Therefore we must consider a state of the form

$$\Phi=(2\pi)^3\left\{\begin{array}{l}\sum\limits_{\nu=1,2}\int dpdk\varphi_{\nu}(p,k)\,b_{\nu}^{*+}(p)\,a^{+}(k)\\ \sum\limits_{\mu=1,2}\int dqdx\psi_{\nu}(q,x)\,c_{\mu}^{*+}(q)\,a^{+}(x)\end{array}\right\}|0\rangle, \tag{30}$$

where $|0\rangle$ is the state function of the vacuum, $a^{+}(k)$ is the operator for creation of a scalar photon,

$$[a^{-}(k),a^{+}(k')]_{-}=\delta(k-k'), \tag{31}$$

$b_{\nu}^{*+}(p)$ is the operator for creation of an electron in a state with rest mass m,

$$[b_{\nu}^{-}(p),b_{\mu}^{*+}(p')]_{+}=\delta_{\mu\nu}\delta(p-p'). \tag{32}$$

$c_{\mu}^{*+}(q)$ is the operator for creation of an electron in a "ghost" state with rest mass M,

$$[c_{\nu}^{-}(q),c_{\mu}^{*+}(q')]_{+}=-\delta_{\mu\nu}\delta(q-q'). \tag{33}$$

We choose the amplitude of the initial physical state in the form

$$\varphi_{\nu}(p,k)=\delta_{\nu\nu_0}\delta(p-p_0)\,\delta(k-k_0). \tag{34}$$

The amplitudes of the "ghost" states are related to the physical states by the required matrix W of Eq. (7):

$$\psi_{\mu}(q,x)=\sum_{\nu=1,2}\int dpdkW_{\mu\nu}(q,x;p,k)\varphi_{\nu}(p,k). \tag{35}$$

Thus the initial state of the system has the form

$$\Phi_{-}=(2\pi)^3\times\left\{\begin{array}{l}b_{\nu_0}^{*+}(p_0)\,a^{+}(k_0)\\ \sum\limits_{\mu_0=1,2}\int dq_0dx_0W_{\mu_0\nu_0}(q_0,x_0;p_0,k_0)\,c_{\mu_0}^{*+}(q_0)\,a^{+}(x_0)\end{array}\right\}|0\rangle. \tag{36}$$

We shall examine the problem in the center-of-mass system, in which the total four-momentum of the system has the form

$$P=p_0+k_0=(E,0). \tag{37}$$

Confining ourselves to the second order of perturbation theory, we write the ordinary S matrix in the form

$$S=1+S^{(2)} \tag{38}$$

so that the final states will have the form

$$\Phi_{+}=\Phi_{-}+\begin{pmatrix}F'_{+}\\ G'_{+}\end{pmatrix}, \tag{39}$$

where

$$\begin{aligned}F'_{+}=&\frac{ig^2}{(2\pi)^2}(2\pi)^3\sum_{\nu=1,2}\int dp_2dk_2a^{+}(k_2)\,b_{\nu}^{*+}(k_2)\\ &\times\left[\frac{1}{\sqrt{2\omega_2}}\frac{1}{\sqrt{2\omega_0}}\bar{u}^{\nu(+)}(p_2)\,Q(mm)\,u^{\nu_0(-)}(p_0)\right.\\ &-\sum_{\mu_0=1,2}\int dq_0dx_0^{\cdot}\frac{1}{\sqrt{2\omega_2 2x_0}}\bar{u}^{\nu(+)}(p_2)\,Q(mM)\,U^{\mu_0(-)}(q_0)\\ &\left.\times W_{\mu_0\nu_0}(q_0x_0;p_0k_0)\right]\delta(p_2+k_2-P)\,|0\rangle;\end{aligned} \tag{40}$$

$$\begin{aligned}G'_{+}=&\frac{ig^2}{(2\pi)^2}(2\pi)^3\sum_{\mu=1,2}\int dq_2dx_2a^{+}(x_2)\,c_{\mu}^{*+}(q_2)\\ &\times\left[\frac{1}{\sqrt{2x_2 2\omega_0}}\bar{U}^{\mu(+)}(q_2)\,Q(Mm)\,u^{\nu_0}(p_0)\right.\\ &-\sum_{\mu_0=1,2}\int dq_0dx_0\frac{1}{\sqrt{2x_2 2x_0}}\bar{U}^{\mu(+)}(q_2)\,Q(MM)\,U^{\mu_0(-)}(q_0)\\ &\left.\times W_{\mu_0\nu_0}(q_0,x_0;p_0,k_0)\right]\delta(q_2+x_2-P)\,|0\rangle.\end{aligned} \tag{41}$$

Here Q is defined as

$$Q=\frac{M\hat{f}_1(\hat{f}_1+M)}{f_1^2(f_1^2-M^2)}+\frac{M\hat{f}_2(\hat{f}_2+M)}{f_2^2(f_2^2-M^2)};$$

$$f_1=p_1+k_1=p_2+k_2;\qquad f_2=p_1-k_2=p_2-k_1, \tag{42}$$

where the indices 1, 2 denote the initial and final states of the system in states with rest mass m or M for the electron.

We look for a matrix W which has the property that simultaneously

$$G_- = WF_1 \tag{43}$$

and

$$G_+ = WF_+. \tag{44}$$

This gives us an equation for W:

$$\frac{1}{\sqrt{2\varkappa_2 2\omega_0}}\bar{U}^{\mu(+)}\,Q(Mm)\,u^{\nu_0}$$

$$-\sum_{\mu_0=1,2}\int d\mathbf{q}_0 d\varkappa_0\,\frac{1}{\sqrt{2\varkappa_2 2\varkappa_0^*}}\bar{U}^{\mu(+)}Q(MM)\,U^{\mu_0(-)}W_{\mu_0\nu_0}$$

$$=\sum_{\nu=1,2}\int d\mathbf{p}_2 d\mathbf{k}_2 W_{\mu\nu}\left[\frac{1}{2\omega_2 2\omega_0}\,\bar{u}^{\nu(+)}\,Q(mm)\,u^{\nu_0(-)}\right.$$

$$\left.-\sum_{\mu_0=1,2}\int d\mathbf{q}_0 d\varkappa_0\,\frac{1}{\sqrt{2\omega_2 2\varkappa_0}}\,\bar{u}^{\nu(+)}\,Q(mM)\,U^{\mu_0(-)}W_{\mu_0\nu_0}\right]. \tag{45}$$

We shall solve this quadratic equation for W near the threshold for creation of "ghosts," with the total energy of the system equal to

$$E = M(1+\varepsilon),\ \varepsilon \ll 1. \tag{46}$$

We shall try to find W in the form

$$W_{\mu\nu}(\mathbf{q}\varkappa;\ \mathbf{pk}) = \bar{U}^{\mu(+)}(\mathbf{q})\,w u^{\nu(-)}(\mathbf{p})\,\delta(q+\varkappa-p-k). \tag{47}$$

We have here to use the facts that

$$\varkappa_2 = \varkappa_0 = \varkappa = M\varepsilon;\ \omega_2 = \omega_0 = \omega = E/2,$$

$$\sum_{\nu=1,2} u^{\nu(-)}\,\bar{u}^{\nu(+)} = \frac{(\hat{p}+m)}{2p_0} \approx \frac{\hat{p}}{E};$$

$$\sum_{\mu=1,2} U^{\mu(-)}\bar{U}^{\mu(+)} = \frac{(\hat{q}+M)}{2q_0} \approx \frac{(\gamma_0+1)}{2},$$

$$Q(mm) \approx Q(mM) \approx Q(Mm)$$

$$\approx \frac{(1+\gamma_0)}{2M\varepsilon} \sim 1/\varepsilon;\ Q(MM) \sim 1,$$

$$\int \delta(q_0+\varkappa_0-P)\,d\mathbf{q}_0 d\varkappa_0 = \varkappa^2 d\mathbf{n}_\varkappa,$$

$$\int \delta(p_2+k_2-P)\,d\mathbf{p}_2 d\mathbf{k}_2 = \frac{\omega^2}{2}\,d\mathbf{n}_k. \tag{48}$$

We note that in Q(Mm) we have dropped the term proportional to $\hat{\mathbf{p}}_1$, because by the Dirac equation $\hat{\mathbf{p}}_1 u(\mathbf{p}_1) = mu(\mathbf{p}_1)$.

Equation (45) takes the form

$$Q(Mm) - \sqrt{\frac{\omega}{\varkappa}}\int d\mathbf{n}_\varkappa \varkappa^2 Q(MM)\,\frac{\hat{q}_0+M}{2q_0}\,w$$

$$-\sqrt{\frac{\varkappa}{\omega}}\int d\mathbf{n}_{k_2}\,\frac{k_2^2}{2}\,w\,\frac{\hat{p}_2}{2}\,Q(mm)$$

$$+\int d\mathbf{n}_{k_2} d\mathbf{n}_\varkappa \varkappa^2\,\frac{k_2^2}{2}\,w\,\frac{\hat{p}_2}{E}\,Q(mM)\,\frac{\hat{q}_0+M}{2q_0}\,w = 0. \tag{49}$$

In this equation the respective orders of magnitude of the terms are

$$\frac{1}{\varepsilon},\ \sqrt{\frac{1}{\varepsilon}}\,\varepsilon^2 w,\quad \sqrt{\varepsilon}\,\frac{1}{\varepsilon}\,w,\ \frac{1}{\varepsilon}\,\varepsilon^2 w^2.$$

This means that $w \sim \epsilon^{-1/2}$. Keeping the main terms in Eq. (49), we get finally

$$Q(Mm) = \sqrt{\frac{\varkappa}{\omega}}\,4\pi\,\frac{\omega^2}{2}\,w\,\frac{\gamma^2}{2}\,Q(mm).$$

From this we get the solution

$$w = 2\sqrt{2}/\pi M^2\sqrt{\varepsilon}. \tag{50}$$

Thus the desired matrix W has the form

$$W_{\mu\nu}(\mathbf{q}\varkappa;\ \mathbf{pk})$$

$$= \frac{2\sqrt{2}}{\pi M^2\sqrt{\varepsilon}}\,\bar{U}^{\mu(+)}(\mathbf{q})\,u^{\nu(-)}(\mathbf{p})\,\delta(q+\varkappa-p-k). \tag{51}$$

This matrix produces a space of state vectors of the form

$$\Phi = (2\pi)^3$$

$$\times\left\{b_\nu^{*+}(\mathbf{p})\,a^+(\mathbf{k}) + \sum_{\mu=1,2}\int d\mathbf{n}_\varkappa\,\frac{2\sqrt{2}\varepsilon^2}{\pi\sqrt{\varepsilon}}\left(\bar{U}^{\mu(+)}(\mathbf{q})\,U^{\nu(-)}(\mathbf{p})\right)c_\mu^{*+}(\mathbf{q})\,a^+(\varkappa)\right\}|0\rangle. \tag{52}$$

These states have positive norm, since the amplitude of the nonphysical states is small, $0(\epsilon^{3/2})$. Therefore the operator U that takes purely physical states over into states of the form (2) exists, and in the approximation in question has the form

$$U = \begin{pmatrix} 1 & W^+ \\ W & 1 \end{pmatrix}. \tag{53}$$

In the opposite limit of very large energies ($E \gg M$), when the difference of the rest masses of the two states of the "electron" can be neglected, the vectors of the required invariant subspace (2) will be vectors of the form

$$\Phi = \begin{pmatrix} F \\ F \end{pmatrix}, \tag{54}$$

i.e., vectors with zero norm. Therefore we may assume that in the general case $M < E < \infty$ these vectors will have positive norm, i.e., that for all energies the matrix U exists (it is obvious that for $E < M$ we have $U = 1$).

5. In conclusion, let us examine the question of the causal property of the matrix S'. Here it is convenient to use the concept of the switching-on function g(x). For the original S matrix

$$S(g) = T\exp\left\{i\int L(x)\,g(x)\,dx\right\} \tag{55}$$

the causality condition can be written in the form[4]

$$S(g_1+g_2) = S(g_1)\,S(g_2), \tag{56}$$

if $G_1 > G_2$, i.e., if the region in which g_1 is different from zero is located later in time than that where g_2 is different from zero. Equation (6),

which defines the transformation U, was derived for the S′ matrix with the interaction completely switched on, i.e., for g(x) = 1 for all x. In the case of incomplete switching-on of the interaction two ways of defining the matrix S′ are possible:

$$S'(g) = U^{+} S(g) U, \tag{57}$$

$$S'(g) = U^{+}(g) S(g) U(g). \tag{58}$$

For the first S′ matrix the condition (56) is satisfied exactly, but this matrix does not contain transitions to nonphysical states only in the case in which g(x) = 1, at least in a macroscopically large region of four-space. For the second S′ matrix Eq. (6) is taken to be satisfied for arbitrary g(x), i.e., it is exactly unitary with respect to physical transitions. On the other hand the causality condition (56) is satisfied only for macroscopically large regions with g(x) = 1, for which one can with arbitrary accuracy replace U(g) by U(1). Thus we come to the conclusion that it is necessary to give up one of the two fundamental properties of the scattering matrix; we must give up either microscopic causality or the exactly unitary character of the matrix. It is important, however, that in the large the matrix S′ is both causal and unitary in both cases.

I thank Professor Ya. A. Smorodinskiĭ for a discussion of the results and for helpful advice in the course of this research.

[1] W. Heisenberg, Nucl. Phys. **4**, 532 (1957).

[2] Bogolyubov, Medvedev, and Polivanov, Научн. докл. Высш. школы (Sci. Reports of the Higher School, Phys.-Math. Series) No. 1 (1958).

[3] L. A. Maksimov, J. Exptl. Theoret. Phys. (U.S.S.R.) **36**, 140 (1959), Soviet Phys. JETP **9**, 97 (1959).

[4] N. N. Bogolyubov and D. V. Shirkov, Введение в теорию квантованных полей (Introduction to the Theory of Quantized Fields), GITTL, Moscow 1957.

[5] A. Pais and G. E. Uhlenbeck, Phys. Rev. **79**, 145 (1950).

Translated by W. H. Furry
78

RELATIVISTIC CORRECTIONS TO PHENOMENOLOGICAL HAMILTONIANS

Yu. M. SHIROKOV

P. N. Lebedev Physics Institute, Academy of Sciences, U.S.S.R.

Submitted to JETP editor June 14, 1958

J. Exptl. Theoret. Phys. (U.S.S.R.) 36, 474-477 (February, 1959)

A general expression has been obtained for the relativistic corrections of order $(v/c)^2$ to a given phenomenological nonrelativistic Hamiltonian describing the interaction between particles of arbitrary mass and spin.

1. In view of the unsatisfactory state of meson theory, phenomenological Hamiltonians for the nucleon-nucleon and meson-nucleon interactions have found wide application at the present time. These Hamiltonians are usually chosen such as to agree with the experimental data on the corresponding two-body problem. The aim of the present paper is to calculate the relativistic corrections to these phenomenological potentials. It turns out that, starting from the general postulate of relativistic invariance, the phenomenological Hamiltonian can be corrected relativistically in a consistent fashion, at least up to terms of order $(v/c)^2$.

2. If the relativistic effects are neglected, the system of two particles with masses κ_1 and κ_2 and spins i and I is described by the Hamiltonian

$$H = \mathbf{p}_1^2/2\varkappa_1 + \mathbf{p}_2^2/2\varkappa_2 + H_{12}, \tag{1}$$

where H_{12} is the nonrelativistic interaction Hamiltonian. The general requirements on the Hamiltonian H_{12} have been analyzed in detail by Okubo and Marshak.[1] In particular, H_{12} must not depend on the total momentum $\mathbf{p}_1 + \mathbf{p}_2 = \mathbf{P}$ as a consequence of conservation law for the nonrelativistic center of intertia (Galilean invariance).

The inclusion of the relativistic effects leads to correction terms which do depend on $\mathbf{P}$.

3. To make the discussion sufficiently rigorous and general, we shall not make use of any special equations of motion. Instead, we start with group theoretical considerations and the invariance properties of the S matrix.

According to the theory of the representations of the inhomogeneous Lorentz group, the system of two free particles is described by the wave function[2,3]

$$\psi^{\varkappa_1\varkappa_2 lI}_{m_i m_I}(\mathbf{p}_1, \mathbf{p}_2), \tag{2}$$

which depends on the variables $\mathbf{p}_1$, $\mathbf{p}_2$ (the momenta) and m_i, m_I (the spin projections). We do not exhibit the other possible variables (isotopic spin, charge, etc.), since they are irrelevant for a discussion of the relativistic invariance. The scattering of two particles is described by the invariant S matrix

$$(\mathbf{p}_1\mathbf{p}_2 m_i m_I \,|\, S \,|\, \mathbf{p}_1'\mathbf{p}_2' m_i' m_I'), \tag{3}$$

which, owing to the conservation law for the 4-momentum, can also be written in the form

$$(\mathbf{p}_1\mathbf{p}_2 m_i m_I \,|\, S \,|\, \mathbf{p}_1'\mathbf{p}_2' m_i' m_I') = \delta(\mathbf{p}_1 + \mathbf{p}_2 - \mathbf{p}_1' - \mathbf{p}_2')$$
$$\times\, \delta(e_{p_1} + E_{p_2} - e_{p_1'} - E_{p_2'})\,(\mathbf{p}_1\mathbf{p}_2 m_i m_I \,|\, V \,|\, \mathbf{p}_1'\mathbf{p}_2' m_i' m_I'),$$

$$e_{p_1} = \sqrt{p_1^2 + \varkappa_1^2}, \quad E_{p_2} = \sqrt{p_2^2 + \varkappa_2^2}. \tag{4}$$

The matrix V is invariant as a consequence of the invariance of the four-dimensional δ function. On the other hand, if perturbation theory is applicable, the S matrix is, in the interaction picture, expressed in terms of the Hamiltonian H_{12} by the relation

$$S = 1 + \frac{1}{i}\int dt H_{12} \exp\{-it(e_{p_1} + E_{p_2} - e_{p_1'} - E_{p_2'})\}$$
$$= 1 - 2\pi i H_{12}\delta(e_{p_1} + E_{p_2} - e_{p_1'} - E_{p_2'}). \tag{5}$$

Since the transformation properties of the Hamiltonian cannot depend on the applicability of perturbation theory to it, and since the expansion in powers of the coupling constant is invariant, it can be concluded from the comparison of (4) and (5) that the Hamiltonian has the form

$$(\mathbf{p}_1\mathbf{p}_2 m_i m_I \,|\, H_{12} \,|\, \mathbf{p}_1'\mathbf{p}_2' m_i' m_I')$$
$$= \delta(\mathbf{p}_1 + \mathbf{p}_2 - \mathbf{p}_1' - \mathbf{p}_2')(\mathbf{p}_1\mathbf{p}_2 m_i m_I \,|\, W \,|\, \mathbf{p}_1'\mathbf{p}_2' m_i' m_I'), \tag{6}$$

where $(\mathbf{p}_1\mathbf{p}_2 m_i m_I \,|\, H_{12} \,|\, \mathbf{p}_1'\mathbf{p}_2' m_i' m_I')$ is an invariant.

The requirement that the operator W be invariant implies that it must commute with the operator $\mathbf{N}$ which generates the infinitesimal Lorentz transformation:

$$[\mathbf{N}, W]_- = 0. \tag{7}$$

The square brackets with a minus sign denote the

commutator. The operator $\mathbf{N}$ has, according to reference 2, the form

$$\mathbf{N} = i\sqrt{e_{p_1}}\frac{\partial}{\partial \mathbf{p}_1}\sqrt{e_{p_1}} - \frac{[\mathbf{i}\times\mathbf{p}_1]}{e_{p_1}+\varkappa_1} + i\sqrt{E_{p_2}}\frac{\partial}{\partial \mathbf{p}_2}\sqrt{E_{p_2}} - \frac{[\mathbf{I}\times\mathbf{p}_2]}{E_{p_2}+\varkappa_2}. \quad (8)$$

The square brackets without a minus sign denote the vector product. The slight difference in the appearance of the operator $\mathbf{N}$ in (8) and in (11) of reference 2 (cf. also reference 3) is due to the fact that, in the present paper, we use a normalization integral without the weight factor $1/e_{p_1}E_{p_2}$.

4. In the nonrelativistic approximation, the operators W, $\mathbf{N}$ can be expanded in powers of $\mathbf{p}_1/\kappa_1$ and $\mathbf{p}_2/\kappa_2$:

$$W = W_0 + W_1, \quad (9)$$

$$\mathbf{N} = \mathbf{N}_0 + \mathbf{N}_1, \quad (10)$$

$$\mathbf{N}_0 = i\varkappa_1\partial/\partial\mathbf{p}_1 + i\varkappa_2\partial/\partial\mathbf{p}_2 \quad (11)$$

$$\mathbf{N}_1 = i\frac{\mathbf{p}_1}{2\varkappa_1} + i\frac{\mathbf{p}_1^2}{2\varkappa_1}\frac{\partial}{\partial\mathbf{p}_1} - \frac{[\mathbf{i}\times\mathbf{p}_1]}{2\varkappa_1} + i\frac{\mathbf{p}_2}{2\varkappa_2} + i\frac{\mathbf{p}_2^2}{2\varkappa_2}\frac{\partial}{\partial\mathbf{p}_2} - \frac{[\mathbf{I}\times\mathbf{p}_2]}{2\varkappa_2}. \quad (12)$$

Substituting (9) and (10) in (7), we obtain, in zeroth order, the condition of Galilean invariance for the interaction Hamiltonian:

$$[\mathbf{N}_0,\ W_0]_- = 0. \quad (13)$$

We now subject the momenta $\mathbf{p}_1$, $\mathbf{p}_2$ to the Jacobi transformation:

$$\mathbf{p}_1 + \mathbf{p}_2 = \mathbf{P},\ \mathbf{p}_1\varkappa_2/(\varkappa_1+\varkappa_2) - \mathbf{p}_2\varkappa_1/(\varkappa_1+\varkappa_2) = \mathbf{p}, \quad (14)$$

and similarly for the momenta $\mathbf{p}_1'$, $\mathbf{p}_2'$. On account of the δ function in (6), one may regard the operator W as independent of $\mathbf{P}'$. In this case, relation (13) takes the form

$$\partial W_0(\mathbf{p}_1, \mathbf{p}', \mathbf{P})/\partial\mathbf{P} = 0. \quad (15)$$

In the zeroth approximation the Hamiltonian does, therefore, not depend on the total momentum, i.e., the requirement of Galilean invariance is satisfied, as was to be expected. In the next nonvanishing approximation, condition (7) has the form

$$\mathbf{N}_0W_1 - W_1\mathbf{N}_0 = W_0\mathbf{N}_1 - \mathbf{N}_1W_0. \quad (16)$$

Substituting (11) and (12) in (16) and using (15), we obtain

$$-i(\varkappa_1+\varkappa_2)\frac{\partial}{\partial\mathbf{P}}W_1(\mathbf{P},\mathbf{p},\mathbf{p}') = \left\{i\frac{\mathbf{p}_1}{2\varkappa_1} + i\frac{\mathbf{p}_2}{2\varkappa_2} + i\frac{\mathbf{p}_1'}{2\varkappa_1} + i\frac{\mathbf{p}_2'}{2\varkappa_2} + i\frac{\mathbf{p}_1^2}{2\varkappa_1}\frac{\partial}{\partial\mathbf{p}_1} + i\frac{\mathbf{p}_2^2}{2\varkappa_2}\frac{\partial}{\partial\mathbf{p}_2} + i\frac{\mathbf{p}_1'^2}{2\varkappa_1}\frac{\partial}{\partial\mathbf{p}_1'} + i\frac{\mathbf{p}_2'^2}{2\varkappa_2}\frac{\partial}{\partial\mathbf{p}_2'} - \frac{[\mathbf{i}\times\mathbf{p}_1]}{2\varkappa_1} - \frac{[\mathbf{I}\times\mathbf{p}_2]}{2\varkappa_2}\right\}W_0(\mathbf{p},\mathbf{p}') + W_0(\mathbf{p},\mathbf{p}')\left\{\frac{[\mathbf{i}\times\mathbf{p}_1']}{2\varkappa_1} + \frac{[\mathbf{I}\times\mathbf{p}_2']}{2\varkappa_2}\right\}. \quad (17)$$

Equation (17) must be written in terms of the $\mathbf{P}$, $\mathbf{p}$, and $\mathbf{p}'$ alone. The operator W_1 can be split up into two parts:

$$W_1 = W_1' + W_1'', \quad (18)$$

where W_1' does not depend on the momentum $\mathbf{P}$:

$$\partial W_1'/\partial\mathbf{P} = 0, \quad W_1' = W_1'(\mathbf{p},\mathbf{p}'), \quad (19)$$

and W_1'' reduces to zero for $\mathbf{P} = 0$. The operator $W_1'(\mathbf{p},\mathbf{p}')$ is not uniquely determined by Eq. (17). This operator does, however, satisfy the nonrelativistic condition (15), and it can always be considered to be included in the operator W_0 of the nonrelativistic approximation. The structure of the phenomenological Hamiltonian H_{12} is significantly affected only by the operator W_1'', which is, however, indeed uniquely defined by equation (17).

Since we are only interested in corrections of order $(v/c)^2$, we write the operator $W_1''(\mathbf{P},\mathbf{p},\mathbf{p}'')$ as a polynomial of no higher than second degree in $\mathbf{P}$:

$$W_1'' = P_iA_i + P_iP_jB_{ij}. \quad (20)$$

Substituting (20) in (17), we can uniquely determine the operators A_i and B_{ij} by using the fact that the operator $(\mathbf{p}_1\mathbf{p}_2\mathbf{m}_i\mathbf{m}_I|\,W_1''\,|\mathbf{p}_1'\mathbf{p}_2'\mathbf{m}_i'\mathbf{m}_I')$ is invariant in three-dimensional space, i.e., that it commutes with the momentum operator $\mathbf{M}$:

$$\mathbf{M} = -i[\mathbf{p}_1\partial/\partial\mathbf{p}_1] - i[\mathbf{p}_2\partial/\partial\mathbf{p}_2] + \mathbf{i} + \mathbf{I}. \quad (21)$$

A simple calculation leads to the following expression for W_1'':

$$W_1'' = -\frac{\mathbf{P}^2W_0}{(\varkappa_1+\varkappa_2)^2} - \frac{(\mathbf{pP})(\mathbf{P}\partial/\partial\mathbf{p}) + (\mathbf{p}'\mathbf{P})(\mathbf{P}\partial/\partial\mathbf{p}')}{2(\varkappa_1+\varkappa_2)^2}W_0 - \frac{(\varkappa_2-\varkappa_1)(\mathbf{p}+\mathbf{p}')\mathbf{P}W_0}{2\varkappa_1\varkappa_2(\varkappa_1+\varkappa_2)} + \frac{i}{2(\varkappa_1+\varkappa_2)}\left\{W_0[\mathbf{P}\times\mathbf{p}']\left(\frac{\mathbf{i}}{\varkappa_1} - \frac{\mathbf{I}}{\varkappa_2}\right) - [\mathbf{P}\times\mathbf{p}]\left(\frac{\mathbf{i}}{\varkappa_1} - \frac{\mathbf{I}}{\varkappa_2}\right)W_0\right\}. \quad (22)$$

5. The operator W_1'' from (22) does not satisfy the nonrelativistic conservation law for the center of inertia and contains all relativistic corrections needed for the phenomenological formulation of the problem[1] (apart from trivial corrections to the kinetic energy). Expression (22) refers to a Hamiltonian which is written in the form of an integral operator. If, as is ordinarily the case, the Hamiltonian is given as a function of the coordinates and the momenta, the correction H_{12}' (derived from the operator W_1'') to the Hamiltonian H_{12} has the form

$$H'_{12} = -\frac{\mathbf{P}^2 H_{12}}{2(\varkappa_1+\varkappa_2)^2} - \frac{\mathbf{Pp}}{2(\varkappa_1+\varkappa_2)^2}\left(\mathbf{P}\frac{\partial H_{12}}{\partial \mathbf{p}}\right)$$
$$+ \frac{i}{2(\varkappa_1+\varkappa_2)^2}\left(\mathbf{P}\frac{\partial H_{12}}{\partial \mathbf{x}}\right)\left(\mathbf{P}\frac{\partial}{\partial \mathbf{p}}\right)$$
$$- \frac{1}{2(\varkappa_1+\varkappa_2)}\left(\frac{\mathbf{i}}{\varkappa_1}-\frac{\mathbf{I}}{\varkappa_2}\right)\left[\frac{\partial H_{12}}{\partial \mathbf{x}}\mathbf{P}\right]$$
$$- \frac{i}{2(\varkappa_1+\varkappa_2)}\left(\frac{\mathbf{i}}{\varkappa_1}-\frac{\mathbf{I}}{\varkappa_2}\right)H_{12}[\mathbf{p}\times\mathbf{P}]$$
$$+ \frac{iH_{12}}{2(\varkappa_1+\varkappa_2)}\left(\frac{\mathbf{i}}{\varkappa_1}-\frac{\mathbf{I}}{\varkappa_2}\right)[\mathbf{p}\times\mathbf{P}] + \frac{\varkappa_2-\varkappa_1}{\varkappa_1\varkappa_2(\varkappa_1+\varkappa_2)}\left\{\frac{i\mathbf{P}}{2}\frac{\partial H_{12}}{\partial \mathbf{x}}\right.$$
$$\left. - \frac{1}{2}\mathbf{p}^2\left(\mathbf{P}\frac{\partial H_{12}}{\partial \mathbf{p}}\right) + \frac{1}{2}\frac{\partial^2 H_{12}}{\partial \mathbf{x}^2}\left(\mathbf{P}\frac{\partial}{\partial \mathbf{p}}\right) + i\left(\frac{\partial H_{12}}{\partial \mathbf{x}}\mathbf{p}\right)\left(\mathbf{P}\frac{\partial}{\partial \mathbf{p}}\right)\right\}. \quad (23)$$

The operator $\mathbf{x}$ in (23) denotes the coordinate difference

$$\mathbf{x} = \mathbf{x}_1 - \mathbf{x}_2 = i\partial/\partial \mathbf{p}_1 - i\partial/\partial \mathbf{p}_2. \quad (24)$$

Including the corrections to the kinetic energy, we arrive at the final result: the relativistic Hamiltonian for the two-body problem has, up to terms of order $(v/c)^2$, the form

$$H = \mathbf{p}_1^2/2\varkappa_1 + \mathbf{p}_2^2/2\varkappa_2 - \mathbf{p}_1^4/8\varkappa_1^3$$
$$- \mathbf{p}_2^4/8\varkappa_2^3 + H_{12} + H'_{12}, \quad (25)$$

The correction term H'_{12} reduces, according to (24), to zero in the center of inertia system. In the two-body problem the relativistic corrections can, therefore, be avoided by going to the center of inertia system. The corrections thus become significant only in the many-body problem.

We emphasize that, according to (18) and (19), the correction term H'_{12} does not contain all corrections, but only those which violate the Galilean invariance of the Hamiltonian. However, these are just the essential corrections to the phenomenological Hamiltonian.

The Hamiltonian (25) can be used for the investigation of the interaction of mesons and nucleons of high energy with nuclei. Besides that, this Hamiltonian is useful for an estimate of the effect of relativistic corrections on the structure of the nucleus.

[1] S. Okubo and R. E. Marshak, Ann. of Phys. (in press).

[2] Yu. M. Shirokov, J. Exptl. Theoret. Phys. (U.S.S.R.) **33**, 1196 (1957); Soviet Phys. JETP **6**, 919 (1958).

[3] Yu. M. Shirokov, J. Exptl. Theoret. Phys. (U.S.S.R.) **35**, 1005 (1958); Soviet Phys. JETP **8**, 703 (1959).

Translated by R. Lipperheide
79

RELATIVISTIC CORRECTIONS TO THE PHENOMENOLOGICAL THEORY OF LEVELS OF LIGHT NUCLEI

F. A. ZHIVOPISTSEV, A. M. PEROLOMOV, and Yu. M. SHIROKOV

Institute of Nuclear Physics, Moscow State University

Submitted to JETP editor June 16, 1958

J. Exptl. Theoret. Phys. (U.S.S.R.) 36, 478-480 (February, 1959)

Relativistic corrections to the phenomenologically prescribed interaction between a pair of nucleons in a nucleus is computed on the basis of the expression obtained by Yu. M. Shirokov for relativistic corrections to the nonrelativistic two-body Hamiltonian. It is found that the relativistic corrections depend strongly on the shape of the potential and are of the order of 0.02 — 0.2 Mev for a pair of nucleons.

1. The question of the role of relativistic effects in the theory of levels of light nuclei was hardly investigated until recently. Blatt and Weisskopf (reference 1, p. 162) express an opinion that these effects can give a contribution on the order of 10 to 20%. At the present state of meson theory we cannot investigate this problem with any degree of reliability. A phenomenological examination, based on general group-theoretical properties of the relativistic invariance of quantum theory, is therefore of interest. The general method for the investigation of problems of this kind is presented in reference 2.

2. Neglecting relativistic effects, the nucleus is described by the non-relativistic Hamiltonian

$$H = \sum_n T_n + \sum_{m>n} H_{mn}, \tag{1}$$

where T_n is the kinetic energy of the n-th nucleon

$$T_n = \mathbf{p}_n^2 / 2M, \tag{2}$$

and H_{mn} is Hamiltonian of the paired interaction between the nucleons m and n. In nuclear physics the Hamiltonian, as a rule, is chosen phenomenologically to satisfy the necessary properties of invariance and to agree with the basic experimental data on the nucleon-interaction. In particular, the Hamiltonian H_{mn} should be galilean-invariant, that is, independent of the total momentum of the interacting nucleons.

It is shown in reference 2 that if relativistic corrections are taken into account with accuracy to (v/c),[2] the Hamiltonian (1) becomes

$$H = \sum_n T_n + \sum_{m>n} H_{mn} + \sum_n T'_n + \sum_{m>n} H'_{mn}, \tag{3}$$

where T'_n is the correction to the kinetic energy of the n-th nucleon,

$$T'_n = -\mathbf{p}_n^4 / 8M^3, \tag{4}$$

and H'_{mn} is the relativistic correction to the interaction Hamiltonian, which equals

$$\begin{aligned} H'_{mn} = (1/8M^2)\{ &- H_{mn}\mathbf{P}^2 \\ &+ i(\mathbf{P}\cdot\partial H_{mn}/\partial\mathbf{x})(\mathbf{P}\cdot\partial/\partial\mathbf{p}) + (\sigma_m - \sigma_n)[\mathbf{P}\times\partial H_{mn}/\partial\mathbf{x}] \\ &- i(\sigma_m - \sigma_n) H_{mn}[\mathbf{p}\times\mathbf{P}] + iH_{mn}(\sigma_m - \sigma_n)[\mathbf{p}\times\mathbf{P}] \\ &- (\mathbf{P}\cdot\partial H_{mn}/\partial\mathbf{p})(\mathbf{P}\cdot\mathbf{p}) + iP_iP_j\partial^2 H_{mn}/\partial x_i\partial p_j\}. \end{aligned} \tag{5}$$

Here

$$\mathbf{P} = \mathbf{p}_m + \mathbf{p}_n, \quad \mathbf{p} = (\mathbf{p}_m - \mathbf{p}_n)/2, \tag{6}$$

and $\mathbf{x}$ is the operator of the difference of nucleon coordinates.

$$\mathbf{x} = \mathbf{x}_m - \mathbf{x}_n; \tag{7}$$

σ_m and σ_n are the spin matrices of the m-th and n-th nucleons, respectively. The nonrelativistic Hamiltonian is assumed specified in the form of a function of the coordinate and momentum operators of the nucleons. In virtue of conservation of the momentum and of the nonrelativistic center of mass, H_{mn} is independent of $\partial/\partial\mathbf{P}$ and $\mathbf{P}$. The Hamiltonian H_{mn} can naturally depend on the ordinary and isotopic spins.

The correction term H'_{mn} does not satisfy the law of conservation of the nonrelativistic center of mass, since it depends explicitly on the total momentum P. H'_{mn} vanishes in the center-of-mass system of the two nucleons, so that an interaction Hamiltonian H_{mn} phenomenologically constructed from on nucleon-nucleon scattering data need not include special allowance for relativistic effects. However, if a Hamiltonian so constructed is applied to the many-body problem, it becomes necessary to take into account the correction term (5), for in this case it is impossible to go over to a system in which the centers of mass of all pairs of particles

are at rest. We note that in expression (5) the additions of order $\mathbf{P}^2/M^2$ and $\mathbf{P}\cdot\mathbf{p}/M^2$ are taken into account exactly, and that the relativistic corrections of order p^2/M^2 are not considered at all. However, the latter do not contradict the nonrelativistic law of conservation of the center of mass. and therefore, when constructing a Hamiltonian from scattering data, they simply enter into the nonrelativistic Hamiltonian H_{mn}.

3. To estimate the influence of relativistic effects on the positions of the levels of light nuclei, the following calculations were performed:

Equation (5) was used to calculate the level shifts for two particles in the states

$$|0s^2_{1/2}01\rangle, \quad |0s^2_{1/2}10\rangle, \quad |1p^2_{3/2}01\rangle, \quad |1p^2_{1/2}01\rangle$$

for a Gaussian potential, a Yukawa potential, and a rectangular well. Oscillator wave functions were used throughout, with $r_0 = 1.65 \times 10^{-13}$ cm (i.e., $h\omega = 15$ Mev). The potentials were chosen in the form

$$V = V_0(0.317 + 0.500P + 0.183PQ)\, f(r/a)$$

with the following constants: for the Gaussian potential:[3]

$$V_0 = -51.9\ \text{Mev}, \quad a = 1.73\cdot 10^{-13}\ \text{cm}, \quad f(x) = e^{-x^2},$$

for the Yukawa potential (reference 1, p. 50)

$$V_0 = -68\ \text{Mev}, \quad a = 1.17\cdot 10^{-13}\ \text{cm}, \quad f(x) = e^{-x}/x,$$

and for the potential well (reference 1, p. 50)

$$V_0 = -33.6\ \text{Mev}, \quad a = 2.1\cdot 10^{-13}\ \text{cm};$$

The potentials are independent of the velocity. P and Q are the permutation operators of the spatial and spin variables respectively. The following results were obtained (in kev):

Potential	State					
	$^2S_{1/2}$ 01	$^2S_{1/2}$ 10	$^2P_{3/2}$ 01	$^2P_{1/2}$ 01	$S_{1/2}$ $P_{1/2}$ 00	$S_{1/2}$ $P_{1/2}$ 01
Gaussian	95	150	52	11	125	—22
Yukawa	96	142	205	51	120	—21
Rectangular well	115	182	62	8	150	—14

4. From the foregoing we can draw the following conclusions as to which relativistic effects on the structure of the nuclear levels are significant for a phenomenological statement of the problem.

The relativistic corrections depend greatly on the form of the potential and are of order 0.02 — 0.2 Mev for individual pairs of nucleons in a nucleus. As a consequence of saturation of the nuclear forces, the correction to the ground state can be considered to be proportional to the number of nucleons in the nucleus, i.e., of the order 0.2 — 2 Mev for light nuclei and 2 — 20 Mev for heavy ones. Corrections to the relative placements of the nuclear levels are of the same order as for a pair of nucleons, i.e., 0.02 — 2 Mev.

Relativistic corrections are thus considerably smaller than given reference 1, and can be disregarded in the less accurate present-day methods. On the other hand, these corrections exceed the errors in the experimental measurements of the nuclear levels, and must therefore be taken into account when developing computational methods of accuracy comparable with that of the experimental measurements.

[1] J. Blatt and V. Weisskopf, Theoretical Nuclear Physics, (Russ. Transl. IIL, 1954), Wiley, N. Y., 1952.

[2] Yu. M. Shirokov, J. Exptl. Theoret. Phys. (U.S.S.R.) **36**, 474 (1959), Soviet Phys. JETP, this issue, p. 330.

[3] R. A. Ferrell and W. M. Visscher, Phys. Rev. **102**, 450 (1956).

Translated by J. G. Adashko
80

ON THE THEORY OF NUCLEAR PARAMAGNETIC RESONANCE IN LIQUIDS

G. V. SKROTSKIĬ and A. A. KOKIN

Submitted to JETP editor June 23, 1958; resubmitted October 28, 1958

J. Exptl. Theoret. Phys. (U.S.S.R.) **36**, 481-487 (February, 1959)

The quantum theory of magnetic resonance absorption due to Kubo and Tomita[1] is used to describe the phenomenon of nuclear paramagnetic resonance in liquids. The thermal motion of the molecules, which leads to a narrowing of the absorption line, is taken into account on the basis of diffusion theory. The transverse and the longitudinal relaxation times and the correction to the gyromagnetic ratio are computed.

1. The general method developed by Kubo and Tomita[1] for the determination of the line shape of magnetic resonance absorption in radio frequency fields has been employed to discuss nuclear magnetic resonance absorption in liquids and exchange narrowing in paramagnetic crystals.

With the aid of this method it has turned out to be possible to take into account the effect of the anisotropy of the g-factor on the line shape[2] and to determine the effect of the exchange interaction on the hyperfine structure in electron paramagnetic resonance.[3] On the basis of this method, Chirkov and Kokin[4] calculated the line shape of electron resonance absorption in powdered free radicals. Skrotskiĭ and Kokin[5] obtained the equations of motion for the magnetization vector and expressions for the coefficients appearing in these equations.

To take thermal motion into account, both Kubo and Tomita[1] and Bloembergen, Purcell, and Pound[6] chose the simplest correlation function

$$f(t) = \exp(-|t|/\tau_c). \tag{1}$$

It is assumed that this form of the function describes both the rotational and the translational Brownian motion. The correlation time τ_c for the rotational Brownian motion is expressed in terms of the temperature, the mobility, and the dimensions of the molecule, while in the case of the translational motion it is expressed in terms of the relative position of the paramagnetic molecules or ions.

Such a choice of $f(t)$ is not general and, strictly speaking, is applicable only to the description of rotational Brownian motion.

The results obtained by Skrotskiĭ and Kokin[5] are employed in this paper for the determination of the transverse and longitudinal relaxation times in liquids. In carrying this out the form of the function is determined on the basis of diffusion theory.

2. In what follows we shall assume that the sample is situated in a constant magnetic field $H_0 = H_z$ and a weak radio frequency field $\mathbf{h}(t)$.

The part of the Hamiltonian $\hat{\mathcal{H}}$ which does not depend on the time may be written in the form of three terms

$$\hat{\mathcal{H}} = \hat{\mathcal{H}}_1 + \hat{\mathcal{H}}_2 + \hat{\mathcal{H}}', \tag{2}$$

where

$$\hat{\mathcal{H}}_1 = -\hbar\omega_0 \sum_j \hat{I}_{jz}; \quad \hbar\omega_0 = g\mu_0 H_0 \tag{3}$$

is the operator for the interaction of the system of magnetic moments with the external constant field H_0. The operator $\hat{\mathcal{H}}_2$ contains the kinetic energy and the interactions which do not depend on the spins I_j. The magnetic dipole-dipole interactions are described by the operator $\hat{\mathcal{H}}'$ which is regarded as a perturbation.

When the condition $\hbar\omega_0 \ll kT$ is satisfied the equilibrium density matrix $\hat{\rho}_0$ does not depend on the spins, and in the case of a homogeneous and isotropic liquid in the first approximation does not depend on the coordinates.

In this case we shall obtain for the relaxation times $T_\perp$ and $T_\parallel$ and for the shift in the resonance frequency $\Delta\omega_0$ in accordance with reference:[5]

$$\frac{1}{T_\alpha} = \sum_\lambda \Omega_{\alpha\lambda}^2 \tau_\lambda', \quad T_{\pm 1} = T_\perp, \quad T_0 = T_\parallel; \tag{4}$$

$$\Delta\omega_0 = \sum_\lambda \Omega_{1\lambda}^2 \tau_\lambda'', \tag{5}$$

where

$$\tau_\lambda' + i\tau_\lambda'' = \int_0^\infty \exp(i\lambda\omega_0\vartheta) f_{\alpha\lambda}(\vartheta)\, d\vartheta, \tag{6}$$

$$\Omega_{\alpha\lambda}^2 f_{\alpha\lambda}(\vartheta) = \langle\{[\hat{M}_\alpha \hat{\mathcal{H}}'_{-\lambda}(\vartheta)]\,[\hat{\mathcal{H}}'^{*}_{-\lambda}(0)\,\hat{M}_\alpha^*]\}\rangle / \hbar^2 \langle|\hat{M}_\alpha|^2\rangle. \tag{7}$$

The angle brackets denote averaging over spins and coordinates using $\hat{\rho}_0 = \text{const}$, the curly brack-

ets denote the symmetrized product of the operators, and $f_{\alpha\lambda}(\vartheta) = 1$.

By utilizing the expressions given in reference 5 for $\hat{\mathcal{H}}'_\lambda(\vartheta)$ and $\hat{\mathcal{H}}'_\lambda(0)$, and by averaging over spins, we obtain for an isotropic liquid:

$$\Omega^2_{12} = \Omega^2_{1-1} = {}^2/_3\Omega^2_{11} = {}^2/_3\Omega^2_{10} = {}^1/_2\Omega^2_{0\pm2} = 2\Omega^2_{0\pm1} = {}^2/_3\Omega^2,$$
$$\Omega^2_{1-2} = \Omega^2_{00} = 0, \tag{8}$$

where

$$\Omega^2 = (12\pi/5)\, I(I+1)\, g^4\mu_0^4\hbar^{-2} \sum_k \langle r_{jk}^{-6} \mid Y_{20}(\vartheta_{jk}\varphi_{jk}) \mid^2 \rangle. \tag{9}$$

The summation over k is carried out for fixed arbitrary j.

The function

$$f_{\alpha\lambda}(\tau) = f_\lambda(\tau)$$
$$= \frac{\sum_k \langle r_{jk}^{-3}(\tau)\, r_{jk}^{-3}(0)\, Y_{2\lambda}(\vartheta_{jk}(\tau)\, \varphi_{jk}(\tau))\, Y^*_{2\lambda}(\vartheta_{jk}\varphi_{jk})\rangle}{\sum_k \langle r_{jk}^{-6} \mid Y_{2\lambda}(\vartheta_{jk}\varphi_{jk}) \mid^2\rangle} \tag{10}$$

will henceforth be called the correlation function.

3. To calculate the relaxation times $T_\perp$ and $T_\parallel$ and the correction to the gyromagnetic ratio it is necessary to obtain the explicit form of the correlation function $f_\lambda(\tau)$.

The direct calculation of $f_\lambda(\tau)$ from (10) does not appear to be possible, since for this it would be necessary to have expressions specifying the motion of each molecule. However, we can get around this difficulty.

We base our discussion on the concept that the molecules in the liquid undergo translational and rotational Brownian motion.

To describe the translational Brownian motion we make use of the equation of free diffusion:

$$\frac{\partial U}{\partial t} - D\Delta U = 0, \quad D = kT/6\pi\eta a, \tag{11}$$

where a is the radius of the molecule.

The probability that at a time t one molecule is contained within a volume element $d\mathbf{r}_1$ at a distance $\mathbf{r}_{12}$ from a second molecule contained within $d\mathbf{r}_2$ is given by the following expression:

$$U(\mathbf{r}_1, \mathbf{r}_{10}, \mathbf{r}_2, \mathbf{r}_{20}, t)\, d\mathbf{r}_1\, d\mathbf{r}_2$$
$$= (4\pi Dt)^{-3} \exp\left(-\frac{(\mathbf{r}_1 - \mathbf{r}_{10})^2 + (\mathbf{r}_2 - \mathbf{r}_{20})^2}{4Dt}\right) d\mathbf{r}_1\, d\mathbf{r}_2, \tag{12}$$

where $\mathbf{r}_{10}$ and $\mathbf{r}_{20}$ define the positions of the molecules at time t = 0.

We write (12) in the form:

$$U(\mathbf{r}_1, \mathbf{r}_{10}, \mathbf{r}_2, \mathbf{r}_{20}, t)\, d\mathbf{r}_1\, d\mathbf{r}_2$$
$$= \frac{1}{(2\pi)^6} \int \exp\left(-k^2 D\mid t\mid - k'^2 D\mid t\mid\right.$$
$$\left. + i\mathbf{k}(\mathbf{r}_1 - \mathbf{r}_{10}) + i\mathbf{k}'(\mathbf{r}_2 - \mathbf{r}_{20})\right) d\mathbf{k}\, d\mathbf{k}'\, d\mathbf{r}_1\, d\mathbf{r}_2 \tag{13}$$

and introduce new variables $\mathbf{r}_1 = \mathbf{r} + \mathbf{r}_2$, $d\mathbf{r}_1 d\mathbf{r}_2 = d\mathbf{r}\, d\mathbf{r}_2$.

Then after integrating over $\mathbf{r}_2$ we obtain:

$$U(\mathbf{r}, \mathbf{r}_0, t) = \left\{\int U(\mathbf{r}_1, \mathbf{r}_{10}, \mathbf{r}_2, \mathbf{r}_{20}, t)\, d\mathbf{r}_2\right\} d\mathbf{r}$$
$$= \frac{1}{(2\pi)^3} \int \exp(-2k^2 D\mid t\mid - i\mathbf{k}(\mathbf{r} - \mathbf{r}_0))\, d\mathbf{k}\, d\mathbf{r}. \tag{14}$$

The last expression gives the probability that during a time $t > 0$ the distance between the molecules will have changed by an amount $\mid \mathbf{r} - \mathbf{r}_0 \mid$.

By making use of the identity

$$\exp(ikr) = \sum_{lm} g_l(kr)\, Y^*_{lm}\left(\frac{\mathbf{k}}{k}\right) Y_{lm}\left(\frac{\mathbf{r}}{r}\right), \tag{15}$$

where

$$g_l(\rho) = (2\pi)^{3/2} i^l\, J_{l+1/2}(\rho)/\sqrt{\rho}, \tag{16}$$

and after carrying out the integration over the angles of $d\mathbf{k}$, we obtain:

$$U(\mathbf{r}, \mathbf{r}_0, t) = \frac{1}{(2\pi)^3} \int_0^\infty \exp(-2k^2 D\mid t\mid)$$
$$\times \sum_{lm} g_l(kr)\, g^*_l(kr_0)\, Y_{lm}(\vartheta\varphi)\, Y^*_{lm}(\vartheta_0\varphi_0)\, k^2 dk. \tag{17}$$

We obtain the average in expression (10) with the aid of the function $U(\mathbf{r}, \mathbf{r}_0, t)$:

$$f_\lambda(\tau) = 3(2a)^3 \int r^{-3} r_0^{-3} Y_{2\lambda}(\vartheta, \varphi)$$
$$\times Y^*_{2\lambda}(\vartheta_0\varphi_0)\, U(\mathbf{r}, \mathbf{r}_0, t)\, d\mathbf{r}\, d\mathbf{r}_0, \tag{18}$$

where we have taken into account the fact that

$$\sum_k \langle r_{jk}^{-6} \mid Y_{2\lambda}(\vartheta_{jk}\varphi_{jk}) \mid^2\rangle = \frac{1}{3(2a)^3}\frac{N}{V}. \tag{19}$$

Now, by utilizing the properties of spherical harmonics and expression (17) for $U(\mathbf{r}, \mathbf{r}_0, t)$, we obtain

$$f_\lambda(\tau) = f(\tau)$$
$$= 3\left(\frac{a}{\pi}\right)^3 \int_0^\infty k^2\, dk \exp(-2k^2 D\mid t\mid) \left|\int_{2a}^\infty g(kr)\frac{dr}{r}\right|^2. \tag{20}$$

The integrals over r and r_0 may be evaluated with the aid of the recurrence relation:[7]

$$-\rho^{-l} g_{l+1}(\rho) = \frac{d}{d\rho}[\rho^{-l} g_l(\rho)]. \tag{21}$$

Then

$$f(\tau) = \frac{3}{(2\pi)^3} \int_0^\infty \exp\left(-\frac{\rho^2\mid\tau\mid}{9\tau_c}\right) \mid g_1(\rho)\mid^2 d\rho, \tag{22}$$

where we have used the notation $\tau_c = (4\pi/3)\, a^3\eta/kT$.

We obtain from (9) and (19):

$$\Omega^2 = \frac{4\pi}{5} I(I+1)\, g^4\mu_0^4\hbar^{-2}\frac{N}{V}(2a)^{-3}. \tag{23}$$

4. The correlation function in the case of rotational Brownian motion can be found in a manner similar to the one utilized above for translational

motion. We consider the molecule as a whole to be a sphere of radius a, and the distance between the magnetic moments b_{jk} within the molecule is assumed constant. Moreover, we assume that the molecule contains two identical nuclei with magnetic moments different from zero.

The solution of the diffusion equation for rotational motion similar to (17) is of the form:

$$v(\vartheta, \varphi, \vartheta_0, \varphi_0, t) = \sum_{lm} Y_{lm}(\vartheta, \varphi) Y^*_{lm}(\vartheta_0, \varphi_0) \exp\left(-\frac{l(l+1)D'|t|}{a^2}\right), \quad (24)$$

where $D' = kT/8\pi\eta a$ is the diffusion coefficient for rotational motion. The expression $v(\vartheta, \varphi, \vartheta_0, \varphi_0, t)\,d\Omega$ determines the probability that the molecule is oriented within the solid angle $d\Omega = \sin\vartheta\, d\vartheta\, d\varphi$, if at time $t = 0$ its orientation is determined by the angles ϑ_0, φ_0.

The evaluation of the correlation function leads in this case to the expression

$$f(\tau) = \exp\left(-\frac{6D'|\tau|}{a^2}\right) = \exp\left(-\frac{|\tau|}{\tau_c}\right), \quad (25)$$

which agrees in form with (1).

Averaging over the angles in (9), we obtain:

$$\Omega^2 = \frac{3}{5} I(I+1) g^4 \mu_0^4 \hbar^{-2} b_{12}^{-6}. \quad (26)$$

5. We now proceed to evaulate the quantities τ'_λ and τ''_λ which appear in the expressions for $T_\perp$, $T_\parallel$, and $\Delta\omega_0$.

In the case of translational Brownian motion we obtain after substituting (22) into (6) and after carrying out the integration over τ:

$$\tau'_\lambda + i\tau''_\lambda = 27\tau_c \int_0^\infty J^2_{3/2}(\rho)\, d\rho / \rho(\rho^2 - 9i\lambda\tau_c\omega_0). \quad (27)$$

This integral can be evaluated if we recall that $J_{3/2}(\rho)$ may be expressed in terms of trigonometric functions.

We denote

$$I(x) = \int_0^\infty J^*_{3/2}(\rho)\, d\rho / \rho\left(\rho^2 - \frac{i}{2}x^2\right)$$

$$= (x^{-3} - 2x^{-5}) + \exp(-x)[\cos x(x^{-3} + 4x^{-4} + 2x^{-5}) + \sin x(x^{-3} - 2x^{-5})]$$

$$\pm i\left\{\left(-\frac{2}{3}x^{-2} + x^{-3} + 2x^{-5}\right) + \exp(-x)[\cos x(x^{-3} - 2x^{-5}) - \sin x(x^{-3} + 4x^{-4} + 2x^{-5})]\right\},$$

$$x = \sqrt{18|\lambda|\tau_c\omega_0}, \quad (28)$$

where both in the above and in the following expressions we choose the upper sign for $\lambda < 0$ and the lower sign for $\lambda > 0$.

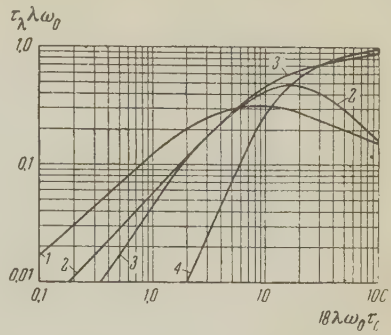

FIG. 1. Curves showing the dependence of $\tau'_\lambda\lambda\omega_0$ and $\tau''_\lambda\lambda\omega_0$ on $18\,\lambda\omega_0\tau_c$ labelled respectively 1 and 3 for translational Brownian motion, and 2 and 4 for rotational Brownian motion.

Thus, in the case of translational Brownian motion

$$\tau'_\lambda = \frac{1}{|\lambda|\omega_0}\frac{3}{2}x^2 \operatorname{Re} I(x), \quad \tau''_\lambda = \frac{1}{|\lambda|\omega_0}\frac{3}{2}x^2 \operatorname{Im} I(x). \quad (29)$$

In weak fields when $\tau_c\omega_0 \ll 1$:

$$\tau'_\lambda = \frac{18}{5}\tau_c - \frac{9}{\sqrt{2}}\tau_c\sqrt{|\lambda|\tau_c\omega_0},$$

$$\tau''_\lambda = \mp\frac{9}{\sqrt{2}}\tau_c\sqrt{|\lambda|\tau_c\omega_0}, \quad (29')$$

while in the case of strong fields when $\tau_c\omega_0 \gg 1$:

$$\tau'_\lambda = \frac{18}{5}\tau_c\delta_{\lambda 0} + \frac{1}{2\sqrt{2}}\tau_c(|\lambda|\tau_c\omega_0)^{-3/2}(1 - \delta_{\lambda 0}),$$

$$\tau''_\lambda = \mp\left(\frac{1}{|\lambda|\omega_0} - \frac{1}{2\sqrt{2}}\tau_c(|\lambda|\tau_c\omega_0)^{-3/2}\right)(1 - \delta_{\lambda 0}). \quad (29'')$$

In the case of rotational Brownian motion, on substituting (25) into (6) and on carrying out the integration with respect to τ, we obtain in a similar fashion

$$\tau'_\lambda = \frac{1}{|\lambda|\omega_0}\frac{18x^2}{x^4 + 324}, \quad \tau''_\lambda = \frac{1}{\lambda\omega_0}\frac{x^4}{x^4 + 324}, \quad (30)$$

which have simple asymptotic expressions.

In the case of weak fields:

$$\tau'_\lambda = \tau_c - \lambda^2\omega_0^2\tau_c^3, \quad \tau''_\lambda = \lambda\omega_0\tau_c^2. \quad (30')$$

In the case of strong fields:

$$\tau'_\lambda = \tau_c\delta_{\lambda 0} + \frac{1}{\lambda^2\omega_0^2\tau_c}(1 - \delta_{\lambda 0}),$$

$$\tau''_\lambda = \left(\frac{1}{\lambda\omega_0} - \frac{1}{\lambda^3\omega_0^3\tau_c^2}\right)(1 - \delta_{\lambda 0}). \quad (30'')$$

The dependence of $\tau'_\lambda|\lambda|\omega_0$ and $\tau''_\lambda|\lambda|\omega_0$ on $\tau_c\omega_0$, both for translational and rotational motion, is shown in Fig. 1.

Using (8), we obtain

$$T_\perp\Omega^2 = (2/3\tau'_2 + 5/3\tau'_1 + \tau'_0)^{-1}; \quad (31)$$

$$T_\parallel\Omega^2 = (2/3\tau'_1 + 8/3\tau'_2)^{-1}; \quad (32)$$

$$\Omega^2/\Delta\omega_0 = (2/3\tau''_2 + 1/3\tau''_1)^{-1}. \quad (33)$$

Thus, to obtain the dependence of $T_\perp$, $T_\parallel$, and $\Delta\omega_0$ on $\tau_c\omega_0$ both for translational and for rotational Brownian motion it is sufficient to know the value of Ω^2, which depends on the structure of the molecules and on the structure of the liquid. Curves

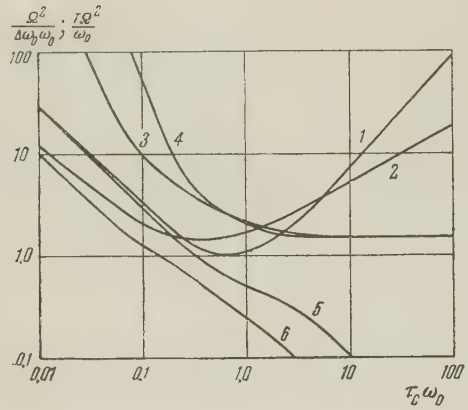

FIG. 2. Curves showing the dependence of $T_{\parallel}\Omega^2/\omega_0$, $T_{\perp}\Omega^2/\omega_0$ and $\Omega^2/\Delta\omega_0\omega_0$ on $\tau_c\omega_0$, labelled respectively 2, 6, and 3 for translational Brownian motion and by 1, 5, 4 for the case of rotational Brownian motion.

of $T_{\perp}\Omega^2/\omega_0$, $T_{\parallel}\Omega^2/\omega_0$, and $\Omega^2/\Delta\omega_0\omega_0$ vs. $\tau_c\omega_0$ are shown in Fig. 2.

6. As an example we consider the case of nuclear magnetic resonance in a liquid whose molecules contain two identical nuclei with magnetic moments differing from zero (water) with spins $I = \frac{1}{2}$.

In this case the operator $\hat{\mathcal{H}}_2$ can be separated into two parts $\hat{\mathcal{H}}_{2t}$ and $\hat{\mathcal{H}}_{2r}$, which describe the motion of the centers of masses of the molecules and the rotation of the molecule as a whole about the common center of mass. The distance b between nuclei belonging to the same molecule is constant.

The rotational Brownian motion leads only to a variation in the angle between the straight line joining these nuclei and the direction of the field H_0.

The translational Brownian motion alters the relative position of nuclei belonging to different molecules.

If we neglect the correlation between the translational and the rotational Brownian motions, each of the expressions for $T_{\perp}^{-1}$, $T_{\parallel}^{-1}$, and $\Delta\omega_0$ defined by (4) and (5) can be separated into two terms corresponding to the translational and the rotational Brownian motion of the molecules.

In calculating Ω^2 for the translational motion of the molecule we should take into account the fact that a fraction of the molecules ($\frac{3}{4}$) has a total nuclear spin equal to unity while the remaining fraction of the molecules ($\frac{1}{4}$) has a spin equal to zero.

Then for the translational motion we have

$$\Omega_t^2 = \frac{3\pi}{20} g^4 \mu_0^4 \hbar^{-2} \frac{N}{V} a^{-3}, \tag{34}$$

where N/V is the number of water molecules per unit volume.

In the case of rotational motion we have:

$$\Omega_r^2 = {}^9/_{20}\ g^4\ \mu_0^4 \hbar^{-2} b^{-6}. \tag{35}$$

Now, by utilizing (29) — (32) and (33) — (35) we can obtain expressions for the relaxation times $T_{\perp}$ and $T_{\parallel}$ and for $\Delta\omega_0$.

In weak fields when $\tau_c\omega_0 \ll 1$ we have:

$$\frac{1}{T_{\perp}} = \frac{1}{T_{\parallel}} = \frac{1}{T} = {}^3/_2\, g^4 \mu_0^4 \hbar^{-2} \tau_c \left(\frac{6\pi}{5} \frac{N}{V} a^{-3} + b^{-6}\right). \tag{36}$$

The transverse and the longitudinal relaxation times are equal.

The effective gyromagnetic ratio is of the form

$$\gamma^* = \gamma\left(1 + \frac{\Delta\omega_0}{\omega_0}\right) = \gamma\left(1 + \frac{6\sqrt{2}+3}{\sqrt{2}} \Omega_t^2 \tau_c \sqrt{\frac{\tau_c}{\omega_0}}\right). \tag{37}$$

In the first approximation the correction is determined by the translational Brownian motion where Ω_t^2 is given by (34).

In the case of strong fields when $\tau_c\omega_0 \gg 1$ we have:

$$\frac{1}{T_{\perp}} = \frac{9}{20} g^4 \mu_0^4 \hbar^{-2} \tau_c \left(\frac{6\pi}{5} \frac{N}{V} a^{-3} + b^{-6}\right); \tag{38}$$

$$\frac{1}{T_{\parallel}} = \frac{\sqrt{2}+1}{20\sqrt{2}} \pi g^4 \mu_0^4 \hbar^{-2} \frac{N}{V} a^{-3} \omega_0^{-3/2} \tau_c^{-1/2}; \tag{39}$$

$$\gamma^* \approx \gamma. \tag{40}$$

Here $T_{\parallel}$ is determined largely by the translational Brownian motion.

7. The expressions for $T_{\perp}$ and $T_{\parallel}$ in the example discussed above have been obtained by Bloembergen, Purcell, and Pound.[6] In reference 1 it was pointed out that these calculations are not accurate.

The expressions for $T_{\perp}$ and $T_{\parallel}$ obtained in reference 6 in the case of weak fields

$$0.88 \frac{1}{T_{\perp}} = \frac{1}{T_{\parallel}} = \frac{9}{10} g^4 \mu_0^4 \hbar^{-2} \tau_c \left(\frac{3}{2}\pi \frac{N}{V} a^{-3} + b^{-6}\right) \tag{41}$$

differ from (36) by numerical coefficients. Taking for water[8] at 20°C $a = 1.45 \times 10^{-8}$ cm, $b = 1.54 \times 10^{-8}$ cm, $\tau_c = 0.32 \times 10^{-11}$ sec, $V/N = 30 \times 10^{-24}$ cm^3, we obtain from (36) $T = T_{\parallel} = T_{\perp} = 3$ sec, which agrees with experimental data ($T_{\parallel} = T_{\perp} = 3.6 \pm 0.4$ sec).[9] For $\Delta\omega_0$ we obtain in this case

$$\Delta\omega_0 = 1.4\sqrt{\omega_0} \cdot 10^{-7}\ \text{sec}^{-1} \tag{42}$$

As can be seen from (39) and Fig. 2, in strong fields $T_{\parallel}$ is proportional to $\tau_c^{1/2}$. Such a dependence is determined by the translational Brownian motion, which makes the principal contribution in the case of strong fields.

For strong fields the dependence of $T_{\parallel}$ on τ_c, determined by (39), is given on a logarithmic scale in the region $\omega_0\tau_c \gg 1$ by a straight line with a slope of 26.5°, and not of 45°, as called for by the

theory of Bloembergen, Purcell, and Pound.[6]

e experimental values given in the paper of Bloembergen, Purcell, and Pound[6] for the relaxation times for glycerine at different values of η/T fall in the case of $\eta/T \gg 1$ on a less steep straight line with a slope of approximately 30°, which is in good agreement with the conclusions reached above. Moreover, it follows from (41) that in strong fields $T_{||}$ is proportional to $\omega_0^{3/2}$, and not to ω_0^2, as in reference 6, which also agrees much better with experimental data.

Thus, for the description of the phenomenon of nuclear resonance in liquids it is necessary to take into account the translational as well as the rotational Brownian motion of the molecules. Moreover the form of the correlation function for the two types of motion turns out to be different. Only in the case of weak fields when $\omega_0\tau_c \ll 1$ do the relaxation times turn out to be not very sensitive to the specific form of the relaxation function.

[1] R. Kubo and K. Tomita, J. Phys. Soc. Japan **9**, 888 (1954).

[2] M. Yokota and S. Koide, J. Phys. Soc. Japan **9**, 953 (1954).

[3] D. Kivelson, J. Chem. Phys. **27**, 1087 (1957).

[4] A. K. Chirkov and A. A. Kokin, J. Exptl. Theoret. Phys. (U.S.S.R.) **35**, 50 (1958), Soviet Phys. JETP **8**, 36 (1958).

[5] G. V. Skrotskiĭ and A. A. Kokin, J. Exptl. Theoret. Phys. (U.S.S.R.) **36**, 169 (1959), Soviet Phys. JETP **9**, 116 (1959).

[6] Bloembergen, Purcell, and Pound, Phys. Rev. **73**, 679 (1948).

[7] L. Schiff, Quantum Mechanics, McGraw-Hill, N. Y., 1955.

[8] R. A. Robinson and R. H. Stokes, Electrolyte Solutions, Butterworths, London, 1955.

[9] Chiarotti, Cristianini, and Ginlotto, Nuovo cimento **1**, 863 (1955).

Translated by G. Volkoff
81

MULTIPLE SCATTERING OF POLARIZED ELECTRONS

I. N. TOPTYGIN

Leningrad Polytechnic Institute

Submitted to JETP editor June 26, 1958

J. Exptl. Theoret. Phys. (U.S.S.R.) **36**, 488-498 (February, 1959)

Multiple elastic scattering of polarized spin-$\frac{1}{2}$ particles in an isotropic homogeneous medium is considered. The kinetic equations determining the distribution function and polarization vector of scattered particles are solved approximately. A solution which is valid for both small and large scattering angles has been obtained as a series expansion in spherical harmonics and spherical vectors.

1. INTRODUCTION

In connection with the testing of parity conservation, electrons and other particles produced in the course of various transformations have recently been found to be polarized. In experiments with polarized particles it is necessary to take into account the effect of multiple scattering on both the magnitude (depolarization) and direction of the polarization vector. The latter effect has been used in a number of investigations[1,2] to transform longitudinal polarization into transverse polarization, which can then be detected from the azimuthal asymmetry of electron scattering in nuclear Coulomb fields.

Bethe and Rose[3] were the first to estimate electron depolarization through multiple scattering. Mühlschlegel and Koppe[4] recently determine the distribution function and polarization of multiply scattered particles for only small angles. However, polarization effects are most significant at large angles, although the scattering cross section is greatly reduced with increase of the angle. In the present work we considered both large and small angles to obtain the angular distribution and polarization of particles passing through a scatterer of limited thickness. Inelastic collisions were disregarded. The equations that were derived agreed with the results obtained by Mühlschlegel and Koppe for small angles.

2. SINGLE SCATTERING

The scattering matrix of electrons in a centrally symmetrical field can, as we know, be represented by

$$\Omega = f(\theta) - ig(\theta)\nu\cdot\sigma, \quad \nu = [\mathbf{n}\times\mathbf{n}']/\sin\theta. \tag{1}$$

Here θ is the scattering angle; $\mathbf{n}$ and $\mathbf{n}'$ are the unit vectors of electron momentum before and after scattering; σ is the Pauli spin operator. The functions f and g for a Coulomb field have been given by Mott.[5] Approximate expressions for these functions up to terms containing $(\alpha Z)^2$ are given in the Appendix.

Before scattering let the state of polarization of the electron beam be given (in its rest frame) by the density matrix $\rho(\zeta) = (1 + \zeta\sigma)/2$, where $\zeta = \mathrm{Sp}(\sigma\rho)$ is the polarization vector. Then the differential cross section for scattering from the state with momentum $\mathbf{p} = p\mathbf{n}$ and polarization ζ to the state with momentum $\mathbf{p}' = p\mathbf{n}'$ and arbitrary polarization is given by

$$S(\mathbf{n}, \zeta; \mathbf{n}') = \mathrm{Sp}(\Omega\rho\Omega^+) = B(\theta) + D(\theta)\nu\cdot\zeta. \tag{2}$$

The polarization vector ζ' of the scattered beam is given by

$$\zeta' = \mathrm{Sp}(\sigma\Omega\rho\Omega^+)/\mathrm{Sp}(\Omega\rho\Omega^+). \tag{3}$$

Using (2) and calculating Sp, we obtain

$$\zeta' S(\mathbf{n}, \zeta; \mathbf{n}') = B\zeta + F[\nu\times\zeta] + C\,\nu\times[\nu\times\zeta] + D\nu. \tag{4}$$

B, C, D and F are given in terms of f and g as follows:

$$B = |f|^2 + |g|^2; \quad C = 2|g|^2,$$

$$D = i(fg^* - f^*g); \quad F = fg^* + f^*g. \tag{5}$$

It is evident from (4) that scattering can change ζ in both magnitude and direction. Polarization effects in both single and double scattering have been considered in detail in many papers (see the review by Tolhoek, reference 6) and will not be considered here.

3. THE KINETIC EQUATIONS

An electron beam scattered in an isotropic homogeneous medium will be characterized by the

intensity $I(\mathbf{n}, \mathbf{r})$ and polarization vector $\zeta(\mathbf{n}, \mathbf{r})$. The equations that determine I and ζ are easily obtained from elementary considerations. Let us consider the product $I\zeta = \mathbf{G}$ which gives the intensity of spin transport. The variation of this quantity per unit length of path is given by the derivative $(\mathbf{n}\cdot\nabla)\mathbf{G}$ and consists of the two parts

$$-N\mathbf{G}(\mathbf{n}, \mathbf{r})\int S(\mathbf{n}, \zeta; \mathbf{n}')\,d\Omega'$$

and

$$N\int \mathbf{G}(\mathbf{n}', \mathbf{r})\,S(\mathbf{n}', \zeta(\mathbf{n}', \mathbf{r}); \mathbf{n})\,d\Omega',$$

where N is the number of scattering centers per unit volume. Using (4) and denoting the total scattering cross section by σ, we obtain

$$\mathbf{n}\cdot\nabla\ \mathbf{G} = -N\sigma\mathbf{G} + N\int(A\mathbf{G}' + DI'\boldsymbol{\nu})\,d\Omega'. \qquad (6)$$

Here $\mathbf{G}' = \mathbf{G}(\mathbf{n}', \mathbf{r})$, $I' = I(\mathbf{n}', \mathbf{r})$, and A denotes the operator

$$A = B + F[\boldsymbol{\nu}\times\dots] + C[\boldsymbol{\nu}\times[\boldsymbol{\nu}\times\dots]]. \qquad (7)$$

An equation for I is obtained analogously:

$$(\mathbf{n}\cdot\nabla)I = -N\sigma I + N\int(BI' + D\boldsymbol{\nu}\cdot\mathbf{G}')\,d\Omega'. \qquad (8)$$

We note that in a paper by Waldmann[7] the kinetic equations for a particle with spin are given in matrix form using the scattering matrix. For the case of electrons these equations can easily be put into the form of (6) and (8).

We shall consider a scatterer in the form of a plane-parallel layer bounded by the planes $z = 0$ and $z = d$. For a beam of finite width I and G will depend on all three coordinates x, y, and z. Both sides of (6) and (8) will be integrated with respect to x and y; the x and y derivatives vanish and ∇ is replaced by $\partial/\partial z$. $I(\mathbf{n}, z)\cos\vartheta\,d\Omega$ will represent the number of particles passing through the plane $z = \text{const}$ in the $\mathbf{n}$ direction per unit time, and $\zeta = \mathbf{G}(\mathbf{n}, z)/I(\mathbf{n}, z)$ will represent the polarization of these particles. Introducing the dimensionless variable $\tau = N\sigma z$, Eqs. (6) and (8) become

$$\cos\vartheta\,\partial I/\partial\tau = -I + \int(BI' + D\boldsymbol{\nu}\mathbf{G}')\,d\Omega',$$

$$\cos\vartheta\,\partial\mathbf{G}/\partial\tau = -\mathbf{G} + \int(A\mathbf{G}' + DI'\boldsymbol{\nu})\,d\Omega'; \qquad (9)$$

B, C, D and F in these equations differ from the expressions in (5) by the factor $1/\sigma$.

The boundary conditions are

$$I(\mathbf{n}, 0) = I^{(0)}\delta(\mathbf{n} - \mathbf{n}_0),\ \mathbf{G}(\mathbf{n}, 0) = I^{(0)}\zeta^{(0)}\delta(\mathbf{n} - \mathbf{n}_0) \quad \text{for } \cos\vartheta > 0,$$

$$I(\mathbf{n}, t) = \mathbf{G}(\mathbf{n}, t) = 0 \quad \text{for } \cos\vartheta < 0; \qquad (10)$$

$\mathbf{n}_0(\vartheta_0, \varphi_0)$ gives the direction of the incident beam; $t = N\sigma d$; the δ function is normalized by $\int\delta(\mathbf{n} - \mathbf{n}_0)\,d\Omega = 1$.

Hereinafter we shall limit ourselves to a beam of normal incidence ($\cos\vartheta_0 = 1$). Instead of (9) with the boundary conditions (10) it is more convenient to consider two system of equations with corresponding boundary conditions:

$$\partial I_0/\partial\tau = -I_0 + \int(BI_0' + D\boldsymbol{\nu}\cdot\mathbf{G}_0')\,d\Omega',$$

$$\partial\mathbf{G}_0/\partial\tau = -\mathbf{G}_0 + \int(A\mathbf{G}_0' + DI_0'\boldsymbol{\nu})\,d\Omega',$$

$$I_0(\mathbf{n}, 0) = I^{(0)}\delta(\mathbf{n} - \mathbf{n}_0);\ \mathbf{G}_0(\mathbf{n}, 0) = I^{(0)}\zeta^{(0)}\delta(\mathbf{n} - \mathbf{n}_0); \qquad \text{(I)}$$

$$\cos\vartheta\,(\partial I_1/\partial\tau) = -I_1 + \int(BI_1' + D\boldsymbol{\nu}G_1')\,d\Omega' + (1 - \cos\vartheta)\,\partial I_0/\partial\tau,$$

$$\cos\vartheta\,\partial\mathbf{G}_1/\partial\tau = -\mathbf{G}_1 + \int(A\mathbf{G}_1' + DI_1'\boldsymbol{\nu})\,d\Omega' + (1 - \cos\vartheta)\,\partial\mathbf{G}_0/\partial\tau,$$

$$I_1(\mathbf{n}, 0) = \mathbf{G}_1(\mathbf{n}, 0) = 0 \quad \text{for } \cos\vartheta > 0,$$

$$I_1(\mathbf{n}, t) = -I_0(\mathbf{n}, t);\ \mathbf{G}_1(\mathbf{n}, t) = -\mathbf{G}_0(\mathbf{n}, t) \quad \text{for } \cos\vartheta < 0. \qquad \text{(II)}$$

When $I = I_0 + I_1$ and $\mathbf{G} = \mathbf{G}_0 + \mathbf{G}_1$ the equations (I) and (II) are equivalent to the original equation (9) and boundary conditions (10).

4. SOLUTION OF SYSTEM (I)

The equations of (I) differ from the exact equations by the fact that $\cos\vartheta$ is replaced by 1 in the left-hand members, which means that the true path $d\tau/\cos\vartheta$ traversed by a particle in the layer $d\tau$ is replaced by a segment $d\tau$ representing its path in the original direction of motion. The distribution function for unpolarized electrons was obtained in this approximation by Goudsmit and Saunderson.[8]

In the small-angle approximation the right-hand members in (I) give equations for I and G in small-angle scattering. However, it is our intention to solve the exact system (9) for all angles, so that we shall first obtain an exact solution of (I).

I_0 and $\mathbf{G}_0$ will be given as series of spherical harmonics and spherical vectors:*

$$I_0(\mathbf{n}, \tau) = \sum_{lm} I_{lm}(\tau)\,Y_{lm}(\mathbf{n}),$$

$$\mathbf{G}_0(\mathbf{n}, \tau) = \sum_{JLM} G^L_{JM}(\tau)\,\mathbf{Y}^L_{JM}(\mathbf{n}). \qquad (11)$$

In order to transform the integrals in the right-hand members we expand the integrands in series of spherical harmonics, as follows:

*We shall use Bethe's definition[9] of spherical harmonics. The definition and properties of spherical vectors have been given by Berestetskii, Dolginov and Ter-Martirosyan.[10]

$$B(\theta) = \Sigma B_l Y^*_{lm}(\mathbf{n}') Y_{lm}(\mathbf{n});$$

$$B_l = 2\pi \int_0^\pi B(\theta) P_l(\cos\theta) \sin\theta \, d\theta. \qquad (12)$$

Considering also that

$$[\mathbf{Y}^L_{JM}]_\mu = (-1)^{1-\mu} C^{JM}_{LM+\mu 1-\mu} Y_{LM+\mu},$$

where $C^{lm}_{l_1 m_1 l_2 m_2}$ is a Clebsch-Gordan coefficient and the index $\mu = 0, \pm 1$ denotes cyclical components of a vector, which are related to its Cartesian components by

$$a_0 = a_z, \; a_{\pm 1} = \mp (a_x \pm i a_y)/\sqrt{2},$$

we obtain

$$\int B(\theta) I'_0 \, d\Omega' = \sum B_l I_{lm}(\tau) Y_{lm}(\mathbf{n}), \; \int B(\theta) \mathbf{G}'_0 \, d\Omega'$$

$$= \sum B_L G^L_{JM}(\tau) \mathbf{Y}^L_{JM}(\mathbf{n}). \qquad (13)$$

For the expansion of $D(\theta)\nu_\mu = D(\theta)[\mathbf{nn}']_\mu / \sin\theta$ in spherical harmonics we note that $D(\theta)/\sin\theta$ transforms as a scalar while $[\mathbf{n}\times\mathbf{n}']_\mu$ transforms as a vector component. We can therefore write

$$D(\theta)[\mathbf{n}\times\mathbf{n}']_\mu/\sin\theta = i \sum D'_l C^{1\mu}_{lm l m'} Y_{lm}(\mathbf{n}) Y_{lm'}(\mathbf{n}'). \quad (14)$$

To determine D'_l we let $\vartheta' = \varphi' = 0$ in this equation. In virtue of the orthogonality of the spherical harmonics and of the Clebsch-Gordan coefficients, we obtain for D'_l:

$$D'_l = (\sqrt{8\pi(2l+1)}/3) \sum C^{1\mu}_{l\mu l 0} C^{1\mu}_{101\mu} \int \frac{D(\vartheta)}{\sin\vartheta} n_\mu Y^*_{l\mu}(\mathbf{n}) \, d\Omega$$

$$= (-1)^l [(2l+1)/3l(l+1)]^{1/2} 2\pi \int_0^\pi D(\theta) P^1_l(\theta) \sin\theta \, d\theta,$$

where P'_l is an unnormalized associated Legendre polynomial.

Making use of (14), we obtain for the integrals contain $D(\theta)$:

$$\int D(\theta) I'_0 \boldsymbol{\nu} \, d\Omega' = -i \sum D_l I_{lm} \mathbf{Y}^l_{lm},$$

$$\int D(\theta) \mathbf{G}'_0 \boldsymbol{\nu} \, d\Omega' = -i \sum D_l G^l_{lm} Y_{lm}; \qquad (15)$$

$$D_l = [2\pi/\sqrt{l(l+1)}] \int_0^\pi D(\theta) P^1_l(\theta) \sin\theta \, d\theta. \qquad (16)$$

The integrals containing $F(\theta)$ and $C(\theta)$ are calculated similarly, using Racah's formula for the summation of Clebsch-Gordan coefficients. We obtain

$$\int F(\theta)[\boldsymbol{\nu}\times\mathbf{G}'_0] \, d\Omega' = \sum_{JLM} F^J_L G^L_{JM} \mathbf{Y}^L_{JM}; \qquad (17)$$

$$F^J_L = -\frac{L(L+1) - J(J+1) + 2}{2L(L+1)} 2\pi \int_0^\pi F(\theta) P^1_l(\theta) \sin\theta \, d\theta; \quad (18)$$

$$\int C(\theta) \boldsymbol{\nu}\times[\boldsymbol{\nu}\times\mathbf{G}'_0] \, d\Omega' = \sum_{JLL'M} C^J_{LL'} G^{L'}_{JM} \mathbf{Y}^L_{JM}, \qquad (19)$$

$$C^l_{ll} = -\pi C_{l0} - \pi C_{l2}/l(l+1),$$

$$C^{l+1}_{ll} = -\pi(3l+4) C_{l0}/(2l+3)$$

$$+ \pi C_{l2}/(l+1)(2l+3), \qquad (20)$$

$$C^{l-1}_{ll} = -\pi(3l-1) C_{l0}/(2l-1) + \pi C_{l2}/l(2l-1),$$

$$C^l_{l-1\,l+1} = C^l_{l+1\,l-1} = [2\pi/(2l+1)\sqrt{l(l+1)}] \int_0^\pi C(\theta) P^1_l(\theta) \, d\theta,$$

$$C_{lm} = \int_0^\pi C(\theta) P^m_l(\theta) \sin\theta \, d\theta.$$

Substituting these values of the integrals into (I), we obtain four first-order differential equations associated in pairs:

$$dI_{LM}/d\tau = -b_L I_{LM} - iD_L G^L_{LM},$$
$$dG^L_{LM}/d\tau = -a^L_L G^L_{LM} - iD_L I_{LM}; \qquad (21)$$

$$dG^{L+1}_{LM}/d\tau = -a^{L+1}_L G^{L+1}_{LM} + c_L G^{L-1}_{LM},$$
$$dG^{L-1}_{LM}/d\tau = -a^{L-1}_L G^{L-1}_{LM} + c_L G^{L+1}_{LM}. \qquad (22)$$

The following notation has been used:

$$b_L = 1 - B_L; \; a^J_L = 1 - B_L - F^J_L - C^J_{LL};$$

$$c_L = C^L_{L+1\,L-1}. \qquad (23)$$

Equations (21) and (22) are easily integrated, the integration constants being determined by the boundary conditions

$$I_{LM}(0) = I^{(0)} \sqrt{(2L+1)/4\pi} \delta_{M0},$$

$$G^L_{JM}(0) = I^{(0)} \sqrt{(2I+1)/4\pi} C^{L0}_{1-M\,JM} \zeta^{(0)}_{-M} \; (J = L, \; L \pm 1). \quad (24)$$

We finally obtain the distribution function of scattered electrons:

$$I_0(\mathbf{n}, \tau) = \frac{I^{(0)}}{4\pi} \sum_l \frac{(2l+1)}{1-k_l^2} (e^{-\alpha_1\tau} - k_l^2 e^{-\alpha_2\tau}) P_l(\cos\vartheta)$$

$$- \frac{I^{(0)} P_0}{4\pi} \sin\chi \sin\varphi \sum_l \frac{(2l+1) k_l}{\sqrt{l(l+1)(1-k_l^2)}} (e^{-\alpha_1\tau} - e^{-\alpha_2\tau}) P^1_l(\vartheta),$$

$$2\alpha_{1,2} = b_l + a^l_l \pm [(b_l - a^l_l)^2 - 4D_l^2]^{1/2},$$

$$k_l = 2D_l/(b_l - a^l_l + \sqrt{(b_l - a^l_l)^2 - 4D_l^2}), \qquad (25)$$

where $P_0 = |\zeta^{(0)}|$ is the degree of polarization of the initial beam, χ is the angle between $\zeta^{(0)}$ and $\mathbf{n}_0$, and the x axis is in the $\zeta^{(0)}$, $\mathbf{n}_0$ plane.

The second term in (25) gives the azimuthal asymmetry due to the transverse polarization component of the incident beam. For $D = 0$, which represents the absence of spin-orbit coupling, α_2 and k_l vanish, while α_1 becomes equal to b_l.

Equation (25) is thus converted into the Goudsmit-Saunderson formula

$$I_0(\vartheta, \tau) = (I^{(0)}/4\pi) \sum (2l+1)\, e^{-b_l \tau} P_l(\cos\vartheta). \quad (26)$$

For the vector $\mathbf{G}_0$ in the case of initial longitudinal polarization ($\xi_z^{(0)} = \xi^{(0)}$, $\xi_x^{(0)} = \xi_y^{(0)} = 0$), we obtain

$$\mathbf{G}_0(\mathbf{n}, \tau) = \frac{I^{(0)}}{\sqrt{4\pi}} \sum \Big\{ \frac{ik_l (2l+1)^{1/2}}{1-k_l^2} (e^{-\alpha_1\tau} - e^{-\alpha_2\tau})\, \mathbf{Y}_{l0}^l$$

$$+ \frac{\xi^{(0)}}{1+s_l^2} [\{(l+1)^{1/2} (e^{-\beta_1\tau} + s_l^2 e^{-\beta_2\tau}) + s_l l^{1/2} (e^{-\beta_1\tau} - e^{-\beta_2\tau})\}\, \mathbf{Y}_{l0}^{l+1}$$

$$- \{l^{1/2}(s_l^2 e^{-\beta_1\tau} + e^{-\beta_2\tau}) + s_l (l+1)^{1/2} (e^{-\beta_1\tau} - e^{-\beta_2\tau})\}\, \mathbf{Y}_{l0}^{l-1}]\Big\},$$

$$2\beta_{1,2} = a_l^{l+1} + a_l^{l-1} \pm [(a_l^{l+1} - a_l^{l-1})^2 + 4c_l^2]^{1/2},$$

$$s_l = 2c_l / (a_l^{l+1} - a_l^{l-1} + \sqrt{(a_l^{l+1} - a_l^{l-1})^2 + 4c_l^2}\,). \quad (27)$$

We also write the projections of $\mathbf{G}_0$ on the rectangular axes χ, η, ζ, which are in the directions of the vectors $\mathbf{n}\times\mathbf{n}_0$, $\mathbf{n}\times[\mathbf{n}\times\mathbf{n}_0]$ and $\mathbf{n}$, as follows:

$$G_\chi = -\frac{I^{(0)}}{4\pi} \sum \frac{k_l (2l+1)}{(1-k_l^2)\sqrt{l(l+1)}} (e^{-\alpha_1\tau} - e^{-\alpha_2\tau})\, P_l^1(\vartheta),$$

$$G_\eta = \frac{I^{(0)}\xi^{(0)}}{4\pi} \sum \frac{1 - s_l^2 - s_l/\sqrt{l(l+1)}}{1+s_l^2} (e^{-\beta_1\tau} - e^{-\beta_2\tau})\, P_l^1(\vartheta),$$

$$G_\zeta = (I^{(0)}\zeta^{(0)}/4\pi) \sum (1+s_l^2)^{-1} \{(l+1)(e^{-\beta_1\tau} + s_l^2 e^{-\beta_2\tau})$$

$$+ l(s_l^2 e^{-\beta_1\tau} + e^{-\beta_2\tau})$$

$$+ 2s_l \sqrt{l(l+1)}/(e^{-\beta_1\tau} - e^{-\beta_2\tau})\} P_l(\cos\vartheta). \quad (28)$$

The projection G_χ is independent of the initial polarization, but gives the polarization of the initially unpolarized electron beam due to multiple scattering (the Mott effect). However, this effect disappears when $D = 0$, which occurs in the first Born approximation.

5. SOLUTION OF SYSTEM (II)

When the scatterer is not very thick each of the functions I_0 and $\mathbf{G}_0$ possesses a very sharp peak in the direction of initial electron motion, since the Coulomb scattering occurs predominantly in the forward direction. I_1 and $\mathbf{G}_1$, which are determined by (II), will have a considerably smoother form, because the functions $(1-\cos\vartheta)\,\partial I_0/\partial\tau$ and $(1-\cos\vartheta)\,\partial\mathbf{G}_0/\partial\tau$ in (II) as well as $I_0(\mathbf{n}, t)$ and $\mathbf{G}_0(\mathbf{n}, t)$ for $\cos\vartheta < 0$, which determine I_1 and $\mathbf{G}_1$ on the boundary, are smooth functions. Successive approximations can therefore be used to solve (II), as in reference 11 for the first equation of (29) with $D = 0$.

We now rewrite (II) in the form

$$\cos\vartheta\,\partial I_1/\partial\tau = J + (1-\cos\vartheta)\,\partial I_0/\partial\tau,$$
$$\cos\vartheta\,\partial\mathbf{G}_1/\partial\tau = \mathbf{Y} + (1-\cos\vartheta)\,\partial\mathbf{G}_0/\partial\tau, \quad (29)$$

where J and $\mathbf{Y}$ denote the differences between the respective integrals and I_1 and $\mathbf{G}_1$. In first approximation we set $J = \mathbf{Y} = 0$. The error thus introduced is the smaller, the smoother the functions I_1 and $\mathbf{G}_1$ and the sharper the forward peak of the single-scattering cross section. A more precise criterion for the applicability of this approximation will be given below.

The equations now have the simple form

$$\cos\vartheta\,\partial I_1/\partial\tau = (1-\cos\vartheta)\,\partial I_0/\partial\tau,$$
$$\cos\vartheta\,\partial\mathbf{G}_1/\partial\tau = (1-\cos\vartheta)\,\partial\mathbf{G}_0/\partial\tau, \quad (30)$$

and their solutions which satisfy the required boundary conditions are as follows:

$$\left.\begin{aligned} I_1^{(1)}(\mathbf{n},\tau) &= (\sec\vartheta - 1)\, I_0(\mathbf{n}, \tau), \\ \mathbf{G}_1^{(1)}(\mathbf{n}, \tau) &= (\sec\vartheta - 1)\, \mathbf{G}_0(\mathbf{n}, \tau), \end{aligned}\right\} \text{ for } \cos\vartheta > 0; \quad (31)$$

$$\left.\begin{aligned} I_1^{(1)}(\mathbf{n}, \tau) &= (\sec\vartheta - 1)\, I_0(\mathbf{n}, \tau) - \sec\vartheta I_0(\mathbf{n}, t), \\ \mathbf{G}_1^{(1)}(\mathbf{n}, \tau) &= (\sec\vartheta - 1)\, \mathbf{G}_0(\mathbf{n}, \tau) - \sec\vartheta \mathbf{G}_0(\mathbf{n}, t) \end{aligned}\right\} \cos\vartheta < 0. \quad (32)$$

These solutions do not apply to the vicinity of the point $\vartheta = \pi/2$, where they possess a singularity; the approximate equations (30) themselves cease to be valid near $\vartheta = \pi/2$. However, the angular region near $\pi/2$ is of least interest since the number of particles moving at such angles is very small

To obtain the next approximation we substitute the values found for I_1 and $\mathbf{G}_1$ into J and $\mathbf{Y}$, which we shall regard as known functions. Then from (29) with the corresponding boundary conditions we obtain for $\cos\vartheta > 0$:

$$I_1^{(2)}(\mathbf{n}, \tau) = (\sec\vartheta - 1)\, I_0(\mathbf{n}, \tau) + \sec\vartheta \int_0^\tau J(\mathbf{n}, \tau')\, d\tau',$$

$$\mathbf{G}_1^{(2)}(\mathbf{n}, \tau) = (\sec\vartheta - 1)\, \mathbf{G}_0(\mathbf{n}, \tau) + \sec\vartheta \int_0^\tau \mathbf{Y}(\mathbf{n}, \tau')\, d\tau'; \quad (33)$$

and for $\cos\vartheta < 0$:

$$I_1^{(2)}(\mathbf{n}, \tau) = (\sec\vartheta - 1)\, I_0(\mathbf{n}, \tau)$$

$$- \sec\vartheta I_0(\mathbf{n}, t) - \sec\vartheta \int_\tau^t J(\mathbf{n}, \tau_,)\, d\tau',$$

$$\mathbf{G}_1^{(2)}(\mathbf{n}, \tau) = (\sec\vartheta - 1)\, \mathbf{G}_0(\mathbf{n}, \tau)$$

$$- \sec\vartheta \mathbf{G}_0(\mathbf{n}, t) - \sec\vartheta \int_\tau^t \mathbf{Y}(\mathbf{n}, \tau')\, d\tau'. \quad (34)$$

The method of estimating corrections containing J and $\mathbf{Y}$ is similar to that by which the Fokker-Planck equation is obtained from the exact kinetic equation. We shall make use of the sharply anisotropic character of the Coulomb cross section and shall consider only small-angle scattering. In this case the first Born approximation can also be applied to heavy nuclei. Replacing $\sin\theta/2$ by $\theta/2$

and cos $\theta/2$ by 1 and retaining the terms with the largest values when θ is small, we obtain from the formulas given in the Appendix:

$$B(\theta) = 16\,\sigma_0 q(\theta)/\theta^4;\quad F(\theta) = 16\,\sigma_0 bq(\theta)/\theta^3,$$
$$C(\theta) = 8\,\sigma_0 b^2 q(\theta)/\theta^2,\quad D(\theta) = 0. \tag{35}$$

Here $q(\theta)$ takes into account the screening of the nuclear field by atomic electrons and removes the divergence at $\theta = 0$.

$I_1^{(1)}(\mathbf{n}', \tau)$ and $\mathbf{G}_1^{(1)}(\mathbf{n}', \tau)$ near the point $\mathbf{n}' = \mathbf{n}$ are expanded in series, keeping terms up to the second order inclusively. We thus obtain

$$\mathbf{G}_1^{(1)}(\mathbf{n}', \tau) = \mathbf{G}_1^{(1)}(\mathbf{n}, \tau) + (\theta\nabla)\,\mathbf{G}_1^{(1)}(\mathbf{n}, \tau)$$
$$+ \tfrac{1}{2}\sum_{ik}\theta_i\theta_k\nabla_i\nabla_k\mathbf{G}_1^{(1)}(\mathbf{n}, \tau) \tag{36}$$

and a similar expansion for $I_1^{(1)}$. In this expression the difference $\mathbf{n}'-\mathbf{n}$ is replaced by θ; $|\theta| = \theta$, the vector θ lying in a plane perpendicular to $\mathbf{n}$. i and k take two values; $\theta_1 = \theta\cos\Phi$, $\theta_2 = \theta\sin\Phi$, $0 \le \Phi \le 2\pi$. ∇ is the portion of the gradient which operates on the angles. When integrating over angles we must replace $d\Omega'$ by $\theta\,d\theta\,d\Phi$. Using (35) and integrating, we obtain

$$J(\mathbf{n}, \tau) = \varkappa\nabla^2 I_1^{(1)}(\mathbf{n}, \tau),$$
$$\mathbf{Y}(\mathbf{n}, \tau) = \varkappa\{\nabla^2\mathbf{G}_1^{(1)} + 2b\times[\mathbf{n}\times\nabla]\times\mathbf{G}_1^{(1)}$$
$$- b^2[\mathbf{G}_1^{(1)} + (\mathbf{n}\cdot\mathbf{G}_1^{(1)})\,\mathbf{n}]\}. \tag{37}$$

Here κ denotes $8\pi(\sigma_0/\sigma)\int_0^\pi q(\theta)\,d\theta/\theta$.

The approximation under discussion can be used when the terms containing J and $\mathbf{Y}$ in (33) and (34) are much smaller than $I_1^{(1)}$ and $\mathbf{G}_1^{(1)}$. It follows from (33), (34), and (37) [see also (41) and (42)] that this condition is satisfied when $\kappa t \ll |\cos^3\vartheta|$, excluding the angular region in the vicinity of $\vartheta = \pi/2$ and limiting the thickness of the scatterer. At small angles $|\vartheta^2 \le \kappa t|$ the solution of (II) need not be considered at all, since in this region a good approximation is given by (25) and (27) or by the equations in reference 4.

We can estimate the order of κ by setting $q(\theta) = 0$ for $\theta < \chi_0$, $q(\theta) = 1$ for $\theta > \chi_0$, where $\chi_0 = \lambda\!\!\!^{-}/a$, $\lambda\!\!\!^{-} = \lambda/p$ is the de Broglie electron wavelength, $a = 0.885\,a_0 Z^{1/3}$ is the Thomas-Fermi atomic radius and a_0 is the Bohr radius. $\chi_0 < 10^{-2}Z^{1/3}$ for electrons of all energies beginning with 150 kev. With σ and κ calculated in the same approximation, we obtain

$$2\varkappa = \chi_0^2 \ln(\pi/\chi_0). \tag{38}$$

Finally, for I and $\mathbf{G}$ we obtain for forward scattering ($\cos\vartheta > 0$):

$$I(\mathbf{n}, t) = \sec\vartheta I_0(\mathbf{n}, t) + \sec\vartheta\int_0^t J(\mathbf{n}, \tau)\,d\tau,$$
$$\mathbf{G}(\mathbf{n}, t) = \sec\vartheta\mathbf{G}_0(\mathbf{n}, t) + \sec\vartheta\int_0^t \mathbf{Y}(\mathbf{n}, \tau)\,d\tau, \tag{39}$$

and for backward scattering ($\cos\vartheta < 0$):

$$I(\mathbf{n}, 0) = -\sec\vartheta I_0(\mathbf{n}, t) - \sec\vartheta\int_0^t J(\mathbf{n}, \tau)\,d\tau,$$
$$\mathbf{G}(\mathbf{n}, 0) = -\sec\vartheta\mathbf{G}_0(\mathbf{n}, t) - \sec\vartheta\int_0^t \mathbf{Y}(\mathbf{n}, \tau)\,d\tau. \tag{40}$$

It is evident from (39) and (40) that, neglecting terms proportional to κ, the vector ξ equals the ratio $\mathbf{G}_0/I_0$, i.e., $\mathbf{G}_0$ and I_0 are good zeroth approximations for the determinations of ξ.

Integration over τ in (39) and (40) can easily be performed when the explicit forms of I_0 and $\mathbf{G}_0$ are used. In obtaining explicit expressions for J and $\mathbf{Y}$ from (37) it is convenient to use the following relations. When $\mathbf{G} = \sec\vartheta\mathbf{G}_0$, where $\mathbf{G}_0 = \Sigma G^L_{JM}\mathbf{Y}^L_{JM}(\mathbf{n})$, we have

$$[\mathbf{n}\times\nabla]\times\mathbf{G} = \sec^2\vartheta[\mathbf{n}_0\times\mathbf{n}]\times\mathbf{G}_0 + \sec\vartheta\sum B^J_L G^L_{JM}\mathbf{Y}^L_{JM}, \tag{41}$$

where $\mathbf{n}_0$ is a unit vector in the z direction;

$$B^L_L = 1,\qquad B^{L+1}_L = L+1,\qquad B^{L-1}_L = -L,$$
$$\nabla^2\mathbf{G} = 2\sec^3\vartheta\mathbf{G}_0 - 2\sec^2\vartheta(\mathbf{n}_0\cdot\nabla)\,\mathbf{G}_0 + \sec\vartheta\nabla^2\mathbf{G}_0. \tag{42}$$

Operation by ∇^2 on a spherical vector or spherical harmonic is equivalent to multiplication by $-L(L+1)$. Use of the operator $(\mathbf{n}_0\cdot\nabla)$ is equivalent to calculating the z-component of the gradient of a spherical harmonic, as was done in reference 9.

6. EVALUATION OF INTEGRALS

We do not know the exact functions f and g which determine the amplitude of electron scattering by an atom. In order to evaluate the integrals in (12), (16), (18), and (20) we take the Coulomb functions f and g as series in (αZ) and consider terms up to $(\alpha Z)^3$ in the scattering cross section. This is the second Born approximation, which is apparently sufficiently good for light and intermediate nuclei, and can be used for approximate evaluation in the case of heavy nuclei.

To allow for screening we shall regard the scattering cross section as vanishing for $\theta < \chi_0$, the angle χ_0 being given in the preceding section.

In calculating the integrals it is convenient to use the representation of associated Legendre polynomials as sums of powers of $\sin(\theta/2)$.[12]

As a result of integration terms of the form

$\ln \sin(\chi_0/2) \approx \ln(\chi_0/2)$ and $1-\sin^n(\chi_0/2)$, $n \geq 1$, appear after the summation signs. The second of these (the difference) can be replaced by unity, after which the corresponding sums will depend only on l and $\ln(\chi_0/2)$ and can easily be computed directly. We finally obtain the following expressions for the integrals:

$$B_l = 1 - 8\pi(\sigma_0/\sigma)\, l(l+1)[\ln(2/\chi_0) - s_0(l) + 1] + 8\pi\beta^2(\sigma_0/\sigma)\, s_0(l) + 8\pi^2\beta\alpha Z(\sigma_0/\sigma)[s_0(l) - 2l]; \quad (43)$$

$$\int_0^\pi F(\theta) P_l^1(\theta) \sin\theta\, d\theta = -(4\sigma_0/\sigma) b^2 + 8b(\sigma_0/\sigma)\{l(l+1)[\ln(2/\chi_0) - s_0(l) + 1] - 1/2 (l+1/2)^2\} - 4\pi\beta\alpha Z(\sigma_0/\sigma)(2l+1)^{-1}\{(1-\beta^2)^{1/2} \times [(l-1)(2l+3)+2] - 2(l-1)(2l+3) - 5\}; \quad (44)$$

$$C_{l0} = 4b^2(\sigma_0/\sigma)\{2\ln(2/\chi_0) - 2s_0(l) - \delta_{l0}\} - 4\pi\beta\alpha Z(\sigma_0/\sigma)\, b\{\delta_{l0} - 2/(2l+1)\}; \quad (45)$$

$$C_{l2} = 4b^2(\sigma_0/\sigma)(l-1)(l+2) + 8\pi\beta\alpha Z(\sigma_0/\sigma)\, b(l-1)(l+2)/(2l+1); \quad (46)$$

$$\int_0^\pi C(\theta) P_l^1(\theta)\, d\theta = 2b^2(\sigma_0/\sigma) \times \{2l(l+1)[\ln(2/\chi_0) - s_0(l) + 1] - (l+1/2)^2\} + 2\pi\beta\alpha Z(\sigma_0/\sigma)\, b\{2l - (l+1/2)^2(\chi_0/2)\}; \quad (47)$$

$$D_l = 8\pi\beta\alpha Z(\sigma_0/\sigma)[(1-\beta^2)/l(l+1)]^{1/2} \times \{1/4 (l+1/2)^2 \chi_0^2 \ln(2/\chi_0) - s_0(l)\}; \quad (48)$$

$$\sigma = 8\pi\sigma_0\{(2/\chi_0^2) - \beta^2\ln(2/\chi_0) + \pi\beta\alpha Z[2/\chi_0 - \ln(2/\chi_0)]\}; \quad (49)$$

$$s_0(l) = \sum_{k=1}^{l} 1/k = \Psi(l+1) + C. \quad (50)$$

$\Psi(l)$ is the logarithmic derivative of the γ function and C is the Euler constant.

Equations (43) — (48) are valid for $l\chi_0 \ll 1$. They contain one parameter which is partly arbitrary — the screening angle χ_0.

7. COMPARISON WITH THE THEORY OF MÜHL-SCHLEGEL AND KOPPE

We shall show that when only small-angle scattering is considered our own Eqs. (25) and (28) go over into the corresponding equations in reference 4. Following Bethe, we replace the Legendre polynomials with Bessel functions through the following familiar formula,[12] which holds true for $\theta \ll 1$:

$$P_l^{-m}(\cos\theta) = (-1)^m (l+1/2)^{-m} J_m((l+1/2)\theta). \quad (51)$$

We shall integrate over θ from 0 to ∞. Also, in the expansion coefficients (16), (18), and (20) we shall neglect all terms except those containing the highest power of l, since terms with large l make the principal contributions to the sums in (25) — (28). These simplifications lead to the following expressions for the expansion coefficients:

$$B_l = 2\pi\int_0^\infty B(\theta) J_0(l\theta)\,\theta\, d\theta,$$

$$C_{ll}^l = -\pi\int_0^\infty C(\theta) J_0(l\theta)\,\theta\, d\theta - \pi\int_0^\infty C(\theta) J_2(l\theta)\,\theta\, d\theta,$$

$$C_{ll}^{l+1} = C_{ll}^{l-1} = -\frac{3\pi}{2}\int_0^\infty C(\theta) J_0(l\theta)\,\theta\, d\theta' + \frac{\pi}{2}\int_0^\infty C(\theta) J_2(l\theta)\,\theta\, d\theta,$$

$$C_{l+1\,l-1}^l = C_{l-1\,l+1}^l = \frac{\pi}{2}\int_0^\infty C(\theta)\{J_0(l\theta) + J_2(l\theta)\}\,\theta\, d\theta,$$

$$F_l^l = 0,\ F_l^{l+1} = -F_l^{l-1} = 2\pi\int_0^\infty F(\theta) J_1(l\theta)\,\theta\, d\theta,$$

$$D_l = 2\pi\int_0^\infty D(\theta) J_1(l\theta)\,\theta\, d\theta. \quad (52)$$

By comparing (52) with the equations (24) of reference 4 we easily obtain the relation between the notation of reference 4 and our notation:

$$\omega(l) = B_l\tau;\quad \omega_0 = \tau;\quad C_{ll}^{l+1}\tau = -2(\gamma+\gamma_1);\ D_l\tau = \delta(l),$$
$$F_l^{l+1}\tau = \varphi(l);\ C_{ll}^l\tau = -2\gamma_1(l);\ c_l\tau = \gamma_1(l). \quad (53)$$

In (25) the summation over l is replaced by an integral and the use of (53) leads to

$$I(\mathbf{n},\tau) = \frac{I_0}{2\pi}\int dl\cdot l\left\{\cosh\sqrt{\gamma_1^2-\delta^2} + \frac{\gamma_1}{\sqrt{\gamma_1^2-\delta^2}}\sinh\sqrt{\gamma_1^2-\delta^2}\right\} e^{\omega-\omega_0-\gamma_1} J_0(l\vartheta) + \frac{I^{(0)}P_0}{2\pi}\sin\chi\sin\varphi\int dl\cdot l \times \frac{\delta}{\sqrt{\gamma_1^2-\delta^2}}\sinh\sqrt{\gamma_1^2-\delta^2}\, e^{\omega-\omega_0-\gamma_1} J_1(l\vartheta), \quad (54)$$

which agrees with (30) of reference 4.

The equations in (32) can be transformed in similar fashion.

The author is deeply grateful to A. Z. Dolginov for valuable suggestions and to V. V. Batygin for discussions.

APPENDIX

Up to terms containing $(\alpha Z)^2$ the functions f and g are given by

$$f = -F' + G;\ g = F'\cot(\theta/2) + G\tan(\theta/2),$$

$$F' = -(Ze^2/2pv)(1-\beta^2)^{1/2}\left[1 - (2i\alpha Z/\beta)\left(C + \ln\sin\frac{\theta}{2}\right)\right],$$

$$G = (Ze^2/2pv)\left\{\cot^2\frac{\theta}{2} + (\pi\beta\alpha Z/2)\left(\operatorname{cosec}\frac{\theta}{2} - 1\right)\right.$$

$$\left. + i\alpha Z\left[(2/\beta)\cot^2\frac{\theta}{2}\left(C + \ln\sin\frac{\theta}{2}\right) - (\beta/2)\ln\operatorname{cosec}^2\frac{\theta}{2}\right]\right\},$$

where C is the Euler constant.

Up to $(\alpha Z)^3$ we have $B(\theta)$, $C(\theta)$, $D(\theta)$, and $F(\theta)$ given by

$$B(\theta) = \sigma_0\operatorname{cosec}^4\frac{\theta}{2}\left[1 - \beta^2\sin^2\frac{\theta}{2} + \pi\beta\alpha Z\sin\frac{\theta}{2}\left(1 - \sin\frac{\theta}{2}\right)\right],$$

$$C(\theta) = 2b^2\sigma_0\cot^2\frac{\theta}{2} + 2\pi\beta b\sigma_0\alpha Z\left(\operatorname{cosec}\frac{\theta}{2} - 1\right),$$

$$D(\theta) = 4\beta\sigma_0\alpha Z(1-\beta^2)^{1/2}\operatorname{cosec}\theta\ln\sin\frac{\theta}{2},$$

$$F(\theta) = 2\sigma_0\cot\frac{\theta}{2}\cdot b\left[(1-\beta^2)^{1/2} + \cot^2\frac{\theta}{2}\right]$$

$$+ 2\pi\beta\sigma_0\alpha Z\tan\frac{\theta}{2}\left\{\left(\operatorname{cosec}^2\frac{\theta}{2} - 1\right)\right.$$

$$\left. + (1-\beta^2)^{1/2}\left(1 - \frac{1}{2}\operatorname{cosec}^2\frac{\theta}{2}\right)\right\}\left(\operatorname{cosec}\frac{\theta}{2} - 1\right),$$

$$b = 1 - (1-\beta^2)^{1/2};\ \sigma_0 = (Ze^2/2pv)^2.$$

[1] Alikhanov, Eliseev, Lyubimov and Érshler, Paper at 8th All-Union Conference on Nuclear Spectroscopy, Leningrad, January 28, 1958.

[2] J. Heintze, Z. Physik **148**, 560 (1957).

[3] M. Rose and H. Bethe, Phys. Rev. **55**, 277 (1939).

[4] B. Mühlschlegel and H. Koppe, Z. Physik **150**, 474 (1958).

[5] N. F. Mott, Proc. Roy. Soc. (London) **A124**, 425 (1929); **A135**, 429 (1932).

[6] H. A. Tolhoek, Revs. Modern Phys. **28**, 277 (1956).

[7] L. Waldmann, Z. Naturforsch. **12a**, 660 (1957).

[8] S. Boudsmit and J. L. Saunderson, Phys. Rev. **57**, 24 (1940).

[9] H. Bethe, Quantenmechanik der Ein- und Zwei-Elektronenprobleme (Russ. Transl.) ONTI, M.-L., 1935. [Handb. Physik XXIV/I, Springer, Berlin, 1933 pp. 273-560]

[10] Berestetskii, Dolginov, and Ter-Martirosyan, J. Exptl. Theoret. Phys. (U.S.S.R.) **20**, 527 (1950).

[11] M. C. Wang and E. Guth, Phys. Rev. **84**, 1092 (1951).

[12] Erdelyi, Magnus, Oberhettinger, and Tricomi, Higher Transcendental Functions, Vol. I, McGraw-Hill Book Company, New York, 1953.

[13] H. A. Bethe, Phys. Rev. **89**, 1256 (1953).

[14] F. Gürsey, Phys. Rev. **107**, 1734 (1957).

Translated by I. Emin
82

ENERGY AND ANGULAR DISTRIBUTION IN DIFFRACTION DISINTEGRATION PROCESSES

I. I. IVANCHIK and V. S. POPOV

P. N. Lebedev Physics Institute, Academy of Sciences (U.S.S.R.)

Submitted to JETP editor June 27, 1958

J. Exptl. Theoret. Phys. (U.S.S.R.) **36**, 499-504 (February, 1959)

The energy and angular distributions have been obtained for particles obtained in diffraction disintegration of a weakly-bound quantum-mechanical system (deuteron etc.). The energy distributions are practically identical with those observed in stripping, whereas the angular distributions are appreciably different. A simple physical explanation of this difference can be proposed, and it may be of importance in interpreting the experimental data.

1. Diffraction disintegration of the deuteron was investigated by Feinberg,[1] Glauber,[2] and Akhiezer and Sitenko,[3] all of whom used a computation method analogous to the Kirchhoff method in the diffraction of light. It yields good results only in the vicinity of the geometric shadow. The most reliable result in the theory of diffraction disintegration is therefore the differential cross section of the process for small angles.

Diffraction disintegration of a deuteron results in simultaneous liberation of two particles, a proton and a neutron. It is possible in principle to set up correlation experiments by measuring the momenta of both liberated particles. Since the neutrons are difficult to observe, the distribution of only one particle (proton) is determined in practice. This raises the question of calculating the angular and energy distributions for one particle.

It was shown by Serber[4] (cf. also reference 5) that in the case of fast particles, to find the distributions over the energies E of one particle it is necessary to calculate the distribution over p_z for this particle (p_z is the projection of the particle momentum along the direction of the initial beam). Then $p_z = (E - E_x/2)/\sqrt{E_d/M}$.

Akhiezer and Sitenko[3] derive a formula [Eq. (16) of reference 3] for the energy distribution. Actually, however, this formula gives the distribution over the modulus of the vector of the relative momentum $f = \sqrt{f_x^2 + f_y^2 + f_z^2}$; the angular distribution of the vector $\mathbf{f}$ is already integrated in this formula, so that the required energy distribution cannot be obtained from it.

2. We proceed to calculate the energy distribution. Consider the wave function of the deuteron in the presence of an absolutely black nucleus. It will have approximately the form of the so-called "modified" function, introduced in reference 3:

$$\psi_0(\boldsymbol{\rho}, \mathbf{r}) = \varphi_0(r)\,\Omega(\boldsymbol{\rho}_n)\,\Omega(\boldsymbol{\rho}_p). \tag{1}$$

Here $\boldsymbol{\rho}$ is the radius vector of the deuteron center of mass in the plane perpendicular to the axis of the incident beam; $\mathbf{r}$ is the radius vector of the relative distance between the proton and neutrons; $\varphi_0(r) = \sqrt{\alpha/2\pi}\; e^{-\alpha r}/r$ is the wave function of the relative motion in the deuteron in the approximation where the nuclear forces radius is zero, and R is the nuclear radius;

$$\Omega(\rho) = \begin{cases} 0 & \text{for } \rho < R \\ 1 & \text{for } \rho > R \end{cases}.$$

The function (1) characterizes a state of the deuteron beam directly after the passage of the nucleus. It contains the deuterons scattered as a whole and deuterons that have experienced a diffraction breakup. It is convenient to separate from ψ_0 the portion orthogonal to $\varphi_0(r)$:

$$\psi_1(\boldsymbol{\rho}, \mathbf{r}) = \psi_0(\boldsymbol{\rho}, \mathbf{r}) - \varphi_0(r)\int d\mathbf{r}'\psi_0(\boldsymbol{\rho}, \mathbf{r}')\,\varphi_0(r'). \tag{2}$$

The function ψ_1 describes only disintegrated deuterons. Henceforth we shall assume $R_d \ll R$. We can then neglect, for deuterons passing near the nucleus at a distance $\sim R_d$, the curvature at the edge of the nucleus, and consider the nucleus to be a plane screen with straight edge, analogous to the procedure used in references 2 and 4.* Here ψ_1 becomes

$$\psi_1(\boldsymbol{\rho}, \mathbf{r}) = \varphi_0(r)\,[\Omega(\boldsymbol{\rho}_n)\,\Omega(\boldsymbol{\rho}_p) - 1] + \varphi_0(r)\,I(\rho), \tag{3}$$

where

*As shown in reference 8, the error introduced thereby is not greater than the error due to an inaccurately selected function $\varphi_0(r)$.

$$I(\rho)=\begin{cases}1 & \text{for } \rho<R\\ \varepsilon_1[4\alpha(\rho-R)] & \text{for } \rho>R\end{cases}$$

The function $\epsilon_1(x)$ is the Gold integral (see reference 6)

$$\varepsilon_1(x)=\int_1^\infty \frac{e^{-xt}}{t^2}dt. \tag{4}$$

We note that

$$\psi_1(\rho, \mathbf{r})\equiv 0 \quad \text{for } \rho<R. \tag{5}$$

At each point of the edge of the nucleus we introduce a local system of coordinates: The deuteron beam travels along the z axis, and the y and x axes lie in the plane of the screen, with the y axis being directed along its edge and the x axis perpendicular to the edge and directed outward from the nucleus. To find the distribution of one nucleon over the momenta, we must expand the function ψ_1 in plane waves of the motion of the center of mass and in the wave functions

$$\varphi_f(\mathbf{r})=e^{i\mathbf{f}\mathbf{r}}-e^{-i\mathbf{f}r}/r(\alpha-if)$$

of relative motion, which correspond to the motion of the nucleons with relative momentum $\mathbf{f}$ at infinity, liberated as a result of the breakup. Since no momentum is transferred to the center of mass of the deuteron in the direction along the edge of the nucleus, it is not necessary to expand ψ_1 in plane waves in the Y direction, and we can calculate instead the cross section per element dY of the length of the edge of the nucleus. Thus

$$\psi_1(k, \mathbf{f}, Y)=(2\pi)^{-2}\int \psi_1(X, Y, \mathbf{r})e^{-ikX}\varphi_{\mathbf{f}}^*(\mathbf{r})\,dX d\mathbf{r}. \tag{6}$$

Here

$$k=p_{px}+p_{nx}=\lambda+\mu,\quad f_x=(p_{px}-p_{nx})/2=(\lambda-\mu)/2,$$
$$f_y=p_{py},\quad f_z=p_{pz}. \tag{7}$$

Formulas (7) result from the fact that we consider here a screen with a straight edge and neglect the momentum transfer in the direction of the primary beam. For a screen with a straight edge we have

$$\psi_1(X, Y, \mathbf{r})$$
$$=\begin{cases}0 & \text{for } X<0\\ -[\omega(x_n)+\omega(x_p)]\varphi_0(r)+\varepsilon_1(4\alpha X)\varphi_0(r) & \text{for } X>0,\end{cases}$$

where

$$\omega(x)=1-\Omega(x)=\begin{cases}0 & \text{for } x>0\\ 1 & \text{for } x<0.\end{cases}$$

Using the Fourier expansion

$$\varphi_0(r)=(2\pi)^{-3}\int \frac{2\sqrt{2\pi\alpha}}{\alpha^2+f^2}e^{-i\mathbf{f}\mathbf{r}}d\mathbf{f}$$

and Eq. (4), we get

$$\psi_1(\lambda, \mu, f_y, f_z)$$
$$=\sqrt{\frac{\alpha}{(2\pi)^3}}\left\{\frac{1}{P(\mu-\lambda-i2P)(\mu-iP)}+\frac{1}{P(\mu-\lambda+i2P)(iP-\lambda)}\right.$$
$$\left.+\frac{1}{\alpha^2+f^2}\int_1^\infty \frac{dt}{t^3\left[2\alpha-2if+i\dfrac{\lambda+\mu}{t}\right]}\right\}. \tag{8}$$

Here $P=\sqrt{\alpha^2+f_y^2+f_z^2}$; $|\psi_1|^2 d\lambda d\mu df_y df_z dY$ gives the effective cross section of process, at which the quantities p_{nx}, p_p, and Y are located in the corresponding intervals. Integration over Y yields $2\pi R$. Integrating over all the momenta, we obtain the total cross section, accurate to within terms of R_d^2:

$$2\pi R\int d\lambda d\mu df_y df_z |\psi_1|^2 = \frac{\pi R R_d}{3}(2\ln 2-{}^1/_2),$$

this agrees with the cross section calculated in references 2 and 3.

To obtain the energy distribution, it is necessary to integrate the expression

$$2\pi R|\psi_1(\lambda, \mu, f_y, f_z)|^2 \tag{9}$$

over the momentum of the neutron, $p_{nx}=\mu$ and also over $p_{px}=\lambda$ and $p_{py}=f_y$. This integration is difficult to perform in exact form, owing to the presence of two different radicals P and f. However, a good approximate expression can be found for the distribution over $p_z=f_z$. In the denominator of the last term of (8) we replace the expression $2\alpha-2if+i(\lambda+\mu)/t$, which is slowly varying, by its value at $t=1$. This does not introduce a great error, owing to the presence of a rapidly diminishing factor $1/t^3$. After this, (8) becomes

$$\psi_2=\sqrt{\frac{\alpha}{(2\pi)^3}}\left\{\frac{1}{P(\mu-\lambda-i2P)(\mu-iP)}+\frac{1}{P(\mu-\lambda+i2P)(iP-\lambda)}\right.$$
$$\left.+\frac{1}{(\alpha^2+f^2)(2\alpha-2if+i(\lambda+\mu))}\right\}. \tag{10}$$

The use of ψ_2 instead of ψ_1 causes the total cross section to deviate 15% from the value $\pi R R_d(2\ln 2-\frac{1}{2})/3$. Furthermore, a special estimate has shown that in the angular range $\lesssim\alpha$ the differential cross section changes merely by 10%. This indeed determines the accuracy of the formula obtained later on. After making the above simplification, the integration over λ, μ, and f_y proceeds without difficulty, and we obtain the following energy distribution:

$$\frac{d\sigma_E}{dq}=\frac{RR_d}{4}\frac{1}{(1+q^2)^{3/2}}\left\{\frac{3}{2}\pi+\pi q^2\right.$$
$$\left.+\frac{2(1+q^2)^{3/2}}{q}\tan^{-1}q-\sqrt{1+q^2}\right\},$$
$$q=(E-E_d/2)/\sqrt{\varepsilon E_d}. \tag{11}$$

Here E is the proton energy, E_d is the energy

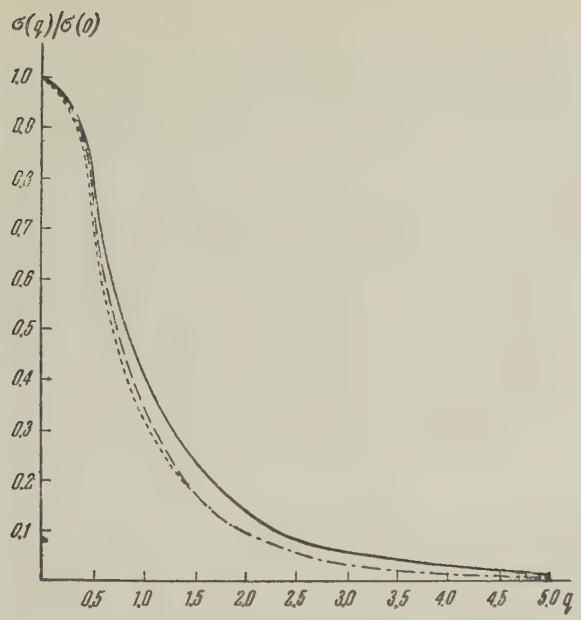

FIG. 1. Energy distributions: Solid line – diffraction disintegration, dotted line – stripping.

of the primary deuteron, and ϵ is the binding energy of the deuteron.

The distribution (11) is shown in Fig. 1 by a solid line. It is seen from (11) that the center of the energy distribution of the proton is $E_d/2$, and that the half-width is $\sqrt{\epsilon E_d}$.

It is interesting to call attention to the following fact. Were it possible to neglect the interaction between the proton and the neutron after the deuteron breakup, then the relative motion of these particles would be described by a plane wave $e^{i\mathbf{f}\cdot\mathbf{r}}$, and in order to find the momentum distribution it would be enough to expand $\psi_1(X, Y, \mathbf{r})$ in a Fourier integral over the coordinates X and $\mathbf{r}$. Calculations with a plane wave are simpler than those using the function $\varphi_{\mathbf{f}}(\mathbf{r})$, and the results are quite close to each other. The energy distribution obtained by replacing $\varphi_{\mathbf{f}}(\mathbf{r})$ with $e^{i\mathbf{f}\cdot\mathbf{r}}$ is shown dotted in Fig. 1. In addition, the same figure shows for comparison the energy distribution for stripping. Obviously, all distributions are practically the same.

3. Let us proceed to find the angular distribution of an individual nucleon. For this purpose it is necessary to integrate in Eq. (9) over μ, f_z, and φ, where $\lambda = p_\perp \cos\varphi$ and $f = p_\parallel \sin\varphi$ (see reference 4). The exact integration leads to very complicated expressions. It is convenient to use the following approximation. Since the integral in the last term of (8) is preceded by a factor $1/(\alpha^2 + f^2)$, which has a sharp maximum, we can put in the integrand $f = 0$ when integrating over f_z. Furthermore, we can replace $2\alpha + 2i\lambda/t$ by $2\alpha + 2i\lambda$, as was done earlier. These simplifications lead to an error on the order of 5% in the total cross section, and to an error of approximately 10% in the angular distribution for $p_\perp \sim \alpha$. We then obtain instead of ψ_1

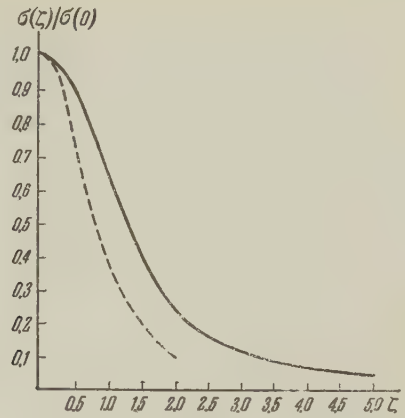

FIG. 2. Angular distribution. ——— diffraction disintegration, – – – – – stripping.

$$\psi_3 = \sqrt{\frac{\alpha}{(2\pi)^3}}\left\{\frac{1}{P(\mu-\lambda-i2P)(\mu-iP)} + \frac{1}{P(\mu-\lambda+i2P)(iP-\lambda)} + \frac{1}{2(\alpha^2+f^2)(\alpha+i\lambda)}\right\}.$$

Substituting this value of ψ_3 for ψ_1 in Eq. (9) and integrating over μ, f_z, and φ, we get

$$\frac{d\sigma}{d\Omega_\zeta} = \frac{RR_d}{4\pi(1+\zeta^2)^{3/2}}\left\{\frac{4}{3} + 4\left(1-\frac{8}{3\sqrt{9+\zeta^2}}\right) - \frac{\pi}{2+\zeta^2} - \frac{1+\zeta^2}{1+\zeta^2/2}\left[\frac{3\pi}{4(1+\zeta^2)}\left(1-\frac{8}{3\sqrt{9+\zeta^2}}\right) + \frac{3\pi/4-2/3}{17+9\zeta^2}\left(1+\frac{8}{3\sqrt{9+\zeta^2}}\right) + \frac{2}{3}\left(1-\frac{8}{3\sqrt{9+\zeta^2}}\right) - \frac{1+\zeta^2/3}{1+\zeta^2}\right]\right\},$$

$$p_\perp = \alpha\zeta, \quad d\Omega_\zeta = 2\pi\zeta d\zeta. \qquad (12)$$

The distribution (12) is shown graphically in Fig. 2. The angular distribution in stripping, shown on the same diagram, is quite different, being "narrower." This can also be understood qualitatively. In stripping, the stripped nucleon does not acquire additional momentum in the transverse direction, and has the same momentum that it had inside the bound deuteron. To the contrary, diffraction disintegration cannot occur without one of the nucleons receiving a momentum $p_\perp \sim \alpha$, sufficient to destroy the weakly-bound deuteron, and this leads to a larger probability of momenta proportional to α.

4. So far we have considered diffraction disintegration of a deuteron, in which the proton and neutron have equal masses. However, there exist weakly bound systems which also can experience diffraction disintegration, but in which the masses of the component particles are quite unequal. An example is Be^9, in which the binding energy of the

last nucleon is merely 0.6 Mev (see reference 7), i.e., even less than in a deuteron. Diffraction disintegration of Be^9 results in the production of a neutron and the nucleus Be^8. This raises the problem of finding the energy and angular distributions of the diffraction-disintegration products of a weakly-bound system, consisting of particles of unequal mass. This calculation is quite analogous to the previously analyzed case of equal masses, where instead of (8) we get

$$\psi_1(\lambda, \mu, f_y, f_z) = \sqrt{\frac{\alpha}{(2\pi)^3}} \left\{ \frac{1}{P(\mu - b\lambda/a + iP/a)(\lambda - iP)} + \frac{1}{P(\lambda - a\mu/b + iP/b)(\mu - iP)} - \frac{1}{\alpha^2 + f^2} \int_1^\infty \frac{dt}{t^3[(\alpha - if)/a + ik/t]} - \frac{1}{\alpha^2 + f^2} \int_1^\infty \frac{dt}{t^3[(\alpha - if)/b + ik/t]} \right\}. \quad (13)$$

The symbols in (13) are the same as in (7), except that now $f_x = b\lambda - a\mu$, where

$$a = m_1/(m_1 + m_2),\ b = m_2/(m_1 + m_2),\ a + b = 1.$$

We note that the shapes of the curves are determined by the parameters a and b. But in cases of practical interest, whenever $a \neq b$, we also have $a \ll b$ (for example, for Be^9 we have $a = b/8$). We shall therefore calculate our curves for two asymptotic cases: when a light particle is observed ($a = 0$, $b = 1$), and when a heavy one is observed ($a = 1$, $b = 0$).

The shape of the energy distribution is the same for a light and heavy particle, and is given by

$$\frac{d\sigma_E}{dq} = \frac{R}{4\alpha(1+q^2)^{3/2}} \left\{ \frac{\pi}{2} - \frac{7}{4}\sqrt{1+q^2} + \pi(1+q^2) - \frac{2(1+q^2)^{3/2}}{q}\tan^{-1} q \right\},$$

$$q = (E - \frac{m}{M}E_{nuc})/\sqrt{2E_{nuc}/M}, \quad (14)$$

where E_{nuc} is the kinetic energy of the incident nucleus, E is the energy of the observed particle, m is its mass, and M is the sum of the masses of the formed particles.

The entire difference in the energy distributions of the light and heavy particles reduces to the fact that the center of the distribution for the light particles lies at mE_{nuc}/M, while that for the heavy nucleus is at $(M-m)E_{nuc}/M$. It can be shown that the distribution (14), expressed in terms of the variable q, hardly differs from the distribution for the case of equal masses, but the meaning of q becomes different.

Let us now proceed to the angular distributions. The angular distributions for the light and heavy particles respectively are given by

$$\frac{d\sigma_l}{d\Omega_\zeta} = \frac{R}{3\alpha}\left\{\left(1 + \frac{3\pi}{16}\right)\frac{1}{(1+\zeta^2)^{3/2}} - \frac{1}{(1+\zeta^2)^2}\right\}, \quad (15)$$

$$\frac{d\sigma_h}{d\Omega_\zeta} = \frac{R}{\alpha}\left\{\frac{1}{(1+\zeta^2)^{3/2}}\left(1 - \frac{1}{3\sqrt{1+\zeta^2}}\right) - \frac{1}{4+2\zeta^2}\left(1 - \frac{1}{3\sqrt{1+\zeta^2}}\right) + \frac{1}{3(1+\zeta^2)^{3/2}(2+\zeta^2)}\left(1 + \frac{1}{5(1+\zeta^2)}\right) - \frac{7\pi - 8}{32(2+\zeta^2)\sqrt{1+\zeta^2}}\right\}. \quad (16)$$

Here $\zeta = p_\perp/\alpha$, $d\Omega_\zeta = 2\pi\zeta\, d\zeta$.

In conclusion, the authors thank E. L. Feĭnberg for guidance and for a detailed evaluation of this work.

[1] E. L. Feĭnberg, J. Exptl. Theoret. Phys. (U.S.S.R.) **29**, 115 (1955), Soviet Phys. JETP **2**, 58 (1956).

[2] R. Glauber, Phys. Rev. **99**, 1515 (1955).

[3] A. I. Akhiezer and A. G. Sitenko, J. Exptl. Theoret. Phys. (U.S.S.R.) **32**, 794 (1957), Soviet Phys. JETP **5**, 652 (1957).

[4] R. Serber, Phys. Rev. **72**, 1008 (1947).

[5] A. I. Akhiezer and I. Ya. Pomeranchuk, Некоторые вопросы теории ядра (Certain Problems in Field Theory), GTTI, 1950.

[6] B. Rossi, High-Energy Particles, (Russ. Trans.) IIL, 1955, p. 619. [Prentice Hall, N. Y., 1952].

[7] B. S. Dzhelepov and L. N. Zyryanova, Usp. Fiz. Nauk **48**, 465 (1952).

[8] I. I. Ivanchik, J. Exptl. Theoret. Phys. **32**, 164 (1957), Soviet Phys. JETP **5**, 133 (1957).

Translated by J. G. Adashko
83

DISPERSION RELATIONS FOR THE ELECTROMAGNETIC FORM FACTOR OF THE PION

I. T. DYATLOV

Leningrad Physico-Technological Institute, Academy of Sciences, U.S.S.R.

Submitted to JETP editor July 4, 1958

J. Exptl. Theoret. Phys. (U.S.S.R.) 36, 505-507 (February, 1959)

Dispersion relations are derived for the electromagnetic form factor of a charged π meson. By including only the contribution to the imaginary part from a state with two π mesons, an equation is obtained which gives the form-factor in terms of the phase shift for scattering of π mesons by π mesons.

FOR the electromagnetic form factor of the π meson one can derive dispersion relations that relate it to the imaginary part of the annihilation amplitude for two π mesons. These may be compared with the relations of the same type for nucleons, which have been considered by Bernstein and Goldberger;[1] the dispersion relations for the π meson do not involve the nonphysical region, and can be simply derived with complete rigor.

We shall consider the analytic properties of the matrix element of the electromagnetic current operator $j_\mu(x)|_{x=0}$ $[\Box A_\mu(x) = -j_\mu(x)]$ between π-meson states with momenta p' and p and isotopic indices i and k — the element $\langle p', i|j_\mu(0)|p, k\rangle$. Such a matrix element enters directly into the expression for the scattering amplitude of π-meson-electron collisions in the lowest approximation in the electromagnetic charge e. From the relativistic and isotopic invariances it follows that the gauge-invariant part of this matrix element can be written in the form

$$\langle p'i|j_\mu(0)|pk\rangle = e(p'+p)_\mu [a_S(q^2) + a_V(q^2)T_3]_{ik}, \quad (1)$$

where $q = p' - p$, T_3 is the operator for the isotopic spin component for $T = 1$, and

$$ca_V(q^2) = \frac{(p'+p)_\mu \langle p'|j_\mu^V(0)|p\rangle}{(p+p')^2} 2\sqrt{\omega_p \omega_{p'}} \quad (2)$$

is the form-factor of the π meson (it will be shown that the factor $a_S(q^2)$ defined by the analogous formula with $j_\mu^S(0)$ is equal to zero). $j_\mu^S(0)$ and $j_\mu^V(0)$ are the isotopic-scalar and the isotopic-vector parts of the current, respectively:

$$j_\mu(0) = j_\mu^S(0) + j_\mu^V(0). \quad (3)$$

It follows from Eq. (1) that the electromagnetic form-factor of the π^0 meson is equal to $a_S(q^2)$, but in virtue of the charge parity of the π^0 meson we have the matrix element

$$\langle p'\pi^0|j_\mu(0)|p\pi^0\rangle = 0, \text{ i.e., } a_S(q^2) = 0. \quad (4)$$

Consequently in the lowest approximation in e there remains only the one form-factor $a_V(q^2)$ for the charged mesons.

Taking the complex conjugate of Eq. (1) and using the fact that for one-particle states $\langle p|^* = |p\rangle$, we show that $a_V(q^2)$ is a real function for real momenta of the particles $(q^2 > 0)$. In addition, $a_V(q^2) \to 1$ for $q^2 \to 0$.

By means of reduction formulas[2] we can write $a_V(q^2) = a(q^2)$ in the form

$$a(q^2) = i\frac{\sqrt{2\omega_p}}{(p+p')^2}\int e^{-ip'x}dx \times \{\langle 0|T(j(x), j_e^V(0)) + [\dot{\Phi}(x), j_e^V(0)]\delta(x_0)|p\rangle\}. \quad (5)$$

$j_e^V(0) = j_\mu^V(0)(p+p')_\mu$; $\dot{\Phi}(x)$ is the time derivative of the meson field $\Phi(x)$ $[(\Box - \mu^2)\Phi(x) = -j(x)]$.

In the physical region $\omega_{p'} \geq \mu$ (μ is the mass of the π meson) the integral of the T product in Eq. (5) is the same as the analogous integrals of the retarded and advanced commutators. Applying the technique of Goldgerger[3] and Bogolyubov[4] we construct a function $F(\omega_{p'})$ analytic in the entire complex plane of $\omega_{p'}(\mathbf{p}' = (\omega_{p'}^2 - \mu^2)^{1/2}\mathbf{e}$, with $\mathbf{e}$ the unit vector in the direction of $\mathbf{p}'$ and fixed vectors $\mathbf{p}$ and $\mathbf{e}$) except on the negative part of the real axis from $-\mu$ to $-\infty$, where it has branch points.

For $\omega_{p'} \geq \mu$

$$F(\omega_{p'}) = a(q^2), \quad q^2 = (p-p')^2 > 0,$$

$$F(-\omega_{p'}) = b_1(q^2) = \frac{1}{e}\frac{((p-p')_\mu \langle 0|j_\nu^V(0)|pp'\rangle)^*}{(p-p')^2} 2\sqrt{\omega_p \omega_{p'}} \quad (6)$$

on the upper edge of the cut and

$$F(-\omega_{p'}) = b_2(q^2) = \frac{1}{e}\frac{(p'-p)_\mu \langle pp'|j_\mu^V(0)|0\rangle}{(p-p')^2} 2\sqrt{\omega_p \omega_{p'}} \quad (7)$$

on the lower edge $(q^2 = (p+p')^2 \leq -4\mu^2)$; $b_1(q^2)$ is the "form-factor" for the annihilation of a pair

of π mesons by the electromagnetic interaction, and $b_2(q^2)$ is the corresponding "form-factor" for the production of a pair of π mesons.

Since $F(\omega_{p'})$ is an analytic function in the cut $\omega_{p'}$ plane and is real on the part of the real axis from μ to ∞, we have by the principle of symmetry for analytic functions

$$b_1(\omega_{p'}) = b_2^*(\omega_{p'}) = b(\omega_{p'}). \tag{8}$$

In the coordinate system in which $\mathbf{p} = 0$, $q^2 = 2\mu q_0 = 2\mu(\omega_{p'} - \mu)$; that is, $F(\omega_{p'})$ is also an analytic function with respect to the variable q^2. In this system we can write the dispersion relations in terms of q^2, and because of relativistic invariance they will be independent of the choice of coordinate system.

Nothing definite can be said about the behavior of $a(q^2)$ and $b(q^2)$ for $|q^2| \to \infty$. It can be hoped that at high energies the cross-sections fall off with increasing q^2 more rapidly than q^{-2}. Then $a(q^2)$ and $b(q^2)$ fall off for $|q^2| \to \infty$, and

$$a(q^2) = -\frac{1}{\pi}\int_{4\mu^2}^{\infty} \frac{\operatorname{Im} b(-\xi^2)d\xi^2}{\xi^2 + q^2}, \quad q^2 > 0, \tag{9}$$

$$\operatorname{Re} b(q^2) = -\frac{1}{\pi} P\int_{4\mu^2}^{\infty} \frac{\operatorname{Im} b(-\xi^2)d\xi^2}{\xi^2 + q^2}, \quad q^2 < -4\mu^2. \tag{10}$$

If $a(q^2)$ and $b(q^2)$ approach constant values or increase for $|q^2| \to \infty$, dispersion relations can be written if we divide a and b by a certain power of q^2. If we confine ourselves to the contribution to $\operatorname{Im} b(q^2)$ from two π mesons only, we get from the unitarity relations for the S matrix

$$\operatorname{Im} b(q^2) = \pm |b(q^2)| \sin\delta(q^2). \tag{11}$$

δ is the pion-pion scattering phase shift for the state with angular momentum $l = 1$ and isotopic spin $T = 1$ (the $\pm$ sign remains undetermined.

The formula (11) is an exact relations for $q^2 \leq -16\mu^2$. If $|b(q^2)|$ falls off rapidly with increasing q^2 we can substitute Eq. (11) in the right members of Eqs. (9) and (10); this gives the relation

$$a(q^2) = \pm\frac{1}{\pi}\int_{4\mu^2}^{\infty} \frac{|b(-\xi^2)|\sin\delta(\sqrt{\xi^2 - 4\mu^2})d\xi^2}{\xi^2 + q^2}. \tag{12}$$

between physical quantities.

In conclusion the writer expresses his deep gratitude to I. M. Shmushkevich for suggesting this topic and to V. N. Gribov for helpful discussions.

[1] J. Bernstein and M. L. Goldberger, Report at the Stanford Conference on the Sizes of Nuclei, 1957.

[2] Lehmann, Symanzik, and Zimmermann, Nuovo cimento 1, 205 (1955).

[3] M. L. Goldberger, Phys. Rev. 99, 979 (1955).

[4] N. N. Bogolyubov and D. V. Shirkov, Введение в теорию квантованных полей (Introduction to the Theory of Quantized Fields), GITTL 1957, pp. 405-407.

Translated by W. H. Furry
84

ON THE THEORY OF ELECTRON PARAMAGNETIC RESONANCE IN ELECTROLYTE SOLUTIONS

A. A. KOKIN

Ural' Polytechnical Institute

Submitted to JETP editor July 4, 1958; resubmitted October 28, 1958

J. Exptl. Theoret. Phys. (U.S.S.R.) **36**, 508-511 (February, 1959)

The transverse and longitudinal relaxation times and the correction to the gyromagnetic ratio are calculated for electron paramagnetic resonance without taking hyperfine structure into account.

1. The theory developed for the case of nuclear resonance in liquids[1] is commonly used to describe the phenomenon of electron paramagnetic resonance in solutions. In doing this, however, the specific characteristic features of the phenomenon are not taken into account.

In nuclear resonance the principal role is played by the interaction of nuclear magnetic moments in the same molecule and between different molecules of the liquid. In the case of electron resonance in solutions, a significant role is played by the nature of the local electric field in the neighborhood of the ion which undergoes random variations both in magnitude and in its symmetry properties.

The mechanism by means of which the translational Brownian movement of the molecules of the liquid affects the line width of electron magnetic resonance is the same as in the case of nuclear magnetic resonance.

The effect of the asymmetry of the local electric field can be easily taken into account by assuming that only the orientation of the axes of symmetry of the local field has random variations, which may be represented by means of a Brownian rotation of a certain static asymmetric field.

Due to the interaction of this field with the electron cloud of the ion and due to the existence of spin-orbit and spin-spin interaction, the degeneracy of the levels in the system of coordinates associated with the local field is removed either partially or completely, depending on the symmetry of the local field and on whether the number of electrons is odd or even. In the laboratory system of coordinates the result of this splitting is an increase in the width of the absorption line.

2. In the majority of cases of the solid salts that have been studied, the local field may be represented by two components: a strong field of cubic symmetry and a weak field of lower, trigonal or tetragonal symmetry.[2]

At ordinary temperatures those levels are populated which are separated from the ground level by $\lesssim 10^2$ cm^{-1}. In many cases in order to describe the lower energy levels of the ion we may introduce the spin-Hamiltonian:[3]

$$\hat{\mathcal{H}}_s = g_{\parallel}\mu_0 \sum_j \hat{\mathbf{S}}_j \cdot \mathbf{H}_0 + \Delta g \mu_0 \sum_j (\hat{S}_{x_j'} H_{0x_j'} + \hat{S}_{y_j'} H_{0y_j'}) + \hbar D \sum_j \left(\hat{S}^2_{z_j'} - \frac{1}{3} S(S+1)\right), \quad (1)$$

where $\Delta g = g_{\perp} - g_{\parallel}$, while the z_j' axis is the axis of symmetry of the local field of the ion. We shall consider that a similar expression will also hold for an ion in solution.

By introducing the angles ϑ_j and φ_j which the z_j' axis makes with the stationary system of coordinates xyz, we obtain

$$\hat{\mathcal{H}}_s = \hat{\mathcal{H}}_1 + \hat{\mathcal{H}}'', \quad (2)$$

where

$$\hat{\mathcal{H}}_1 = \hbar\omega_0 \sum_j \hat{S}_{jz}, \quad (3)$$

$$\hbar\omega_0 = g'\mu_0 H_0, \quad (3')$$

$$g' = g_{\parallel} + \frac{2}{3}\Delta g. \quad (3'')$$

The operator $\hat{\mathcal{H}}''$ may be regarded as a perturbation if $\Delta g/g \ll 1$, $D/\omega_0 \ll 1$.

3. In addition to $\hat{\mathcal{H}}_S$, the complete Hamiltonian of the system also includes $\hat{\mathcal{H}}_2$, which contains the kinetic energy and the interactions independent of the spins (we do not take exchange interactions into account), and $\hat{\mathcal{H}}'$ — the dipole-dipole magnetic interaction between ions, which is also treated as a perturbation.

If we neglect the correlation between the translational and the rotational motion then the inverse relaxation times and the correction to the gyromagnetic ratio can be separated into two parts, which correspond to the translational and the rotational Brownian motion of the ions. In this procedure

the part that corresponds to the translational Brownian motion determined by $\hat{\mathcal{H}}'$ and by the thermal motion of the ions will in the case of electron resonance be the same as in the case of nuclear resonance. The other part of the inverse relaxation times and of the correction to the gyromagnetic ratio due to the rotational Brownian motion must be calculated differently.

The perturbation which depends on the orientation of the local field with respect to the external field is given by $\hat{\mathcal{H}}''$ which can be written in the form

$$\hat{\mathcal{H}}'' = \sum_{\lambda} \hat{\mathcal{H}}''_{\lambda} \quad (\lambda = 0, \pm 1, \pm 2), \tag{4}$$

where

$$\hat{\mathcal{H}}_0 = -\sqrt{16\pi/45}\,\hbar \times \sum_j{}' \left(C\hat{S}_{0j} - D\frac{3\hat{S}_{0j}^2 - S(S+1)}{2} \right) Y_{20}(\vartheta_j \varphi_j); \tag{5}$$

$$\hat{\mathcal{H}}_{\pm 1} = \pm i\sqrt{4\pi/15}\,\hbar \sum_j{}' (C\hat{S}_{\pm 1 j} - D(\hat{S}_{\pm 1 j}\hat{S}_{0j} + \hat{S}_{0j}\hat{S}_{\pm 1 j}))\, Y_{2\mp 1}(\vartheta_j \varphi_j); \tag{6}$$

$$\hat{\mathcal{H}}_{\pm 2} = -\sqrt{2\pi/15}\,\hbar D \sum_j{}' \hat{S}_{\pm 1 j}^2 Y_{2\mp 2}(\vartheta_j \varphi_j); \tag{7}$$

$$\hat{S}_{\pm 1} = \mp (1/\sqrt{2})(\hat{S}_x \pm i\hat{S}_y),\ S_0 = S_z,$$

$$C \quad (\Delta g/g')\omega_0.$$

Now, by making use of expressions (7) of reference 4 and by assuming the distribution of z'_j to be isotropic, we obtain for $\Omega^2_{\alpha\lambda}$ and $f_\lambda(\tau)$ the following expressions:

$$\Omega^2_{00} = \Omega^2_{\pm 1 \mp 2} = 0,$$
$$\Omega^2_{0\pm 1} = {}^1/_{15}[C^2 + D^2(4S(S+1) - 3)/5],$$
$$\Omega^2_{0\pm 2} = {}^4/_{75} D^2 (4S(S+1) - 3),$$
$$\Omega^2_{10} = {}^4/_{45}[C^2 + {}^9/_4 D^2 (4S(S+1) - 3)/5], \tag{8}$$
$$\Omega^2_{1-1} = \Omega^2_{12} = {}^2/_{75} D^2 (4S(S+1) - 3),$$
$$\Omega^2_{11} = {}^1/_{15}[C^2 + {}^3/_5 D^2 (4S(S+1) - 3)],$$
$$f_\lambda(\tau) = \frac{4\pi}{N} \left\langle \sum_j{}' Y_{2\lambda}(\vartheta_j(\tau)\varphi_j(\tau))\, Y^*_{2\lambda}(\vartheta_j \varphi_j) \right\rangle. \tag{9}$$

In the above the angle brackets denote averaging over the angle coordinates.

We choose the correlation function $f_\lambda(\tau)$ to be of the same form as in the case of rotational Brownian motion in nuclear resonance:[4]

$$f_\lambda(t) = f(t) = \exp(-t/\tau'_c). \tag{10}$$

By utilizing the results of reference 4, we can easily obtain expressions for the inverse relaxation times and for the correction to the gyromagnetic ratio in arbitrary fields.

We shall write them down for the case of weak fields when $\omega_0\tau_c \ll 1$, and for the case of strong fields when $\omega_0\tau_c \gg 1$.

In the case of weak fields:

$$\frac{1}{T_\perp} = \frac{6\pi}{5} S(S+1)\, g^4\mu_0^4\hbar^{-2} \frac{N}{V} a^{-3}\tau_c + \left\{ \frac{7}{45} C^2 + \frac{2}{15} D^2 (4S(S+1) - 3) \right\} \tau'_c; \tag{11}$$

$$\frac{1}{T_\parallel} = \frac{6\pi}{5} S(S+1)\, g^4\mu_0^4\hbar^{-2} \frac{N}{V} a^{-3}\tau_c + \left\{ \frac{2}{15} C^2 + \frac{2}{15} D^2 (4S(S+1) - 3) \right\} \tau'_c; \tag{12}$$

$$\gamma^* = \gamma \left\{ 1 + \frac{6\sqrt{2} + 3}{\sqrt{2}} \frac{\pi}{10} S(S+1) \times g^4\mu_0^4\hbar^{-2} \frac{N}{V} a^{-3}\tau_c \sqrt{\tau_c/\omega_0} \right\}. \tag{13}$$

In strong fields:

$$\frac{1}{T_\perp} = \frac{9\pi}{25} S(S+1)\, g^4\mu_0^4\hbar^{-2} \frac{N}{V} a^{-3}\tau_c + \left\{ \frac{4}{45} C^2 + \frac{1}{25} D^2 (4S(S+1) - 3) \right\} \tau'_c; \tag{14}$$

$$\frac{1}{T_\parallel} = \frac{\sqrt{2}+1}{30\sqrt{2}} \pi S(S+1)\, g^4\mu_0^4\hbar^{-2} \frac{N}{V} a^{-3}\tau_c\, (\tau_c\omega_0)^{-1/2}; \tag{15}$$

$$\gamma^* = \gamma \left(1 + \frac{1}{15} (\Delta g/g')^2 \right). \tag{16}$$

Here, just as in the case of nuclear resonance, $T_\parallel$ has a minimum in the neighborhood of $\omega_0\tau_c \sim 1$.

4. It is known from experiment that the line width in solution decreases with increasing degree of dilution down to a certain concentration.[2] Thus, in the case of aqueous solutions of salts of Cr^{+++}, VO^{++}, Cu^{++} and Mn^{++} the decrease in line width ceases at a concentration of ~ 0.1 mole/l, with the limiting line width being of the order of 30 Oe in the case of Mn^{++} and 200 Oe in the case of Cr^{+++} at room temperature and for $\omega_0 \sim 7.8 \times 10^7$ sec^{-1}.

The particularly small line width in the case of a solution of Mn^{++} is associated with the high symmetry of the local field of the ion. Since in this case the Mn^{++} ion is in an S state, we have $\Delta g = 0$.

Assuming in the case of Mn^{++} $a = 2.4 \times 10^{-8}$ cm^5, $g = 2$, $S = 5/2$, we shall obtain, in accordance with (11)

$$1/T_\perp = 0.25\tau_c N/V + (64/15) D^2 \tau'_c. \tag{17}$$

By utilizing experimental values[6] for the variation of the half width of the line with concentration ~ 80 for 1 mole/l at 20°C we obtain $\tau_c = 1 \times 10^{-11}$ sec and $D = 0.08$ cm^{-1}. If we take in the case of water $\eta = 0.01$ poise, then in the case of the Mn^{++} ion the correlation time corresponding to the rotational motion of the ion is given by $\tau_c = 1.4 \times 10^{-11}$ sec ($\tau_c \approx \tau'_c$).

The value of the constant indicates a stronger asymmetry of the local field in the neighborhood of the ion than in the case of the solid salts of Mn^{++} ($D = 0.01\ cm^{-1}$).

To determine the constants D and Δg for other salts it is necessary to have also the frequency dependence of that part of the half-width of the absorption line which does not depend on the concentration.

In conclusion, it is my duty to express my gratitude to G. V. Skrotskiĭ for discussing this work.

[1] Bloembergen, Purcell, and Pound, Phys. Rev. **73**, 679 (1948).

[2] S. A. Al'tshuler and B. M. Kozyrev, Usp. Fiz. Nauk. **63**, 533 (1957).

[3] M. H. L. Pryce, Proc. Phys. Soc. **A63**, 25 (1950).

[4] G. V. Skrotskiĭ and A. A. Kokin, J. Exptl. Theoret. Phys. **36**, 481 (1959), Soviet Phys. JETP **9**, 335 (1959), this issue.

[5] R. A. Robinson and R. H. Stokes, Electrolyte Solutions, Butterworths, London, 1955.

[6] B. M. Kozyrev, Izv. Akad. Nauk. S.S.S.R., Ser. Fiz. **21**, 828 (1957) [Columbia Tech. Transl. p. 828].

Translated by G. Volkoff
85

ON THE SHAPE OF ALPHA-ACTIVE NUCLEI

L. L. GOL' DIN, G. I. NOVIKOVA, and K. A. TER-MARTIROSYAN

Submitted to JETP editor July 9, 1958

J. Exptl. Theoret. Phys. (U.S.S.R.) **36**, 512-516 (February, 1959)

The shape of a heavy nucleus can be determined from the rate of alpha decay to successive levels of the main rotational band of the daughter nucleus. The quantities α_2 and α_4 which are the coefficients in the expansion of the nuclear shape in Legendre polynomials, are computed. The calculations are performed for four even and three odd nuclei. The results of the calculations agree satisfactorily with each other and indicate that the contribution of the term $\alpha_4 P_4(\cos\vartheta)$ to the nuclear shape is significant.

SEVERAL recent theoretical papers[1-5] are devoted to the calculation of the intensity of the rate of α decay to levels belonging in the same rotational band. Calculations show that the rates of decay are very sensitive to the shape of the nucleus. It is therefore natural to use the experimental rates of α decay to determine not only the dimensions of the atomic nuclei, but also their configurations. In the present article we use for the calculation the intensities of α transitions only to levels that belonged to the main rotational bands, since the theory has been derived precisely for these transitions. By main rotational band we understand the band of the daughter nucleus, beginning with the level that is characterized by the same momentum I and the same parity as the main level of the parent nucleus. The α transitions to these levels are not connected with a change in K (the projection of I on the symmetry axis of the nucleus) and are favored transitions.

It was shown in reference 5 that the intensities of the α transitions to the levels of the main rotational bands are given by the formula

$$W_I = 4\pi^2 \frac{\hbar k_I}{\mu} \sum_{l=|I-I_0|}^{I+I_0} |C^{I\,I_0}_{l\,0;\;I_0}|^2 \left| \int_{-1}^{1} \frac{R(\vartheta)\chi(\vartheta)}{\varphi_{Il}[R(\vartheta)]} Y_{l0}(\vartheta)\, d(\cos\vartheta) \right|^2, \tag{1}$$

where W_I is the probability of α decay to a level with spin I (I_0 is the spin of the parent nucleus), k_I is the wave number of the α particles whose emission leads to the excitation of this level, μ is the mass of the α particle, $C^{IM}_{I_1M_1,I_2M_2}$ are the Clebsch-Gordan coefficients, l is the angular momentum carried away by the α particle, $R = R(\vartheta)$ is the equation for the surface of the nucleus (outside of which the nuclear forces are assumed to vanish) in a coordinate system fixed at the nucleus, $\chi(\vartheta)$ is the wave function of the α particle on the surface of the nucleus, $Y_{l_0}(\vartheta)$ is a spherical harmonic, and $\varphi_{Il}(r)$ is the radial eigenfunction of an α particle with a momentum l (for a transition to a level with spin I).

The theoretical problem is to find a nuclear shape $R(\vartheta)$ compatible with the experimental values of W_I. It is natural to assume in the calculation that the unknown function $\chi(\vartheta)$ is constant on the surface of the nucleus.

The greatest difficulties are involved in the calculation of $\varphi_{Il}(r)$. Exact calculations of $\varphi_{Il}(r)$ have been carried out thus far only for even nuclei, and necessitate the use of high-speed electronics computers. It was shown in reference 5 that the use of an approximate function $\varphi^{(0)}_{Il}(r)$ in Eq. (1), at least in the case of even nuclei, produces no substantial error in the calculation of the probability of the α decay to the rotational levels. The function $\varphi^{(0)}_{Il}(r)$ is the radial eigenfunction, calculated without allowance for the quadrupole term (in the higher multipoles) in the Coulomb potential of the nonspherical nucleus, and is determined with sufficient accuracy from a simple analytical formula. Although a comparison of the exact functions $\varphi_{Il}(r)$ and the approximate ones $\varphi^{(0)}_{Il}(r)$ has never been performed for odd nuclei, one can hardly expect the odd nuclei to behave in this respect substantially differently from the even ones. This has caused the authors of reference 5 to propose the substitution of $\varphi^{(0)}_{Il}(r)$ for $\varphi_{Il}(r)$ in the formulas, as is indeed done in the present paper.

In the calculations we have computed the first two terms that describe the deviation of the nuclear shape from spherical

$$R(\vartheta) = r_0[1 + \alpha_2 P_2(\cos\vartheta) + \alpha_4 P_4(\cos\vartheta)], \tag{2}$$

where P_2 and P_4 are Legendre polynomials, and

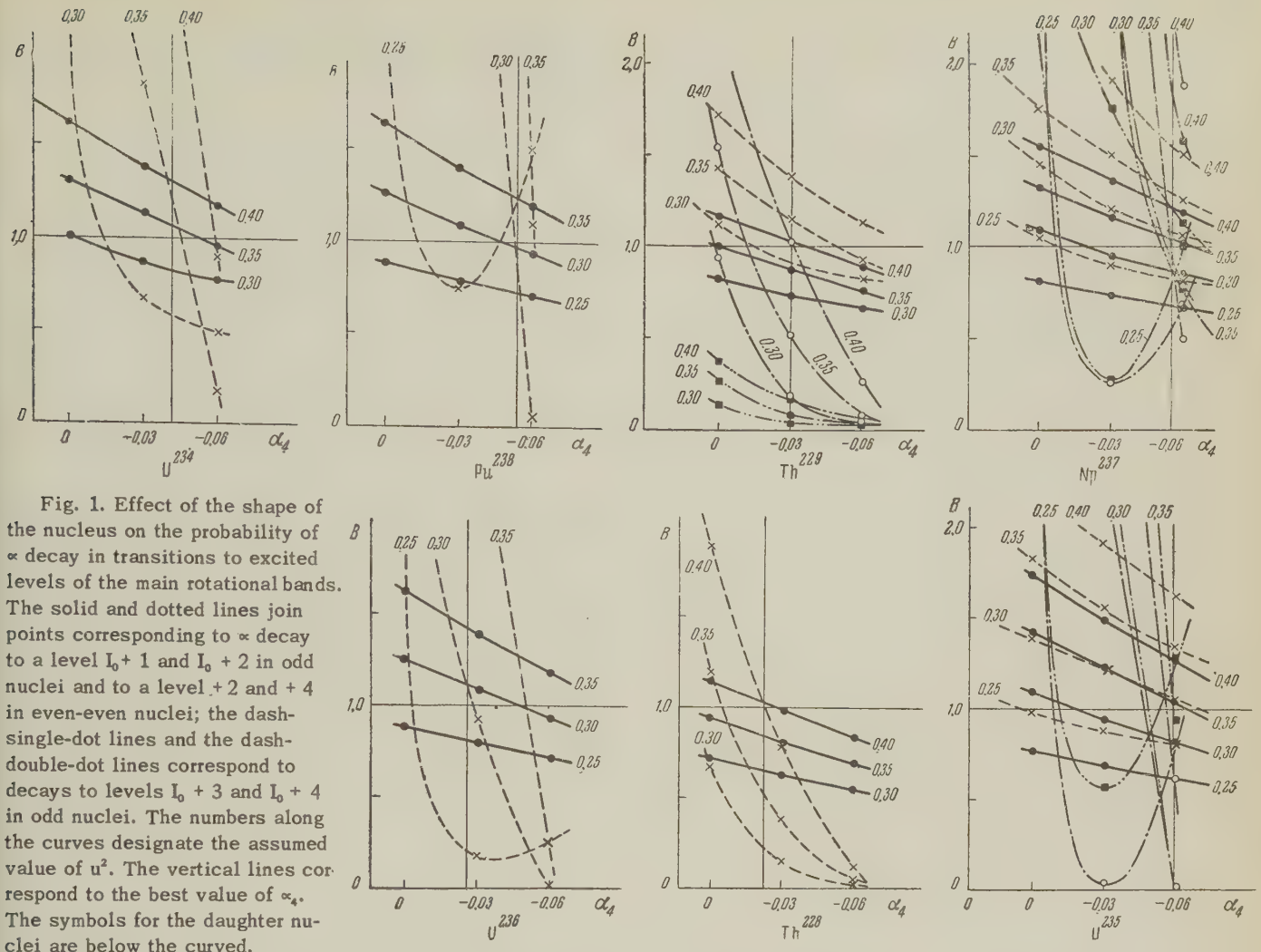

Fig. 1. Effect of the shape of the nucleus on the probability of α decay in transitions to excited levels of the main rotational bands. The solid and dotted lines join points corresponding to α decay to a level $I_0 + 1$ and $I_0 + 2$ in odd nuclei and to a level $+2$ and $+4$ in even-even nuclei; the dash-single-dot lines and the dash-double-dot lines correspond to decays to levels $I_0 + 3$ and $I_0 + 4$ in odd nuclei. The numbers along the curves designate the assumed value of u^2. The vertical lines correspond to the best value of α_4. The symbols for the daughter nuclei are below the curved.

α_2 and α_4 are coefficients that must be determined. We have preferred to use instead of α_2 the quantity $u^2 = (a^2 - b^2)/a^2 \approx 2\Delta R/R$ (a is the major semiaxis of the nucleus and b is the minor one).

Figure 1 shows the results of the calculations, performed for four even-even and three odd nuclei. The calculations were made under differing assumptions concerning the shape of the nucleus: u^2 assumed the values 0.25, 0.30, 0.35, and 0.40 while α_4 was assigned values 0, -0.03, and -0.06. The optimum values of u^2 and α_4 were found by interpolation.

To determine the size of the nucleus we used the rate of α decay to the lower level of the band. In determining the shape, the most useful quantities were the ratios W_I/W_{I_0} of the α-decay rates to the level with spin I and to the lowest level of the band. Figure 1 shows the quotients of these ratios divided by the experimental values, as functions of α_4, i.e.,

$$B = (W_I / W_{I_0})_{\text{calc}} / (W_I / W_{I_0})_{\text{exptl}}.$$

The table contains the the theoretical curves for the optimum values of u^2 and α_4 and a comparison of the calculated and experimental values of W_I/W_{I_0} for these parameters. Since the nuclear spin in the transition to a higher level increases successively, the levels are identified in the table by the spin.

As can be seen from the table, the intensities of the α transitions at $l_{\min} \leq 4$ agree well with the theory and lead to an almost identical shape for all the considered nuclei. The values listed in the table show a striking discrepancy for the levels $I_0 + 4$ and $I_0 + 5$ in Th^{229}. The rotational nature of these levels is not established with full assurance, however, since it merely follows from the fact that the energies of the levels fit well the rotational formula. The experiments specially set up by E. F. Tretyakov to investigate the internal-conversion electrons that accompany the α decay of U^{233} have confirmed the rotational nature of the $I_0 + 3$ level, but have contributed nothing so far for the $I_0 + 4$ and $I_0 + 5$ levels.

The calculated rate of α decay to the levels of

Nucleus	u^2	α_2	α_4	B						Q_0 (barns)	Q_4 (barn^2)	$\hbar^2 2J_{en}$ (kev)	J_{en} (10^{-46} g – cm^2)	J_{sol} (10^{-46} g – cm^2)	J_{irr} (10^{-46} g – cm^2)
				$l_{min}=2$		$l_{min}=4$		$l_{min}=6$							
				I_0+1	I_0+2	I_0+3	I_0+4	I_0+5	I_0+6						
U^{235}*	0.34	0.161	—0.058	1	1.3	1	1			13.7	—3.6	5.29	0.66	1.18	0.034
Np^{237}*	0.34	0.160	—0.056	1	1.2	1	1			14.5	—3.6	6.20	0.57	1.20	0.035
Th^{229}	0.39	0.177	—0.030	1	1.3	1	0.1**	$2 \cdot 10^{-4}$**		14.7	+2.0	6.20	0.57	1.16	0.044
Pu^{238}	0.31	0.138	—0.052		1		1		4	12.3	—3.9	7.5	0.47	1.21	0.027
U^{236}	0.28	0.119	—0.026		1		1		26	10.9	—0.7	7.5	0.47	1.29	0.025
U^{234}	0.33	0.148	—0.041		1		1		23	11.7	—0.9	7.3	0.48	1.10	0.030
Th^{228}	0.39	0.173	—0.025		1		1		29	14.1	—3.0	9.6	0.37	1.13	0.043

* All the nuclear characteristics listed in the table pertain to the lower level of the main rotational band, which does not coincide with the ground state of the nucleus.

** The rotational nature of this level follows only from the excitation energy and is not confirmed by other data.

the $I_0 + 6$ type is in substantial disagreement with experiment. This discrepancy must, however, not be given any particular significance. The intensity of α radiation with $l = 6$ depends both on u^2 and α_4, and also on the term α_6 which has not been calculated. The contributions of the terms that depend on u^2 and on α_4 to the probability amplitude are almost equal in magnitude and opposite in sign when $l = 6$. The accuracy of calculations under such cancellation is naturally quite unsatisfactory. The discrepancy noted is apparently merely an example of the roughness of the theory.

Knowledge of the shape of the nucleus makes it possible to calculate its multipole moments. Column 11 of the table lists the values of the intrinsic quadrupole moment Q_0, calculated under the assumption that the protons are uniformly distributed. The calculations were carried out using the approximate formula

$$Q_0 = {}^6/_5 Zr_0^2 \alpha_2 (1 + {}^4/_7 \alpha_2), \qquad (3)$$

which follows directly from the usual definition

$$Q_0 = \frac{2Z}{V} \int r^2 P_2 (\cos \vartheta)\, d\tau$$

with allowance for Eq. (2). Direct measurements of Q_0 with which to compare our results are unfortunately lacking for these nuclei. The measurements available for U^{235} and Np^{237} pertain to the ground states of these nuclei and not to the lower level of the main rotational bands, for which our calculations were made. We give below for comparison data by Newton,[6] which show that our calculations give the correct order of magnitude for the quadrupole moments:

Nucleus:	U^{233}	U^{235}	U^{238}	Np^{237}	Pu^{238}
Q_0 (barns):	13.7	10.1	10.3	9.0	9.2

That the theoretical values of Q_0 exceed somewhat the experimental ones is apparently the result of our using in our calculations the nuclear radii obtained from the α decay (from the intensity of the zero level). These radii are known to be some 20% greater than the electrical radii of the nuclei measured by scattering of fast electrons; this should yield, approximately, a 40% increase in the calculated values over the true ones.

Column 12 of the table gives the values of the 2^4-pole moment, calculated from the formula

$$Q_4 = \frac{Z}{V} \int r^4 P_4 (\cos \vartheta)\, d\tau \simeq \frac{1}{3} Zr_0^4 (\alpha_4 + 1.54\, \alpha_2^2). \qquad (4)$$

In formula (4) the negative term α_4 partially offsets the positive term $1.54\, \alpha_2^2$, thus reducing substantially the accuracy of the results. Direct experimental measurements of Q_4 for heavy nuclei are unfortunately still not available.

Column 13 of the table gives the values of $\hbar^2/2J_{en}$ calculated from the excitation energy of the rotational levels, while the next column gives the values of the moment of inertia J_{en} thus determined. In the last two columns of the table are listed the values of the moment of inertia, calcu-

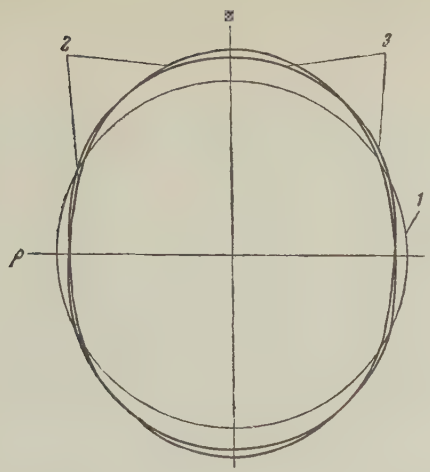

FIG. 2. Shape of U^{234} nucleus. 1– circle, 2– without allowance for α_4, 3– with allowance for α_4.

lated from the model of the "solid nucleus," J_{sol}, and for the "drop nucleus" with irrotational motion of the liquid, J_{irr}.

As expected, J_{sol} is several (2 or 3) times greater the experimentally observed value of J_{en}. We cannot establish here a connection between the variations of J_{sol} and J_{en} from nucleus to nucleus. J_{irr} is found to be substantially smaller than J_{en}, so that the "irrotational" model is apparently too rough.

In conclusion we show in Fig. 2 the shape of the U^{234} nucleus, calculated with and without the term α_4. For comparison the figure shows a circle representing a fully spherical nucleus. As follows from the figure, the contribution of the term $\alpha_4 P_4$ is far from small.

We are glad to make use of this opportunity to thank G. M. Adel'son-Vel'skiĭ and A. P. Brizgal for the mathematical calculations.

[1] J. O. Rasmussen and B. Segal, Phys. Rev. **103**, 1298 (1956).

[2] V. M. Strutinskiĭ, J. Exptl. Theoret. Phys. (U.S.S.R.) **30**, 411 (1956) and **32**, 1412 (1957), Soviet Phys. JETP **3**, 450 (1956) and **5**, 1150 (1957).

[3] V. G. Nosov, Dokl. Akad. Nauk SSSR **112**, 414 (1957), Soviet Phys. "Doklady" **2**, 48 (1957); J. Exptl. Theoret. Phys. (U.S.S.R.) **33**, 226 (1957), Soviet Phys. JETP **6**, 176 (1958).

[4] Gol'din, Adel'son-Vel'skiĭ, Birzgal, Piliya, and Ter-Martirosyan, J. Exptl. Theoret. Phys. (U.S.S.R.) **35**, 184 (1958), Soviet Phys. JETP **8**, 127 (1959).

[5] J. O. Newton, Nucl. Phys. **3**, 345 (1957); Preprint, 1958.

Translated by J. G. Adashko
86

POLARIZATION OF BETA-ELECTRONS FROM RaE

B. V. GESHKENBEĬN, S. A. NEMIROVSKAYA, and A. P. RUDIK

Submitted to JETP editor July 24, 1958; resubmitted October 28, 1958

J. Exptl. Theoret. Phys. (U.S.S.R.) **36**, 517-525 (February, 1959)

Effects due to parity nonconservation in the β decay of RaE are studied. A formula is derived for the longitudinal polarization of the β electrons. It is found that the magnitude of the longitudinal polarization does not equal v/c. Throughout the calculation the possibility of violation of time reversal invariance is allowed for. The experimental data on the magnitude of the polarization of RaE β electrons severely restrict the region of possible violation of time reversal invariance.

EVER since the discovery of parity nonconservation in weak interactions the β decay of RaE has aroused a lot of interest.

First, Lewis[1] and Fujita et al.[2] pointed out the sensitivity of the β spectrum of RaE to a possible violation of time-reversal invariance. Secondly Alikhanov made the suggestion, confirmed by experiment,[3] that the longitudinal polarization of β electrons from RaE should differ from v/c and the amount of this difference should, generally speaking, depend on the possible violation of time reversal invariance.

Below we derive an expression for the longitudinal polarization of β electrons from RaE taking into account possible violation of time reversal invariance.

1. BETA SPECTRUM OF RaE

The β spectrum of RaĖ (a $1^- \to 0^+$ transition) is the only known example among first forbidden transitions of this type which does not have an allowed shape. This fact was successfully explained within the framework of modern β decay theory which takes into account the variation of the electron wave function within the nucleus.[4-7] In these calculations β decay was assumed to be invariant under time reversal.

Below we follow the procedure of Takebe, Nakamura and Taketani,[7] but without assuming that β decay is invariant under the parity (or, possibly, time reversal) operation. Using the two-component theory of the neutrino and the methods of Berestetskiĭ, Ioffe, Rudik, and Ter-Martirosyan[8] we find the following expression for the correction factor of the RaE spectrum shape (see Appendix I):

$$C(Z, R_0, W) = C_0(Z, R_0, W) + \Delta C.$$

S and T Interaction

$$C_0(Z, R_0, W) = \bar{M}_1(1+x)^2 + \bar{L}_1[{}^1/_3 q^2 x^2 + y^2 + {}^1/_6 q^2 + {}^2/_3 qy(x-1)] + \bar{N}_1[{}^2/_3 q(x^2-1) + 2y(1+x)] + {}^1/_2 \bar{L}_2(2x-1)^2, \quad (1')$$

$$\Delta C = [\bar{M}_1 + 2\bar{L}_2 + {}^1/_3 q^2 \bar{L}_1 + {}^2/_3 q \bar{N}_1] x^2 F^2. \quad (1'')$$

Here $\bar{M}_1$, $\bar{L}_1$, $\bar{L}_2$, and $\bar{N}_1$ are tabulated[7] functions of the total electron energy W (in the following W is given in units of mc^2). If variation of the electron wave function in the nucleus is ignored we have $\bar{M}_1 = M_0$, $\bar{L}_1 = L_0$, $\bar{L}_2 = L_1$ and $\bar{N}_1 = N_0$, where M_0, L_0, L_1, and N_0 are given in references 9 and 10. The two arbitrary parameters x and y denote ratios of matrix elements:

$$x = ig_S \int \beta \mathbf{r} / g_T \int \beta [\sigma \times \mathbf{r}]; \qquad y = \int \beta \boldsymbol{\alpha} / \int \beta [\sigma \times \mathbf{r}].$$

It is assumed that violation of time reversal invariance manifests itself in a complex value of the scalar interaction coupling constant: $G_S = g_S(1 + iF)$, $G_T = g_T$, where g_S, g_T and F are real.

V and A Interaction

$$C_0(Z, R_0, W) = \bar{M}_1(1+x)^2 + \bar{L}_1[{}^1/_3 q^2 x^2 + y^2 + {}^1/_6 q^2 - {}^2/_3 qy(x-1)] + \bar{N}_1[-{}^2/_3 q(x^2-1) + 2y(1+x)] + {}^1/_2 \bar{L}_2(2x-1)^2 \quad (2')$$

$$\Delta C = [\bar{M}_1 + {}^1/_2 \bar{L}_2 + {}^1/_6 q^2 \bar{L}_1 + {}^2/_3 q \bar{N}_1] F^2. \quad (2'')$$

Now x and y are given by

$$x = ig_V \int \mathbf{r} / g_A \int [\sigma \times \mathbf{r}]; \qquad y = g_V \int \boldsymbol{\alpha} / g_A \int [\sigma \times \mathbf{r}].$$

and it is assumed that violation of time reversal invariance manifests itself in a complex value of

the axial vector interaction coupling constant; $G_V = g_V$, $G_A = g_A(1 + iF)$ (g_V, g_A, F — real).

2. POLARIZATION OF BETA ELECTRONS FROM RaE

We write the polarization of the β electrons from RaE in the form

$$\langle\sigma\rangle = (D_0(Z, R_0, W) + \Delta D)/(C_0(Z, R_0, W) + \Delta C), \quad (3)$$

where C_0 and ΔC are given by Eqs. (1′), (1″), (2′), and (2″) while D_0 and ΔD are given respectively by (see Appendix 1):

For S and T Interaction

$$D_0(Z, R_0, W) = \sin[\delta_1 - \delta_{-1}]\{(\overline{M}_1^2 - \overline{M}_{-1}^2)^{1/2}(1 + x)^2$$
$$+ (\overline{L}_1^2 - \overline{L}_{-1}^2)^{1/2}(\tfrac{1}{3}q^2x^2 + y^2 + \tfrac{1}{6}q^2 + \tfrac{2}{3}qy(x - 1))$$
$$- \tfrac{1}{2}[(\overline{L}_1 + \overline{L}_{-1})^{1/2}(\overline{M}_1 + \overline{M}_{-1})^{1/2}$$
$$+ (\overline{L}_1 - \overline{L}_{-1})^{1/2}(\overline{M}_1 - \overline{M}_{-1})^{1/2}](\tfrac{2}{3}q(x^2 - 1)$$
$$+ 2y(1 + x))\} + \sin[\delta_2 - \delta_{-2}](\overline{L}_2^2 - \overline{L}_{-2}^2)^{1/2}(2x - 1)^2/2, \quad (4')$$

$$\Delta D = \sin[\delta_1 - \delta_{-1}]\{(\overline{M}_1^2 - \overline{M}_{-1}^2)^{1/2} + \tfrac{1}{3}q^2(\overline{L}_1^2 - \overline{L}_{-1}^2)^{1/2}$$
$$- \tfrac{1}{3}q[(\overline{L}_1 + \overline{L}_{-1})^{1/2}(\overline{M}_1 + \overline{M}_{-1})^{1/2}$$
$$+ (\overline{L}_1 - \overline{L}_{-1})^{1/2}(\overline{M}_1 - \overline{M}_{-1})^{1/2}]\}x^2F^2$$
$$+ 2\sin[\delta_2 - \delta_{-2}](\overline{L}_2^2 - \overline{L}_{-2}^2)^{1/2}x^2F^2$$
$$+ \cos[\delta_1 - \delta_{-1}]\{(\overline{L}_1 + \overline{L}_{-1})^{1/2}(\overline{M}_1 + \overline{M}_{-1})^{1/2}$$
$$- (\overline{L}_1 - \overline{L}_{-1})^{1/2}(\overline{M}_1 - \overline{M}_{-1})^{1/2}\}(y - \tfrac{2}{3}q)xF; \quad (4'')$$

For V and A Interaction

$$D_0(Z, R_0, W) = \sin[\delta_1 - \delta_{-1}]\{(\overline{M}_1^2 - \overline{M}_{-1}^2)^{1/2}(1 + x^2)$$
$$+ (\overline{L}_1^2 - \overline{L}_{-1}^2)^{1/2}[\tfrac{1}{3}q^2x^2 + y^2 + \tfrac{1}{6}q^2 - \tfrac{2}{3}qy(x - 1)]$$
$$- \tfrac{1}{2}[(\overline{L}_1 + \overline{L}_{-1})^{1/2}(\overline{M}_1 + \overline{M}_{-1})^{1/2} + (\overline{L}_1 - \overline{L}_{-1})^{1/2}(\overline{M}_1 - \overline{M}_{-1})^{1/2}]$$
$$\times[-\tfrac{2}{3}q(x^2 - 1) + 2y(1 + x)]\}$$
$$+ \sin(\delta_2 - \delta_{-2})(\overline{L}_2^2 - \overline{L}_{-2}^2)^{1/2}(2x - 1)^2/2, \quad (5')$$

$$\Delta D = \sin[\delta_1 - \delta_{-1}]\{(\overline{M}_1^2 - \overline{M}_{-1}^2)^{1/2} + \tfrac{1}{6}q^2(\overline{L}_1^2 - \overline{L}_{-1}^2)$$
$$- \tfrac{1}{3}q[(\overline{L}_1 + \overline{L}_{-1})^{1/2}(\overline{M}_1 + \overline{M}_{-1})^{1/2}$$
$$+ (\overline{L}_1 - \overline{L}_{-1})^{1/2}(\overline{M}_1 - \overline{M}_{-1})^{1/2}]\}F^2$$
$$+ \tfrac{1}{2}\sin[\delta_2 - \delta_{-2}](\overline{L}_2^2 - \overline{L}_{-2}^2)^{1/2}F^2$$
$$+ \cos[\delta_1 - \delta_{-1}][(\overline{L}_1 + \overline{L}_{-1})^{1/2}(\overline{M}_1 + \overline{M}_{-1})^{1/2}$$
$$- (\overline{L}_1 - \overline{L}_{-1})^{1/2}(\overline{M}_1 - \overline{M}_{-1})^{1/2}](y - \tfrac{2}{3}qx)F. \quad (5'')$$

All roots in Eqs. (4′), (4″), (5′), and (5″) are to be taken as positive. The functions $\overline{M}_{-1}$, $\overline{L}_{-1}$ and $\overline{L}_{-2}$ are given in Appendix II.

The symmetry between the functions C_0 and D_0 should be noted. Indeed, wherever C_0 contains the quantities $\overline{M}_1$, $\overline{L}_1$, $\overline{L}_2$ and $\overline{N}_1$, D_0 contains instead

$$\overline{M}_1' = [\overline{M}_1^2 - \overline{M}_{-1}^2]^{1/2}\sin(\delta_1 - \delta_{-1});$$
$$\overline{L}_1' = [\overline{L}_1^2 - \overline{L}_{-1}^2]^{1/2}\sin(\delta_1 - \delta_{-1});$$
$$\overline{L}_2' = [\overline{L}_2^2 - \overline{L}_{-2}^2]^{1/2}\sin(\delta_2 - \delta_{-2});$$
$$\overline{N}_1' = -\tfrac{1}{2}[(\overline{L}_1 + \overline{L}_{-1})^{1/2}(\overline{M}_1 + \overline{M}_{-1})^{1/2}$$
$$+ (\overline{L}_1 - \overline{L}_{-1})^{1/2}(\overline{M}_1 - \overline{M}_{-1})^{1/2}]\sin(\delta_1 - \delta_{-1});$$

If in the expansion of $\overline{M}_1$, $\overline{L}_1$, etc. and $\overline{M}_{-1}$, $\overline{L}_{-1}$, etc. only terms up to first order in pR_0 are kept (and further if the nuclear charge distribution is approximated by a point charge and the electron wave function is assumed to be constant within the nuclear volume) then, as was shown by Lee-Whiting,[11]

$$\overline{M}_1'/\overline{M}_1 \approx \overline{L}_1'/\overline{L}_1 \approx \overline{L}_2'/\overline{L}_2 \approx \overline{N}_1'/\overline{N}_1 \approx v/c.$$

This leads to a longitudinal polarization of the β electrons equal to v/c. In the case of RaE, however, the above approximations are not valid and the longitudinal polarization of the β electrons differs from v/c.

3. RESULTS OF CALCULATIONS AND DISCUSSION

We consider first the case when time reversal invariance is valid.

Using the values of x and y determined by Takebe, Nakamura, and Taketani[7] from requiring the best possible agreement between the theoretical and experimental C_0, we obtain in the case of S and T interaction the values listed in Table I for the deviation of the polarization from v/c.

TABLE I. Values of $\langle\sigma\rangle/(v/c)$ for S, T interaction ($r_0 = 1.17 \times 10^{-13}$)

x	y	W			
		1.2	1.8	2.4	3.0
0.2	18.8	0.53	0.43	0.28	0.13
0.4	22.4	0.67	0.64	0.57	0.44
0.6	25.7	0.71	0.69	0.63	0.50
1.0	32.35	0.76	0.75	0.71	0.62
1.2	35.6	0.77	0.76	0.72	0.65
3.0	64.8	0.80	0.80	0.78	0.75
5.5	104	0.80	0.80	0.77	0.76

For the V and A interaction a region of values of x and y was determined by requiring a satisfactory agreement between the theoretical and experimental values of C_0. As was to be expected, this region turned out to be somewhat different from the corresponding region for the S and T interaction. The deviation of the polarization from v/c in the case of V and A inter-

TABLE II. Values of $\langle\sigma\rangle/(v/c)$ for V, A interaction ($r_0 = 1.17 \times 10^{-13}$)

x	y	W = 1.2	W = 1.8	W = 2.4	W = 3.0
0.2	19.85	0.83	0.83	0.81	0.76
0.5	24.6	0.80	0.80	0.77	0.70
1.0	32.35	0.76	0.75	0.71	0.62
1.3	37	0.74	0.73	0.68	0.60
1.7	42.95	0.71	0.68	0.62	0.56
2.0	47.3	0.69	0.65	0.58	0.54

action is listed in Table II (it is clear that for for $x = 1$ there is no difference between the S, T, and V, A interactions).

The dependence of the polarization of the β electrons on x allows, in principle, a unique determination of x. The experimental data[3] available at this time do not contradict the theoretical calculations for $x \approx 1.7$ (V, A interaction) or $x \approx 0.6$ (S, T interaction).

The different x-dependence of $\langle\sigma\rangle/(v/c)$ should be noted: for the S, T interaction $\langle\sigma\rangle/(v/c)$ increases, and for the V, A interaction it decreases as x increases. However, for all interactions and for any x and y which permit the fitting of the experimental spectrum shape of RaE by the theoretical one, we have $(-\langle\sigma\rangle/(v/c))_{max} \lesssim 0.84$.

Let us next take into account the possibility of violation of time-reversal invariance in β decay. Before quoting the results of the calculations for various admissible values of F let us explain why it is impossible to reconcile theory and experiment for large F ($F \sim 1$) in the β decay of RaE. We make use of the well-known fact that the experimentally required energy dependence of $C = C(Z, R_0, W)$ can only be obtained provided there are strong interference effects in $C(Z, R_0, W)$ (with a simultaneous decrease of $C(Z, R_0, W)$ by about two orders of magnitude).

Let us solve for y in the equation $C_{exp} = C(Z, R_0, W)$, for some fixed x. From Eqs. (2′) and (2″) we have for the V, A interaction:

$$y = (1/\bar{L}_1)\{\varepsilon_0 \pm (\varepsilon_0^2 - \varepsilon_1\bar{L}_1 + C_{exp}\bar{L}_1 - F^2\varepsilon_2\bar{L}_1)^{1/2}\}, \quad (6)$$

where

$$\varepsilon_0 = {}^1/_3 q(x-1)\bar{L}_1 - (1+x)\bar{N}_1,$$

$$\varepsilon_1 = x^2(\bar{M}_1 + {}^1/_3 q^2\bar{L}_1 + 2\bar{L}_2 - {}^2/_3 q\bar{N}_1) + 2x(\bar{M}_1 - \bar{L}_2) + \varepsilon_2,$$

$$\varepsilon_2 = \bar{M}_1 + {}^1/_2\bar{L}_2 + {}^1/_6 q^2\bar{L}_1 + {}^2/_3 q\bar{N}_1.$$

We give below values of $\epsilon_0^2 - \epsilon_1\bar{L}_1$ and $\epsilon_2\bar{L}_1$ for various x and W.

As was mentioned above, $\bar{L}_1 C_{exp} \sim \epsilon_0^2 - \epsilon_1\bar{L}_1$. On the other hand, we have from Tables III and IV that $\epsilon_0^2 - \epsilon_1\bar{L}_1 \ll \epsilon_2\bar{L}_1$. It then follows from Eq. (6) that F cannot be of the order of magnitude of unity (since y is to be real). It is important to note that the above considerations remain valid for slight changes in the functions $\bar{L}_1$, $\bar{L}_2$, $\bar{M}_1$, and $\bar{N}_1$ (such changes could be due to insufficiently accurate knowledge of the nuclear charge distribution, to corrections arising from third forbidden matrix elements, etc.).

TABLE III. Values of $(\epsilon_0^2 - \epsilon_1\bar{L}_1)$

x	W = 1.2	W = 1.8	W = 2.4	W = 3.0
0.2	0.37	0.26	0.20	0.20
1.0	1.56	0.98	0.65	0.56
2.0	4.33	2.93	2.36	2.62

TABLE IV. Values of $\epsilon_2\bar{L}_1$

W	1.2	1.8	2.4	3.0
$\epsilon_2\bar{L}_1$	121.70	126.77	130.80	134.38

However, for small values of F ($F < 10^{-2}$) one finds from numerical calculations that a satisfactory theoretical fit to the experimental spectrum shape of RaE is possible. The longitudinal polarization of β electrons in the allowed region for x and y and for $F^2 = 6 \times 10^{-3}$ and $F^2 = 3 \times 10^{-3}$ is listed in Tables V and VI for V, A interaction. As can be seen from Eq. (5″) the polarization depends not only on the magnitude of F^2 but also on the sign of F.

TABLE V. Values of $\langle\sigma\rangle/(v/c)$ for V, A interaction with $F^2 = 6 \times 10^{-3}$

		W = 1.2		W = 1.8		W = 2.4		W = 3.0	
x	y	F<0	F>0	F<0	F>0	F<0	F>0	F<0	F>0
0.2	19	0.94	0.67	0.90	0.72	0.89	0.70	0.87	0.68
1.3	36.25	0.86	0.59	0.80	0.61	0.74	0.55	0.69	0.50
1.7	42.4	0.84	0.58	0.77	0.59	0.71	0.53	0.67	0.51

TABLE VI. Values of $\langle\sigma\rangle/(v/c)$ for V, A interaction with $F^2 = 3 \times 10^{-3}$

		W							
		1.2		1.8		2.4		3.0	
x	y	$F<0$	$F>0$	$F<0$	$F>0$	$F<0$	$F>0$	$F<0$	$F>0$
0.2	19.4	0.89	0.73	0.87	0.76	0.85	0.73	0.81	0.68
1.3	36.55	0.81	0.64	0.76	0.65	0.71	0.59	0.64	0.51
1.9	45.76	0.79	0.62	0.73	0.61	0.67	0.55	0.63	0.53

TABLE VII. Values of $\langle\sigma\rangle/(v/c)$ for S, T interaction with various F

			W						
			1.2		1.8		2.4		3.0	
F^2	x	y	$F<0$	$F>0$	$F<0$	$F>0$	$F<0$	$F>0$	$F<0$	$F>0$
$10\cdot10^{-3}$	0.4	21.94	0.82	0.47	0.72	0.47	0.62	0.36	0.49	0.23
	0.8	27.96	0.92	0.51	0.84	0.54	0.78	0.49	0.73	0.45
$6\cdot10^{-3}$	1.2	34.66	0.89	0.61	0.84	0.64	0.80	0.60	0.75	0.55
	2.0	47.20	0.92	0.65	0.88	0.69	0.86	0.67	0.84	0.67
$3\cdot10^{-3}$	1.2	35.00	0.84	0.66	0.80	0.67	0.75	0.62	0.68	0.54
	3.0	62.65	0.89	0.67	0.85	0.69	0.83	0.66	0.82	0.67

In Table VII the deviation of the polarization from v/c is listed in the case of S, T interaction for various values of F^2 (in the S, T case values of F^2 up to $F^2 = 10^{-2}$ are allowed). The irregular variation of $\langle\sigma\rangle/(v/c)$ as a function of F^2 is apparently due to the fact that for various values of x and F the theoretical and experimental spectrum shapes do not agree to the same degree of accuracy. (This irregularity is also present in the V, A case but only at high electron energies and to a much smaller extent.)

The following statements can be made based on a comparison of Tables V, VI, and VII with reference 3:

1. For V, A interaction: assuming that time reversal invariance is violated in β decay the experimental data exclude $F < 0$ for $F^2 = 6 \times 10^{-3}$ and $F^2 = 3 \times 10^{-3}$. For $F > 0$ theory and experiment can be made to agree for $x \approx 0.2$ ($F^2 = 6 \times 10^{-3}$) or $x \approx 0.7$ ($F^2 = 3 \times 10^{-3}$).

2. For S, T interaction: the value of $F^2 = 10^{-2}$, which is admissible as far as comparison of experimental and theoretical spectrum shapes is concerned, is excluded by the experimental data on electron polarization.[3] For $F^2 = 6 \times 10^{-3}$ and $F^2 = 3 \times 10^{-3}$ the case $F < 0$ is excluded, and the case $F > 0$ with either value for F^2 is allowed if $x \approx 1.7$.

The authors express their sincere appreciation to Academician A. I. Alikhanov, who stimulated this research, for many discussions and to B. L. Ioffe and V. A. Lyubimov for advice.

APPENDIX I

We shall use the methods of reference 8 (referred to hereafter as I). We write the electron wave function, with finite nuclear size effects taken into account, as

$$\Psi_{p,\xi}(r) = \begin{pmatrix} \varphi_p V_\xi \\ \chi_p V_\xi \end{pmatrix}. \qquad \text{(A1.1)}$$

where V_ξ is the two-component unit spinor determining the electron polarization,

$$\varphi_p = \alpha_0 + i\mathbf{p}\cdot\mathbf{r}\,\alpha_1 + i(\sigma\cdot\mathbf{r})(\sigma\cdot\mathbf{n})\beta_c,$$

$$\chi_p = [\beta_0 + i\mathbf{p}\cdot\mathbf{r}\,\beta_1 + i(\sigma\cdot\mathbf{r})(\sigma\cdot\mathbf{n})\alpha_c](\sigma\cdot\mathbf{n}), \qquad \text{(A1.2)}$$

$\mathbf{p}$ is the electron momentum, and $\mathbf{n} = \mathbf{p}/p$.

The quantities α_i and β_i are chosen as follows:

$$\alpha_0 = aie^{-i\delta_{-1}} g_{-1}; \qquad \alpha_1 = a\frac{3}{pr} e^{-i\delta_{-2}} g_{-2};$$

$$\beta_c = a\frac{1}{r}(e^{-i\delta_1} g_1 - e^{-i\delta_{-2}} g_{-2});$$

$$\beta_0 = ae^{-i\delta_1} f_1; \qquad \beta_1 = a\frac{3}{ipr} e^{-i\delta_2} f_2;$$

$$\alpha_c = a\frac{1}{ir}(e^{-i\delta_{-1}} f_1 - e^{-i\delta_2} f_2), \quad a = \sqrt{\pi/2p\overline{W}}. \qquad \text{(A1.3)}$$

In the actual calculations we used the phase shifts given in reference 12. The relation of these phase shifts to the ones in Eq. (A1.3) is as follows:

$$\delta_{-1} = \delta_{1/2,-1/2} + \pi/2; \qquad \delta_1 = \delta_{1/2,1/2};$$

$$\delta_{-2} = \delta_{3/2,-1/2}; \qquad \delta_2 = \delta_{3/2,1/2} - \pi/2$$

The values of the phase shifts are tabulated below.

Values of phase shifts

W	1.2	1.8	2.4	3.0
$\delta_{1/2\ 1/2}$	0.0208	0.2618	0.3228	0.3604
$\delta_{1/2-1/2}$	0.7647	0.6646	0.6101	0.5713
$\delta_{3/2\ 1/2}$	−0.8175	−0.4438	−0.3643	−0.3204
$\delta_{3/2-1/2}$	−0.3847	−0.2323	−0.2161	−0.2124

The functions $C(Z, R_0, W)$ and $D(Z, R_0, W)$ according to Eq. (I.35), are given by

$$C(Z, R_0, W) = \lambda_{ik} A_{ik} - \chi_{ik} b_{ik},$$

$$D(Z, R_0, W) = \lambda_{ik} b_{ik} - \chi_{ik} A_{ik},$$

$$D(Z, R_0, W) = D(Z, R_0, W) + \Delta D; \quad \mathbf{B}_{ik} = \mathbf{n}\, b_{ik}. \qquad \text{(A1.4)}$$

After averaging over the direction of emission of the neutrino, summing over the final and averaging over the initial nuclear spin states, according to Eqs. (I.32), (I.38), and (I.39) we have for the V, A interaction (where the fact that the RaE β decay is a $1^- \to 0^+$ transition has been taken into account)*

$$A_{0c} = -[C_\tau - {}^1/_3 q C_b]\, C_a^*; \quad b_{0c} = 0;$$

$$A_{1c} = 0; \quad b_{1c} = -{}^1/_3 p C_a C_a^*;$$

$$A_{01} = 0; \quad b_{01} = {}^1/_3 p\,[C_\tau - {}^1/_3 q C_b]\, C_a^*;$$

$$A_{cc} = C_a C_a^*; \quad b_{cc} = 0;$$

$$A_{11} = {}^1/_3 p^2 |C_R|^2 + {}^1/_6 p^2 |C_T|^2; \quad b_{11} = 0;$$

$$A_{00} = {}^1/_3 q^2 |C_R|^2 + |C_\tau|^2 + {}^1/_6 q^2 |C_T|^2$$
$$- {}^2/_3 q\,[\mathrm{Re}\, C_R C_\tau^* - \mathrm{Im}\, C_T C_\tau^*]; \qquad b_{00} = 0, \qquad \text{(A1.5)}$$

where

$$\mathbf{a} = G_V \int \mathbf{r} - i G_A \int [\sigma \times \mathbf{r}]; \quad \mathbf{b} = G_V \int \mathbf{r} + i G_A \int [\sigma \times \mathbf{r}];$$

$$\mathbf{R} = G_V \int \mathbf{r}; \quad \tau = -i G_V \int \boldsymbol{\alpha}; \quad \mathbf{T} = G_A \int [\sigma \times \mathbf{r}].$$

Assuming that violation of time reversal invariance is connected with the A-interaction coupling constant and introducing the ratios x and y of matrix elements we obtain (here in all A_{ik} and b_{ik} the common factor $g_A^2 |\int \sigma \times \mathbf{r}|^2$ is omitted; $\int \sigma \times \mathbf{r}$ and $\int \alpha$ are purely imaginary, $\int \mathbf{r}$ is purely real):

$$A_{0c} = -[y(1+x) - {}^1/_3 q (x^2 - 1 - F^2)$$
$$- iF(y - {}^2/_3 q x)]; \quad b_{0c} = 0;$$

$$A_{1c} = 0; \quad b_{1c} = -{}^1/_3 p A_{cc}; \quad A_{01} = 0; \quad b_{01} = -{}^1/_3 p A_{0c};$$

$$A_{cc} = (1+x)^2 + F^2; \quad b_{cc} = 0;$$

$$A_{11} = {}^1/_3 p^2 x^2 + {}^1/_6 p^2 (1 + F^2); \quad b_{11} = 0;$$

$$A_{00} = {}^1/_3 q^2 x^2 + y^2 + {}^1/_6 q^2 (1 + F^2)$$
$$- {}^2/_3 q (x - 1) y; \quad b_{00} = 0. \qquad \text{(A1.6)}$$

Noting that for the S and T interactions q goes into −q and assuming that violation of time reversal invariance is connected with the S-interaction coupling constant we get analogous expressions for A_{ik} and b_{ik} in the S, T case.

In the determination of λ_{ik} and χ_{ik} we note the connection between the functions $g_{\pm i}$ and $f_{\pm i}$ and the functions L_0, P_0, M_0, Q_0, L_1, P_1, and N_1.[9,10] Then, omitting factors entering into the phase space factor and the Fermi function, we find

$$\lambda_{00} = L_0; \quad \chi_{00} = (L_0^2 - P_0^2)^{1/2} \sin[\delta_{-1} - \delta_1];$$

$$\lambda_{11} = (9/p^2) L_1; \quad \chi_{11} = (9/p^2)(L_1^2 - P_1^2)^{1/2} \sin[\delta_{-2} - \delta_2];$$

$$\lambda_{cc} = M_0 + L_1 + (M_0 - Q_0)^{1/2}(L_1 - P_1)^{1/2} \cos(\delta_{-1} - \delta_2)$$
$$- (M_0 + Q_0)^{1/2}(L_1 + P_1)^{1/2} \cos(\delta_1 - \delta_{-2});$$

$$\chi_{cc} = (M_0^2 - Q_0^2)^{1/2} \sin(\delta_{-1} - \delta_1) + (L_1^2 - P_1^2)^{1/2} \sin(\delta_{-2} - \delta_2)$$
$$+ (L_1 - P_1)^{1/2}(M_0 + Q_0)^{1/2} \sin(\delta_2 - \delta_1)$$
$$+ (L_1 + P_1)^{1/2}(M_0 - Q_0)^{1/2} \sin(\delta_{-2} - \delta_{-1});$$

$$\lambda_{01} = -(3i/2p)\{(L_0 + P_0)^{1/2}(L_1 + P_1)^{1/2} e^{i(\delta_{-1} - \delta_{-2})}$$
$$+ (L_0 - P_0)^{1/2}(L_1 - P_1)^{1/2} e^{i(\delta_1 - \delta_2)}\};$$

$$\chi_{01} = -(3/2p)\{(L_0 + P_0)^{1/2}(L_1 - P_1)^{1/2} e^{i(\delta_{-1} - \delta_2)}$$
$$- (L_0 - P_0)^{1/2}(L_1 + P_1)^{1/2} e^{i(\delta_1 - \delta_{-2})}\};$$

$$\lambda_{0c} = -{}^1/_2\{2N_0 - (L_0 + P_0)^{1/2}(L_1 - P_1)^{1/2} e^{i(\delta_{-1} - \delta_2)}$$
$$+ (L_0 - P_0)^{1/2}(L_1 + P_1)^{1/2} e^{i(\delta_1 - \delta_{-2})}\};$$

$$\chi_{0c} = {}^1/_2 i\{-(L_0 + P_0)^{1/2}(M_0 + Q_0)^{1/2} e^{i(\delta_{-1} - \delta_1)}$$
$$+ (L_0 - P_0)^{1/2}(M_0 - Q_0)^{1/2} e^{-i(\delta_{-1} - \delta_1)}$$
$$+ (L_0 + P_0)^{1/2}(L_1 + P_1)^{1/2} e^{i(\delta_{-1} - \delta_{-2})}$$
$$+ (L_0 - P_0)^{1/2}(L_1 - P_1)^{1/2} e^{i(\delta_1 - \delta_2)}\};$$

$$\lambda_{1c} = (3/2p)\{-2(L_1^2 - P_1^2)^{1/2} \sin(\delta_{-2} - \delta_2) + i(L_1 + P_1)^{1/2}$$
$$\times (M_0 - Q_0)^{1/2} e^{i(\delta_{-2} - \delta_{-1})} + i(L_1 - P_1)^{1/2}(M_0 + Q_0)^{1/2} e^{i(\delta_2 - \delta_1)}\};$$

$$\chi_{1c} = (3/2p)\{(M_0 + Q_0)^{1/2}(L_1 + P_1)^{1/2} e^{i(\delta_{-2} - \delta_1)}$$
$$- (M_0 - Q_0)^{1/2}(L_1 - P_1)^{1/2} e^{i(\delta_2 - \delta_1)} - 2L_1\}. \qquad \text{(A1.7)}$$

Using the above expressions for A_{ik}, b_{ik}, λ_{ik} and χ_{ik} we obtain, after some simple manipulations, the values of $C(Z, R_0, W)$ and $D(Z, R_0, W)$. In the case of RaE which is of interest here one must make the replacements $M_0 \to \overline{M}_1$, $L_0 \to \overline{L}_1$, $L_1 \to \overline{L}_2$, $N_0 \to \overline{N}_1$, $Q_0 \to -\overline{M}_{-1}$, $P_0 \to -\overline{L}_{-1}$ and $P_1 \to -\overline{L}_{-2}$.

*We take this opportunity to point out an error in reference 8 in the definition of a: the correct definition is a = m − it (and not a = m + it).

APPENDIX II

From the definitions of the functions $\overline{M}_1$, $\overline{L}_1$, and $\overline{L}_2$[7] it is easy to obtain the following expressions for the functions $\overline{M}_{-1}$, $\overline{L}_{-1}$, and $\overline{L}_{-2}$:

$$2\overline{M}_{-1} = (X_{-1}^2 + Y_1^2) M_1^{(S)} + (X_{-1}^2 - Y_1^2) M_1^{(L)},$$

$$2\overline{L}_{-1} = (X_1^2 + Y_{-1}^2) L_1^{(S)} + (X_1^2 - Y_{-1}^2) L_1^{(L)},$$

$$2\overline{L}_{-2} = (X_2^2 + Y_{-2}^2) L_2^{(S)} + (X_2^2 - Y_{-2}^2) L_2^{(L)}. \quad \text{(A2.1)}$$

We give below values of $\overline{M}_{-1}$, $\overline{L}_{-1}$, and $\overline{L}_{-2}$ obtained using the functions tabulated in reference 7.

Values of $\overline{M}_{-1}$, $\overline{L}_{-1}$, and $\overline{L}_{-2}$
($r_0 = 1.17 \times 10^{-13}$)

W	$\overline{M}_{-1}$	$\overline{L}_{-1}$	$\overline{L}_{-2}$
1.2	104.270	—0.52366	—0.02967
1.8	67.211	—0.34027	—0.07549
2.4	48.663	—0.24878	—0.12031
3.0	37.527	—0.19404	—0.16538

[1] R. R. Lewis, Phys. Rev. **108**, 904 (1957).

[2] Fujita, Yamada, Matumoto, and Nakamura, Phys. Rev. **108**, 1104 (1957).

[3] Alikhanov, Eliseev, and Lyubimov, J. Exptl. Theoret. Phys. (U.S.S.R.) **35**, 1061 (1958), Soviet Phys. JETP **8**, 740 (1959).

[4] M. Yamada, Progr. Theoret. Phys. (Japan) **10**, 252 (1953).

[5] G. E. Lee-Whiting, Phys. Rev. **97**, 463 (1955).

[6] E. A. Plassmann and L. M. Langer, Phys. Rev. **96**, 1593 (1954).

[7] Takebe, Nakamura, and Taketani, Progr. Theoret. Phys. (Japan) **14**, 317 (1955).

[8] Berestetsky, Joffe, Rudik and Ter-Martirosyan, Nuclear Phys. **5**, 464 (1958).

[9] E. J. Konopinski and G. E. Uhlenbeck, Phys. Rev. **60**, 308 (1941).

[10] A. M. Smith, Phys. Rev. **82**, 955 (1951).

[11] G. E. Lee-Whiting, Canad. J. Phys. **36**, 252 (1958).

[12] L. A. Sliv and B. A. Volchok, Таблицы кулоновских фаз и амплитуд с учетом конечных размеров ядра (Tables of Coulomb Phase Shifts and Amplitudes including Finite Nuclear Size Effects), M.-L., Acad. Sci. Press, 1956.

Translated by A. M. Bincer
87

DIRECT NEUTRON-EXCHANGE INTERACTION OF COMPLEX NUCLEI

V. I. GOL' DANSKIĬ

P. N. Lebedev Physics Institute, Academy of Sciences, U.S.S.R.

Submitted to JETP editor July 24, 1958

J. Exptl. Theoret. Phys. (U.S.S.R.) **36**, 526-528 (February, 1959)

It is shown that it should be possible to observe the process of direct interaction between complex nuclei, in which the nuclei exchange neutrons when located on the external boundary of the Coulomb potential barrier. For large values of neutron moments in the outer shells, this process may result in a large range of the spins of the interacting nuclei and in excitation of all levels, which practically would not be attainable in any other way. The exponent that characterizes the probability of the processes under consideration is estimated.

ACCELERATION of heavy ions makes timely at present the observation of a unique nuclear process, namely the direct (i.e., not involving compound nucleus) exchange of neutrons between complex nuclei. We cite two possible examples of such a process:

$$\underset{0^+}{{}_8O^{18}_{10}} + \underset{0^+}{{}_{10}Ne^{20}_{10}} \longrightarrow \underset{0,\,2,\,4^+}{{}_8O^{18*}_{10}} + \underset{0,\,2,\,4^+}{{}_{10}Ne^{20*}_{10}}$$

(neutron exchange in the $d_{5/2}$ shell)

$$\underset{0^+}{{}_{36}Kr^{84}_{48}} + \underset{0^+}{{}_{36}Kr^{84}_{48}} \longrightarrow \underset{0,\,2,\,4,\,6,\,8^+}{{}_{36}Kr^{84*}_{48}} + \underset{0,\,2,\,4,\,6,\,8^+}{{}_{36}Kr^{84*}_{48}}$$

(neutron exchange in the $g_{9/2}$ shell).

It is obvious that at large moments of the neutrons in the outer shells, such an exchange may lead to a very strong change in the spins of the interacting nuclei, i.e., to an excitation of levels which differ greatly from the ground state in the value of the moment, but which are relatively weakly excited ($\lesssim$ Mev). Since the excitation of such levels by any other means is of very low likelihood, it is not excluded that this process, in spite of its uniqueness, may be of interest also for the study of new, still unknown nuclear levels.

To estimate the probability of this process we can use the general method proposed by Landau[1] to describe transitions in quasi-classical system and applied by E. M. Lifshitz to interactions between deuterons and nuclei[2] and to neutron transfer from one complex nucleus to another.[3] We use Landau's method for the analysis of this case in complete analogy with the method used by Lifshitz, the only difference being that one must consider not one act of neutron transfer from nucleus 1 to nucleus 2, but two such acts (transfer one neutron from 1 to 2 and of another from 2 to 1), the aggregate of which comprises the neutron-exchange interaction.

We used in the calculations the same approximations as in reference 3, namely that the nuclei are considered concentrated in a point, the neutron mass m is assumed small compared with the nuclear masses ($m \ll M_i$, $i = 1, 2$), and the energy of the relative motion E_0 of the nuclei is sufficiently large ($E_0 \gg J_i m/M_i$, where J_1 and J_2 are the binding energies in nucleus 1 or 2). Without dwelling here on the intermediate derivations, we cite only the final result: the sought probability of direct neutron-exchange interaction is proportional to

$$\Phi = \exp\{-2\sqrt{2}\,Z_1Z_2e^2\sqrt{m}(\sqrt{J_1}+\sqrt{J_2})/\hbar E_0\}. \quad (1)$$

If the energy J_1' of the detachment of the neutron from nucleus 1, which is the first to join the additional neutron, is less than the energy J_1, or if an analogous relationship ($J_2' < J_2$) is satisfied for nucleus 2, then the most probable process is one in which the neutron first joins nucleon 1 or nucleon 2, and only then does this nucleus emit the neutron that goes into "exchange." Then the term $\sqrt{J_1} + \sqrt{J_2}$ in the final expression for Φ should be replaced by the smaller of the two sums, $\sqrt{J_1'} + \sqrt{J_2}$ or $\sqrt{J_1} + \sqrt{J_2'}$.

The relations obtained (like the omitted intermediate derivations) are quite analogous to those obtained by Lifshitz for the transfer of a neutron from one complex nucleus to another. The final result — the quantity Φ — differs in our case from that given in reference 3 only in the presence of two terms $\sqrt{J_i}$ instead of a single one, either $\sqrt{J_1}$ or $\sqrt{J_2}$. To test the applicability of these relations and to estimate the effective values of

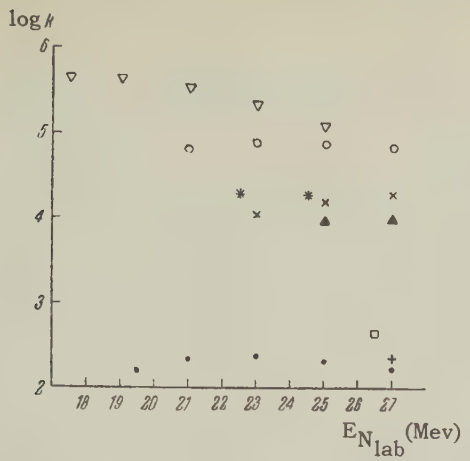

● — Be^9, + — C^{12}, □ — O^{16}, × — Na^{23}, ○ — Mg^{24}, ▽ — Mg^{25}, ▲ — Mg^{26}, * — Al^{27}

the factors in front of the exponents it is necessary to compare the formulas obtained in reference 3 with the large experimental material accumulated recently on the transfer of neutrons from N^{14} nuclei to various bombarded targets.[4-9] For N^{14} we have: $Z_1 = 7$, $J = 10.55$ Mev, $E_0 = \{(14/(14 + M_2)\} E_{N\ lab}$.

The experimental dependence[5-8] of the cross sections for the neutron transfer to various nuclei by the nitrogen nuclei on the energy of the nitrogen nuclei is illustrated in the diagram in the form of the logarithms of the factor in front of the exponent [$\text{Log } k = \log \sigma_{(mbn)} + \alpha/2.3\, E_{N\ lab}$] at various values of $E_{N\ lab}$. The diagram shows that, at least for six nuclei (Be^9, Na^{23}, Al^{27} and the three isotopes of Magnesium) the sum $\log \sigma + \alpha/2.3\, E_{N\ lab}$ is actually constant, thus confirming qualitatively the applicability of the discussed relationships.

Data on neutron transfer from N^{14} to B^{10} and N^{14} do not fit into the relation obtained in reference 3, since the cross sections of these reactions increase with energy rather slowly (α_{exp} is less than that cited above), and the values of $\log \sigma + \alpha/2.3\, E_{N\ lab}$ diminish with increasing energy of the nitrogen ions. However, even in these cases the discrepancy between the experimental data and the ordinary formula for the probability of penetrating through the Coulomb barrier is considerably greater.

The values of the factors in front of the exponents, obtainable from the diagram (0.2 to 0.4 barns for Be, C, and O and 10 to 100 barns for Na, Mg, and Al) are naturally too high, since in the derivation of these relations the nuclei were assumed to be concentrated in a point.

Without dwelling in greater detail on the role of the finite dimensions of the nuclei in the exact calculations, we point out only that the region in which the sharp increase in the cross section of neutron transfer by the N^{14} nuclei increases rapidly with energy is shown experimentally to extend to energies somewhat in excess of the usually employed Coulomb potential barrier. However, the exact contribution of the barrier factors to the foregoing effective values of the factors in front of the exponents is immaterial. All that is important is that the true values of the factors in front of the exponents are close in order of magnitude to those proposed for the direct neutron-exchange interaction. In the latter case we can expect only a relatively small reduction in the factor in front of the exponent for the production of each of the final states with different spins, owing to the large number of these possible states. A comparison of the geometrical cross sections with the cross sections of the neutron-transfer processes, together with a comparison of the values of Φ for neutron exchange and for neutron transfer, give therefore grounds for assuming that the direct neutron-exchange cross sections of complex nuclei may reach values on the order of $10^{-30} - 10^{-29}$ cm^2 near the limiting barrier energy and that such an interaction can be thus observed by recording the subsequent γ radiation (in particular, the coincidences between γ quanta from both final nuclei) and in some cases by detecting hitherto-unknown isomer transitions (relative to the long-lived low-energy E2 transitions).

The author expresses sincere gratitude to A. S. Kompaneets and E. M. Lifshitz for valuable advice.

[1] L. D. Landau, Sow. Phys. **1**, 88 (1932).

[2] E. M. Lifshitz, J. Exptl. Theoret. Phys. (U.S.S.R.) **8**, 930 (1938).

[3] E. M. Lifshitz, J. Exptl. Theoret. Phys. (U.S.S.R.) **9**, 1 (1939).

[4] K. F. Chackett and J. H. Fremlin, Phil. Mag. **45**, 735 (1954).

[5] H. Reynolds and A. Zucker, Phys. Rev. **101**, 166 (1956).

[6] Reynolds, Scott, and Zucker, Phys. Rev. **102**, 237 (1956).

[7] Webb, Reynolds, and Zucker, Phys. Rev. **102**, 749 (1956).

[8] Halbert, Handley, Pinajian, Webb, and Zucker, Phys. Rev. **106**, 251 (1957).

[9] Volkov, Pasyuk, and Flerov, J. Exptl. Theoret. Phys. (U.S.S.R.) **33**, 595 (1957), Soviet Phys. JETP **6**, 459 (1958).

Translated by J. G. Adashko
88

POLARIZATION OF BETA PARTICLES AND BETA-GAMMA CORRELATION FOR FIRST-FORBIDDEN TRANSITIONS OF ORIENTED NUCLEI

A. Z. DOLGINOV and N. P. POPOV

Leningrad Physical and Technological Institute, Academy of Sciences, U.S.S.R.

Submitted to JETP editor July 29, 1958

J. Exptl. Theoret. Phys. (U.S.S.R.) **36**, 529-538 (February, 1959)

Explicit formulas are obtained for the polarization of β particles and the β-γ correlation for first-forbidden transitions of oriented nuclei. All five types of β interaction are considered, and nonconservation of parity is taken into account. Effects of the Coulomb field of the extended nucleus are included. Unoriented nuclei are treated as a special case.

In an earlier paper by one of the writers[1] general formulas were obtained for the angular and polarization correlations of the particles from β decay transitions of any order of forbiddenness. Here we shall examine first-forbidden transitions in detail, and shall give for this case explicit formulas suitable for practical calculations. Since the method of the calculation has been described in reference 1, we shall present at once the final expressions for the correlations.

We take a right-handed system of coordinates with the z axis along the preferred direction of orientation of the nuclear spin $\mathbf{j}_0$. We introduce the notations: $\mathbf{p}(p, \vartheta, \varphi)$ is the momentum of the electron; $\mathbf{k}(k, \theta, \Phi)$ is the momentum of the γ quantum; I is the multipole order of the γ quantum; j_0, j_1, and j_2 are the angular momenta of the nuclear levels for the β-γ transition $j_0(\beta)\, j_1(\gamma)\, j_2$; μ_0, μ_1, and μ_2 are the z components of the angular momenta of the nuclear levels; and $\boldsymbol{\zeta}(1, \chi, \omega)$ is the polarization vector of the electron is the system of coordinates in which it is at rest. χ and ω are the polar angles of the vector $\boldsymbol{\zeta}$ in the right-handed system of coordinates formed by the vectors

$$z_p \| \mathbf{p},\ x_p \| \mathbf{p} \times \mathbf{j}_0,\ y_p \| [\mathbf{p} \times \mathbf{j}_0] \times \mathbf{p}. \tag{1}$$

The probability of finding the electron with the polarization $\boldsymbol{\zeta}$ and the momentum $\mathbf{p}$ from the first-forbidden β decay of the oriented nucleus is given by the formula:*

$$W(\mathbf{j}_0 \mathbf{p} \boldsymbol{\zeta}) = \sum_{g,\ L \leqslant L'} A^g_{LL'} h_g(\mathbf{j}_0)\, W(j_1 L' j_0 g; j_0 L), \tag{2}$$

$$h_g(\mathbf{j}_0) = \sum_{\mu_0} (-1)^{j_0 - \mu_0} C^{g0}_{j_0 \mu_0 j_0 - \mu_0}\, w(\mu_0), \tag{3}$$

$$A^g_{LL'} = z^g_{LL'} \sqrt{2g+1}\, P_g(\cos\vartheta) + (-1)^g \sum_m y^m_{LL'} f_m(x, \omega, \vartheta). \tag{4}$$

Here L and L′ = 0, 1, and 2; g = 0, 1, 2, 3, but with $g \leq 2j_0$; m = 0, 1, ... 9, with m = 0 for g = 0, m = 1, 2, 3 for g = 1, m = 4, 5, 6 for g = 2, and m = 7, 8, 9 for g = 3. Common factors have been omitted throughout. If the polarization of the electrons is not observed, we have

$$A^g_{LL'} = z^g_{LL'} \sqrt{2g+1}\, P_g(\cos\vartheta). \tag{5}$$

For aligned nuclei (obtained, for example, by the method of Bleaney[3] or Pound[4]) only even values of g are possible. For arbitrarily oriented nuclei (obtained, for example, by the Gorter-Rose method[5]) odd values of g are also possible. $C^{a\alpha}_{b\beta c}$ are Clebsch-Gordan coefficients,[6] W(abcd; ef) are Racah functions,[7] and $w(\mu_0)$ is the probability of a given value μ_0 for the angular-momentum component of the oriented nucleus. The values of $z^g_{LL'}$ and $y^m_{LL'}$ are given in Appendix 1. The values of $f_m(\chi, \omega, \vartheta)$ are given in Appendix 5, and $P_g(\cos\vartheta)$ is the Legendre polynomial. The values of $j_g(j_0) \equiv j_0^{-g} h_g(j_0)$ are given in reference 8.

The angular β-γ correlation for first-forbidden transitions in oriented nuclei has the form

$$W(\mathbf{j}_0, \mathbf{p}, \mathbf{k}) = \sum_{SJg} \sum_{L \leqslant L'} z^J_{LL'} U^{LL'}_{SgJ} h_g(\mathbf{j}_0)\, B_S F_{SgJ}(\mathbf{p}, \mathbf{k}), \tag{6}$$

$$U^{LL'}_{SgJ} = (-1)^{g+J} \sqrt{(2g+1)(2S+1)} \times X(j_1 j_1 S,\ j_0 j_0 g,\ L' L J), \tag{7}$$

*The expression $W(\mathbf{j}_0 \mathbf{p} \boldsymbol{\zeta})$ for the STP interactions and without inclusion of the effect of the finite dimensions of the nucleus has also been obtained by Berestetskii, Rudik, Ioffe, and Ter-Martirosyan.[2] We have learned that they have generalized their result, but have neglected in their calculations terms of the order $(pR)^2$ and v_{nuc}^2; these can however, have an important effect for certain values of the nuclear matrix elements.

$$B_S = \sqrt{(2j_1+1)(2I+1)}\,[1 - S(S+1)/2I(I+1)]$$

$$\times W(j_2 I j_1 S; j_1 I)\, C^{I0}_{I0S0}. \qquad (8)$$

Here L and L′ = 0, 1, 2; J = 0, 1, 2, 3; $0 \le g \le 2j_0$, with $|S-J| \le g \le S+J$. As before, only even values of g are possible for aligned nuclei. The quantities X(abc, def, ghi) are Fano functions; their properties and explicit form, together with a number of particular values, are given in reference 6. The $F_{SgJ}(\mathbf{p}, \mathbf{k})$ are given in Appendix 5.

If we are interested in the correlation between the direction of the β particle and the circular polarization of the subsequent γ quantum, we must insert in Eq. (6) or Eq. (14) instead of B_S the quantity

$$B_{SM} = \sqrt{(2I+1)(2j_1+1)}\, C^{IM}_{IMS0}\, W(j_2 I j_1 S; j_1 I), \qquad (9)$$

where M = 1 or −1, respectively, for right or left circular polarization of the γ quantum. In the particular case in which S = 1,

$$B_{1M} = M[j_1(j_1+1) - j_2(j_2+1)$$

$$+ I(I+1)]\,[2I(I+1)\sqrt{j_1(j_1+1)}]^{-1}. \qquad (10)$$

If the observed β-γ cascade has the form $j_0(\beta)\, j_1(\gamma_1)\, j_2(\gamma_2) \ldots j_{N-1}(\gamma)\, j_N$, and an experiment is made to study the angular distribution of the γ quantum of the $j_{N-1}(\gamma)\, j_N$ transition, then we must take j_{N-1} instead of j_1, j_N instead of j_2 in the expressions for B_S or B_{SM} and multiply these expressions by the product

$$\prod_{k=2}^{N-1} \sqrt{(2j_k+1)(2j_{k-1}+1)}\, W(j_k I_k S j_{k-1}; j_{k-1} j_k). \qquad (11)$$

If the γ transition is of mixed nature (for example, E2 and M1), then instead of B_S we must take the expression of Eq. (13) of reference 9.

If the nuclei are unoriented, g = 0, and the expression (2) determines the total polarization of the electrons. The degree of polarization can be characterized by the quantity

$$\langle\zeta\rangle = \frac{W(\chi=0) - W(\chi=\pi)}{W(\chi=0) + W(\chi=\pi)}\,\frac{\mathbf{p}}{p}. \qquad (12)$$

Using Eq. (2), we get

$$\langle\zeta\rangle = (\mathbf{p}/p) \sum_L' y^0_{LL} \Big/ \sum_L' z^0_{LL}. \qquad (13)$$

Setting g = 0 in Eq. (6), we get the expression for the β-γ correlation for unoriented nuclei:*

$$W(\mathbf{p}, \mathbf{k}) = \sum_{S=0,2}' \sum_{L \le L'}' (2S+1)\, z^S_{LL'}$$

$$\times W(j_0 j_1 L S; L' j_1)\, B_S P_S(\cos\vartheta_{pk}). \qquad (14)$$

In the case in which the nuclear charge $Z \gg 2A^{1/3}E$ the expression (2) can be considerably simplified:

$$W(\mathbf{j}_0, \mathbf{p}, \boldsymbol{\zeta}) = z^0_{00} + \sqrt{1/3}\, z^0_{11} + (y^0_{00} + \sqrt{1/3}\, y^0_{11}) \cos\chi$$
$$+ \{\sqrt{3}\,(z^1_{11}U - z^1_{01}) \cos\vartheta + 3[(y^1_{11} - \sqrt{2/5}\, y^3_{11})U$$
$$- (y^1_{01} - \sqrt{2/5}\, y^3_{01})] \cos\chi \cos\vartheta - 3[(y^1_{11} + \sqrt{1/10}\, y^3_{11})U$$
$$- (y^1_{01} + \sqrt{1/10}\, y^3_{01})] \sin\vartheta \sin\chi \cos\omega$$
$$- 3\sqrt{1/2}\,(y^2_{11}U - y^2_{01}) \sin\vartheta \sin\chi \sin\omega\}$$
$$\times [j_0(j_0+1)]^{-1/2} \sum_{\mu_0}' \mu_0 w(\mu_0),$$
$$\sqrt{2}\,U = [j_0(j_0+1) - j_1(j_1+1) + 2]$$
$$\times [2\sqrt{j_0(j_0+1)}]^{-1}. \qquad (15)$$

The values of $z^g_{LL'}$ and $y^m_{LL'}$ as used in Eq. (15) are as follows:

$$\sqrt{3}\, z^0_{11} = \varkappa^2 \xi^-_1 (b_{11} + 2b_{66} - 2\sqrt{2}\, b_{16}),$$
$$3\sqrt{3}\, z^1_{11} = \sqrt{6}\, y^0_{11} = \sqrt{2}\, \varkappa^3 \xi^0_3 (c_{11} + 2c_{66} + 2\sqrt{2}\, c_{16}),$$
$$27 y^1_{11} = \sqrt{2}\, \varkappa^2 [\xi^-_1] (b_{11} + 2b_{66} + 2\sqrt{2}\, b_{16}),$$
$$27 y^3_{11} = 4\sqrt{5}\, \varkappa^2 \lambda^-_1 (b_{11} + 2b_{66} + 2\sqrt{2}\, b_{16}),$$
$$9 y^2_{11} = -2\varkappa^3 \xi^0_3 (c_{11} + 2c_{66} + 2\sqrt{2}\, c_{16}),$$
$$3 z^1_{01} = 2\varkappa^3 \xi^0_3 (c_{12} + \sqrt{2}\, c_{26}),$$
$$9\sqrt{6}\, y^3_{01} = 8\sqrt{5}\, \varkappa^2 \lambda^-_1 (b_{12} + \sqrt{2}\, b_{26}),$$
$$9\sqrt{3}\, y^1_{01} = 2\varkappa^2 [\xi^-_1] (b_{12} + \sqrt{2}\, b_{26}),$$
$$3\sqrt{6}\, y^2_{01} = -4\varkappa^3 \xi^0_3 (c_{12} + \sqrt{2}\, c_{26}),$$
$$z^0_{00} = \varkappa^2 \xi^-_1 b_{22}, \quad y^0_{00} = \varkappa^3 \xi^0_3 c_{22}.$$

Here

$$\varkappa^2 \xi^-_1 b_{ii'} = (W-1)^2 (E+\gamma)\, \mathrm{Re}\, b^+_{ii'} + (W+1)^2 (E-\gamma)\, \mathrm{Re}\, b^-_{ii'},$$

$$\varkappa^2 [\xi^-_1]\, b_{ii'} = -3(W-1)^2 (E+\gamma)\, \mathrm{Re}\, b^+_{ii'}$$
$$+ (W+1)^2 (E-\gamma)\, \mathrm{Re}\, b^-_{ii'},$$
$$\varkappa^2 \lambda^-_1 b_{ii'} = (W+1)^2 (E-\gamma)\, \mathrm{Re}\, b^-_{ii'},$$
$$E\xi^0_3 c_{ii'} = p\, \mathrm{Re}\,(c^+_{ii'} + c^-_{ii'}) - \alpha Z\, \mathrm{Im}\,(c^-_{ii'} - c^+_{ii'}).$$

*$W(\mathbf{p}, \mathbf{k})$ agrees with Eq. (10) of reference 9 if we note that in the notations of reference 9 the quantities $z^S_{LL'}$ are $(2S+1)^{-1}(2L'+1)^{1/2} \sum_{i \le k}' [\mathrm{Re} M_{Li} M^*_{L'k}]\, C^{SLL'}_{ik}$. Unlike those of reference 9, our expressions $z^S_{LL'}$ are given for the β interaction of general type with parity nonconservation.

We get the values of $\kappa^2\epsilon_1^-b_{ii'}$ and $E\epsilon_3^0c_{ii'}$ from $\kappa^2\xi_1^-b_{ii'}$ and $E\xi_3^0c_{ii'}$ if in the latter we replace $\mathrm{Re}\, x_{ii'}^{\pm}$ by $\mathrm{Im}\, x_{ii'}^{\pm}$ and $\mathrm{Im}\, x_{ii'}^{\pm}$ by $-\mathrm{Re}\, x_{ii'}^{\pm}$. The values of $b_{ii'}$ and $c_{ii'}$ are given in Appendix 1. The forbiddenness of the β transition that comes from the smallness of pR is removed for large values of Z, since instead of p the integrand contains the quantity $\kappa = [(E + V)^2 - 1]^{1/2}$, and $\kappa \gg p$. Since $\kappa \approx V$, where V is the effective depth of the Coulomb well in the region of the nucleus, the dependence on the energy drops out, and the β transition becomes similar to an allowed one. A comparison of Eq. (15) with the formula for the polarization of the β particles from allowed transitions of oriented nuclei[1] shows that the character of the polarization is the same in the two cases (the nuclear matrix elements are of course different).

For $Z \gg 2A^{1/3}E$ the expression (6) also becomes simpler.

$$W(\mathbf{j}_0, \mathbf{p}, \mathbf{k}) = \sum_{S,g} \sqrt{2S+1}\,\{[(2j_0+1)^{-1} z_{00}^0 + \sqrt{1/3}\, W(Sj_0j_1 1;\ j_0 j_1) z_{11}^0]\, \delta_{Sg} P_S(\cos\theta) - (-1)^g \sqrt{2g+1}\,[z_{01}^1 W(j_0 S j_0 1;\ j_0 g)\sqrt{1/3,(2j_0+1)}\,(-1)^g + z_{11}^1 X(j_1 j_1 S, j_0 j_0 g,\ 111)]\, F_{Sg1}(\mathbf{p},\mathbf{k})\}\, h_g(j_0)\, B_S. \quad (16)$$

For the case of an even value of the quantity S + g + J the values of $z_{LL'}^J$ are the same as the corresponding values of $z_{LL'}^g$ in Eq. (16), and in the case of odd values they are obtained from them if we replace $\kappa^2\xi_1^-b_{ii'}$ by $\kappa^2\epsilon_1^-b_{ii'}$ and $E\xi_3^0c_{ii'}$ by $E\epsilon_3^0c_{ii'}$. In allowed transitions of unoriented nuclei there is no β-γ correlation. Thus it is to be expected that for $Z \gg 2A^{1/3}E$ the correlation will also be small for first-forbidden transitions. This result can be obtained directly from the explicit form of the $z_{LL'}^S$ appearing in Eq. (14). On the other hand, for β-γ transitions of oriented nuclei we must expect a large correlation in the case $Z \gg 2A^{1/3}E$, since there is such a correlation for allowed transitions. Comparison of Eq. (16) with the expression for the β-γ correlation in allowed transitions[1] shows that the character of the correlation is the same in the two cases.

For aligned nuclei with $Z \gg 2A^{1/3}E$ the correlation between the directions of $\mathbf{j}_0$, $\mathbf{p}$, and $\mathbf{k}$ can be large only if the invariance of the theory under time reversal is violated.

APPENDIX 1

Values of $z_{LL'}^g$ in Eqs. (4) and (5) and, for the case of even values of the quantity S + g + J, in Eqs. (6) and (14):

$$z_{00}^0 = \varkappa^2\varphi_1\xi_1^- b_{22} - 6\varkappa^2\varphi_2\xi_1^0 b_{23} + 9\varphi_0\xi_1^+ b_{33} - 2q\varkappa^2\varphi_2\xi_1^0 a_{22} + 6q\varphi_0\xi_1^+ a_{23} + q^2\varphi_0\rho_1^- b_{22},$$

$$\sqrt{3}\, z_{11}^0 = \varkappa^2\varphi_1[(\xi_1^- + 2\xi_2^-) b_{11} + (2\xi_1^- + \xi_2^-) b_{66} + 2\sqrt{2}(\xi_1^- - \xi_2^-) b_{16}] + 6\sqrt{3}\varkappa^2\varphi_2\xi_1^0(\sqrt{2} b_{46} + b_{14}) + 27\varphi_0\xi_1^+ b_{44} - 2q\varkappa^2\varphi_2\xi_1^0[a_{11} - 2a_{66} + 4\sqrt{2}(a_{61} - a_{16})] - 6\sqrt{3} q\varphi_0\xi_1^+(a_{14} - \sqrt{2} a_{46}) + 3q^2\varphi_0\rho_1^-(b_{11} + b_{66}),$$

$$\sqrt{15}\, z_{11}^2 = -\varkappa^2\varphi_1[2\xi_5^-(\sqrt{2} b_{11} - \sqrt{2} b_{66} + 2b_{16} - b_{61}) + \xi_2^-(\sqrt{2} b_{11} + \sqrt{1/2} b_{66} - 2b_{16})] - 6\sqrt{3}\varkappa^2\varphi_2\xi_5^0(\sqrt{2} b_{14} - b_{64}) + 2q\varkappa^2\varphi_2\rho_5^0(\sqrt{2} a_{11} + \sqrt{2} a_{66} - 2a_{16} - a_{61}),$$

$$z_{22}^0 = \sqrt{5}(\varkappa^2\varphi_1\xi_2^- + q^2\varphi_0\rho_1^-) b_{55}, \quad 2\sqrt{5}\, z_{22}^2 = -\sqrt{14}\,\varkappa^2\varphi_1\xi_2^- b_{55}$$

$$\sqrt{5}\, z_{02}^2 = -2\sqrt{2}\{\varkappa^2\varphi_1\xi_5^- b_{52} - 3\varkappa^2\varphi_2\xi_5^0 b_{53} - q\varkappa^2\varphi_2\rho_5^0 a_{52}\},$$

$$\sqrt{5}\, z_{12}^2 = -\sqrt{2}\{\varkappa^2\varphi_1[\xi_5^-(\sqrt{2} b_{51} + 2b_{56}) + \xi_2^-(b_{56} - \sqrt{2} b_{51})] + 3\sqrt{6}\varkappa^2\varphi_2\xi_5^0 b_{54} - q\varkappa^2\varphi_2\rho_5^0(\sqrt{2} a_{51} - 2a_{56})\},$$

$$3\sqrt{3}\, z_{11}^1 = \sqrt{2}\{\varkappa^3\varphi_1[\xi_3^0(c_{11} + 2c_{66} + 2\sqrt{2} c_{16}) + 2\xi_4^0(c_{66} - c_{11} - \sqrt{2} c_{16} + \sqrt{1/2} c_{61}) + \xi_6^0(c_{11} + 1/2\, c_{66} - \sqrt{2} c_{16})] + 6\sqrt{3}\varkappa\varphi_2[\xi_3^+(c_{14} + \sqrt{2} c_{64}) - \xi_4^+(c_{14} - \sqrt{1/2} c_{64})] + 27\varkappa\varphi_0\xi_3^0 c_{44} - 2q\varkappa\varphi_2[\rho_3^-(d_{11} - 2d_{66} - \sqrt{2} d_{16} + \sqrt{2} d_{61}) - \rho_4^-(d_{66} + d_{11} - \sqrt{2} d_{16} - \sqrt{1/2} d_{61})] - 6\sqrt{3} q\varkappa\varphi_0\xi_3^0(d_{14} - \sqrt{2} d_{64}) + 3q^2\varkappa\varphi_0\rho_3^0(1/2\, c_{66} - \sqrt{2} c_{16})\},$$

$$\sqrt{35}\, z_{22}^3 = -3\sqrt{2}\,\varkappa^3\varphi_1\xi_6^0 c_{55},$$

$$\sqrt{30}\, z_{22}^1 = (3\varkappa^3\varphi_1\xi_6^0 + 5q^2\varkappa\varphi_0\rho_3^0) c_{55},$$

$$3z_{01}^1 = 2\{\varkappa^3\varphi_1[\xi_3^0(c_{12} + \sqrt{2} c_{26}) + \xi_4^0(2c_{12} - \sqrt{2} c_{62})] + 3\varkappa\varphi_2[\xi_3^+(\sqrt{3} c_{24} - \sqrt{2} c_{63} - c_{13}) + \xi_4^+(\sqrt{2} c_{63} - 2c_{13})] - 2q\varkappa\varphi_2[\rho_3^-(d_{12} + \sqrt{1/2} d_{26} - \sqrt{1/2} d_{62}) + \rho_4^-(d_{12} - \sqrt{1/2} d_{62})] - 3q\varkappa\varphi_0\xi_3^0(\sqrt{3} d_{42} - d_{31} + \sqrt{2} d_{36}) - 9\sqrt{3}\varkappa\varphi_0\xi_3^0 c_{34} + q^2\varkappa\varphi_0\rho_3^0(c_{12} - \sqrt{2} c_{26})\},$$

$$3z_{12}^1 = -\sqrt{5}\{\varkappa^3\varphi_1\xi_4^0(2c_{51} + \sqrt{2} c_{56}) - 6\sqrt{3}\varkappa\varphi_2\xi_4^+ c_{54} - q\varkappa\varphi_2\rho_4^-(2d_{51} - \sqrt{2} d_{56}) + 2q^2\varkappa\varphi_0\rho_3^0(2c_{15} + \sqrt{2} c_{56})\},$$

$$\sqrt{35}\, z_{12}^3 = 6\varkappa^3\varphi_1\xi_6^0(c_{65} - \sqrt{2} c_{15}).$$

Values of $y_{LL'}^m$ in Eq. (4):

$$y_{00}^0 = \varkappa^3\varphi_1\xi_3^0 c_{22} - 6\varkappa\varphi_2\xi_3^+ c_{23} + 9\varkappa\varphi_0\xi_3^0 c_{33} - 2q\varkappa\varphi_2\rho_3^- d_{22} + 6q\varkappa\varphi_0\xi_3^0 d_{23} + q^2\varkappa\varphi_0\rho_3^0 c_{22},$$

$$9\sqrt{6}\, y_{01}^3 = 4\sqrt{5}\{\varkappa^2\varphi_1[2\xi_1^-(b_{12} + \sqrt{2} b_{26}) + \xi_5^-(b_{12} - \sqrt{1/2} b_{26})] + 3\varkappa^2\varphi_2[2\xi_1^0(\sqrt{3} b_{24} - \sqrt{2} b_{36} - b_{13}) + \xi_5^0(\sqrt{1/2} b_{36} - b_{13})] - q\varkappa^2\varphi_2[2\rho_1^0(a_{21} + a_{12} - \sqrt{2} a_{26} + \sqrt{2} a_{62}) + \rho_5^0(a_{12} - \sqrt{1/2} a_{62})] - 6q\varphi_0\xi_1^+(\sqrt{3} a_{24} - a_{13} + \sqrt{2} a_{63}) - 18\sqrt{3}\varphi_0\xi_1^+ b_{34} + 2q^2\varphi_0\rho_1^-(b_{12} - \sqrt{2} b_{26})\},$$

$$5\sqrt{5}\,y^4_{02} = 2\{\varkappa^3\varphi_1\xi^0_4 c_{52} - 3\varkappa\varphi_2\xi^+_4 c_{53} - q\varkappa\varphi_2\rho^-_4 d_{52}\},$$
$$-15\sqrt{14}\,y^4_{22} = 30\,y^5_{22} = 7\sqrt{7}\,z^3_{22},$$
$$27\,y^1_{11} = \sqrt{6}\,m^0_{11} - 2\sqrt{15}\,m^2_{11} - 3\sqrt{2}\,Q_1,$$
$$27\,y^3_{11} = 5\sqrt{6}\,n^2_{11} + 4\sqrt{15}\,n^0_{11} - 12\sqrt{5}\,P_1,$$
$$\sqrt{2}\,y^0_{11} = 3m^1_{11} - \sqrt{3}\,Q_3,$$
$$3y^2_{11} = -\sqrt{6}\,s^1_{11}, \quad 5\sqrt{10}\,y^4_{11} = 3t^1_{11}, \quad 5\sqrt{5}\,y^1_{11} = -3\sqrt{7}\,n^1_{11},$$
$$3y^7_{22} = -2s^3_{22}, \quad y^0_{22} = \sqrt{6}\,m^1_{22}, \quad 3\sqrt{2}\,y^1_{22} = -m^0_{22},$$
$$\sqrt{3}\,y^2_{22} = -\sqrt{2}\,s^1_{22}, \quad 3\sqrt{5}\,y^3_{22} = n^0_{22}, \quad 7y^8_{22} = -2\sqrt{5}\,m^2_{22},$$
$$49y^9_{22} = 24\sqrt{3}\,n^2_{22}, \quad \sqrt{6}\,y^2_{01} = -2s^1_{01}, \quad \sqrt{2}\,y^6_{02} = s^2_{02},$$
$$\sqrt{6}\,y^2_{12} = 2s^1_{12}, \quad \sqrt{2}\,y^6_{12} = s^2_{12}, \quad 3y^7_{12} = -2s^3_{12},$$
$$7\sqrt{35}\,y^8_{12} = 5\sqrt{2}\,t^2_{12}, \quad 9\sqrt{3}\,y^1_{12} = 5m^2_{12} - 2\sqrt{5}\,Q_2,$$
$$9\sqrt{6}\,y^3_{12} = 5(\sqrt{5}\,n^2_{12} - 8P_2), \quad 25\sqrt{2}\,y^4_{12} = 3n^1_{12} - {}^1\!/_3\sqrt{14}\,z^3_{12},$$
$$5y^5_{12} = {}^7\!/_3\sqrt{{}^1\!/_2}\,z^3_{12} + {}^6\!/_5\sqrt{7}\,m^1_{12}.$$

In the expressions for $z^g_{LL'}$ and $y^m_{LL'}$ the following notations are used: $\kappa^2 = W^2 - 1$, $W = E + V$, where E is the energy of the electron in units mc^2, including the rest energy ($\hbar = m = c = 1$). For the case of a surface distribution of charge $V = \alpha Z/R$, where R is the radius of the nucleus; for a uniform volume distribution $V = 3\alpha Z/2R$. The energy of the neutrino is denoted by q.

$$\xi^\pm_l x_{il'} \equiv (W \pm 1)(\beta^+_l \operatorname{Re} + \alpha^+_l \operatorname{Im})\, x^\pm_{il'}$$
$$+ (W \mp 1)(\beta^-_l \operatorname{Re} + \alpha^-_l \operatorname{Im})\, x^\mp_{il'},$$

$$\xi^0_l x_{il'} \equiv (\beta^+_l \operatorname{Re} + \alpha^+_l \operatorname{Im})\, x^+_{il'} + (\beta^-_l \operatorname{Re} + \alpha^-_l \operatorname{Im})\, x^-_{il'}.$$

The quantities $\beta^\pm_l$ and $\alpha^\pm_l$ are determined from the condition of smooth joining of the electron wave function at the surface of the nucleus. The explicit forms for these quantities are given in Appendix 3. The quantity $x_{ii'}$ is any one of the quantities $a_{ii'}$, $b_{ii'}$, $c_{ii'}$, or $d_{ii'}$.

For the STP or VA interactions $\rho^0_l = \xi^0_l$ and $\rho^\pm_l = \xi^\pm_l$. The meanings of $\rho^\pm_l x_{ii'}$ and $\rho^0_l x_{ii'}$ become the same as those of $\xi^\pm_l x_{ii'}$ and $\xi^0_l x_{ii'}$, respectively, if one replaces all the β^+_l by β^-_l, all the α^+_l by α^-_l, and vice versa. The expressions for $z^J_{LL'}$ for odd $S + g + J$ can be obtained if in the values of $z^g_{LL'}$ given above one replaces $\operatorname{Re} x^\pm_{ii'}$ by $\operatorname{Im} x^\pm_{ii'}$ and $\operatorname{Im} x^\pm_{ii'}$ by $-\operatorname{Re} x^\pm_{ii'}$. In calculating y^3_{01} one must replace β^+_5 and α^+_5 by $3\beta^+_5$ and $3\alpha^+_5$ and set $\beta^+_1 = \alpha^+_1 = 0$. In the calculation of y^4_{02} one must put $-5\beta^+_4$ and $-5\alpha^+_4$ instead of β^+_4 and α^+_4. We get y^1_{01} from y^3_{01} if we multiply β^-_5 and α^-_5, β^-_1 and α^-_1 by $-2({}^2\!/_5)^{1/2}$, $({}^2\!/_5)^{1/2}/4$, respectively, and set $\beta_1 = -3\beta^-_1$, $\alpha^+_1 = -3\alpha^-_1$, and $\beta^+_5 = \alpha^+_5 = 0$. We get y^5_{02} from y^4_{02} if we set $\beta^+_4 = \alpha^+_4 = 0$ and multiply β^-_4 and α^-_4 by $2(14)^{1/2}$. We get $m^g_{LL'}$, $n^g_{LL'}$, and $t^g_{LL'}$ in the corresponding $z^g_{LL'}$ we replace $\beta^\pm_l$ by $\gamma^\pm_l\beta^\pm_l$ and $\alpha^\pm_l$ by $\gamma^\pm_l\alpha^\pm_l$, using the values of $\gamma^\pm_l$ from the table. We get $s^g_{LL'}$ if in addition to this we replace $\operatorname{Re} x^\pm_{ii'}$ by $\operatorname{Im} x^\pm_{ii'}$ and $\operatorname{Im} x^\pm_{ii'}$ by $\operatorname{Re} x^\pm_{ii'}$.

Odd values of g

$\gamma^\pm_l$	m^1_{11}	s^1_{11}	n^1_{11}	t^1_{11}	m^1_{22}	s^1_{22}	s^1_{01}	n^1_{12}	m^1_{12}	s^1_{12}
$\gamma^\pm_3$	1	1	0	0	1	1	1	0	0	1
γ^+_4	0	−1/2	0	−5			−1/2	−5	0	1/2
γ^-_4	0	1/2	−2	1			1/2	1	1	−1/2
$\gamma^\pm_6$	2	2	1	2	5/3	2				

Even values of g

$\gamma^\pm_l$	m^0_{11}	m^2_{11}	n^2_{11}	n^0_{11}	m^0_{22}	m^2_{22}	n^0_{22}	n^2_{22}	s^2_{02}	m^2_{12}	n^2_{12}	s^2_{12}	t^2_{12}
γ^+_1	−3			0	1		0						
γ^-_1	1			1	−1/3		10/3						
γ^+_2	3/2	0	−3	0	−3/5	−1/7	3	1		−3/5	−6/5	0	1
γ^-_2	−5/2	0	1	0	1	1	−1	0		1	2/5	0	−7
γ^+_5		0	3/2						−1	0	3	−1	0
γ^-_5		1	1/2						1	−2	1	1	0

$$Q_1 = q^2\varphi_0[\rho_1^-](b_{11} + {}^1/_2 b_{66} + \sqrt{2}b_{16}),$$
$$Q_2 = q^2\varphi_0[\rho_1^-](b_{15} + \sqrt{{}^1/_2}b_{65}),$$
$$Q_3 = q^2\varkappa\varphi_0\rho_3^0(c_{11} + {}^1/_2 c_{66} + \sqrt{2}c_{16}).$$

We get $[\rho_1^-]$ if in the expressions for ρ_1^- we replace the quantities β_1^+ and α_1^+ by $-3\beta_1^+$ and $-3\alpha_1^+$. We get the values of P_1 and P_2 from Q_1 and Q_2 if we set $\beta_1^- = \alpha_1^- = 0$ and do not multiply β_1^+ and α_1^+ by -3. All the other $z^g_{LL'}$ and $y^m_{LL'}$ are zero. The quantities $x_{ii'}$ for the STP interaction have the form:

$$a^{\pm}_{ii'} = b^{\pm}_{ii'} = \eta_{ii'}K_iK_{i'}^*, \quad c^{\pm}_{ii'} = d^{\pm}_{ii'} = \eta'_{ii'}K_iK_{i'}^*,$$
$$\eta_{ii'} = C_iC_{i'}^* + C'_iC'^*_{i'}, \quad \eta'_{ii'} = C_iC'^*_{i'} + C'_iC_{i'}^*,$$
$$\eta_{11} = |C_S|^2 + |C'_S|^2, \quad \eta_{33} = |C_P|^2 + |C'_P|^2,$$
$$\eta_{13} = C_SC_P^* + C'_SC'^*_P.$$
$$\eta_{1k} = C_SC_T^* + C'_SC'^*_T, \quad \eta_{3k} = C_PC_T^* + C'_PC'^*_T \text{ for } k \neq 1, 3.$$
$$\eta_{kk'} = |C_T|^2 + |C'_T|^2 \text{ for } k, k' = 2, 4, 5, 6,$$
$$\eta_{ii'} = \eta^*_{i'i}.$$

The quantities C_S, C_T, C_P, C_V, and C_A are the constants for the scalar, tensor, pseudoscalar, vector, and axial-vector β interactions; C'_S, C'_T, and so on are the analogous constants for the terms that can be admitted only since there is parity nonconservation (i.e., the terms containing an additional factor $\gamma_5 = \gamma_1\gamma_2\gamma_3\gamma_4$, $\gamma_4 = -\beta$); the K_i are the nuclear matrix elements for the β interaction. Their explicit form is given in Appendix 2. For the VA interaction

$$b^{\pm}_{ii'} = -a^{\pm}_{ii'} = \zeta_{ii'}L_iL_{i'}^*, \quad d^{\pm}_{ii'} = -c^{\pm}_{ii'} = \zeta'_{ii'}L_iL_{i'}^*,$$
$$\zeta_{ii'} = C_iC_{i'}^* + C'_iC'^*_{i'}, \quad \zeta'_{ii'} = C_iC'^*_{i'} + C'_iC_{i'}^*,$$
$$\zeta_{11} = \zeta_{44} = \zeta_{14} = C_V{}^2 + C'_V{}^2,$$
$$\zeta_{kk'} = C_A{}^2 + C'_A{}^2 \text{ for } k, k' \neq 1, 4,$$
$$\zeta_{1k} = \zeta_{4k} = C_VC_A^* + C'_VC'^*_A \text{ for } k \neq 1, 4,$$
$$\zeta_{ii'} = \zeta^*_{i'i}.$$

The nuclear matrix elements L_i differ from the corresponding K_i by an additional matrix β in the integrand. The expressions for $x_{ii'}$ in the general case of STPVA interactions are given in Appendix 4. Equations (2) and (6) contain the imaginary part of $x_{ii'}$ because we have not assumed the invariance of the β interaction with respect to time reversal. If we make this assumption all terms containing $\mathrm{Im}\, x^{\pm}_{ii'}$ must be thrown out, and comparison with experiment becomes considerably simpler. To settle the question of the invariance of the theory with respect to time reversal it is better to study the β-γ correlation and the polarization of the β particles from allowed transitions of oriented nuclei,[1] since in that case the interpretation of experiments is simpler and more unambiguous.

The values of $z_{LL'}$ and $y_{LL'}$ given above are for the case of a surface distribution of the nuclear charge. If we assume a volume charge distribution, we must make the following replacements:

$$\varphi_0 \to \varphi_3, \quad \varphi_1\xi_1^- \to \varphi_4\xi_1^- - (3\alpha Z/5R)\,\xi_1^0 + (3\alpha Z/10\varkappa R)^2\,\xi_1^+,$$
$$\varphi_2\xi_1^0 \to \varphi_5\xi_1^0 - (3\alpha Z/10\varkappa^2 R)\,\xi_1^+, \quad \varphi_1\xi_2^- \to \varphi_6\xi_2^-,$$
$$\varphi_1\xi_5^- \to \varphi_7\xi_5^- - (3\alpha Z/10R)\,\xi_5^0, \quad \varphi_2\xi_5^0 \to \varphi_8\xi_5^0,$$
$$\varphi_1\xi_3^0 \to [\varphi_4 - 3\alpha ZW/5R\varkappa^2 + (3\alpha Z/10\varkappa R)^2]\xi_3^0,$$
$$\varphi_1\xi_4^0 \to \varphi_7\xi_4^0 - (3\alpha Z/10\varkappa^2 R)\,\xi_4^-, \quad \varphi_2\rho_5^0 \to \varphi_8\rho_5^0,$$
$$\varphi_2\xi_3^+ \to \varphi_5\xi_3^+ - (3\alpha Z/10R)\,\xi_3^0, \quad \varphi_1\xi_6^0 \to \varphi_6\xi_6^0,$$
$$\varphi_2\rho_3^- \to \varphi_5\rho_3^- - (3\alpha Z/10R)\,\rho_3^0, \quad \varphi_2\xi_4^+ \to \varphi_8\xi_4^+,$$
$$\varphi_2\rho_4^- \to \varphi_8\rho_4^-;$$
$$V = \alpha Z/R \to 3\alpha Z/2R.$$

The values of the φ_i are given in Appendix 3. Apart from terms of the order $(\alpha Z)^2/4$ one can set $\varphi_i = 1$.

To go over to the case of a point nucleus one must take the formulas for the surface charge distribution and set $V = 3\alpha Z/2R$.

APPENDIX 2

$$K_i = \sqrt{4\pi}\int \psi^*_{j_1\mu_1}\tau O_i\psi_{j_0\mu_0}d\mathbf{r}, \quad L_i = \sqrt{4\pi}\int \psi^*_{j_1\mu_1}\tau\beta O_i\psi_{j_0\mu_0}d\mathbf{r},$$
$$O_1 = C_1 r\beta Y_{1\lambda}, \quad O_2 = C_0 r\beta\,(\sigma\cdot\mathbf{Y}'_{00}),$$
$$O_3 = -iC_0\beta\gamma_5 Y_{00}, \quad O_4 = iC_1\beta\,(\boldsymbol{\alpha}\cdot\mathbf{Y}^{-1}_{1\lambda}),$$
$$O_5 = C_2 r\beta\,(\sigma\mathbf{Y}^{-1}_{2\lambda}), \quad O_6 = -C_1 r\beta\,(\sigma\cdot\mathbf{Y}^0_{1\lambda}),$$
$$C_L \equiv [C^{j_1\mu_1}_{L\lambda j_0\mu_0}]^{-1},$$
$$K_1 = \sqrt{3}\int\beta\mathbf{r}, \quad K_2 = \int\beta\,\sigma\cdot\mathbf{r}, \quad K_3 = -i\int\beta\gamma_5,$$
$$K_4 = \int i\beta\boldsymbol{\alpha}, \quad K_5 = \frac{\sqrt{3}}{2}\int B^{\beta}_{ij}, \quad K_6 = -\sqrt{\frac{3}{2}}\int\beta[\sigma\times\mathbf{r}],$$
$$L_1 = \sqrt{3}\int\mathbf{r}, \quad L_2 = \int\sigma\cdot\mathbf{r}, \text{ and so on.}$$

$\psi_{j_0\mu_0}$ and $\psi_{j_1\mu_1}$ are the wave functions of the initial and final states of the nucleus; τ is an operator that acts on the isotopic spin variables; β, γ_5, σ, and α are Dirac matrices; Y_{JM} is a vector spherical harmonic (cf. reference 1).

APPENDIX 3

$$\beta_1^{\pm} = a^2_{l_2\mp 1/2}[(W \pm 1)\varkappa]^{-1},$$
$$\beta_2^{\pm} = 9a^2_{l_2\pm 1/2}[(W \pm 1)\varkappa^3]^{-1},$$
$$\beta_3^{\pm} = a_{l_2 1/2}a_{l_2-1/2}\varkappa^{-2}\cos(\delta_{l_2\mp 1/2} - \delta_{l_2\pm 1/2}),$$
$$\beta_4^{\pm} = 3a_{l_2\mp 1/2}a_{l_2\mp 1/2}[(W \pm 1)\varkappa^2]^{-1}\cos(\delta_{l_2\mp 1/2} - \delta_{s_2|_2\mp 1/2}),$$
$$\beta_5^{\pm} = 3a_{l_2\mp 1/2}a_{l_2\pm 1/2}\varkappa^{-3}\cos(\delta_{l_2\mp 1/2} - \delta_{s_2\pm 1/2}),$$
$$\beta_6^{\pm} = 9a_{s_2 1/2}a_{l_2-1/2}\varkappa^{-4}\cos(\delta_{s_2|_2\pm 1/2} - \delta_{s_2|_2\mp 1/2}).$$

Here the $a_{j\lambda}$ are the coefficients for joining-on the electron wave function at the edge of the nucleus;

j is the total angular momentum and $l = j + \lambda$ the orbital angular momentum of the electron, $\lambda = \pm\frac{1}{2}$. Tables of the numerical values are given in the book of Sliv and Volchek.[10] The $\delta_{j\lambda}$ are the phase shifts of the electron wave function in the Coulomb field of the nucleus. Tables of the $\delta_{j\lambda}$ are also given in reference 10.

The quantities $\alpha_l^{\pm}$ differ from the corresponding $\beta_l^{\pm}$ only by the fact that they contain $\sin(\delta_{j\lambda} - \delta_{j'\lambda'})$ instead of $\cos(\delta_{j\lambda} - \delta_{j'\lambda'})$, and $\alpha_1^{\pm} = \alpha_2^{\pm} = 0$. Neglecting terms smaller than the order of $(\alpha Z)^2$, we can obtain simple expressions for $\beta_l^{\pm}$ and $\alpha_l^{\pm}$:

$$\beta_1^{\pm} = (E \pm \gamma)/(W \pm 1), \quad \beta_2^{\pm} = [p^2 + (\alpha ZE)^2]\varkappa^{-2}\beta_1^{\mp},$$

$$\beta_3^{\pm} = p^2/\varkappa\sqrt{p^2 + (\alpha Z)^2}, \quad \beta_4^{\pm} = \sqrt{p^2 + (\alpha ZE)^2}\varkappa^{-1}\beta_1^{\pm}\cos\omega_1^{\pm},$$

$$\beta_5^{\pm} = \sqrt{p^2 + (\alpha ZE)^2}p\varkappa^{-2}\cos\omega_2^{\pm},$$

$$\beta_6^{\pm} = 2p^2[p^2 + (\alpha ZE)^2]/\varkappa^3\sqrt{4p^2 + (\alpha Z)^2}, \quad \alpha_3^{\pm} = \pm\alpha Z\beta_3^{\pm}/p,$$

$$\alpha_4^{\pm} = \beta_4^{\pm}\tan\omega_1^{\pm}, \quad \alpha_5^{\pm} = \beta_5^{\pm}\tan\omega_2^{\pm}, \quad \alpha_6^{\pm} = \mp\frac{\alpha Z}{2p}\beta_6^{\pm},$$

$$\tan\omega_1^{+} = \left[\frac{3}{4}\frac{\alpha ZE}{p} - \frac{1}{4}\frac{\alpha Z}{p}\right]$$

$$\times\left[1 + \frac{3}{8}\left(\frac{\alpha Z}{p}\right)^2 - (\alpha Z)^2 + \frac{1}{8}\left(\frac{\alpha Z}{p}\right)^2 E - \left(\frac{\alpha ZE}{p}\right)^2\right]^{-1},$$

$$\tan\omega_2^{\mp} = \left[\frac{3}{4}\frac{\alpha ZE}{p} \mp \frac{3}{4}\frac{\alpha Z}{p}\right]$$

$$\left[1 - \frac{1}{8}\left(\frac{\alpha Z}{p}\right)^2 - (\alpha Z)^2 \mp \frac{3}{8}\left(\frac{\alpha Z}{p}\right)^2 E + \left(\frac{\alpha ZE}{p}\right)^2\right]^{-1},$$

$$\gamma = \sqrt{1 - (\alpha Z)^2}.$$

$$\varphi_0 = 1 - (\varkappa R)^2/5, \quad \varphi_1 = 1 - 3(\varkappa R)^2/25, \quad \varphi_2 = 1 - 4(\varkappa R)^2/25,$$

$$\varphi_3 = 1 - 11(\varkappa R)^2/75, \quad \varphi_4 = 1 - 2(\varkappa R)^2/35, \quad \varphi_5 = 1 - 7(\varkappa R)^2/75,$$

$$\varphi_6 = 1 - 3(\varkappa R)^2/35, \quad \varphi_7 = 1 - 12(\varkappa R)^2/175,$$

$$\varphi_8 = 1 - 4(\varkappa R)^2/35.$$

APPENDIX 4

For the STPVA interactions the quantities $a_{ii'}$, $b_{ii'}$, and so on have the forms:

$$a_{ii'}^{\pm} = (\eta_{ii'}K_iK_{i'}^* - \zeta_{ii'}L_iL_{i'}^*) \pm (\chi_{ii'}K_iL_{i'}^* - \chi_{i'i}^*L_iK_{i'}^*),$$
$$b_{ii'}^{\pm} = (\eta_{ii'}K_iK_{i'}^* + \zeta_{ii'}L_iL_{i'}^*) \pm (\chi_{ii'}K_iL_{i'}^* + \chi_{i'i}^*L_iK_{i'}^*),$$
$$c_{ii'}^{\pm} = (\eta'_{ii'}K_iK_{i'}^* - \zeta'_{ii'}L_iL_{i'}^*) \pm (\chi'_{ii'}K_iL_{i'}^* - \chi'^*_{i'i}L_iK_{i'}^*),$$
$$d_{ii'}^{\pm} = (\eta'_{ii'}K_iK_{i'}^* + \zeta'_{ii'}L_iL_{i'}^*) \pm (\chi'_{ii'}K_iL_{i'}^* + \chi'^*_{i'i}L_iK_{i'}^*).$$

The values of $\eta_{ii'}$, $\eta'_{ii'}$, $\zeta_{ii'}$, and $\zeta'_{ii'}$ are the same as in Appendix 1. For $\chi_{ii'}$ we get:

$$\chi_{11} = \chi_{14} = C_SC_V^* + C'_SC'^*_V; \quad \chi_{31} = \chi_{34} = C_PC_V^* + C'_PC'^*_V;$$
$$\chi_{k1} = \chi_{k4} = C_TC_V^* + C'_TC'^*_V, \quad k \neq 1, 3, \quad \chi_{ii'} \neq \chi_{i'i}^*;$$
$$\chi_{1k} = C_SC_A^* + C'_SC'^*_A, \quad \chi_{3k} = C_PC_A^* + C'_PC'^*_A, \quad k \neq 1, 4;$$
$$\chi_{kk'} = C_TC_A^* + C'_TC'^*_A, \quad k \neq 1, 3, k' \neq 1, 4.$$

If $\chi_{ii'} = C_iC_{i'}^* + C'_iC'^*_{i'}$, then $\chi'_{ii'} = C_iC'^*_{i'} + C'_iC_{i'}^*$.

APPENDIX 5

Values of $f_m(\chi, \omega, \vartheta)$ in (4) and $F_{SgJ}(p, k)$ in (6).

$$f_0 = \cos\chi, \quad f_1 = 3\{\cos\chi\cos\vartheta - \sin\chi\sin\vartheta\cos\omega\},$$

$$f_2 = 3\sqrt{1/2}\sin\chi\sin\vartheta\sin\omega,$$

$$f_3 = -3\sqrt{1/10}\{2\cos\chi\cos\vartheta + \sin\chi\sin\vartheta\cos\omega\},$$

$$f_4 = -\sqrt{5/2}\{\cos\chi(3\cos^2\vartheta - 1) - 3\sin\chi\sin\vartheta\cos\vartheta\cos\omega\},$$

$$f_5 = {}^3/_2\sqrt{5/7}\{\cos\chi(3\cos^2\vartheta - 1) + 2\sin\chi\sin\vartheta\cos\vartheta\cos\omega\},$$

$$f_6 = -3\sqrt{5/2}\sin\chi\sin\vartheta\cos\vartheta\sin\omega,$$

$$f_7 = {}^3/_4\sqrt{7}\sin\chi\sin\vartheta(5\cos^2\vartheta - 1)\sin\omega,$$

$$f_8 = {}^3/_2\sqrt{7/5}\{\cos\chi(5\cos^3\vartheta - 3\cos\vartheta)$$
$$- \sin\chi\sin\vartheta(5\cos^2\vartheta - 1)\cos\omega\},$$

$$f_9 = -{}^1/_4\sqrt{7/3}\{4\cos\chi(5\cos^3\vartheta - 3\cos\vartheta)$$
$$+ 3\sin\chi\sin\vartheta(5\cos^2\vartheta - 1)\cos\omega\},$$

$$F_{SgJ}(p, k) = 4\pi i^{\gamma}\sum C^{J\sigma}_{g_e S\sigma}Y_{S\sigma}(\theta\Phi)Y^*_{J\sigma}(\vartheta\varphi),$$

where $2\gamma = 1 - (-1)^{S+g+J}$.

Some particular values of $F_{SgJ}(p, k)$ can be expressed in terms of the values of $f_m(-\theta, \varphi - \Phi, \vartheta)$:

$$F_{110} = -f_0, \quad F_{101} = f_1,$$
$$F_{111} = -f_2, \quad F_{121} = f_3, \quad F_{112} = -f_4,$$
$$F_{132} = -f_5, \quad F_{122} = f_6, \quad F_{133} = -f_7, \quad F_{123} = f_8, \quad F_{143} = f_9.$$

[1] A. Z. Dolginov, J. Exptl. Theoret. Phys. (U.S.S.R.) **33**, 1363 (1956), Soviet Phys. JETP **6**, 1047 (1958). Nucl. Phys. **5**, 512 (1958).

[2] Berestetsky, Ioffe, Rudik, and Ter-Martirosyan, Nucl. Phys. **5**, 464 (1958).

[3] B. Bleaney, Proc. Phys. Soc. **A64**, 315 (1951).

[4] R. V. Pound, Phys. Rev. **76**, 1410 (1949).

[5] Simon, Rose, and Jauch, Phys. Rev. **84**, 1155 (1951).

[6] E. Condon and G. Shortley, The Theory of Atomic Spectra (Macmillan, N. Y. 1935). H. Matsunobu and H. Takebe, Prog. Theor. Phys. **14**, 589 (1955).

[7] L. C. Biedenharn and M. E. Rose, Revs. Modern Phys. **25**, 729 (1953). H. Jahn, Proc. Roy. Soc. **205**, 192 (1951).

[8] J. A. M. Cox and H. A. Tolhoek, Physica **19**, 673 (1953).

[9] A. Z. Dolginov and I. N. Toptigin, Nucl. Phys. **2**, 147 (1956/57).

[10] L. A. Sliv and B. A. Volchek, Таблицы кулоновских фаз и амплитуд с учетом конечных размеров ядра (Tables of Coulomb Phases and Amplitudes, Including Effects of the Finite Dimensions of the Nucleus), AN SSSR Press 1956.

Translated by W. H. Furry
89

INVESTIGATION OF THE AVERAGE NUCLEAR POTENTIAL PARAMETERS

L. A. SLIV and B. A. VOLCHOK

Leningrad Physico-Technical Institute, Academy of Sciences, U.S.S.R.

Submitted to JETP editor July 29, 1958

J. Exptl. Theoret. Phys. (U.S.S.R.) **36**, 539-553 (February, 1959)

The parameters of the average nuclear potential have been found on the basis of data on the levels of nuclei with doubly-closed shells plus or minus one nucleon. It is shown that the potential parameters are the same for all nuclei lying on the nuclear stability curve. A formula has been derived for the depth of the potential for prescribed values of N and Z. An expansion of the nucleon functions in terms of spherical oscillator functions is considered.

THE wealth of experimental data leaves no doubt that there exists in the nucleus a self-consistent field that determines the approximately independent motion of the nucleons and the formation of nuclear shells. So far it has not been possible to derive the self-consistent field from the nucleon interactions. One is, therefore, limited to finding an average field close to the self-consistent field on the basis of the known experimental information.

A detailed knowledge of the form of the potential of this field is not very important for obtaining qualitative results. For example, to determine the level ordering, one may use an oscillator or square-well potential with the right choice of parameters. However, the correct level spacing cannot be obtained in this way.

On the other hand, it is known that the differential cross sections for the scattering of nucleons from nuclei agree with experiment only if the diffuseness of the potential at the boundary is taken into account.[1] The proton distribution in the nucleus has, according to the scattering experiments with fast electrons, a diffuse boundary, and so does the corresponding potential.[2] The analytic form of this potential, as proposed by Woods and Saxon,[3] is

$$V(r) = V_0 / (1 + e^{\alpha (r - r_0)}), \qquad (1)$$

where $r_0 = R_0 A^{1/3} \times 10^{-13}$ cm is the nuclear radius; α is a parameter determining the diffuseness of the nuclear boundary (in units of 10^{13} cm^{-1}); V_0 is the depth of the potential at the center of the nucleus. To the potential (1) one must add a spin-orbit term of the form

$$-\lambda \left(\frac{\hbar}{2Mc}\right)^2 \frac{1}{r} \frac{\partial V(r)}{\partial r} (\mathbf{l} \cdot \mathbf{s}), \qquad (2)$$

where λ indicates the relative strengths of the nuclear spin-orbit interaction and the relativistic Thomas term. The potential, then, contains four parameters: α, λ, V_0, and R_0, which must be determined from the experimental data.

There already exists a series of papers devoted to the determination of the potential parameters from an analysis of various experiments.[4] It is, however, difficult to make the obtained parameter values agree with each other, since the dispersion of the results is so bad that it is even impossible to detect any regularity in it. In this connection, principal doubts have been raised as to the existence of a common potential for all nuclei or even for one and the same nucleus in different reactions.

We made the attempt to determine the average potential parameters for a number of nuclei distributed over the entire periodic system. If the parameters are subject to any variations, we give the physical reasons for these changes.

The determination of the parameters is based on the data on the ground and excited levels of nuclei. The lower levels are useful for our purposes, as their energies and spins are now known with good accuracy. We restrict ourselves to nuclei with doubly closed shells plus or minus one nucleon. In this way we are certain that the levels contain only one particle and that their energies are not altered by interactions between nucleons in unfilled shells nor by interactions with the core. To be sure, a nucleus with one odd nucleon will be weakly polarized; but this polarization will be so small that its effect on the position of the levels will not exceed 100 kev. It must also be kept in mind that the levels may deviate from their single particle position by a large measure for excitations of more than 2 Mev. We regard the excited states as real excitations of the last odd nucleon in the potential of type (1).

METHOD OF CALCULATION

The equation of motion for a neutron (or a "hole") in the potential $V(r)$ with spin-orbit coupling has the form

$$\left[\frac{\hat{p}^2}{2M} + V(r) - \lambda\left(\frac{\hbar}{2Mc}\right)^2 \frac{\mathbf{l}\cdot\mathbf{s}}{r}\frac{\partial V(r)}{\partial r}\right]\psi = E\psi. \qquad (3)$$

In the case of a proton the additional Coulomb term

$$V_c = \begin{cases} [3/2 - 1/2\,(r/r_0)^2]\,(Z-1)\,e^2/r_0 & \text{for } r \leqslant r_0, \\ (Z-1)\,e^2/r & \text{for } r \geqslant r_0. \end{cases} \qquad (4)$$

must be introduced. This choice of V_C is not entirely correct, since the charge radius is always smaller than the range of the nuclear forces. Furthermore, the proton density is not necessarily constant over the nucleus, but may fall off towards the center and may certainly have a diffuse boundary. The main effect of such refinements, which we shall not consider, would be a change in the depth of the proton potential by a few percent.

Among the four parameters to be determined, the radius R_0 is to be singled out as a constant. The linear substitution $R_0 \to R_0'$ has the following effect on Eq. (3) for neutrons: the equation remains invariant under the substitution

$$\alpha R_0 = \alpha' R_0', \quad (V_0 + E)\,R_0^2 = (V_0' + E')\,R_0'^2, \quad \lambda V_0 = \lambda' V_0, \qquad (5)$$

For the eigenvalue E_i we have the following relation:

$$E_i(\alpha, \lambda, V_0, R_0) = E_i^{\exp}, \qquad (5a)$$

where $E_i^{\exp}$ is the experimental energy of the level.

The hypersurface (5a) is different for different levels of the same nucleus. The optimal parameters for all levels of a given element must be chosen such as to correspond to the point of intersection of all the hypersurfaces, if such exists. In the region under consideration, $1.2 \leq R_0 \leq 1.4$, these surfaces can be significantly different only if $|E_i/V_0| \sim 1$. In our case $|E_i/V_0| \ll 1$, so that the surfaces (5a) coincide within the limits of accuracy, and all R_0 are equivalent. Thus, for Pb^{207}, the parameter R_0 is varied along with the others, and a preference for any value of R_0 is impossible in the light of the foregoing considerations.

The most consistent way to obtain R_0 would be the following: from Eq. (3) with the potential (1) we could determine all the nucleon wave functions in the given nucleus; we then could calculate the density distribution of the nucleons, and determine R_0 by comparing the latter with experiment. Since we only calculated the wave function for one nucleon, we had to choose a different method. As usual, we assumed that $R_0 = 1.3$.*

The determination of the energy levels of the excited states of the nucleon in a given potential reduces mathematically to finding the eigenvalues of the second order differential equation

$$-\frac{\hbar^2}{2M}\frac{1}{r^2}\frac{d}{dr}\left[r^2\frac{dR(r)}{dr}\right] + \left[V + V_c - E + \frac{\hbar^2}{2M}\frac{l(l+1)}{r^2} - \lambda\frac{\hbar^2}{4M^2c^2}\frac{\mathbf{l}\cdot\mathbf{s}}{r}\frac{dV}{dr}\right]R(r) = 0, \qquad (6)$$

where $R(r)$ is the radial part of the wave function.

For neutrons with $l = 0$, Eq. (6) reduces to the hypergeometric equation. The eigenvalues E are determined by a certain transcendental equation. In the general case it is not possible to express the solutions to (6) through special functions. The eigenfunctions and eigenvalues must then be found by numerical integration.

We chose the Runge-Kutta method for our calculations.[5] We used this method for the integration in the whole interval, except at $r \to 0$, where the potential is singular. Ordinary power expansions were used for the integration in the region $r \approx 0$. The eigenvalues were found in the following order. For a tentative energy value E the corresponding wave function was determined. If the function had k zeros in the interval $(0 \div +\infty)$, after which it grew beyond all limits, then $E_k < E < E_{k+1}$. Changing E gradually, we found the interval in which E lies. The error in E did not exceed 0.03 Mev. The eigenfunctions were, at each point, determined with a relative accuracy $\epsilon \leq 10^{-5}$; they were computed up to values of r at which $|R(r)| \leq 5 \times 10^{-3}$ of the last extremum.

By varying the potential parameters α, λ, and V_0 we obtained a series of eigenvalues for each level with given n, l. If three or more levels are known in the nucleus under consideration, it is possible to find the optimal values for all three parameters, for which the eigenvalues give the best agreement with the experimental data. The calculations showed that the level energy E_{nl} depends linearly on λ and V_0 with good accuracy. We therefore list, in Table I, only the values of the derivatives $\partial E/\partial\lambda$, $\partial E/\partial V_0$ for each nucleus. To determine the dependence of E_{nl} on α, we had to compute a sufficient number of points for the construction of the diagram (see, for example, Fig. 2). As a result of the interpolations, the accuracy of the calculations of the levels dropped to 0.1 and possibly 0.2 Mev for the levels with large

*If necessary, one can always convert the neutron levels to a different R_0 by making use of the relations (5).

TABLE I. Determination of the potential parameters from the experimental data on the energy levels*

$_{82}Pb^{207}_{125}$

$\varkappa$	1.05	1.15	1.4	1.15				
λ	39	39	39	28	Δ	E_b	$\frac{\partial E}{\partial V_0}$	$\frac{\partial E}{\partial \lambda}$
V_0, Mev	41.8	41.8	41.8	41.8				
$3p^{1}/_{2}$	—6.8	—6.8	—6.8	—7.0	—0.2	—6.8	—0.62	0.02
$2f^{5}/_{2}$	—7.0	—7.1	—7.4	—7.5	—0.1	—7.42	—0.66	0.04
$3p^{3}/_{2}$	—7.75	—7.75	—7.80	—7.6	0.2	—7.75	—0.66	—0.01
$1i^{13}/_{2}$	—6.9	—7.3	—8.4	—6.5	1.9	—8.41	—0.75	—0.07
$2f^{7}/_{2}$	—9.4	—9.6	—9.9	—9.3	—0.2	—9.13	—0.75	—0.025

$_{8}O^{15}_{7}$

$\varkappa$	1.00	1.15	1.25	1.15				
λ	44	47	47	33	Δ	E_b	$\frac{\partial E}{\partial V_0}$	$\frac{\partial E}{\partial \lambda}$
V_0, Mev	54.1	54.1	54.1	54.1				
$1p^{1}/_{2}$	—13.3	—13.3	—13.4	—13.3	—1.00	—13.3	—0.52	0.075
$1d^{5}/_{2}$	—8.0	— 8.0	— 7.9	—7.00	0.9	— 8.03	—0.44	—0.06
$1p^{3}/_{2}$	—18.8	—19.4	—19.7	—19.0	0.4	—19.44	—0.58	—0.038

$_{7}N^{15}_{8}$

α	1.00	1.125	1.25	1.15				
λ	41	42	47	34	Δ	E_b	$\frac{\partial E}{\partial V_0}$	$\frac{\partial E}{\partial \lambda}$
V_0, Mev	53.6	53.6	53.6	53.6				
$1p^{1}/_{2}$	—10.2	—10.2	—10.2	—10.9	—0.7	—10.2	—0.50	0.075
$1d^{5}/_{2}$	—5.05	— 4.9	— 4.9	— 4.4	0.5	— 4.9	—0.42	—0.055
$1p^{3}/_{2}$	—15.8	—16.2	—16.5	—16	0.6	—16.53	—0.60	—0.038

$_{82}Pb^{209}_{127}$

α	1.05	1.15	1.4			
λ	28	28	28	E_b	$\frac{\partial E}{\partial V_0}$	$\frac{\partial E}{\partial \lambda}$
V_0, Mev	42.6	42.6	42.6			
$2g^{9}/_{2}$	—3.8	—3.9	—4.1	—3.87	—0.66	—0,031
$2i^{11}/_{2}$	—2.7	—3.1	—4.2	—3.12	—0.66	0,075
$3d^{5}/_{2}$	—2.7	—2.5	—2.2	—2.31	—0.53	—0.011
$2g^{7}/_{2}$	—1.7	—1.6	—1.4	—1.85	—0.53	0.042
$3d^{3}/_{2}$	—1.6	—1.5	—1.2	—1.33	—0.46	0.015

*The first three columns give the values of the level energies and the corresponding parameters. The fourth column for the elements Pb^{207}, O^{15}, and N^{15} gives the level energies computed with parameter values α and λ, which are optimal for Pb^{209}, O^{17}, and F^{17}, respectively. The fifth column gives the difference, Δ, between these energies and the experimental values. The last three columns give E_b, the binding energy of the level, and $\partial E/\partial\lambda$ and $\partial E/\partial V_0$, the partial derivatives of the energy with respect to the parameters λ and V_0. The experimental decay schemes are shown in Fig. 1.

TABLE I (continued)

$_{20}Ca^{41}_{21}$

α	1.05	1.15	1.23	E_b	$\frac{\partial E}{\partial V_0}$	$\frac{\partial E}{\partial \lambda}$
λ	34	27	20			
V_0, Mev	49.3	49.6	50.0			
$1f_{7/2}$	—8.5	—8.5	—8.5	—8.4	—0.62	—0.08
$2p_{3/2}$	—6.5	—6.5	—6.5	—6.45	—0.48	—0.016
$2p_{1/2}$	—4.3	—4.5	—4.7		—0.39	0.028

$_{39}Y^{89}_{50}$

α	1.125	1.25	1.40	E_b	$\frac{\partial E}{\partial V_0}$	$\frac{\partial E}{\partial \lambda}$
λ	43	40	38			
V_0, Mev	54.5	53.9	53.2			
$2p_{1/2}$	—7.3	—7.3	—7.3	—7.3	—0.70	0.033
$1g_{9/2}$	—6.4	—6.4	—6.4	—6.39	—0.75	—0.09
$2p_{3/2}$	—9.7	—9.5	—9.4	—8.83	—0.75	—0.017

$_{21}Sc^{49}_{28}$

α	1.05	1.15	1.25	E_b	$\frac{\partial E}{\partial V_0}$	$\frac{\partial E}{\partial \lambda}$
λ	36	28	21			
V_0, Mev	56.4	56.6	56.8			
$1f_{7/2}$	—9.5	—9.5	—9.5	—9.5	—0.68	—0.09
$2p_{3/2}$	—6.4	—6.4	—6.4	—6.43	—0.58	—0.023
$1f_{5/2}$	—1.9	—3.4	—4.7		—0.58	0.13

$_{83}Bi^{209}_{126}$

α	1.0	1.15	1.25	E_b	$\frac{\partial E}{\partial V_0}$	$\frac{\partial E}{\partial \lambda}$
λ	18,5	25	28			
V_0, Mev	57.8	56.9	56.4			
$1h_{9/2}$	—3.72	—3.72	—3.72	—3.72	—0.77	0,075
$2f_{7/2}$	—2.81	—2.81	—2.81	—2.82	—0.77	—0,035

$_{8}O^{17}_{9}$

α	1.00	1.125	1.25	E_b	$\frac{\partial E}{\partial V_0}$	$\frac{\partial E}{\partial \lambda}$
λ	45	35	26			
V_0, Mev	43.0	44.2	45.9			
$1d_{5/2}$	—4.14	—4.14	—4.14	—4.14	—0,46	—0.0625
$2s_{1/2}$	—3.27	—3.27	—3.27	—3.27	—0.36	0

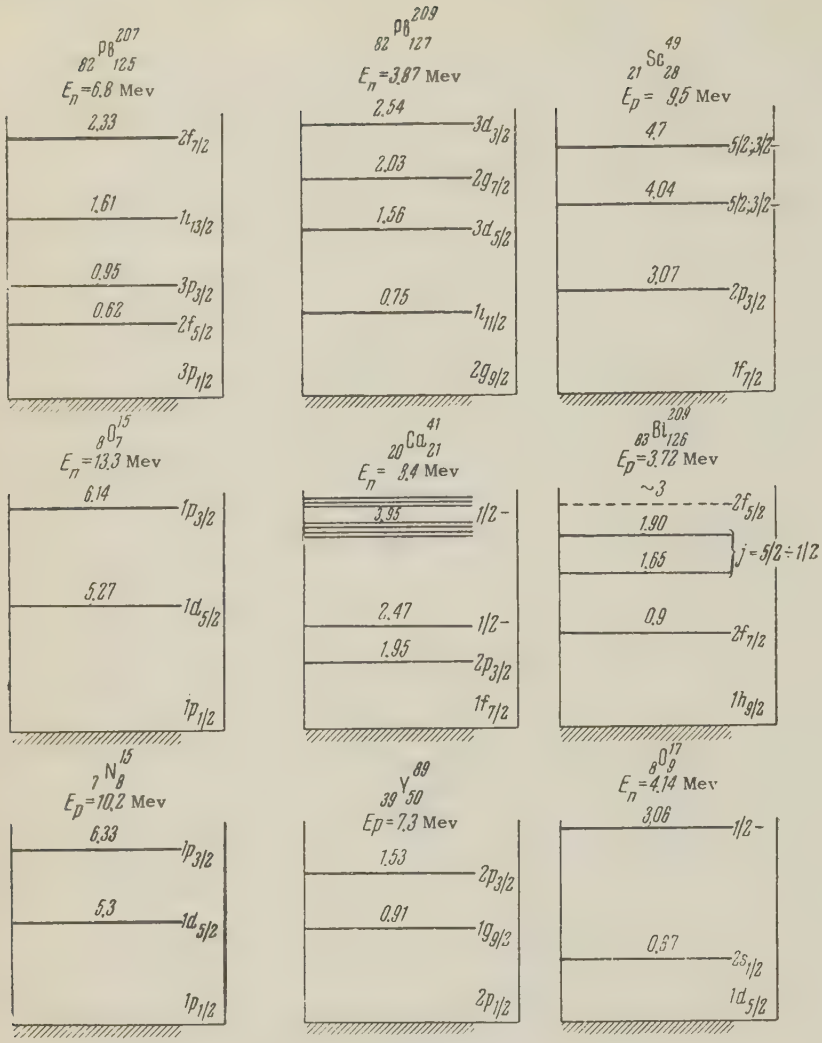

FIG. 1. Nuclear Decay Schemes (cf. Table I).

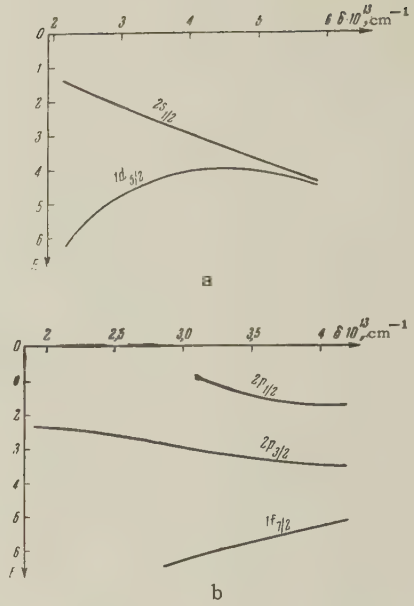

FIG. 2. Dependence of the level energy on the surface thickness $\delta = (2/\alpha)\ln g/\alpha$. (a) Levels of O^{17}: $2s_{1/2}$ and $1d_{5/2}$, (b) levels of Ca^{41}: $1f_{7/2}$, $2p_{3/2}$, $2p_{1/2}$. V_0 = 42.8 Mev, λ = 42, R_0 = 1.3.

l. We therefore determined the optimal choice of potential parameters for each nucleus separately.

RESULTS OF THE CALCULATIONS

$_{82}Pb^{209}_{127}$. The spectrum of Pb^{209} may serve as an example for a single particle neutron excitation. The levels of Pb^{209} were investigated in the reaction (d, p).[6] The level ordering found is in agreement with the shell model. The magnitude of the spin-orbit splitting conforms to the semi-empirical formula of Leventov.[7] Five levels were computed. The final results are listed in Table I. The best agreement with the experimental data is obtained for α = 1.15, λ = 28, V_0 = 42.6 Mev. The deviation of the last level by 0.3 Mev may prove to be fictitious, as the position of this level is not known exactly. Even if the level energy is confirmed, one should keep in mind that possible deviations from the single particle character of the excitation may show up more strongly for such a high level.

$_{82}Pb^{207}_{125}$. The spectrum of Pb^{207} (reference 6) may serve as an example for a neutron "hole" excitation. The excited levels are the result of the transition of a neutron from a filled lower level to the ground level, which earlier contained one neutron. The energy of such an excited state will be given by the energy difference between the ground state and the lower level from which the neutron made its transition. With the experimental energies and spins of the excited and ground states it is possible to determine the energies and spins of the filled states. We must, however, assume that the binding energies of nucleon pairs is the same for all levels. Below we shall return to the question of a possible discrepancy in the pair energy and make estimates for it. The three best choices for the parameters are listed in Table I. For the first and second choice the level $1\,i_{13/2}$ should lie considerably higher. For the third set of parameters the first four levels agree well with experiment; only the last level, $2\,f_{7/2}$, lies below

the experimental value by 0.8 Mev. As in the case of Pb^{209}, the discrepancy in the last level may be explained by a deviation from the single particle state.

$_{20}Ca^{41}_{21}$. In contrast to the other nuclei with a single nucleon above the closed shells, Ca^{41} has a large group of levels following after the first excited level $2\,p_{3/2}$ (references 8, 9). The spins and measured capture cross sections of these levels indicate that they cannot be single particle levels, with the exception, perhaps, of the level $E = 3.95$ Mev, which may be identified with the $2\,p_{1/2}$ level. Using these three levels for the determination of the parameters, we obtain $\alpha = 1.15$, $\lambda = 27$, and $V_0 = 49.6$ (see Table I). If the level $E = 2.47$ Mev is taken to be the $2\,p_{1/2}$ state, we obtain the absurd value $\lambda \sim 5$. The value of V_0 for Ca^{41} is remarkably high: it is larger than in the Pb^{209} case by 7 Mev. For an explanation we consider the levels of Ca^{49}. Since 28 neutrons also form a shell (which, however, is less tight than the 20-neutron shell), one may expect that the levels of Ca^{49} are single particle levels. Two levels of Ca^{49} are known: the ground level with the neutron binding energy ~ 5 Mev and an excited level 2 Mev above the former. Using these data and setting $\alpha = 1.15$, we obtain for the two other parameters the values $V_0 = 43.4$ Mev and $\lambda = 22$. Since the number of neutrons per proton is higher in Ca^{49} than in Ca^{41}, there is reason for the assumption that the depth of the neutron potential depends on the relative number of protons in the nucleus.

$_{8}O^{17}_{9}$. The nucleus O^{17} has only two single particle levels, $1\,d_{5/2}$ and $2\,s_{1/2}$. The third level $(-\frac{1}{2})$ cannot be a single particle level, even if it would correspond to a hole. From the two levels we find $V_0 = 44.5$ and $\lambda = 33$, with α chosen to be $\alpha = 1.15$.

$_{8}O^{15}_{7}$. The first three levels were used for the determination of the parameters. The levels were identified on the basis of references 8 and 9. We found $\alpha = 1.15$, $\lambda = 47$, and $V_0 = 54.1$ Mev.

We now turn to the analysis of the single particle proton levels.

$_{83}Bi^{209}_{126}$ (see Table I). The first two levels are $1\,h_{9/2}$ and $2\,f_{7/2}$. The spins and the parities of the following levels are not exactly known. Therefore only the first two levels were used for the determination of the potential parameters. Taking $\alpha = 1.15$, we found $\lambda = 25$, $V_0 = 56.9$. A larger value for V_0 results if the Coulomb potential is taken into account, which has a height of about 15 Mev for Bi^{209}. With the above-mentioned parameters the energy of the level $2\,f_{5/2}$ can be computed; it is found to be 3 Mev (the levels $E = 1.65$ and $E = 1.9$ Mev should rather correspond to $1\,i_{13/2}$ and $3\,p_{3/2}$). It is very important to obtain more detailed information on the levels of Bi^{209}, before any conclusive statements can be made about the potential or even the single particle character of the levels themselves. We recall that the quadrupole moment, which is twice as large as in the single particle case, can be consistently explained by the weak polarization of the core. The anomalous magnetic moment can, however, not be interpreted in this fashion, which casts some doubt on the pure single particle character of even the ground level.

$_{81}Tl^{207}_{126}$. The ground level is $3\,s_{1/2}$, the excited level, representing a hole, is $2\,d_{3/2}$. The binding energy has not been measured exactly. The optimal parameters, for $\alpha = 1.375$, are $\lambda = 38$ and $V_0 = 55.8$ Mev.

$_{21}Sc^{49}_{28}$. As in the case of Ca^{49}, we may assume that the 28 neutrons form a closed shell and that the levels of Sc^{49} are possibly single particle levels. The first two levels are known to be $1\,f_{7/2}$ and $2\,p_{3/2}$. The spins of the other two levels are not known exactly. From the two levels we obtained the parameters $V_0 = 56.6$ and $\lambda = 29$. The third level, $1\,f_{5/2}$, will then have the binding energy $E_b = 4.7$ Mev, which almost coincides with the excited level $E = 4.7$ Mev $(^5/_2, ^3/_2^-)$.

$_{21}Sc^{41}_{20}$. This nucleus is radioactive. The binding energy of the proton is small (1.62 Mev). The great number of relatively close lying levels points to their non-single particle character. If one can speak of a single-particle level at all, it is only of the ground level. The ground level has led only to the determination of the depth $V_0 = 49$ Mev.

$_{9}F^{17}_{8}$. Only the two bound states $1\,d_{5/2}$ and $2\,s_{1/2}$ were taken into account. Taking $\alpha = 1.15$, we obtained $\lambda = 34$ and $V_0 = 53.6$ Mev.

$_{7}N^{15}_{8}$. In analogy to the case of O^{15}, we obtained the optimal values for all three parameters from the first three levels: $\alpha = 1.25$, $\lambda = 44$, $V_0 = 53.6$ Mev.

To investigate the proton shell "40", we scanned the levels of the nuclei $_{39}Y^{89}_{50}$, $_{40}Zr^{89}_{49}$, $_{40}Zr^{91}_{51}$, and $_{41}Nb^{91}_{50}$. The ground and first excited levels of Y^{89} led to reasonable parameters for the potential (with $\alpha = 1.40$): $\lambda = 38$, $V_0 = 53.2$ Mev. The next excited level, however, does not fit in any more. All excited levels of Nb^{91}, Zr^{89}, and Zr^{91} must be assumed to have lost their single-particle character. Otherwise anomalous parameters would be obtained (for example, $\lambda \sim 60$).

Considering only the ground states to be single particle states and fixing α and λ, we obtain

TABLE II. Optimal parameters α, λ of the potential $V(r)$ for which the energies of the ground and low excited single particle levels coincide with the experimental values

Nucleus with an "extra" nucleon			Nucleus with a "hole"		
	α	λ		α	λ
$_8O_9^{17}$	1.15	33	$_7N_8^{15}$	1.25	44
$_9F_8^{17}$	1.15	34	$_8O_7^{15}$	1.15	47
$_{20}Ca_{21}^{41}$	1.15	27	$_{40}Zr_{49}^{89}$	1.375	38
$_{21}Sc_{20}^{41}$	1.15	27	$_{39}Y_{50}^{89}$	1.40	38
$_{20}Ca_{29}^{49}$	1.15	22	$_{81}Tl_{126}^{207}$	1.375	38
$_{21}Sc_{28}^{49}$	1.15	28	$_{82}Pb_{125}^{207}$	1.4	39
$_{41}Zr_{50}^{91}$	1.15	27			
$_{41}Nb_{50}^{91}$	1.15	27			
$_{82}Pb_{127}^{209}$	1.15	28			
$_{83}Bi_{126}^{209}$	1.15	25			

TABLE III. Depth of the potential V_0

Nucleus with an odd neutron				Nucleus with an odd proton				
Element	ΔZ	V_0, calculated	V_0 according to (8)	Element	ΔN	V_c	V_0, calculated	V_0 according to (8)
$_8O_7^{15}$	2.0	54.1	54.6	$_7N_8^{15}$	1.0	2.7	53.6	52.0
$_8O_9^{17}$	0	44.6	44	$_9F_8^{17}$	—1.0	3.6	43.4	42.9
$_{20}Ca_{21}^{41}$	2.2	49.6	48.3	$_{21}Sc_{28}^{49}$	2.6	6.0	56.6	55.3
$_{40}Zr_{49}^{89}$	2.2	43.2	46.0	$_{39}Y_{50}^{89}$	—0.2	9.4	53.2	53.2
$_{40}Zr_{51}^{91}$	0.6	46.2	44.5	$_{41}Nb_{50}^{91}$	—2.6	9.8	53.6	52
$_{82}Pb_{125}^{207}$	—0.8	41.8	43.7	$_{81}Tl_{126}^{207}$	2.8	14.9	55.8	60.0
$_{82}Pb_{127}^{209}$	2.2	42.6	43.2	$_{83}Bi_{126}^{209}$	0.2	15.3	56.9	59.3

$Nb^{91}: V_0 = 53.6$; $Zr^{91}: V_0 = 46.2$; $Zr^{89}: V_0 = 43.2$.

With all these data, 40 nucleons do not form a shell, but a subshell, which is sufficiently tight only for the ground state of the odd nucleon.

DISCUSSION OF THE RESULTS OF THE CALCULATION OF THE NUCLEAR POTENTIAL PARAMETERS

In Table II we collect the results of the computation of the parameters α and λ for nuclei with closed shells plus or minus a single nucleon. We call attention to the fact that these parameters remain constant for the elements from O^{15} to Pb^{209}. The average value of α is 1.15, the average value of λ is 28. The somewhat larger fluctuations of λ are, in part, due to the fact that we fixed α in a number of cases, so that λ also includes any possible fluctuations in α. Consequently, the observed deviations of α and λ from the average do not exceed 10%.

The foregoing refers to nuclei with one extra nucleon. For nuclei with one missing nucleon, we have, on the average, $\alpha = 1.4$ and $\lambda = 40$. To investigate the reasons for the increase in the values of the parameters, we computed the energies of the hole levels, say for Pb^{207}, using the values of α and λ taken from Pb^{209} (cf. the fifth column in Table I). The resulting deviations of the calculated levels from the experimental ones do not exceed 0.2 Mev, where the deviations go in both directions. An exception is the level $1\,i_{13/2}$, for which the discrepancy reaches 2 Mev. We recall that, in the calculation of the hole levels, we have assumed that the pair binding energy is the same for different levels. In reality this is, of course, not the case, and the discrepancies can therefore be viewed as a criterion for the validity of this assumption. In the cases of O^{15} and N^{15} the difference in the pair binding energy for different levels, Δ, is greater than or equal to ~ 0.6 Mev. This increase was to be expected, for the pair energy, as well as the fluctuations in it, is larger for light nuclei than for heavy nuclei.

We may thus consider the parameters α and λ to be identical for all nuclei, with the values $\alpha = 1.15$ and $\lambda \approx 28$, whereas the observed discrepancies for the hole levels are to be regarded as a numerical measure of the difference in the pair energies at different levels.

For the depth of the potential, V_0, the picture is more complicated. In Table III we list the results of the calculation of V_0 for 16 nuclei. First of all, we note the approximate equality of V_0 for O^{17}, F^{17}, and Pb^{209}. For O^{15} and N^{15}, on the other hand, the potential increases by ~ 10 Mev, and for Ca^{41}, by 6 Mev. This increase in V_0 cannot possibly be explained by a variation in the radius, for then one would have to set $R_0 \approx 1.0$ instead of $R_0 = 1.3$, for the case of O^{15}. Better founded is the assumption that the neutron potential depends on the relative number of protons, and the proton potential depends on the relative number of neutrons in the nucleus. The depth of the potential is the same for all those nuclei in which the number of neutrons and the number of protons are in statistical equilibrium. These nuclei lie on the stability curve, which may be obtained from the semi-empirical mass formula[10] by setting $(\partial M/\partial Z)_A = 0$:

$$A = 2Z + 0.0146\, A^{2/3} Z. \tag{7}$$

The values of N and Z for the nuclei on the stability curve correspond to the stable neutron and proton numbers. We denote them by N_{st} and Z_{st}. A deviation of N or Z from their stable values

leads to a change in the depth of the potential V_0. The following semi-empirical formula may be written down for V_0:

$$V_0^n = V_0^{stab} + (a/A)(Z - Z_{st}). \quad (8)$$

The proton potential will be deeper than the neutron potential by the Coulomb energy:

$$V_0^p = V_0^{stab} + (a/A)(N - N_{st}) + V_c. \quad (8a)$$

In Table III we list the values of $\Delta Z = Z - Z_{st}$ and $\Delta N = N - N_{st}$ obtained with formula (7). The experimental values of ΔZ and ΔN were used only for the lightest nuclei, $A = 15$ and $A = 17$, since it is known that (7) yields incorrect values for these nuclei. In the fourth and last columns of Table III we list the values of V_0 computed from (8) and (8a), with $V_0^{stab} = 44$ Mev and $a = 80$ Mev for both V_0^n and V_0^p. The agreement between the two values for V_0 is better for neutrons. The value of V_c entering into the proton potential was taken to be the value of the Coulomb energy of the last proton at the nuclear boundary $r = r_0$. To obtain $V_0 - V_c = 44$ Mev (with V_0 from (8a)) for Bi^{209}, as it should be, the value of V_c must be lowered by 3 Mev. On the other hand, we obtain a somewhat larger value for the average Coulomb energy, if we use the wave functions obtained for the ground state of Bi^{209}. As mentioned earlier, we did not treat the Coulomb energy in an entirely accurate way. Furthermore, it is not quite clear how one should properly compute the Coulomb energy from V_0. Despite these inaccuracies in V_c, formula (8a) gives satisfactory agreement within 4%.

The value $a = 80$ Mev indicates that each nucleon of a different kind above or below the stable number gives a contribution of $(80/A)$ Mev to the potential. This is twice as large as the average value for one nucleon $(44/A)$. This result is not surprising, since the nucleons interact with each other mainly over small distances, and the number of interacting states for nucleons of different kind is, on account of the Pauli principle, twice as large.

The second term in (7) indicates the excess of neutrons necessary for the compensation of the Coulomb potential in the nucleus with Z protons. The neutron excess is equal to the ratio $V_c/(a/A)$. Taking $V_c = (Z-1)e^2/r_0$ and $a = 80$ Mev, we obtain $V_c/(a/A) \approx 0.014 A^{2/3}(Z-1)$, which is in good agreement with the semi-empirical formula (7).

This analysis of the nuclear potential supports the hypothesis of the charge independence of nuclear forces.

TABLE IV. Depth of the neutron potential V_0 for the isotopes of Ca

Element	ΔZ	V_0,* calculated	V_0,** according to (8)
$_{20}Ca^{41}_{21}$	2.2	49.6	48.3
$_{20}Ca^{43}_{23}$	0.6	46.6	45.1
$_{20}Ca^{45}_{25}$	—1.2	45.0	41.8
$_{20}Ca^{47}_{27}$	—3	42.5	38.9
$_{20}Ca^{49}_{29}$	—4.6	42.5	36.5

*Computed with the experimental binding energies of the last neutron.

**The depths V_0, calculated with formula (8).

Another point deserves attention. The depth of the potential for Pb^{207} was calculated to be less than for Pb^{209}, despite the fact that Pb^{207} lies closer to the equilibrium isotope Pb^{206}. The reason for this is to be sought in the difference between the experimental binding energy and the depth of the ground level of the odd nucleon. Usually these two quantities are equal. However, the binding energy also contains part of the energy of the other nucleons, which is given off as a result of the removal of the particle. In particular, the contraction of the nuclear radius $(A^{1/3} \rightarrow (A-1)^{1/3})$ leads to a raising of the levels of all other nucleons. The energy contributed by the other nucleons will be larger for the nucleus Pb^{207}, which has an unfilled neutron shell, than for the nucleus Pb^{209}, which has a tight core.

We have determined the effective potential for one-nucleon motions in the nucleus. However, if the nucleus contains several nucleons above the closed shells, the last nucleon will not be in a single-particle state, owing to the remaining interactions. This is clearly evident from the calculation of V_0 for the ground state of the isotopes of Ca. As the number of nucleons above the shell increases, the potential deviates more and more from the single particle potential of formula (8) in that it becomes deeper (cf. Table IV).

THE NUCLEON WAVE FUNCTIONS

In this section we consider the nucleon wave functions calculated with the average nuclear potential. These functions are expanded into a series in terms of spherical oscillator functions, in order to simplify the further computations. The wave equation for the wave functions with an average diffuse proton potential has the form

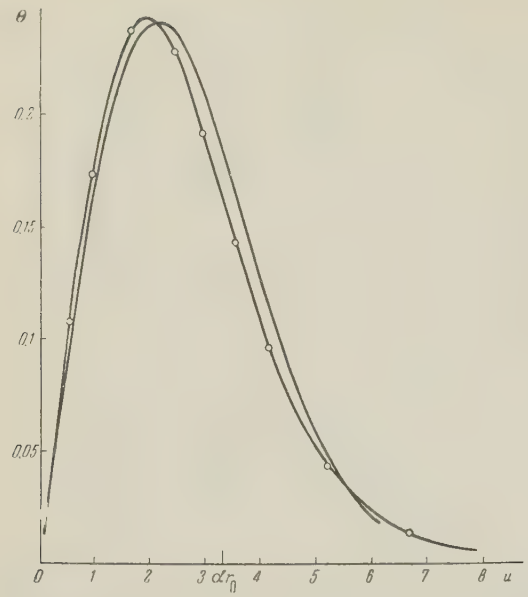

FIG. 3. Normalized neutron function for the $1p_{1/2}$ level of O^{15} (curve with points; $\alpha = 1 \times 10^{13}$ cm^{-1}, $\lambda = 25$, $V_0 = 43.8$ Mev, $R_0 = 1.3$) and normalized oscillator function $\Theta_1^1(u/u_0)$ ($u_0 = 1.5$).

$$-\frac{\hbar^2}{2M}\frac{1}{u^2}\frac{d}{du}\left[u^2\frac{dR^l(u)}{du}\right]+\left[\frac{V+V_c-E}{\alpha^2}+\frac{\hbar^2}{2M}\frac{l(l+1)}{u^2}\right.$$
$$\left.-\lambda\left(\frac{\hbar}{2Mc}\right)^2\frac{\mathbf{l}\cdot\mathbf{s}}{u}\frac{dV}{du}\right]R^l=0, \qquad (9)$$

where

$$V=-V_0/(1+e^{u-b}); \quad u=\alpha r;$$

$$b=\alpha r_0=1.3\alpha A^{1/3}\cdot 10^{13}\ \text{cm}.$$

For the protons we have

$$V_c=\begin{cases}[3/2-1/2(u/b)^2]\,\alpha(Z-1)/137\,b & \text{for } u\leqslant b,\\ \alpha(Z-1)/137\,u & \text{for } u\geqslant b.\end{cases} \qquad (10)$$

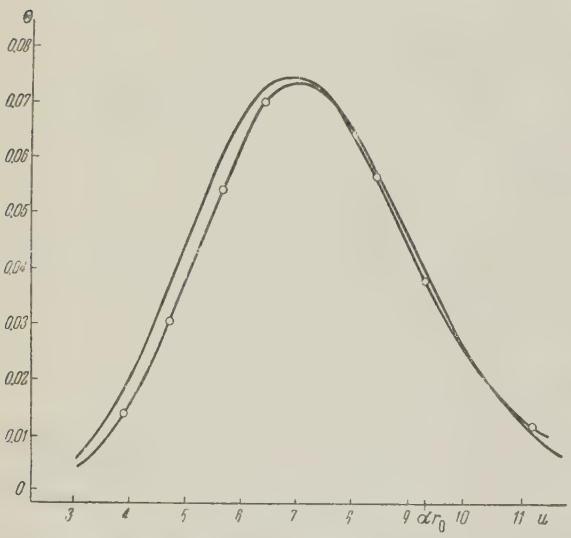

FIG. 4. Normalized neutron function for the $1i_{13/2}$ level of Pb^{209} (curve with points; $\alpha = 1.15 \times 10^{13}$ cm^{-1}, $\lambda = 28$, $V_0 = 42.6$ Mev, $R_0 = 1.3$) and normalized oscillator function $\Theta_1^6(u/u_0)$ ($u_0 = 2$).

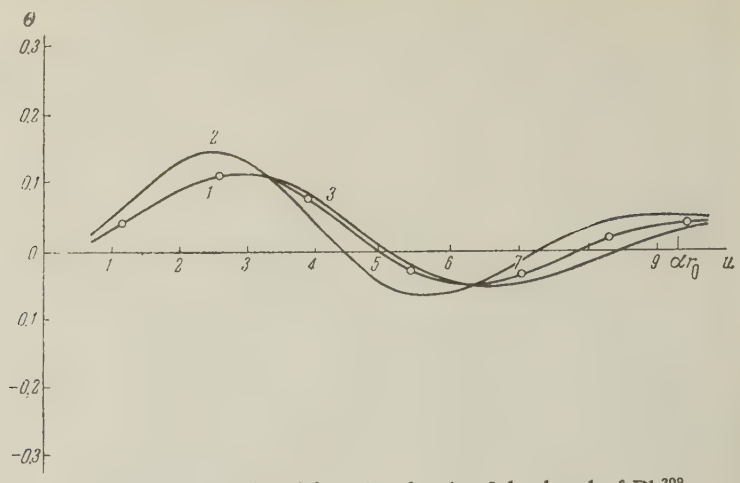

FIG. 5. Normalized function for the $3d_{5/2}$ level of Pb^{209} (curve 1; $\alpha = 1.15 \times 10^{13}$ cm^{-1}, $\lambda = 28$, $V_0 = 42.6$ Mev, $R_0 = 1.3$) and normalized oscillator function $\Theta_3^2(u/u_0)$ for two values of u_0 (curve 2: $u_0 = 2$, curve 3: $u_0 = 2.32$).

For neutrons, $V_C = 0$.

The normalized oscillator functions are

$$\Theta_n^l\left(\frac{u}{u_0}\right)=\frac{\exp\left[-1/2\,(u/u_0\sqrt{2})^2\right](u/u_0\sqrt{2})^l}{[u_0^3\sqrt{2}\,\Gamma(n)\,\Gamma(n+l+1/2)]\,2^{1/2}}\,L_{n-1}^{l+1/2}\left[\left(\frac{u}{u_0\sqrt{2}}\right)^2\right],$$

$$\int_0^\infty \Theta_n^l\left(\frac{u}{u_0}\right)\Theta_m^l\left(\frac{u}{u_0}\right)u^2du=\delta_{n,m},$$

$$n=1,\ 2,\ 3\ldots; \quad u_0=\alpha\sqrt{\hbar/2M\omega}. \qquad (11)$$

$L_n^p(x)$ is the Laguerre polynomial, which satisfies the relation

$$L_n^p(x)=x^{-p}e^x\frac{d^n}{dx^n}(e^{-x}x^{n+p}), \qquad (12)$$

$\hbar\omega$ is the distance between two neighboring levels. The normalized solution, $R^l(u)$, of Eq. (1), corresponding to the momentum l and k zeros in the interval $(0 < u < \infty)$, is expanded in terms of the corresponding functions $\Theta_n^l(u/u_0)$:

$$R^l(u)=\sum_{n=1}^{\infty}C_n\Theta_n^l(u/u_0), \qquad (13a)$$

$$C_n=\int_0^\infty R^l(u)\,\Theta_n^l(u/u_0)\,u^2\,du, \qquad (13b)$$

$$1=\int_0^\infty[R^l(u)]^2u^2\,du=\sum_{n=1}^{\infty}C_n^2. \qquad (13c)$$

The system of functions (11) is complete for arbitrary finite u_0, but the convergence properties of the series (13) depend on the choice of u_0. We chose u_0 such as to make the contribution of the function $\Theta_{k+1}^l(u/u_0)$ (which has k zeroes) to the normalization integral (13c) maximal. This means, graphically, that we superpose the first maxima of the functions $R^l(u)$ and $\Theta_{k+1}^l(u/u_0)$.

In this way the optimal scale will be different for different levels of the same nucleus. In Figs.

TABLE V. Dependence of the expansion coefficients C_i of the normalized neutron function for the 1 $p_{1/2}$ level of O^{15} on the scale u_0 (parameter values: $\alpha = 1.00$, $\lambda = 25$, $V_0 = 43.9$; energy $E = -9.4$)

u_0	1.0	1.5	2.0	5.0	10
C_1	0.8456	0.9832	0.9055	0.2821	0.130
C_2	—0.4416	0.0206	0.3573	0.3478	0.190
C_3	0.2352	0.0866	0.2019	0.3648	0.2350
C_4	—0.1376	—0.0133	0.0954	0.3600	0.2700
C_5	0.0866	0.0111	0.0488	0.3429	0.3000
C_6	—0.0555	—0.0067	0.0244	0.3210	0.320
C_7	0.0377	0.0020	0.0113	0.2967	0.335
C_8	—0.0266	—0.0016	0.0051	0.2724	0.350
C_9	0.0178	—0.0002	0.0024	0.2505	0.355
C_{10}	—0.0111	0.0005	0.0009	0.2286	0.365
C_{11}	0.0089	—0.0005	—0.0002	0.2067	0.370

3 and 4 we plot the functions corresponding to the levels 1 $p_{1/2}$ (O^{15}) and 1 $i_{11/2}$ (Pd^{209}), as calculated on the "Strela" computer, and the corresponding oscillator functions. The approximation turns out to be satisfactory. A slight change in u_0 would result in even better agreement. The vertical mark on the abscissa indicates the nuclear boundary r_0 in the given scale. Figure 5 shows the curve for 3 $d_{5/2}$ (Pb^{209}), as computed on the machine, and the oscillator function for two values of u_0. Here the agreement is already worse, especially in the "tail." This indicates that, independently of the choice of u_0, one cannot restrict oneself to only a single term in the expansion of functions $R^l(u)$ with several zeros according to formula (13a).

Table V shows the dependence of the coefficients C_n^l on u_0 for the 1 $p_{1/2}$ level of O^{15}.

CONCLUSIONS

The above calculations of the ground and low excited levels of 16 nuclei with doubly closed shells plus or minus one nucleon show that:

1. The average nuclear potential of the form (1) with the appropriate choice of parameters gives the correct level ordering, and, with good accuracy, the correct spacing.

2. The parameters α and λ, which determine the diffuseness of the boundary of the potential and the magnitude of the spin-orbit interaction, are approximately equal for all nuclei. This result is in agreement with the known data on the scattering of fast electrons from nuclei with spin-orbit splitting of the levels.

3. The depth of the potential, V_0, is the same for all nuclei lying on the stability curve. It is equal to ~ 44 Mev. For the other nuclei, V_0 is determined by formulas (8) and (8a).

4. The presence of several nucleons above closed shells leads to an increase in the depth of the potential over that given by (8) and (8a), owing to the residual interaction between the nucleons.

5. The investigation of the properties of nuclei with a proton shell $Z = 40$ shows that the excited levels of these nuclei are not single particle levels. This indicates that the shell "40" is less tight than the shells "20", "50", and others.

6. The wave function of the last odd nucleon is close to the corresponding oscillator function only in the first quantum states (1p, 1i, and similar levels). For these, a good approximation can be obtained with an appropriate choice of the scale u_0. Wave functions with several zeros (2p, 3p, and similar levels) cannot be satisfactorily approximated by a single oscillator function.

It is our pleasure to express our deep gratitude to S. B. Mostinskaya, who guided us in all the calculations, and also to I. S. Berezin and N. P. Trifonov. We further thank G. V. Podgaiskaya, G. G. Vasil'eva, and E. F. Kobzeva for participating in the final phases of the calculations.

[1] B. L. Cohen and R. V. Neidigh, Phys. Rev. **93**, 282 (1954), Beyster, Walt, and Salmi, Phys. Rev. **104**, 1319 (1956).

[2] Hahn, Ravenhall, and Hofstadter, Phys. Rev. **101**, 1131 (1956).

[3] R. D. Woods and D. S. Saxon, Phys. Rev. **95**, 577 (1954).

[4] R. M. Sternheimer, Phys. Rev. **97**, 1314 (1955). Ross, Mark, and Lawson, Phys. Rev. **102**, 1613 (1956) and **104**, 401 (1956). P. É. Nemirovskiĭ, J. Exptl. Theoret. Phys. (U.S.S.R.) **30**, 551 (1956) and **33**, 746 (1957), Soviet Phys. JETP **3**, 484 (1956) and **6**, 573 (1958).

[5] L. Collatz, Numerical Methods for the Solution of Differential Equations (Russ. Transl.), IIL, 1953.

[6] J. A. Harvey, Canad. J. Phys. **31**, 278 (1953).

[7] I. I. Levintov, Dokl. Akad. Nauk SSSR **107**, 240 (1956), Soviet Phys. "Doklady" **1**, 175 (1956). Doctoral Dissertation, 1957.

[8] R. U. Nussbaum, Revs. Modern Phys. **28**, 423 (1956).

[9] L. V. Groshev and A. M. Demidov, Атомная энергия (Atomic Energy) **3**, 91 (1957).

[10] C. F. v. Weizsaecker, Z. Physik **96**, 431 (1953).

Translated by R. Lipperheide
90

RENORMALIZATION OF THE VERTEX PART IN PSEUDOSCALAR MESON THEORY

V. N. GRIBOV

Leningrad Physico-Technical Institute

Submitted to JETP editor August 15, 1958

J. Exptl. Theoret. Phys. (U.S.S.R.) 36, 554-559 (February, 1959)

The renormalization of the vertex part in pseudoscalar meson theory is investigated with the aid of the spectral representations of the vacuum average of the T-product of three Heisenberg operators proposed by Schwinger[1] and by Gribov.[2] The problem of the magnitude of the renormalization constants is discussed. An expression for Z_1 in terms of the spectral functions is obtained and the relation between these spectral functions and the spectral functions in the Källen-Lehmann representations for single particle Green's functions is established.

1. The spectral representations for the Green's functions proposed by Schwinger[1] and by the author[2] contain a number of the essential properties of these functions in a simple and clear form, and therefore they may turn out to be useful both for establishing different kinds of dispersion relations and for the further study of the structure of contemporary theory. In spite of the fact that the derivation of these representations based only on the conditions of causality and on the structure of the spectrum of the system has met with serious objections (Källen), the fact that they are valid in the case of perturbation theory suggests that they are actually correct (a more detailed discussion of this point will be given in a subsequent paper). However, it remains unclear as to what particular requirement must be imposed in order to limit the class of possible representations. One such requirement might be the requirement of renormalizability of the theory. In this paper it is shown that the representations referred to above satisfy these requirements.

With the aid of these representations it is possible to discuss in a simple way the problem of the magnitude of the renormalization constants, to obtain an expression for the constant Z_1 in terms of the spectral functions, and to establish the relation of these spectral functions with the spectral functions in the Källen-Lehmann representation for the single particle Green's functions.

2. We start from the following relation which is obtained by simple differentiation taking into account the renormalized field equations and the commutation relations:

$$\left(\gamma_\lambda \frac{\partial}{\partial x_{1\lambda}} + m\right)\left(\Box_2 - \mu^2\right)$$
$$\times \langle 0 \mid T\psi(x_1)\, \varphi_i(x_2)\, \bar{\psi}(x_2) \mid 0 \rangle \left(\gamma_\nu \frac{\overleftarrow{\partial}}{\partial x_{3\nu}} - m\right)$$
$$= \langle 0 \mid Tu(x_1)\, j_i(x_2)\, \bar{u}(x_3) \mid 0 \rangle + gZ_1Z_2^{-1}Z_3^{-1}\tau_i\gamma_5\delta(x_1 - x_2)$$
$$\times \langle 0 \mid T\psi(x_1)\bar{\psi}(x_3) \mid 0 \rangle \left(\gamma_\nu \frac{\overleftarrow{\partial}}{\partial x_{3\nu}} - m\right)$$
$$- gZ_1Z_2^{-1}Z_3^{-1}(\gamma_\lambda \partial/\partial x_{1\lambda} + m)$$
$$\times \langle 0 \mid T\psi(x_1)\bar{\psi}(x_3) \mid 0 \rangle \tau_i\gamma_5\delta(x_2 - x_3)$$
$$+ gZ_1Z_2^{-2}\gamma_5\tau_i(\Box_2 - \mu^2) \langle 0 \mid T\varphi_j(x_1)\varphi_i(x_2) \mid 0 \rangle$$
$$- 2ig\gamma_5\tau_i Z_1Z_2^{-2}Z_3^{-1}\delta(x_1 - x_2)\delta(x_2 - x_3);$$
$$u(x) = (\gamma_\mu \partial/\partial x_\mu + m)\psi(x); \qquad j_i(x) = (\Box - \mu^2)\varphi_i(x). \quad (1)$$

In the momentum representation this relation has the form:

$$ig(i\hat{p}_1 + m)G(\hat{p}_1)\tau_i\Gamma_5(\hat{p}_1, k, \hat{p}_3)$$
$$\times G(p_3)(i\hat{p}_3 + m)(k^2 + \mu^2)\Delta(k^2) = T_i(\hat{p}_1, k, \hat{p}_3)$$
$$+ igZ_1Z_2^{-1}Z_3^{-1}\gamma_5\tau_i G(\hat{p}_3)(i\hat{p}_3 + m) + igZ_1Z_2^{-1}Z_3^{-1}$$
$$\times (i\hat{p}_1 + m)G(\hat{p}_1)\gamma_5\tau_i + igZ_1Z_2^{-2}\gamma_5\tau_i(k^2 + \mu^2)\Delta(k^2)$$
$$- 2igZ_1Z_2^{-2}Z_3^{-1}\gamma_5\tau_i; \qquad p_1 + k - p_3 = 0; \quad (2)$$

$G(\hat{p})$ and $\Delta(k^2)$ are the renormalized Green's functions; $T(\hat{p}_1, k_1, \hat{p}_3)$ is the Fourier component of the vacuum average of the T-product of the operators $u(x_1)\, j_i(x_2)\, \bar{u}(x_3)$. In reference 2 the following expression was obtained for this quantity

$$T_i(\hat{p}_1, k, \hat{p}_3)$$

$$= i\gamma_5\tau_i \int_0^\infty d\varkappa_1^2\, d\varkappa_2^2\, d\varkappa_3^2 \int_0^1\int_0^1\int_0^1 d\alpha\, d\beta\, d\gamma\, \delta(\alpha+\beta+\gamma-1)$$

$$\times \left\{ \frac{f_0(\varkappa_1^2,\varkappa_2^2,\varkappa_3^2) + (\gamma\hat{p}_1+\alpha\hat{p}_3)\, f_1(\varkappa_1^2,\varkappa_2^2,\varkappa_3^2) + \beta(\hat{p}_1+\hat{p}_3) f_2(\varkappa_1^2,\varkappa_2^2,\varkappa_3^2)}{p_1^2\beta\gamma + k^2\alpha\gamma + p_3^2\alpha\beta + \alpha\varkappa_1^2 + \beta\varkappa_2^2 + \gamma\varkappa_3^2 - i\varepsilon} \right.$$

$$\left. - \frac{(\beta/2i)\,[\hat{p}_1, \hat{p}_3]\, f_3(\varkappa_1^2,\varkappa_2^2,\varkappa_3^2)}{p_1^2\beta\gamma + k^2\alpha\gamma + p_3^2\alpha\beta + \alpha\varkappa_1^2 + \beta\varkappa_2^2 + \gamma\varkappa_3^2 - i\varepsilon} \right\}. \quad (3)$$

Here a small change in notation has been introduced, and an error made in reference 2 has been corrected. $f_i(\kappa_1^2, \kappa_2^2, \kappa_3^2)$ are real functions symmetric with respect to an interchange of κ_1^2 and κ_3^2, equal to zero if $\kappa_1 + \kappa_2 < m + \mu$ or $\kappa_2 + \kappa_3 < m + \mu$, or $\kappa_1 + \kappa_3 < 3\mu$. The integral over κ_1^2, κ_2^2, and κ_3^2 in (3) may be either convergent or divergent depending on whether the combinations of the renormalization constants appearing in (2) are finite or infinite, but the functions $f_i(\kappa_1^2, \kappa_2^2, \kappa_3^2)$ are necessarily finite. This follows from the fact that (cf. reference 2) they are simply related to the Fourier-component $\rho_{uj\bar{u}}(\hat{p}_1, \hat{p}_3)$ of the unordered product of the operators $u(x_1)$, $j_i(x_2)$, $\bar{u}(x_3)$. The latter differs from the Fourier component $\rho_{\psi\varphi\bar{\psi}}(\hat{p}_1, \hat{p}_3)$ of the average product of the operators $\psi(x_1)$, $\varphi_i(x_2)$, $\bar{\psi}(x_3)$, which is finite, only by the factor

$$\rho_{uj\bar{u}}(\hat{p}_1, \hat{p}_3)$$

$$= (i\hat{p}_1 + m)\,\rho_{\psi\varphi\bar{\psi}}(\hat{p}_1, \hat{p}_3)\,(i\hat{p}_3 + m)\,[(p_1 - p_3)^2 + \mu^2]. \quad (4)$$

If the normalizing constants are finite then the integral (3) must be convergent. From its convergence it follows (cf. the analogous discussion in reference 3) that, for example, for $\hat{p}_1 = im$, $\hat{p}_3 = im$ and $k^2 \to \infty$, $T_i(im, k^2, im) \to 0$. We then obtain under the conditions stated above

$$\Gamma_5(im, k^2, im) \to \gamma_5 Z_1 Z_2^{-1}(2 - Z_2^{-1}). \quad (5)$$

Having this asymptotic expression for Γ_5, it is easy to show by utilizing the Källen-Lehmann expression for Z_3^{-1}, that $Z_3^{-1} \to \infty$. This represents the substance of Källen's proof[3] that one of the renormalization constants is infinite. We shall not discuss the special case $Z_2^{-1} = 2$ (cf. reference 3).

If the renormalization constants themselves are infinite, but their combinations appearing in (2) are finite, then, since in this case $\Delta(k^2)$ falls off slower than $1/k^2$, we can neglect all the terms in (2) with the exception of the penultimate one, and obtain:

$$\Gamma_5(im, k^2, im) \to \gamma_5 Z_1 Z_2^{-2} \quad (6)$$

and, similarly,

$$\Gamma_5(\hat{p}_1, -\mu^2, im) \to \gamma_5 Z_1 Z_2^{-1} Z_3^{-1}. \quad (6a)$$

But, as has been shown by Lehmann, Symanzik, and Zimmerman,[4] in a consistent theory $\Gamma_5(im, k^2, im) \to 0$, $\Gamma_5(\hat{p}, -\mu^2, im) \to 0$ and, consequently, $Z_1 Z_2^{-2} = 0$, $Z_1 Z_2^{-1} Z_3^{-1} = 0$. But in this case those terms of the field equations which describe the interaction are equal to zero. Therefore, such a case is not very probable. On the other hand that case is most probable when the combinations of the constants appearing in (2) are infinite. In this case the integral (3) must diverge, and it is necessary to obtain a finite expression for the vertex part. To do this we first determine the constant Z_1 in terms of the functions $f_i(\kappa_1^2, \kappa_2^2, \kappa_3^2)$. We define Z_1 by the condition

$$\Gamma_5(im, -\mu^2, im) = \gamma_5. \quad (7)$$

This condition corresponds to the determination of the coupling constant by means of the dispersion relations. The fact that the conditions $\hat{p}_1 = \hat{p}_3 = im$, $k^2 = -\mu^2$ cannot be satisfied for real momenta does not lead to any difficulties since we have an explicitly analytic expression for $T_i(\hat{p}_1, k^2, \hat{p}_3)$.

It follows from (7) that

$$T_i(im, -\mu^2, im)$$

$$= ig\gamma_5\tau_i[1 - 2Z_1 Z_2^{-1} Z_3^{-1} - Z_1 Z_2^{-2} + 2Z_1 Z_2^{-2} Z_3^{-1}]. \quad (8)$$

By utilizing this relation we can write the right hand side of (2) in the form:

$$T_i'(\hat{p}_1, k^2, \hat{p}_3) + ig Z_1 Z_2^{-1} Z_3^{-1}\gamma_5\tau_i[(i\hat{p}_1 + m)\,G(\hat{p}_1) - 1]$$
$$+ ig Z_1 Z_2^{-1} Z_3^{-1}[G(\hat{p}_3)(i\hat{p}_3 + m) - 1]\gamma_5\tau_i$$
$$+ ig Z_1 Z_2^{-2}\gamma_5\tau_i[(k^2 + \mu^2)\Delta(k^2) - 1] + ig\gamma_5\tau_i.$$
$$T_i'(\hat{p}_1, k^2, \hat{p}_3) = T_i(\hat{p}_1, k^2, \hat{p}_3) - T_i(im, -\mu^2, im). \quad (9)$$

However, T_i' is not yet, generally speaking, a convergent expression, since the subtraction of $T_i(im, -\mu^2, im)$ does not yet regularize even the first term in the integral of (3). Indeed, let us consider this first term in T_i', which contains the function $f_0(\kappa_1^2, \kappa_2^2, \kappa_3^2)$. It has the form:

$$\int d\varkappa_1^2\, d\varkappa_2^2\, d\varkappa_3^2\, f_0(\varkappa_1^2, \varkappa_2^2, \varkappa_3^2) \int d\alpha\, d\beta\, d\gamma$$

$$\times \frac{\delta(\alpha+\beta+\gamma-1)\,[\alpha\beta(p_3^2 + m^2) + \alpha\gamma(k^2 + \mu^2) + \beta\gamma(p_1^2 + m^2)]}{[\alpha\beta p_3^2 + \beta\gamma p_1^2 + \alpha\gamma k^2 + \varkappa^2]\,[-\alpha\beta m^2 - \alpha\gamma\mu^2 - \beta\gamma m^2 + \varkappa^2]},$$
$$\varkappa^2 = \alpha\varkappa_1^2 + \beta\varkappa_2^2 + \gamma\varkappa_3^2. \quad (10)$$

At first sight it might appear that the integral (10) cannot be divergent, since if the integral diverges then only large values of κ_1^2, κ_2^2 and κ_3^2 are of importance in it, and the terms containing p_1^2, p_3^2, and k^2 in the denominator may be neglected. Then the infinite part of this integral must be of the form

$$A_1(p_1^2 + m^2) + A_2(k^2 + \mu^2) + A_3(p_3^2 + m^2), \quad (11)$$

where A_1, A_2, and A_3 are infinite. But these terms could not cancel against other infinite terms in (9) since $\Delta(k^2)$, $G(\hat{p}_1)$, and $G(\hat{p}_3)$ fall off for large momenta. However, this conclusion is not correct since, for example, for large values of κ_2^2 in the integral over β the region of small $\beta \sim 1/\kappa_2^2$ is important. In this region the denominators are not large. But the size of the region is of order $1/\kappa_2^2$, so that the whole integral over β behaves like $1/\kappa_2^2$ for large values of κ_2^2. It is also important that for $\beta \sim 1/\kappa_2^2$ the integrand in (10) becomes dependent only on the momentum k^2.

However, from these arguments it follows that the divergence of the integral (10) may be due only to regions of correspondingly small β, α, and γ and that in order to regularize it, it is sufficient to subtract from the integrand its limiting values in these regions, viz. to subtract from the integrand the expression

$$\frac{\alpha\beta\,(p_3^2+m^2)}{(\alpha\beta p_3^2+\varkappa^2)(-\alpha\beta m^2+\varkappa^2)}$$

$$+\frac{\alpha\gamma\,(k^2+\mu^2)}{(\alpha\gamma k^2+\varkappa^2)(-\alpha\gamma\mu^2+\varkappa^2)}+\frac{\beta\gamma\,(p_1^2+m^2)}{(\beta\gamma p_1^2+\varkappa^2)(-\beta\gamma m^2+\varkappa^2)}. \quad (12)$$

After this subtraction the integral (10) will be convergent, and it now remains only to discuss the divergences produced by the integration of expression (12). Since each of the terms of (12) depends on only one of the momenta there exists a possibility for its infinite parts to cancel against the infinite parts contained in the remaining terms of (9).

If we believe in the renormalizability of the theory, then we must conclude that such a cancellation does indeed take place. In principle we could terminate at this point our investigation of the representation (10), since after subtraction we obtain a representation of the contribution to the vertex part made by $f_0(\kappa_1^2, \kappa_2^2, \kappa_3^2)$ in the form of a convergent integral, plus finite terms which have the same analytic properties as the original integral. However, it is of interest to establish the requirements which are imposed on the function $f_0(\kappa_1^2, \kappa_2^2, \kappa_3^2)$ by the condition of renormalizability.

3. We consider the second term in (12) and carry out the integration over β and γ. We obtain

$$\int d\varkappa_1^2 d\varkappa_2^2 d\varkappa_3^2 f_0(\varkappa_1^2, \varkappa_2^2, \varkappa_3^2) \int_0^1 (1-\alpha)\frac{d\alpha}{\varkappa_2^2(1-\alpha)+\varkappa_1^2\alpha}$$

$$\times\left\{\ln\frac{\varkappa_1^2\alpha+\varkappa_3^2(1-\alpha)+\alpha(1-\alpha)k^2}{\varkappa_1^2\alpha+\varkappa_3^2(1-\alpha)-\alpha(1-\alpha)\mu^2}\right.$$

$$\left.+\text{terms of order } \varkappa_2^{-4}\ln\varkappa_2^2\right\}. \quad (13)$$

This integral diverges when the integration over κ_2^2 is carried out. This means that $f_0(\kappa_1^2, \kappa_2^2, \kappa_3^2)$ does not fall off sufficiently rapidly as $\kappa_2^2 \to \infty$. However, it cannot increase faster than κ^{2q}, where $q < 1$, since in this case the integral (10) would diverge when the integration over κ_2^2 is carried out not only for small values of β, and this would contradict the previous conclusions.

For the sake of simplicity we consider the case $f_0(\kappa_1^2, \kappa_2^2, \kappa_3^2) \to \varphi_0(\kappa_1^2, \kappa_3^2)$ as $\kappa_2^2 \to \infty$. It is simple to make generalizations to other possible cases. We consider that the integral containing $f_0(\kappa_1^2, \kappa_2^2, \kappa_3^2) - \varphi_0(\kappa_1^2, \kappa_3^2)$ in place of $f_0(\kappa_1^2, \kappa_2^2, \kappa_3^2)$ converges. Then after integrating over κ_2^2, and after introducing the cut-off limit λ, we shall obtain for the divergent part (13) the following expression:

$$\int d\varkappa_1^2 \int d\varkappa_3^2\, \varphi_0(\varkappa_1^2, \varkappa_3^2)$$

$$\times\int \ln\frac{\alpha\varkappa_1^2+(1-\alpha)\varkappa_3^2+\alpha(1-\alpha)k^2}{\alpha\varkappa_1^2+(1-\alpha)\varkappa_3^2-\alpha(1-\alpha)\mu^2}\ln\left(\frac{\lambda}{\varkappa_3^2}\frac{1-\alpha}{\alpha}\right)d\alpha. \quad (14)$$

In order that the infinite part of (14) should cancel against the fourth term in (9), it is necessary to have

$$\int d\varkappa_1^2 d\varkappa_3^2\,\varphi_0(\varkappa_1^2, \varkappa_3^2)\int_0^1 d\alpha \ln\frac{\alpha\varkappa_1^2+(1-\alpha)\varkappa_3^2+\alpha(1-\alpha)k^2}{\alpha\varkappa_1^2+(1-\alpha)\varkappa_3^2-\alpha(1-\alpha)\mu^2}$$

$$= C\,[(k^2+\mu^2)\,\Delta(k^2)-1], \quad (15)$$

where C is a finite constant.

In order that (15) should hold it is necessary, first, that its left hand side should increase slower than the first power of k^2. If $\varphi(\kappa_1^2, \kappa_3^2)$ is such that this holds, then by equating the imaginary parts on the right and on the left hand sides we easily obtain the relation between the function $\varphi_0(\kappa_1^2, \kappa_3^2)$ and the function $\kappa(\sigma^2)$ in the Kallen-Lehmann representation for $\Delta(k^2)$. If

$$\Delta(k^2) = \frac{1}{k^2+\mu^2}+\int_{9\mu^2}^{\infty}\frac{\sigma(\varkappa^2)\,d\varkappa^2}{k^2+\varkappa^2-i\varepsilon},$$

then after integration over α we get from (15)

$$C(\varkappa^2-\mu^2)\,\sigma(\varkappa^2)$$

$$=\frac{1}{\varkappa^2}\int d\varkappa_1^2 d\varkappa_3^2\,\vartheta(\varkappa-\varkappa_1-\varkappa_3)\,S(\varkappa, \varkappa_1, \varkappa_3)\,\varphi_0(\varkappa_1^2, \varkappa_3^2), \quad (16)$$

where

$$S(\varkappa, \varkappa_1, \varkappa_3)$$

$$=[(\varkappa-\varkappa_1-\varkappa_3)(\varkappa-\varkappa_1+\varkappa_3)(\varkappa+\varkappa_1-\varkappa_3)(\varkappa+\varkappa_1+\varkappa_3)]^{1/2},$$

$$\vartheta(x)=1 \text{ for } x>0 \text{ and } \vartheta(x)=0 \text{ for } x<0. \quad (17)$$

We note that formula (16) is self consistent in the sense that in virtue of the condition $f_0(\kappa_1^2, \kappa_2^2, \kappa_3^2) = 0$ for $\kappa_1+\kappa_3 < 3\mu$ the right hand side differs

from zero only for $\kappa^2 > 9\mu^2$.

To obtain a similar relation between $f_i(\kappa_1^2, \kappa_2^2, \kappa_3^2)$ and the spectral functions in the representation for $G(\hat{p})$ it is necessary to investigate the remaining terms in (3) containing f_1, f_2, and f_3. These terms cannot give a contribution to (16) since they depend on the Dirac matrices, but they can give a contribution to the relation for $G(\hat{p})$.

Actually it is easy to see, by taking into account the fact that each of the infinite terms in (9) depends on only one of the momenta and increases slower than $\hat{p}_1$, $\hat{p}_3$, and k^2, that the integrals containing f_2 and f_3 cannot diverge at all, while the integral containing f_1 can diverge only as a result of integration over κ_1^2, or over κ_3^2. We write out the contribution to $T_i'(\hat{p}_1, k^2, \hat{p}_3)$ of the terms containing f_1 in a more detailed manner. It has the form:

$$\int d\varkappa_1^2 d\varkappa_2^2 d\varkappa_3^2 f_1(\varkappa_1^2, \varkappa_2^2, \varkappa_3^2)$$

$$\times \int \frac{d\alpha\, d\beta\, d\gamma\, \delta(\alpha+\beta+\gamma-1)}{(\alpha\beta p_3^2 + \alpha\gamma k^2 + \beta\gamma p_1^2 + \varkappa^2)(-\alpha\beta m^2 - \alpha\gamma\mu^2 - \beta\gamma m^2 + \varkappa^2)}$$

$$\times\{[\gamma(i\hat{p}_1 + m) + \alpha(i\hat{p}_3 + m)]\varkappa^2 + m(\alpha+\gamma)(\alpha\beta p_3^2 + \alpha\gamma k^2 + \beta\gamma p_1^2)$$

$$-(\alpha\beta m^2 + \alpha\gamma\mu^2 + \beta\gamma m^2)(i\alpha\hat{p}_3 + i\gamma\hat{p}_1)\}. \qquad (18)$$

Owing to the presence of κ^2 in the numerator the regions of small values of α, γ and of the values of α, γ of order of magnitude of unity give contributions, generally speaking, of the same order of magnitude to the divergent part of $T_i'(\hat{p}_1, k^2, \hat{p}_3)$. However, the contribution from the region in which α, γ are of the order of magnitude of unity behaves for large $\hat{p}_1$ or $\hat{p}_3$ as the first power of $\hat{p}_1$ or $\hat{p}_3$, and consequently cannot cancel against the remaining terms of (9) due to the falling off of $G(\hat{p})$ for large values of $\hat{p}$. Therefore the function $f_1(\kappa_1^2, \kappa_2^2, \kappa_3^2)$ must have such properties that the contribution of this region to the divergent part will be equal to zero. If again we make the simplest assumption that as $\kappa_1^2 \to \infty$ $f_0(\kappa_1^2, \kappa_2^2, \kappa_3^2) \to \varphi_0(\kappa_2^2\ \kappa_3^2)$, while $f_1(\kappa_1^2, \kappa_2^2, \kappa_3^2) \to \varphi_1(\kappa_2^2, \kappa_3^2)$, then the divergent part of $T_i'(\hat{p}_1, k^2, \hat{p}_3)$ which must cancel the second term in (9) may be written in the form

$$(i\hat{p}_1 + m)\int d\varkappa_1^2\, d\varkappa_2^2\, d\varkappa_3^2 \int \gamma\, d\alpha\, d\beta\, d\gamma\, \delta(\alpha+\beta+\gamma-1)$$

$$\times \frac{\beta(m - i\hat{p}_1)\varphi_0(\varkappa_2^2, \varkappa_3^2) + (\varkappa^2 - \beta\gamma i\hat{p}_1 m)\varphi_1(\varkappa_2^2, \varkappa_3^2)}{(\beta\gamma\hat{p}_1 + \varkappa^2)(-\beta\gamma m^2 + \varkappa^2)}. \qquad (19)$$

Carrying out the integration in (19) first over α, β and then over κ_1^2 with the cut-off limit λ, we shall obtain for its infinite part the expression:

$$\int d\varkappa_2^2\, d\varkappa_3^2 \int_0^1 d\gamma \left\{\left[\varphi_0(\varkappa_2^2, \varkappa_3^2) - \frac{i\hat{p}_1 m}{m - i\hat{p}_1}\varphi_1(\varkappa_2^2, \varkappa_3^2)\right] \ln\frac{\varkappa_2^2(1-\gamma) + \varkappa_3^2\gamma + p_1^2\gamma(1-\gamma)}{\varkappa_2^2(1-\gamma) + \varkappa_3^2\gamma - m^2\gamma(1-\gamma)} \cdot \ln\lambda + \varphi_1(\varkappa_2^2, \varkappa_3^2)\gamma(i\hat{p}_1 + m)\right.$$

$$\left.\times\left[\frac{1}{2}\ln^2\lambda(1-\gamma) - \frac{m^2\ln(\varkappa_2^2(1-\gamma) + \varkappa_3^2\gamma - m^2\gamma(1-\gamma)) + p_1^2\ln(\varkappa_2^2(1-\gamma) + \varkappa_3^2\gamma + p_1^2\gamma(1-\gamma))}{m^2 + p_1^2} \cdot \ln\lambda\right]\right\} \qquad (20)$$

The condition given above for the slowness of increase for large values of $\hat{p}_1$ leads to the requirement

$$\int d\varkappa_2^2\, d\varkappa_3^2\, \varphi_1(\varkappa_2^2, \varkappa_3^2) = 0. \qquad (21)$$

When (21) holds it is easy to obtain the relation between $\varphi_0(\kappa_2^2, \kappa_3^2)$ and $\varphi_1(\kappa_2^2, \kappa_3^2)$ and the functions $\sigma_1(\kappa^2)$ and $\sigma_2(\kappa^2)$ in the representation for $G(\hat{p})$. If

$$G(\hat{p}) = \frac{1}{i\hat{p} + m} + \int_{(m+\mu)^2}^{\infty} d\varkappa^2 \frac{-i\hat{p}_1\sigma_1(\varkappa^2) + \sigma_2(\varkappa^2)}{p^2 + \varkappa^2 - i\varepsilon}, \qquad (22)$$

then

$$\sigma_1(\varkappa^2) = \frac{1}{2\varkappa^4}\int d\varkappa_2^2\, d\varkappa_3^2\, \vartheta(\varkappa - \varkappa_2 - \varkappa_3)$$

$$S(\varkappa, \varkappa_2, \varkappa_3)(\varkappa_2^2 - \varkappa_3^2 - \varkappa^2)\varphi_1(\varkappa_2^2, \varkappa_3^2), \qquad (23)$$

$$\sigma_2(\varkappa^2) = \frac{1}{2\varkappa^2}\int d\varkappa_2^2\, d\varkappa_3^2\, \vartheta(\varkappa - \varkappa_2 - \varkappa_3)$$

$$S(\varkappa, \varkappa_2, \varkappa_3)\varphi_0(\varkappa_2^2, \varkappa_3^2). \qquad (24)$$

These relations are also self consistent in the sense that the right hand side differs from zero only for $\kappa^2 > (m+\mu)^2$.

In conclusion I would like to express my thanks to I. T. Dyatlov for an exceedingly useful discussion.

[1] J. Schwinger, Paper given at the 7-th Rochester Conference on High Energy Physics.

[2] V. N. Gribov, J. Exptl. Theoret. Phys. (U.S.S.R.) **34**, 1310 (1958), Soviet Phys. JETP **7**, 903 (1958).

[3] G. Källen, Dan. Mat.-Fys. Medd. **27**, 12 (1953).

[4] Lehmann, Symanzik, and Zimmerman, Nuovo cimento **2**, 3 (1955).

Translated by G. Volkoff
91

BEHAVIOR OF A CONDUCTING GASEOUS SPHERE IN A QUASI-STATIONARY ELECTROMAGNETIC FIELD

V. V. YANKOV

P. N. Lebedev Physics Institute, Academy of Sciences, U.S.S.R.

Submitted to JETP editor August 16, 1958

J. Exptl. Theoret. Phys. (U.S.S.R.) 36, 560-564 (February, 1959)

The stability of a homogeneous plasma sphere of infinite conductivity in an external quasi-stationary electromagnetic field is investigated by perturbation-theory methods.

In recent years a number of papers have appeared which consider the equilibrium states of an isolated plasma in an external electromagnetic field (cf. references 1 — 3). Equilibrium between the field and the bound plasma configuration obtains by virtue of equilibration of the electrodynamic and hydrostatic forces. The behavior of an equilibrium system of this type, in particular as it pertains to problems of stability, are of great interest.[4] The stability of a plasma is also of great interest in connection with methods of radiation acceleration of charged-particle bunches.[5]

In the present work perturbation theory is used to investigate the stability of a conducting sphere comprising a completely ionized gas which is located in an external quasi-stationary field.

It is assumed that the electrical conductivity of the plasma is infinite. The plasma sphere itself is considered a uniform adiabatic system which obeys the equation of state of an ideal gas and is characterized by one external parameter — the radiation pressure at the surface (gravitational forces are neglected).

PLASMA SPHERE IN A UNIFORM FIELD

For simplicity we first consider a gaseous sphere of infinite conductivity located in a quasi-stationary spatially uniform electromagnetic field; the field components are given functions of time:

$$\mathbf{E} = \{E_x, E_y, E_z\} = E_0\{\exp(i\Omega_{1e}t), \exp(i\Omega_{2e}t), \exp(i\Omega_{3e}t)\},$$
$$\mathbf{H} = \{H_x, H_y, H_z\} = H_0\{\exp(i\Omega_{1m}t), \exp(i\Omega_{2m}t), \exp(i\Omega_{3m}t)\}, \quad (1)$$

where all frequencies Ω differ from each other. The effective amplitude of this alternating (rotating) field is independent of direction; thus the mean pressure is uniform everywhere over the surface of the sphere and equilibrium obtains for the spherical shape. Obviously the field in (1) can only be an approximation to any actual electromagnetic fields of this form and is actually a superposition of standing or traveling waves which are polarized in various directions. Actually, if the dimensions of the bunch are small compared with the wavelength (quasi-stationary case) the inhomogeneity and wave properties of the field can be neglected in considering all problems except those which relate to the behavior of the bunch as a whole (these will be considered separately).

The investigation of the stability of a plasma sphere in the field given by (1) is carried out by means of an energy approach. Since the quasi-stationary conditions are satisfied we can determine the electromagnetic energy of a bunch in the external field (1) starting from well-known formulas of electrostatics magnetostatics.* An ideally conducting plasma bunch which cannot be penetrated by an alternating electromagnetic field ($\mathbf{E}^{int} = 0$, $\mathbf{B}^{int} = \mu$, $\mathbf{H}^{int} = 0$) may be considered phenomenologically as a body with infinite dielectric susceptibility $\epsilon \to \infty$ and zero magnetic permeability $\mu = 0$. Then the potential energy in the external field at any instant of time is given by

$$U(t) = \frac{1}{8\pi}\int (\mathbf{H}^{int}\cdot\mathbf{H} - \mathbf{D}^{int}\cdot\mathbf{E})\, dv. \quad (2)$$

In Eq. (2) the integration is carried out over the volume of the bunch while the magnetic field $\mathbf{H}^{int} = -\operatorname{grad}\psi_m^{int}$ and the electric induction $\mathbf{D}^{int} = -\operatorname{grad}\psi_e^{int}$ inside the bunch are found from the solutions of the Laplace equation

$$\Delta\psi_m = 0, \quad \Delta\psi_e = 0 \quad (3)$$

for potentials which satisfy the boundary conditions

$$\psi_m^{int} = \psi_m^{ext}, \quad \psi_e^{ext} = 0,$$
$$\partial\psi_m^{ext}/\partial n = 0, \quad \partial\psi_e^{int}/\partial n = \partial\psi_e^{ext}/\partial n \quad (4)$$

at the surface of the bunch. The basic problem

*Our attention was directed to this fact by M. L. Levin.

now becomes the determination of the mean potential energy of the bunch in a given external field as a function of the variables which characterize arbitrarily small deformation of the sphere. Let the surface be characterized by a function $R(\vartheta, \varphi)$ which characterizes the distance from the center of the sphere to a point on the surface given by the angles ϑ and φ in a spherical system of coordinates; the origin is taken at the center of the sphere. $R(\vartheta, \varphi)$ can be expanded in spherical functions:

$$R(\vartheta, \varphi) = R_0\Big[1 + \sum_{l=0}^{\infty}\sum_{m=-l}^{l} \alpha_{lm} Y_l^m(\vartheta, \varphi)\Big].$$

The expansion coefficients α_{lm} are generalized coordinates; at any instant of time these determine uniquely a definite arbitrary configuration of the surface of the bunch. In analyzing the motion in the neighborhood of the equilibrium configuration we limit ourselves to weak perturbations of the sphere, in which case $\alpha_{lm} \ll 1$.

In accordance with perturbation theory, the solutions of Eq. (3) which satisfy (4) at the boundary of the bunch are sought as a series in increasing powers of the small deformation parameters α_{lm}. We limit ourselves to second-order perturbations and neglect intermediate contributions, giving only the final result. The time average of the electromagnetic potential energy of an infinitely conducting plasma bunch in a quasi-stationary external field (1) is given by the expression

$$\bar{U} = \frac{9H_0^2}{32\pi} V_0 \left\{\left(1 - 2\frac{E_0^2}{H_0^2}\right)\frac{V}{V_0} + \sum_{l=2}^{\infty}\sum_{m=-l}^{l} \frac{3}{4\pi} N_{lm} \frac{(2l-1)(l-1)}{2(2l+1)} \times \left[1 - \frac{4}{3}\frac{(l+1)l}{l-1}\frac{E_0^2}{H_0^2}\right]\alpha_{lm}^2\right\}, \quad (5)$$

where $V_0 = 4\pi R_0^3/3$ is the equilibrium volume of the bunch, N_{lm} is the index of the spherical function $Y_l^m(\vartheta, \varphi)$. The summation in (5) starts with $l = 2$. When $l = 0$ only the volume of the sphere is changed and the deformation corresponding to $l = 1$ is associated with the displacement of the sphere as a whole, which makes no contribution to the energy in the case of a uniform field.

Writing the deformation parameters α_{lm} in the form of functionals

$$\alpha_{lm} = N_{lm}^{-1}\int_0^{2\pi}\int_0^{\pi} (R/R_0)\, Y_l^m \sin\vartheta\, d\vartheta\, d\varphi \approx N_{lm}^{-1} R_0^{-3}\int_S RY_l^m d\sigma,$$

where the integration is carried out over the surface of the bunch, we find the mean pressure as a variational derivative of the potential energy:

$$P(\vartheta, \varphi) = \frac{\delta\bar{U}}{\delta R} = \frac{9H_0^2}{32\pi}\left\{\left(1 - 2\frac{E_0^2}{H_0^2}\right) + \sum_{l=2}^{\infty}\sum_{m=-l}^{l} \frac{(2l-1)(l-1)}{2l+1} \times \left[1 - \frac{4}{3}\frac{(l+1)l}{l-1}\frac{E_0^2}{H_0^2}\right]\alpha_{lm} Y_l^m(\vartheta, \varphi)\right\}. \quad (6)$$

The term in Eq. (6) which is independent of deformation is the constant electromagnetic pressure

$$P_0 = \frac{9H_0^2}{32\pi}\left(1 - 2\frac{E_0^2}{H_0^2}\right),$$

which is directed along the normal to the surface (inward or outward). Adding to Eq. (5) the expression for potential energy corresponding to the work performed by the gas in the adiabatic process we obtain the total potential energy of a uniform plasma bunch near equilibrium:

$$\bar{U} + W_g = \frac{9H_0^2}{32\pi} V_0 \left\{\left(1 - 2\frac{E_0^2}{H_0^2}\right)\left[1 + \frac{1}{\gamma - 1} + \frac{\gamma}{2}\left(\frac{V - V_0}{V_0}\right)^2\right] + \sum_{l=2}^{\infty}\sum_{m=-l}^{l} \frac{3}{4\pi} N_{lm} \frac{(2l-1)(l-1)}{2(2l+1)}\left[1 - \frac{4}{3}\frac{(l+1)l}{l-1}\frac{E_0^2}{H_0^2}\right]\alpha_{lm}^2\right\}, \quad (7)$$

where $\gamma = c_p/c_v$ is the ratio of the specific heats. An analysis of the last expression yields certain conclusions regarding the behavior of a conducting gaseous sphere in electromagnetic fields such as those described by Eq. (1).

We first consider the effect of a uniform quasi-stationary magnetic field (a field of this type was used in the work reported by Knox[3]). In Eq. (7) we set $E_0 = 0$, thereby obtaining a situation of minimum potential energy for $V = V_0$; then all the $\alpha_{lm} = 0$. Whence it follows that a spherical bunch of radius R_0 is stable against an arbitrary small deformation.

In the case in which only an electric field operates the surface of the sphere is subject to forces of negative electric pressure, $P_0 < 0$; thus a bunch in a void cannot be in equilibrium.

In the general case of superposition of electric and magnetic fields a stable volume for a bunch in a void is possible only if the fixed radiation pressure is positive, $P_0 > 0$, i.e., the following relation must be satisfied: $H_0^2 > 2E_0^2$. The nature of the stability with respect to various deformations is determined by the sign of the quantity

$$\gamma_l = 1 - \frac{4}{3}\frac{(l+1)l}{(l-1)}\frac{E_0^2}{H_0^2},$$

which depends on the ratio of the electric and magnetic field amplitudes and on the deformation index l. A bunch is stable against elementary deforma-

tion characterized by the indices l and m if $\eta > 0$ and is unstable if $\eta < 0$. In particular, in order for a spherical bunch to be stable against a simple ellipsoidal deformation[6] ($l = 2$) the inequality $H_0^2 > 8E_0^2$ must be satisfied (the same applies for $l = 3$). As the value of l increases, denoting more complicated deformations, the relation between the electric and magnetic fields becomes more stringent; when $l \gg 1$ this relation becomes $H_0^2 > 4E_0^2 l/3$. Whence it follows that in the presence of an electric field an ideally conducting bunch can be stable only against deformations which are characterized by a finite number of first surface harmonics satisfying the relation

$$\eta > 0. \tag{8}$$

The nature of the stability criterion (8) is intimately related to the basic assumptions made at the beginning of this paper concerning the ideal electrical conductivity of the plasma. As applied to a real bunch this supposition is valid as long as the wavelength $\lambda = 2\pi R_0/l$ of the corresponding surface harmonics is much greater than the skin depth d.

STABILITY IN A QUASI-UNIFORM FIELD

Above we have investigated the stability of a plasma bunch in an idealized spatially uniform field (1). In treating actual cases we must take account of the small inhomogeneity in the external field.

We consider a conducting plasma sphere in an external quasi-uniform field which may conveniently be written as follows:

(1) Quasi-uniform electric field

$$\mathbf{E}_e(\mathbf{r}) = \mathbf{E}_0 + \mathbf{E}_{1e}(\mathbf{r}), \quad \mathbf{H}_e(\mathbf{r}) = \mathbf{H}_{1e}(\mathbf{r}); \tag{9}$$

(2) Quasi-uniform magnetic field

$$\mathbf{H}_m(\mathbf{r}) = \mathbf{H}_0 + \mathbf{H}_{1m}(\mathbf{r}), \quad \mathbf{E}_m(\mathbf{r}) = \mathbf{E}_{1m}(\mathbf{r}), \tag{10}$$

where $\mathbf{E}_0$ and $\mathbf{H}_0$ are given by (1) as before and the small fields denoted by the subscript "1" are not considered in detail but merely characterize the small inhomogeneity of the applied field. We now use Eqs. (9) and (10) in place of (1) in the original expression for the potential energy. Taking account of the small variation of the external field over the bunch, we obtain an approximate expression for the mean potential energy in a quasi-uniform field:

$$\overline{U}(\mathbf{r}, V, \alpha) = \overline{U}(\mathbf{r}) + \overline{U}(V, \alpha),$$

where $\overline{U}(V, \alpha)$ corresponds to the formula derived earlier (7), while

$$\overline{U}(\mathbf{r}) = \frac{3}{16\pi} V_0 [2(\mathbf{H}_0 \cdot \mathbf{H}_{1m} - 2\mathbf{E}_0 \cdot \mathbf{E}_{1e}) + (H_{1e}^2 - 2E_{1m}^2) + (H_{1m}^2 - 2E_{1e}^2)]_{av}$$

depends on the position of the bunch as a whole in the quasi-uniform field ($\mathbf{r}$ is the relative coordinate of the center of the bunch). The forces which act on a spherical bunch, at the center of which the amplitudes of the external fields reach their maximum values E_0 and H_0, vanish when integrated over the volume; thus, the bunch as a whole is in a state of quilibrium in the inhomogeneous field. The nature of the stability is determined by the sign of $\overline{U}(\mathbf{r})$ in the neighborhood of equilibrium.

We may illustrate the application of this analysis by a simple example, using the superposition of six standing plane waves with different wave numbers $k = \Omega/c$ in an appropriate configuration. It is not difficult to show that in this quasi-uniform wave field

$$\overline{U}(\mathbf{r}) = \frac{9H_0^2}{32\pi} V_0 \left[\left(\frac{E_0^2}{H_0^2} k_{2e}^2 - k_{2m}^2 \right) x^2 + \left(\frac{E_0^2}{H_0^2} k_{3e}^2 - k_{3m}^2 \right) y^2 + \left(\frac{E_0^2}{H_0^2} k_{1e}^2 - k_{1m}^2 \right) z^2 \right],$$

where x, y, z denotes the departure of the center of the sphere from the location of the common antinode of the standing waves. From this follows the stability criterion:

$$H_0^2/E_0^2 < (k_{je}/k_{jm})^2, \quad j = 1, 2, 3. \tag{11}$$

Comparing Eq. (11) with the criterion for internal stability of a highly conducting bunch ($d \ll R_0$) with respect to a change of volume and shape:

$$H_0^2/E_0^2 > 4(l+1)\,l/3(l-1), \quad 2 \leqslant l < \pi R_0/2d,$$

we see that these inequalities are incompatible with respect to field amplitudes. However, since the first relation involves amplitudes which are related to the wave properties of the fields while the second involves only quasi-static properties, over a wide region of wave numbers for which

$$k_{je}^2/k_{jm}^2 > 4(l+1)\,l/3(l-1),$$

both inequalities can be satisfied simultaneously and a spherical bunch is characterized by stability with respect to all simple types of small perturbations of volume, shape, and position in an external field.

Similar results can be obtained in fields which are more complicated than plane-wave fields; for example we may consider fields which are formed by an appropriate configuration of axially symmetric electric and magnetic waves.

In conclusion we may point out that in a general

consideration of bunches of charged particles one must inevitably encounter difficulties which stem from the fact that the system has a limited number of degrees of freedom. The rather crude phenomenological model used in the present paper does, however, indicate the basic features of the behavior of plasma in quasi-stationary fields.

Inasmuch as the purpose of the present note was to investigate the stability of a highly conducting gaseous sphere in an external field we have limited ourselves to small deformation of the surface and have not considered transient effects.

The author wishes to thank Prof. M. S. Rabinovich for valuable discussions of this work.

[1] M. Krushkal and M. Schwarzschild, Proc. Roy. Soc. (London), **A223**, 348 (1954); V. D. Shafranov, Атомная энергия (Atomic Energy) **5**, 38 (1956).

[2] V. D. Shafranov, J. Exptl. Theoret. Phys. (U.S.S.R.) **33**, 710 (1957), Soviet Phys. JETP **6**, 545 (1958).

[3] F. B. Knox, Australian J. Phys. **10**, 221, 565 (1957).

[4] V. I. Veksler, L. M. Kovrizhnykh, M. S. Rabinovich and V. V. Yankov, Possibility of Using Electromagnetic Waves for Stabilization of Plasma Bunches, Report of the Inst. Phys. Acad. Sci. August, 1956.

[5] V. I. Veksler, Атомная энергия (Atomic Energy) **2**, 427 (1957).

[6] V. V. Yankov, The Stability of a Quasi-Ellipsoidal Plasma Bunch in an Alternating Electromagnetic Field, Report of the Inst. Phys. Acad. Sci., 1957.

Translated by H. Lashinsky
92

THE INFLUENCE OF THE ELECTRON-PHONON INTERACTION ON THE CYCLOTRON RESONANCE FREQUENCY

A. V. TULUB

Leningrad State University

Submitted to JETP editor August 22, 1958

J. Exptl. Theoret. Phys. (U.S.S.R.) 36, 565-573 (February, 1959)

The electron-phonon interaction in polar crystals leads to a non-linear dependence of the cyclotron resonance frequency on the magnetic field strength. An evaluation of the non-linear terms shows that they are small for the magnetic fields used in practice. The polaron effect also gives a correction to the diamagnetic susceptibility. In this paper we perform a mass renormalization in a magnetic field without assuming that the coupling constant is small.

THE cyclotron-resonance phenomenon takes place in a uniform magnetic field, provided the frequency of the additional, variable field is equal to twice the Larmor frequency $2\omega_0 = eH/m^*$. From experiments on cyclotron resonance one can find the magnitude of the effective mass m^*, or, in the general case, of the mass tensor. In the present paper the influence of the electron-phonon interaction on the cyclotron resonance frequency is considered. If the periodic field of the lattice is taken into account, as is usually done, by the introduction of an effective mass, the interaction with the lattice leads to a change (renormalization) of that mass. If there is an external magnetic field, this renormalized mass will in that case depend on the field strength H. The frequency ω_0 will thus be a nonlinear function of H. The problem consists in evaluating the nonlinear terms. These terms will also influence the magnetic properties of the electrons.

In the following we shall consider the case of polar crystals, and for the sake of simplicity we shall assume the effective mass to be isotropic.

The interaction of the electrons with the lattice cannot be considered as a perturbation in the case of polar crystals. For large values of the coupling constant α the adiabatic approximation[1] is valid, and for $\alpha = 1$ to 4 the intermediate coupling approximation. We shall consider the latter case below.

The method of mass renormalization when a magnetic field is present which is developed in the present paper is based upon the approximate elimination of the variables of the phonon field from the energy operator. One can find the action of the phonon absorption operator a_k on the eigenfunctional Ω of the energy operator by evaluating the commutator of a_k with the Hamiltonian $\mathcal{H}$. This method was proposed in meson theory by Chew, Low, and Wick.[2] The result of the action of a_k on Ω is the multiplication of the functional Ω by some function which will depend on the electron momentum as a parameter. Thus in the evaluation of the average value of the energy the phonon field operators give additional terms depending on the electron momentum. The terms quadratic in the momentum will determine the magnitude of the renormalized mass.

In the evaluation of $a_k\Omega$ there arises a difficulty connected with the fact that the action of a_k on Ω is expressed in terms of the momentum operator of the phonon field which arises when recoil is taken into account. This operator is replaced in the expression for $a_k\Omega$ by its average value which is evaluated below.

This method to take the momentum into account is in the case of a free polaron equivalent to the following model. It is assumed that all phonons which form a cloud around the electron possess identical "radial functions" which can be found from a variational principle.[3] For the case of a polaron at rest a more exact variational principle[4] was proposed.

THE ELIMINATION OF THE PHONON FIELD VARIABLES FROM THE ENERGY OPERATOR

We consider the electron energy operator in a magnetic field, taking into account the interaction between the electron and the field of the longitudinal optical phonons, which is known from the polaron theory[1,3]

$$\mathcal{H} = \frac{\pi^2}{m} + \sum_k \omega a_k^+ a_k + \sum_k (V_k a_k e^{ikx} + V_k^* a_k^+ e^{-ikx}), \quad (1.1)$$

a_k are the second-quantization operators,

$$V_k = -\frac{i\omega}{k}\left(\frac{4\pi\alpha}{L^3}\right)^{1/2}(2m\omega)^{-1/4}, \quad \alpha = e^2\left(\frac{m}{2\omega}\right)^{1/2}\left(\frac{1}{n^2} - \frac{1}{\epsilon}\right),$$
$$\pi = -i\nabla - eA, \quad (1.2)$$

ω is the limiting frequency of the longitudinal optical vibrations, ϵ the static dielectric constant, and n the refractive index for light.*

We assume that the magnetic field is directed along the 3-axis. The commutation relations for the operators π_i will have the form

$$[\pi_1, \pi_2] = ieH; \quad (1.3)$$

the other commutators being equal to zero.

We shall write the eigenfunctional Ψ of the energy operator (1.1) in the form

$$\Psi\{a\} = \exp\left\{i\left(\pi_3 x_3 - \sum_k (\mathbf{k}\cdot\mathbf{x})\, a_k^+ a_k\right)\right\}\Omega\{a\}. \quad (1.4)$$

Substituting (1.4) into (1.1) we get the following equation for the functional Ω:

$$\left\{\pi^2/2m + \sum_k (\omega + k^2/2m - (\mathbf{k}\pi)/m)\, a_k^+ a_k + \sum_k (V_k a_k + V_k^* a_k^+)\right.$$
$$\left. + (1/2m)\sum_{k,k'} (\mathbf{k}\cdot\mathbf{k}')\, a_k^+ a_{k'}^+ a_k a_{k'}\right\}\Omega = E\Omega. \quad (1.5)$$

In Eq. (1.5) π_3 is a number, and not an operator, since the quantity

$$\pi_3 = -i\nabla_3 + \sum_k k_3 a_k^+ a_k$$

is an integral of motion.

To eliminate the phonon field variables from the energy operator we shall evaluate the commutator of the energy operator with the operator a_k:

$$[\mathcal{H}, a_k] = -V_k^* - (k^2 + c^2 - 2\mathbf{k}\cdot\boldsymbol{\pi})/2m - (\mathbf{k}\cdot\mathbf{q})\, a_k/m,$$
$$\mathbf{q} = \sum_k \mathbf{k} a_k^+ a_k, \quad c^2 = 2m\omega. \quad (1.6)$$

Letting the operators in the left hand and the right hand side of (1.6) act on the functional Ω we get

$$a_k\Omega = -2mV_k^*\{2m(\mathcal{H} - E)$$
$$+ k^2 + c^2 - 2\mathbf{k}\cdot\boldsymbol{\pi} + 2\mathbf{k}\cdot\mathbf{q}\}^{-1}\Omega. \quad (1.7)$$

Since V_k^* is a function it is immaterial in what order V_k^* is written down, and this is taken into account in (1.7).

For the following it is convenient to use the following integral transform for the inverse operator L^{-1}:

$$L^{-1} = i\int_0^\infty e^{-isL}ds. \quad (1.8)$$

*We use a system of units for which $\hbar = 1$, $c = 1$.

The transform (1.8) is analogous to V. A. Fock's eigen time method in relativistic quantum mechanics. The integral on the right hand side of (1.8) must be considered to be the limiting value of the expression

$$\lim_{\delta\to 0} i\int_0^\infty e^{-isL-\delta s}ds.$$

We shall rewrite (1.7) in the form

$$a_k\Omega = -2miV_k^*\int_0^\infty ds \exp\{-is(k^2 + c^2)$$
$$- is[2m(\mathcal{H} - E) - 2\mathbf{k}\cdot\boldsymbol{\pi} + 2\mathbf{k}\cdot\mathbf{q}]\}\,\Omega \quad (1.7a)$$

taking (1.8) into account. The next transformations raises the problem of "disentangling" the operator $\exp\{-is\,2m\,(\mathcal{H} - E)\}$ from the exponent in (1.7a) in the form of a factor.

To ascertain the character of the next approximation we shall consider to begin with that case where there is no magnetic field and where one can thus manipulate the operators π_i as numbers. The intermediate coupling method used by Lee, Low, and Pines[3] is equivalent to the following simplification of Eq. (1.7a). If we neglect the commutator $[q, \mathcal{H}]$, the action of the absorption operator a_k on the state functional is expressed by the equation

$$a_k\Omega = -2mi\,V_k^*\int_0^\infty ds$$
$$\times\exp\{-is(k^2 + c^2 - 2\mathbf{k}\cdot\boldsymbol{\pi} + 2\mathbf{k}\cdot\mathbf{q})\}\,\Omega. \quad (1.9)$$

Replacing the operator q in (1.9) by its average value, evaluated with the functionals Ω, and taking into account that because of symmetry the average value of the phonon field momentum will be directed solely along the only vector which occurs in the problem, π ($\langle q\rangle = \eta\pi$), we obtain from (1.9) an approximate expression for $a_k\Omega$, where the parameter η is evaluated from the above-mentioned relation $\langle q\rangle = \eta\pi$. If a variational method is used for the functional of the phonon field, this approximation corresponds, according to reference 3, to the assumption that all phonons are in the same state.

The renormalization of the mass when there is a magnetic field proceeds in the same approximation: we assume that after disentangling the exponent in (1.9) we can assume $[q, \mathcal{H}] = 0$ and after that replace q by its average value.

We shall now return to Eq. (1.7a). We first of all single out the operator $\exp\{2isk\cdot\pi\}$, taking into account that the operators π_1 and π_2 do not commute with one another. We shall use the equations (see Appendix A).

$$\exp\{-is(k^2+\pi^2-2\mathbf{k}\cdot\boldsymbol{\pi}-2\mathbf{q}\cdot\boldsymbol{\pi})\}$$

$$=\exp\{-is[k_3^2+\xi(k_1^2+k_2^2)]\}\exp\{2is(\mathbf{k},\boldsymbol{\Pi}-\mathbf{Q}+\mathbf{q})\}$$

$$\times\exp\{-is(\pi^2-2\boldsymbol{\pi}\cdot\mathbf{q})\}. \qquad (1.10)$$

where

$$\xi(x)=(2x)^{-1}\sin 2x, \qquad (1.11)$$

$$\Pi_1(x)=x^{-1}(\sin x)(\pi_1\cos x-\pi_2\sin x), \qquad (1.12)$$

$$\Pi_2(x)=x^{-1}(\sin x)(\pi_2\cos x+\pi_1\sin x),\quad \Pi_3=\pi_3,$$

$$[\Pi_1,\Pi_2]=ieH(x^{-1}\sin x)^2. \qquad (1.13)$$

The quantities Q_i are expressed in terms of the q_i in the same way as the Π_i are expressed in terms of the π_i in (1.12) and (1.13). In Eq. (1.10) and in the following equations Π_1 and Π_2 are functions of the argument $x = eHs$ which we shall drop for the sake of simplicity.

Neglecting the commutator of q with $\mathcal{H}$ we obtain from (1.7a) the following expression for $a_k\Omega$:

$$a_k\Omega=-2miV_k^*\int_0^\infty ds$$

$$\times\exp\{-is(c^2+k_3^2+\xi(k_1^2+k_2^2)-2\mathbf{k}(\boldsymbol{\Pi}-\mathbf{Q}))\}\Omega. \qquad (1.14)$$

As was pointed out above, the quantity Q will in the following be replaced by its average value where the average value is understood to be the average over the phonon field variables. If we write the functional Ω in the form $\Omega=\Phi\{a\}\psi(x)$, after this averaging the quantity $\langle q_i\rangle=\langle\Phi, q_i\Phi\rangle$ is still an operator, acting upon the function ψ.

There is in this way a connection between the average values of the phonon field operator and the operators π_i arising from taking the properties of the state functional Ω into account. By themselves, of course, the operators a_k and π are dynamically independent.

We shall now turn to the evaluation of the average value of the phonon field momentum operator.

EVALUATION OF THE CONSTANTS DETERMINING THE MASS RENORMALIZATION

We shall assume that $\langle q_i\rangle$ and π_i are also in the case of a free polaron proportional to one another:

$$\langle q_1\rangle=\eta_1\pi_1,\quad \langle q_2\rangle=\eta_1\pi_2,\quad \langle q_3\rangle=\eta_3\pi_3. \qquad (2.1)$$

The validity of this assumption is confirmed by the following consideration: if we substitute (2.1) into (1.14) and evaluate the average value of q_i with the $a_k\Omega$ defined in that way, it turns out that, indeed, the average value of q_i is proportional to π_i.

From (1.7a) we have

$$\langle\Omega, q_i\Omega\rangle=-4m^2\sum_k k_i|V_k|^2\int_0^\infty s\,ds$$

$$\times\langle\Omega,\exp\{-is[c^2+k^2-2\mathbf{k}\cdot\boldsymbol{\pi}$$

$$+2\mathbf{k}\cdot\mathbf{q}+2m(\mathcal{H}-E)]\}\Omega\rangle. \qquad (2.2)$$

The operator $\exp\{-2is(\mathcal{K}-E)\}$ in (2.2) can with equal convenience be taken out as a factor to the right as to the left of the other operators. Taking half of the sum of these two expressions and using (1.2) and the relation

$$k^{-2}=i\int_0^\infty e^{-i\tau k^2}d\tau \qquad (2.3)$$

we get the following expression

$$\langle\Omega, q_i\Omega\rangle=-i\frac{4\pi\alpha}{(2\pi)^3}c^3\int k_i d^3k\int_0^\infty d\tau$$

$$\times\int_0^\infty sds\,\langle\Omega,\exp\{-isc^2-i(\tau+s)k_3^2-i(\tau+\xi s)(k_1^2+k_2^2)\}$$

$$\times\frac{1}{2}[\exp\{2isk\widetilde{\Pi}(eHs)\}+\exp\{2isk\widetilde{\Pi}(-eHs)\}]\Omega\rangle, \qquad (2.4)$$

where

$$\widetilde{\Pi}_i=(1-\eta_i)\Pi_i \text{ for } i=1,2;\quad \widetilde{\Pi}_3=(1-\eta_3)\Pi_3.$$

It is clear from (2.4) that $\langle q_i\rangle$ is an even function of H. In evaluating the integral over d^3k (see Appendix B) we used the formula

$$e^Ae^B=e^{A+B}e^{[A,B]/2}; \qquad (2.5)$$

where [A, B] is a number

In the integration over $d\tau\,ds$ we expanded the integrand in powers of H, after which the integrals were evaluated using

$$\int_0^\infty d\tau\int_0^\infty ds\,s^n\frac{e^{-isc^2}}{(\tau+s)^{m/2}}=\frac{\sqrt{\pi}(2k-1)!!}{2^kc^{2k+1}(m/2-1)}e^{-i\pi(2k+1)/4}; \qquad (2.6)$$

where n and m are integers, $2k = 2n - m + 3$.

In the asymptotic expansion so obtained we retain the quadratic terms in $(\omega_0/\omega)^2$. As a result we get the following equation to determine η

$$\eta_i=(1-\eta_i)\frac{\alpha}{6}\left\{1-\left(\frac{\omega_0}{\omega}\right)^2\left[\frac{1}{2}-\frac{45}{56}(1-\eta_i)^4\right]\right\}. \qquad (2.7)$$

Assuming moreover that

$$\eta_i=\eta_i^{(0)}+\eta_i^{(1)},\qquad \eta_i^{(0)}=\frac{\alpha}{6}\Big/\left(1+\frac{\alpha}{6}\right),$$

we find

$$\eta_i=\eta_i^{(0)}\left\{1-\left(1+\frac{\alpha}{6}\right)^{-1}\left(\frac{\omega_0}{\omega}\right)^2\left[\frac{1}{2}-\frac{45}{56}\left(1+\frac{\alpha}{6}\right)^{-4}\right]\right\}. \qquad (2.8)$$

The function η_3 turns out to be equal to

$$\eta_{l3} = \eta_l^{(0)} \left\{1 - 3\left(1+\frac{\alpha}{6}\right)^{-1}\left(\frac{\omega_0}{\omega}\right)^2\left[\frac{1}{2} - \frac{15}{56}\left(1+\frac{\alpha}{6}\right)^{-4}\right]\right\}. \quad (2.9)$$

The action of a_k upon Ω is thus in the approximation under consideration completed determined.

The problem now consists in evaluating the average values of the phonon field operators in the Hamiltonian (1.5).

We shall consider the expression $\langle \sum_k a_k^+ (\mathbf{k}\cdot\boldsymbol{\pi}) a_k \rangle$.

From (1.7) and (1.8) we have

$$\langle \sum_k a_k^+ (\mathbf{k}\cdot\boldsymbol{\pi})\, a_k \rangle$$

$$= -4m^2 \sum_k |V_k|^2 \int_0^\infty ds \int_0^\infty ds' \, \langle e^{-isL} (\mathbf{k}\cdot\boldsymbol{\pi}) e^{-is'L} \rangle. \quad (2.10)$$

Expression (2.10) can conveniently be evaluated as follows. We shift the operator $(\mathbf{k}\cdot\boldsymbol{\pi})$ first to the right of $\exp(-is'L)$ and then to the left of $\exp(-isL)$ and take half the sum of the expressions thus obtained which will be an even function of H as can easily be ascertained.

Using the formula

$$(\mathbf{k}\cdot\boldsymbol{\pi})\, e^{-is(\pi^2 - 2\mathbf{p}\cdot\boldsymbol{\pi})} = e^{-is(\pi^2 - 2\mathbf{p}\cdot\boldsymbol{\pi})} (\mathbf{k}\cdot\boldsymbol{\pi}' (2eHs) - eHs\,[\mathbf{k}\times\mathbf{p}]_3),$$

$$\pi_1'(x) = \pi_1 \cos x + \pi_2 \sin x,$$

$$\pi_2'(x) = \pi_2 \cos x - \pi_1 \sin x, \quad \pi_3'(x) = \pi_3, \quad (2.11)$$

we get after some transformations the following expression for the terms quadratic in the momenta π_1^2 and π_2^2

$$-i \frac{4\pi\alpha}{(2\pi)^3} c^3 \pi^{3/2} e^{-3i\pi/4} \int_0^1 d\nu \int_0^\infty d\tau \int_0^\infty ds \cdot s e^{-isc^2} \frac{s}{(\tau+s)^{1/2}(\tau+\xi s)^2}$$

$$\times \left(1 + \frac{s^2}{(\tau+\xi s)^2} \frac{\sin^4 eHs}{(eHs)^2} (1-\eta_l)^4\right)^{-1/2}$$

$$\times \frac{1}{2} \{\pi_1(-\nu sH)\, \tilde{\Pi}_1(esH)$$

$$+ \tilde{\Pi}_1(-esH)\, \pi_1'(\nu sH) + (1 \to 2)\}. \quad (2.12)$$

Integration over $d\nu$ gives

$$\int_0^1 d\nu \, \frac{1}{2} \{\ldots\} = (1-\eta_l)\left(\frac{\sin eHs}{eHs}\right)^2 (\pi_1^2 + \pi_2^2). \quad (2.13)$$

The remaining integration is carried out by means of (2.6).

After evaluating the average values of the field operators we obtained the following values for the renormalized mass:

$$m_{11}^* = m_{22}^* = m_\perp = m_0 \left\{1 + \left(\frac{\omega_0}{\omega}\right)^2 \left[\frac{29}{24}\alpha \left(1+\frac{\alpha}{6}\right)^{-1} - \frac{5}{12}\alpha - \frac{15}{14}\alpha\left(1+\frac{\alpha}{6}\right)^{-5}\right]\right\}; \quad (2.14)$$

$$m_{33}^* = m_\parallel = m_0 \left\{1 + \left(\frac{\omega_0}{\omega}\right)^2 \left[\frac{\alpha}{2}\left(1+\frac{\alpha}{6}\right)^{-1} - \frac{45}{112}\alpha\left(1+\frac{\alpha}{6}\right)^{-5}\right]\right\}; \quad (2.15)$$

$$m_0 = m\left(1+\frac{\alpha}{6}\right).$$

For $H = 0$ we get the renormalized mass value obtained in reference 3.

The ratio of the unrenormalized cyclotron resonance frequency to the renormalized one is, according to (2.14),

$$(\omega_0/\omega_0^*) = [1 + d_\perp(\alpha)(\omega_0/\omega)^2]. \quad (2.16)$$

In the intermediate coupling region the function $d_\perp(\alpha)$ is, apart from a factor of the order of unity, equal to

$$d(1) = 0.12; \; d(2) = 0.46; \; d(3) = 0.74; \; d(4) = 0.90.$$

Since the energies of the longitudinal optical phonons are about 0.01 ev the correction term in (2.16) is for all practically used fields vanishingly small, i.e., cyclotron resonance experiments give $m|_{H=0}$.

CORRECTION TO THE DIAMAGNETIC SUSCEPTIBILITY

As the result of the elimination of the phonon field variables, the energy operator takes the following form

$$\mathcal{H} = (\pi_1^2 + \pi_2^2)/2m_\perp + \pi_3^2/2m_\parallel. \quad (3.1)$$

We consider the problem of evaluating the density matrix $\rho(x, x', \beta)$ for an ideal gas, when the Hamiltonian of the system is given by Eq. (3.1). We write the matrix $\rho(x, x', \beta)$ in the form

$$\rho(x, x', \beta) = \langle x | \exp(-\beta\mathcal{H}) | x' \rangle, \quad (3.2)$$

where x stands for the three coordinates x_1, x_2, x_3. If we introduce the variable s, equal to $s = -i\beta$, instead of β, we can formally consider expression (3.2) as the transformation function $\langle x(s) | x'(0) \rangle$. The latter can be found from the following equations:[5,6]

$$i \frac{\partial}{\partial s} \langle x(s) | x'(0) \rangle = \langle x(s) | \mathcal{H} | x'(0) \rangle; \quad (3.3)$$

$$(-i\partial/\partial x - eA(x)) \langle x(s) | x'(0) \rangle = \langle x(s) | \pi(s) | x'(0) \rangle;$$

$$(i\partial/\partial x' - eA(x') \langle x(s) | x'(0) \rangle = \langle x(s) | \pi(0) | x'(0) \rangle \quad (3.4)$$

and the boundary condition

$$\lim_{s\to 0} \langle x(s) | x'(0) \rangle = \delta(x - x'). \quad (3.5)$$

To evaluate the transformation function it is necessary to solve the Heisenberg equations of motion

for the operators π and x. These equations have in the case considered the following form

$$dx/ds = P\pi;\ d\pi/ds = 2\omega_0 Q\pi; \tag{3.6}$$

$$P = \begin{pmatrix} m_\perp^{-1} & 0 & 0 \\ 0 & m_\perp^{-1} & 0 \\ 0 & 0 & m_\parallel^{-1} \end{pmatrix},\quad Q = \begin{pmatrix} 0 & 1 & 0 \\ -1 & 0 & 0 \\ 0 & 0 & 0 \end{pmatrix}. \tag{3.7}$$

The solution of equations (3.6) can be written in the form

$$\pi(s) = e^{2\omega_0 Qs}\pi(0);$$

$$x(s) = x(0) + (2\omega_0 Q)^{-1}(e^{2\omega_0 Qs} - 1)P\pi(0). \tag{3.8}$$

Using expression (3.8) we can express the energy operator as a function of the operators x(s) and x(0). Shifting x(s) to the left and x(0) to the right, we get after some transformations (see reference 5) the following equation

$$i\frac{\partial}{\partial s}\langle x(s)\,|\,x'(0)\rangle = \left\{\frac{1}{2}\omega_0^2(x-x')\,P^{-1}\frac{Q^2}{\sinh^2\omega_0 Qs}(x-x')\right.$$

$$\left. - i\omega_0 \mathrm{Sp}\,Q\,(1-e^{-2\omega_0 Qs})^{-1}\right\}\langle x(s)\,|\,x'(0)\rangle. \tag{3.9}$$

Taking the properties of the matrix Q into account we find

$$2\ \mathrm{Sp}\,Q\,(1-e^{-2\omega_0 Qs})^{-1} = \mathrm{Sp}\,Q\ \coth\omega_0 Qs$$

$$= 2\cot\omega_0 s + 1/\omega_0 s. \tag{3.10}$$

Integration of Eq. (3.9) gives the following value for the partition function Z

$$Z = \mathrm{Sp}\,\rho(x,\ x',\ \beta) = \frac{2V}{h^3}(2\pi kT)^{3/2} m_\perp m_\parallel^{1/2}\frac{\beta\hbar\omega_0}{\sinh\beta\hbar\omega_0}, \tag{3.11}$$

where V is the volume of the system.

Using (2.14) and (2.15), the diamagnetic susceptibility turns out to be equal to

$$\chi = -N\mu^2/3kT$$

$$+ NkT(2d_\perp + d_\parallel)\mu^2/\hbar^2\omega^2 = \chi_1 + \chi_2, \tag{3.12}$$

where $\mu = e\hbar/2mc$.

The relative order of magnitude is given by

$$|\chi_2/\chi_1| \sim (kT/\hbar\omega)^2.$$

The polaron effect leads thus to a change in the diamagnetic susceptibility. The correction term is appreciable at temperatures of the order of $kT \sim \hbar\omega$.

In conclusion I wish to express my gratitude to Academician V. A. Fock for discussing the present paper.

APPENDIX A

Introducing the operators

$$c = (2eH)^{-1/2}(\pi_1 + i\pi_2),\ c^+ = (2eH)^{-1/2}(\pi_1 - i\pi_2) \tag{A.1}$$

and using the notation

$$q' = (2eH)^{-1/2}(q_1 + iq_2),\ k' = (2eH)^{-1/2}(k_1 + ik_2), \tag{A.2}$$

we can rewrite $\exp\{-is(\pi^2 - 2\mathbf{k}\cdot\pi - 2\mathbf{q}\cdot\pi)\}$ in the form

$$\exp\{-is(\pi_3^2 - 2k_3\pi_3 - 2q_3\pi_3 + eH)\}$$

$$\times \exp\{-2ieHs(c^+c - q'c^+ - q'^+c - k'c^+ - k'^+c)\}.$$

We consider moreover the function

$$\Phi(\varepsilon) = \exp\varphi(\varepsilon) = \exp\{-2ieHs\ (c^+c - q'c^+$$

$$- q'^+c - \varepsilon(k'c^+ + k'^+c))\}. \tag{A.3}$$

To disentangle the operator $\exp\{2\mathrm{ieHs}(\mathrm{k}'\mathrm{c}^+ + \mathrm{k}'^+\mathrm{c})\}$ we write down the derivative[7]

$$\frac{d\Phi}{d\varepsilon} = \Phi(\varepsilon)\left\{\varphi' + \frac{1}{2!}[\varphi',\ \varphi] + \frac{1}{3!}[[\varphi',\ \varphi]\varphi] + \ldots\right\}. \tag{A.4}$$

After evaluating the commutators, one can sum the series. Integrating the equation thus obtained over ϵ from zero to unity we get the result given in the text.

APPENDIX B

We consider the evaluation of the integral

$$I = \int_{-\infty}^{+\infty} k_1 dk_1 \int_{-\infty}^{+\infty} dk_2 \exp\{-is\xi(k_1^2 + k_2^2)$$

$$+ 2is(k_1\Pi_1 + k_2\Pi_2)\}, \tag{B.1}$$

where $[\Pi_1, \Pi_2] = \mathrm{ieH}\lambda^2$.

Using (2.5) the integral over dk_2 is equal to

$$\exp(2isk_1\Pi_1)\int_{-\infty}^{+\infty} dk_2 \exp\{-is\xi k_2^2 + 2isk_2\ (\Pi_2 + k_1 eHs\lambda^2)\}$$

$$= \exp(2isk_1\Pi_1)\,e^{-i\pi/4}$$

$$\times (\pi/s\xi)^{1/2}\exp\{is_\xi^{-1}(\Pi_2 + k_1 eHs\lambda^2)^2\},$$

In integrating over dk_1 we must use (2.5) again.

After averaging the operators over the phonon field variables we must pick out the terms quadratic in the momenta. It is advisable first to symmetrize the exact values of the integrals. In (B.1), for instance, one can in the integration over dk_2 place the operator $\exp\{2\mathrm{isk}_1\Pi_1\}$ both to the left and to the right of the terms with the operator Π_2.

One can, finally, evaluate first of all the integral over dk_1 and then the integral over dk_2. The expressions obtained by that means differ by the arrangement of the operators Π_1 and Π_2 with

respect to one another. As a result the value of the integral (B.1) turns out to be equal to

$$I = -i\pi(\xi')^{-1}(s\xi)^{-1}(\Pi_1 T + T\Pi_1)/2, \quad \text{(B.2)}$$

$$T = \exp(is\Pi_1^2/2\xi)\exp(is\xi\Pi_2^2/\xi'^2)\exp(is\,\Pi_1^2/2\xi) + (1 \to 2),$$

$$(\xi')^2 = \xi^2 + (eHs)^2\lambda^4. \quad \text{(B.3)}$$

up to terms of the order $(eH)^3$. To simplify the expressions obtained we used the formula[7]

$$\exp(-ap^2)\exp(bq^2)\exp(ap^2)$$

$$= \exp\{b(q + 2iap)^2\}, \quad [q, p] = i. \quad \text{(B.4)}$$

[1] S. I. Pekar, Исследования по электронной теории кристаллов (Investigations on the Electronic Theory of Crystals) Gostekhizdat, 1951, [Untersuchungen über die Elektronentheorie der Kristalle, Akademie Verlag, Berlin, 1954.

[2] G. F. Chew and F. E. Low, Phys. Rev. **101**, 1570 (1956).

[3] Lee, Low, and Pines, Phys. Rev. **90**, 297 (1953).

[4] G. R. Allcock, Adv. Phys. **5**, 412 (1956).

[5] J. Schwinger, Phys. Rev. **82**, 664 (1951).

[6] P. A. M. Dirac, The Principles of Quantum Mechanics (Oxford, 1935).

[7] R. G. Newton, Phys. Rev. **96**, 523 (1954).

Translated by D. ter Haar
93

SCATTERING OF NEUTRONS BY ORIENTED NONSPHERICAL NUCLEI

G. L. VISOTSKIĬ, E. V. INOPIN, and A. A. KRESNIN

Physico-Technical Institute, Academy of Sciences, Ukrainian S.S.R.

Submitted to JETP editor August 23, 1958

J. Exptl. Theoret. Phys. (U.S.S.R.) **36**, 574-580 (February, 1959)

We consider the scattering of neutrons by oriented nonspherical nuclei. To calculate the scattering cross section we use the black-nucleus model. It is shown that nonsphericity effects are much more pronounced on oriented nuclei than on unoriented ones. It is also shown that a considerable azimuthal asymmetry appears in the angular distribution of neutrons scattered by oriented nonspherical nuclei.

1. INTRODUCTION

THE investigation of neutron scattering by nonspherical nuclei may yield much valuable information on the structure of atomic nuclei. However, as shown in many papers,[1,2] the nonsphericity under ordinary experimental conditions does not manifest itself strongly enough to permit reliable interpretation of the experimental results. For example, at neutron energies of several tens of Mev, the total neutron cross sections are changed by nonsphericity of the nuclei by only two or three percent (at the experimentally-observed values of nonsphericity).

The effects due to nonsphericity increase if the targets employed are oriented nuclei. Actually, we consider, for example, a black nucleus in the shape of an ellipsoid of revolution with semi-axes a and b (a is the major semi-axis, directed along the axial symmetry axis of the nucleus). If the nuclei are now oriented so that the symmetry axis of the nucleus coincides with the direction of the incident beam of neutrons, we obtain for the total cross section $\sigma_t^{\parallel} = 2\pi b^2$, but if the symmetry axis is directed perpendicular to the incident beam, we get $\sigma_t^{\perp} = 2\pi ab$. Thus $\sigma_t^{\perp}/\sigma_t^{\parallel} = a/b$. We can thus determine directly whether the nucleus is prolate or oblate. In the former case $\sigma_t^{\perp}/\sigma_t^{\parallel} > 1$, and in the latter $\sigma_t^{\perp}/\sigma_t^{\parallel} < 1$. For the nonsphericities observed experimentally, a typical ratio of the semi-axis is $1.3 - 1.4$ and the estimate made here shows that the nonsphericity effects may reach 30 or 40%.

Actually this estimate is somewhat too high, since it is impossible in practice to attain complete orientation of the nuclear spins along a specified direction. Furthermore, the symmetry axis of the nucleus undergoes a quantum-mechanical precession about the direction of the spin and this leads to a further decrease in the effect. It is obvious that the last circumstance will manifest itself less, the greater the nuclear spin. In very large spins, i.e., in the quasi-classical case, the precession can be neglected.

If the direction of the nuclear spin orientation does not coincide with the direction of the incident beam, an azimuthal asymmetry may occur in the angular distribution of the scattered neutrons. This phenomenon is connected with the fact that there exists a definite plane, determined by the direction of the incident beam and by the direction of the nuclear spins of the target. The appearance of azimuthal asymmetry is directly connected with the nonsphericity of the nuclei and therefore a study of this phenomenon can yield interesting information on the parameters of the nucleus.

In the present paper we examine a neutron scattering by oriented nonspherical nuclei. In the calculations we use the adiabatic approximation,[1-3] i.e., the motion of the neutron is assumed sufficiently fast to permit neglecting the rotation of the nucleus during the collision time. This is true if the neutron energy exceeds several Mev.

In the calculation of the specific examples we used the model of the black nucleus, which limits the applicability of the numerical results obtained to neutron energies of several tens of Mev. When using the corresponding expressions for the scattering amplitude, similar calculations can be performed in complete analogy for other energies, too.

2. DESCRIPTION OF THE SPIN STATE OF THE NUCLEUS

The spin state of an ensemble of nuclei with spin I is characterized by a $(2I + 1)$-row density matrix,[4] which can be represented in the form of an expansion in the irreducible spin tensors

T^{JM}, which transform under rotations of the quantization axis according to the irreducible representation of the rotation group D_J. Defining the mm′-th matrix element of T^{JM} in the form

$$T^{JM}_{mm'} = (-1)^{I+m'}\,(IIm - m' \mid IIJM), \qquad (1)$$

so that the normalization condition assumes the form

$$\mathrm{Sp}\, T^{JM}(T^{J'M'})^{+} = \delta_{JJ'}\delta_{MM'}, \qquad (2)$$

we obtain the following expansion of the density matrix ρ in irreducible spin tensors

$$\rho = \sum_{J=0}^{2I}\sum_{M=-J}^{J} \langle (T^{+})^{JM}\rangle\, T^{JM}. \qquad (3)$$

In cases of practical interest, when the spin orientation of the nuclei is caused by an axially-symmetrical field, the density matrix (assuming that the direction of the orienting field is taken to be the same as the quantization axis) is diagonal and can be written

$$\rho = \sum_{J=0}^{2I} \langle (T^{+})^{J0}\rangle\, T^{J0}. \qquad (4)$$

The 2I quantities $\langle (T^{+})^{J_0}\rangle$, which characterize the spin state of a system of nuclei with spin I, can be expressed in terms of the parameters f_k, which describe the degree of orientation of the nuclei, for example, for I = 1:

$$T^{10} = (1/\sqrt{2})\, f_1,$$
$$T^{20} = (1/\sqrt{6})\, f_2.$$

De Groot[5] and Khutsishvili[6] give the explicit form and a detailed description of the properties of the parameters f_k. We note that the system in which at least one parameter $f_{2p+1} \neq 0$ (p is an integer) is called polarized; but if all $f_{2p+1} = 0$, but at least one parameter $f_{2p+1} \neq 0$, the system is called aligned. The alignment is possible only if $I \geq 1$. For non-oriented nuclei all $f_k = 0$; the normalization is so chosen that the maximum values of f_k are +1.

As is known, the average value of a certain physical quantity A is defined with the aid of the density matrix in the following form:

$$\bar{A} = \mathrm{Sp}\,\rho A.$$

Taking into account the fact that the density matrix is diagonal, we can write the average value of the cross section of any scattering process in the following form:

$$\bar{\sigma} = \sum_{M=-I}^{I} \rho_{MM}\sigma_M = \sum_{M=-I}^{I}\sum_{J=0}^{2I} \langle T^{J0}\rangle\, T^{J0}_{MM}\sigma_M, \qquad (5)$$

where σ_M is the cross section of the particular process on a nucleus with spin and spin projection along the quantization axis M. Since $\sigma_M = \sigma_{-M}$, the expression for $\bar{\sigma}$ will contain only f_k with even k, i.e., the scattering cross section will depend only on the degree of alignment, but not on the degree of polarization of the target nuclei.

The effect of the orientation of the nuclear spins on the cross section of any scattering process is best characterized by a ratio of the scattering cross section $\sigma(f_k)$ on nuclei with an orientation specified by a certain set of parameters f_k, to the section $\sigma(0)$ of the same process on unoriented nuclei.

We introduce the notation

$$\gamma^{I}_{MK} = (\sigma^{I}_{MK} - \sigma^{I}_{M,K})/\sigma^{I}_{M,K}, \qquad (6)$$

where M is the projection of the nuclear spin on the direction of the orienting field, M_0 vanishes for integral spin and equals $\frac{1}{2}$ for half-integral spin, and K is the projection of the nuclear spin along the direction of the symmetry axis of the ellipsoid. The indices I and K we shall omit in the future wherever it causes no misunderstanding. Using (1), (5), and (6) we obtain for the quantities $\bar{\sigma}(f_k)/\bar{\sigma}(0)$, under specific cases of different spins, the expressions given in the table. The explicit form of the expression for the multiplier of f_6 is not given, since an estimate has shown that the terms containing f_6 give a negligible contribution.

3. TOTAL CROSS SECTION

Drozdov[1] and Inopin[2] have shown that in the adiabatic approximation the total cross section of all process σ_t is determined by the amplitude for scattering on a stationary nucleus. If the nucleus is characterized by quantum numbers I, M, and K, the total cross section can be expressed as follows

$$\sigma^{I}_{tMK} = \frac{4\pi}{k}\,\mathrm{Im}\int f(\Omega,\ \omega)\,|\Psi^{I}_{MK}(\omega)|^2\, d\omega\,|_{\theta=0}, \qquad (7)$$

where ω is a unit vector that defines the orientation of the nucleus in space, Ω a unit vector defining the direction of the wave vector k′ of the scattered neutron, and θ is the scattering angle. The wave functions that describe the rotational state of the nucleus is of the form

$$\Psi^{I}_{MK}(\omega) = \sqrt{(2I+1)/8\pi^2}\, D^{I}_{MK}(\omega), \qquad (8)$$

where $D^{I}_{MK}(\omega)$ is an element of the (2I + 1)-dimensional irreducible representation of the rotation group. The expression for the scattering amplitude, assuming a black nucleus, can be obtained from Eq. (4) of reference 7, and is of the form

$$f(\Omega, \omega) = ikb^2\zeta(\vartheta) J_1(\varkappa)/\varkappa, \quad \zeta(\vartheta) = \sqrt{1+\varepsilon\sin^2\vartheta},$$

$$\varepsilon = \frac{a^2}{b^2} - 1, \quad \varkappa = 2kb\sin\frac{\theta}{2}\sqrt{1+\varepsilon\cos^2\gamma}, \qquad (9)$$

where k is the wave vector of the incident neutron, and γ is the angle between the vector $\mathbf{k'-k}$ and the symmetry axis of the nucleus.

Putting the scattering angle θ equal to zero and using an expansion in Legendre polynomials

$$\sqrt{1+\varepsilon\sin^2\vartheta} = \sum_l (2l+1) A_l P_l(\cos\vartheta), \qquad (10)$$

where the expansion coefficients are determined by the expression

$$A_l = \frac{1}{2}\int_0^\pi \sqrt{1+\varepsilon\sin^2\vartheta}\, P_l(\cos\vartheta)\sin\vartheta\, d\vartheta, \qquad (11)$$

we get

$$\sigma^I_{tMK} = \frac{2I+1}{4\pi}\cdot\frac{R_0^2}{(1+\varepsilon)^{1/3}}$$

$$\times\sum_l\int (2l+1) A_l P_l(\cos\vartheta)\,|D^I_{MK}(\omega)|^2\, d\omega, \qquad (12)$$

where R_0 is the radius of a spherical nucleus of equal volume. Using the properties of the functions D^I_{MK}:

$$|D^I_{MK}|^2 = \sum_{L=0}^{2I}(-1)^{M-K}(IIM-M\,|\,L0)$$

$$\times(IIK-K\,|\,L0)\,D^L_{00}, \qquad (13)$$

$$D^L_{00}(\omega) = P_L(\omega), \qquad (13a)$$

we obtain after simple transformations

$$\sigma^I_{tMK} = 2\pi(2I+1)\frac{R_0^2}{(1+\varepsilon)^{1/3}}(-1)^{M-K}$$

$$\times\sum_{L=0}^{2I}(IIM-M\,|\,L0)(IIK-K\,|\,L0)\,P_L(\cos\psi)\,A_L, \qquad (14)$$

where ψ is the angle between the vector k and the direction of the orienting field H.

Correspondingly, the quantities γ^I_{MK} can be represented as follows:

$$\gamma^I_{MK} = (-1)^{M-M_0}$$

$$\times\frac{\sum_L (IIM-M\,|\,L0)(IIK-K\,|\,L0)P_L(\cos\psi)\,A_L}{\sum_L (IIM_0-M_0\,|\,L0)(IIK-K\,|\,L0)\,P_L(\cos\psi)A_L} - 1. \qquad (15)$$

As already mentioned in the introduction, the total neutron cross section for an unoriented nucleus depends very little on the deformation. Furthermore, it is entirely independent of the nuclear spin[8] if the nucleus is not oriented. It is therefore convenient to study the behavior of the quantity

$$\Lambda_t = \bar{\sigma}_t(f_k)/\bar{\sigma}_t(0),$$

i.e., of the ratio of the total neutron cross section on an oriented nucleus to the total neutron cross section on an unoriented one.

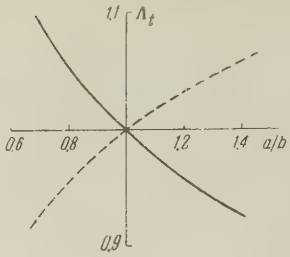

FIG. 1

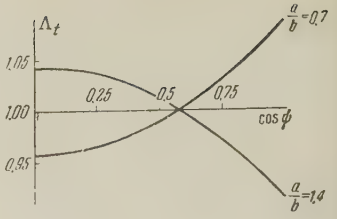

FIG. 2

After calculating the quantity γ^I_{MK} and using the expressions in the table, we obtain the numerical values of the ratio Λ_t of interest to us. The calculation of the coefficients A_l can be either by direct computation of the integrals (11) or by expanding the expression $\sqrt{1+\epsilon\sin^2\vartheta}$ in powers of ϵ.

An estimate shows that the contribution due to the term containing f_4 is only several percent of the main contribution of the term containing f_2. The term containing f_6, as already mentioned, yields a negligible contribution. It is also clear that the effect is nonlinearly related to the value of f_2.

The dependence of Λ_t on the ratio of semi-axis a/b is illustrated in Fig. 1. The solid curve corresponds to the case $I = K = 5/2$, $\psi = 0$, and $f_2 = +1$. We see that the ratio of the cross section diminishes monotonically with increasing a/b; when $a/b < 1$, we get $\Lambda_t > 1$, and vice versa, in full agreement with what was said in the introduction. The dotted curve corresponds to the same parameters, but for $K = 1/2$ rather than $5/2$ as in the first case. Such a case, as is known, occurs when the sequence of the levels in the rotational band is reversed. The resultant curve can be obtained from the curve for $K = 5/2$ by reversing the sign of the deformation. In other words, in this case a prolate nucleus behaves like an oblate one, and vice versa. This result is connected with the fact that when $K = 1/2$ and $I > 1/2$ the spin is perpendicular to the symmetry axis of the nucleus.

The characteristic variation of Λ_t with ψ, the angle between the orienting field and the incident beam, is shown in Fig. 2 for the case $I = K = 5/2$, $f_2 = +1$ and for two values of the semi-axis ratio a/b, namely 1.4 and 0.7 (i.e., b/a = 1.4). In both cases the effect reaches a maximum value when the orienting field is parallel to **K** (i.e., $\psi = 0$). Obviously the effect manifests itself most fully if the measurements are made at $\psi = 0$ and $\psi = \pi/2$. In accordance with the remarks made in the introduction, the curves corresponding to the different signs of deformation differ in the sign of the effect.

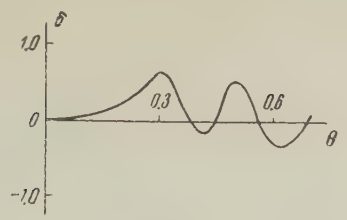

FIG. 3

We give the values of Λ_t for a/b = 0.7, $\psi = 0$, and $f_2 = +1$ and for various nuclear spins:

$I = 1$	$3/2$	2	$5/2$	$7/2$
$\Lambda_t = 1.024$	1.049	1.070	1.087	1.113

As expected, the effect increases monotonically with increasing spin.

In the foregoing examples a typical value of the effect was ~10%. However, the attainment of 100% orientation of nuclei in the experiment is of little likelihood, i.e., we always have $f_2 < 1$, and the observed effects are correspondingly decreased.

4. ANGULAR DISTRIBUTION OF SCATTERED NEUTRONS

Let us consider the differential cross section of scattering of neutrons in a direction defined by a unit vector Ω, by a nucleus characterized by quantum numbers I, M, and K. This cross section is given by

$$\sigma^I_{MK}(\Omega) = \int |f(\Omega, \omega)|^2 |\Psi^I_{MK}(\omega)|^2 d\omega. \qquad (16)$$

The scattering amplitude f and the wave function of the rotational state of the nucleus Ψ^I_{MK} are determined as before by expressions (9) and (8). The calculations yield the following expression for the sought cross section

$$\sigma^I_{MK}(\Omega) = k^2 R_0^4 (1 + \varepsilon^2)^{1/2} \sum_{L=0}^{2I} (-1)^{M-K} \times (IIM - M | IIL\,0)(IIK - K | IIL\,0)$$
$$\times \left\{ \left(1 - \frac{1}{3}\frac{\varepsilon}{1+\varepsilon}\right) P_L(\cos\beta) B_L - \frac{2}{3}\frac{\varepsilon}{1+\varepsilon}\left[P_L(\cos\beta) P_2(\cos\eta) \times \sum_{l=|L-2|}^{L+2} (L\,200|L\,2l\,0)^2 B_l + 2\sum_{\mu=1}^{2} (-1)^\mu \times \sqrt{\frac{(L-\mu)!\,(2-\mu)!}{(L+\mu)!\,(2+\mu)!}} P_L^\mu(\cos\beta) \times P_2^\mu(\cos\eta)\cos\mu \times \sum_{l=|L-2|}^{L+2} (L\,200\,|\,L2l0)(L2\mu - \mu\,|\,L2l0) B_l \right] \right\}. \qquad (17)$$

Here

$$B_\lambda = \int Y_{\lambda 0}(\omega) \frac{J_1^2(kb\theta\sqrt{1+\varepsilon\cos^2\gamma})}{(kb\theta\sqrt{1+\varepsilon\cos^2\gamma})^2} d\omega, \qquad (18)$$

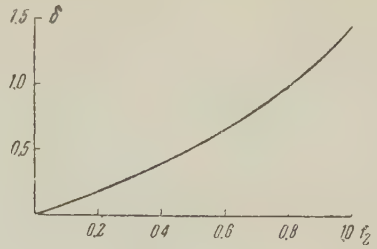

FIG. 4

β is the angle between $\mathbf{k}' - \mathbf{k}$ and $\mathbf{H}$, η is the angle between $\mathbf{k}' - \mathbf{k}$ and $\mathbf{k}$. The angle ξ is determined by the relation

$$\cos\xi = -\cot\beta\cot\eta. \qquad (19)$$

The angles β and γ can be expressed in terms of the scattering angle θ, the azimuth angle φ, and the angle ψ

$$\cos\eta = -\sin(\theta/2),$$
$$\cos\beta = -\cos\psi\sin(\theta/2) + \sin\psi\cos(\theta/2)\cos\varphi. \qquad (20)$$

If the orienting field is perpendicular to the direction of the incident neutron beam, i.e., if $\psi = \pi/2$, we get

$$\cos\eta = -\sin(\theta/2),$$
$$\cos\beta = \cos(\theta/2)\cos\varphi, \quad \tan\xi = \tan\varphi/\sin(\theta/2). \qquad (20a)$$

The expressions (16) and (20) yield the dependence of $\sigma^I_{MK}(\Omega)$ on the azimuth angle φ. In case of unoriented nuclei this dependence vanishes in the averaging over M, but in the case of oriented nuclei an azimuthal asymmetry occurs in the angular distribution of the scattered neutrons. If we denote by $\bar{\sigma}(\theta, \varphi)$ the angular distribution of the neutrons scattered in a direction defined by the angles θ and φ, averaged over M, then the azimuthal asymmetry can be characterized by the following quantity

$$\delta = (\bar{\sigma}(\theta, \pi/2) - \bar{\sigma}(\theta, 0))/\bar{\sigma}(\theta, 0). \qquad (21)$$

After calculating the differential cross section with equation (17) (in which the coefficients B_λ are calculated numerically) and averaging it over M, for which we must use expression (15) for γ'_{MK} and the expressions for $\bar{\sigma}(f_k)/\bar{\sigma}(0)$, listed in the table, we obtain the value of the azimuthal asymmetry from (21). Figure 3 shows the dependence of the azimuthal asymmetry on the scattering angle θ for the case $I = K = 5/2$, a/b = 1.3, $f_2 = +0.5$, and kR = 12. The azimuthal asymmetry reaches a considerable value at $\theta \approx 0.3$, i.e., near the first diffraction minimum.

The dependence of the azimuthal asymmetry on the degree of alignment of the nuclei f_2 is shown in figure 4 for $\theta = 0.5$, $I = K = 5/2$, a/b = 1.3, and kR = 12. It is seen there that the azimuthal asym-

j	$\bar{\sigma}(f_k)/\bar{\sigma}(0)$
1	$1+f_2\,\frac{\gamma_1}{3+2\gamma_1}$
$^3/_2$	$1+f_2\,\frac{\gamma_{3/2}}{2+\gamma_{3/2}}$
2	$1+\frac{10}{7}f_2\,\frac{2\gamma_2-\gamma_1}{5+2\gamma_1+2\gamma_2}+\frac{1}{7}f_4\,\frac{\gamma_2-4\gamma_1}{5+2\gamma_1+2\gamma_2}$
$^5/_2$	$1+\frac{5}{14}f_2\,\frac{5\gamma_{5/2}-\gamma_{3/2}}{3+\gamma_{3/2}+\gamma_{5/2}}-\frac{3}{14}f_4\,\frac{\gamma_{5/2}-3\gamma_{3/2}}{3+\gamma_{3/2}+\gamma_{5/2}}$
$^7/_2$	$1+\frac{1}{3}f_2\,\frac{7\gamma_{7/2}+\gamma_{5/2}-3\gamma_{3/2}}{4+\gamma_{3/2}+\gamma_{5/2}+\gamma_{7/2}}-\frac{1}{11}f_4\,\frac{7\gamma_{7/2}-13\gamma_{5/2}-3\gamma_{3/2}}{4+\gamma_{3/2}+\gamma_{5/2}+\gamma_{7/2}}+\frac{1}{33}c_6f_6$

metry increases monotonically with increasing f_2, and at $f_2 \lesssim 0.4$ this dependence is close to linear.

[1] S. I. Drozdov, J. Exptl. Theoret. Phys. (U.S.S.R.) **28**, 734 and 736 (1958), Soviet Phys. JETP **1**, 588 and 591 (1955).

[2] É. V. Inopin, Dissertation, Physico-Tech. Inst. Acad. Sci. U.S.S.R. (1958).

[3] E. V. Inopin, J. Exptl. Theoret. Phys. (U.S.S.R.) **34**, 1455 (1958), Soviet Phys. JETP **7**, 1007 (1958).

[4] U. Fano, Phys. Rev. **93**, 121 (1954).

[5] S. R. de Groot, Physica **18**, 1201 (1952).

[6] G. R. Khutsishvili, J. Exptl. Theoret. Phys. (U.S.S.R.) **28**, 496 (1955), Soviet Phys. JETP **1**, 390 (1955).

[7] E. V. Inopin, J. Exptl. Theoret. Phys. (U.S.S.R.) **30**, 210 (1956), Soviet Phys. JETP **3**, 134 (1956).

[8] S. I. Drozdov, J. Exptl. Theoret. Phys. (U.S.S.R.) **30**, 786 (1956), Soviet Phys. JETP **3**, 759 (1956).

Translated by J. G. Adashko
94

ON THE WEAK-INTERACTION TYPES POSSIBLE IN THE SCHEME OF FEYNMAN AND GELL-MANN

V. M. SHEKHTER

Leningrad Physico-Technical Institute, Academy of Sciences, U.S.S.R.

Submitted to JETP editor September 2, 1958

J. Exptl. Theoret. Phys. (U.S.S.R.) 36, 581-584 (February, 1959)

It is shown that the β-decay current is uniquely determined by the requirement that the divergence of its vector part vanish; along with this we have the fact that the current responsible for the decay of hyperons is not conserved. If this were not so the Lagrangian of the strong interactions would have a symmetry that would be in contradiction with experimental results on the associated production of strange particles. As a consequence of this the reaction $\Sigma \to \Lambda + e + \nu$ can go only through the A-type interaction, and the result of the experiment proposed in reference 6 must be negative.

To explain the fact that the vector coupling constant for β decay does not undergo renormalization, despite the existence of the strong interactions, Feynmann and Gell-Mann[1] have suggested that the vector part of the β-decay Lagrangian involves only currents that are conserved in the presence of strong interaction (cf. also reference 2). In this connection the question arises as to the extent to which the current responsible for β decay is uniquely determined by the requirement that its divergence vanish. Furthermore it is not obvious a priori whether the current responsible for the decay of hyperons is conserved. At the beginning one can only assert that the existence of a current with a vanishing divergence means the conservation of a certain vector, and consequently means an additional symmetry of the interaction Lagrangian. Pais[3] has shown that certain classes of such symmetries lead to contradictions with the experiments on associated production of strange particles. It will be shown here that from the results of Pais it follows that the β-decay current is uniquely determined and the current responsible for the decay of hyperons is not conserved.

The strong-interaction Lagrangian can be written in the form (boldface letters denote isovectors, i.e., vectors in the isotopic space)

$$L = \{g_1(\bar{N}i\gamma_5\boldsymbol{\tau}N) + g_2(\bar{\Lambda}i\gamma_5\boldsymbol{\Sigma} + \bar{\boldsymbol{\Sigma}}i\gamma_5\Lambda) - ig_3[\bar{\boldsymbol{\Sigma}}i\gamma_5\boldsymbol{\Sigma}] + g_4(\bar{\Xi}i\gamma_5\boldsymbol{\tau}\Xi)\}\boldsymbol{\pi} + \{g_5(\bar{N}i\gamma_5\Lambda)K + g_6(\bar{N}i\gamma_5\boldsymbol{\tau}\boldsymbol{\Sigma})K + g_7K(\bar{\Lambda}i\gamma_5\tau_2\Xi) + g_8K(\bar{\boldsymbol{\Sigma}}i\gamma_5\tau_2\boldsymbol{\tau}\Xi) + \text{Herm. conj.}\}. \quad (1)$$

The only difference from the notations of the paper of d'Espagnat, Prentki, and Salam[4] is that the sign of g_2 is changed, whereas in Pais's notation[3] $g_i = G_i$ $(i = 1, 2, 3, 4)$, $g_5 = F_1$, $g_6 = F_2$, $g_7 = -iF_3$, $g_8 = -iF_4$. The assumption that K has a parity different from that of Λ and Σ is immaterial.

It is not hard to see that in virtue of the conservation laws for baryon number, strangeness, and charge and the isotopic invariance of the theory with the Lagrangian (1), we have for arbitrary values of the g_j conservation of the isoscalar currents

$$J_\mu^S = (\bar{N}i\gamma_\mu N) + (\bar{\Lambda}i\gamma_\mu\Lambda) + (\bar{\boldsymbol{\Sigma}}i\gamma_\mu\boldsymbol{\Sigma}) + (\bar{\Xi}i\gamma_\mu\Xi), \quad (2)$$

$$J^\mu = -(\bar{\Lambda}i\gamma_\mu\Lambda) - (\bar{\boldsymbol{\Sigma}}i\gamma_\mu\boldsymbol{\Sigma}) - 2(\bar{\Xi}i\gamma_\mu\Xi) + i\left(K^*\frac{\partial K}{\partial x_\mu} - \frac{\partial K^*}{\partial x_\mu}K\right), \quad (3)$$

and also the isovector current

$$\mathbf{J}_\mu^V = (\bar{N}i\gamma_\mu\boldsymbol{\tau}N) - 2i[\bar{\boldsymbol{\Sigma}}i\gamma_\mu\boldsymbol{\Sigma}] + (\bar{\Xi}i\gamma_\mu\boldsymbol{\tau}\Xi) + 2\left[\boldsymbol{\pi}\frac{\partial\pi}{\partial x_\mu}\right] + i\left(K^*\boldsymbol{\tau}\frac{\partial K}{\partial x_\mu} - \frac{\partial K^*}{\partial x_\mu}\boldsymbol{\tau}K\right). \quad (4)$$

Furthermore the Lagrangian for the electromagnetic interactions has the form $\frac{1}{2}(J_\mu^S + j_\mu^G + (J_\mu^V)_3) \times A_\mu$.

If the bare masses of the Λ and the Σ are equal, and the coupling constants satisfy the relations

$$g_2 = \varepsilon g_3, \quad g_5 = \varepsilon g_6, \quad g_7 = \varepsilon g_8; \quad m_\Lambda = m_\Sigma; \quad \varepsilon = \pm 1, \quad (5)$$

then in addition to (4) we can construct another conserved current isovector

$$\mathbf{J}_\mu^P = \varepsilon(\bar{\Lambda}i\gamma_\mu\boldsymbol{\Sigma} + \bar{\boldsymbol{\Sigma}}i\gamma_\mu\Lambda) + i[\boldsymbol{\Sigma}i\gamma_\mu\boldsymbol{\Sigma}] - i\left(K^*\boldsymbol{\tau}\frac{\partial K}{\partial x_\mu} - \frac{\partial K^*}{\partial x_\mu}\boldsymbol{\tau}K\right). \quad (6)$$

The equations in (5) agree exactly with the conditions obtained in reference 4 for the invariance of the theory with respect to rotations in a four-dimensional Euclidean isotopic space. On the other hand, Pais[3] has shown that from precisely these conditions there follow consequences that are in contradiction with experiment. In fact, for $\epsilon = 1$* the vanishing of the divergence of the component $(J_\mu^P)_3$ corresponds to the conservation of the operator

$$\hat{N}_Y - \hat{N}_Z + \hat{N}_{K^+} - \hat{N}_{K^0}, \tag{7}$$

where

$$Y^+ \equiv \Sigma^+, \quad Y^0 \equiv (\Lambda^0 - \Sigma^0)/\sqrt{2};$$
$$Z^0 \equiv (\Lambda^0 + \Sigma^0)/\sqrt{2}, \quad Z^- \equiv \Sigma^-, \tag{8}$$

and $\hat{N}$ is the operator for a number of particles ($\hat{N}_Y = \hat{N}_{Y^+} + \hat{N}_{Y^0}$, $\hat{N}_Z = \hat{N}_{Z^0} + \hat{N}_{Z^-}$). Together with the vanishing of the divergence of the expression (3), i.e., the conservation of

$$-\hat{N}_Y - \hat{N}_Z - 2\hat{N}_\Xi + \hat{N}_{K^+} + \hat{N}_{K^0}, \tag{9}$$

Eq. (7) at once means also the conservation of the operators introduced by Pais,

$$\hat{S}_1 \equiv -\hat{N}_Z - \hat{N}_\Xi + \hat{N}_{K^+}, \quad \hat{S}_2 \equiv -\hat{N}_Y - \hat{N}_\Xi + \hat{N}_{K^0}, \tag{10}$$

which, for example, directly forbids the reaction $\pi^+ + p \to \Sigma^+ + K^+ \equiv Y^+ + K^+$, which has been observed experimentally. Therefore we can regard it as established that the conditions (5) are not satisfied, and that there is no possibility of including J_μ^P and J_μ^V in the β-decay Lagrangian.

Direct calculation shows that it is impossible to construct any other conserved isovectors; consequently the β-decay current $(J_\mu^V)_+ = (J_\mu^V)_1 + i(J_\mu^V)_2$ is uniquely determined.

Since furthermore there is no term $(\bar{\Lambda} i\gamma_\mu \Sigma)$ in Eq. (4), the decays $\Sigma^+ \to \Lambda^0 + e^+ + \nu$, $\Sigma^- \to \Lambda^0 + e^- + \tilde{\nu}$ can occur only owing to the renormalized axial-vector interaction. For this reason there should be no polarization of the Λ in such reactions if the Σ are not polarized, and the Λ is emitted asymmetrically for polarized Σ.

Feynman and Gell-Mann suggested that the decay of hyperons is due to the existence of currents with change of the strangeness. Such currents will have half-integral isotopic spin, since from the quantities of the theory one can construct only expressions of the types $(\bar{\Lambda} i\gamma_\mu N)$ or $(\bar{\Lambda} i\gamma_\mu \tau N)$. It is easy to see tha, generally speaking, such currents are not conserved. Only under the conditions

$$g_1 = -\varepsilon g_2 = -g_3 = g_4 = \varepsilon'' g_5 = \varepsilon\varepsilon'' g_6 = \varepsilon'\varepsilon'' g_7 = \varepsilon\varepsilon'\varepsilon'' g_8,$$
$$m_N = m_\Lambda = m_\Sigma = m_\Xi; \quad m_K = m_\pi; \quad \varepsilon, \varepsilon', \varepsilon'' = \pm 1 \tag{11}$$

*If $\varepsilon = -1$, N_{Y^0} and N_{Z^0} are interchanged in Eqs. (7)–(10).

which are stronger than Eq. (5), do we get conservation of the current

$$J_\mu^\psi = (\bar{\Lambda} i\gamma_\mu \tau N) + \varepsilon[(\bar{\Sigma} i\gamma_\mu N) - i[\bar{\Sigma} i\gamma_\mu \tau N]] - \varepsilon'(\bar{\Xi} i\gamma_\mu \tau\tau_2 \Lambda)$$
$$- \varepsilon\varepsilon'[(\bar{\Xi} i\gamma_\mu \tau_2 \Sigma) - i[\bar{\Xi} i\gamma_\mu \tau\tau_2 \Sigma]] + 2i\varepsilon''\left(K\frac{\partial\pi}{\partial x_\mu} - \frac{\partial K}{\partial x_\mu}\pi\right), \tag{12}$$

and also of the currents

$$-\frac{i}{2}[\tau J_\mu^\psi] = (\bar{\Lambda} i\gamma_\mu N) - \varepsilon(\bar{\Sigma} i\gamma_\mu N) - \varepsilon'(\bar{\Xi} i\gamma_\mu \tau\tau_2 \Lambda)$$
$$+ \varepsilon\varepsilon'(\bar{\Xi} i\gamma_\mu \tau_2 \Sigma) + \varepsilon''\left(\left[\tau K\frac{\partial\pi}{\partial x_\mu}\right] - \left[\tau\frac{\partial K}{\partial x_\mu}\pi\right]\right), \tag{13}$$

$$\tau J_\mu^\psi = -\frac{i}{2}\tau[\tau J_\mu^\psi] = 3(\bar{\Lambda} i\gamma_\mu N) - \varepsilon(\bar{\Sigma} i\gamma_\mu \tau N) + 3\varepsilon'(\bar{\Xi} i\gamma_\mu \tau_2 \Lambda)$$
$$- \varepsilon\varepsilon'(\bar{\Xi} i\gamma_\mu \tau\tau_2 \Sigma) + 2i\varepsilon''\left(\tau K\frac{\partial\pi}{\partial x_\mu} - \tau\frac{\partial K}{\partial x_\mu}\pi\right). \tag{14}$$

If there exist also other mesons besides π and K, other currents besides the expressions (12) — (14) can be conserved. For example, if one introduces into the theory a pseudoscalar ρ meson having zero charge and isotopic spin and interacting with the baryons through the additional Lagrangian terms

$$L' = g_\rho[(\bar{N} i\gamma_5 N) - (\bar{\Lambda} i\gamma_5 \Lambda) - (\bar{\Sigma} i\gamma_5 \Sigma) + (\Xi i\gamma_5 \Xi)]\rho \tag{15}$$

and impose the conditions

$$g_1 = \varepsilon g_2 = g_3 = g_4; \quad g_5 = \varepsilon g_6 = \varepsilon' g_7 = \varepsilon\varepsilon' g_8 = \varepsilon'' g_\rho;$$
$$m_N = m_\Lambda = m_\Sigma = m_\Xi; \quad m_\rho = m_K; \quad \varepsilon, \varepsilon', \varepsilon'' = \pm 1, \tag{16}$$

we find that the current

$$J_\mu^\chi = (\bar{\Lambda} i\gamma_\mu N) + \varepsilon(\bar{\Sigma} i\gamma_\mu \tau N) + \varepsilon'(\bar{\Xi} i\gamma_\mu \tau_2 \Lambda)$$
$$+ \varepsilon\varepsilon'[\bar{\Xi} i\gamma_\mu \tau\tau_2 \Sigma) + 2i\varepsilon''\left(\frac{\partial\rho}{\partial x_\mu}K - \rho\frac{\partial K}{\partial x_\mu}\right). \tag{17}$$

is conserved.

The introduction of the ρ meson has the result that $\partial J_\mu^\psi/\partial x_\mu \neq 0$, so that the simultaneous conservation of J_μ^χ and the currents (12) — (14) is impossible. It can be noted that if one uses in Eq. (1) the same spatial parities for Λ, Σ, and K, the current (17) can be conserved as before (the ρ meson would then be scalar), and the currents (12) — (14) are then not conserved. The conditions (11), however, and also the conditions (16), contain the relations (5) which are in contradiction with experiment. Consequently both sets of conditions are incapable of fulfillment, the current responsible for the decay of hyperons is not conserved, and, accordingly, the decay coupling constants are subject to renormalization. This explains the fact that hyperon decays with lepton emission has so far not been observed, whereas in the absence of the renormalization several percent of the total number of Λ and Σ decays should be accompanied by the emission of electrons or μ mesons (cf. e.g., reference 5). In addition, because of the nonconservation of the pion-neutrino decay current the correlation in the $K_{\mu 3}$ decay cannot be de-

scribed by the expression obtained in reference 6.

Up to now we have been speaking only about vector currents. Since in ordinary β decay the experimental ratio of the axial-vector and vector coupling constants[7] is $|C_A/C_V| = 1.14$, i.e., close enough to unity, the question of the conservation of axial-vector currents is also of interest. The construction of such currents is impossible, however, in the theory with the interaction (1) unless one introduces additional particles. If, for example, we introduce a σ meson that is scalar in the ordinary and isotopic spaces[8] with the interaction

$$L' = g_\sigma [(\bar{N}N) + (\bar{\Lambda}\Lambda) + (\bar{\Sigma}\Sigma) + (\bar{\Xi}\Xi)]\,\sigma, \qquad (18)$$

then with conditions on the bare masses and coupling constants given by

$$g_1 = g_2 = g_3 = g_4 = g_\sigma \equiv g;$$

$$m_N = m_\Lambda = m_\Sigma = m_\Xi \equiv m; \qquad m_\sigma = m_\pi = 0, \qquad (19)$$

and only apart from effects of the K-meson interactions, we have conservation of the current

$$(\bar{N} i\gamma_5\gamma_\mu \tau N) + (\bar{\Lambda} i\gamma_5\gamma_\mu \Sigma) + (\bar{\Sigma} i\gamma_5\gamma_\mu \Lambda) - i\,[\bar{\Sigma} i\gamma_5\gamma_\mu \Sigma]$$

$$+ (\bar{\Xi} i\gamma_5\gamma_\mu \tau \Xi) + 2\left(\frac{\partial\sigma}{\partial x_\mu}\pi - \sigma\frac{\partial\pi}{\partial x_\mu}\right) - \frac{2m}{g}\frac{\partial\pi}{\partial x_\mu}. \qquad (20)$$

The conditions (19), which differ from the Gell-Mann scheme[9] by the addition of the σ meson, do not impose the limitations (5) on the K-meson interaction constants, and therefore do not contradict experiment. Nevertheless the addition (20) to the vector current J_μ^V would mean a violation of the assumption[1] that the weak-interaction Lagrangian involves only fermion operators of definite spirality.

In conclusion I express my deep gratitude for a discussion to I. M. Shmushkevich and S. S. Gershteĭn.

[1] R. P. Feynman and M. Gell-Mann, Phys. Rev. **109**, 193 (1958).

[2] S. S. Gershteĭn and Ya. B. Zel'dovich, J. Exptl. Theoret. Phys. (U.S.S.R.) **29**, 698 (1955), Soviet Phys. JETP **2**, 576 (1956).

[3] A. Pais, Phys. Rev. **110**, 574 (1958).

[4] d'Espagnat, Prentki, and Salam, Nucl. Phys. **3**, 446 (1957).

[5] V. M. Shekhter, J. Exptl. Theoret. Phys. (U.S.S.R.) **35**, 458 (1958), Soviet Phys. JETP **8**, 316 (1959).

[6] Weinberg, Marshak, Okubo, Sudarshan, and Teutsch, Phys. Rev. Let. **1**, 25 (1958).

[7] A. Winther and O. Kofoed-Hansen, Dansk. Mat.-Fys. Medd. (in press).

[8] J. C. Polkinghorne, Nuovo cimento **8**, 179 (1958).

[9] M. Gell-Mann, Phys. Rev. **106**, 1296 (1957).

Translated by W. H. Furry
95

CORRELATION BETWEEN THE DIRECTION OF AN INTERNAL BREMSSTRAHLUNG QUANTUM AND CIRCULAR POLARIZATION OF A GAMMA QUANTUM EMITTED BY AN EXCITED NUCLEUS AFTER K CAPTURE

G. M. GANDEL' MAN

Submitted to JETP editor August 23, 1958

J. Exptl. Theoret. Phys. (U.S.S.R.) **36**, 585-587 (February, 1959)

The correlation between the γ quantum from radiative K capture and the circularly-polarized γ quantum from an excited nucleus is studied. A general formula is derived for the correlation and for its dependence on the spins of the initial, excited, and final states of the nuclei.

IT is well known that along with ordinary K capture one observes radiative K capture, which is frequently called internal bremsstrahlung, in which a continuous spectrum of γ quanta, up to the maximum energy W_0, is produced. If the nucleus is produced here in the excited state, circular polarization of the γ quantum of the excited nucleus can be observed in the direction of emission of the bremsstrahlung γ quantum. This offers an interesting possibility of determining the spin of excited states of nuclei formed in K capture.

In the case of electronic β decay, the spins of the excited nuclei can be determined by studying the correlation of the electrons and the circular polarization of the γ quantum of the excited nucleus.[1]

The correlation considered by us occurs unconditionally only if parity is not conserved in K capture. It is not necessary here to measure the energy of the bremsstrahlung quantum. This finds its expression in the fact that the considered correlation is of the form

$$W(\theta) \approx 1 + A\tau \cos\theta, \tag{1}$$

where θ is the angle between the directions of the two γ quanta, and τ equals $+1$ or -1 respectively for right- and left-handed polarized γ quanta.

Let us dwell briefly on a derivation of this formula for the case of the A, V variant of the β interaction.

The matrix element for radiation K capture is:

$$R = \sqrt{4\pi / 2k_0}\,(ge / 2mk_0)\,\Phi(0)\,\{\bar{\nu}\Lambda\hat{k}\hat{\varepsilon}e\}; \tag{2}$$

$\Phi(0)$ is the wave function of the K electron in the nuclear region, ϵ is the polarization vector of the bremsstrahlung γ quantum, k and k_0 are respectively the momentum and energy of bremsstrahlung γ quantum, and Λ is the matrix of the β interaction:

$$\Lambda = (\psi_f \mid 1 \mid \psi_i)\,\gamma_0 (C_V^* - iC_V'^*\gamma_5) - i(\psi_f \mid \sigma_\alpha \mid \psi_i)\,(C_A^* + iC_A'^*\gamma_5)\,\gamma_\alpha\gamma_5. \tag{3}$$

We have to find the density matrix ρ_R for the radiation K capture, and then multiply it by the density matrix ρ_γ for the γ transition $J_f \to J_{ff}$.

The density matrix ρ_R of the radiative K capture is

$$(\rho_R)_{M_f M_f'} \sim \sum_{s_\nu,\, s_l} (J_f M_f \mid H_R \mid J_i M_i)\,(J_f M_f' \mid H_R \mid J_i M_i)^*, \tag{4}$$

$$H_R = \bar{\nu}\Lambda\hat{k}\hat{\varepsilon}e. \tag{5}$$

The summation extends over the spins of the emitted neutrino and the captured electron. M_f is the magnetic quantum number of the excited nucleus, J_i is the initial spin of the nucleus, J_f is the spin of the excited state, and J_{ff} is the spin of the final nucleus after emission of the γ quantum.

We shall not perform a complete calculation of ρ_R, and will write the result for the interference term (between A and V) of the ρ_R matrix. This term equals

$$-2mk_0\,4q_0 M_F (C_V^* C_A' + C_A C_V'^*)\,(J_f M_f' \mid \sigma_\alpha \mid J_i M_i)^*\,k_\alpha \delta(M_f, M_f' \ldots$$

$$-2mk_0\,4q_0 M_F^* (C_V C_A'^* + C_A^* C_V')$$

$$\times (J_f M_f \mid \sigma_\alpha \mid J_i M_i)\,k_\alpha \delta(M_f', M_i); \tag{6}$$

M_F is the Fermi matrix element.

A similar result is obtained when calculating the matrix ρ for positron β decay, but k_α is replaced by the corresponding positron momentum component p_α. This pertains also to other terms of the density matrix ρ.

Starting with the above we can write an expression for the coefficient A in (1), using the results of Alder, Stech, and Winther[2] on β-γ correlation

Here the electron momentum must be replaced by the bremsstrahlung γ-quantum momentum, and since $k/k_0 = 1$, A is independent of the energy of the bremsstrahlung γ quantum:

$$A = \frac{\frac{1}{2\sqrt{3}}\left[\sum_{\lambda,\lambda'} \delta_\lambda \delta_{\lambda'} F_1(\lambda, \lambda', J_{ff}, J_f)\right] \left\{\frac{J_f(J_f+1) - J_i(J_i+1) + 2}{[J_f(J_f+1)]^{1/2}} |M_{GT}|^2 (C_A C_A'^* + C_A' C_A^*) + 4 M_F M_{GT} \operatorname{Re}(C_V C_A'^* + C_V' C_A^*)\right\}}{\left\{|M_F|^2 (|C_V|^2 + |C_V'|^2) + |M_{GT}|^2 (|C_A|^2 + |C_A'|^2)\right\} \sum_\lambda \delta_\lambda^2} \quad (7)$$

By way of an interesting example, let us consider the K capture

$$Be^7 \to Li^{7*} + \nu + \gamma_{brem.}$$
$$\downarrow$$
$$Li^7 + \gamma$$

There are two possibilities, $3/2 \xrightarrow{\beta} 1/2 \xrightarrow{\gamma} 3/2$ or $3/2 \xrightarrow{\beta} 3/2 \xrightarrow{\gamma} 3/2$. The excited state, in all probability, emits a quadrupole γ quantum, i.e., $\lambda = \lambda' = 2$.

In the first case of a pure Gamow-Teller transition (for the 2-component neutrino and real C_V and C_A), $A = 1/6$. In the second case

$$A = -0.13 \frac{(4/\sqrt{15}) C_A^2 |M_{GT}|^2 + 4 M_F M_{GT} C_V C_A}{G_V^2 M_F^2 + C_A^2 M_{GT}^2}$$
$$x = M_F C_V / M_{GT} C_A.$$
$$= -0.13 \frac{1.03 + 4x}{1 + x^2}, \quad (8)$$

In the second case A is close to $1/6$ and is positive only when $x \sim -1$. The contribution of the interference terms is quite large here.

Thus, an investigation of the correlation of the γ quantum of radiative K capture and of a circularly-polarized γ quantum of an excited nucleus can yield interesting information on the spin of the excited state, or else, if J_f is known, it yields data on the role of the interference terms in the β interaction. The correlation considered is analogous in many respects to the β-γ correlation.

In conclusion, I thank Ya. B. Zel'dovich for attention to and interest in this work.

[1] F. Boehm and A. H. Wapstra, Phys. Rev. **106**, 1364 (1957).

[2] Alder, Stech, and Winther, Phys. Rev. **107**, 728 (1957).

Translated by J. G. Adashko
96

CALCULATION OF POLARIZATION OF MEDIUM-ENERGY NEUTRONS

P. E. NEMIROVSKIĬ

Submitted to the JETP editor August 23, 1958

J. Exptl. Theoret. Phys. (U.S.S.R.) 36, 588-593 (February, 1959)

The polarization of 0.1 — 1 Mev neutrons scattered by heavy nuclei is investigated. It is shown that the polarization can be described with satisfactory accuracy by introducing in the optical potential and additional term of the form $-\frac{\kappa}{r}\frac{dV}{dr}(\sigma\cdot l)$, where $\kappa = 3\times 10^{-27}$ cm^2. The best agreement between theory and experiment is obtained when the imaginary part of the ordinary potential is 2.5 Mev.

1. INTRODUCTION

EXPERIMENTS on neutron polarization are a very important means of determining the interaction between nucleons and nuclei. Experiments made at relatively small energies are the most interesting, since they yield a clearly pronounced dependence on the atomic weight and a readily interpretable angular dependence.

Naturally, the theory can yield good agreement with experiment only for spherical nuclei. In addition, an agreement with theory can be expected only at energies for which the inelastic scattering is small or, to the contrary, so large that the fraction of elastic scattering in the reaction cross section is negligible. Thus, the most suitable energy intervals are $E < 0.5$ Mev and $E > 3$ Mev. In the intermediate region between 0.6 and 3 Mev the comparison cannot be so reliable.

The optical model were used by us to investigate the polarization found in the experiments of Darden et al.[1,2] The phases were calculated with a "Strela" computer. The results of the calculations was a total cross sections, the absorption cross sections, and the angular distributions were published elsewhere.[3] We wish to dwell here specially on problems of polarization.

2. METHOD OF PHASE CALCULATION

The potential was chosen in the following form

$$V = V_1(1 + i\zeta) + V_2, \qquad (1)$$

where

$$V_1 = -V_0/(1 + e^{\alpha(r-R_0)}), \qquad (2)$$

$$V_2 = -\frac{\varkappa}{r}\frac{dV_1}{dr}(\sigma\cdot\mathbf{l}),$$

$$V_0 = 50 \text{ Mev}, \quad 1/\alpha = 0.65\cdot 10^{-13}, \quad \varkappa = 2.8\cdot 10^{-27} \text{ cm}^2,$$

$$R_0 = (1.16A^{1/3} + 0.36)\cdot 10^{-13} \text{ cm}; \qquad (3)$$

with $k_0 = (1/\hbar)\sqrt{2mV_0} = \alpha$.

The Schrödinger equation with this potential was solved on a "Strela" computer. In this case the solutions of the Schrödinger radial equation, in the region where the potential vanishes, can be represented as

$$\psi = A\{r^{-1/2}H^{(2)}_{l+1/2}(kr) + \eta_l r^{-1/2}H^{(1)}_{l+1/2}(kr)\}. \qquad (4)$$

For the functions $J_{l+1/2}(x)$ and $J_{l-1/2}(x)$ tables are available and therefore to determine η_l it is enough to know ψ in two points at which the potential vanishes within the interval. Such a method of solution accelerates considerably the operation of the computer, since the calculation of the asymptotic form of ψ would necessitate a considerably longer operation. The values of η_l for different energies were then computed manually.

The values obtained for η_l were used to calculate the polarization. At energies of 0.25 and 0.5 Mev, we took into account only waves with $l = 0$, 1, and 2. At 1.25 Mev we performed the calculation also for $l = 3$. The polarization was calculated here from the formula

$$P = \frac{\lambda\!\!\!^{-2}\,\mathrm{Im}\sum_l [(l+1)(1-\eta_{l+1/2}) + l(1-\eta_{l-1/2})]P_l(\cos\vartheta)}{2d\sigma_{\mathrm{tot}}/d\Omega} \times \sum_{l'}(\eta^*_{l'-1/2} - \eta^*_{l'+1/2})P^{(1)}_{l'}(\cos\vartheta)$$

where $\lambda\!\!\!^{-}$ is the wavelength of the neutron, divided by 2π, σ_{tot} is the total cross section, and $d\Omega$ is the element of solid angle.

3. COMPARISON WITH EXPERIMENT

A comparison with experiment can be made only for the data of Darden et al. The 380-kev energy is quite suitable for comparison with experiment. The radiative capture at this energy is small and the inelastic scattering is insignificant. Therefore

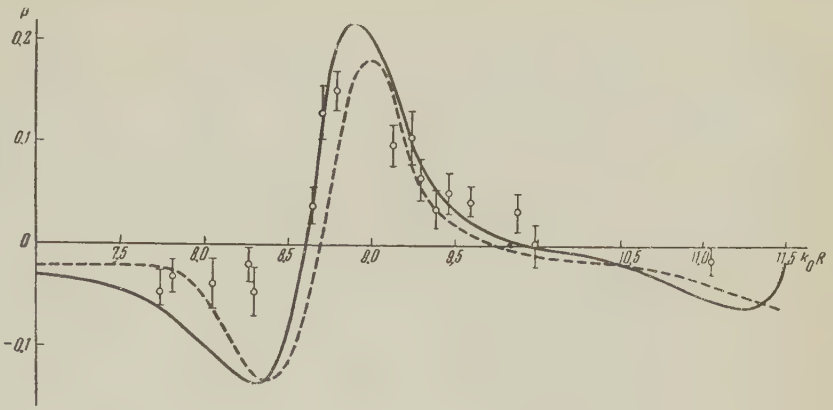

FIG. 1. Polarization of neutrons scattered at an angle of $\pi/2$. The abscissas represent k_0R. The solid curve corresponds to an energy of 0.5 Mev, the dotted one to 0.25 Mev for $\zeta = 0.05$; the experimental points pertain to 380 kev.

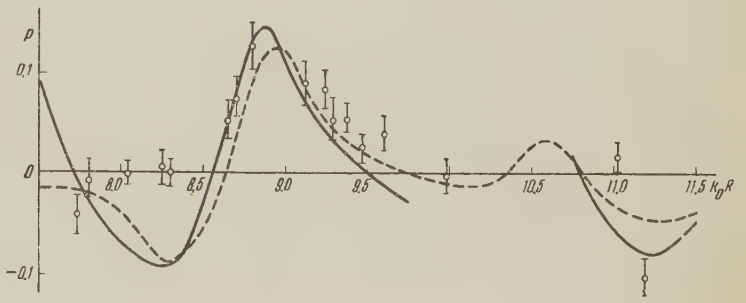

FIG. 2. Polarization of neutrons scattered at 55°. Symbols are the same as in Fig. 1.

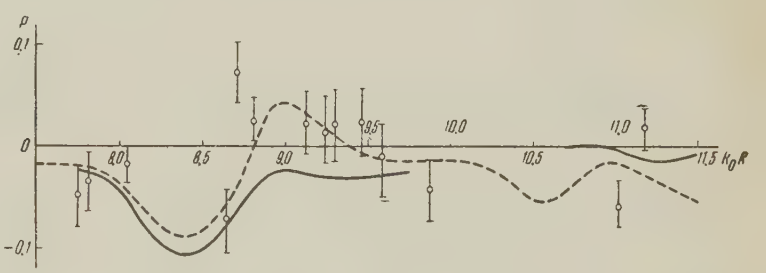

FIG. 3. Polarization of neutrons scattered at 130°. Symbols are the same as in Fig. 1.

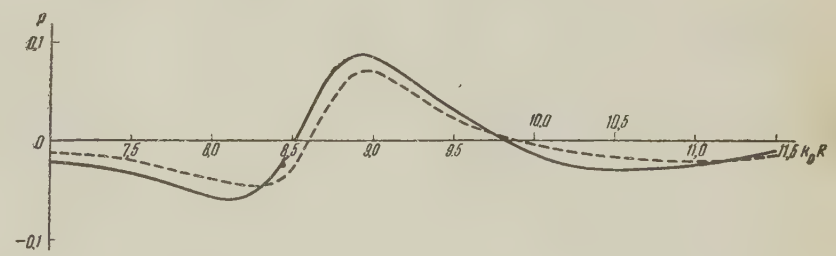

FIG. 4. Polarization of neutrons scattered at 90°. The solid curve corresponds to an energy of 0.5 Mev, the dotted one to 0.25 Mev, for $\zeta = 0.1$.

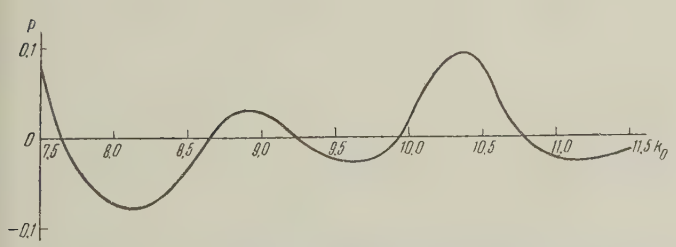

FIG. 5. Polarization of neutrons scattered at 55°. Symbols the same as in Fig. 4, energy 0.5 Mev.

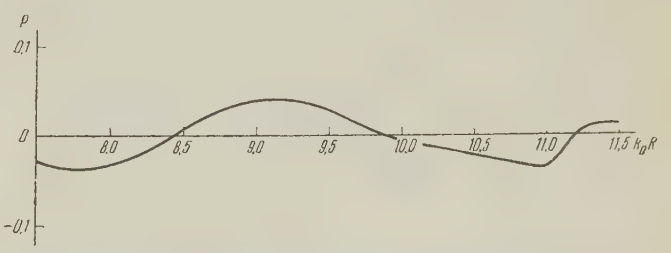

FIG. 6. Polarization of neutrons scattered at 130°. Symbols the same as in Fig. 4. Energy 0.5 Mev.

the assumption that the intermediate system breaks up only elastically is close to reality. We assume that there are no inelastic processes. The curves are given for angles.55, 90, and 180° for two values of the absorption coefficient and for two energies, 250 and 500 kev (Figs. 1 — 6).

The simplest curve is that for 90° (Figs. 1 and 4). It has one maximum A = 100 and two minima at A = 80 and 200. The course of the curve is determined essentially by the phase of difference* $\eta_{3/2}$-

* The phases of $p_{3/2}$ and $p_{1/2}$ are denoted $\eta_{3/2-}$ and $\eta_{1/2-}$.

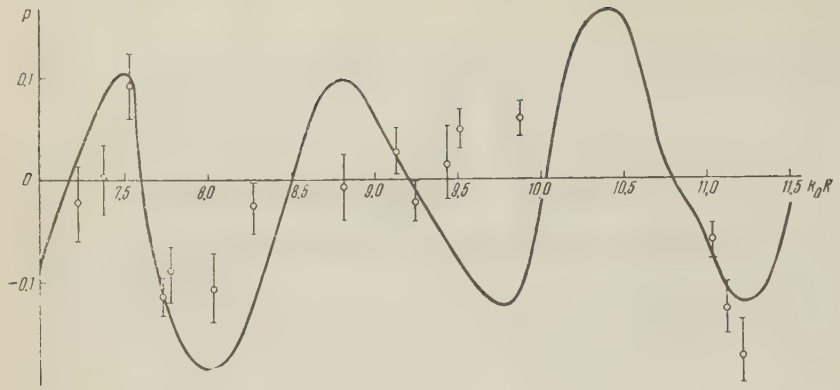

FIG. 7. Polarization of neutrons scattered at 55°. The curve corresponds to an energy of 1.25 Mev and $\zeta = 0.05$. The experimental points pertain to energy of 0.98 Mev.

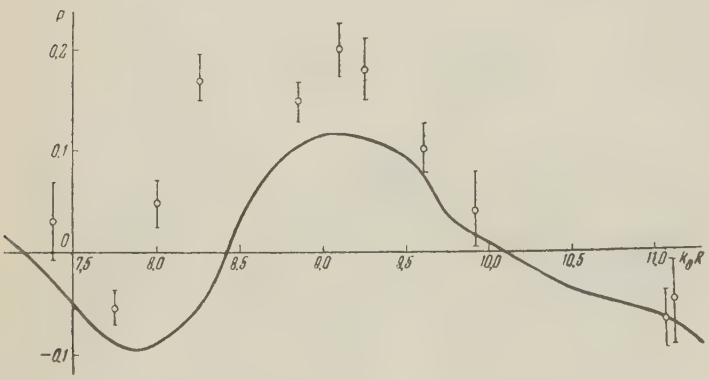

FIG. 8. Polarization of neutrons scattered at 90°. The curve corresponds to energy of 1.25 Mev and $\zeta = 0.05$.

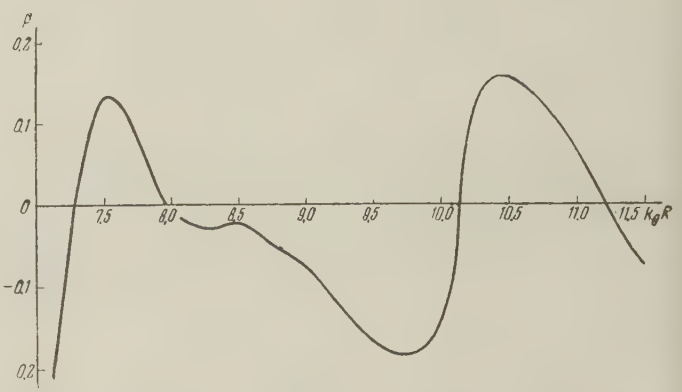

FIG. 9. Polarization of neutrons scattered at 125°. The curve corresponds to energy of 1.25 Mev and $\zeta = 0.05$.

and $\eta_{1/2}$-, i.e., with $l = 1$. As the energy is increased, the width of the maximum at A = 100 increases. If the coefficient of absorption is large the maximum is lower, but not wider. The experimental maximum at A = 100 is in agreement with the curve for $\zeta = 0.05$, although, possibly, the experimental values of the polarization are somewhat lower than the theoretical ones.

Of the 18 experimental points (5 points correspond to nuclei with static deformations), 12 agree with the theoretical curves. The deviation is particularly large for Se and Br. The reason of the deviation in the case of these nuclei must be sought apparently in their structure, since the discrepancies occur also at different angles and energies.

The 500-kev curve for 55° has three maxima (Figs. 1 and 4), one corresponding to the p wave and two corresponding to the d wave. One of the d maxima is at A = 50, where measurements were not performed, while the second occurs for nonspherical nuclei. We have therefore noted on the experimental curve only the maximum at A = 90 — 100. For this angle the agreement is somewhat poorer, Se, Br and Hg being in particularly poor agreement with the theory. The sign of polarization for the case of Hg disagrees with experiment.

For 130° both the theoretical and experimental values of the polarization are small. The experiment confirms the theory in this respect. However, the errors in the experimental values are so large, that the comparison with experiment can hardly be given any great weight.

The comparison for 980 kev is considerably more complicated (Figs. 7-9). Inelastic scattering can occur at this energy. For comparison with theory, nuclei with small inelastic scattering cross sections are the most suitable. From this point of view, nuclei with A = 50 — 60 are of interest. At an angle of 55° one should observe in the case of these nuclei a narrow maximum (large positive polarizations) followed by a broad minimum (large negative polarizations) (at $\zeta = 0.05$). Actually, measurements for V, Mn, Co, Cu, and Zn gave a picture close to that expected theoretically. The maximum at A = 100 is not clearly pronounced for $\vartheta = 55°$, but is quite clear at $\vartheta = 90°$. Here the polarizations are quite larger than the theoretical (at $\zeta = 0.05$), if elastic scattering is assumed as the only process. However, in nuclei with A ~ 100 inelastic scattering is very large, so that only a small portion of scattering goes into elastic scattering via the intermediate nucleus. Then the denominator in the expression for the polarization decreases and the experimental data generally do not disagree with the theory. For A = 200 agree-

ment with experiment at $\vartheta = 55°$ is also satisfactory.

The experimental errors in the 125° case are so large, that it hardly makes sense to make comparisons with experiment. Again, the data for selenium are in sharp disagreement with the theory.

In conclusion we can state that a total analysis of the existing data on polarization shows the following:

(1) The spin-orbit constant $\kappa \approx 3 \times 10^{-27}$ cm^2, selected from data on the stationary states,[4] describes fairly well the polarization of slow neutrons.

(2) The imaginary portion of the potential for low-energy neutrons is close to 3 Mev, in good agreement with experiments on the total cross sections and on radiative-capture cross sections.

The causes of disagreement between theory and experiment are still not clear in the case of several nuclei.

The author is greatly indebted to Academician A. A. Dorodnitsyn and to A. I. Sragovich for performing the operations on the "Strela" computer, and also laboratory assistants M. P. Shustova and L. V. Moiseeva for performing the numerical computations.

[1] Adair, Darden, and Fields, Phys. Rev. **96**, 503 (1954).

[2] Clement, Borelli, Darden, Haeberly, and Striebel, Nucl. Phys. **6**, 188 (1958).

[3] P. É. Nemirovskiĭ, Paper delivered at Conference on Nuclear Reactions, Moscow, November, 1957 (in press).

[4] I. I. Levintov, Dokl. Akad. Nauk SSSR **107**, 240 (1956), Soviet Phys. "Doklady" **1**, 175 (1956); J. Exptl. Theoret. Phys. (U.S.S.R.) **30**, 988 (1956), Soviet Phys. JETP **3**, 484 (1956); P. É. Nemirovskiĭ, J. Exptl. Theoret. Phys. (U.S.S.R.) **33**, 746 (1957), Soviet Phys. JETP **6**, 573 (1958).

Translated by J. G. Adashko
97

CALCULATION OF SCATTERING PHASE SHIFTS WITH INCLUSION OF THE SECOND APPROXIMATION

A. A. SOKOLOV, V. M. ARUTYUNYAN, and R. M. MURADYAN

Moscow State University

Submitted to JETP editor August 26, 1958

J. Exptl. Theoret. Phys. (U.S.S.R.) **36**, 594-599 (February, 1959)

The elastic scattering phase shifts for Dirac particles are determined from the interaction potential with inclusion of the second approximation. The results of the Born approximation and of damping theory, and also the McKinley-Feshbach formula, which is a generalization of the Rutherford-Mott formula, can be obtained as special cases.

1. INTRODUCTION

As is well known, in the theory of scattering one has the following exact formula for the angular distribution of a beam of unpolarized Dirac particles scattered by a stationary center of force:[1]

$$d\sigma/d\Omega = |f(\theta)|^2 + |g(\theta)|^2; \tag{1}$$

$$f(\theta) = \frac{1}{2ik}\sum_{l=0}^{\infty}[(l+1)(\exp\{2i\delta_l^{(1)}\}-1) + l(\exp\{2i\delta_l^{(2)}\}-1)]P_l(\cos\theta),$$

$$g(\theta) = \frac{1}{2ik}\sum_{l=1}^{\infty}[-\exp\{2i\delta_l^{(1)}\} + \exp\{2i\delta_l^{(2)}\}]P_l^1(\cos\theta). \tag{2}$$

For the total effective cross-section we have:

$$\sigma = \frac{4\pi}{k^2}\sum_{l=0}^{\infty}[(l+1)\sin^2\delta_l^{(1)} + l\sin^2\delta_l^{(2)}]. \tag{3}$$

In the general case of an arbitrary interaction potential no exact expression has been found for the angles $\delta_l^{(1)}$ and $\delta_l^{(2)}$, which are the phase differences between the asymptotic expressions for the radial functions with the scattering center present and the radial functions of the free motion. There are various methods for the approximate calculation of the phase shifts $\delta_l^{(1)}$ and $\delta_l^{(2)}$, in particular the Born approximation and the semi-analytical method of Wentzel, Kramers, and Brillouin. Recently the phase shifts have been calculated by means of a damping theory.[2] In the present paper the phase shifts are calculated correct to the second approximation in the interaction potential. We note that if we confine ourselves to just the first approximation we shall get again the results of the damping theory.

2. SOLUTION OF THE DIRAC EQUATION FOR THE FREE PARTICLE

In studying the phase shifts for the elastic scattering of spinning particles it is convenient to take the solution of the free-particle Dirac equation

$$(E - c\,\mathbf{p}\cdot\boldsymbol{\alpha} - \rho_3 mc^2)\psi(\mathbf{r}) = 0, \tag{4}$$

without restriction by boundary conditions at infinity or at the origin, in the form:

$$\psi(\mathbf{r}) = \sum_l \begin{Bmatrix} \sqrt{1+k_0/K}\{(l+1)A_l[j_l(kr) - \tan\delta_l^{(1)} n_l(kr)] \\ + lB_l[j_l(kr) - \tan\delta_l^{(2)} n_l(kr)]\} i^l P_l(\cos\theta) \\ \sqrt{1+k_0/K}\{A_l[j_l(kr) - \tan\delta_l^{(1)} n_l(kr)] \\ - B_l[j_l(kr) - \tan\delta_l^{(2)} n_l(kr)]\} i^l e^{i\varphi} P_l^1(\cos\theta) \\ \sqrt{1-k_0/K}\{lA_{l-1}[j_l(kr) - \tan\delta_{l-1}^{(1)} n_l(kr)] \\ + (l+1)B_{l+1}[j_l(kr) - \tan\delta_{l+1}^{(2)} n_l(kr)]\} i^l P_l(\cos\theta) \\ \sqrt{1-k_0/K}\{-A_{l-1}[j_l(kr) - \tan\delta_{l-1}^{(1)} n_l(kr)] \\ + B_{l+1}[j_l(kr) - \tan\delta_{l+1}^{(2)} n_l(kr)]\} i^l e^{i\varphi} P_l^1(\cos\theta) \end{Bmatrix} \tag{5}$$

For $\delta_l^{(1)} = \delta_l^{(2)} = 0$ this solution describes a particle with positive energy and its momentum and spin directed along the z axis. Here

$$j_l(kr) = (\pi/2kr)^{1/2} J_{l+1/2}(kr); \quad n_l(kr) = (\pi/2kr)^{1/2} N_{l+1/2}(kr).$$

The quantity $\hbar\mathbf{k}$ is the momentum, $E = c\hbar K$ is the energy, and $m = \hbar k_0/c$ is the mass of the particle. We note that, for $A_l = B_l = 1$ and $\delta_l^{(1)} = \delta_l^{(2)} = 0$, Eq. (5) is the expression of a plane wave in spherical coordinates.

The free-particle solution (5) is at the same time also an asymptotic expression for the solution of the Dirac equation in the presence of a spherically symmetrical center of short-range forces. In this case $\delta_l^{(1)}$ and $\delta_l^{(2)}$ are no longer arbitrary constants, and depend in a definite way on the form of the interaction potential.

3. APPROXIMATE SOLUTION OF THE DIRAC EQUATION FOR A PARTICLE IN A CENTRAL FIELD

In scattering problems the most important case is that in which there is no vector potential and the scalar potential is spherically symmetrical.

In this case it is convenient to consider instead of the Dirac equation

$$(E - c\,\mathbf{p}\cdot\boldsymbol{\alpha} - \rho_3 mc^2 - V(r))\,\psi(\mathbf{r}) = 0 \qquad (6)$$

the equivalent integral equation

$$\psi(\mathbf{r}) = \psi_0(\mathbf{r}) + \hat{D}(\mathbf{r})\int G(\mathbf{r},\mathbf{r}')\,V(r')\,\psi(\mathbf{r}')\,d\mathbf{r}', \qquad (7)$$

where

$$G(\mathbf{r},\mathbf{r}') = -\frac{1}{4\pi}\frac{\cos k\,|\mathbf{r}-\mathbf{r}'|}{|\mathbf{r}-\mathbf{r}'|}, \qquad (8)$$

$$\hat{D}(\mathbf{r}) = c^{-2}\hbar^{-2}(E + c\mathbf{p}\cdot\boldsymbol{\alpha} + \rho_3 mc^2). \qquad (9)$$

Furthermore for the zeroth approximation $\psi_0(\mathbf{r})$ we take not a plane wave, but the solution (5) of the free-particle Dirac equation, with the condition $\delta_l^{(1)} = \delta_l^{(2)} = 0$, which secures the finiteness of $\psi_0(\mathbf{r})$ at the origin:

$$\psi_0(\mathbf{r}) = \sum_l \begin{Vmatrix} \sqrt{\alpha}[(l+1)A_l + lB_l]\,i^l j_l(kr)\,P_l(\cos\theta) \\ \sqrt{\alpha}\,(A_l - B_l)\,i^l j_l(kr)\,e^{i\varphi}P_l^1(\cos\theta) \\ \sqrt{\beta}\,[lA_{l-1} + (l+1)B_{l+1}]\,i^l j_l(kr)\,P_l(\cos\theta) \\ \sqrt{\beta}\,(-A_{l-1} + B_{l+1})\,i^l j_l(kr)\,e^{i\varphi}P_l^1(\cos\theta) \end{Vmatrix} \qquad (10)$$

where for convenience we have introduced the notations

$$\alpha = 1 + k_0/K, \qquad \beta = 1 - k_0/K.$$

Assuming that the interaction energy can be regarded as a perturbation, we carry out a successive-approximation calculation to the second order. In this approximation the wave function has the form:

$$\psi(\mathbf{r}) = \psi_0(\mathbf{r}) + \psi_1(\mathbf{r}) + \psi_2(\mathbf{r})$$

$$= \psi_0(\mathbf{r}) + \hat{D}(\mathbf{r})\int G(\mathbf{r},\mathbf{r}')\,V(r')\,\psi_0(\mathbf{r}')\,d\mathbf{r}'$$

$$+ \hat{D}(\mathbf{r})\int G(\mathbf{r},\mathbf{r}')\,V(r')d\mathbf{r}'\,\hat{D}(\mathbf{r}')\int G(\mathbf{r}',\mathbf{r}'')\,V(r'')\,\psi_0(\mathbf{r}'')\,d\mathbf{r}''. \qquad (11)$$

By using the arbitrariness of A_l and B_l, and also the choice of the Green's function (8), we try to identify the asymptotic form of the wave function with the conditions at infinity, Eq. (5), in first and second approximations. In what follows we use the following expansion of the Green's function:

$$-\frac{1}{4\pi}\frac{\cos k\,|\mathbf{r}-\mathbf{r}'|}{|\mathbf{r}-\mathbf{r}'|}:$$

$$= \frac{k}{4\pi}\sum_{l=0}^{\infty}(2l+1)\,G(r,r')\Big\{P_l(\cos\theta)\,P_l(\cos\theta')$$

$$+ 2\sum_{m=1}^{\infty}\frac{(l-m)!}{(l+m)!}P_l^m(\cos\theta)\,P_l^m(\cos\theta')\cos m(\varphi-\varphi')\Big\}, \qquad (12)$$

$$G(r,r') = \begin{cases} j_l(kr')\,n_l(kr) & \text{for } r > r', \\ j_l(kr)\,n_l(kr') & \text{for } r < r'. \end{cases}$$

Here $\mathbf{r}$, θ, φ and $\mathbf{r}'$, θ', φ' respectively are the spherical coordinates for the position vectors $\mathbf{r}$ and $\mathbf{r}'$.

(a) First approximation. In the first approximation

$$\psi(\mathbf{r}) = \psi_0(\mathbf{r}) + \psi_1(\mathbf{r})$$

$$= \psi_0(\mathbf{r}) + \hat{D}(\mathbf{r})\int G(\mathbf{r},\mathbf{r}')\,V(r')\,\psi_0(\mathbf{r}')\,d\mathbf{r}'. \qquad (13)$$

By taking into account Eqs. (10), (12), and (13), and also the well known orthogonality and normalization relations of the Legendre polynomials, we can carry out the integration over the angles in $\psi_1(\mathbf{r})$. This gives:

$$\psi_1(\mathbf{r}) = k\hat{D}(\mathbf{r})\sum_l \begin{Vmatrix} \sqrt{\alpha}[(l+1)A_l + lB_l]\,i^l\Phi_l^l(r)P_l(\cos\theta) \\ \sqrt{\alpha}\,(A_l - B_l)\,i^l\Phi_l^l(r)e^{i\varphi}P_l^1(\cos\theta) \\ \sqrt{\beta}\,[lA_{l-1} + (l+1)B_{l+1}]\,i^l\Phi_l^l(r)P_l(\cos\theta) \\ \sqrt{\beta}\,(-A_{l-1} + B_{l+1})\,i^l\Phi_l^l(r)e^{i\varphi}P_l^1(\cos\theta) \end{Vmatrix} \qquad (14)$$

where we have used the notation:

$$\Phi_l^m(r) = n_l(kr)\int_0^r j_m^2(kr')\,V(r')\,r'^2dr'$$

$$+ j_l(kr)\int_r^{\infty} n_m(kr')j_m(kr')V(r')\,r'^2dr'. \qquad (15)$$

To get the final form of the wave function in first approximation, we must work out the application of the operator $\hat{D}(\mathbf{r})$ in the expression (14); we find as the result

$$\psi_1(\mathbf{r}) = \frac{kK}{c\hbar}\sum_l \begin{Vmatrix} \sqrt{\alpha}\{(l+1)A_l[\alpha\Phi_l^l(r) + \beta\Phi_l^{l+1}(r)] \\ + lB_l[\alpha\Phi_l^l(r) + \beta\Phi_l^{l-1}(r)]\}i^l P_l(\cos\theta) \\ \sqrt{\alpha}\{A_l[\alpha\Phi_l^l(r) + \beta\Phi_l^{l+1}(r)] - B_l[\alpha\Phi_l^l(r) \\ + \beta\Phi_l^{l-1}(r)]\}i^l e^{i\varphi}P_l^1(\cos\theta) \\ \sqrt{\beta}\{lA_{l-1}[\alpha\Phi_l^{l-1}(r) + \beta\Phi_l^l(r)] \\ + (l+1)B_{l+1}[\alpha\Phi_l^{l+1}(r) + \beta\Phi_l^l(r)]\}i^l P_l(\cos\theta) \\ \sqrt{\beta}\{-A_{l-1}[\alpha\Phi_l^{l-1} + \beta\Phi_l^l(r)] \\ + B_{l+1}[\alpha\Phi_l^{l+1}(r) + \beta\Phi_l^l(r)]\}i^l e^{i\varphi}P_l^1(\cos\theta) \end{Vmatrix} \qquad (16)$$

In obtaining Eq. (16) from Eq. (14) we have used

the differential relations

$$(p_1 + ip_2)\,\Phi_l^l(r)\,P_l(\cos\theta)$$

$$= \frac{\hbar k e^{i\varphi}}{i(2l+1)}\,[\Phi_{l-1}^l(r)\,P_{l-1}^1(\cos\theta) + \Phi_{l+1}^l(r)P_{l+1}^1(\cos\theta)]$$

$$p_3\Phi_l^l(r)\,P_l(\cos\theta)$$

$$= \frac{\hbar k}{i(2l+1)}\,[l\Phi_{l-1}^l(r)\,P_{l-1}(\cos\theta) - (l+1)\Phi_{l+1}^l(r)P_{l+1}(\cos\theta)],$$

$$(p_1 - ip_2)\,\Phi_l^l(r)P_l^1(\cos\theta)e^{i\varphi}$$

$$= -\frac{\hbar k}{i}\,\frac{l(l+1)}{2l+1}\,[\Phi_{l-1}^l(r)P_{l-1}(\cos\theta)$$

$$+ \Phi_{l+1}^l(r)\,P_{l+1}(\cos\theta)],$$

$$p_3\Phi_l^l(r)P_l^1(\cos\theta)\,e^{i\varphi} = \frac{\hbar k e^{i\varphi}}{i(2l+1)}\,[(l+1)\Phi_{l-1}^l(r)\,P_{l-1}^1(\cos\theta)$$

$$- l\Phi_{l+1}^l(r)P_{l+1}^1(\cos\theta)], \qquad (17)$$

which can easily be obtained by direct differentiation if one uses the connections between the successive Legendre polynomials that are well known from the theory of spherical harmonics.

We note that in Eq. (16) only Legendre functions of order l appear; this formulation is obtained by replacements of the summation index l by $l-1$ and $l+1$.

Recalling the asymptotic behavior of the function $\Phi_l^m(\mathbf{r})$ for large r

$$\Phi_l^m(r) \to n_l(kr)\int_0^\infty j_m^2(kr')V(r')\,r'^2dr', \qquad (18)$$

and using Eqs. (10) and (16), we can easily write out the asymptotic expression for the first-approximation wave function $\psi(\mathbf{r}) = \psi_0(\mathbf{r}) + \psi_1(\mathbf{r})$. Identifying this with the expression (5), we determine the following values for the scattering phase shifts:

$$\tan\delta_l^{(1)} = -\frac{kK}{c\hbar}\left\{\alpha\int_0^\infty j_l^2(kr)\,V(r)\,r^2dr + \beta\int_0^\infty j_{l+1}^2(kr)\,V(r)\,r^2dr\right\},$$

$$\tan\delta_l^{(2)} = -\frac{kK}{c\hbar}\left\{\alpha\int_0^\infty j_l^2(kr)\,V(r)\,r^2dr\right.$$

$$\left.+\beta\int_0^\infty j_{l-1}^2(kr)\,V(r)\,r^2dr\right\}. \qquad (19)$$

This same result is given also by the damping theory developed in the papers of reference 2. These papers contain a more detailed discussion of the results that follow from the formulas (19).

(b) Second approximation. The exact calculation of

$$\psi_2(\mathbf{r}) = \hat{D}(\mathbf{r})\int G(\mathbf{r},\mathbf{r}')\,V(r')\,\psi_1(\mathbf{r}')\,dr' \qquad (20)$$

involves rather cumbersome manipulations. We shall be interested in only the asymptotic behavior of $\psi(\mathbf{r}) = \psi_0(\mathbf{r}) + \psi_1(\mathbf{r}) + \psi_2(\mathbf{r})$, which is enough for the calculation of the scattering phase shifts in second approximation.

Substituting Eq. (16) in Eq. (20) and carrying out the angular integrations, we get by using Eq. (18) the asymptotic expression for $\psi_2(\mathbf{r})$ for $r \to \infty$:

$$\psi_2(\mathbf{r}) \approx \hat{D}(\mathbf{r})\sum_l \frac{Kk^2}{c\hbar}\left\{\begin{array}{c} \sqrt{\alpha}\,[(l+1)A_l\varepsilon_l^{(2)} \\ + lB_l\varepsilon_l^{(1)}]i^l n_l(kr)P_l(\cos\theta) \\ \sqrt{\alpha}[A_l\varepsilon_l^{(2)} - B_l\varepsilon_l^{(1)}]\; i^l n_l(kr)\,e^{i\varphi}P_l^1(\cos\theta) \\ \sqrt{\beta}[lA_{l-1}\varepsilon_l^{(4)} \\ +(l+1)\,B_{l+1}\varepsilon_l^{(3)}]i^l n_l(kr)P_l(\cos\theta) \\ \sqrt{\beta}[-A_{l-1}\varepsilon_l^{(4)} \\ +B_{l+1}\varepsilon_l^{(3)}]\; i^l n_l(kr)\,e^{i\varphi}P_l^1(\cos\theta), \end{array}\right\} \qquad (21)$$

where

$$\varepsilon_l^{(1)} = \int_0^\infty j_l(kr')[\alpha\Phi_l^l(r') + \beta\Phi_l^{l-1}(r')]r'^2dr',$$

$$\varepsilon_l^{(2)} = \int_0^\infty j_l(kr')\,[\alpha\Phi_l^l(r') + \beta\Phi_l^{l+1}(r')]\,r'^2dr',$$

$$\varepsilon_l^{(3)} = \int_0^\infty j_l(kr')[\alpha\Phi_l^{l+1}(r') + \beta\Phi_l^l(r')]\,r'^2dr',$$

$$\varepsilon_l^{(4)} = \int_0^\infty j_l(kr')[\alpha\Phi_l^{l-1}(r') + \beta\Phi_l^l(r')]\,r'^2dr'. \qquad (22)$$

Equation (21) does not differ in its structure from Eq. (14), since the relations (17) also hold for the function $n_l(kr)$. Therefore we omit the computations and give the expressions for the phase shifts in second approximation:

$$\tan\delta_l^{(1)} = -\left(\frac{kK}{c\hbar}\right)\left\{\alpha\int_0^\infty j_l^2(kr)\,V(r)\,r^2dr\right.$$

$$\left.+\beta\int_0^\infty j_{l+1}^2(kr)\,V(r)r^2dr\right\}$$

$$-\left(\frac{kK}{c\hbar}\right)^2\left\{\alpha^2\int_0^\infty j_l(kr)\,\Phi_l^l(r)\,V(r)\,r^2\,dr\right.$$

$$+2\alpha\beta\int_0^\infty j_l(kr)\,\Phi_l^{l+1}(r)\,V(r)\,r^2dr$$

$$\left.+\beta^2\int_0^\infty j_{l+1}(kr)\,\Phi_{l+1}^{l+1}(r)\,V(r)\,r^2dr\right\},$$

$$\tan\delta_l^{(2)} = -\left(\frac{kK}{c\hbar}\right)\left\{\alpha\int_0^\infty j_l^2(kr)V(r)r^2dr + \beta\int_0^\infty j_{l-1}^2(kr)V(r)r^2\,dr\right\}$$
$$-\left(\frac{kK}{c\hbar}\right)^2\left\{\alpha^2\int_0^\infty j_l(kr)\,\Phi_l^l(r)V(r)r^2\,dr + 2\alpha\beta\int_0^\infty j_l(kr)\,\Phi_l^{l-1}(r)V(r)r^2dr + \beta^2\int_0^\infty j_{l-1}(r)\,\Phi_{l-1}^{l-1}(r)V(r)r^2dr\right\}. \quad (23)$$

From (23) we can obtain previous results as special cases. For example, neglecting the terms quadratic in $V(r)$, we get the results found from the damping theory for the scattering of Dirac particles, Eq. (19). In the case of small values of the scattering phase shifts ($\tan\delta_l \approx \delta_l$) we find the results of the first Born approximation (cf. reference 3)

$$\delta_l^{(1)} = -\left(\frac{kK}{c\hbar}\right)\left\{\alpha\int_0^\infty j_l^2(kr)V(r)r^2dr + \beta\int_0^\infty j_{l+1}^2(kr)V(r)r^2dr\right\},$$
$$\delta_l^{(2)} = -\left(\frac{kK}{c\hbar}\right)\left\{\alpha\int_0^\infty j_l^2(kr)V(r)r^2dr + \beta\int_0^\infty j_{l-1}^2(kr)V(r)r^2dr\right\}.$$

The formulas in (23) can also be used to study the scattering by a center of Coulomb forces ($V(r) = -Ze^2/r$). In this case it must be noted that the integrated values of the phase shifts diverge. Nevertheless, we get correct results if in the formulas (2) we first carry out the summation over l, which gives the following values for the scattering amplitudes in second approximation:

$$f(\theta) = \left(\frac{Ze^2}{c\hbar}\right)\frac{K}{8k^2}\left(\frac{2\alpha}{\sin^2(\theta/2)} + \frac{2\beta\cos\theta}{\sin^2(\theta/2)}\right) + \left(\frac{Ze^2}{c\hbar}\right)^2\frac{\pi K^2}{4k^3}\frac{\alpha\beta}{\sin(\theta/2)}\left(1-\sin\frac{\theta}{2}\right),$$
$$g(\theta) = \left(\frac{Ze^2}{c\hbar}\right)\frac{K}{8k^2}\frac{4\beta\cos(\theta/2)}{\sin(\theta/2)} + \left(\frac{Ze^2}{c\hbar}\right)^2\frac{\pi K^2}{4k^3}\frac{\alpha\beta}{\cos(\theta/2)}\left(1-\sin\frac{\theta}{2}\right).$$

From this we get for the differential cross section the well known formula which takes into account not only relativistic and spin effects but also terms of the second order in $V(r)$, which characterize the asymmetry of the scattering of electrons and positrons[4]

$$\frac{d\sigma}{d\Omega} = \left(\frac{Ze^2}{2mc^2}\right)^2\frac{1-v^2/c^2}{v^4/c^4}\sec^4\frac{\theta}{2}\left[1-\frac{v^2}{c^2}\sin^2\frac{\theta}{2} + Z\pi\frac{v}{c}\left(\frac{e^2}{c\hbar}\right)\sin\frac{\theta}{2}\left(1-\sin\frac{\theta}{2}\right)\right].$$

[1] N. F. Mott and H. S. W. Massey, Theory of Atomic Collisions, Clarendon Press, Oxford, 1933.

[2] A. A. Sokolov and B. K. Kerimov, Nuovo cimento **5**, 921 (1957). Sokolov, Kerimov, and Guseinov, Nucl. Phys. **5**, 390 (1958).

[3] G. Parzen, Phys. Rev. **80**, 261 (1950).

[4] W. A. McKinley, Jr. and H. Feshbach, Phys. Rev. **74**, 1759 (1948).

Translated by W. H. Furry
98

TWO CASES OF UNSTABLE COMBUSTION

K. I. SHCHELKIN

Submitted to JETP editor August 28, 1958

J. Exptl. Theoret. Phys. (U.S.S.R.) 36, 600-606 (February, 1959)

A criterion has been derived for instability of the flame zone of a plane detonation wave; this criterion determines the conditions for the occurrence of a spin detonation. Conditions have been derived for the occurrence of single-headed spin detonations, and for oscillations of the combustion front in a detonation wave. It is shown that the criterion for unstable combustion which is derived for detonation waves is also applicable to forced combustion chambers.

The instability of the flame zone plane is considered as a source of high-frequency oscillations of the flame. The order of magnitude of the fundamental frequency of these oscillations has been determined, and the conditions for the appearance of higher harmonics have been found. The origin of resonance vibrations in a furnace is explained qualitatively, and an estimate is made of the maximum pressure during the oscillations.

1. INSTABILITY OF THE FLAME FRONT PLANE IN A DETONATION WAVE

LET us consider a stationary detonation wave. Gas, originally in a state represented by point O in the P-V diagram (Fig. 1), is rapidly compressed (by the shock wave) along the dynamic adiabatic to the state A. The high density and temperature of the gas in state A gives rise to chemical combustion reactions in the gas, whose final state is the Jouguet point J in the P-V diagram — the point where the Hugoniot adiabatic H is tangent to the line OA. At the point J, the sound velocity a is just equal to the velocity of the detonation front with respect to the compressed gas (the Jouguet condition):

$$a = D - W_J ,$$

where D is the velocity of detonation and W_J is the velocity of the gas in the pressure wave.

The chemical reactions going on in the detonation wave require a certain amount of time. Therefore the plane at which the combustion is completed does not coincide geometrically with the density discontinuity at A. Figure 2 shows schematically the distribution of pressure behind the front in a detonation wave. From A to J the pressure decreases in accordance with the rate at which heat is being generated. All the intermediate states on curve AJ in Fig. 2 are represented by points on the straight line AJ in Fig. 1; this follows from the requirement that all parts of the burning zone travel with the same velocity. The distribution of the states and velocities of the gas behind a detonation front has been dealt with exhaustively by Ya. B. Zel'dovich.[1]

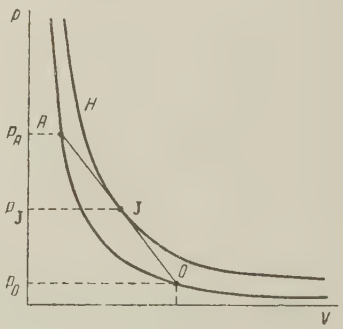

FIG. 1

The time required for a chemical reaction depends, as a rule, on the temperature and pressure according to the relation

$$\tau \sim p^{-n} e^{E/RT}, \qquad (1)$$

where E is the activation energy for the reaction, R is the gas constant, and n is a constant.

To simplify the discussion, it will be assumed in what follows that during the induction period τ there is no reaction at all, but that all the heating occurs instantaneously at the time τ. The distribution of pressure in the detonation wave for this approximation is shown in Fig. 3. The temperature

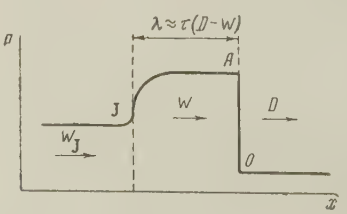

FIG. 2

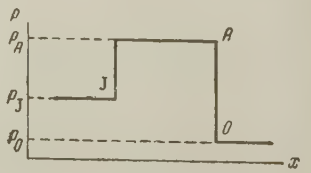

FIG. 3

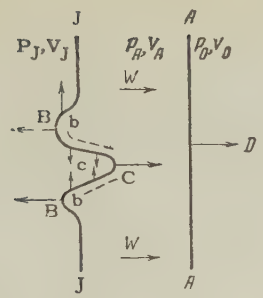

FIG. 4

and density distributions for the gas in the wave are analogous.

In Fig. 4 the compression shock front of the detonation wave is shown as a plane AA, perpendicular to the plane of the paper, and the heating front is represented by the surface JJ. On the heating front there is a perturbation BCB. This will arise if the flame induction period is lengthened in the regions marked b, and shortened in the region c — as a result of the non-uniformity of the burning mixture entering the flame zone, for example. To the right of this wavy surface JBCBJ, the gas is compressed to the pressure P_A, while to the left the pressure is equal to the lower value P_J. The values of P_A and P_J can be found from the P-V diagram, Fig. 1.

During the first few moments after the formation of a perturbation, the Jouguet conditions are fulfilled at points B, C, and B; along the direction of wave motion, the state and velocity of the gas remain the same as they were before the perturbation. However, in the direction perpendicular to the direction of propagation, the gas is set into motion and the pressure discontinuity that has been built up across the combustion surface begins to break up. The gas at the locations bb, being at the higher pressure, will expand adiabatically, and rarefaction waves will move into these regions, as shown by the dashed lines. The gas expanding out of bb will flow into the region c, compressing the gas in it. On the plane J-J, the pressure will be smoothed out to some value intermediate between P_A and P_J. In the neighborhood of the points B, B the gas b expands to the pressure P_J, while near point C the gas c is compressed to the pressure P_A.

In the regions b the detonation wave expands as if it were in a divergent cone. The compression at c, on the other hand, is equivalent to the concentration of a wave in a converging cone. To the right of the region c the induction period is decreased, because of the overcompression of the detonation wave; while in the regions bb the induction period is lengthened because of the reduced pressure. The original perturbation BCB spreads out, as shown by the arrows in Fig. 4, and the ignition front loses its stability.

It should be noted that, when the gas in the regions bb begins to expand and the gas at c is compressed, the Jouguet conditions at the points BB and C are destroyed and waves of pressure and rarefaction travel up to the plane AA and distort the shock-wave front. For a strong wave in a diatomic gas, the lateral extension of the disturbance along JJ is approximately three times as wide as the length of the burning zone by the time the initial disturbance has reached the shock front AA.

Even if an initial disturbance of the type BCB is suddenly formed, the burning zone will become unstable only if the perturbation grows sufficiently rapidly; otherwise the gas, in spite of its initial heterogeneity, will be able to escape from the vicinity of the ignition front, and the perturbation BCB will disappear.

The relationship can be formulated quantitatively as follows: if the adiabatic expansion of the gas from zone b into zone c, which lowers the temperature of the gas, increases the induction period of the reaction by an amount of the same order of magnitude as the induction period itself, or more, then any initial curvature of the front will be increased, and a plane front will not be stable. Reasoning in this way, and neglecting the dependence of the induction period on pressure or density, one is led to the expression

$$(d\tau/dT)|_{T_A}(T - T_A) \geqslant \tau, \qquad (2)$$

where T is the temperature of the unburned gas in region b after its expansion.

From (1) and (2) we can obtain the criterion for the instability of a plane flame zone in a detonation wave:

$$(E/RT_A)(1 - T/T_A) \geqslant 1. \qquad (3)$$

It has already been mentioned that near the point B the gas b expands to the pressure P_J of point J (Figs. 1 and 2), while near the point C the burning gas is compressed to the pressure P_A. Formula (3) can therefore be re-written as

$$(E/RT_A)[1 - (P_J/P_A)^{(\gamma-1)/\gamma}] \geqslant 1. \qquad (4)$$

The quantities occurring in equation (4) can be calculated readily for any concrete case.

As an example, let us estimate the value of expression (4) for a detonation wave in a diatomic gas with an activation energy of 40,000 cal/mole, propagating with a velocity of 1700 m/sec (M = 5).

For an initial temperature of $T_0 = 290°K$, the temperature of the unburned gas behind the pres-

sure front will be equal to 1650°K. In the detonation wave, the ratio of the pressure of the burned gas to the pressure of the unburned gas, P_J/P_A, is close to one-half, so that

$$\frac{E}{RT_A}\left[1-\left(\frac{P_J}{P_A}\right)^{(\gamma-1)/\gamma}\right]=\frac{40\,000}{2\cdot1650}[1-(1/2)^{0.4/1.4}]=2.2>1.$$

The loss of stability of the flame front, as we have said, leads to disturbances in the shock wave front AA. This results in the formation of wrinkles in the compression front. Details of the surface irregularities and the formation of spin detonations can be found in references 1 to 4.

If the width of the detonation wave front λ (the distance from the plane AA to the plane JJ in Figs. 2, 3, and 4) is small is comparison with the tube diameter d, then a large number of wrinkles may form in the compression front, over the whole cross-section of the tube. A total of $(d/3\lambda)^2$ wringles may be formed in the whole area. Because there is no a priori tendency for the disturbances to move in any one direction, they will propagate randomly in different directions with respect to the shock front surface. They will mutually interfere and will ignite the gas, particularly in the regions of constructive interference. As a result, the detonation wave front will take on the appearance of a pulsating brush. As the diameter of the tube decreases, or as the chemical reaction time increases (i.e., as the composition or the pressure of the mixture approach the detonation limit) the tube cross-section will contain fewer and fewer irregularities, until finally only one remains — a classical single-headed spin detonation.

Intermediate between the single-headed spin detonation and the brush-like detonation front are the cases of spin detonation with two, three, and more heads.

From the above considerations it is possible to derive the conditions for the formation of a single-headed spin detonation in a diatomic gas: the reaction zone thickness must be of the order of one-third of the tube diameter, or greater.

$$3\lambda/d=3\tau(D-W)/d\geqslant 1, \qquad (5)$$

where W is the gas velocity in the density discontinuity, and d is the tube diameter.

Instability of the ignition zone and a "brushlike" fine structure of the detonation front can also occur in the detonation of condensed explosives. Spin detonations are not observed in condensed explosives, apparently because the conditions for a single-headed spin are very close to the conditions for the failure of detonation near the limiting diameter for an unconfined charge. It is possible that spin might be observed in a small-diameter charge encased in a very strong confining tube.

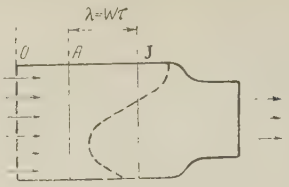

FIG. 5

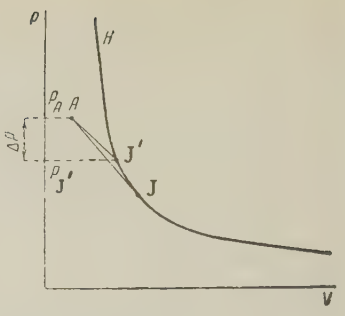

FIG. 6

Some years ago Apin[5] put forward a "jet" mechanism for the propagation of detonations in condensed explosives. He, too, proposed a brush-like structure for the front of his jet detonations. Apin ascribed the formation of the "brush" to the projection of gas jets into the unburned material. The jets were assumed to be formed either by microscopic non-uniformities in the material or by microcavitation in blisters or bubbles.

It is probably more natural to explain the "brush-like" structure of the burning or detonation zone of condensed explosives by the instability of the plane ignition zone, and the formation of many irregularities in the wave front, which interfere with each other and ignite the unreacted explosive, just as in the case of gaseous detonations.

To conclude this section, it should be mentioned that the instability of a plane ignition front in a detonation wave was first considered by the author[4] in 1949. Zel'dovich and Kompaneets,[1] speaking of the conditions for the existence of spin detonations, remarked that during the ignition of a gas the burning should be faster in a convex compression wave than in a plane wave. On the other hand, a convex front will not be concentrated as the detonation proceeds. The existence of a spin is therefore possible only if the magnitude of E/RT is sufficiently large. The critical value of this quantity is not to be found in the cited references.

2. INSTABILITY OF THE IGNITION ZONE AS THE SOURCE OF HIGH-FREQUENCY VIBRATIONS IN FORCED COMBUSTION CHAMBERS

Forced combustion chambers, e.g., in rockets, may (very schematically, of course) be represented as shown in Fig. 5. In the region O-A the components are mixed and preheated. In the space from A to J the mixture reacts by self-ignition; at the plane J the combustion reaction has been completed.

The combustion process in a furnace is hydrodynamically and thermodynamically analogous to

the combustion in a detonation wave. The state of the gas at the plane A can be described by some point A in Fig. 1. Its state when it reaches J is given by the point J in the same figure, lying below A on a branch of the Hugoniot adiabatic, or (depending upon the burning rate of the mixture) by some other point J′ (Fig. 6) which lies above J but below A. The gas thermodynamics of furnace combustion have been considered in detail by Troshin.[6]

For the case in which a preheated mixture is subsequently ignited in a furnace, the reaction time (the induction period for ignition) is found from an expression of the type (1). Because of the similarity between combustion in a furnace and combustion in a detonation, we may carry over to a furnace all the considerations and conclusions of the preceding section about the instability of a plane ignition front.

We can write down the same criterion for the instability of a plane ignition zone:

$$\frac{E}{RT}\left[1-\left(\frac{P_A-\Delta P}{P_A}\right)^{(\gamma-1)/\gamma}\right]\geqslant 1. \qquad (6)$$

Here T is the temperature of the heated mixture, P is the pressure drop along the furnace due to the burning. In Fig. 6, if the state of the combustion products is characterized by the point J′, the pressure drop $P = P_A - P_{J'}$.

Just as in the previous case, the loss of stability in the plane front leads to the formation of a pulsating combustion zone. In view of the fact that in furnaces the velocity of the unburned mixture is always considerably less than the speed of sound, the width of the disturbances in the combustion front will be of the order of twice the width of the burning zone. We may therefore have

$$(d/2\lambda)^2 = (d/2\tau W)^2 \qquad (7)$$

disturbances of the combustion front over the cross-sectional area of the furnace.

We can now estimate the frequency of the pulsations. Since this frequency will depend on the ratio (7), it is useful to begin by estimating the lowest possible frequency. This is the case where the expression (7) is numerically equal to unity, i.e., when the length of the burning zone is about equal to, or greater than, half the diameter of the chamber. This can be considered to be the fundamental frequency of the furnace oscillations.

The time required to develop a single pulse is of the order of $\lambda/a = \tau W/a$, since the instability is propagated with the speed of sound, a, because the disturbances which lengthen or shorten the induction period are propagated with the speed of sound. However, the recovery of the perturbed front varies with the rate at which the unignited gas replenishes the combustion zone:

$$t_{rec} \approx \lambda/W = \tau W/W \approx \tau,$$

i.e., the time taken for the front to recover from a perturbation is of the order of the ignition induction period, τ. Since W is always small compared to a, and the time interval $\tau W/a$ can be neglected, the order of magnitude of the fundamental frequency is

$$\nu_0 = 1/\tau. \qquad (8)$$

If the length of the combustion zone $\lambda = \tau W$ is noticeably less than the chamber diameter, and if we consider the pulsations to be random and unsynchronized over the cross section of the chamber, then the upper limit of frequency can be obtained by multiplying (7) and (8):

$$\nu_{max} = \frac{1}{\tau}\left(\frac{d}{2\tau W}\right)^2 = \frac{1}{\tau}\left(\frac{d}{2\lambda}\right)^2. \qquad (9)$$

It is easy to estimate the order of magnitude of these frequencies. For a light gasoline, for example, which we may take to be composed entirely of heptane, in a furnace where the mixture is preheated to 700°K, the induction period is

$$\tau = 10^{-14.4}e^{38000/2\cdot 700} = 2.5\cdot 10^{-3} \text{ sec.}$$

The fundamental frequency is therefore 400 cycles per second. The length of the burning zone for this case, if the velocity of the unburned gases is assumed to be 50 m/sec, is equal to $\lambda = 50 \times 2.5 \times 10^{-3} = 0.125$ m. In a chamber one meter in diameter the maximum attainable frequency is:

$$\nu_{max} = \frac{1}{2.5\cdot 10^{-3}}\left(\frac{1}{2\cdot 0.125}\right)^2 = 6400 \text{ cps.}$$

Each pulse in the combusion front produces a pressure wave in the chamber with an amplitude of the order of ΔP (Fig. 6). This wave will spread out from the location of the disturbance, decaying rapidly. In themselves, waves such as these apparently constitute no danger to the furnace. However, if the oscillation of the flame front resonates with one of the proper frequencies of the gas in the furnace (either longitudinal or transverse) dangerous vibrational forces may be set up in the chamber, with a large pressure drop across the wave fronts.

The resonant frequencies are of the order of magnitude of

$$\nu_p = k\bar{a}/L, \qquad (10)$$

where a is a quantity close to the mean speed of sound in the chamber, L is a characteristic dimension (length or diameter) of the chamber,

and k is the order of the harmonic.

It can be seen from a consideration of the instability condition (6) that resonance could produce dangerous results. Expression (6) shows that the flame will begin to oscillate if a rarefaction wave with an amplitude of the order of ΔP would noticeably increase the induction period for combustion; a compressive wave of the same strength would decrease the induction period. Consequently, compressive waves with amplitude ΔP moving through the hot gas will accelerate its combustion. As they pass through the unburned mixture, they "ignite" it in their paths, picking up the energy of combustion as they go, and so increasing in amplitude. This provides a mechanism for increasing the amplitude of resonance oscillations.

We can now attempt to estimate the order of magnitude of the pressure drop attainable in a compression wave during resonance oscillation in a combustion chamber. For this purpose we may use a crude, almost unreasonable model: waves travelling in the region of hot, unignited gas will be assumed to compress the mixture at almost constant volume, while waves in the remaining parts of the chamber will be treated as simple decaying shock waves.

The maximum pressure drop in a travelling wave can be approximated (very roughly, of course) by

$$\Delta P_{max} = P_A (\pi - 1) W/a, \qquad (11)$$

where π is the increase in pressure which would result from combustion at constant volume. One of the crudest approximations made in the derivation of equation (11) is the assumption that the flow rate of gas out of the chamber, and consequently the pressure in the chamber, are not affected by the oscillation. A number of other factors are also ignored.

Using formula (11) with $\pi = 10$, for the same numerical example used above, one obtains

$$\Delta P_{max} = P_A (10 - 1)\,{}^{50}/_{600} = 0.75\ P_A \sim P_A.$$

During resonance oscillations, therefore, the pressure drop in the compression waves can, if the chamber is strong enough, reach a value of the same order of magnitude as the total chamber pressure itself.

It must be emphasized again that throughout this entire second section, we have been considering the combustion very schematically, and that the conclusions are of a qualitative rather than a quantitative nature.

In conclusion, it must be remembered that qualitative evidence for the role which the induction period for combustion plays in setting up high-frequency oscillations in combustion chambers has already been presented. See, for instance, the work of Crocco which is mentioned in reference 7.

[1] Ya. B. Zel'dovich and A. S. Kompaneets, Теория детонации (Theory of Detonation) GITTL, Moscow (1955).

[2] K. I. Shchelkin, Dokl. Akad. Nauk SSSR **47**, 501 (1945)

[3] Ya. B. Zel'dovich, Dokl. Akad. Nauk SSSR **52**, 147 (1946).

[4] K. I. Shchelkin, Быстрое горение и спиновая детонация газов (Rapid Combustion and Spin Detonation of Gases) Voenizdat, Moscow (1949).

[5] A. Ya. Apin, Dokl. Akad. Nauk SSSR **50**, 285 (1945); A. Ya. Apin and V. K. Bobolev, Dokl. Akad. Nauk SSSR **58**, 241 (1947).

[6] Ya. K. Troshin, Izv. Akad. Nauk SSSR, Otdel. Tekh. Nauk (in press).

[7] Sin-I Cheng, Jet Propulsion **26**, 92 (1956).

Translated by D. C. West
99

ON THE COMPENSATION EQUATION IN SUPERCONDUCTIVITY THEORY

D. V. SHIRKOV

The V. A. Steklov Mathematics Institute, Academy of Sciences, U.S.S.R.

Submitted to JETP editor September 1, 1958

J. Exptl. Theoret. Phys. (U.S.S.R.) 36, 607-612 (February, 1959)

A relation between the matrix elements of the variational derivatives of the scattering matrix and the energy operator is established. With its aid the kernel of the integral equation for the compensation of "dangerous" diagrams is expressed in terms of the usual Green functions.

1. INTRODUCTORY REMARKS

AN analysis of the influence of the Coulomb interaction between electrons in superconductivity theory was given in a paper by Bogolyubov, Tolmachev, and the author.[1] The structure of the kernel $Q(k, k')$ of the integral equation for the compensation of dangerous electron diagrams was also investigated (§5). This kernel was expressed in terms of the characteristics of the auxiliary model problem which describes the Coulomb interaction between the electrons and also their interaction with the auxiliary classical external field. The above-mentioned characteristics of the model problem were strictly determined only in one case through the method of approximate second quantization (§6.1). In the remaining cases expressions for these characteristics, containing "radiative" Coulomb corrections, were estimated, in the region of the infrared catastrophe, from qualitative considerations (§6.2). The reason for this was that the method of expressing the kernel Q in terms of the energy operator

$$R = H_{\text{int}} T\left(\exp\left\{-i\int_{-\infty}^{0} H_{\text{int}}(t)dt\right\}\right) = H_{\text{int}} S^{0}_{-\infty} \quad (1.1)$$

which was used in that paper, leads for a number of cases to inconvenient and asymmetric expressions.

It is, however, well known that the energy characteristics of a many-body system can be expressed in terms of the "total" S-matrix[2,3]

$$S = S^{\infty}_{-\infty} = T\left(\exp\left\{-i\int_{-\infty}^{\infty} H_{\text{int}}(t)dt\right\}\right). \quad (1.2)$$

In the present investigation such an approach is used as the basis of the discussion. Through this the kernel $Q(k, k')$ is expressed in terms of the vacuum matrix elements of the variational derivatives of S, i.e., in terms of the usual Green functions for which explicit expressions can be obtained, for instance, by the method of approximate second quantization.[5]

2. THE RELATION BETWEEN THE OPERATORS S AND R AND THEIR VARIATIONAL DERIVATIVES

The connection of the energy levels of a system which has undergone second quantization and the total scattering matrix S was recently investigated by Sucher[2] and Rodberg.[3] The most convenient formula was obtained by Rodberg (Eq. (16) of reference 3).* From this formula follows, in particular, a connection between the matrix elements of the total S-matrix (1.2) and those of the energy operator R (1.1) which can be written in the form

$$\langle \Phi_n^* S \Phi_n \rangle_c = -2\pi i \delta(E - E_n) \langle \Phi_n^* R \Phi_n \rangle_c. \quad (2.1)$$

The index "c" indicates here that only connected diagrams are taken into account in the evaluation of the matrix elements.

Equations of the type (2.1) can also be established for the commutators of the quantities S, R with the particle creation and annihilation operators, and also for the variational derivatives of S and R with respect to those operators.

Let $a^+_{k,\sigma}$ be the creation operator for an electron with momentum k, energy $\epsilon(k)$ and spin σ. We can then connect the commutator [see Eq. (47.13) of reference 4]

$$[a^+_{k,\sigma}, S]_- = -\sum_{k',\sigma'}\int_{-\infty}^{\infty} \frac{\delta S}{\delta a_{k',\sigma'}(t)} [a^+_{k,\sigma}, a_{k',\sigma'}(t)]_+ dt$$

$$= -\int_{-\infty}^{\infty} \frac{\delta S}{\delta a_{k,\sigma}(t)} e^{-i\varepsilon(k)t}\, dt \quad (2.2)$$

with the commutator

$$[a^+_{k,\sigma}, R] = -\int_{-\infty}^{0} \frac{\delta R}{\delta a_{k,\sigma}(t)} e^{-i\varepsilon(k)t}\, dt \quad (2.3)$$

*A similar formula was independently obtained by V. V. Tolmachev (unpublished).

through the relation

$$[a^+_{k,\sigma}, S]\,\Phi_E = -i\int\limits_{-\infty}^{\infty} e^{it(H_0+\varepsilon(k)-E)}\,dt\,[a^+_{k,\sigma}, R]\,\Phi_E. \quad (2.4)$$

To show that, we write (2.1) in the form

$$S\Phi_E = -i\int\limits_{-\infty}^{\infty} e^{it(H_0-E)}\,dt\,R\Phi_E. \quad (2.5)$$

From (2.5) follows also that

$$Sa^+_{k,\sigma}\,\Phi_E = -i\int\limits_{-\infty}^{\infty} e^{it(H_0-E-\varepsilon(k))}\,dt\,Ra^+_{k,\sigma}\Phi_E. \quad (2.6)$$

On the other hand,

$$a^+_{k,\sigma}\,S\Phi_E = -ia^+_{k,\sigma}\int\limits_{-\infty}^{\infty} e^{it(H_0-E)}\,dtR\Phi_E$$

$$= -i\int\limits_{-\infty}^{\infty} e^{it(H_0-\varepsilon(k)-E)}\,dt\,a^+_{k,\sigma}R\Phi_E. \quad (2.7)$$

The difference between Eqs. (2.6) and (2.7) gives (2.4).

Considering more complicated commutators we arrive at the formula

$$\int\limits_{-\infty}^{\infty}\left\langle\Phi_1^*\frac{\delta^{n+m}S}{\delta a^+_{k_1\sigma_1}(t_1)\ldots\delta a^+_{k_n\sigma_n}(t_n)\,\delta a_{l_1s_1}(\tau_1)\ldots\delta a_{l_ms_m}(\tau_m)}\Phi_2\right\rangle_c$$

$$\times\exp\left\{i\sum_i\varepsilon(k_i)t_i - i\sum_j\varepsilon(l_j)\tau_j\right\}dt_1\ldots d\tau_m$$

$$= -2\pi i\delta\left(E_1-\sum_i\varepsilon(k_i)+\sum_j\varepsilon(l_j)-E_2\right)$$

$$\times\int\limits_{-\infty}^{0}\left\langle\Phi_1^*\frac{\delta^{n+m}R}{\delta a^+_{k_1\sigma_1}(t_1)\ldots\delta a_{l_ms_m}(\tau_m)}\Phi_2\right\rangle_c$$

$$\times\exp\left\{i\sum_i\varepsilon(k_i)t_i - i\sum_j\varepsilon(l_j)\tau_j\right\}dt_1\ldots d\tau_m. \quad (2.8)$$

We note next that we can use the property of the translational invariance of the matrix element of the variational derivative of the S-matrix to perform in the left hand side one integration over time and to split off explicitly the δ-function. This gives

$$i\int\limits_{-\infty}^{\infty}\left\langle\Phi_1^*\frac{\delta^{n+m}S}{\delta a^+_{k_1\sigma_1}(0)\,\delta a^+_{k_2\sigma_2}(t_2)\ldots\delta a_{l_ms_m}(\tau_m)}\Phi_2\right\rangle_c$$

$$\times\exp\left\{i\sum_{i=2}^{n}\varepsilon(k_i)t_i - i\sum_j\varepsilon(l_j)\tau_j\right\}dt_2\ldots d\tau_m$$

$$= \int\limits_{-\infty}^{0}\left\langle\Phi_1^*\frac{\delta^{n+m}R}{\delta a^+_{k_1\sigma_1}(t_1)\ldots\delta a_{l_ms_m}(\tau_m)}\Phi_2\right\rangle_c$$

$$\times\exp\left\{i\sum_{i=1}^{n}\varepsilon(k_i)t_i - i\sum_j\varepsilon(l_j)\tau_j\right\}dt_1\,dt_2\ldots d\tau_m \quad (2.9)$$

where

$$\sum_{i=1}^{n}\varepsilon(k_i) - \sum_{j=1}^{m}\varepsilon(l_j) = E_1 - E_2. \quad (2.10)$$

Equation (2.9) is most convenient for further applications.

3. TRANSFORMATIONS OF THE KERNEL Q OF THE COMPENSATION EQUATION

We go now to the transformation of the kernel $Q(k, k')$ of the equation of compensation of dangerous electron diagrams, determined by Eq. (I.5.36).* In reference 1 it was shown that the kernel Q can be written in the form of a sum of two terms

$$Q(k, k') = Q_c(k, k') + Q_{ph}(k, k'). \quad (3.1)$$

The first term Q_c corresponds to Coulomb effects only and can be obtained from (I.5.36) by replacing R by R_c [Eq. (I.5.49)], i.e., by assuming $H_{ph} = 0$. Using the fact that in the case considered the momenta k, k′ are near the Fermi surface, so that the energies $\tilde{\varepsilon}(k)$, $\tilde{\varepsilon}(k')$ are small, we obtain using (2.9)

$$Q_c(k, k') = \begin{cases} i\int\limits_{-\infty}^{\infty}\langle\delta^4S_c/\delta a^+_{k',+}(0)\,\delta a^+_{-k',-}(t_1)\,\delta a_{k,+}(t_2)\,\delta a_{-k,} \\ \qquad -(t_3)\rangle_c dt_1\,dt_2\,dt_3 \\ \qquad \text{if} \quad k < k_F, \\ i\int\limits_{-\infty}^{\infty}\langle\delta^4S_c/\delta a^+_{k,+}(0)\,\delta a^+_{-k,-}(t_1)\,\delta a_{k',+}(t_2)\,\delta a_{-k'}, \\ \qquad -(t_3)\rangle_c dt_1\,dt_2\,dt_3 \\ \qquad \text{if} \quad k > k_F, \end{cases} \quad (3.2)$$

where

$$S_c = T\left(\exp\left\{-i\int\limits_{-\infty}^{\infty}H_c(t)\,dt\right\}\right). \quad (3.3)$$

To transform the second term in (3.1) which is proportional to g^2 it is convenient to start not from Eq. (I.5.36) but from the earlier Eq. (I.5.31).

We shall use (2.9) to write the coefficient of u_k^2 on the right hand side of that equation which is according to (I.5.34) equal to

$$\int\limits_{-\infty}^{0}dt\,dt'\exp\{i\tilde{\varepsilon}(k)(t+t')\}\langle\delta^2R'/\delta a^+_{k,+}(t')\,\delta a^+_{-k,-}(t)\rangle_c$$

$$= \sum_{k'}u_{k'}v_{k'}Q(k, k'), \quad (3.4)$$

in the form

$$i\int\limits_{-\infty}^{\infty}\langle\delta^2S/\delta a^+_{k,+}(0)\,\delta a^+_{-k,-}(t)\rangle_c\,e^{i\tilde{\varepsilon}(k)t}\,dt.$$

In accordance with (2.10) this is possible, if

*I.e., Eq. (5.36) of reference 1.

$$\tilde{\varepsilon}(k) + \tilde{\varepsilon}(k) = 2\tilde{\varepsilon}(k) = 0, \tag{3.5}$$

i.e.,

$$\sum_{k'} u_{k'} v_{k'} Q(k, k') = i \int_{-\infty}^{\infty} \langle \delta^2 S / \delta a^+_{k',+}(0)\, \delta a^+_{-k',-}(t) \rangle_c \, dt \tag{3.6}$$

if (3.5) is satisfied.

The matrix element which enters into the right hand side can be written in the form of a time-ordered product of two "currents" $(\delta S/\delta a^+) S^+$:

$$\left\langle \frac{\delta^2 S}{\delta a^+_{k',+}(0)\, \delta a^+_{-k',-}(t)} \right\rangle_c = \left\langle \frac{\delta^2 S}{\delta a^+_{k',+}(0)\, \delta a^+_{-k',-}(t)} S^+ \right\rangle_{\alpha_0}$$

$$= \left\langle T \left(\frac{\delta S}{\delta a^+_{k',+}(0)} S^+ \right) \left(\frac{\delta S}{\delta a^+_{-k',-}(t)} S^+ \right) \right\rangle_{\alpha_0} \tag{3.7}$$

if we take the causality properties of the S-matrix [see, for instance, Eq. (48.15) of reference 4] into account. The index α_0 denotes here an averaging over the α-vacuum.

The time-ordered product of "currents" thus obtained is for any fixed order of the time arguments ($t > 0$ or $t < 0$) the ordinary product of these "currents". This product can be expanded in a series in terms of a complete set of functions. If we restrict ourselves in this expansion to terms corresponding to states containing one α-electron and one β-phonon we split off the "main terms" containing small denominators $\{\tilde{\omega}(q) + \tilde{\varepsilon}(k) + \tilde{\varepsilon}(k')\}$.

By this means we get, for instance for $t < 0$, using the property of translational invariance,

$$\left\langle \frac{\delta^2 S}{\delta a^+_{k',+}(0)\, \delta a^+_{-k',-}(t)} \right\rangle_c = \sum_{k',s} \left\langle \frac{\delta S}{\delta a^+_{k',+}(0)} S^+ \alpha^+_{k',s} \beta^+_{k-k'} \right\rangle_{\alpha_0}$$

$$\times \left\langle \alpha_{k's} \beta_{k-k'} \frac{\delta S}{\delta a^+_{-k',-}(t)} S^+ \right\rangle_{\alpha_0} = \sum_{k',s} \exp\{it[\tilde{\omega}(k-k') + \tilde{\varepsilon}(k')]\}$$

$$\times \left\langle \frac{\delta S}{\delta a^+_{k',+}(0)} \alpha^+_{k's} \beta^+_{k-k'} \right\rangle_{\alpha_c} \left\langle \alpha_{k's} \beta_{k-k'} \frac{\delta S}{\delta a^+_{-k',-}(t)} \right\rangle_{\alpha_c} \tag{3.8}$$

Commuting after that the operators α^+, α, β^+, β with $\delta S/\delta a^+$ we can go to the limit as $\alpha \to a$. Combining the results for $t < 0$ and $t > 0$, taking into account the symmetry of the Hamiltonian H_{ph} with respect to β and β^+ we get, using (3.7) and (3.8)

$$i \int_{-\infty}^{\infty} \langle \delta^2 S / \delta a^+_{k',+}(0)\, \delta a^+_{-k',-}(t) \rangle_c \, dt$$

$$= -2 \sum_{k'} \frac{u_{k'} v_{k'}}{\tilde{\varepsilon}(k') + \tilde{\omega}(k-k')} \Gamma(k, k', q)\, \Gamma(-k, -k', -q);$$

$$(q = k - k'), \tag{3.9}$$

where

$$\Gamma(k, k', q) = \int_{-\infty}^{\infty} d\tau\, d\theta \langle \delta^3 S / \delta a_{k',+}(\tau)\, \delta a^+_{k',+}(0)\, \delta\beta_q(\theta) \rangle_{a_c}. \tag{3.10}$$

Expression (3.10) is written down in the limit of small $\tilde{\epsilon}(k')$ and $\tilde{\omega}(q)$.

Before comparing Eqs. (3.6) and (3.9), we make the following substitution. According to condition (3.5), Eq. (3.6) permits us to evaluate Q in the limiting case $\tilde{\epsilon}(k) = 0$. Since the momentum k is near the Fermi surface, the energy $\tilde{\epsilon}(k)$ will in actual fact be a small quantity. In the representation of the kind (I.5.57) which we have used, the energy $\tilde{\epsilon}(k)$ is everywhere put equal to zero except in the energy denominator $\tilde{\omega}(q) + \tilde{\epsilon}(k) + \tilde{\epsilon}(k')$. To obtain the required expression for Q_{ph} we must thus add $\tilde{\epsilon}(k)$ in the energy denominator of the right hand side of (3.9). In this way we get from (3.6) and (3.9)

$$Q_{ph}(k, k') = -2 \frac{\Gamma(k, k', q)\, \Gamma(-k, -k', -q)}{\tilde{\omega}(q) + \tilde{\varepsilon}(k) + \tilde{\varepsilon}(k')}. \tag{3.11}$$

Performing in (3.10) the variation over β and the transition to the limit $g = 0$, we have also

$$Q_{ph}(k, k') = 2 \frac{g^2(q)\, \omega(q)\, (\lambda_q + \mu_q)^2}{\tilde{\omega}(q) + \tilde{\varepsilon}(k') + \tilde{\varepsilon}(k)}$$

$$\times \Lambda(k, k', q)\, \Lambda(-k, -k', -q), \tag{3.12}$$

where

$$\Lambda(k, k', q)$$

$$= \int_{-\infty}^{\infty} d\tau\, d\theta \langle \delta^2 [T(H_q(\theta) S_c)] / \delta a_{k',+}(\tau)\, \delta a^+_{k',+}(0) \rangle_{a_c}, \tag{3.13}$$

$$H_q(\theta) = \frac{1}{V 2V} \sum_{l,s} a^+_{l+q,s}(\theta)\, a_{l,s}(\theta). \tag{3.14}$$

The quantity Λ can be expressed simply in terms of one-electron Green functions of the above-mentioned model problem. On the other hand, performing explicitly in (3.13) the functional differentiation and using the "generalized Wick theorem" [see Eq. (34.11) of reference 4] we get a representation of Λ in terms of the one-electron Green functions and the four-vertex Green function of the pure Coulomb problem. We have

$$\Lambda = \frac{1}{V 2V} \Big\{ 1 + \int_{-\infty}^{\infty} dt\, d\tau \overrightarrow{a^+_{k',+}(t)}\, a_{k',+}(0)$$

$$\times \langle \delta^2 S_c / \delta a^+_{k',+}(t)\, \delta a_{k',+}(\tau) \rangle_c$$

$$+ \int_{-\infty}^{\infty} dt\, d\tau \overrightarrow{a^+_{k',+}(\tau)}\, a_{k,+}(t) \langle \delta^2 S_c / \delta a^+_{k,+}(0)\, \delta a_{k,+}(t) \rangle_c$$

$$+ \sum_{l,s} \int_{-\infty}^{\infty} d\theta\, d\tau\, dt_1 dt_2 \overrightarrow{a^+_{l+q,s}(\theta)}\, a_{l+q,s}(t_1)\, \overrightarrow{a^+_{l,s}(t_2)}\, a_{l,s}(\theta)$$

$$\times \langle \delta^4 S_c / \delta a^+_{l,s}(t_2)\, \delta a^+_{k,+}(0)\, \delta a_{l+q,s}(t_1)\, \delta a_{k',+}(\tau) \rangle_c \Big\}. \tag{3.15}$$

The time-ordered pairing which occurs here has the form

$$\overrightarrow{a^{+}_{k,+}(t)\,a_{k,+}(\tau)} = \begin{cases} \theta_F(k)\, e^{-i\tilde{\varepsilon}(k)(t-\tau)} & \text{if } t > \tau, \\ -\theta_G(k)\, e^{-i\tilde{\varepsilon}(k)(\tau-t)} & \text{if } t < \tau, \end{cases} \quad (3.16)$$

where

$$\theta_F(k) = 1 - \theta_G(k) = \begin{cases} 1 & \text{if } k < k_F, \\ 0 & \text{if } k > k_F. \end{cases} \quad (3.17)$$

In conclusion the author expresses his gratitude to N. N. Bogolyubov and V. V. Tolmachev for helpful discussions.

[1] Bogolyubov, Tolmachev, and Shirkov, Новый метод в теории сверхпроводимости (A New Method in Superconductivity Theory), Acad. Sci. Press, 1958; [Fortschr. Physik, in press].

[2] J. Sucher, Phys. Rev. **107**, 1448 (1957).

[3] L. S. Rodberg, Phys. Rev. **110**, 277 (1958).

[4] N. N. Bogolyubov and D. V. Shirkov, Введение в теорию квантованных полей (Introduction into the Theory of Quantum Fields) GTI, 1957 [translation published by Interscience, 1959].

[5] Chen Chun-Sian and Chow Shih-Hsun, J. Exptl. Theoret. Phys. (U.S.S.R.) **34**, (1958), Soviet Phys. JETP **7**, 1080 (1958).

Translated by D. ter Haar
100

Letters to the Editor

STATISTICAL DELAY OF DISCHARGE IN NaCl *AND* KBr

M. A. MEL' NIKOV

Tomsk Polytechnic Institute

Submitted to JETP editor June 9, 1958; resubmitted November 10, 1958

J. Exptl. Theoret. Phys. (U.S.S.R.) 36, 613-614 (February, 1959)

THE fact that x-ray treated and untreated crystals have the same value of pulse breakdown voltage[1,2] leads to the conclusion that an increase in the number of free electrons does not influence either the electric strength or the delay time t_d of the discharge, and that there is no statistical delay time t_{st}. In NaCl exposed for 10^{-8} sec, t_{st} is almost zero.[3,4] In mica and glass, the statistical delay is either zero or less than 10^{-8} sec.[5] According to reference 6, $t_{st} > 10^{-8}$ in KCl, but the procedure employed in this reference, whereby the specimen was exposed to multiple pulses, was not faultless. Thus, at exposures of 10^{-8} sec and longer, there is no statistical delay in solid dielectrics.

We have developed a procedure for obtaining high-voltage pulses (up to 27 kv) with wavefronts of 10^{-9} sec, and for recording these pulses with a pulsed[7] cathode-ray oscillograph. We attempted to estimate t_{st} with the aid of this procedure of NaCl and KBr crystals. The breakdown was produced between a hemisphere and a plane (spaced 100 μ at the thinnest point), with the front of a single pulse, applied for intervals ranging from 4 to 6 millimicroseconds. The specimens were either untreated or previously treated with x-rays for four hours and illuminated during the time of breakdown. The diagram shows the dependence of

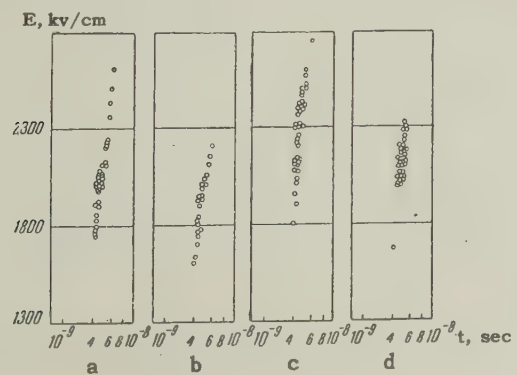

Dielectric	E_b, kv/cm	t_d	ΔE		Δt_d	
		10^{-9} sec	kv/cm	%	10^{-9} sec	%
Untreated NaCl	2420	2.7				
X-ray treated NaCl	2130	2.2	290	12	0.5	18.5
Untreated Kbr	2570	2.85				
X-ray treated Kbr	2280	2.38	290	11.6	0.47	16.5

the electric strength E_b on the time prior to breakdown of the untreated and x-ray treated specimens of NaCl and KBr. The table lists the values of the strength for a breakdown probability $\psi = 90\%$, the discharge delay time t_d, the reduction in strength ΔE_b, and the reduction in the discharge delay time Δt_d for x-ray treated and untreated specimens. The value of t_d was determined by the Vorb'ev procedure.[3] The static strength, used to determine t_d, was assumed to be the same for treated and untreated specimens, namely the value of E_b of untreated specimens when the voltage was applied for 10^{-6} sec, before space charge could manifest itself.

To ascertain whether the difference in the values of E_b and t_d for treated and untreated specimens lies within the experimental error, we analyzed the possible errors. A detailed analysis of the errors that arise in experiments similar to ours was made in reference 3. We give a brief analysis of the errors in our experiments. We measured the thickness of the specimen with the IZV-1 instrument, which reads 1μ per scale division, and in which the relative error is $a_1 = 1\%$ for both treated and untreated specimens. The errors a_2 and a_3, which can arise in the oscillographic determination of the amplitude of the voltage pulse and of the time prior to breakdown, do not exceed 2% and 5% respectively. The divider and tube were calibrated with measuring spheres. However, since we used the same calibration curve for both x-ray treated and untreated specimens, the error in the calibration of the tube is automatically allowed for in the calibration curve. Errors may result from distortion in the oscillograms. At a tube accelerating voltage of 42 kv the electron velocity was 1.22×10^{10} cm/sec and the time of flight in the deflecting field was 3.28×10^{-10} sec. The reduction in the amplitude, allowing from the effect of the electron time of flight between deflecting plates, is not more than 0.2%. The distortion due to the asymmetry of the potential of the deflecting plates (cf. reference 8) does not affect the results of the measurements.

Thus, the error in the pulse amplitude amounted to $a_1 + a_2 = 1 + 2 = 3\%$. It follows therefore that the difference in the values of E_b and t_d for untreated and treated specimens does not lie within

the experimental error and probably indicates the presence of a statistical delay in the discharge of untreated NaCl and KBr specimens. If $t_{st} = 0$ for treated specimens, the difference in the discharge delay time will be the statistical delay time for untreated specimens, with values 5×10^{-10} sec for NaCl and 4.7×10^{-10} sec for KBr. If $t_{st} \neq 0$ for the treated specimens, the differences in the delay time are the differences in the statistical delay times of the discharge in untreated and x-ray treated specimens of NaCl and KBr.

The author takes this opportunity to thank Prof. A. A. Vorob'ev for guiding this research.

[1] A. F. Walther and L. D. Inge, Dokl. Akad. Nauk SSSR **2**, 65 (1934).

[2] A. Walther and L. Inge, Arch. Elektrotechn. **28**, 72 (1934).

[3] G. A. Vorob'ev, Dissertation, Tomsk Polytechn. Inst., 1956.

[4] K. K. Sonchik, Изв. Высшей школы СССР, Физика (News of the Higher Schools, Phys. Ser.) No. 4, 73 (1958).

[5] E. A. Konorova, J. Exptl. Theoret. Phys. (U.S.S.R.) **32**, 603 (1957), Soviet Phys. JETP **5**, 497 (1957).

[6] Kawamura, Ohkira, and Kichi, J. Phys. Soc. Japan **9**, 541 (1954).

[7] G. A. Vorob'ev, Изв. Высшей школы СССР, Физика (News of the Higher Schools, Phys. Ser.) No. 4, 174 (1958).

[8] Voznesenskiĭ, Korotkikh, Chernetskiĭ, and Koporskiĭ, Usp. Fiz. Nauk **62**, 4, 497 (1957).

Translated by J. G. Adashko
101

ON THE QUESTION OF COLLECTIVE EFFECTS IN LIGHT NUCLEI

V. V. BALASHOV and A. F. TULINOV

Institute of Nuclear Physics, Moscow State University

Submitted to JETP editor June 27, 1958

J. Exptl. Theoret. Phys. (U.S.S.R.) **36**, 615-616 (February, 1959)

In the region of light nuclei, the shell model gives good agreement with experiment for the magnetic moments and the probabilities of the magnetic dipole γ transitions. On the other hand, there is no such agreement for the probabilities of the E2 transitions and the electric quadrupole moments (cf. the table; the energy of the levels, E, is given in Mev).

The values for τ_{theor} for the transitions in C^{12} taken from the paper of Kurath,[5] corrected for the value $\langle r^2 \rangle = 5.7 \times 10^{-26}$ cm^2 obtained by Hofstadter.[6] It is seen from the table that in all three cases the measured transition probability is higher than the calculated one. The analysis of the relative intensities of the E2 and M1 transitions leads to the same result.[5,7]

If we further consider that the measured nuclear quadrupole moments lie well above those calculated with the shell model,[8] we are driven to the conclusion that the shell model always gives too low values for the corresponding matrix elements.

It is believed that this situation is connected with the collective motion of the nucleons in the nucleus. This effect was accounted for in the nucleus O^{17} by introducing an additional effective nucleon charge $e' = \alpha e$, which is connected with the excitation of collective quadrupole oscillations in the nucleus.[9] α was found to be ≈ 0.6. We note that better agreement with experiment is indeed obtained by using approximately this value for the effective charge in the calculation of the matrix elements for the transitions in the nuclei C^{12} and B^{10}. However, the concept of an effective charge is closely connected with the formalism of the unified nuclear model of Bohr and Mottelson,[10] whose applicability to light nuclei is doubtful. In this sense the use of an effective charge in the region of light nuclei corresponds to the formal introduction of additional parameters; the question of the role of collective effects in E2 transitions in light nuclei, therefore, remains open.

In view of this it is of interest to consider the collective effects in the nucleus in a general way, independently of the specific mechanism of the collective intensification of the electric quadrupole transitions and, hence, of the introduction of any additional parameters.

In the absence of the single-particle operator, the operator for the quadrupole transition connected with the collective motion contains, owing to the charge independence of nuclear forces, only the scalar component of the isotopic spin. (In the framework of the unified nuclear model this follows immediately from relation (7.12) of refer-

Nucleus	Transition $E(J, T) \to E(J', T')$	τ, experiment	τ, theory	
			$L-S$	$j-j$
C^{12}	4.43 (2.0) → 0 (0.0)	$5.25 \cdot 10^{-14}$ sec [1]	$1.8 \cdot 10^{-13}$ sec	$4.2 \cdot 10^{-12}$ sec
B^{10}	0.72 (1.0) → 0 (3.0)	$1.05 \cdot 10^{-9}$ sec [2]	∞	$4.5 \cdot 10^{-9}$ sec
Be^{10}	3.37 (2.1) → 0 (0.1)	$< 8 \cdot 10^{-14}$ sec [3]	$1.4 \cdot 10^{-13}$ sec	∞ [4]

ence 10.) Collective effects are therefore absent in E2 transitions in which the isotopic spin changes, and one may assume that the shell model theory gives the correct values for the probabilities of these transitions. We note that the conclusion that the shell model theory cannot give the probabilities of quadrupole transitions is based on the analysis of transitions in which the isotopic spin does not change (see above).

The verification of the above assertion is of special interest in the region of light nuclei, where the isotopic spin may be considered a good quantum number and where, moreover, the shell model successfully explains the spectrum of energy levels. Within the p shell only a few pure E2 transitions with a change in the isotopic spin can be observed:

B^{10}	3.58 (2.0) → 1.74 (0.1),	C^{12}	16.1 (2.1) → 0 (0.0),
B^{10}	4.77 (2.0) → 1.74 (0.1),	N^{14}	? (2.0) → 2.31 (0.1).
B^{10}	6.02 (4.2) → 5.16 (2.1),		

For the first three transitions experimental values are available only for the total Γ width of the level.[7,11] Γ, the width for the transition $16.1 \rightarrow 0$ in C^{12}, is equal to 0.72 ev (reference 12). In the limit of j-j coupling (the intermediate coupling parameter $\xi = \infty$) the ground state of C^{12} corresponds to the closed shell $p_{3/2}$, and the excited state at 16.1 Mev corresponds to the configuration $|p_{3/2}^{-1}p_{1/2}; 21>$. Using the value $<r^2> = 5.7 \times 10^{-26}$ cm² (reference 6), we obtain, in this approximation, $\Gamma_{theor} = 0.87$ ev. Perturbation theoretical calculations show that Γ_{theor} decreases for deviations from strict j-j coupling, with $d\Gamma_{theor}/d(1/\xi) = 0.24$ ev in the limit of j-j coupling.

This example therefore confirms our previous contention that the increase in the probability of quadrupole transitions is connected with collective effects and that these effects vanish in transitions in which the isotopic spin changes. Unfortunately, experimental data are available only for the single case 16.1 (C^{12}).

In this connection the following experiments are of interest: (a) A measurement of τ for the transitions 3.58 → 1.74 Mev and 4.77 → 1.74 Mev in B^{10}. This can be done either by the Doppler method, e.g., in the reaction $C^{12}(d, \alpha)B^{10}$, or by measuring the relative transition probabilities from the states 3.58 and 4.77 Mev to the lower lying states. (b) A measurement of the relative probabilities in the mixed M1 + E2 transitions, in particular, in the transition 17.63 → 2.9 Mev in the nucleus Be^8, for which an experimental value for the total Γ width is available.[11]

[1] Swann, Metzger, and Rasmussen, Bull. Am. Phys. Soc., Ser. II 2, 29 (1957).

[2] Bloom, Turner, and Wilkinson, Phys. Rev. 105, 232 (1957).

[3] A. N. Boyarkina and A. F. Tulinov, J. Exptl. Theoret. Phys. (U.S.S.R.) 36, 353 (1959); Soviet Phys. JETP 9, 244 (1959) this issue.

[4] V. V. Balashov, Доклады на Всесоюзной конференции по ядерным реакциям при малых и средних энергиях (Proceedings of the All Union Conference on Nuclear Reactions at Low and Intermediate Energies) Moscow, 1957.

[5] D. Kurath, Phys. Rev. 106, 975 (1957).

[6] R. Hofstadter, Revs. Modern Phys. 28, 214 (1956).

[7] L. Meyer-Schuetzmeister and S. Hanna, Phys. Rev. 108, 1506 (1957).

[8] M. Mayer and J. Jensen, Elementary Theory of Nuclear Shell Structure, N. Y. 1955.

[9] B. H. Flowers, Доклады на Всесоюзной конференции по ядерным реакциям при малых и средних энергиях (Proceedings of the All Union Conference on Nuclear Reactions at Low and Intermediate Energies) Moscow, 1957.

[10] A. Bohr and B. Mottelson, Kgl. Danske. Vid. Selskab, Mat.-fys. Medd. 27, No.16 (1953).

[11] F. Ajzenberg and T. Lauritsen, Revs. Modern Phys. 27, 77 (1955).

[12] A. Lane and L. Radicati, Proc. Phys. Soc. 67, 167 (1954).

Translated by R. Lipperheide
102

DIFFRACTION STRIPPING OF RELATIVISTIC PARTICLES

I. I. IVANCHIK

P. N. Lebedev Physics Institute, Academy of Sciences, U.S.S.R.

Submitted to JETP editor June 27, 1958

J. Exptl. Theoret. Phys. (U.S.S.R.) 36, 617-618 (February, 1959)

IN a number of papers[1-4] various authors have considered the diffraction dissociation of the deuteron on a "black" nucleus in the deuteron energy region $E_d \sim 100$ to 200 Mev. The nucleus is also black when $E_d \gtrsim 6$ Bev. We first show that the results obtained earlier[1-4] also apply for a relativistic deuteron.

First we consider diffraction scattering. If φ is the wave function for free motion the wave func-

tion for a deuteron which suffers diffraction at the nucleus is $\psi = \varphi\Omega(\rho_n)\Omega(\rho_p)$ (cf. reference 3). The subscripts n and p refer to the neutron and proton respectively, ρ is the radius vector of the particle in the plane perpendicular to the beam axis; $\Omega(\rho) = 0$ or 1 when $\rho \gtrless R$, where R is the radius of the nucleus.

We find the expression for φ. Since the relative motion in the deuteron is nonrelativistic the wave function of the deuteron in the rest system is known. This wave function is

$$\xi_i \sqrt{\alpha/2\pi}\, e^{-iM\tau} e^{-\alpha r}/r,$$

where ξ_i denotes the spin state of the function for spin 1, $\alpha = 1/2 R_d$, R_d is the radius of the deuteron, M is the deuteron mass, τ is the characteristic time and r is the distance between the proton and neutron. Considered as a whole the deuteron is a particle of spin 1. Hence it may be assumed that the part of the deuteron wave function which depends on its motion as a whole is transformed by a Lorentz transformation for the irreducible representation for spin 1, for example the representation given by Shirokov.[5] The part of the wave function which describes the relative motion is a scalar in the sense of the Lorentz transformation. Hence in the system in which the deuteron moves as a unit with a 4-velocity u_μ its wave function is of the form:

$$\varphi_i = \xi_i \exp(ip_\mu x_\mu) \sqrt{\alpha/2\pi} \exp\left(-\alpha\sqrt{y_\mu^2}\right)/\sqrt{y_\mu^2}.$$

Here $p_\mu = Mu_\mu$, $x_\mu^{p(n)}$ are the coordinates of the proton (neutron), $x_\mu = (x_\mu^p + x_\mu^n)/2$ and $y_\mu = x_\mu^p - x_\mu^n$. From the equality $y_\mu u_\mu = 0$, we have $y_0 = (u_i y_i)/u_0$, i.e., the characteristic contraction for a relativistic particle. The amplitude for the elastic scattering of the deuteron is written in a way similar to that used in reference 3. The only difference is that in place of the expression $\exp(-2\alpha r)/r^2$, after some simple transformations we obtain

$$\frac{\exp(-\alpha r)\exp\left(-\alpha\sqrt{r^2+\lambda^2 z^2 - 2\lambda z(\rho\cdot\nu)}\right)}{r\sqrt{r^2+\lambda^2 z^2 - 2\lambda z(\rho\cdot\nu)}}.$$

Here ν is a unit vector parallel to the projection of the velocity of the scattered deuteron on the plane perpendicular to the axis of the beam (z-axis); $\kappa' = p_0\theta R$, where p_0 is the initial momentum of the deuteron; $\lambda = \kappa'(\mu v/cMA^{1/3})$; μ is the mass of the π meson; A is the atomic number of the target nucleus.

For a given κ' the difference from the nonrelativistic scattering amplitude is determined by the parameter $\eta = \mu v/cMA^{1/3}$. When A = 216 we have $\eta \sim 1/80$; on the other hand the non-relativistic distributions have been computed in references 1—4 with an accuracy $1/p^2 \sim 1/9$ (for the same value of A). Completely analogous arguments may be invoked for diffraction stripping. On this basis it can be shown that when $E_d \gtrsim 6$ Bev the earlier formulas for diffraction scattering and stripping still apply.

These considerations can also be applied to the process of diffraction production, for example the production of a charged π meson by a relativistic proton. The possibility of such a process was first indicated by Pomeranchuk and Feĭnberg.[6] In emulsions irradiated by protons with energies greater than several Bev (approximately 10 Bev), this effect can appear as the scattering of a relativistic particle. The nucleus on which the break in the track would occur would not undergo any change but the scattering angle would be large (cf. below). To estimate the angular and energy distributions of the π-mesons this process can be considered as the diffraction of a deuteron-like system consisting of the π meson and the neutron. Part of the time a proton is in the state $\pi^+ + n$. The binding energy for this state is approximately μc^2 while the wave function for the internal motion, at least at a distance $r \gtrsim \hbar/\mu c$, is essentially the same as the wave function for the deuteron. For this reason quantitative estimates can be made on the basis of the results found for deuteron splitting. The system spends only approximately 1/10 of the total time in the state described by this wave function but we can still estimate the total cross section. Since the masses of the π meson and the neutron are different it is necessary to apply the formulas for unequal masses used in reference 4. The energy and angular distributions of the emitted π-mesons should be given by Eqs. (14) and (15) of reference 4. In accordance with Eq. (14) the maximum lies at a π-meson energy $E_\pi \sim \mu E_p/M \sim E_p/7$ while the mean momentum transferred to the nucleus is of order μc. In simple scattering at this same angle the proton would transfer a momentum of approximately Mc to the nucleus, in which case the nucleus should disintegrate.

In conclusion the author wishes to thank E. L. Feĭnberg for discussions of this problem.

[1] E. L. Feĭnberg, J. Exptl. Theoret. Phys. (U.S.S.R.) **29**, 115 (1955), Soviet Phys. JETP **2**, 58 (1956).

[2] R. Glauber, Phys. Rev. **99**, 1515 (1955).

[3] A. I. Akhiezer and A. G. Sitenko, J. Exptl. Theoret. Phys. (U.S.S.R.) **32**, 794 (1957), Soviet Phys. JETP **5**, 652 (1957).

[4] I. I. Ivanchik and Ya. S. Popov, J. Exptl. Theoret. Phys. (U.S.S.R.) this issue, p. 509 Soviet Phys. JETP?

[5] Yu. M. Shirokov, Dokl. Akad. Nauk SSSR **94**, 857 (1954).

[6] I. Ya. Pomeranchuk and E. L. Feĭnberg, Dokl. Akad. Nauk SSSR **93**, 439 (1953).

Translated by H. Lashinsky
103

SCATTERING OF 240-Mev AND 270-Mev NEGATIVE PIONS ON HYDROGEN

V. G. ZINOV and S. M. KORENCHENKO

Joint Institute for Nuclear Research

Submitted to JETP editor August 26, 1958

J. Exptl. Theoret. Phys. (U.S.S.R.) **36**, 618-619 (February, 1959)

THE elastic and exchange scattering of π^- mesons on hydrogen at 240 and 270 Mev energy was studied, using the π^- meson beam of the Joint Institute for Nuclear Research synchrocyclotron. The measurements were carried out by means of scintillation counters. Liquid hydrogen was used as the target.

The measured values of the differential cross sections are given in Tables I and II (in units of 10^{-27} cm^2/sterad).

If we assume that only the S and P waves take part in the scattering, then the angular distributions can be written in the form

$$d\sigma/d\omega = AP_0 + BP_1 + CP_2,$$

where P_0, P_1, and P_2 are the Legendre polynomials. The coefficients of the expression, found by means of the least-mean-square method, are given in Table III (in units of 10^{-27} cm^2/sterad).

TABLE I

(240±7) MeV			
$\vartheta_{c.m.s.}^{\circ}$	$\left(\frac{d\sigma}{d\omega}\right)_{\pi^- \to \pi^-}$	$\vartheta_{c.m.s.}^{\circ}$	$\left(\frac{d\sigma}{d\omega}\right)_{\pi^- \to \gamma}$
39.9	1.60±0.16	19.7	9.91±1.21
58.7	1.40±0.12	38.8	7.96±0.93
76.3	1.01±0.09	57.2	6.63±0.77
97.8	0.82±0.09	74.5	4.53±0.53
117.1	0.89±0.08	95.7	4.05±0.49
138.6	1.48±0.12	114.9	3.47±0.43
158.1	1.97±0.19	136.8	3.58±0.51
		157.0	4.56±0.60

TABLE II

(270±7) Mev			
$\vartheta_{c.m.s.}^{\circ}$	$\left(\frac{d\sigma}{d\omega}\right)_{\pi^- \to \pi^-}$	$\vartheta_{c.m.s.}^{\circ}$	$\left(\frac{d\sigma}{d\omega}\right)_{\pi^- \to \gamma}$
40.6	1.40±0.13	20.0	7.78±0.94
59.6	1.17±0.11	39.6	6.19±0.73
77.3	0.83±0.08	58.1	4.90±0.59
98.8	0.60±0.06	75.5	3.42±0.41
117.9	0.77±0.08	96.8	2.52±0.32
139.3	1.09±0.10	115.9	2.31±0.30
158.4	1.56±0.16	137.6	2.65±0.36
		157.4	3.10±0.42

TABLE III

	240 Mev			270 Mev		
	$\pi^- \to \pi^-$	$\pi^- \to \gamma$	$\pi^- \to \pi^0$	$\pi^- \to \pi^-$	$\pi^- \to \gamma$	$\pi^- \to \pi^0$
A	1.28±0.046	5.12±0.22	2.56±0.11	1.04±0.039	3.73±0.18	1.86±0.09
B	0.23±0.089	2.72±0.41	1.82±0.27	0.27±0.077	2.35±0.31	1.53±0.20
C	0.93±0.12	2.30±0.50	2.18±0.47	0.79±0.094	2.01±0.36	1.81±0.32

The total cross sections for the interaction of π^- mesons with hydrogen at 240 and 270 Mev energy equal $(48.3 \pm 3.3) \times 10^{-27}$ cm^2, and $(36.5 \pm 2.4) \times 10^{-27}$ cm^2 respectively.

Translated by H. Kasha
104

ACCELERATION OF CHARGED PARTICLES IN RUNNING OR STANDING ELECTROMAGNETIC WAVES

G. A. ASKAR' YAN

P. N. Lebedev Physics Institute, Academy of Sciences U.S.S.R.

Submitted to JETP editor September 5, 1958

J. Exptl. Theoret. Phys. (U.S.S.R.) **36**, 619-621 (February, 1959)

THE average Lorentz force acting on a charged particle in the field of, say, a plane electromagnetic wave depends not only on the amplitudes but also on the phase shift between the oscillating-particle velocity and the magnetic field of the wave. For example, in the absence of free-particle momentum spread this average force is zero in a traveling wave. In a standing wave it is different from zero and is directed towards the nodes of the wave field (cf., for example, references 1 — 3), but the spatial sinusoidal variation of this force does not allow us to utilize it for prolonged acceleration over distances exceeding $\frac{1}{4}$ of a wavelength. It is therefore of interest to investigate in general the conditions that can give rise to the existence of a unidirectional average force of sufficient magnitude acting on particles in a traveling or in a standing wave.

The average force depends on the resonance properties of the motion of the particles (arising as a result of the application of special kinds of external fields or of the utilization of plasma resonances etc.) and on the spread in the transverse momentum of the particles (as a result of radiation or of collisions with other particles in the bunch, in the plasma stream, or in the stationary plasma). In the general case, the resonance frequency ω_0 and the dissipation coefficient γ may vary spatially. It will be shown that a special choice of these two quantities may lead to a directed continuous acceleration of particles, independent of the sign of the charge, through the spatially periodic field of the standing wave.

It can be easily shown that the average Lorentz force acting on each charge in the running wave is given by

$$f_{av} = {}^1/_2 r_0 E_0 H_0 \gamma \omega^2 c / \{(\omega_0^2 - \omega^2)^2 + \gamma^2 \omega^2\}$$

(E_0, H_0 — are the field amplitudes, $r_0 = e^2/mc^2$ is the "classical radius" of the charge), i.e., if the frequency of the wave and the characteristic parameters of the oscillations are chosen appropriately acceleration becomes possible even for unbunched particles.

Let us consider the case when dissipation predominates over the inertial and resonance factors, which occurs, in particular, near resonance. When $|\omega_0^2 - \omega^2| \ll \gamma\omega$; $f_{av} \sim r_0 E_0 H_0 c/\gamma$, i.e., as damping decreases the force increases. The possibility of accelerating particles near resonance in the case of small damping associated not with radiation by particles, but, for example, with small collision losses, will make it unnecessary to bunch the particles compactly, which is difficult to achieve, and will also allow direct acceleration of heavy weakly-radiating particles. However, if the losses are associated with radiation, then $\gamma = {}^2/_3 \omega^2 N r_0 / c$ (N is the number of particles in the bunch), therefore the total force is given by $f_{av} \approx E_0 H_0 c^2/\omega^2 N$; for $N r_0 \omega / c > |1 - \omega_0^2/\omega^2|$. In this case bunching the particles increases the range of working frequencies, but a further increase in the number of particles in the bunch diminishes the force acting on each particle of the bunch.

In the opposite case when the frequency spread is sufficiently great the acting force is proportional to the dissipation coefficient. For example, if damping is associated with radiative processes, then

$$f_{av} = N r_0^2 E_0 H_0 \omega^4 / 3(\omega_0^2 - \omega^2)^2.$$

This case leads to the expression for the force acting on each particle: $f \sim N$, which is characteristic of the coherent method of acceleration proposed by V. I. Veksler.

The use of bunches also permits one to achieve, in order to produce the required phase shift, a large dissipation of the transverse components of the momenta of the particles on collisions within the bunch without any appreciable dissipation of forward motion.

It is evident from the above that it is possible by various methods to vary within wide limits the phase shift between the velocity of oscillation and the electric field of the wave. This circumstance may be utilized not only in order to increase the efficiency of acceleration in a traveling wave, but also for the production of a spatially variable phasing of particle oscillations needed for continuous acceleration in a standing-wave field. The transition to standing waves not only allows a sharp reduction in the power of the power supply, but also guarantees efficient acceleration of a rarefied unbunched plasma or one that is weakly bunched (in order for the ions to be entrained by the electrons).

The average Lorentz force acting on each particle in a high-frequency standing wave depends on

the longitudinal coordinate z

$$f_{av} \approx {}^1/_2 r_0 E_0 H_0 \{(\omega_0^2 - \omega^2)\,\omega c / [(\omega_0^2 - \omega^2)^2 + \gamma^2\omega^2]\} \sin 2hz.$$

In order to achieve cumulative acceleration of particles it is necessary that in those regions of space where sin 2hz changes sign the factor $\{\ldots\}$ should either change sign or have a different magnitude. (In estimating the average force we can, as before, restrict ourselves in certain cases to a consideration of the effect on the forced vibrations, since the possible excitation of characteristic oscillations gives no average contribution not only in the presence of real damping or of a spread in the phases of excitation of free oscillations, but also as a result of the fact that the characteristic oscillations have a frequency different from the frequency of the magnetic field of the wave.) In the case of a more complicated, say sinusoidal, spatial variation of the resonance parameters, we can easily demonstrate the fact that the space average of the accelerating force is different from zero by making use of solutions of the Mathieu equation, or by assuming for the sake of simplicity that the variations of the resonant frequency are small and by restricting ourselves to the first approximation. The cumulative contribution in the latter case will be determined by integrals of terms of the type $\sin\{2\pi(2/\lambda - 1/l)\,z + \varphi\}$ in the case when the spatial period l of the frequency variation is equal to one half of the wavelength of the radiation λ. Such zonal damping of the reverse acceleration by local constant external fields or by a local choice of the regime of dissipation will enable us to obtain continuous acceleration of plasma particles over long paths within the stationary field of a standing wave of large amplitude.

The simplest choice of the spatial variation of the oscillation parameters may be made by means of increasing or decreasing the axial magnetic field in those "quarter wavelength" regions in which it is required to alter the direction or the magnitude of the acceleration. This field will give rise to spatially-periodic variation of the amplitudes and the phases of the forced oscillations either because of a change in the cyclotron resonance frequencies, or because of a change in the characteristic plasma resonances (these changes may occur due to a change in plasma density when it is compressed in the regions of increased magnetic field) etc. Such a "corrugated field" may also help the focusing of the beam of particles undergoing acceleration.

In the method of acceleration under discussion the effective accelerating field intensity acting on the electrons may be made sufficiently large compared to the amplitude of the electric wave field. The efficiency of acceleration can also be increased by a transition from a linear resonator to a circular resonator utilizing repeated traversals of the wave field.

It is evident that similar devices may be used not only for the acceleration of plasma, but also for retarding and for turning back charged particles leaking out of storage systems.

[1] Veksler, Kovrizhnykh, Rabinovich, and Yankov, Report, Physics Institute, Academy of Sciences, U.S.S.R., 1956.

[2] A. V. Gaponov and M. A. Miller, J. Exptl. Theoret. Phys. (U.S.S.R.) **34**, 242 (1958), Soviet Physics JETP **7**, 168 (1958).

[3] H. Boot and R. Harvie, Nature **180**, 1187 (1957).

Translated by G. Volkoff
105

CONCERNING THE PRODUCTION OF COMPOUND NUCLEI IN THE INTERACTION BETWEEN ATOMIC NUCLEI

A. S. KARAMYAN, Yu. B. GERLIT, and B. F. MYASOEDOV

Submitted to JETP editor September 16, 1958

J. Exptl. Theoret. Phys. (U.S.S.R.) **36**, 621-623 (February, 1959)

IT is natural, when investigating the interaction between multiply-charged ions and nuclei of various elements, to inquire about the extent to which these reactions proceed by complete fusion of the colliding nuclei with subsequent evaporation of neutrons. A useful criterion for such a reaction are the curves of the cross section of a reaction involving the emission of a specified number of

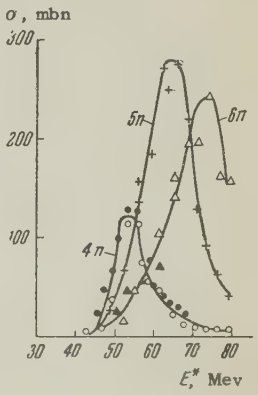

FIG. 1. Dependence of the cross sections of the reactions Au(N, (4–6)n) on the excitation energy of the compound nucleus Em^{211}.

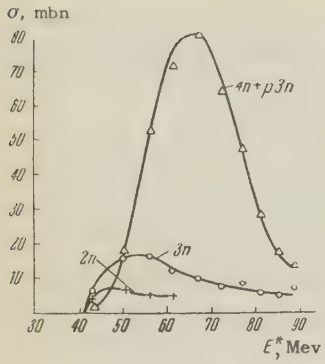

FIG. 2. Dependence of the cross sections of the reactions V(N, xn) on the exitation energies of the compound nucleus Zn^{65}.

neutrons vs. the energy of excitation of the compound nucleus.

Baraboshkin et al.[1] obtained the excitation functions of the reactions $Au^{197}(N^{14}, xn)$ where x = 4, 5, and 6. New literature data[2] on branching in the α-decay and K-capture "forks," and more exact measurements of the energies of accelerated nitrogen ions have enabled us to refine somewhat these data. The excitation functions of the reactions that involve emission of 4, 5, or 6 neutrons in the interaction between accelerated nitrogen ions with gold nuclei, shown in Fig. 1, have a behavior that is characteristic of the production of a compound nucleus. The absolute values of the cross sections show that the reactions proceed in this manner with high probability. However, when the nitrogen-ion energies exceed 70 Mev, the compound Em^{211} nuclei are fissioned, a fact that makes difficult the study of deviations from the formation of compound nuclei at high excitation energies. It is obvious that it is necessary to employ for this purpose targets of lighter nuclei, for which the fission of compound nuclei has a low probability. Furthermore, there are indications[3] that the character of the interaction between multiply-charged ions and nuclei depends substantially on the region of mass numbers of the target nuclei. Irradiation of a lighter element by multiply charged ions will therefore simultaneously permit us to determine the extent to which reactions with formation of a compound nucleus occur at other regions of mass numbers, and to investigate possible deviations from this mechanism. For this purpose, we investigated interactions between accelerated ions of N^{14}, N^{15}, C^{12}, and C^{13} and nuclei of vanadium. The experiments were carried out in the following manners: stacks comprising 10 — 12 aluminum foils, 8μ thick with a spattered layer of 0.1 to 0.2 mg/cm^2 of vanadium were irradiated by monoenergetic beams in the internal test chamber of the cyclotron. The zinc and copper were separated from each foil after the exposure. The isotopes were identified by the half-lives of the beta-active

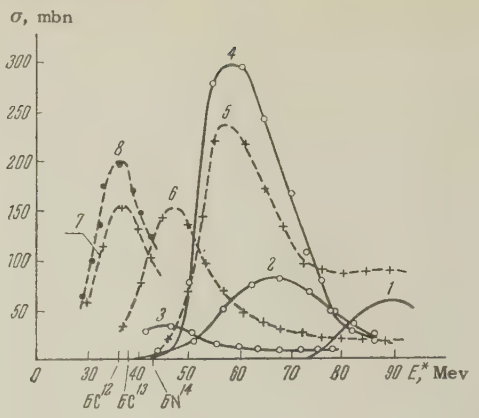

FIG. 3. Comparison of the energy relations of the cross sections of evaporation reactions on multiply-charged protons, resulting in compound nuclei. o — data of this paper, • — data of reference 5, + — data of reference 6. Curve 1 — $V(N^{15}, 5n)$, 2 — $V(N^{14}, p3n + 4n)$, 3 — $V(C^{12}, 2n)$, 4 — $V^{51}(C^{13}, 3n)$, 5 — Cu^{65} (p, p3n + 4n), 6 — Cu^{65}(p3n), 7 — Cu^{63}(p2n), 8 — Cu^{63}(p2n).

products. The ion energies corresponding to each foil were determined from the range-energy curves obtained in reference 4.

Figure 2 shows the variation of the cross sections of the reactions with emission of 2, 3, and 4 neutrons on the excitation energy of the compound nucleus Zn^{65} ($V^{51} + N^{14} \rightarrow Zn^{65}$). In view of the fact that Zn^{61} has a very short half-life and is entirely converted into Cu^{61} during the time of chemical separation, it has been impossible to separate reactions with emission of 4 neutrons from the possible reaction whereby Cu^{61} is produced directly through the emission of 3 neutrons and 1 proton. The diagram shows therefore the summary cross section of both reactions.

Figure 3 shows analogous curves for the reactions, in which the emission of a various number of particle was investigated relative to the same reaction product Cu^{61}, obtained by irradiation with various ions. For comparison, the same diagram shows curves for the cross sections of several reactions investigated by Ghoshal[5] and Meadows.[6] If the distortion due to the presence of the Coulomb barrier at low energies is taken into account (BC^{12}, BC^{13}, and BN^{14} in the diagram), it is easy to see that the cross section vs. energy curve on Figs. 2 and 3 has a form characteristic of reactions with formation of a compound nucleus. A striking fact is that the curves for the emission of 2 and 3 neutrons do not break off on the high-energy side, but become almost parallel to the axis. While a similar behavior (see reference 6) of the cross sections is readily explained by the presence of direct collisions between the protons and the nuclei, in our case this may be an indication of the occurrence

of some other reactions, say those connected with the so-called local heating.

In addition, it is seen from Fig. 3 that our curves corresponding to the evaporation of 2, 3, or 4 neutrons from the excited nuclei are shifted towards the high-energy side by approximately 8 or 10 Mev relative to the similar curves obtained in references 5 and 6. It is possible that this shift is caused by the large angular momentum acquired by the compound nucleus from the multiply-charged ion. However, we do not have enough accurate data to ascertain complete reliability of this shift, let alone to estimate its magnitude.

Without going into the details of the variation of the excitation function, as manifested by the presence of the foregoing segments of the curves and with their shifts, it can be apparently stated at present that when the target mass numbers range from 50 to 200 the interaction with multiply-charged ions proceeds to a considerable extent via production of compound nuclei.

The authors are indebted to Prof. G. N. Flerov for guidance of this research. The authors are grateful to diploma students A. A. Pleve and V. A. Fomichev for aid in the measurements and for processing the results.

[1] Baraboshkin, Karamyan, and Flerov, J. Exptl. Theoret. Phys. (U.S.S.R.) **32**, 1294 (1957), Soviet Phys. JETP **5**, 1055 (1957).

[2] A. W. Stoner and E. K. Hyde, Inorg. Nuc. Chem. **4**, 77 (1957).

[3] Chackett, Fremlin, and Walker, Phil. Mag. **45**, 173 (1954).

[4] Yu. G. Oganesyan, J. Exptl. Theoret. Phys. (U.S.S.R.) **36**, 936 (1959), Soviet Phys. JETP (in press).

[5] Ghoshal, Phys. Rev. **80**, 939 (1950).

[6] J. W. Meadows, Phys. Rev. **91**, 885 (1953).

Translated by J. G. Adashko
106

CONCERNING THE ρ^0 MESON

Ya. I. GRANOVSKIĬ

Institute of Nuclear Physics, Academy of Sciences, Kazakh S.S.R.

Submitted to JETP editor October 22, 1958

J. Exptl. Theoret. Phys. (U.S.S.R.) **36**, 623-624 (February, 1959).

IN the compound model of elementary particles, based on the Fermi-Yang idea,[2] the pion is represented as a system comprising a nucleon in strong interaction with an antinucleon.[2,3] However, along with a tripiet of pions, the same "bare" particles can form an isotopic singlet[4]

$$\rho^0 = (\langle p\bar{p}\rangle + \langle n\bar{n}\rangle)/\sqrt{2}. \qquad (1)$$

The fact that no such particle has yet been observed experimentally necessitates a special explanation. Okun'[3] has proposed that the mass of the ρ^0 meson is sufficiently large. On the other hand, Perel'man has remarked recently[5] that $M_{\rho 0} \approx M_{\pi 0}$.

We wish to note that, in view of the difference in the isotopic spins, the forces that bind the nucleon and antinucleon into π^0 and ρ^0 mesons will also be different. For example, in the symmetrical variant, the interaction potential $V = a\tau_1\tau_2$ equals a when $t = 1$ and $-3a$ when $T = 0$. In this case the existence of a π meson would exclude the existence of a ρ^0 meson. Addition of a term independent of T to the potential cannot change this conclusion, since these forces are small.

The mass differences calculated by Perel'man pertain to particles having equal isotopic spins. In particular, the quantity $\Delta M = 12.7\, m_e$ is the mass difference between $\pi^{\pm}$ and π^0 mesons. Allowance for the magnetic interaction, which has an opposite sign but a somewhat smaller magnitude, brings the calculated mass difference closer to the experimental value $M = 9\, m_e$.

[1] E. Fermi and C. N. Yang, Phys. Rev. **76**, 1739 (1949).

[2] S. Sakata, Progr. Theoret. Phys. **16**, 686 (1956).

[3] L. B. Okun', J. Exptl. Theoret. Phys. (U.S.S.R.) **34**, 469 (1958), Soviet Phys. JETP **7**, 322 (1958).

[4] H. A. Bethe and J. Hamilton, Nuovo cimento **4**, 1 (1956).

[5] M. G. Perel'man, J. Exptl. Theoret. Phys. (U.S.S.R.) **35**, 508 (1958), Soviet Phys. JETP **8**, 350 (1959).

[6] P. S. Signell and R. E. Marshak, Phys. Rev. **106**, 832 (1957). J. Ball and G. Chew, Phys. Rev. **109**, 1385 (1958).

Translated by J. G. Adashko
107

HYSTERESIS AND NON-STATIONARY EFFECTS IN THE ELECTRON TEMPERATURE IN PLASMA IN INERT GASES

A. V. GUREVICH

P. N. Lebedev Physics Institute, Academy of Sciences, U.S.S.R.

Submitted to JETP editor October 23, 1958

J. Exptl. Theoret. Phys. (U.S.S.R.) **36**, 624-626 (February, 1959)

In an earlier paper[1] we have indicated certain features characteristic of the heating of an electron gas in a highly ionized plasma which result from the fact that the frequency of collisions between electrons and ions falls off sharply with increasing electron velocity.* It was found that in a fixed electric field the electron gas is in a stationary state with respect to the ions only at small values of the field ($E < E_k$); when $E \geq E_k$ this state becomes unstable. A similar instability is found in a low-frequency alternating electric field. In this case, however, there is a second stable state characterized by a high electron temperature. The transition between the first and second states takes place at various field amplitudes and leads to hysteresis in the dependence of electron temperature on field.

Similar effects can occur in a weakly ionized plasma; all that is necessary is that the frequency of electron collisions be a sufficiently rapidly decreasing function of velocity: $\nu \sim v^{-\alpha}$, where $\alpha > 1$. In general this condition is not satisfied because the frequency of collisions between electrons and molecules increases rapidly with increasing v. However, an inverse relationship is possible. An inverse relation can obtain, for example, in heavy inert gases such as argon, krypton and xenon at small electron velocities $v \lesssim 5 \times 10^7$ cm/sec (Ramsauer effect).

The calculation of the stationary electron temperature T_e is carried out for a weakly ionized plasma in the same way as for the highly ionized plasma considered in reference 1.† The figure shows the dependence of T_e on the electric field intensity in krypton at a gas temperature of 27°C (p is the pressure in mm Hg). (In this calculation we have used the data of Ramsauer and Kollath[2] and Holtsmark.[3]) It is apparent from the figure that the weakly heated state of the electron gas (the lower curve) becomes unstable at some value of the field intensity in the same way as in a highly ionized plasma. In contrast with the latter, however, in the case being considered here there is a

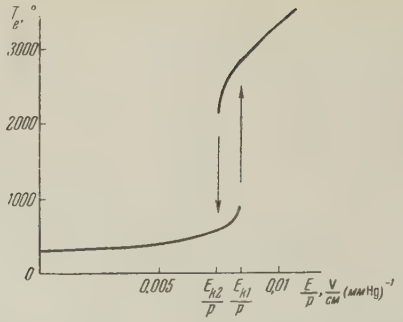

second stable state at a high electron temperature: this state arises because of the increased frequency of collisions between the electrons and krypton ions at high velocities ($v > 5 \times 10^7$ cm/sec). The critical field values associated with the transition from the first state to the second state vary slightly ($E_{k1} = 8.4 \times 10^{-3} p$, $E_{k2} = 7.4 \times 10^{-3} p$ (v/cm): here p is the gas pressure in mm Hg). As a consequence the hysteresis loop is small. The electron temperature changes by approximately a factor of 3 in the transition. There is a corresponding change in electronic conductivity: this conductivity increases by a factor of 2.4 in the transition from the first state to the second state but is reduced by a factor of 3 for the reverse transition. The time required for the transition is $10^{-3} p^{-1}$ sec. In an alternating electric field the effect is suppressed at higher frequencies ω and vanishes completely when $\omega > 1.5 \times 10^8 p$ sec^{-1}.

It should be pointed out that the present calculation applies only when the electron velocity distribution is Maxwellian. As is well-known, this condition is not satisfied in the case of a slightly ionized plasma ($N_e/N_m \lesssim 10^{-10}$), in which case the frequency of collisions with molecules is more than a factor of 10^5 greater than the frequency of collisions between electrons. In the latter case, as is clear, for example, from reference 4, the mean electron temperature is always uniquely related to the electric field intensity so that the effect being discussed here is not obtained.

The author is indebted to V. L. Ginzburg for his interest in this work.

*By a highly ionized plasma we mean one in which collisions between electrons and ions predominate; by a weakly ionized plasma we mean one in which collisions between molecules (or atoms) predominate.

†In computing the complex conductivity of a plasma one introduces the coefficients K_σ and K_ϵ which have been considered earlier in references 1 and 4. It should be noted that if the dependence of ν on v is given by a power law the coefficients K_σ and K_ϵ depend only on the parameter ω/ν_{eff}. In the general case, however, they also depend on T_e. This dependence is found to be important in the exam-

ple considered here. We also note that the assumption that the heavy-particle temperature is stationary, necessary for the validity of the entire analysis (cf. reference 1), is always satisfied in a weakly ionized plasma.

[1] A. V. Gurevich, J. Exptl. Theoret. Phys. (U.S.S.R.) **35**, 392 (1958), Soviet Phys. JETP **8**, 271 (1959).

[2] C. Ramsauer and R. Kollath, Ann. Phys. **5**, 536 (1929).

[3] J. Holtsmark, Z. Physik **66**, 49 (1930).

[4] A. V. Gurevich, J. Exptl. Theoret. Phys. (U.S.S.R.) **30**, 1112 (1956), Soviet Phys. JETP **3**, 895 (1956).

Translated by H. Lashinsky
108

ON SOME SYMMETRY PROPERTIES OF THE EIGENFUNCTIONS OF THE SCHRÖDINGER EQUATION

D. A. BOCHVAR, N. P. GAMBARYAN, I. V. STANKEVICH, and A. L. CHISTYAKOV

Institute of Organometallic Compounds, Academy of Sciences, U.S.S.R.

Submitted to JETP editor October 25, 1958

J. Exptl. Theoret. Phys. (U.S.S.R.) **36**, 626-627 (February, 1959)

IN the present note we wish to call attention to two facts which have not, so far as we know, been noted in the literature: the fact that the symmetry groups of the eigenfunctions of the Schrödinger equation are subgroups of the symmetry group G_H of the corresponding Hamiltonian $\hat{H}$, and the fact that the converse statement is not valid, i.e., the existence of subgroups of the group G_H that are not symmetry groups of the eigenfunctions of the given Schrödinger equation.

The first statement has been made by Melvin,[1] who introduced the concept of the cokernel K^{ij} of the i-th row of the j-th irreducible representation of the group G_H, to which there correspond in the j-th irreducible representation matrices with all the elements in the i-th row equal to zero except for the diagonal element, which is unity. It is easy to see that the symmetry transformations occurring in the cokernel K^{ij} leave the i-th function in the list of eigenfunctions $\psi_1, \psi_2, \ldots, \psi_l$ invariant, and that they form a subgroup of the group G_H.[1] Contrary to Melvin's statement, however, this still does not mean that the cokernel K^{ij} is identical with the symmetry group of the functions ψ_i, since it remains unproved that an eigenfunction of the Hamiltonian $\hat{H}$ with the symmetry group G_H cannot be invariant with respect to some symmetry operator s which does not belong to the group G_H.

We shall prove this last assertion on the assumption that the set (L) of the nodal points of the eigenfunctions of the equation

$$\hat{H}\psi = (\hat{T} + \hat{V})\psi = E\psi, \qquad (1)$$

has no internal points and that the value of the potential at any point ζ of the configuration space can be represented as the limit of the values of the potential at a sequence of points ζ_n that converges to ζ, i.e.,

$$V(\zeta) = \lim V(\zeta_n) \quad \text{for } \zeta_n \to \zeta.$$

Suppose that s does not belong to G_H. We shall show that no eigenfunction of the operator $\hat{H}$, which satisfies our assumptions, can be invariant with respect to the symmetry operation s. Let us assume the opposite, i.e., that there exists a function (whose set of nodal points has no internal points) for which $s\psi = \psi$. Then $s\hat{H}\psi = s(\hat{T} + \hat{V})\psi = \hat{T}s\psi + s\hat{V}\psi = E\psi$ and, on the other hand, $\hat{T}s\psi + \hat{V}s\psi = Es\psi$. Consequently $s\hat{V}\psi = \hat{V}s\psi = \hat{V}\psi$, so that $sV = V$ at points where $\psi \neq 0$.*

On our assumption about the set L of the nodal points, for any point ζ in L we can always find a set of points ζ_n not belonging to L that converge to ζ. Obviously $\psi(\zeta_n) \neq 0$. Therefore from $sV(\zeta_n)\psi(\zeta_n) = V(\zeta_n)\psi(\zeta_n)$ it follows that $sV(\zeta_n) = V(\zeta_n)$. Going to the limit, we get $sV(\zeta) = V(\zeta)$, and consequently the equation $sV = V$ is valid for every point of the configuration space, which contradicts the hypothesis of our argument.

Thus on the assumptions indicated it has been shown that the symmetry groups of the eigenfunctions of the Schrödinger equation are subgroups of the symmetry group G_H of the Hamiltonian $\hat{H}$, namely they are the corresponding cokernels.

We shall show the incorrectness of the converse statement for the example of a Hamiltonian with the symmetry group C_{6v}. The group C_{6v} has as one of its subgroups the group $(E, C_3^{\pm})$. We shall show that this subgroup cannot be a cokernel of the group C_{6v}. From the table of characters[2] of the group C_{6v} it can be seen that the only subgroups that are cokernels corresponding to one-dimensional representations are: for $A_1(C_{6v})$, for $A_2(E, C_2, C_3^{\pm}, C_6^{\pm})$, for $B_1(E, C_3^{\pm}, \sigma_{d_1}, \sigma_{d_2}, \sigma_{d_3})$, and for $B(E, C_3^{\pm}, \sigma_{v_1}, \sigma_{v_2}, \sigma_{v_3})$. In the two-dimensional representation E_1 there corre-

spond to the elements C_3, independently of the choice of basis, matrices of the form

$$\begin{vmatrix} -1/2 & \pm\sqrt{3/2} \\ \mp\sqrt{3/2} & -1/2 \end{vmatrix},$$

which follows from the value of the character $\chi^{E_1}(C_3^{\pm}) = -1$ and the unitary nature of the matrices; this means that these elements cannot occur in the cokernel of the representation E_1. In the two-dimensional representation E_2, with any basis, a unit matrix corresponds to the element C_2. This follows from the value of the character $\chi^{E_2}(C_2) = 2$ and the fact that $C_2^2 = E$. Consequently any cokernel corresponding to the representation E_2 will contain the element C_2, and the subgroup $(E, C_3^{\pm})$ cannot be identical with it.

Thus the subgroup $(E, C_3^{\pm})$ cannot be a cokernel of the group C_{6V}, i.e., cannot be a symmetry group of any of the solutions of the Schrödinger equation with a Hamiltonian of that symmetry.

In conclusion we note that solutions of the Schrödinger equation that possess the full symmetry of the system of eigenfunctions (for the case of a finite number of particles see reference 3) have as their symmetry groups all possible cokernels of the symmetry group of the Hamiltonian.

*Division by the function ψ is possible because the effect of the potential energy operator $\hat{V}$ reduces to multiplication by the potential function V.

[1] M. A. Melvin, Revs. Modern Phys. 28, 18 (1956).

[2] H. Eyring, J. Walter, and G. Kimball, Quantum Chemistry (Russ. Transl.), IIL 1948.

[3] T. Kato, Trans. Am. Math. Soc. 70, 195 (1951).

Translated by W. H. Furry
109

ON THE PROBLEM OF TESTING PARITY CONSERVATION IN THE STRONG INTERACTIONS

V. G. SOLOV' EV

Joint Institute of Nuclear Studies

Submitted to JETP editor October 27, 1959

J. Exptl. Theoret. Phys. (U.S.S.R.) 36, 628-629 (February, 1959)

In the analysis of the problem of the conservation of parity in individual interactions we shall start from the following postulates: (1) the law of conservation of the combined parity reflects fundamental properties of space-time and is the basic symmetry law in nature; (2) the conservation of spatial parity in individual interactions is a consequence of additional invariance requirements.

In fact, as has been shown in references 1—3, in the case of the renormalized quantum electrodynamics, owing to the gauge-invariance condition, the requirement of invariance with respect to the combined-inversion operation PC (or the time reversal T) leads to invariance with respect to the spatial-inversion operation P. In the case of the renormalized pseudoscalar meson theory, owing to the condition of isotopic invariance, the requirement of invariance with respect to the combined-inversion transformation PC also leads to invariance with respect to the spatial-inversion operation P. The requirement of the invariance with respect to the transformation PC of the renormalized and isotopically invariant interaction Lagrangian of the K mesons and baryons does not lead to invariance with respect to the operation P. In this connection it is of interest to examine whether parity is conserved in processes of production of K mesons and hyperons.

It is known that parity is conserved with great precision in nucleon-nucleon collisions and nuclear reactions. If there is no departure from isotopic invariance, then parity nonconservation in these processes can appear both as a consequence of the participation of virtual K mesons and hyperons, and also owing to the nonrenormalizability (nonlocal character) of the interaction. As is shown by a calculation carried out in reference 5, the contribution of the K-meson forces to the nucleon-nucleon potential is small, so that the (very precise) parity conservation in nucleon-nucleon interactions is not in contradiction with violation of parity conservation in interactions involving K mesons and hyperons.*

Let us consider the process $\pi + N \rightarrow K + Y$ with the subsequent decay $Y \rightarrow N + \pi$ (Y can be a Λ or a Σ hyperon). As has been shown in reference 4, if parity is not conserved in the production of the K meson and hyperon, there is a longitudinal component of the polarization vector of the hyperon, and this leads to the appearance of an asymmetry in the distribution of the π mesons from the decay of the hyperons (in the center-of-mass system), both relative to the plane perpendicular to the plane of production and containing the direction of the initial π meson, and also relative to the plane perpendicular to the plane of production and perpendicular to the direction of the initial π meson. It is found[4,5] that if there is a longitudi-

nal polarization of the hyperon, then there must be asymmetry relative to at least one of these planes. It must be noted that since the properties of the longitudinal polarization (if there is any) are unknown, it may possibly be different (in magnitude and sign) for different angles of production of the hyperon, and the effect may be cancelled out to some extent in integrating over the angles. In this connection it would be interesting to study this process in a narrow range of angles of production of the hyperons.

At high π-meson energies the most probable processes will be those with three or more particles in the final state. In this case the reaction $\pi^- + p \rightarrow \Sigma^- + K^+ + \pi^0$ is of great interest. If parity is not conserved in the production of hyperons and K mesons, there will be an asymmetry in the distribution of the K mesons relative to the plane (in the center-of-mass system) containing the directions of the incident π meson and the Σ particle. It must be pointed out that this reaction is a very convenient one from the point of view of the processing of the experimental data. The advantage of this and analogous reactions ($K^- + d \rightarrow \Lambda + p + \pi^-$; $\pi^- + p \rightarrow Y^0 + K^+ + \pi^-$) lies in the fact that the asymmetry does not depend on the properties of the longitudinal polarization, so that one can obtain better statistics by totalling the experimental data for all angles of production of the hyperons.

*The writer is grateful to Professor Drell for sending a preprint and an account of his work on the problem of PC conservation.

[1] V. G. Solov'ev, J. Exptl. Theoret. Phys. (U.S.S.R.) **33**, 796 (1957), Soviet Phys. JETP **6**, 613 (1958).

[2] V. G. Solov'ev, Nucl. Phys. **6**, 618 (1958).

[3] S. Gupta, Canadian J. of Phys. **35**, 1309 (1957).

[4] V. G. Solov'ev, A Possible Test of Parity Conservation in the Production of K Mesons and Hyperons. Preprint P-147 (R-147), Joint Institute for Nuclear Research, February, 1958.

[5] Drell, Frautschi, and Lockett, preprint.

Translated by W. H. Furry.
110

ON THE EMISSION MECHANISM OF PROMPT FISSION NEUTRONS

V. S. STAVINSKIĬ

Submitted to JETP editor October 30, 1958

J. Exptl. Theoret. Phys. (U.S.S.R.) **36**, 629-630 (February, 1959)

RECENTLY the energy and angular distributions of fission neutrons have been determined with respect to a system in which a fission fragment is at rest.[1] They are in disagreement with the mechanism hitherto usually considered for the emission of prompt fission neutrons, namely the analog of the evaporation of molecules from the surface of hot materials. The measurements show that the neutron angular distributions are strongly anisotropic with respect to the direction of motion of the fission fragment in the system of coordinates in which the fission fragment is at rest, and the energy distribution of the neutrons shows a sharp maximum at an energy of the order 0.1 to 0.2 Mev, with a width of the same order. As is well known the evaporation mechanism leads to an isotropic distribution with a Maxwellian energy spectrum. A possibility of an anisotropic neutron angular distribution can be understood from the point of view of Hill and Wheeler.[2] However, the motion of the nuclear surface can modulate the neutron evaporation spectrum only weakly and essentially cannot explain the sharp peak observed in reference 1.

The foregoing characteristics of the spectra of prompt fission neutrons can be explained by assuming that the surface energy, contained in the outgrowths which remain after the "neck" breaks at the instant of fission, is liberated in the form of a shock wave, which then propagates in the direction of motion of the fragment. Such a shock wave can lead to emission of almost monoenergetic neutrons along the direction of motion of the fission fragment.

To estimate the effect one has to know the form of the deformed fragments at the instant at which the "neck" breaks. At present there does not exist any experimental indications concerning this form. We therefore shall utilize the results of Hill,[3] which were derived within the framework of the liquid drop model. These computations show that right after the instant of fission each fragment has an outgrowth with linear dimensions exceeding the nuclear radius by a factor 1.5 to 2. Utilizing the commonly accepted value for the surface energy one can estimate that each outgrowth contains a deformation energy of the order 20 to 30 Mev. Knowing the number of nucleons in the outgrowth one can easily calculate the velocity of contraction of the outgrowths. This turns out to be of the order

0.1 c, where c is the velocity of light. The sound velocity in nuclear matter can be calculated from the estimates of the nuclear compressibility.[4] It also turns out to be of order 0.1 c. The mean free path of the nucleons is evidently shorter within the outgrowth than within usual undeformed nuclei, which is $\sim 5 \times 10^{-13}$ cm if one takes the imaginary part of the optical potential to be approximately 0.2 of the real part.

These considerations evidently show that the conditions for the appearance and the propagation of shock waves in the fission fragments are fulfilled. Concerning the damping of the shock wave, one would have first to determine its emergence from the outgrowth. However, the damping is clearly rather large and the energy contained in the shock wave will suffice on the average just for the emission of one neutron of very low energy. Part of the energy contained originally in the deformation of the outgrowth will be used up in achieving the equilibrium shape of the fragment, and in its heating. The latter will lead to a background in the observed neutron spectrum, which is not in disagreement with the evaporation mechanism.

If the proposed fission neutron emission mechanism actually occurs, then a more accurate measurement of the fission neutron spectrum and angular distribution will be able to provide information on the deformation of the fragments at a time just prior to the fission. It further could improve our knowledge on the compressibility of nuclear matter, which plays an important part in the mechanism of nuclear fission.

The author is deeply grateful to A. I. Leipunskiĭ for his critique of this paper and I. P. Stakhanov and A. A. Rukhadze for valuable suggestions and discussions.

[1] H. R. Bowman and S. G. Thompson, Proceedings of the Second Conference of Peaceful Uses of Atomic Energy, 1958 Vol. 15, p. 652.

[2] D. L. Hill and J. A. Wheeler, Phys. Rev. 89, 1102 (1953).

[3] D. L. Hill, Proceedings of the Second Conference of Peaceful Uses of Atomic Energy, 1958, Vol. 15, p. 660.

[4] W. I. Swiatecki, Phys. Rev. 83, 178 (1951).

Translated by M. Danos
111

LINE WIDTH OF THE CHLORINE QUADRUPOLE RESONANCE IN CHLORATES OF BARIUM, SODIUM, AND POTASSIUM

V. S. GRECHISHKIN

Leningrad State University

Submitted to JETP editor November 1, 1958

J. Exptl. Theoret. Phys. (U.S.S.R.) 36, 630-632 (February, 1959)

THE large number of factors that tend to broaden the nuclear quadrupole resonance line make difficult the interpretation of absorption line shapes in crystals. However, in a number of cases it is possible to obtain information because mechanical stresses do not play an important role in powders if there are no temperature gradients. In the present work we have studied the width of the quadrupole resonance line in chlorates of barium, sodium, and potassium. The quadrupole resonances in sodium chlorate and potassium chlorate have been reported earlier;[1,2] however, in this work no precise measurements or interpretations of the line width were made.

These observations have been carried out using frequency or Zeeman modulation[3] a superregenerative circuit, a narrow-band, low-frequency amplifier, and a phase-sensitive detector. The reference voltage at the phase-sensitive detector was applied through a reference voltage amplifier which was provided with a phase shifter. The frequency modulation was obtained by means of a vibrating condenser and the Zeeman modulation was produced by means of a coil which was driven by rectangular pulses. All the measurements were carried out at room temperature. In the frequency-modulation measurements the second derivative of the absorption line was recorded since by this means it is possible to suppress spurious amplitude modulation. The correction to the second moment for the second derivative was obtained by the method proposed by Andrew

$$S^* = S_0 + \nu_m^2/6, \qquad (1)$$

where S* is the second moment of the absorption line observed in the experiment, S_0 is the true second moment, and ν_m is the amplitude of the frequency modulation. Equation (1) applies in the case in which the amplitude of the frequency modu-

lation is much smaller than the line width. Starting from the Duhamel formula it can be shown that distortions due to rapid passage through the resonance region and the time constant of the phase detector are given by the following when frequency or Zeeman modulation are used:

$$S^* = S_0 + 2(v\tau)^2, \qquad (2)$$

where v is the rate of passage through the resonance region and τ is the time constant of the detector. The final measurements were made with Zeeman modulation. The use of a superregenerative system makes it possible to use a convenient frequency scale since the signals follow the quenching frequency. The quadrupole resonance signals of Cl^{35} and Cl^{37} were observed in $Ba(ClO_3)_2$, $NaClO_3$, and $KClO_3$ powders. At the present time we have also observed the quadrupole resonance in calcium chlorate. The observed signal amplitudes are in good agreement with the natural abundances of the chlorine isotopes. The amplitude of the rf field was rather small in order to avoid the additional broadening, which exceeds the nuclear magnetic resonance broadening by a factor of 4. In spite of the low level of the rf field the signal-to-noise ratio in potassium chlorate was of the order of 60 for Cl^{35}. The total width of the lines were measured at half heights.

The results of the experiment are shown in the table; it is apparent that in these chlorates the line width is determined basically by nuclear dipole-dipole interactions since the ratio of magnetic moments of the chlorine isotopes is 1.2. An estimate of relaxation-time broadening shows that this quantity is less than 0.03 kcs.[4] Because $NaClO_3$ is a cubic crystal, a simple expression can be used for the second moment[5]

$$h^2\langle\Delta\nu^2\rangle_{av} = 60q^4\beta^4d^{-6}, \qquad (3)$$

where h is Planck's constant, g is the gyromagnetic ratio, β is the nuclear magneton and d is the size of an elementary cell.

It should be noted that Eq. (2) applies in the case in which the center of the line is not shifted. When making corrections, however, one must take account of the displacement of the center. With the introductions of corrections for broadening due to the magnetic field of the earth, the rate of passage through the resonance region, and effects due to sodium atoms, the second moment for Cl^{35} in $NaClO_3$ is found to be

$$\langle\Delta\nu^2\rangle_{av} = 0.42\cdot10^5 \text{ cs}^2.$$

Whence we find that d = 6.9 A. This result is in good agreement with the x-ray data,[6] according to

Material	Isotope	Frequency, Mcs.	Δν, kcs	$\frac{\Delta\nu\,(Cl^{35})}{\Delta\nu\,(Cl^{37})}$
$Ba(ClO_3)_2$	Cl^{35}	29.6	2.8	1.07
	Cl^{37}	23.2	2.6	
$KClO_3$	Cl^{35}	28.1	1.1	1.2
	Cl^{37}	22.2	0.9	
$NaClO_3$	Cl^{35}	29.9	1.3	1.13
	Cl^{37}	23.6	1.15	

which d = 6.5 A in $NaClO_3$. The calculation which has been carried out on the basis of well-known crystal structures shows that the line shapes in chlorates are amenable to straight-forward interpretation.

In conclusion we wish to thank F. I. Skripov for discussions and his interest in this work.

[1] T. C. Wang, Phys. Rev. **99**, 566 (1955).
[2] G. B. Benedek and T. Kushida, Rev. Sci. Instr. **28**, 92 (1957).
[3] H. C. Allen, J. Phys. Chem. **57**, 501 (1953).
[4] V. S. Grechishkin, J. Exptl. Theoret. Phys. (U.S.S.R.) **35**, 364 (1958), Soviet Phys. JETP 8, 253 (1959).
[5] A. Abragam and K. Kambe, Phys. Rev. **91**, 894 (1953).
[6] G. Kartha, Proc. Ind. Acad. Sci. **A36**, 501 (1952).

Translated by H. Lashinsky
112

CROSS SECTION OF Te^{125m} *PRODUCTION VIA THE (n, γ) REACTION*

V. S. GVOZDEV and Yu. L. KHAZOV

Leningrad Physico-technical Institute, Academy of Sciences, U.S.S.R.

Submitted to JETP editor November 6, 1958

J. Exptl. Theoret. Phys. (U.S.S.R.) **36**, 632-633 (February, 1959)

WHEN an isomer pair is produced via the (n, γ) reaction, the more probable of the two isomers is the one whose spin is closest to that of the initial nucleus.[1] It has been established that for isotopes of tin, tellurium, and zenon the production cross section of an isomer state with spin $^{11}/_2$ amounts to several dozens of millibarns. Exceptions are the isotopes of tellurium 122 and 124, for which

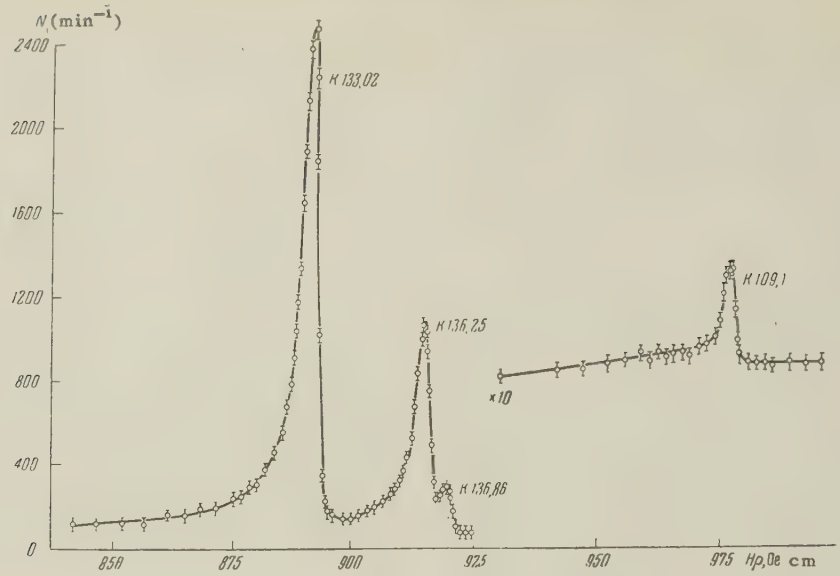

Hughes and Harvey[2] lists cross sections of 1.0 ± 0.3 and 5 ± 3 barns.

In the present investigation we measured the cross section for the production of the isomer state of Te^{125} with spin $^{11}/_{2}$ via the (n, γ) reaction. The cross section was determined by comparison with the cross section of the $Hf^{180}(n,\gamma)Hf^{181}$ reaction, which were taken to be 10 ± 3 barns, as in reference 2. Separated Te^{124} and Hf^{180} sources were prepared for the measurements and irradiated simultaneously in the neutron beam.

The internal-conversion electron spectrum of Te^{125m} and Ta^{181}, produced in the β^- decay of Hf^{181}, was investigated with a beta spectrometer. The figure shows the internal-conversion electron K lines of the gamma transitions of energies 133.02, 136.25, and 136.85 kev (Ta^{181}) and 109.1 kev (Te^{125m}, for which the ordinate scale is magnified ten times). By determining the intensity ratio of the 109.1 and 133.02 kev K lines, it is possible to calculate the cross section for the production of Te^{125m} via the (n, γ) reaction; it was found to be 40 ± 25 millibarns.

According to reference 1, the cross section for the production of the ground state of Te^{125} via the (n, γ) reaction is 6.5 ± 1.2 barns. The ratio of the Te^{125m} (spin $^{11}/_{2}$) and Te^{125} (spin $^{1}/_{2}$) cross sections is 0.006.

[1] E. Segrè and A. Helmholz, Rev. Modern Phys. 21, 274 (1949).

[2] D. J. Hughes and J. A. Harvey, Neutron Cross Sections, N. Y., 1955.

Translated by J. G. Adashko
113

THE REACTION T (p, n) He^3 AT 7—12 Mev PROTON ENERGY

G. F. BOGDANOV, N. A. VLASOV, C. P. KALININ, B. V. RYBAKOV, L. N. SAMOĬLOV, and V. A. SIDOROV

Submitted to JETP editor November 17, 1958

J. Exptl. Theoret. Phys. (U.S.S.R.) **36**, 633-636 (February, 1959)

THE reaction T (p, n) He^3 is a convenient source of monochromatic neutrons and is widely used in many laboratories. From the results of the study of the reaction in the proton energy range from the reaction threshold (1.019 Mev) to 7 Mev,[1,2] it was possible to deduce the existence of excited levels of the α particle at 22 Mev and 24 — 25 Mev.[1,3] Several experimental works have been published recently[4] confirming the existence of excited states of the α particle.

The cross section and the angular distribution of neutrons in the reaction T (p, n) He^3 in the proton energy range 7 — 12 Mev were measured in the course of the present experiment. It was also attempted to measure the polarization of the neutrons.

A solid tritium-zirconium target of 20 μ thickness was bombarded by 12 Mev protons from a cyclotron. The neutron flux was measured by a telescope consiting of four proportional counters,[5]

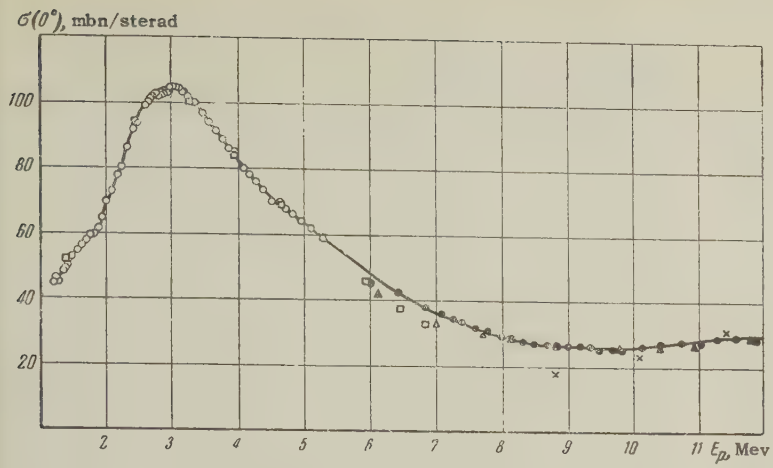

FIG. 1. The cross section of the reaction T (p, n) He^3 at the angle 0°, ● – telescope of proportional counters, ▲ – time-of-flight spectrometer, o – data of reference 2, □ – data of reference 1, × – data of reference 8.

E_p, Mev	A	B	C	D	E	σ_t (mbn)
6.8	11.1	11.3	24.4	—51.4	25.3	305
8.9	13.3	1.0	1.3	—28.4	27.3	241
12.0	13.0	7.5	—23.7	—24.9	44.6	176

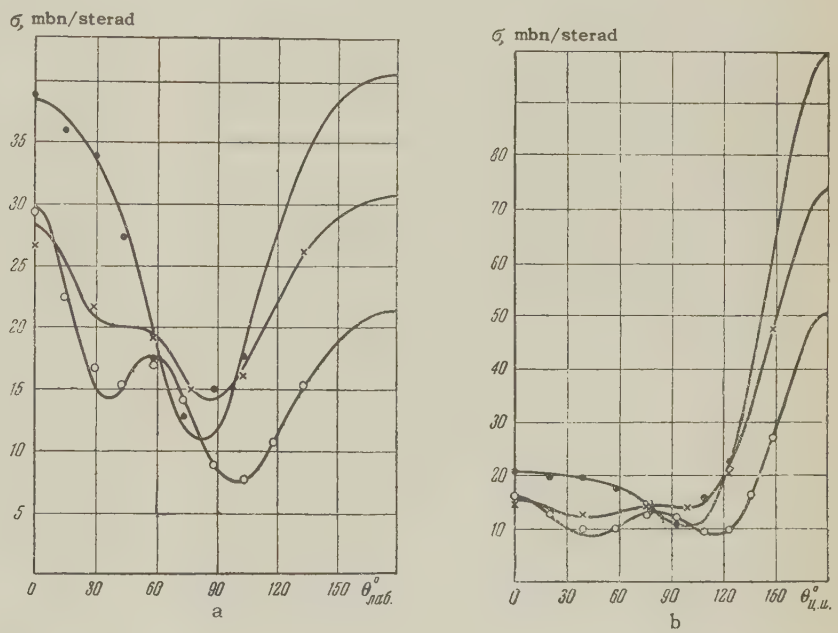

FIG. 2. Angular distribution of neutrons from the reaction T (p, n) He^3. a – in the laboratory system of coordinates, b – in the c.m.s., ● – E_p = 6.8 Mev, × – E_p = 8.9 Mev, o – E_p = 12 Mev.

and was also analyzed by a time-of-flight spectrometer.[6,7] The accuracy of the cross section measurements amounted to 10%.

The reaction cross section measured at 0° and those measured in the energy range 1 — 7 Mev (published earlier[1,2]) are shown in Fig. 1. In the energy range under investigation, the cross section is approximately constant and increases slightly at 11 — 12 Mev. Three experimental points taken from the work of Steward et al.[8] are also shown in Fig. 1. The discrepancy between the results of that work and our results lies outside the limits of errors.

The angular distributions of neutrons of 6.8, 8.9, and 12 Mev are shown in Fig. 2a. The same angular distributions in the center-of-mass system are shown in Fig. 2b. The forward-backward anisotropy indicates a strong interference of states with different parity. The curves in the figures correspond to expressions of the form

$$\sigma(\theta) = A + B\cos\theta + C\cos^2\theta + D\cos^3\theta + E\cos^4\theta$$

in the c.m.s. The coefficients in these expressions have been obtained by the least-squares method and are given in the table. The values of the total cross section for the reaction T (p, n) He^3 obtained by the integration of these equations are also given in the table.

The dependence of the total reaction cross section on energy is shown in Fig. 3.

The study of the polarization of neutrons produced in the reaction T (p, n) He^3 is of great importance for the study of the excited states of the

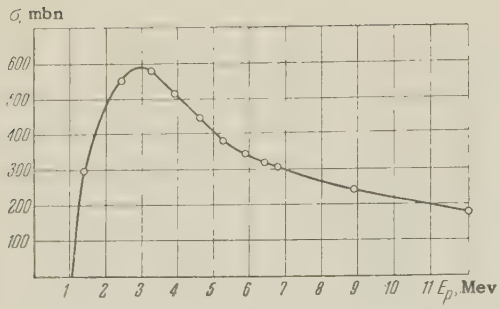

FIG. 3. Dependence of the total cross section for the reaction T (p, n) He^3 on proton energy.

α particle. The method of inverse reactions proposed by Barshall[9] was used for the measurement of the polarization. In our case, the inverse reaction is the reaction He^3 (n, p) T. A chamber filled with He^3 to a pressure of 10 atmospheres was placed at an angle θ_1 to the beam of neutrons originating from the reaction T (n, P) He^3, and the right-left asymmetry of the proton yield from the reaction He^3 (n, p) T was measured by the proportional-counter telescope[5] at an angle θ_2. In the c.m.s., a single angle $\theta_{c.m.}$ corresponds to the angles θ_1 and θ_2. The angle θ_1 was chosen from the condition of equality of the excitation energy of the intermediate nucleus He^4 in the direct and inverse reactions. This angle is uniquely determined by the energy of the reaction $Q = -0.764$ Mev and by the energy E_p of protons bombarding the tritium target:

$$\cos\theta_1 = (6E_p - 5.348) / \sqrt{12E_p(3E_p - 3.056)}.$$

Such a method makes it possible to measure the absolute values of the polarization without an analyzer of known properties.

Polarization measurements require a very exact geometry, since the measured azimuthal asymmetry may be due to the inequality of the right and left deviation angles with respect to the neutron beam. To check the geometry of our experimental setup, we measured the scattering of neutrons on hydrogen by means of recoil protons under the same geometrical conditions. In order to increase the angle sensitivity, the detection of recoil protons was carried out on the falling portion of the spectrum, where the counting rate decreases with the angle, both owing to the decrease in intensity and owing to the decrease in energy.

The measurements showed that, for $E_p \lesssim 10$ Mev, the asymmetry at angles corresponding to the condition of Barshall is not larger than 5%. For the angle $\theta_1 = \theta_2 = 40°$, large asymmetry has been found indicating that the neutrons are polarized.

[1] Vlasov, Kalinin, Oglobin, Samoĭlov, Siderov, and Chuev. J. Exptl. Theoret. Phys. (U.S.S.R.) **28**, 639 (1955), Soviet Phys. JETP **1**, 500 (1955).

[2] Willard, Bair, and Kington, Phys. Rev. **90**, 865 (1953).

[3] A. I. Baz' and Ia. A. Smorodinskiĭ, J. Exptl. Theoret. Phys. (U.S.S.R.) **27**, 382 (1954).

[4] Bogdanov, Vlasov, Kalinin, Ribakov, Samoĭlov, and Sidorov, Труды Всесоюзной конференции по ядерным реакциям при малых и средних энергиях (Trans. All-Union Conference on Low and Medium Energy Nuclear Reactions), Acad. Sci. Press, 1958, p. 7.

[5] Kondrashev, Kurashov, Linev, Sidorov, Sokolov, and Khaldin, Приборы и техника эксперимента (Instruments and Meas. Engg.) **1**, 17 (1958).

[6] Bogdanov, Kurashov, Rybakov, and Sidorov, Атомная энергия (Atomic Energy) **1**, 66 (1956).

[7] Bogdanov, Vlasov, Kalinin, Rybakov, and Sidorov, Атомная энергия (Atomic Energy) **3**, 204 (1957).

[8] Steward, Frye, and Rosen, Bull. Am. Phys. Soc. **2**, 93 (1956).

[9] H. H. Barshall, Helv. Phys. Acta **29**, 145 (1956).

Translated by H. Kasha
114

ISOTOPIC SHIFT OF THE CURIE POINT IN URANIUM HYDRIDE AND DEUTERIDE

A. I. KARCHEVSKII, E. V. ARTYUSHKOV, and L. I. KIKOIN

Submitted to JETP editor November 18, 1959

J. Exptl. Theoret. Phys. (U.S.S.R.) **36**, 636-637 (February, 1959)

THE observed ferromagnetism of uranium hydride and deuteride[1-3] makes possible an investigation of the isotopic shift of the Curie temperature.

One possible cause of such a shift is the difference in distance between the uranium ions in these two compounds. Actually, crystallographic investigations[4] have shown that the constants a of the cubic lattices of uranium hydride and deuteride are equal to 6.6310 and 6.625 A respectively. So noticeable a distance between the lattice constants of the two compounds should undoubtedly influence the value of the volume integral with which the value of the Curie temperature is directly connected.

There exist several methods capable of deter-

mining the Curie temperature in a ferromagnet with sufficient accuracy. In the present investigation, aiming to obtain preliminary data on the shifts of the Curie points, we investigated the temperature variation of the residual magnetism of samples of uranium hydride and deuteride. It is known that as the Curie point (close to 180° for the compounds of interest to us) is approached from the low-temperature side, the residual magnetism experiences a rapid decrease, linear over a sufficiently wide temperature interval. The intercept of the magnetization vs. temperature curve with the temperature axis can be assumed to be the Curie temperature of the specimen only in the first approximation. However, the difference in the so obtained "extrapolated" temperatures of the two specimens is apparently equal, with sufficient accuracy, to the true difference of the Curie temperatures of these specimens.

The residual magnetism of the specimens was measured with an astatic magnetometer. The temperatures of the specimens were determined in the various experiments either with a copper-constantan thermocouple, or with a platinum resistance thermometer. Approximately 20 specimens of uranium hydride and deuteride were prepared. The impurities in the initial uranium fluctuated from 0.4 to 0.12 percent. All the hydride and deuteride specimens were obtained through a direct reaction between the uranium and hydrogen or deuterium at approximately 250°C. The hydrogen and deuterium were produced by decomposition of a suitable amount of uranium hydride or deuteride at a temperature near 400°C.

In all the specimens investigated, an isotopic shift of the Curie temperature was observed in going from the hydride to the deuteride. This shift is practically independent of the purity of the initial uranium and consequently is not due to chemical impurities. Typical curves of the temperature dependence of the residual magnetism J_R of the hydride and deuteride samples are shown in the figure. It is seen from these curves that the difference in the Curie temperatures of uranium hydride and deuteride is 4°. The average error, obtained in the measurement of 10 pairs of specimens, is 0.5°. The Curie-temperature shift $\Delta\Theta$ in going from the hydride to the deuteride of uranium is thus

$$\Theta_{UH_3} - \Theta_{UD_3} = \Delta\Theta = +(4.0 \pm 0.5)°K.$$

The method described is not suitable for the determination of the absolute Curie temperature. The Curie temperature obtained by the extrapolation method depends on the magnetic "prior history" of the specimen. In our experiments, residual

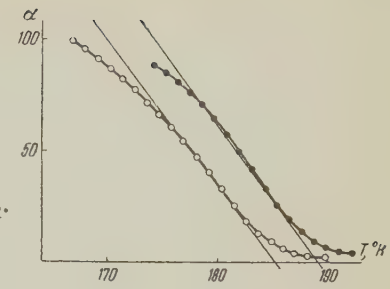

● – UH_3, ○ – UD_3; α – magnetometer deflection, proportional to the residual magnetism of the specimen, J_R.

magnetism was produced by slowly cooling (for one hour) the specimens, placed in a magnetic field of approximately 200 oersteds, from room temperature to that of liquid nitrogen, after which the magnetic field was turned off and the specimen remained magnetized. The value of the residual magnetism depends, naturally, on the intensity of the magnetic field in which the specimen is cooled and on the lowest cooling temperature.

The extrapolated Curie point, obtained from the residual magnetism vs. temperature curve for the given specimen, remained constant within 0.1 or 0.2° under considerable variations of the external conditions (magnetizing field and temperature).

We are planning an investigation of the absolute value of the Curie temperature of uranium hydride and deuteride.

In conclusion, we thank Academician I. K. Kikoin for suggesting the problem and for great help in the investigation.

[1] Trzebiatowski, Stalinski, and Sliwa, Roczniki Chem. **26**, 110 (1952), **28**, 12 (1954).

[2] S. T. Lin and A. R. Kaufman, Phys. Rev. **102**, 640 (1956).

[3] W. E. Henry, Phys. Rev. **109**, 1976 (1958).

[4] J. J. Katz and E. Rabinowitch, The Chemistry of Uranium, (Russ. Transl.) M. IIL, 1954, p 174 [McGraw-Hill, N. Y., 1951].

Translated by J. G. Adashko
115

MAGNETOCALORIC EFFECT IN URANIUM HYDRIDE AND DEUTERIDE

A. I. KARCHEVSKII

Submitted to JETP editor November 18, 1958

J. Exptl. Theoret. Phys. (U.S.S.R.) **36**, 638-639 (February, 1959)

THE investigation of the magnetic properties of the ferromagnets uranium hydride and uranium deuteride is of great interest, because it discloses

how replacement of one element by its isotope affects the properties of the ferromagnet. It was shown, in particular,[1] that uranium hydride had a Curie temperature noticeably different from that of the deuteride (by approximately 4°).

Henry[2] has shown that even the saturation magnetizations of uranium hydride and deuteride are different. His value of the Curie temperature of uranium hydride (168°K) differs substantially from the value given by Lin and Kaufman (181°K).[3]

The procedure used in reference 1 made it possible to observe only the shift in the Curie temperature in going from the hydride to the deuteride of uranium; the absolute values of the Curie temperatures were determined in these experiments quite roughly.

One of the most reliable methods of determining the Curie temperature is to investigate the temperature dependence of the magnetocaloric effect, in which the temperature of a body is changed by adiabatic magnetization. This temperature change is equal to where J is the magnetization of the specimen, T the temperature, C_H the heat capacity, and H the intensity of the magnetic field. Since $(dJ/dT)_H$ of ferromagnetic bodies has its maximum at the Curie point, the temperature variation at this point has a clearly pronounced maximum, which permits an accurate determination of the Curie temperature.

$$dT = -\frac{T}{C_H}\left(\frac{dJ}{dT}\right)_H dH,$$

An investigation of the magnetocaloric effect has additional interest in that its value, together with the temperature dependence of the magnetization, permits a determination of the constant of the molecular field of the investigated ferromagnet.

Uranium hydride, like uranium deuteride, is obtainable only in finely-powdered form. A method was therefore developed of measuring the magnetocaloric effect in powdered specimens. To check this method, we measured the magnetocaloric effect in ferromagnetic chromium-tellurium (CrTe) and manganese-antimony (MnSb) alloys. The data obtained were found to agree well with measurements made by others on monolithic samples of these substances. We compared our results with the data of Weiss and Forrer[4] for nickel, with the data of A. K. Kikoin[5] for CrTe, and with the data of O. A. Shakalis (private communication) for MnSb. The method of obtaining specimens of uranium hydride and deuteride was analogous to that described in references 1, 3, and 6. The amount of impurities in the initial uranium did not exceed 0.12%. The magnetocaloric effect was measured

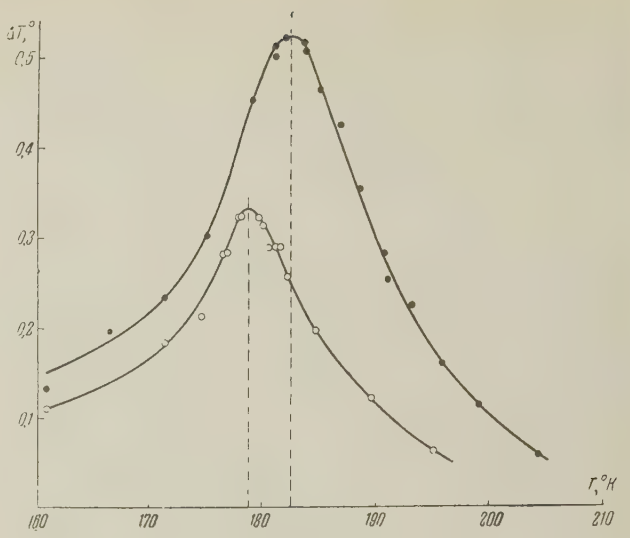

●–UH_3, ○–UD_3

at various values of magnetic field intensity, up to 17,000 oersteds.

The diagram shows curves for the dependence of the magnetocaloric effect on the temperature, plotted in a magnetic field of 17,000 oersteds. The maxima of the curves correspond to the ferromagnetic Curie temperatures $\Theta_{UH_3} = 182.0°K$ and $\Theta_{UD_3} = 178.4°K$. The difference in the Curie temperatures, $\Delta\Theta = 3.6 \pm 0.4°$, is in good agreement with the results of reference 1. The absolute Curie temperature for uranium hydride is nearly the same as obtained by Lin and Kaufman,[3] but differs considerably from the value of 168°K given by Henry for uranium hydride,[2] a value that must be considered erroneous.

It follows from the curves that uranium hydride and deuteride have not only different Curie temperatures, but also different magnetocaloric effects. In particular, the maximum temperature change ΔT_m in adiabatic magnetization (at the Curie point) is 1.6 times greater in uranium hydride than in deuteride.

Whether this difference in the magnetocaloric effects is due only to the difference in the saturation magnetisms of these compounds[2] or partly to the difference in the molecular-field constants can be ascertained only by detailed magnetic investigations, which are now in progress. In any case, the measurements of the magnetocaloric effect make it possible to determine the magnitude of the spontaneous magnetization for these new ferromagnetic substances.

A. G. Orlov, a student at the Moscow Engineering-Physics Institute, participated in the preliminary experiments on the magnetocaloric effect.

In conclusion, I thank the supervisor of this project, Academician I. K. Kikoin, for continuous inter-

est in the problem and for much valuable advice.

[1] Karchevskii, Artyushkov, and Kikoin, J. Exptl. Theoret. Phys. (U.S.S.R.) **36**, 646 (1959), Soviet Phys. JETP this issue, p 442.

[2] W. E. Henry, Phys. Rev. **109**, 1976 (1958).

[3] S. T. Lin and A. R. Kaufman, Phys. Rev. **102**, 640 (1956).

[4] P. Weiss and R. Forrer, Ann Physik, **5**, 153 (1926).

[5] I. K. Kikoin, Труды института физики металлов (Trans. Metal Physics Inst.) No. 15, 1954, p. 70.

[6] J. J. Katz and E. Rabinowitch, The Chemistry of Uranium, (Russ. Transl.) M., IIL, 1954, pp 157-175 [McGraw-Hill, N. Y., 1951].

Translated by J. G. Adashko
116

POLARIZATION OF THE μ^+ MESON CURRENT AT SEA LEVEL

B. A. DOLGOSHEIN and B. I. LUCHKOV

Moscow Engineering-Physics Institute

Submitted to JETP editor July 31, 1958

J. Exptl. Theoret. Phys. (U.S.S.R.) **36**, 640-641 (February, 1959)

THE violation of the law of parity conservation in weak interactions is known to lead to the longitudinal polarization of the μ meson in the $\pi \to \mu$ decay in the center-of-mass system. The μ mesons observed at sea level are produced in the decay of π mesons in flight. A current of μ mesons with energy E_μ is generated by π mesons in a certain energy interval ΔE_π. Since the energy spectrum of the π mesons in the atmosphere decreases fast with the energy ($\sim E^{1-\gamma_\pi}$), there will be an excess of μ mesons flying, in the center-of-mass system, into the forward hemisphere relative to the direction of motion of the π mesons, i.e., the μ-meson current will be polarized. The degree of polarization of the the μ mesons was theoretically determined by Gol'dman (reference 1).* It is given by the expression

$$\gamma_i = \frac{1}{v} - \frac{\gamma}{\gamma - 1}\frac{1-v}{v}\left[1 - \left(\frac{1-v}{1+v}\right)^{\cdot}\right] \Big/ \left[1 - \left(\frac{1-v}{1+v}\right)^{\gamma}\right], \quad (1)$$

where v is the velocity of the μ meson in the center-of-mass system, measured in units of c; γ is a parameter characterizing the energy spectrum of the particles which generate the μ mesons. It was further shown[1,2] that the depolarization due to scattering of the μ meson before it comes to rest is negligibly small. The polarization of the μ mesons can be determined by studying the asymmetry in the electron emission in the $\mu \to e$ decay.

In the two-component theory of the neutrino, this asymmetry is determined by the formula of Lee, Yang, and Landau:

$$W(\varepsilon, \theta)\, d\varepsilon\, d\Omega = \frac{\varepsilon^2}{2\pi}\left[(3 - 2\varepsilon) + \xi\eta(2\varepsilon - 1)\cos\theta\right] d\varepsilon\, d\Omega, \quad (2)$$

where ϵ is the energy of the positron in units of the maximal energy, ξ is a theoretical parameter which is close to unity and depends on the coupling constants, η is the degree of polarization, and θ is the angle between the polarization vector of the μ meson and the direction of emission of the electron.

The present note is devoted to the experimental determination of the degree of polarization of the cosmic μ^+ mesons at sea level. The measured quantity is the relative yield of decay positrons emitted into the upper hemisphere in the decay of the μ^+ meson as it comes to rest. The $\mu \to e$ decays were observed in a large rectangular Wilson chamber containing 9 copper plates each 4 mm thick. The presence of 550 g/cm^2 of material on top of the chamber determined the momentum of the μ mesons decaying in the chamber as $p_\mu \gtrsim 1.2$ Bev/c. In total, 202 meson decays were observed. In 122 events the positron was emitted into the upper hemisphere and in 80 events, into the lower hemisphere. The relative number of decays in which the positron was emitted into the upper hemisphere is thus $\beta_{Cu} = 0.604 \pm 0.034$,† which corresponds to a degree of polarization $\eta = 0.98^{+0.02}_{-0.32}$. To ascertain that no coarse systematic errors were incurred which might lead to an asymmetry, a control experiment was run in which the copper plates in the chamber were replaced by iron plates, which were so magnetized in the horizontal direction as to depolarize the μ mesons completely. In this experiment the relative number of decays with the positron emitted into the upper hemisphere was $\beta_{Fe} = 0.516 \pm 0.052$, which is in good agreement with an isotropic distribution $\beta = 0.5$.

Theoretical calculations[1] of the degree of polarization of the μ mesons produced by π mesons give the value $\eta = 0.3$. The experimental result is therefore not in agreement with the theoretical value. It also contradicts the experimental value $\eta = 0.19 \pm 0.06$ of Clark and Hersil.[4]

This discrepancy may be due to statistical fluctuations, which have a probability of ~1%. If further investigations confirm the results of our experiment, one may be led to the assumption that the μ mesons within the considered range of momenta are produced in the atmosphere not only on account of the $\pi \to \mu$ decay. In our experiment we studied the polarization of μ mesons with momenta $\gtrsim 1.2$ Bev/c at sea level. Muons with these momenta are mainly produced at heights of several kilometers and have momenta of 4 — 5 Bev/c at the moment of their creation. The $K_{\mu 2}$ decay, which makes up 60% of all K decays, may play an essential role in the production of μ mesons with such momenta. The μ mesons in the $K_{\mu 2}$ decay are practically completely polarized, if the energy spectrum of the K mesons in the atmosphere falls off with the energy corresponding to a parameter value $\gamma \geq 2$ (reference 1). For satisfactory agreement with experiment it is sufficient to assume that, at energies of ~10 Bev, the number of K mesons amounts to 20% of that of the π mesons. The disagreement with the results of reference 4 is then explained by submitting that the μ mesons whose polarization was measured in reference 4 had significantly lower momenta (~2 Bev/c at the moment of creation), to which the contribution from the $K_{\mu 2}$ decay is small.

In this way it is possible to obtain information about the mechanism of the production of μ mesons of high energy by investigating the dependence of the degree of polarization on the μ meson energy.

The authors are grateful to A. I. Alikhanyan for his constant interest in this work and valuable advice.

*Hayakawa made a similar calculation.[2]

†In the calculation of the transmission coefficient of the positrons in the plates and of the number of positrons exiting into the upper hemisphere, we used the Wilson's[3] theoretical energy-range and scattering-range relations.

[1] L. I. Gol'dman, J. Exptl. Theoret. Phys. (U.S.S.R.) **34**, 1017 (1958), Soviet Phys. JETP **7**, 702 (1958).

[2] S. Hayakawa, Phys. Rev. **108**, 1533 (1957).

[3] R. R. Wilson, Phys. Rev. **84**, 100 (1951).

[4] G. W. Clark and J. Hersil, Phys. Rev. **108**, 1538 (1957).

Translated by R. Lipperheide
117

THERMODYNAMIC PROPERTIES OF A DEGENERATE PLASMA

A. A. BEDENOV

Moscow State University

Submitted to JETP editor November 13, 1958

J. Exptl. Theoret. Phys. (U.S.S.R.) **36**, 641-642 (February, 1959)

USING the diagram technique developed by Matsubara[1] for statistical Green's functions in quantum statistical mechanics, we have calculated the interaction correction for the thermodynamic potential of a completely ionized degenerate plasma in the case in which the electron plasma is a Fermi gas while the nuclei form a Boltzmann gas.

The calculation is carried out under the assumption that the mean scattering amplitude in the Coulomb field $e^2/\overline{E}$ is small, compared to the mean distance between particles $R : e^2/R\overline{E} \equiv \alpha \ll 1$. We consider the case in which the chemical potential of the electrons μ and the temperature T are of the same order of magnitude; in this case the mean energy $\overline{E}$ is of the same order of magnitude as the temperature T. We may note that under these conditions the plasma is highly compressed; from the inequality

$$e^2/T \sim e^2/\mu \sim e^2/(\hbar^2/mR^2) \ll R$$

it follows that R, the mean distance between particles is much smaller than the Bohr radius: $R \ll \hbar^2/me^2$.

If these conditions are satisfied the thermodynamic potential Ω is expanded in terms of the small parameter α and with accuracy to terms of order $\alpha^{3/2}$ is given by the expression:

$$\Omega = \Omega_0 - \int V_q n_p^e n_{p+q}^e \, dp dq - \frac{2}{3} V\overline{\pi} e^3 \left(2\frac{\partial n_e}{\partial \mu_e} + \frac{\partial n_i}{\partial \mu_i}\right)^{3/2},$$
$$n_p = [1 + \exp(p^2/2m - \mu)/T]^{-1}, \quad n = \int n_p \, dp. \qquad (1)$$

Here Ω_0 is the thermodynamic potential of an ideal gas of electrons and nuclei, $V_q = 4\pi e^2/q^2$ is the Fourier component of the potential of the Coulomb interaction $e^2/|x|$, μ_e and μ_i are the chemical potentials for the electrons and for the nuclei.

The second term in Eq. (1) represents the ex-

change energy of the electrons which, since it refers to a single particle, is e^2/R in magnitude. The third term in Eq. (1) is the result of the self-consistent interaction between the particles; its order of magnitude is $(e^2/R)(e^2/RT)^{1/2}$ (for a single particle).

We may note that the result given in reference 2 is not correct: this result does not take account of the exchange energy of the electrons and the self-consistent term has been computed incorrectly. This term was computed by means of the Debye-Hückel method; however, this approach cannot be used because the mean wavelength of an electron in a compressed plasma is comparable to the mean distance between particles R.

We are indebted to Academician L. D. Landau for discussion of this problem.

[1] T. Matsubara, Progr. Theoret. Phys. **14**, 351 (1955).

[2] L. D. Landau and E. M. Lifshitz, Статистическая физика (Statistical Physics) GTTI, 1951, §74 [Addison Wesley Cambridge, 1958.]

Translated by H. Lashinsky
118

INTERACTION BETWEEN K AND π MESONS

V. I. OGIEVETSKIĬ

Joint Institute for Nuclear Research

Submitted to JETP editor November 20, 1958

J. Exptl. Theoret. Phys. (U.S.S.R.) **36**, 642-643 (February, 1959)

THE question of the existence of a direct interaction between K and π mesons has been discussed in several papers.[1-5] Because of the pseudoscalar nature of π mesons, a direct three-boson coupling of the type $KK\pi$ is possible only if the K mesons do not have a definite parity[2] or if only combined parity IC is conserved in this interaction.

In a recent paper, Pais[5] discussed the original hypothesis that the parity of charged and neutral K mesons is different. In this case, the demand of charge independence in the pion-nucleon system places strong restrictions on the Lagrangian for strong interactions. Many reactions, for example, the charge exchange one $K^+ + n \to K^0 + p$, turn out to be forbidden. In order to avoid this difficulty, the parity-conserving $[K\pi]$-interaction

$$[K\pi] = f(2m_K)[\bar{K}^+K^0\pi^+ + \bar{K}^0K^+\pi^-], \qquad (1)$$

is introduced. Here m_K is the mass of the K meson. This coupling violates, of course, the symmetry property of strong interactions.[5,6*] Pais considers that the coupling of Eq. (1) makes the main contribution to the "forbidden" reaction noted above. The coupling constant f evaluated from the charge-exchange reaction, turns out to be of the order of the electromagnetic constant e (the real expansion parameter is $(f^2/4\pi)(m_K/m_\pi)^2 \sim 0.3$).

In discussing the consequences of his hypothesis, Pais finds it necessary not only to resort to perturbation theory for the $[K\pi]$- and $[NKY]$-couplings, but also to make assumptions about the behavior of the S matrix far from the energy shell.

The pair production of K mesons

$$\pi^- + p \to K^- + K^0 + p. \qquad (2)$$

seems to us to be of interest in verifying the existence of the $[K\pi]$-interaction (1). This reaction is, according to Pais,[6] forbidden by the symmetry properties of the baryon-meson interactions, and would occur only as a result of the interaction (1). Therefore, the pair production (2) can be represented by the graph (see the figure): after virtual

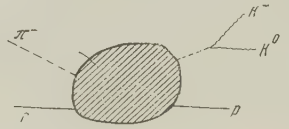

π^--p scattering; the π^- turns into K^- and K^0. If we go over into the system A in which the momentum of the final proton is equal to the sum of momenta of the π^- meson and the initial proton, then the momenta of the K mesons will be equal in magnitude and opposite in direction.

If, in fact, a pair of K mesons is produced as a result of the reaction (1), in the system A the angular distribution of K mesons should be isotropic. Such a reference system always exists. Its velocity relative to the laboratory system is

$$v = c^2(l - p)/(\omega + Mc^2 - E), \qquad (3)$$

where l, ω, and $\mathbf{p}$, E are the momenta and total energy of the π^- meson and final proton, respectively, in the laboratory system; M is the mass of the proton.†

There will not, of course, be complete isotropy, since the final state interaction has not been taken into account, and the $[K\pi]$-coupling was calculated only to first order. However, here it is not neces-

sary to resort to assumptions about the behavior of the S matrix off the energy shell.

Such assumptions can lead to more detailed predictions. For example, if the virtual π^- meson goes off mainly in the direction of the initial π^- meson, just as a real π^- meson resulting from shadow scattering at high energies, then in the center-of-mass system, the summed K-meson momentum is directed mainly forward. Similar assumptions have been used widely by Pais[5] in describing the reaction $\pi + N \rightarrow Y + K$ and others.

The author is deeply grateful to Chou Kuang-Chao for valuable discussion.

*If the K^+ and K^0 have the same parity, then only the combined parity IC is conserved in the interaction of Eq. (1).

†If the K^+ and K^0-mesons have the same parity and strong baryon-meson couplings are symmetrical according to Pais,[6] then one might introduce a 4-boson coupling to avoid the difficulties. Then for non-derivative couplings, for example, $\overline{K}(\tau, \pi)K\pi^0$, considerations about the isotropy of K^- and K^0 in the system A remain valid.

[1] M. Goldhaber, Phys. Rev. **101**, 433 (1956).
[2] J. Schwinger, Phys. Rev. **104**, 1164 (1956).
[3] V. G. Solov'ev, J. Exptl. Theoret. Phys. (U.S.S.R.) **33**, 796 (1957), Soviet Phys. JETP **6**, 613 (1958).
[4] S. Barshay, Phys. Rev. **109**, 2160 (1958); Phys. Rev. **110**, 743 (1958).
[5] A. Pais, Preprint, 1958.
[6] A. Pais, Phys. Rev. **110**, 574 (1958).

Translated by G. E. Brown
119

POLARIZATION OF Au^{198} *NUCLEI IN A SOLUTION OF GOLD IN IRON*

B. N. SAMOĬLOV, V. V. SKLYAREVSKIĬ, and E. P. STEPANOV

Submitted to JETP editor November 25, 1958

J. Exptl. Theoret. Phys. (U.S.S.R.) **36**, 644 (February, 1959)

KHUTSISHVILI[1] proposed a method for the polarization of ferromagnetic nuclei. We undertook to apply this method to nuclei of non-ferromagnetic elements introduced into a ferromagnet. In this communication we report the results of experiments on the polarization of nuclei of Au^{198} in a gold-iron alloy. A specimen (with 0.3% gold by weight), made into a disk 0.3 cm in diameter and 0.01 cm thick, was exposed to thermal neutrons in a reactor. The activity of the Au^{198} nuclei formed in the specimen was approximately 4 microcurie during the time of the experiment. After irradiation, the specimen was annealed in vacuo and soldered to the end of a copper "cold pipe," joined to copper plates pressed into a potassium-chrome-alum block. The salt was adiabatically demagnetized at initial field and temperature values of 20000 gauss and 1.05°K. The gamma rays were registered by two scintillation counters with CsI crystals (diameter 40 mm, height 40 mm).

The Au^{198} disintegrates via β decay ($2^- \rightarrow 2^+$ transition), followed by emission of 411-kev gamma rays ($2^+ \rightarrow 0^+$ transition). At a temperature near 0.015°K the anisotropy of this gamma radiation is $\epsilon = 1 - N(0)/N(\pi/2)$ (where $N(0)$ and $N(\pi/2)$ are the readings of the counters placed parallel and perpendicular to the direction of the polarizing field of the permanent magnet) was found to be 3.3%. The magnetization of the specimen in the field of the permanent magnet was ~ 0.6 of saturation. The true value of the anisotropy, corresponding to 100%magnetization of the specimen, was therefore $\epsilon = 3.3/0.6 = 5.5\%$. It follows from this value of ϵ that the quantity $\beta = \mu H/kTI$ (μ is the magnetic moment of Au^{198}, I the spin of Au^{198}, and H the magnetic field on the Au^{198} nucleus) ranges from 0.3 to 0.4, while the polarization f_1 of Au^{198} ranges from 0.25 to 0.35. The values of β and f_1 were computed from the values of ϵ by the Tolhoek and Cox formulas.[2] The indeterminacy in β and f_1 is caused by the fact that the parameter λ, which depends on the matrix elements of the forbidden Au^{198} transition ($2^- \rightarrow 2^+$), is unknown.

The magnetic moment of Au^{198} is 0.5 ± 0.04 nuclear magnetons.[3] This, together with a value $\beta = 0.3$ to 0.4 measured at $T = 0.015°$, makes $H = (0.5 \text{ to } 0.7) \times 10^6$ oe.

So strong a field can be apparently explained only by the presence of a magnetic moment at the electron shells of the gold atoms in the gold-iron alloy (unlike the gold atoms in the metallic gold, which are diamagnetic). This magnetic moment may be due to an exchange interaction between the electron shells of the gold and iron atoms in the alloy, similar to the interaction between the electrons of the iron atoms. However, it is not impossible for the gold atoms in the alloy to be paramagnetic ions having no exchange bonds with the iron atoms.

It is hoped that the method of introducing nuclei into ferromagnetic alloys will increase considerably the number of elements capable of polariza-

tion. In addition, an investigation of the polarization of nuclei in various alloys may yield information on the magnetic properties of the atoms in these alloys.

The authors express their deep gratitude to E. K. Zavoĭskiĭ for interest in the work and for much valuable advice, and to L. V. Groshev for a review of the results.

[1] G. R. Khutsishvili, J. Exptl. Theoret. Phys. (U.S.S.R.) **29**, 894 (1955), Soviet Phys. JETP **2**, 744 (1956).

[2] H. A. Tolhoek and J. A. M. Cox, Physica, **19**, 101, 673 (1953).

[3] Christensen, Hamilton, Lemonick, Pipkin, Reynolds, and Stroke, Phys. Rev. **101**, 1989 (1956).

Translated by J. G. Adashko
120

DEPOLARIZATION OF μ^- MESONS IN THE FORMATION OF μ-MESIC ATOMS

I. M. SHMUSHKEVICH

Leningrad Physico-Technical Institute

Submitted to JETP editor December 7, 1958

J. Exptl. Theoret. Phys. (U.S.S.R.) **36**, 645-646 (February, 1959)

IN the formation of μ-mesic atoms, the μ^- mesons initially fall into highly excited states. Therefore, during the cascade transitions into the ground state, the mesic atom, on the average, passes through a large number of intermediate states. At lower levels, the inequality

$$\Delta_{nl} \gg \Gamma_{nl}, \tag{1}$$

is valid, where Δ_{nl} is the distance between fine-structure levels with the quantum numbers n and l, but different j ($j = l \pm \frac{1}{2}$), and Γ_{nl} is the width of the corresponding level and is equal to the sum of the radiative width and the width with respect to Auger transitions (the greater Z, the greater the values of n for which condition 1 is satisfied). Physically, inequality (1) signifies that the time during which the μ-mesic atom remains at a given level is considerably greater than the time required for a change of the μ-meson spin under the action of the field of the nucleus. This leads to depolarization of the μ^- mesons, if they were initially polarized. Below, we will estimate the degree of polarization of the μ^- mesons falling into the K shell of the mesic atom. In order not to complicate the question by the necessity of taking hyperfine structure into account, we limit ourselves to the considerations of μ-mesic atoms formed with nuclei of zero spin.

Considering radiative or Auger transitions between levels for which Eq. (1) is satisfied, and remembering that these transitions are essentially dipole transitions, we obtain the following relation between the average values of $\sigma = 2\mathbf{s}$ ($\mathbf{s}$ is the spin operator of the μ^--meson), $\bar{\sigma}_1$ and $\bar{\sigma}_2$, in the initial and final states:

$$\bar{\sigma}_2 = \beta\bar{\sigma}_1, \tag{2}$$

where

$$\beta = \frac{[j_2(j_2+1) - l_2(l_2+1) + 3/4]\,[j_1(j_1+1) + j_2(j_2+1) - 2]}{[j_1(j_1+1) - l_1(l_1+1) + 3/4]\,2j_2(j_2+1)}. \tag{3}$$

The bar over σ signifies that the average is taken firstly over states with given nlj and μ (μ is the projection of j), and secondly over all μ for given nlj.

Let us now consider some excited level of the μ-mesic atom with sufficiently large quantum numbers $n_0 l_0 j_0$, for which condition (1) is still satisfied. Let $\bar{\sigma}_0$ be the average value of σ at this level. The successive application of Eqs. (2) and (3) to the cascade transition from the given level to the K shell leads to a relation between the average values of the spin in the K shell and $\bar{\sigma}_0$ with a definite set of intermediate states passed through by the μ-mesic atom. Averaging over the various possible cascades by using the formulas for the probabilities of radiative[1] and Auger transitions,[2,3] we obtain

$$\bar{\sigma}_K = \beta_K \bar{\sigma}_0. \tag{4}$$

for $\bar{\sigma}_K$, the average value of σ in the K shell.

Analysis of the result thus obtained indicates that if n_0 and l_0 are large and $j_0 = l_0 + \frac{1}{2}$, then for all practical purposes, $\beta_K \approx 1$. But if under the same conditions $j_0 = l_0 - \frac{1}{2}$, then $\beta_K = 0$.[4]

Initially, in the formation of a mesic atom, the μ^- mesons fall into states with large n ($n \approx 14$, 15) and large l. In these excited states, the sign of inequality (1) is reversed, owing to Auger transitions. Therefore, depolarization does not occur in these states. It does not begin until the μ^- meson falls to a level at which Eq. (1) holds. This makes it possible to evaluate $\bar{\sigma}_0$ in the following way: at the instant at which the polarized μ^- meson drops into the level with the quantum numbers $n_0 l_0$, the wave function has the form

$$\Psi_0 = \sum_m a_m \chi_{1/2}\, \varphi_{n_0 l_0 m} = \sum_{m j_0} a_m C^{j_0 m + 1/2}_{l_0 m, 1/2\, 1/2}\, \Phi_{n_0 l_0 j_0 m + 1/2}. \tag{5}$$

where $\varphi_{n_0 l_0 m}$ is the wave function of the mesic atom without taking spin into account, $\chi_{1/2}$ is the spin function of the μ^- meson polarized along the z axis, $\Phi_{n_0 l_0 j_0 m+\frac{1}{2}}$ is the wave function of the mesic atom with the quantum numbers $n_0 l_0 j_0$, and finally, $\mu_0 = m + \frac{1}{2}$. For $t > 0$,

$$\Psi = \sum_{mj_0} a_m C^{j_0 m+1/2}_{l_0 m, 1/2 1/2} \Phi_{n_0 l_0 j_0 m+1/2} \exp(-iE_{n_0 l_0 j_0} t/\hbar). \quad (6)$$

In view of Eq. (1), the states with $j_0 = l_0 + \frac{1}{2}$ and $j_0 = l_0 - \frac{1}{2}$ must be considered independently. Considering that all values of m are equally probable, it is not hard to find that for given n_0 and $l_0 \gg 1$, the probability of falling into states with $j_0 = l_0 + \frac{1}{2}$ and $j_0 = l_0 - \frac{1}{2}$ is equal to $\frac{1}{2}$. Here, the average value $\overline{\sigma}_z$ in each of these states (for $l_0 \gg 1$) is equal to $\frac{1}{3}$. From states with $j_0 = l_0 + \frac{1}{2}$, the μ mesons reach the K shell, retaining the value of $\overline{\sigma}_z$ ($\beta_K \approx 1$) equal to $\frac{1}{3}$. But from states with $j_0 = l_0 - \frac{1}{2}$, the μ^- mesons, in dropping into the K shell, are almost completely depolarized ($\beta \approx 0$). Consequently, the average value of σ_z, i.e., the degree of polarization of the μ^- mesons in the K shell, must be equal to $\frac{1}{6} \approx 17\%$. This agrees approximately with the experimentally-observed value.[5,6]

I would like to express my sincere thanks to S. S. Gershteĭn, V. N. Gribov, and A. Z. Dolginov for their interest in the work and for useful discussions.

[1] H. A. Bethe, Quantum Mechanics of Simple Systems (Russ. transl.). ONTI, 1935.

[2] G. R. Burbridge and A. H. de Borde, Phys. Rev. **89**, 189 (1953).

[3] A. H. de Borde, Proc. Phys. Soc. **67**, 57 (1954).

[4] I. M. Shmushkevich, Nucl. Phys. (in press).

[5] Garwin, Lederman and Weinrich, Phys. Rev. **105**, 1415 (1957).

[6] Ignatenko, Egorov, Khalupa, and Chultem, J. Exptl. Theoret. Phys. (U.S.S.R.) **35**, 894, 1131 (1958), Soviet Phys. JETP **8**, 621 792 (1959).

Translated by D. Lieberman
121

ON $\mu^+\mu^-$ ANNIHILATION AND THE DECAY OF NEUTRAL MESONS

Ya. B. ZEL'DOVICH

Institute of Theoretical and Experimental Physics, Academy of Sciences, U.S.S.R.

Submitted to JETP editor December 10, 1958

J. Exptl. Theoret. Phys. (U.S.S.R.) **36**, 646-647 (February, 1959)

BY analogy with e^+e^- annihilation (see reference 1), it can be expected that the $\mu^+\mu^-$ "atom" will yield two quanta in the para-state and three quanta in the ortho-state.

Berestetskii and Pomeranchuk[2] have pointed out the possibility of the direct transformation of an e^+e^- pair into $\mu^+\mu^-$ through one virtual quantum.* Considering the inverse process, we come to the conclusion that in addition to $\mu^+\mu^-$ annihilation with emission of quanta, the transformation of $\mu^+\mu^-$ into an e^+e^- pair is also possible. This process is of the same order with respect to $e^2/\hbar c$ as two-quantum annihilation.

It is easy to convince oneself that the transformation of $\mu^+\mu^-$ into e^+e^- in this order cannot occur in the para-state. On the other hand, in the ortho-state of $\mu^+\mu^-$, the transformation into e^+e^- proceeds with a probability three times smaller than the probability of two-quantum annihilation of the para-state. Thus, the probability of the transformation of ortho-$\mu^+\mu^-$ into e^+e^- is approximately 400 times greater than the probability of the three-quantum annihilation of ortho-$\mu^+\mu^-$.

The pseudoscalar neutral meson π^0 is similar (see reference 3) to the para-state of $\mu^+\mu^-$ or e^+e^-; the decay of π^0 into two quanta conforms to this analogy. The ortho-state of $\mu^+\mu^-$ would be similar to a neutral odd-parity meson with spin 1. As is clear from what has been presented above, such a meson would decay not into three quanta, but directly into an e^+e^- pair, with a lifetime of the order of the lifetime of the π^0 (compare reference 4).

Careful measurements of e^+e^- pairs during energetic collisions of cosmic particles with nuclei were performed[5,6] in connection with measurements of the lifetime of the π^0. The results of these measurements apparently rule out the existence of a nuclearly-active neutral meson with spin 1, because the number of e^+e^- pairs produced in the vicinity of the collision agrees with Dalitz's calculation[7] of the relative probability of the process $w(\pi^0 = \gamma + e^+ + e^-)$ namely $w(\pi^0 = 2\gamma) = 1/80$.

Clearly, no electromagnetic processes, including production of an e^+e^- pair, can be observed in the $\pi^+\pi^-$ "atom," because the transformation of $\pi^+\pi^-$ into $2\pi^0$ will occur with overwhelming probability.

I would like to thank I. Ya. Pomeranchuk for opportunely calling my attention to reference 2.

*As noted by the authors, the expressions for the cross section, given in reference 2, must be multiplied by 4.

[1] I. Ya. Pomeranchuk, Dokl. Akad. Nauk SSSR **60**, 218 (1947).

[2] V. B. Berestetskiĭ and I. Ya. Pomeranchuk, J. Exptl. Theoret. Phys. (U.S.S.R.) **29**, 864 (1955), Soviet Phys. JETP **2**, 580 (1956).

[3] E. Fermi and C. N. Yang, Phys. Rev. **76**, 1739 (1949).

[4] S. Sakafa and Y. Tanikawa, Phys. Rev. **57**, 548 (1940).

[5] B. M. Anand, Proc. Roy. Soc. **A220**, 183 (1953).

[6] Brisbout et al., Phil. Mag. **1**, 605 (1956).

[7] R. H. Dalitz, Proc. Phys. Soc. **A64** 667 (1957).

Translated by D. Lieberman
122

ELECTRON PARAMAGNETIC RESONANCE OF Co^{2+} IN CORUNDUM

G. M. ZVEREV and A. M. PROKHOROV

Institute of Nuclear Physics, Moscow State University

Submitted to JETP editor December 16, 1958

J. Exptl. Theoret. Phys. (U.S.S.R.) **36**, 647-648 (February, 1959)

LINES of electron paramagnetic resonance of the cobalt ion were observed at frequencies of 9800 and 37500 Mcs at $T = 4.2°K$ in a monocrystal of corundum containing cobalt as an impurity. All the lines have a superfine structure of eight components in accordance with the value of the spin of the Co^{59} nucleus, $I = 7/2$.

When the magnetic field is parallel to the trigonal axis of the crystal, an intense line is observed; the components of this line are strongly non-equidistant at the frequency 9800 Mcs. When the magnetic field is perpendicular to the trigonal axis, the components of the superfine structure of this line are equidistant at both frequencies.

The observed spectrum can be ascribed to Co^{2+} with an effective spin of $S' = 1/2$. The superfine structure was not studied in detail; the g-factors, measured with respect to the center of the line, are $g_{\parallel} = 2.27$ and $g_{\perp} = 4.95$.

In addition to the intense line, several weak lines with a superfine structure characteristic of cobalt are observed.

As compared with the ions Cr^{3+}, Fe^{3+}, and V^{3+}, the ion Co^{2+} in corundum has a considerably longer relaxation time, so that at $T = 4.2°K$ the saturation effect occurs at powers $\sim 10^{-8}$ w.

Translated by D. Lieberman
123

SOVIET PHYSICS JOURNALS

Published in English by the American Institute of Physics

Soviet Physics – JETP

A translation, beginning with 1955 issues of "Journal of Experimental and Theoretical Physics" of the USSR Academy of Sciences. Leading physics journal of Soviet Union. Similar to "The Physical Review" in quality and range of topics. Outstanding new work is most likely to appear in this journal.

Twelve issues, approximately 3,500 pages. $75 domestic, $79 foreign. Libraries $35 domestic, $39 foreign. Single copies, $8.*

Soviet Physics – SOLID STATE

A translation, beginning with 1959 issues of "Fizika Tverdogo Tela" of the USSR Academy of Sciences. Offering results of theoretical and experimental investigations in the physics of semiconductors, dielectrics, and on applied physics associated with these problems. Also publishes papers on electronic processes taking place in the interior and on the surface of solids.

Twelve issues, approximately 2,000 pages. $55 domestic, $59 foreign. Libraries $25 domestic, $29 foreign. Single copies, $8.*

Soviet Physics – TECHNICAL PHYSICS

A translation, beginning with the 1956 issues of the "Journal of Technical Physics" of the USSR Academy of Sciences. Contains work on plasma physics and magnetohydrodynamics, aerodynamics, ion and electron optics and radio physics. Also publishes articles in mathematical physics, the physics of accelerators and molecular physics.

Twelve issues, approximately 2,000 pages, $55 domestic, $59 foreign. Libraries $25 domestic, $29 foreign. Single copies, $8.*

Soviet Physics– ACOUSTICS

A translation, beginning with 1955 issues of "Journal of Acoustics" of USSR Academy of Sciences. Devoted principally to physical acoustics but includes electro, bio, and psycho acoustics. Mathematical and experimental work with emphasis on pure research.

Four issues, approximately 400 pages. $12 domestic, $14 foreign. (No library discounts) Single copies, $4.

Soviet Physics – DOKLADY

A translation, beginning with 1956 issues of "Physics Sections" of Proceedings of USSR Academy of Sciences. All-science journal offering four-page reports of recent research in physics and borderline subjects.

Six issues, approximately 1,500 pages. $35 domestic, $38 foreign. Libraries $15 domestic, $18 foreign. Single copies Vols. 1 and 2, $5; Vol. 3 and later issues, $7.*

Soviet Physics – CRYSTALLOGRAPHY

A translation, beginning with 1957 issues of the journal "Crystallography" of USSR Academy of Sciences. Experimental and theoretical papers on crystal structure, lattice theory, diffraction studies, and other topics of interest to crystallographers, mineralogists, and metallurgists.

Six issues, approximately 1,000 pages. $25 domestic, $27 foreign. Libraries $10 domestic, $12 foreign. Single copies, $5.*

SOVIET ASTRONOMY – AJ

A translation, beginning with 1957 issues of "Astronomical Journal" of USSR Academy of Sciences. Covers various problems of interest to astronomers and astrophysicists including solar activity, stellar studies, spectroscopic investigations of radio astronomy.

Six issues, approximately 1,100 pages. $25 domestic, $27 foreign. Libraries $10 domestic, $12 foreign. Single copies, $5.*

Soviet Physics – USPEKHI

A translation, beginning with September, 1958 issue of "Uspekhi Fizicheskikh Nauk" of USSR Academy of Sciences. Offers reviews of recent developments comparable in scope and treatment to those carried in "Reviews of Modern Physics." Also contains reports on scientific meetings within the Soviet Union, book reviews, and personalia.

Six issues, approximately 1,700 pages. (Contents limited to material from Soviet sources.) $45 domestic, $48 foreign. Libraries $20 domestic, $23 foreign. Single copies, $9.*

*For libraries of non-profit degree-granting academic institutions.

Subscription prices subject to annual variation depending on size of Russian originals.

Please send orders and inquiries to

American Institute of Physics

335 East 45 Street, New York 17, N. Y.